

**The Synthesis of Functionalized Glycosides:
Coordination Chemistry, Antiparasitic Activity, Precursors to
Conformationally Constrained Macrocyclic
Architectures and Photophysical Properties**

A thesis submitted to Maynooth University in fulfilment of the
requirements for the degree of

Doctor of Philosophy

by

Andrew Reddy B.Sc.



**Maynooth
University**
National University
of Ireland Maynooth

Department of Chemistry,

Maynooth University,

Maynooth,

Co. Kildare,

Ireland.

February 2017

Research Supervisor: Dr Trinidad Velasco-Torrijos

Head of Department: Dr John Stephens

Dedication

To my parents, Eileen and Seamus. Thank you for everything.

Table of Contents

Declaration	i
Acknowledgments.....	ii
Abstract	iv
Abbreviations	vi
Chapter 1: Introduction	
1.1 Biological Role of Carbohydrates	2
1.1.1 Carbohydrates as a Source of Energy	2
1.1.2 Carbohydrates as Information Carrying Molecules.....	2
1.1.3 Structural Functions of Carbohydrates.....	3
1.2 Chemical Attributes of Carbohydrates.....	3
1.2.1 Carbohydrates as Scaffolds in Synthesis	3
1.2.2 Carbohydrate Conjugation	4
Chapter 2: Design, Synthesis and Characterization of Novel Amino- and Iminopyridyl Antiparasitic Agents	
2.1. Introduction.....	6
2.1.1 Leishmaniasis.....	6
2.1.1.1 Current Therapies	7
2.1.1.2 Metallodrugs as Novel Antileishmanial Therapeutics	10
2.1.2 Chagas' Disease	16
2.1.2.1 Current Therapies	18
2.1.2.2 Metallodrugs as Novel Antichagasic Therapeutics.....	20
2.1.3 Carbohydrate Conjugation in Drug Design:.....	24
2.1.3.1 Carbohydrate Conjugated Metal Chelators.....	25
2.2 Aim.....	31
2.3 Results and Discussion	33
2.3.1 Synthesis of the N ₂ Ligand Series	33
2.3.1.1 Imine ligands.....	33
2.3.1.2 Amine Ligands.....	37
2.3.2 Coordination complexes of the N ₂ Series	42
2.3.3 Synthesis of the N ₂ O Series	59
2.3.4 Coordination Chemistry of the N ₂ O Series	65
2.4 Conclusion	80

Chapter 3: Biological Evaluation of Novel Antiparasitic Agents

3.1 Aim.....	83
3.2 Results and Discussion	84
3.2.1 Evaluation of <i>In Vitro</i> Cytotoxicity to Macrophage Cells.....	84
3.2.2 Evaluation of Antileishmanial Activity	86
3.2.2.1 <i>In Vitro</i> Studies on <i>L. amazonensis</i> Viability	86
3.2.2.2 <i>L. amazonensis</i> Promastigote Morphology Studies.....	91
3.2.2.3 Insights Gained from Biological Studies of <i>L. amazonensis</i>	92
3.2.2.4 Conclusion of <i>L. amazonensis</i> Studies	95
3.2.3 Evaluation of Antitrypanosomal Activity	95
3.2.3.1 <i>In Vitro</i> Studies on <i>T. cruzi</i> Viability	95
3.2.3.2 <i>T. cruzi</i> Trypomastigote Morphology Studies	99
3.2.3.3 Insights Gained from Biological Studies of <i>T. cruzi</i>	101
3.2.3.4 Conclusions of <i>T. cruzi</i> Biological Studies	103
3.2.4 <i>In Vivo</i> Immunogenicity in <i>G. mellonella</i>	103
3.2.4.1 <i>Galleria Mellonella</i> as a Toxicology Model for the Analysis of Drug Candidates	103
3.2.4.2 <i>G. mellonella</i> Studies.....	104
3.2.5 Susceptibility of Compounds to Enzymatic Hydrolysis.....	107
3.2.5.1 Results of Enzymatic Hydrolysis Studies	108
3.2.5.2 Conclusion of Glucosidase Studies	119
3.3 Conclusion	119

Chapter 4: Studies Towards the Synthesis of a Galactosyl-1,2,3-Triazolyl Derived Macrocycle

4.1 Introduction.....	123
4.1.1 Carbohydrate functionalized macrocycles	123
4.1.2 Carbohydrates as Pendant Groups.....	123
4.1.3 Carbohydrates as Internal Ring Constituents	125
4.1.4 Carbohydrate Macrocycles Containing Triazole Rings	128
4.1.5 Macrocyclization Strategies.....	130
4.2 Aim.....	132
4.3 Results and Discussion	134
4.3.1 Investigations into the Synthesis of a Serine Derived Macrocycle 4.1a	134
4.3.1.1 Synthesis of Peracetylated Galactosyl Donor 4.2	134

4.3.1.2	Glycosylation Studies with <i>N</i> -Fmoc-L-Serine Methyl Ester.....	137
4.3.2	Investigations into the Synthesis of a 1, 2, 3-Triazolyl-Ethylene Derived Macrocycle	147
4.3.2.1	CuAAC Macrocyclization Approach (Route A)	148
4.3.2.2	Intramolecular Glycosylation Route (Route B)	154
4.4	Conclusion	162
Chapter 5: Investigations into the Fluorescent Properties of Functionalized Imino- Pyridyl Compounds		
5.1	Introduction.....	165
5.1.1	Fluorescence Spectroscopy	165
5.1.2	Structural Attributes of Fluorophores	166
5.1.3	Fluorescent glycosides.....	167
5.2	Aim.....	173
5.3	Results and Discussion	175
5.3.1	Synthesis	175
5.3.1.1	Synthesis of Mannoside 5.1	175
5.3.1.2	Synthesis of Galactoside 5.2	176
5.3.1.3	Synthesis of THP Derivative 5.3	177
5.3.1.4	Synthesis of Menthol Derivative 5.4	177
5.3.2	Fluorescence Studies	179
5.3.2.1	Fluorescence Studies of 2.33	179
5.3.2.2	Fluorescence Studies of 2.34	180
5.3.2.3	Fluorescence Studies of 2.35	181
5.3.2.4	Fluorescence Studies of 5.1	182
5.3.2.5	Fluorescence Studies of 5.2	183
5.3.2.6	Fluorescence Studies of 5.3	185
5.3.2.7	Fluorescence Studies of 5.4	186
5.3.3	DFT Studies	188
5.4	Conclusion	192
Chapter 6: Experimental Details		
6.1	General Procedures.....	194
6.2	Chapter 2	195
6.2.1	N ₂ Series.....	195
6.2.2	N ₂ O Series	214

6.3 Chapter 3	228
6.4 Chapter 4	230
6.5 Chapter 5	241
6.5.1 Synthesis	241
6.5.2 Fluorescence Studies	248

Chapter 7: Conclusions and Future Work

Appendix

Publications	281
Oral Presentations	281
Poster Presentations	281
Crystallographic Data	282
2.18	282
2.19	287
2.21	296
2.33	301
2.34	305
2.44	309
2.46	313

Declaration

I hereby certify that this thesis has not been submitted before, in whole or in part, to this or any other university for any degree and is, except where otherwise stated, the original work of the author.

Signed: _____

Date: _____

Acknowledgments

I would firstly like to thank my supervisor Dr Trinidad Velasco-Torrijos for her help and constant support throughout my PhD, and for letting me follow my own research interests. Thank you to the head of the department Dr John Stephens for all his assistance. I owe a sincere debt of gratitude to Dr Malachy McCann, for all his advice throughout my PhD, and for giving me a love of coordination chemistry. Thanks to all the other academic staff who have helped me throughout my studies, in particular Dr Frances Heaney and Dr Denise Rooney. Thank you also Dr John McGinley, for originally agreeing to take me on and continuing to offer advice after you moved.

Thanks to all the technical staff of the department, in particular Ria, Barbara, Ken, Ollie and Walter. Your help with analysis and advice has been invaluable to me. Many thanks to Donna and Carol for all your help. A special thank you to Noel, for recovering my data when my hard drive crashed and solving countless problems for me during my PhD. You are a treasure to the department.

I would also like to thank Dr Brendan Twamley for solving X-ray crystal structures and Prof Kevin Kavanagh and his lab for letting me pretend to be a biologist while I did my *Galleria* studies. Also, a huge debt of gratitude is owed to Prof André Luis Souza dos Santos and his research group for their collaboration on the antiparasitic work.

A massive thank you all the postgrads of the department, past and present, you've made my PhD an absolute pleasure. I am incredibly lucky to have worked with such great people. Thanks for all the nights out, nights in, department parties and banter. I don't think I will ever be able to repeat the craic that I've had in the tea room. Thanks to the other members of the TVT group, Jessica (dinner ideas, *that* song), Harlei (carb binges) and Matthew. To the old TVT crowd, Gama, Roisin and Lorna, thanks for welcoming me to the lab. To the rest of the lad(ie)s, it's been fantastic. Chigstopher (the degenerate pest in my office, tea drinker extraordinaire and occasionally useful computational chemist), Jack (cyka blyat) and Ross (shut up Driver), Barry and Adam, thanks for the laughs. Many thanks to the girls in the writing room, Michelle D (for feeding me), Jacinta (Endnote help and all round legend) and Sam (for putting up with my moaning).

A massive thank you to everyone else in the department, Muhib (for putting up with my stupid questions), Michelle Q, Mark, Karen, Michelle K everyone else I didn't mention. I don't think I will ever work with people as funny, and entertaining again. Thanks also to Isabel for looking after my crystals and making sure they got to Trinity safe and sound.

"The chymists are a strange class of mortals, impelled by an almost insane impulse to seek their pleasures amid smoke and vapour, soot and flame, poisons and poverty; yet among all these evils I seem to live so sweetly that may I die if I were to change places with the Persian king."

— Johann Joachim Becher (1667)

This is certainly true. Thanks to everyone in the department for making my time here as enjoyable as it was.

Finally, a huge thank you to my family and friends back home. Mam and Dad, I could not have gotten through this without your constant support and encouragement. Thank you.

Abstract

The research presented in this thesis focuses on the synthesis of functional glycosides and the investigation of their properties. This included the study of their ability to form metal complexes and the study of the antiparasitic activity of both the free glycosides and metal complexes, the use of glycosides to serve as precursors to conformationally constrained macrocyclic molecules and a preliminary investigation of the photophysical properties of a collection of glycosidic compounds.

Two novel classes of glycosylated chelators were synthesized and characterized; one containing a dinitrogen aminopyridyl chelating motif and another containing a dinitrogen/oxygen phenoxy-iminopyridyl metal binding unit. The ability of these compounds to form stable metal complexes with several metals (Cu(II), Zn(II) and Fe(II)) was investigated and the coordination complexes obtained were characterized.

The anti-chagasic and anti-leishmanial activity of a selection of these compounds were evaluated in collaboration with the group of Prof André Luis Souza dos Santos at the Microbiology Institute Paulo de Góes in Universidade Federal do Rio de Janeiro (UFRJ), in addition to their toxicity towards mammalian macrophage cells. Several compounds with antiparasitic activity with excellent selectivity indexes were identified. From the analysis of these preliminary investigations, structural features were identified that appear to be necessary for their antiparasitic activity. Preliminary investigations into the probably mode of action involving the study of the susceptibility of the glycosylated compounds to enzymatic hydrolysis by β -glycosidase were carried out. The toxicity of the most potent compounds was also investigated using the *Galleria Mellonella* model.

The use of carbohydrates as scaffolds to synthesize conformationally constrained macrocycles was also explored. To this end, several galactosyl donors were synthesized and their reactivity towards glycosylation with a serine derivative and 2-chloroethanol was investigated. Two different synthetic strategies were compared to highlight the intramolecular glycosylation as the most suitable route for macrocyclization.

Finally, the photophysical properties of a collection of glycosides and structural analogues was examined. This involved the synthesis of a family of substituted iminopyridyl compounds and the preliminary analysis of their fluorescent properties. Based on these studies, a plausible explanation for the fluorescent behaviour of glycoside functionalised iminopyridyl compounds is proposed.

Abbreviations

a.u: Absorbance Units

Ar: Aromatic

BODIPY: Boron dipyrromethene

Bipy: Bipyridine

COSY: Homonuclear Correlation spectroscopy

CuAAC: Copper catalysed azide-alkyne cycloaddition

DBU: 1, 8-Diazabicyclo[5.4.0]undec-7-ene

DCM: Dichloromethane

DEPT: Distortionless enhancement by polarization transfer

DFT: Density functional theory

DIAD: Diisopropyl azodicarboxylate

DMF: Dimethyl formamide

DMTST: Dimethyl(thiomethyl)sulfonium triflate

DMSO: Dimethyl sulfoxide

Dtmp: 5,7-Dimethyl-s-triazolo[1,5-a]pyrimidine

Et₂O: Diethyl ether

EtOH: Ethanol

ESI: Electrospray ionisation

EtOAc: Ethyl acetate

Fmoc: 9-Fluorenylmethyloxycarbonyl

FRET: Förster resonance energy transfer

HMBC: Heteronuclear multiple bond correlation

HOMO: Highest occupied molecular orbital

HPLC: High performance liquid chromatography

HRMS: High resolution mass spectroscopy

HSQC: Heteronuclear single quantum correlation

IPA: Isopropanol

IR: Infrared

ISC: Intersystem crossing

LUMO: Lowest unoccupied molecular orbital

MeCN: Acetonitrile

MeOH: Methanol

MO: Molecular orbital

Mp: Melting point

MTT: 3-(4,5-dimethylthiazol-2-yl)-2,5-diphenyltetrazolium bromide

NBS: N-Bromosuccinimide

NIS: N-Iodosuccinimide

NKT: Natural killer cells

NMR: Nuclear magnetic resonance

Phen: Phenanthroline

PPTS: Pyridinium *p*-toluenesulfonate

PSYCHE: Pure shift yielded by chirp excitation

Pyr: Pyridine

ROS: Reactive oxygen species

TBAB: Tetrabutylammonium bromide

TBAI: Tetrabutylammonium iodide

TFA: Trifluoroacetic acid

THF: Tetrahydrofuran

THP: Tetrahydropyran

TLC: Thin layer chromatography

TOCSY: Total correlation spectroscopy

TPPO: Triphenylphosphine oxide

UV-vis: Ultraviolet-visible spectroscopy

Chapter 1: Introduction

1.1 Biological Role of Carbohydrates

Carbohydrates are a class of biological molecules consisting of carbon, hydrogen and oxygen and generally conform to the formula $C_nH_{2n}O_n$. They are found ubiquitously in nature and perform many roles in biology. Some of these primary functions are as sources of energy, information transfer and as structural molecules.

1.1.1 Carbohydrates as a Source of Energy

Carbohydrates are the primary source of energy in nature. Every year, 10 billion metric tons of CO_2 and H_2O are converted by photosynthesis into cellulose and other carbohydrate derived plant products.¹ In plants, energy is primarily stored as starch, a polymer formed primarily of $\alpha(1\rightarrow4)$ linked glucose monomers. Animals utilize the structurally related carbohydrate polymer glycogen as the primary polysaccharide used to store energy. Like starch, this is comprised of $\alpha(1\rightarrow4)$ linked glucose monomers. However, unlike starch, glycogen is highly branched with $\alpha(1\rightarrow6)$ bonds occurring every 24 to 30 glucose units. These polymers are degraded enzymatically and release energy upon cellular respiration which oxidizes the carbohydrates to CO_2 and H_2O .²

1.1.2 Carbohydrates as Information Carrying Molecules

Carbohydrates serve as information carrying molecules in nature and are involved in the majority of cell-cell interactions. They are well suited to this task due to the multitude of complex structures that carbohydrates can exist as; a pyranose sugar with 5 stereocenters has 2^5 isomers possible, without considering other forms that sugar can exist in. This array of distinct structures originating from such a small molecule makes them unique biomolecules in terms of information storage. Carbohydrates, often conjugated to a protein or other biomolecule, serve as mediators for a range of signalling processes such as immune signalling, blood clotting and microbial adhesion.^{1,3} These interactions occur primarily by the recognition of the carbohydrate motif by protein based receptors, known as lectins.⁴

1.1.3 Structural Functions of Carbohydrates

Carbohydrates play an essential role in providing rigid structures in plants. Cellulose, the most abundant polymer on earth, is produced at a rate of approximately 1.5×10^{12} tons per year.⁵ It is a tough, fibrous material that is found in wood and the plant cell wall. Like glycogen and starch, it is comprised of glucose monomers however it is linked in a $\beta(1 \rightarrow 4)$ fashion unlike the $\alpha(1 \rightarrow 4)$ linkage found in the above polymers. Most animals cannot utilize cellulose as a fuel source as they lack the enzymes necessary to digest it. Some animals such as cows and sheep have a symbiotic relationship with bacteria that live in their rumen which possess enzymes to break down cellulose which is then digested by the animal.¹

1.2 Chemical Attributes of Carbohydrates

1.2.1 Carbohydrates as Scaffolds in Synthesis

Carbohydrates are extremely useful as scaffolds upon which to build highly specific structures with control over the final stereochemistry and conformation of the molecule. A typical hexose can exist as an open chain structure with 4 chiral centres, a 6-membered heterocyclic ring (pyranose) with 5 chiral centres, or as a 5-membered heterocyclic ring (furanose), also with 5 chiral centres. This extra chiral centre present in the cyclic form of saccharides occurs at the anomeric carbon, termed the C-1 position. This chiral centre has a significant effect on the reactivity and behaviour in biological systems and are denoted as α or β , depending on their relationship to the configuration of a reference group. This reference group is the stereocenter furthest from the C-1 position (typically C-5). An α -anomer is one which the C-1 OH group is on the same side as the reference group when the sugar is drawn as a Fischer projection, while a β anomer has the anomeric OH group on the opposite side. As described above, there is an enormous variety of possible structures available, depending on the sugar and the form it adopts. This feature, together with the abundance of synthetic methodologies available for the selective manipulation of the sugars functional groups, make carbohydrates ideal synthetic building blocks.

1.2.2 Carbohydrate Conjugation

Carbohydrates are extremely attractive as pendant groups to conjugate to a molecule with the intention of modifying its physicochemical properties. Quite often, this attribute is solubility, as the hydroxyl groups present in the carbohydrate greatly improve the solubility of the compound in water and other hydrophilic solvents.⁶

Carbohydrates are also utilized to modulate the biological properties of molecules of interest. As described above, carbohydrates are involved in a multitude of highly specific biological recognition processes. This can be taken advantage of to target specific receptors by conjugating the sugar motif of interest to a molecule and thereby utilize naturally occurring biological processes such as active transport or recognition by the immune system in conjunction with the activity of the conjugated molecule.⁷, The highly specific nature of carbohydrate recognition *in vivo* makes them uniquely effective as activity modifying conjugates in the design of biologically active molecules.

**Chapter 2: Design, Synthesis and Characterization of Novel
Amino- and Iminopyridyl Antiparasitic Agents**

2.1 Introduction

2.1.1 Leishmaniasis

Leishmaniasis is a group of tropical diseases resulting from infection of protozoan parasites of the genus *Leishmania*. It occurs in several forms, of which the three most important are cutaneous, mucocutaneous and visceral leishmaniasis. The cutaneous form presents with skin ulcers, while the mucocutaneous form presents with ulcers of the skin, mouth, and nose. Visceral Leishmaniasis, the most severe form, begins with skin ulcers and then later presents with fever, low count of red blood cells and enlarged spleen and liver.⁸ This disease is fatal if left untreated.

Leishmaniasis affects more than 12 million people worldwide in 88 countries, primarily in South America, Africa and Asia.⁹ It is transmitted by the bite of infected female sandflies which can transmit the infective stage of the parasite, metacyclic promastigotes, during the blood meal. The promastigotes then develop into amastigotes inside host macrophages where they multiply and spread to different tissues in the host. The cycle of infection continues when they are ingested by another sandfly during a blood meal and they go on to develop into metacyclic promastigotes inside the midgut of the sandfly. (Figure 2. 1)

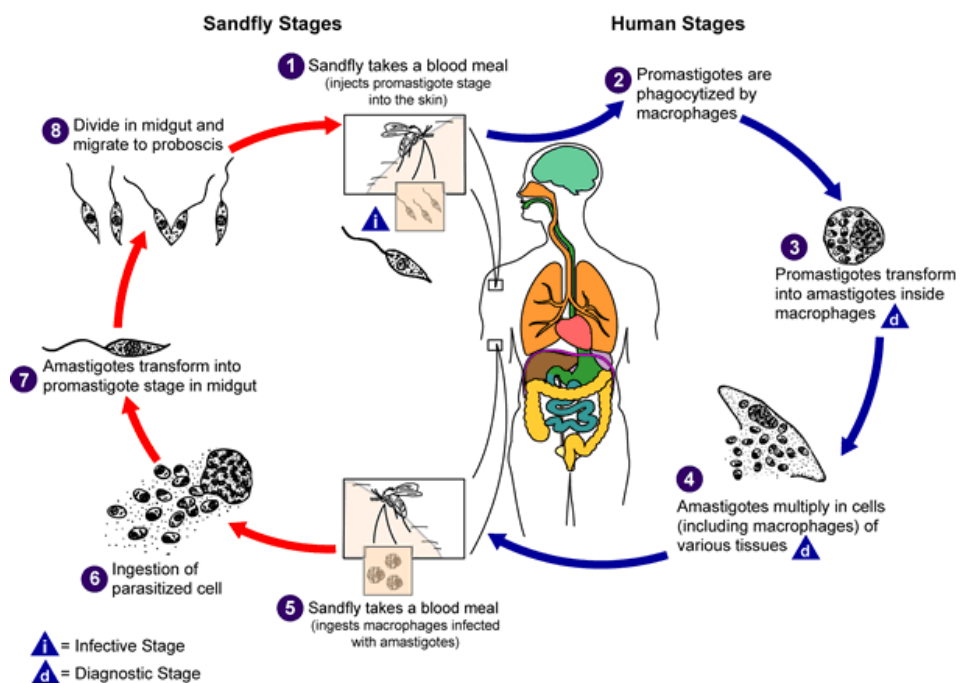


Figure 2. 1. Life cycle of leishmania parasite.³

2.1.1.1 Current Therapies

Pentavalent Antimonials:

First line treatment of leishmaniasis typically employs pentavalent antimonial based therapeutics. These were first introduced in 1945 building upon the work of Prof. Upendranath Brahmachari. He discovered urea stibamine in 1912, the first effective drug against *L. donovani*, for which he was nominated for the Nobel Prize in Physiology and Medicine in 1929 and again in 1949. The most common drugs prescribed are sodium stibogluconate and meglumine antimoniate (**Figure 2.2**) although these present with several problems. The first of which is the route of administration; these drugs are not orally active and require intramuscular or intralymphatic injection every day for up to 3 days.¹⁰ In addition to this, there are several unwanted side effects which include pancreatitis, peripheral neuropathy, gastrointestinal problems, hepatotoxicity, renal toxicity and cardiotoxicity leading to sudden death.¹¹ Due to their widespread use over the last 60 years there has been widespread resistance to these drugs with more than 60% of patients in the Indian state of Bihar presenting with cases that are unresponsive to antimony based drugs.¹²

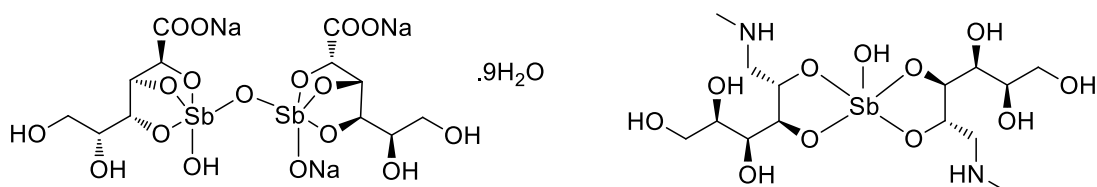


Figure 2. 2. Chemical structures of sodium stibogluconate and meglumine antimoniate.¹³

Amphotericin B:

In the areas where resistance to antimonial antileishmanial treatment is common, amphotericin B (**Figure. 2.3**), a macrolide polyene antibiotic, is the preferred drug of choice.¹⁴ Its mode of action involves the complexation with ergosterol, a major component of the cell wall of leishmania parasites. Pores in the cell membrane are formed following this complexation which causes increased membrane permeability

Miltefosine:

Miltefosine (**Figure 2.4**) is the first orally administered drug available for the treatment of leishmaniasis. It was originally developed as a treatment for skin metastasis of breast cancer and its use as an antileishmanial therapy began in the mid 1980's in India. Several clinical trials were conducted throughout the 1990's and it achieved FDA approval in 2014 for treatments of all forms of leishmaniasis making it the first approved drug for cutaneous and mucosal leishmaniasis.¹⁸

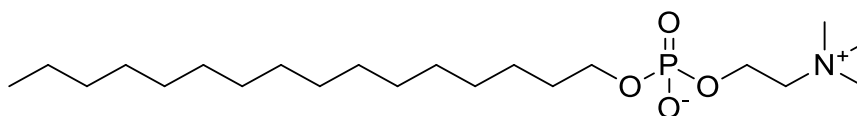


Figure 2. 4. Chemical structure of Miltefosine.¹⁹

Miltefosine shows high activity in several strains of Leishmaniasis with a cure rate of above 90% in India and Colombia. However, against *L. braziliensis* and *L. mexicana* it only showed activity in approximately 50% of cases.²⁰ The mechanism of action is unknown but several mechanisms have been proposed including inhibition of phosphatidylcholine biosynthesis, alteration of phospholipid and sterol composition of the parasite membrane and inhibition of calcium homeostasis.¹⁹ As with other treatments for leishmaniasis, miltefosine is not without its drawbacks. It is known to be teratogenic in addition to causing hepatotoxicity, gastrointestinal problems and nephrotoxicity.

Paromomycin:

Paromomycin (**Figure 2.5**) is a broad spectrum aminoglycoside antibiotic which is used for the treatment of visceral and cutaneous leishmaniasis although it does display reduced activity against visceral leishmaniasis. It can be administered both as a parenteral injection for visceral leishmaniasis and as a topical ointment for the treatment of cutaneous leishmaniasis. It is now off patent and is recognised as an orphan drug by both the FDA and EMEA and was approved in India in 2006 as a treatment for visceral leishmaniasis on the recommendation of the WHO.¹¹ The precise mode of action of paromomycin against *leishmania* is not fully elucidated, it has been observed that it inhibits protein synthesis of the parasites by promoting

ribosomal subunit association following a low Mg^{2+} concentration induced dissociation. This association of the ribosomal subunits prevents subunit recycling and ultimately leads to the death of the parasite.²¹ Other proposed mechanisms include the alteration of membrane fluidity and the induction of respiratory dysfunction.^{22,23} Paromomycin has exhibited adverse reactions in patients such as ototoxicity, diarrhoea, abdominal cramps and nausea. Resistance has not been observed in the clinic but has been shown in a laboratory strain of *L. donovani*.²⁴

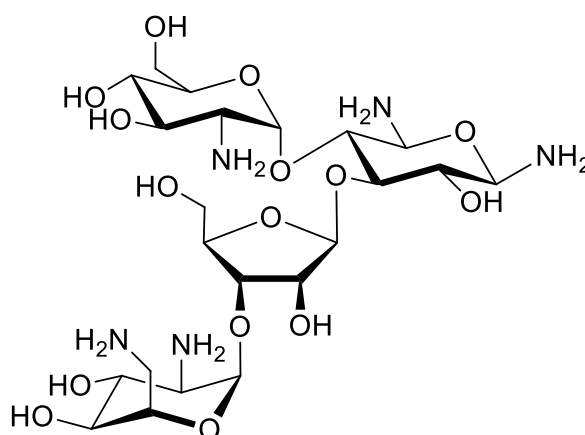


Figure 2. 5. Chemical structure of paromomycin.¹¹

2.1.1.2 Metallodrugs as Novel Antileishmanial Therapeutics

Metallodrugs have been drawing increasing interest in recent years for the development of new antiparasitic drugs. Three main strategies have emerged to best utilise metals in this regard;

- 1) The complexation of a metal to a known antiparasitic agent to modify and improve its pharmacodynamics properties e.g. Incorporating a redox active metal centre to generate reactive oxygen species (ROS) to induce parasite death.²⁵
- 2) The complexation of a metal to known antiparasitic agent to modulate its pharmacokinetic profile e.g. The complexation of ruthenium to benznidazole to improve solubility and cellular uptake.²⁶
- 3) The use of novel metal complexes as antiparasitic therapeutics.

A wide variety of metal containing compounds have been investigated as novel antileishmanial agents.

2.1.1.2.1 Cu(II) Complexes

Cu(II) complexes are attractive candidates for the development of novel antimicrobial drugs as Cu(II) is an endogenously occurring metal in mammalian biology. Humans therefore possess pathways for the regulation of copper levels *in vivo* which reduces the likelihood of metal induced toxicity.²⁷ There have been many Cu(II) compounds reported in the literature with the ability to inhibit the growth of *Leishmania* parasites, several of which show good potency and selectivity.

Moreno *et al.* have synthesized Cu(II) complexes of 5,7-dimethyl-s-triazolo[1,5-a]pyrimidine (dtmp), a ligand known to form metal complexes with antiparasitic effects.²⁸ These were assayed against *L. braziliensis* and *L. infantum* and the complex $[\text{Cu}(\text{dtmp})_4(\text{H}_2\text{O})_2](\text{ClO}_4)_2 \cdot 2\text{H}_2\text{O}$ (**Figure 2.6**) displayed IC_{50} values of 39.6 and 10.3 μM respectively with selectivity indexes of 15 and 54 when compared to their toxicity towards mammalian Vero cells. The IC_{50} value is a measure of how much of a substance is required to inhibit the growth of an organism by 50% and is used to describe the toxicity of a compound towards an organism.

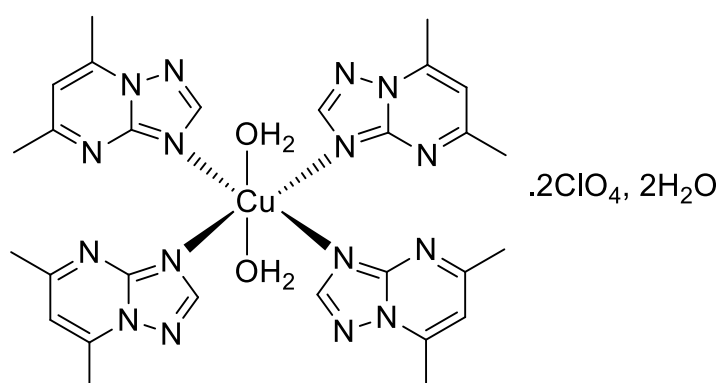


Figure 2. 6. Complex prepared by Cabellero *et al.*²⁸

A Cu(II) complex of a limonene-thiosemicarbazone ligand has been prepared by Britta *et al*, termed BenzCo, and its effect on *L. amazonensis* was studied.²⁹ It was discovered that this complex (**Figure 2.7**) has potent antileishmanial properties and is effective against several stages of the parasite, namely leishmania promastigotes,

axenic amastigotes and intracellular amastigotes with IC_{50} values of 3.8, 9.5 and 10.7 μ M respectively. The effect that this compound has on the parasites has been studied in detail and it was found that it primarily effects the mitochondria of the promastigotes. Depolarization of mitochondrial membrane potential in the cells was observed which suggests interference with the proton potential of the mitochondrial membrane. Transmission electron spectroscopy was used to inspect the parasites following administration of BenzCo at its IC_{50} value. This revealed protrusion in the flagellar pocket of the promastigotes, which would further support this hypothesis.

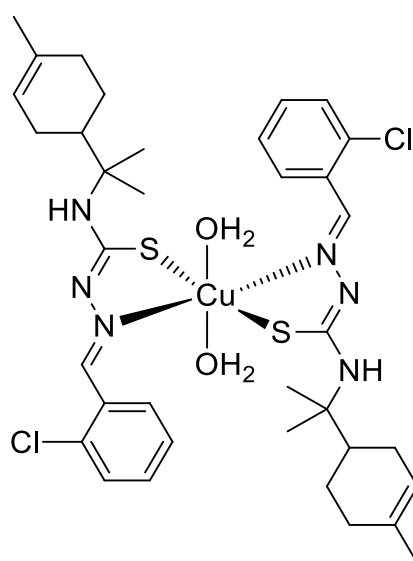


Figure 2. 7. Chemical structure of BenzCo.²⁹

Espósito *et al.* have prepared a series of α -hydroxycarboxylate Cu(II) complexes (**Figure 2.8**) and examined their antileishmanial effects.³⁰ These complexes produced dose dependent leishmania inhibition with the highest activity observed when R = CH_3 with an IC_{50} value of 242 μ M. This figure is similar to that of $CuSO_4$ (IC_{50} : 218 μ M) which indicates that the complexes retain the biocidal activity of the 'free' Cu(II) ion. While the ligands do not enhance the antiparasitic activity of the metal, it is proposed that chelating the copper with the ligands will prevent off target binding of the copper if administered to a mammal, considering the high binding affinity site on the abundant plasma protein albumin for Cu(II) *in vivo*.³¹

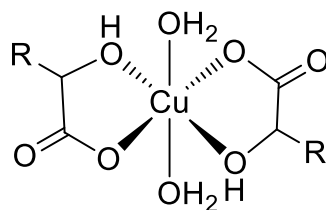
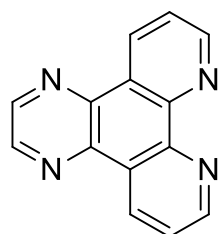
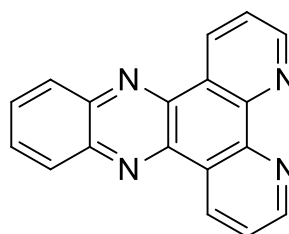


Figure 2.8. Complexes prepared by Esposito *et al.*³⁰

Metal complexes of polyaromatic ligands have been widely studied in bioinorganic chemistry due to their ability to act as DNA intercalators. Navarro *et al.* have investigated Cu(II) complexes of dipyrido[3,2-a:2',3'-c]phenazine (dppz) and dipyrido[3,2-a:2',3'-h]quinoxaline (dpq) (**Figure 2.9**) as agents against leishmaniasis.³² They found these complexes to be highly effective DNA intercalators and as agents for killing *L. braziliensis*. With the exception of [Cu(dpq)(NO₃)](NO₃), all of the compounds studied were successful at killing 100% of the parasites after 64 h at 10 μM. [Cu(dppz)₂(NO₃)]NO₃ showed the highest activity with all of the parasites dead after 1.5 h at a concentration of 10 μM.



dpq



dppz

Figure 2. 9. Ligands used by Navarro.³²

2.1.1.2.2 Zn(II) Complexes

Zn(II) has been shown to be highly effective in combatting *Leishmania* infections. The most simple Zn(II) compound investigated and found to be effective is the simple salt zinc sulfate which has been shown to be an effective therapy for visceral leishmaniasis when administered orally for 45 days.³³

Work has been carried out by Peniche *et al.* on the co-administration of zinc sulfate and zinc chloride with disulfiram (**Figure 2.10**), a drug used to treat alcoholism with known antiprotazoal activity,³⁴ as a strategy to enhance its leishmaniacidal effects.³⁵ This was found to be very successful, with an IC₅₀ value of 0.003 μ M against *L. major* with an *in vitro* therapeutic index of 8337 when co-administered with ZnCl₂ to infected RAW murine macrophage cells. The metal salts alone did not produce any significant antiparasitic effects nor did they prove to be toxic to the mammalian cells used.

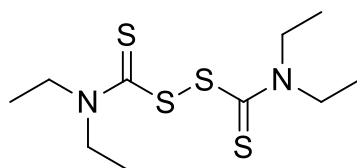


Figure 2.10. Chemical structure of disulfiram.³⁵

2-picolylamine Zn(II) complexes (**Figure 2.11**) have been recently reported and their effects on *L. major* have been studied in depth.³⁶ These compounds showed potent antileishmanial properties with IC₅₀ values as low as 0.3 μ M. The researchers fluorescently labelled these compounds in order to establish their localisation when administered to parasitized mice. This revealed that the compounds rapidly accumulate in the promastigote cytosol. The fluorescent label, when administered without conjugation to the Zn(II) complex, did not show any uptake into the parasites. This would suggest that the Zn(II) is required for the complex to cross the parasite membrane. It is suggested that the selectivity of the compounds is due to their cationic nature, which allows them to distinguish the negatively charged parasite cell surface from the near neutral surface of mammalian cells. The compounds did not exhibit appreciable toxic effects towards mammalian cells and were successful at eradicating the parasitic infection after 12 days of treatment in a mouse model. The mode of action for these compounds has not yet been deduced but it is suggested that it involves the disruption of the parasites membrane.

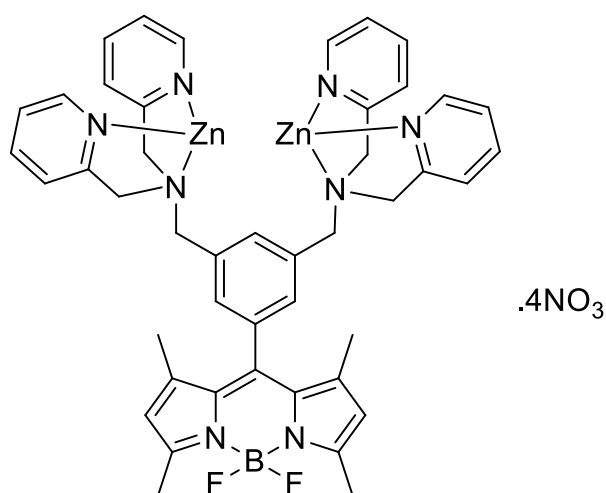


Figure 2.11. Structure of fluorescently labelled Zn(II) complex studied by Rice *et al.*³⁶

Carbonic anhydrase has recently been shown by Pal *et al.* to be the target of metal dithiocarbamate complexes.³⁷ They examined the effect of several Mn(II) and Zn(II) dithiocarbonate complexes and found them to be effective inhibitors of β -carbonic anhydrase from several different microbial species including *M. tuberculosis*, *Legionella pneumophila*, and *C. neoformans*. Following this discovery, they investigated the use of the complexes as antileishmanial compounds. All of the compounds studied were effective at inhibiting the growth of *L. major*. The complex utilizing Propineb as a ligand (**Figure 2.12**) exhibited the highest activity with an IC₅₀ value of 0.27 μ M with a selectivity index of 50.

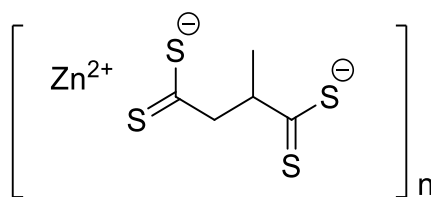


Figure 2. 12. Zn(II) complex of Propineb.³⁷

Tosylsulfonamide ligands have been shown to possess potent antileishmanial activity which is further enhanced by complexation to Zn(II) (**Figure 2.13**).³⁸ IC₅₀ values as low as 0.32 μ M were reported which are comparable to the activity of amphotericin B (0.29 μ M). In addition, these compounds showed low toxicity in mammalian Vero cells. Their interaction with carbonic anhydrase, a Zn(II) containing metalloenzyme, was studied in depth *in vitro* and *in silico*. Inhibition studies show that both the

ligands and corresponding Zn(II) complexes are efficient inhibitors of bovine carbonic anhydrase with the Zn(II) complexes exhibiting enhanced activity when compared to the ligands alone. Docking studies revealed that the tosylsulfonamide ligands bind quite well to the active site of the enzyme with a strong interaction between the carboxylic acid OH and Zn(II) present in the enzyme. While the Zn(II) complex did show higher activity than the ligands alone, no docking studies were performed on these metal complexes to elucidate the cause of this increase of activity.

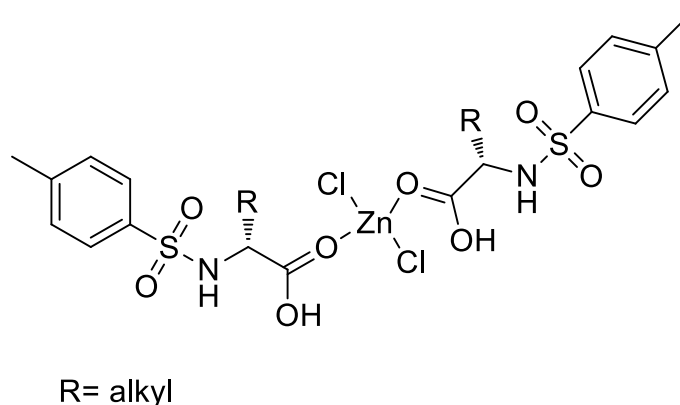


Figure 2.13. Zinc tosylsulfonamide complexes used as carbonic anhydrase inhibitors.³⁸

2.1.2 Chagas' Disease

Chagas' disease (CD) is a chronic, debilitating parasitic disease caused by *Trypanosoma Cruzi* and is primarily transmitted by blood-sucking insects of the subfamily Triatominae, most commonly the kissing bug, although transmission from blood donations, consumption of contaminated food and vertical transmission have also been reported.³⁹

Following the bite of a kissing bug, metacyclic trypomastigotes are transferred into the host and find their way into cells near the bite where they develop into amastigotes. These amastigotes then multiply by binary fission and continue to infect surrounding tissue. Following this, they grow into trypomastigotes and enter into the blood stream where they can infect other sites in the host or be consumed by a kissing bug during a blood meal. Once consumed by a kissing bug, they transform into epimastigotes in the midgut of the insect where they multiply. The epimastigotes

move into the triatomine hindgut where they can then infect a new host when the fly takes a blood meal of another human (**Figure 2.14**).

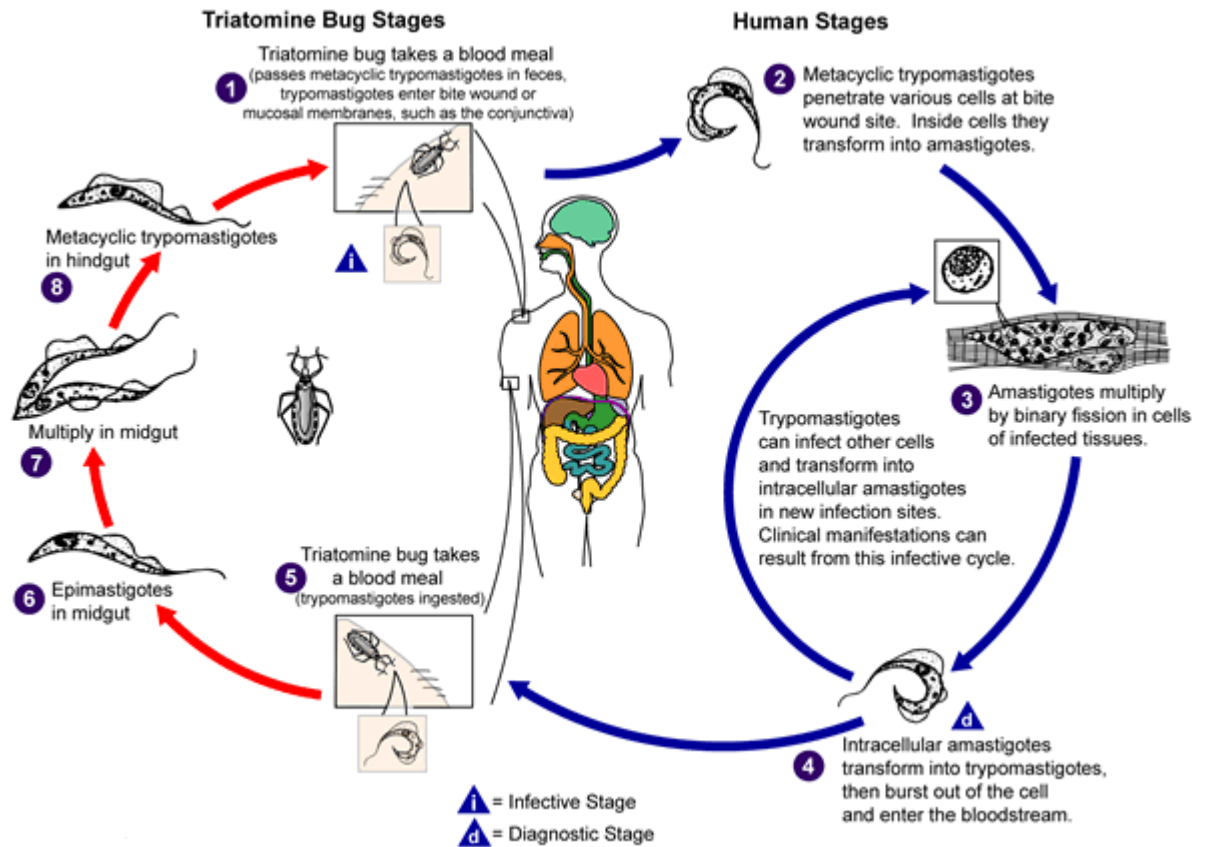


Figure 2.14. Life cycle of the *T. cruzi* parasite.⁴⁰

CD is a significant healthcare problem and is estimated to infect more than 10 million people worldwide. It presents a substantial socioeconomic burden in addition to a high mortality rate.⁴¹ The disease does not always initially present with symptoms; however, when it does they are typically mild symptoms such as fever, swollen lymph nodes, headaches, or swelling at the site of the bite. After several weeks, individuals enter the chronic phase of disease in which 60–70% of patients do not present further symptoms. The other 30 to 40% of people develop further symptoms 10 to 30 years after the initial infection. These include enlargement of the ventricles of the heart which can lead to heart failure in addition to the enlargement of the oesophagus or colon which may also occur.

2.1.2.1 Current Therapies

Nifurtimox:

Nifurtimox (**Figure 2.15**) is an orally available medication used for the treatment of CD and is typically administered over the course of 30-60 days. It was first introduced in 1967 and its use is currently discouraged due to the numerous and severe side effects. It is known to cause gastrointestinal side effects, central nervous system issues, birth defects and increase the risk of heart failure.⁴²

Nifurtimox is only effective during the initial stages of infection. In the chronic stages of the diseases it is ineffective due to its poor pharmacokinetic profile which does not allow for a sufficiently high concentration in all tissues where the infection is present.⁴³

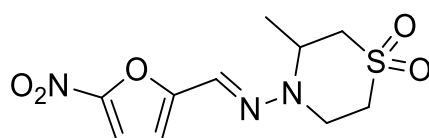
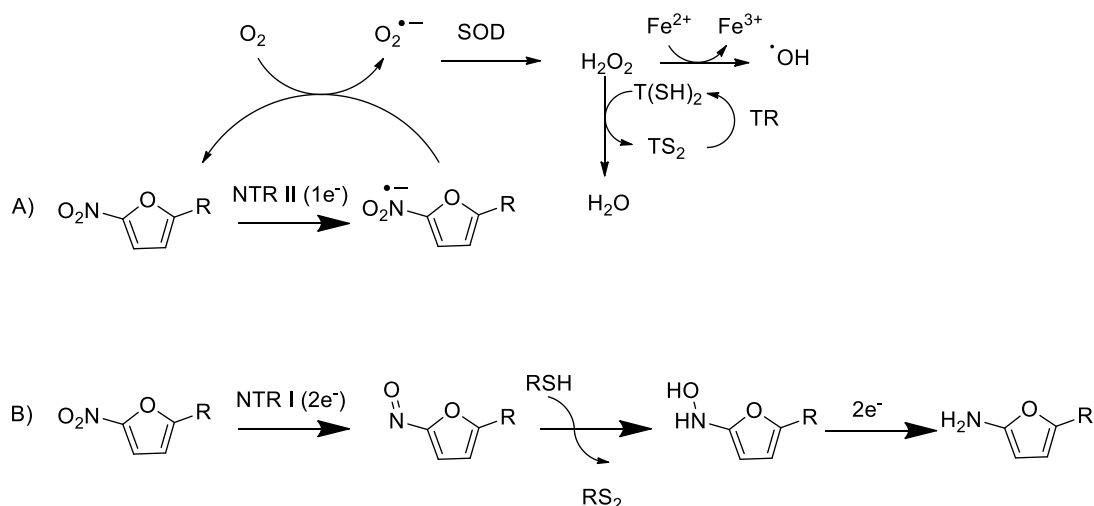


Figure 2.15. Chemical structure of Nifurtimox.⁴²

Nifurtimox is thought to exert its effects *in vivo* by undergoing enzymatic reduction and generating oxidative stress, which the trypanosome parasites are extremely sensitive to. This is due to their lack of the catalase enzyme which protects mammalian cells in addition to the absence of a glutathione-dependent hydrogen peroxide metabolism.⁴⁴ This reduction can be effected by two nitroreductases found in the parasite which leads to either the generation of hydroxyl radicals or the oxidation of trypanosomal thiol species (**Scheme 2.1**).⁴⁵ It is proposed that the primary mode of antitrypanosomal activity is the oxygen cycling pathway to generate hydroxyl radicals.



Scheme 2.1. Bioreduction of nitroaromatic drugs (ArNO₂). (A) One-electron reduction by type II nitroreductases (NTR) promoting redox-cycling with superoxide/H₂O₂ formation and drug regeneration. ROS production oxidizes parasite thiols. (b) Two-electron reduction by type I NTR yielding the nitroso-compound (ArNO), a good scavenger of thiols. SOD = superoxide dismutase; T(SH)₂= reduced trypanothione, TS₂= oxidized trypanothione; TR = trypanothione reductase.⁴⁵

Benznidazole:

Benznidazole is a 2-nitroimidazole derivative first introduced in 1972 and is used as the first line treatment of CD (Figure 2.16). It is orally available and it is typically administered daily for a period of 60 days and cures up to 80% of patients in the acute phase of infection and 5-20% of chronic cases.⁴⁶ While it is currently the preferred treatment for CD, benznidazole is known to cause side effects such as gastrointestinal problems, rashes, anorexia, insomnia, immunosuppression and peripheral neuropathy.⁴⁷ The efficacy and tolerance of benznidazole is inversely related to the age of the patient, with adverse effects seen more frequently and severely among elderly patients.⁴⁸



Figure 2.16. Chemical structure of Benznidazole.

Similar to nifurtimox, benznidazole is a prodrug which exerts its trypanocidal effects following the reduction of the nitro group by nitroreductases *in vivo*. However, the antikinestoplastic effects of benznidazole do not depend on the generation of oxygen radicals as nifurtimox does. The generation of H_2O_2 or O_2^- have not been observed in amastigotes when benznidazole is administered at concentrations significant enough to inhibit the growth of the parasite. Homogenates of *T. Cruzi* administered with benznidazole exhibit EPR signals corresponding to the nitrate anion which further supports the hypothesis of a different reduction pathway than nifurtimox.⁴⁹ It is likely that the pathway involves the covalent binding of the electrophilic metabolites with trypanosome macromolecules, but there is no single accepted pathway for the drugs mode of action and it is likely that several are involved.^{50, 51}

2.1.2.2 Metallodrugs as Novel Antichagasic Therapeutics

As with leishmaniasis, many researchers have been exploring metal based drugs in the quest to find new treatments for CD. The use of DNA intercalating ligands such as phenanthroline or the conjugation of a known antiparasitic compound with a metal have been exhaustively studied. To this end a wide variety of metal-based compounds have been explored as novel antichagasic agents.

2.1.2.2.1 Cu(II) Complexes

Heteroleptic Cu(II) complexes of norfloxacin (NOR), an antimicrobial quinolone, have been prepared by Martins *et al.* using either bipyridine (bipy) or phenanthroline (phen).⁵² It was found that the $[\text{CuCl}_2(\text{phen})]$ and $[\text{CuCl}_2(\text{phen})(\text{NOR})] \cdot 3\text{H}_2\text{O}$ (**Figure 2.17**) had significant activity against *T. Cruzi* trypomastigotes. Further studies indicate that the norfloxacin ligand is quite labile; *in vitro* experiments with bovine serum

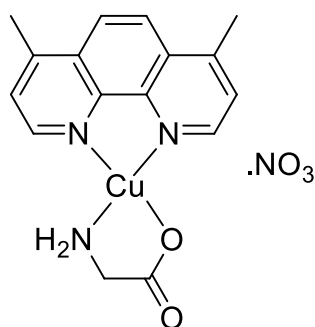


Figure 2.18. *Cu(II)* complex prepared by Becco *et al.*⁵⁴

Extensive studies were performed to examine the interactions of the compounds with DNA and proteins in order to establish the mechanism of their trypanocidal activity. These studies revealed that the primary inhibitory effects arise from the intercalation of the complex with the target DNA, followed by radical mediated cleavage of the DNA. Interactions with tubulin, integrin and fibronectin, which cause protein misfolding, are also observed. This would suggest that these interactions may also play a role in the activity of the compounds.

Risedronate, a bisphosphonate compound currently being used as a drug for several bone diseases, has been investigated as a ligand for the synthesis of antiparasitic metal complexes (**Figure 2.19**) by Demoro *et al.*⁵⁵ This work found that the copper complex was effective at reducing the growth of both *T. cruzi* promastigotes and epimastigotes. The antiproliferative effects of the metal complexes of risedronate exceeded that of the free risedronate ligand, which indicates that the coordination of metal ions significantly contributes to its effectiveness against the parasites.

The target of bisphosphonate compounds in kinetoplasts has been identified as farnesyl diphosphate synthase enzyme.⁵⁶ The authors studied the interaction of the compounds with this enzyme and found that they were effective inhibitors of its activity. Furthermore, they found that their enzyme inhibition effects correlated with their ability to inhibit the growth of *T. cruzi*, which indicates that this is the likely mode of action of the drugs.

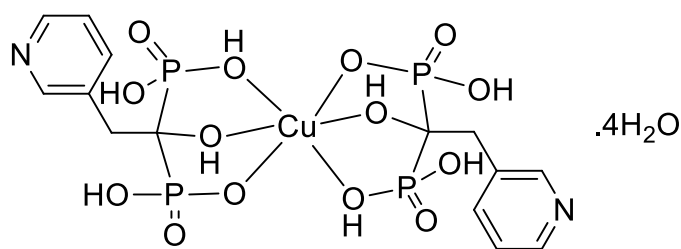


Figure 2.19. *Cu(II) risedronate complex.*⁵⁵

2.1.2.2.2 Zinc(II) Complexes

Gouvea *et al.* has investigated Zn(II) complexes of the antibacterial compound norfloxacin as antichagasic agents (**Figure 2.20**).⁵⁷ It was found that while norfloxacin and its Zn(II) complex exhibited little activity against *T. cruzi*, the corresponding $[\text{ZnCl}_2(\text{NOR})(\text{phen})] \cdot 2\text{H}_2\text{O}$ complex showed good activity with an IC_{50} value of 12 μM . The analogous $[\text{ZnCl}_2(\text{phen})]$ complex showed a similar activity of 14 μM , which would suggest that incorporation of the norfloxacin has little effect on the mode of action of the complex. Studies into the interaction of the complexes with DNA and BSA show that the $[\text{Zn}(\text{phen})]^{2+}$ moiety is able to intercalate with DNA, which is likely the cause of growth inhibition observed.

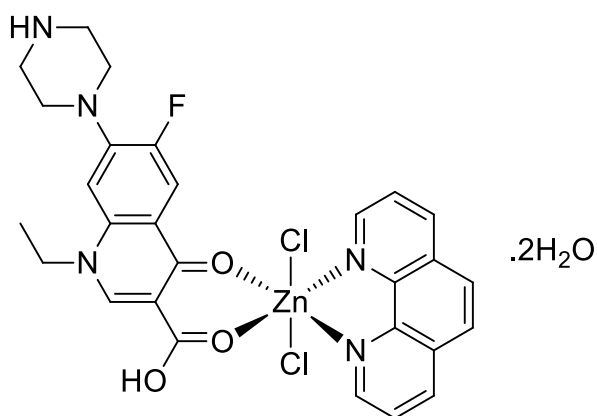


Figure 2.20. *Zn(II) complex synthesized by Gouvea et al.*⁵⁷

Work by Cabellero's group into the antiparasitic activity of previously mentioned dtmp metal complexes revealed that the Zn(II) complex showed the highest activity of the compounds screened against *T. cruzi* (**Figure 2.21**).²⁸ However, the IC_{50} value and selectivity index were inferior to the therapies currently used to treat the disease.

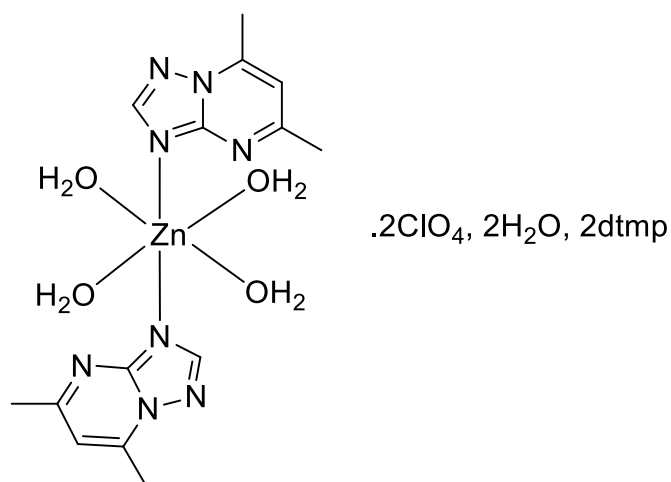


Figure 2.21. Zn(II) complex synthesized by Cabellero et al.²⁸

2.1.3 Carbohydrate Conjugation in Drug Design:

Glycoconjugation is an attractive strategy in drug design as carbohydrates can confer superior biological activities to a potential drug through a variety of mechanisms. They can act as targeting groups and increase the uptake of the compound into cells by taking advantages of specific glucose transporters such as GLUT or SLC2A which actively transport the glycosylated compound into the cell. This approach avoids absorption problems caused by unsatisfactory lipophilicity profiles.⁵⁸ A further advantage to using glycosylated compounds is the marked increase in water solubility, which can be up to 700 times more soluble when compared to the aglycon compound.⁵⁹ Glycosylation also allows for the use of a prodrug strategy which uses the sugar moiety to mask a pharmacologically significant group within the molecule which is only revealed after the sugar is cleaved enzymatically *in vivo* by glycosidases.⁶⁰

Interestingly, a pro-prodrug scheme is emerging as a more favourable alternative to the traditional prodrug method. This uses an ester-protected sugar as the pendant group on the compound of interest which must first undergo hydrolysis by esterases *in vivo* to reveal the deprotected per-hydroxylated sugar. This can then undergo active transport into the cell before glycolysis to reveal the active compound. This offers the advantage of increasing the lipophilicity of the compound, assisting with

absorption via passive diffusion and can improve oral bioavailability which can be compromised by the use of deprotected sugars.⁷

2.1.3.1 Carbohydrate Conjugated Metal Chelators

The investigation of metal complexes bearing pendant sugar groups has been an area of intense research over the past number of years. Glycosylated coordination compounds have generated significant interest in the area of targeted diagnostic agents for positron emission topography (PET) and computed topography (CT) applications. The sugar moiety can serve as both a solubilizing agent and as a targeting unit in complexes containing radioactive nuclides such as $^{99m}\text{Tc(I)}$, $^{186}\text{Re(I)}$ and $^{55}\text{Co(II)}$ (**Figure 2.22**).^{61,62,63,64}

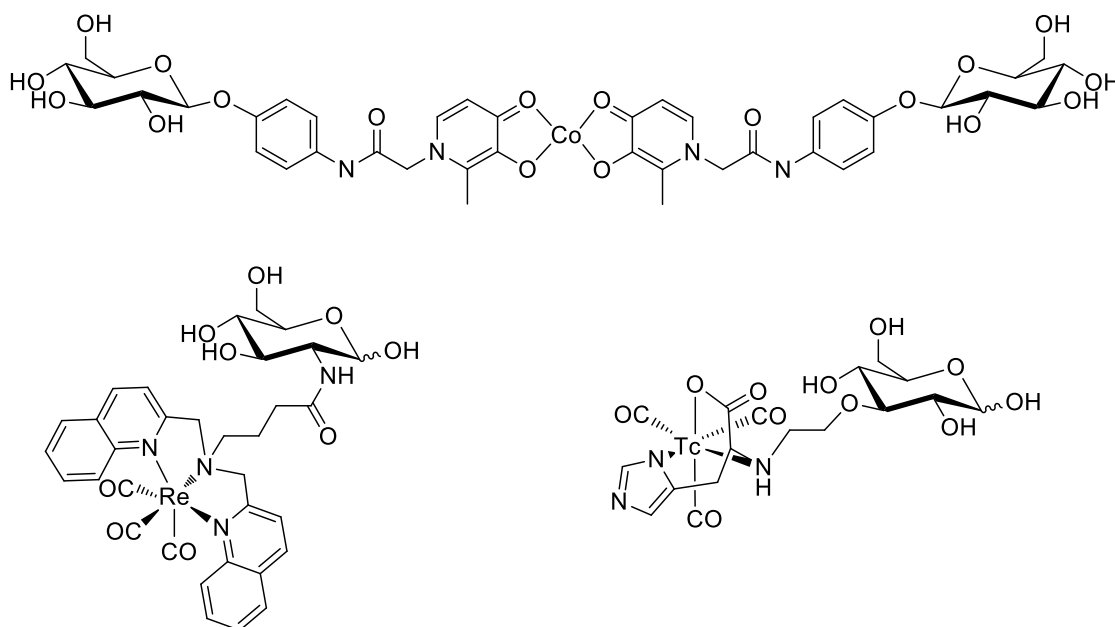


Figure 2.22. Examples of carbohydrate conjugated radiotracers investigated by Schibli, Ferreira and Banerjee.^{61,62,63}

This strategy has also been extended to the design of novel contrast agents for magnetic resonance imaging (MRI). This technique utilises lanthanide ions, typically Gd(III), to modulate local water-proton T1 and T2 relaxation times which improves the image obtained. These typically feature a macrocyclic core with additional coordinating pendant groups to ensure the stability of the compound given the toxicity associated with free lanthanide cations. A range of targeting moieties have

been investigated and some are widely used in the clinic such as Gadofosveset (**Figure 2.23**), trade name Vasovist, which targets the blood. This uses a biphenylcyclohexyl unit that has a high affinity for human serum albumin and therefore gives a higher concentration of the agent in the blood than the surrounding tissue, thereby improving its appearance in the MRI image.⁶⁵

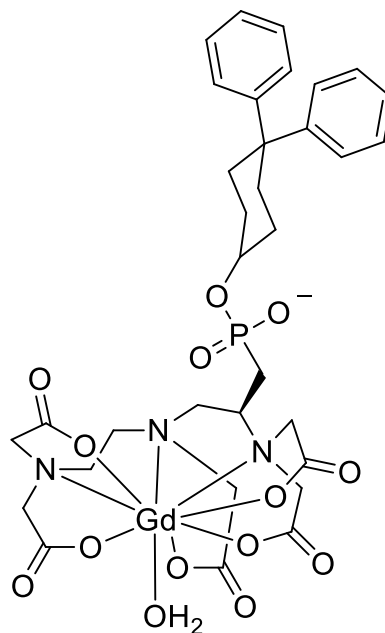


Figure 2.23. Chemical structure of Vasovist.⁶⁶

Glycosylation has been widely explored in this area.^{67,68,69,70,71} In particular, galactose conjugates have attracted attention due to their ability to target liver cells by selective uptake by the hepatic asialoglycoprotein receptor (ASGP-R) which is found on hepatic cells, liver cancers and in some cases, metastases of hepatic tumours. Gerald *et al.* have studied complexes of Gd(III) and the γ -emitting ¹⁵³Sm(III) nuclide coordinated to ligands bearing galactose moieties conjugated via a thioglycosidic bond to prevent enzymatic cleavage. They found that increasing the number of galactose residues on the molecule increase the affinity for ASGP-R *in vitro* while substituting galactose for glucose or lactose inhibits this targeting behaviour.⁶⁷ This has lead other researchers to explore polyglycosylated ligands and dendritic glycoclusters as targeting agents (**Figure 2.24**).^{68,72}

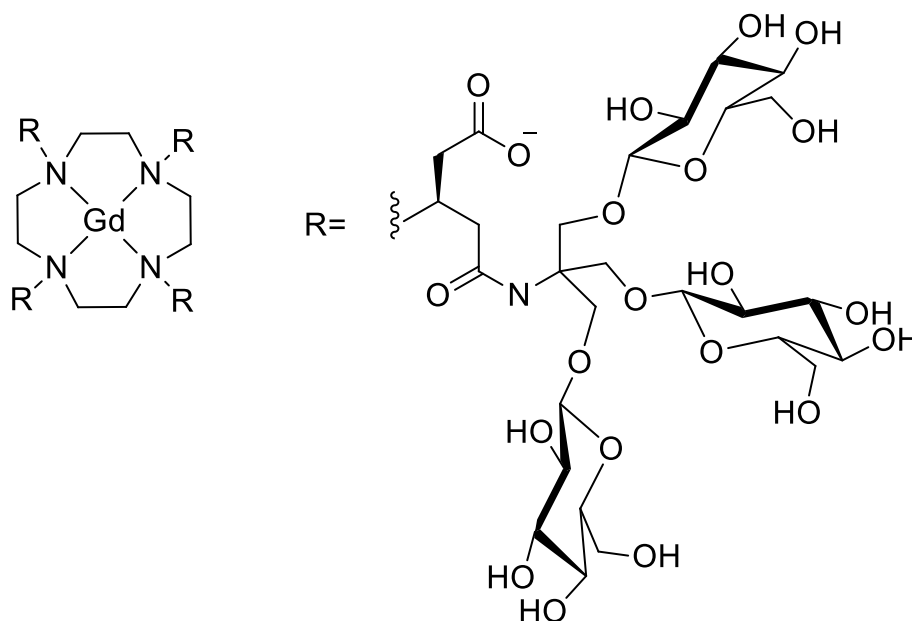


Figure 2.24. Complex used by Parker et al.⁶⁸

The use of carbohydrate conjugated metal complexes as therapeutics, however, is an underdeveloped yet emerging area of medicinal chemistry. The most well-known example is Auranofin, an organogold complex derived from 2,3,4,6-O-tetraacetyl- β -D-glucopyranosyl-1-thiol (**Figure 2.25**). It was originally used as an antirheumatic agent, however, it is currently undergoing investigation as a potential antibacterial agent.^{73,74} The exact mechanism of action of this compound is still being studied; current hypothesis is that Au(I) is released from the drug and can bind to the redox-active dithiol group of thioredoxin reductase (TrxR). Au(I) binding in the active site is thought to prevent electron transfer to the downstream substrate thioredoxin (Trx), thus interfering with redox homeostasis in the parasite.⁷⁵

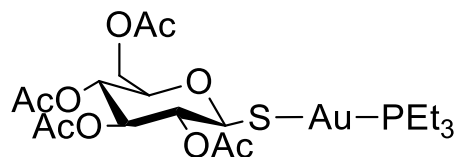


Figure 2.25. Chemical structure of Auranofin.⁷³

Carbohydrates have been used to modulate the activity of anticancer Pt(II) compounds. Research by Wang's group involved the investigation of a glucose derived cisplatin analogue (**Figure 2.26**).⁷⁶ While this work did not show significant improvement over the parent Pt(II) compound, it was the first example of a

carbohydrate conjugated metal complex that did not feature the sugar as a coordinating ligand.

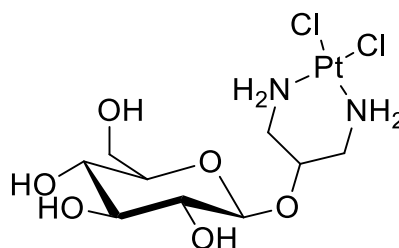


Figure 2.26. Cisplatin analogue prepared by Wang *et al.*⁷⁶

Work by Ma *et al.* has investigated glycoconjugates of anticancer terpyridine Pt(II) complexes using a wide variety of peracetylated sugars (**Figure 2.27**).⁷⁷ They discovered that these compounds can be up to 100 times more cytotoxic against human cancer cell lines than cisplatin. Their studies indicate that the compounds exert their effect by interaction with ctDNA by a non-intercalating binding mode, which may explain why the activity is much higher than other derivatives which typically follow a DNA intercalation mechanism of activity.

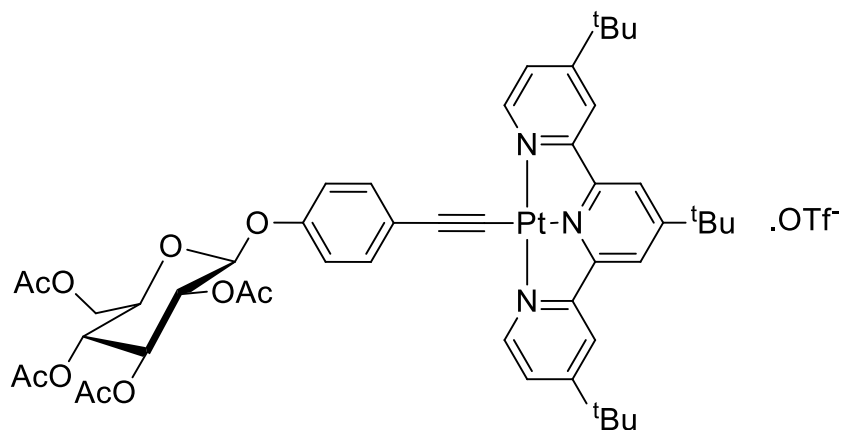


Figure 2.27. Example of Pt(II) complex synthesised by Ma *et al.*⁷⁷

Goa *et al.* have made significant advances in the field of carbohydrate conjugated Pt(II) anticancer compounds.^{59,78,6,79} This work has shown substantial improvements in both the efficacy of the compounds and the *in vivo* tolerance of the compounds when compared to the currently used drug Oxaliplatin. The improved anticancer activity can be attributed to the targeting action of the sugar moiety which exploits the Warburg effect (**Figure 2.28**). The Warburg effect is the significantly increased

uptake of glucose by tumours compared to healthy tissue. Exploiting this effect by use of a targeting sugar moiety provides a higher local concentration of the drug in the tumour than the rest of the body. The side effects caused by Pt(II) compounds can in part be attributed to their insolubility which impedes excretion by the kidney and often leads to nephrotoxicity. The solubilizing nature of the carbohydrate moiety is thought to be a key factor in the reduced toxicity observed in these compounds.⁶

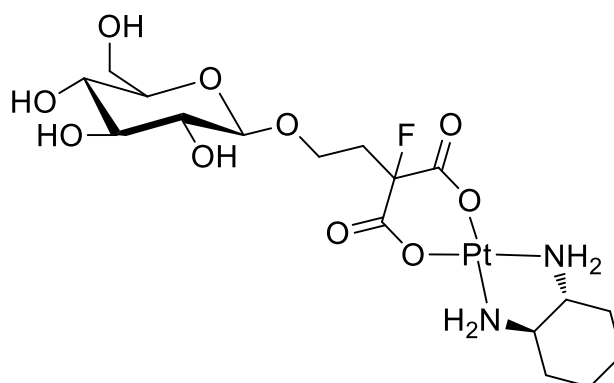


Figure 2.28. Chemical structure of Pt(II) complex prepared by Gao *et al.*⁷⁹

Ru(II) complexes bearing ligands based on galactose and fructose have been synthesized by Fernandes *et al.* (**Figure 2.29**).⁸⁰ These were assayed against HeLa cells and showed dose dependent activity with IC₅₀ values lower than cisplatin. Further studies of these complexes and their Fe(II) analogues revealed that these compounds act by increasing activity of caspase-3 and caspase-7 which trigger apoptosis.⁸¹ Their work revealed that the Fe(II) complexes were significantly less active than their Ru(II) analogues. The nature of the carbohydrate ligand also proved to be significant to the activity of the compounds; the cyclic glucose and galactose ligands were significantly more active than the open chained ligands which were also studied.

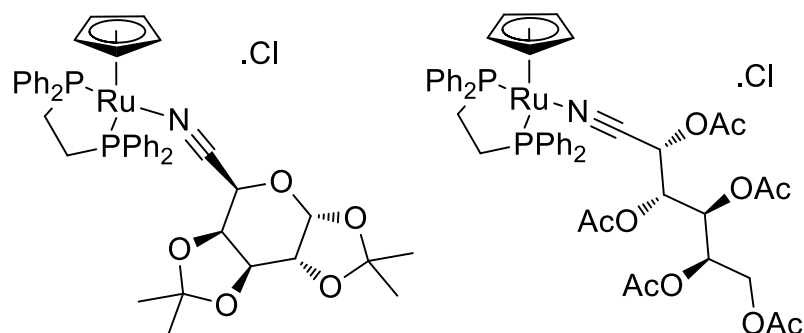


Figure 2.29. Compounds studied by Fernandes *et al.*⁸¹

Fructose derived cobalt carbonyl complexes have been investigated as novel therapeutics against a breast cancer cell line.⁸² These proved only moderately effective and the potency of the compound was correlated to the number of isopropylidene protecting groups present on the sugar. The highest activity was observed when the fructose contained two protecting groups (**Figure 2.30**) which suggests that the lipophilicity of the compound is important for cellular uptake. This was investigated by means of atomic absorption spectroscopy to quantify the levels of Co present 24 h after administration of the compound. This showed that only low amounts of the deprotected compound was able to cross into the cell while the mono- and diprotected compounds presented a much higher uptake, clearly demonstrating the advantage of using protected carbohydrates as drug conjugates than their perhydroxylated analogues.

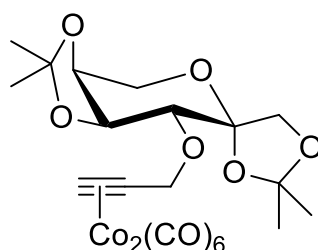


Figure 2.30. Cobalt complex prepared by Ott *et al.*⁸²

Ag(I) complexes of thiosugar derived tripodal ligands have been synthesized and evaluated as antibacterial agents by Gottschaldt *et al.* (**Figure 2.31**).⁸³ These complexes proved to be active against a broad range of bacteria and significantly less toxic to human cells than the simple salts used as a control. However, the activity was independent of the type of sugar used which suggests that they cross the cell wall by non-specific diffusion and the activity arises solely from the Ag(I) cation.

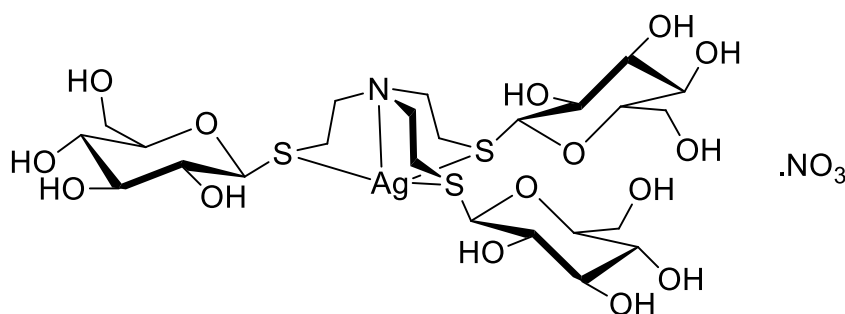


Figure 2.31. Silver complex prepared by Gottschaldt *et al.*⁸³

The above compounds represent almost the entirety of the carbohydrate conjugated metalloterapeutics reported in the literature. As can be seen, a wide variety of metals and coordination environments have been studied using these ligands, primarily for cancer, but also for antibacterial uses. While this area is still in its infancy, the potential for carbohydrate conjugation as a strategy for designing novel metallodrugs is clearly demonstrated.

2.2 Aim

The aim of this work was to:

- i. Design and synthesize a library of novel amino- and iminopyridyl ligands and their corresponding glycosylated derivatives.
- ii. Investigate the coordination chemistry of these novel ligands to form Cu(II), Zn(II) and Fe(II) complexes.

As demonstrated *vide supra*, both Cu(II) and Zn(II) have been shown to be highly efficacious at increasing both the potency and selectivity of antikineto-plastic compounds. The incorporation of a dinitrogen chelating ligand has proven successful in the design of metal-based therapeutics with the widespread use of bipyridine and phenanthroline based compounds reported in the literature. However, the ability of these compounds to intercalate DNA can also cause cytotoxic effects due to the non-specific nature of the interactions. We therefore sought to investigate novel dinitrogen chelating ligands which do not have these structural features associated with their cytotoxicity, ie. a rigid, extended aromatic surface, to act as efficient DNA intercalators as a means to avoid this.

We decided to explore the use of aryl-picolylamine based chelating motif as the core of the ligands described in this work. The aryl moiety features a *para*-phenolic group; this serves a dual purpose: (i) to act as a redox active site and (ii) to provide a point of functionalisation to append pharmacokinetic modulating groups (**Figure 2.32**).

As previously outlined, carbohydrate conjugation is an extremely attractive strategy to modulate bioactivity. In order to investigate the importance of the phenolic OH group, several compounds featuring both metabolically labile and stable ether

linkages were prepared. Glucosidases are known to effect hydrolysis at the anomeric position and yield a hydroxylated sugar and the aglycon unit as an alcohol.⁸⁴ Therefore, two types of glucosylated ligand were studied:

- i) Aryl glucosides whereby the phenolic oxygen is directly linked to the anomeric centre. Enzymatic hydrolysis would liberate this redox active ligand.
- ii) Glucoconjugates with an ethylene linker incorporated between the sugar and the aryl ring. Enzymatic hydrolysis of these species would liberate a primary alcohol with the linker still attached to the phenolic oxygen and thus inhibit its potential redox activity.

The aryl ring can also incorporate an additional phenolic hydroxyl group to provide a third coordination point with the aim of increasing the metal binding ability of the ligand. Thus, two distinct series of compounds with different coordination sites were investigated; namely, a dinitrogen N₂ series and the N₂O series which features an additional OH phenolic group.

The coordination chemistry of the ligands with divalent cations Cu(II), Zn(II) and Fe(II) salts was then explored.

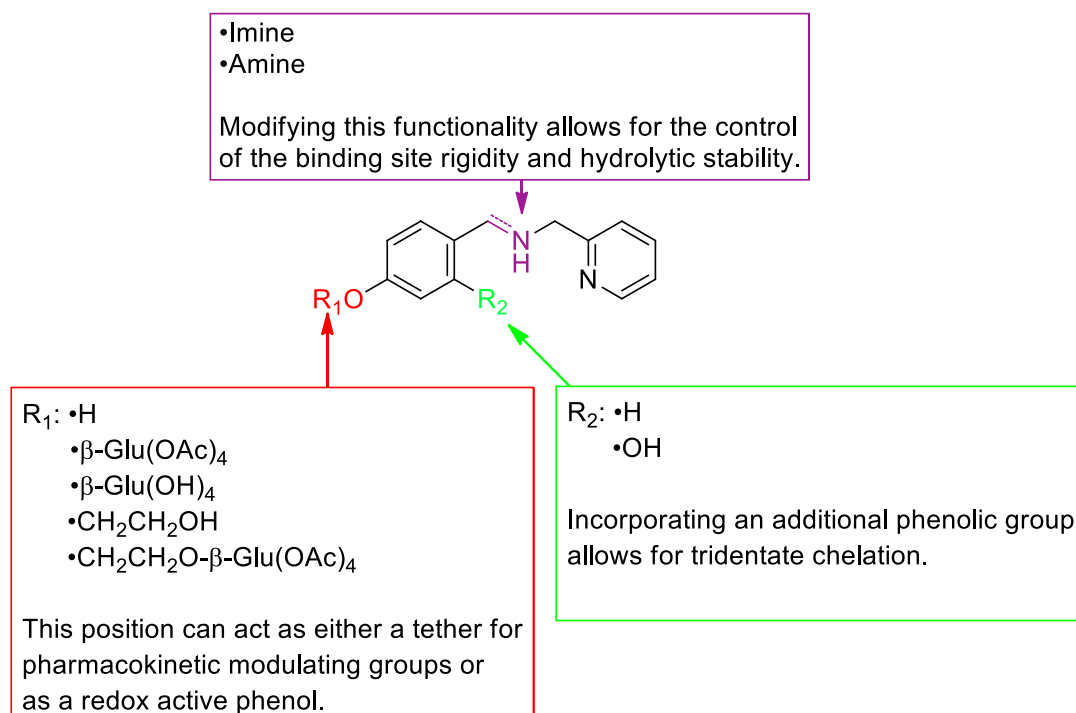
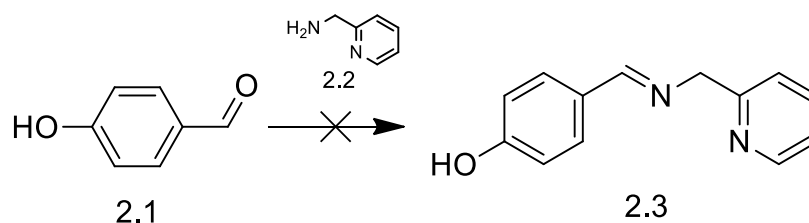


Figure 2.32. Chemical structure of the ligand scaffold under investigation.

2.3 Results and Discussion

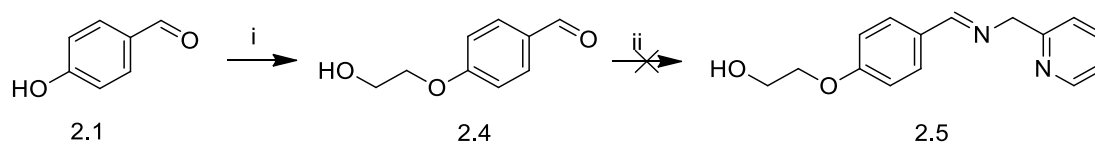
2.3.1 Synthesis of the N₂ Ligand Series

2.3.1.1 Imine ligands



Scheme 2.2. Reagents and conditions: i) MgSO₄, EtOH

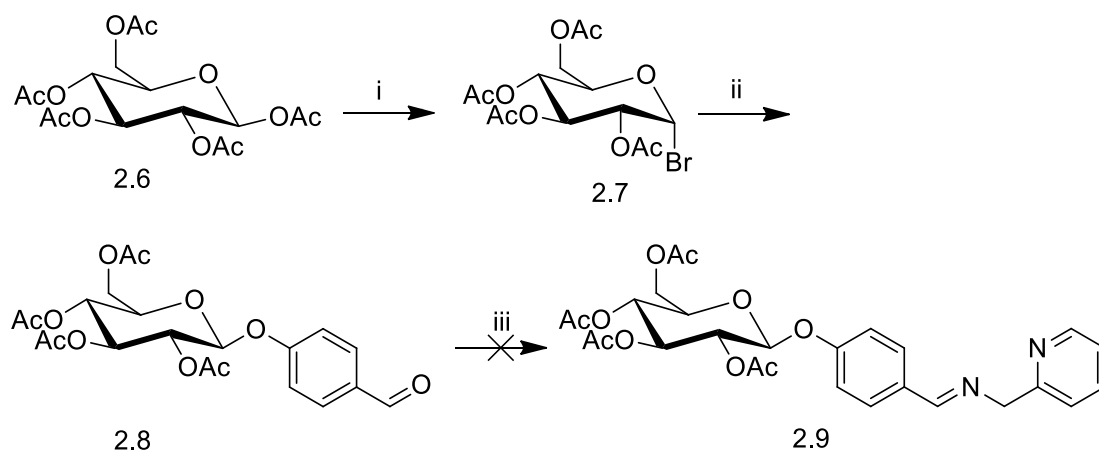
The initial investigations focused on ligands featuring a dinitrogen iminopyridine chelating unit with a *para*-phenoxy group. The synthesis of ligand **2.3** was attempted by the direct reaction of 2-picolylamine (**2.2**) with 4-hydroxybenzaldehyde (**2.1**) (**Scheme 2.2**). These proved to be unsatisfactory as the desired compounds could not be isolated in sufficient purity. Efforts were made in a wide variety of solvents using anhydrous conditions and different techniques to remove the water generated, such as Dean-Stark distillation and the addition of desiccating agents such as MgSO₄ in order to drive the reaction to completion. Formation of the imine could be observed by TLC and NMR but they proved to be unstable and immediately begin to decompose to the corresponding amine and aldehyde starting materials upon isolation.



Scheme 2.3. Reagents and conditions: i) 2-chloroethanol, DBU, NaI, 4 h, isopropanol, 120 °C (microwave), 59%; ii) 2-picolylamine (**2.2**), MgSO₄, EtOH, 6 hr.

The synthesis of ligand **2.5** was attempted by the reaction of 4-(2-hydroxyethoxy)benzaldehyde (**2.4**) with **2.2** (**Scheme 2.3**). **2.4** was prepared by a microwave promoted Williamson ether synthesis between 2-chloroethanol and 4-

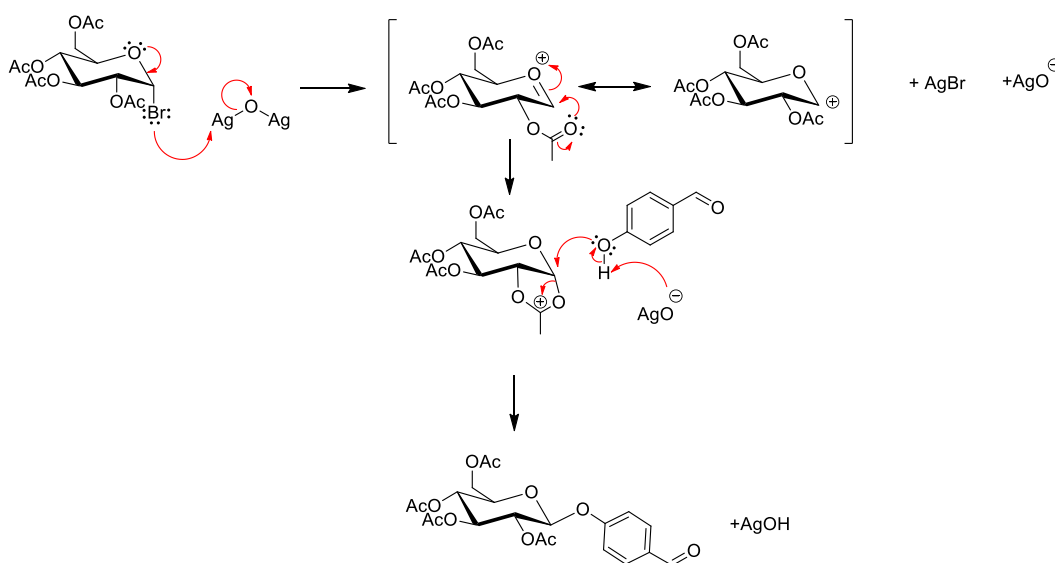
hydroxybenzaldehyde, utilizing DBU as the base and NaI as a nucleophilic catalyst in isopropanol. This route offered higher yields and easier purification than the analogous reaction using conventional heating, which necessitates the use of DMF or DMSO as the solvent due to the high temperature required to obtain sufficient conversion. As was observed with ligand **2.3**, the imine proved to be highly unstable under ambient conditions and could not be satisfactorily isolated.



Scheme 2.4. Reagents and conditions: i) HBr/AcOH, rt, 4 h, 87%; ii) 4-hydroxybenzaldehyde (**2.1**), Ag₂O, rt, 18h, 63%; iii) 2-picolyamine (**2.2**), MgSO₄, 80°C, 6 h.

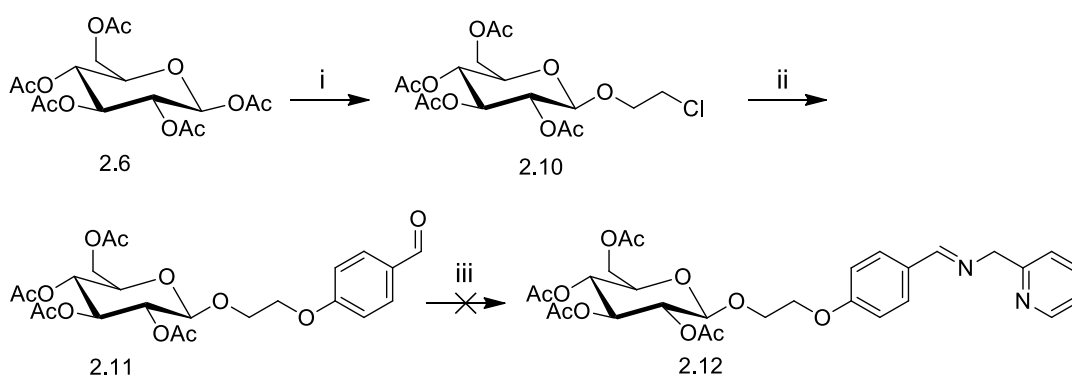
The synthesis for glycosylated ligand **2.9** utilizes the reaction of a glycosylated phenoxyaldehyde **2.8** with **2.2**, as can be seen in **Scheme 2.4**. It follows a Koenigs-Knorr glycosylation of **2.1** with glucosyl bromide **2.7** for the functionalization of the phenolic hydroxyl group of **2.1**. Attempts were made to directly glycosylate **2.1** using an acetate glucosyl donor **2.6**. However, this did not produce the target intermediate in sufficiently high yield. A glucosyl bromide donor **2.7** was therefore used to obtain the target glycosylated aldehyde **2.8**. **2.7** was prepared by the stereospecific bromination of glucose pentaacetate with 33% HBr in AcOH to furnish the α anomer in high yield. The glycosylation was carried out in the dark under inert conditions using Ag₂O as the halophilic promoter to activate the glucosyl donor. This generated the target aldehyde stereospecifically as the β anomer in good yield. Both Ag(OTf) and Ag₂CO₃ were screened as reaction promoters, however, these did not produce appreciable conversion of the starting material.

The stereoselectivity of this glycosylation is governed by the acetyl group in the two position which participates in anchimeric assistance (**Scheme 2.5**). Following the abstraction of bromide by Ag(I), the carbonyl oxygen of the acetate group acts as a nucleophile to attack the resulting oxocarbenium intermediate to form a five membered acetoxonium ring. This ring blocks nucleophilic attack of 4-hydroxybenzaldehyde from the bottom face which results in the formation of the beta anomer exclusively.



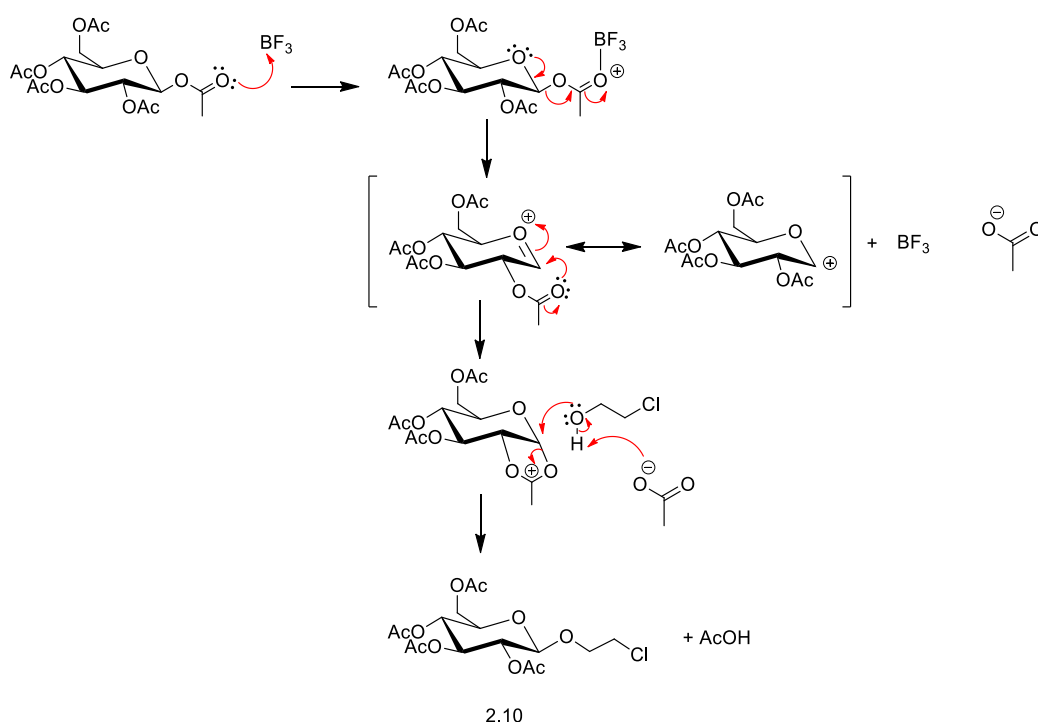
Scheme 2.5. Mechanism for the formation of **2.6**.

As with the previously studied N_2 imine compounds, the desired imine could not be obtained due to its instability under ambient conditions.



Scheme 2.6. Reagents and conditions: i) 2-chloroethanol, $BF_3 \cdot OEt_2$, $0^\circ C - rt$, 17 h, 55%; ii) 4-hydroxybenzaldehyde, K_2CO_3 (**2.1**), TBAI, $110^\circ C$, 17 h, 87%; iii) 2-picolylamine (**2.2**), $MgSO_4$, $80^\circ C$, 6 h.

Ligand **2.12** was envisaged to be obtained from the route shown above (**Scheme 2.6**). The glycosyl donor **2.6** was the commercially available β -D-glucose pentaacetate which was glycosylated with 2-chloroethanol in good yield using $\text{BF}_3 \cdot \text{OEt}_2$ to give the β -anomer exclusively. In this reaction, the oxocarbenium ion is generated by the Lewis acid activation of the anomeric acetyl group and subsequent abstraction by BF_3 . The acetyl group at the 2-position participates in anchimeric assistance in the same manner as described in **Scheme 2.5**. This anchimeric assistance controls the stereochemical outcome of the reaction and explains the stereospecificity observed in the reaction (**Scheme 2.7**). This stereochemistry is confirmed by both the chemical shift of the H-1 signal at 4.68 ppm which occurs significantly lower than the α -anomer and also by the coupling constant of $^3J_{1,2} = 8$ Hz, which is larger than would be expected for an α -glucoside.

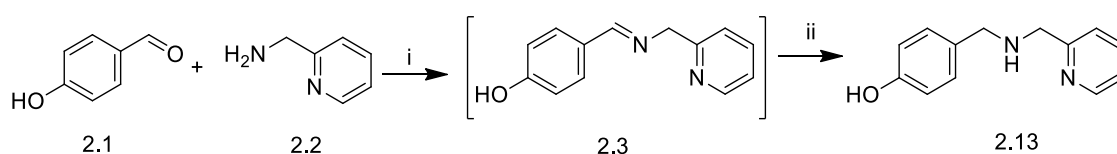


Scheme 2.7. Mechanism of BF_3 promoted glycosylation of peracetylated glucose.

The ether linkage in **2.10** was formed in high yield using a Williamson ether synthesis in DMF using tetrabutylammonium iodide (TBAI) as a nucleophilic catalyst. The yield for this reaction is higher than the analogous reaction using 2-chloroethanol in place of the glucoside. This may be explained by the competing self-reaction of 2-

prevents the formation of the imine. Instead, the compounds were synthesized by the formation of the imine in refluxing anhydrous ethanol under N₂ with MgSO₄. The imine is then directly reduced by the addition of a solution of NaBH₄ in anhydrous ethanol to generate the corresponding amine following an aqueous quench and extractive work up.

It is worth noting that extensive optimization of the reaction conditions was required. It is necessary to stir the NaBH₄ solution for at least 15 min before addition to the reaction as several undesirable byproducts are formed if NaBH₄ is added directly to the reaction. This suggests that partial ethanolsis of the reducing agent is necessary to attenuate the reducing ability of the reagent. The diminished reducing ability may grant it selectivity to preferentially reduce imines which mirrors the selectivity observed with the triacetoxyborohydride reducing agent.⁸⁶ The reaction requires rigorously dry conditions in order to cleanly reduce the imine to yield only a single product. This necessitates the drying of all glassware and MgSO₄ at 150 °C for 24 h and carrying out the reaction and filtration of desiccating agent under a stream of N₂.



Scheme 2.9. Reagents and conditions: i) MgSO₄, ethanol, 3 h; ii) AcOH, NaBH₄, 16 h, 68% over two steps.

As discussed above, ligand **2.13** was synthesized via the direct reaction of 4-hydroxybenzaldehyde **2.1** and 2-picolylamine **2.2** and subsequent reduction using NaBH₄ (**Scheme 2.9**). This produces the target amine as a single product in high purity as indicated by the elemental analysis. During the optimization of this synthetic procedure, a tertiary amine byproduct **2.18** was isolated and characterized by X-ray crystallography (**Figure 2.33**). This compound is obtained by the reaction of the desired product **2.13** with a second molecule of 4-hydroxybenzaldehyde to form a second iminium species. This is subsequently reduced to yield the observed tertiary amine **2.18**. This takes place when the imine formation step has not gone to completion or if there is water present in the reaction mixture to shift the equilibrium

from the imine towards the more thermodynamically favored amine and aldehyde. This demonstrates the need for rigorously anhydrous conditions in order to achieve full conversion of the starting materials and ensure the synthesis of only a single product.

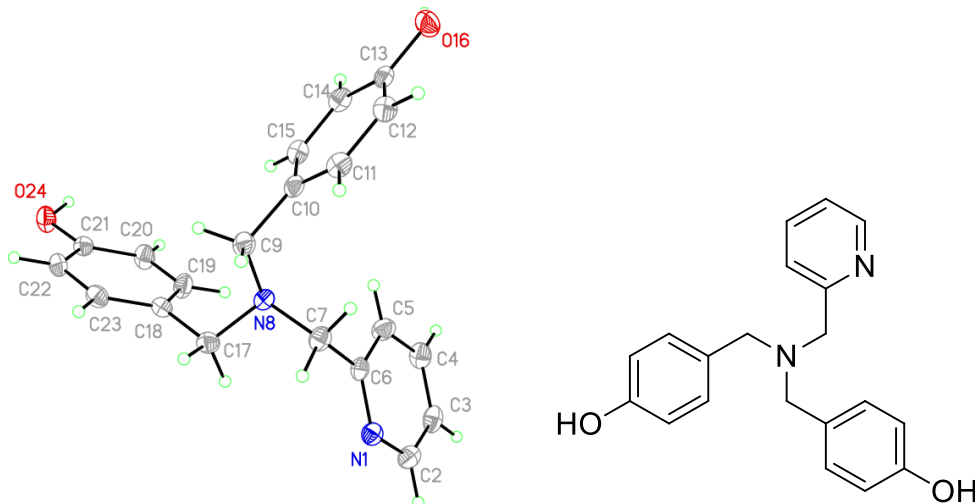
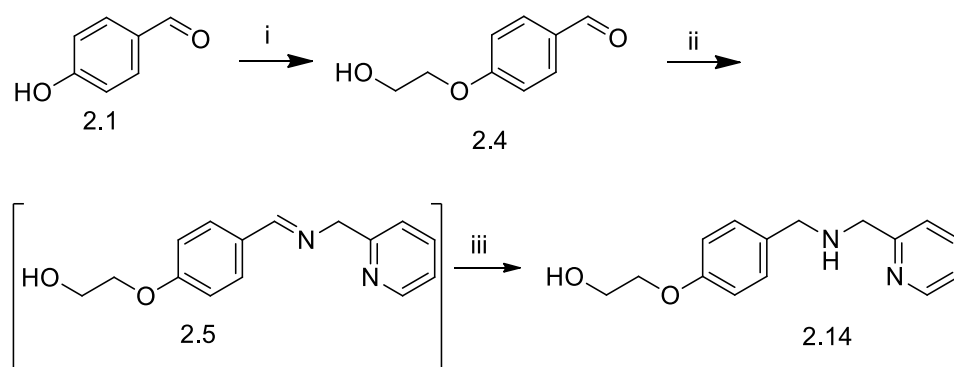
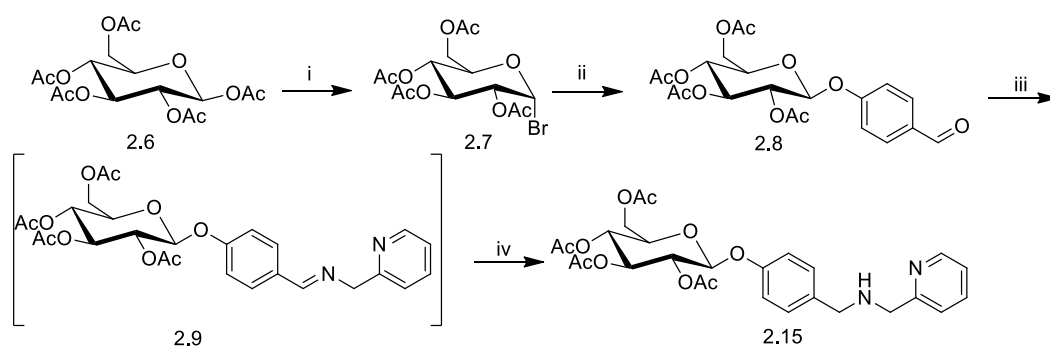


Figure 2.33. X-ray crystal structure of **2.18**



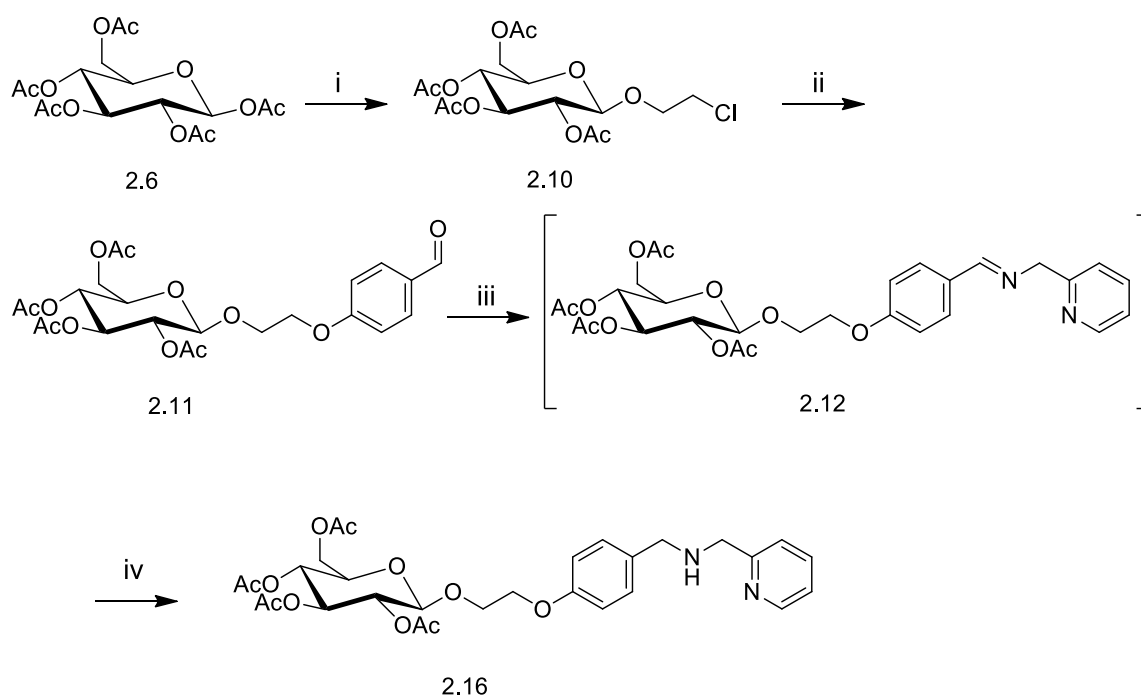
Scheme 2.10. Reagents and conditions: i) 2-chloroethanol, DBU, NaI, 4 h, isopropanol, 120 °C (microwave), 59%; ii) 2-picolyamine, MgSO₄, EtOH, 3 h; iii) AcOH, NaBH₄, 68% over two steps.

Compound **2.14** was prepared in a similar manner to **2.13** following an identical reductive amination protocol (**Scheme 2.10**). This utilized the previously described aldehyde **2.4** to generate the imine intermediate **2.5** which was then reduced *in situ*. Following protocol optimized for **2.13**, the reaction yielded the target compound as a single product in good yield and high purity.



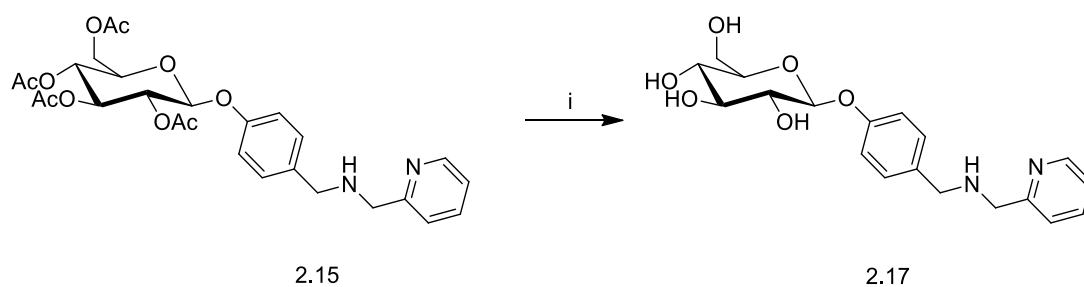
Scheme 2.11. Reagents and conditions: i) HBr/AcOH , rt, 4 h, 87%; ii) 4-hydroxybenzaldehyde, Ag_2O , rt, 18h, 63%; iii) 2-picolyamine, MgSO_4 , 80°C , 4h; iv) AcOH , NaBH_4 , 16 h, rt, 76% over two steps.

The glycosylated analogue N_2 ligand **2.15** was obtained by the *in situ* reduction of **2.9** (Scheme 2.11). The reductive amination followed a similar procedure to the other compounds in this series. The reaction quench did prove problematic however. Earlier iterations of the reductive amination procedure utilized HCl to quench the reaction. However, for this compound it promoted the formation of unwanted by products. After further optimization, the best conditions to quench the reaction were identified as the addition of water to the reaction and heating the mixture to deactivate unreacted NaBH_4 prior to the work up. The protocol was used for all subsequent syntheses of the N_2 ligands.



Scheme 2.12. Reagents and conditions: i) 2-chloroethanol, $BF_3 \cdot OEt_2$, $0^\circ C - rt$, 17 h, 55%; ii) 4-hydroxybenzaldehyde, K_2CO_3 , TBAI, $110^\circ C$, 17 h, 87%; iii) 2-picolyamine, $MgSO_4$, $80^\circ C$, 4 h; iv) $NaBH_4$, AcOH, rt, 16 h, 42% over two steps.

Compound **2.16** was prepared by the formation of the glucosylated linker followed by etherification with 4-hydroxybenzaldehyde and subsequent reductive amination (**Scheme 2.12**). Using the same method as described for **2.15** with the water quenched reductive amination, the compound was obtained in a reasonable yield with a sufficiently high purity.



Scheme 2.13. Reagents and conditions: i) NaOMe, MeOH/ H_2O , rt, 1 h, 98%

Deprotected ligand **2.17** was prepared in a quantitative yield using a Zemplén deprotection to hydrolyze the acetyl protecting groups (**Scheme 2.13**). This initially yielded the target compound as a hygroscopic, tar-like substance but upon lyophilization for 48 h the product was obtained as an air stable solid.

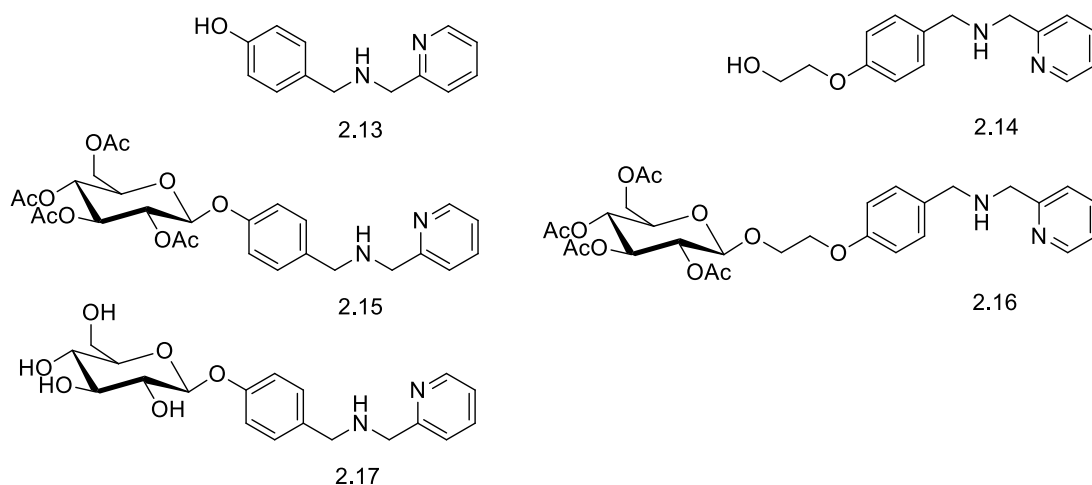
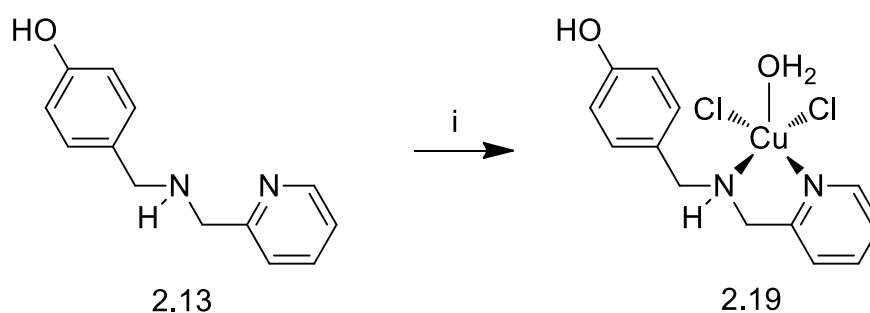


Figure 2.34. N_2 ligands synthesized

2.3.2 Coordination complexes of the N_2 Series



Scheme 2.14. Reagents and conditions: i) $\text{CuCl}_2 \cdot 2\text{H}_2\text{O}$, EtOH, 18 h, 69%

The 1:1 Cu(II) complex **2.19** was generated from the reaction of ligand **2.13** with one equivalent of $\text{CuCl}_2 \cdot 2\text{H}_2\text{O}$ in ethanol at room temperature (**Scheme 2.14**). This produced a green precipitate which was collected by vacuum filtration and dried *in vacuo* to yield the product as a green powder. Elemental analysis indicates that the Cu(II) is bound in a 1:1 ratio with the ligand in addition to one molecule of water. The IR spectrum of the free ligand shows a broad, poorly defined band at 3430 cm^{-1} representing the $\nu_{\text{N-H}}$ and $\nu_{\text{O-H}}$ stretches, whereas the Cu(II) complex shows distinct bands at 3495 , 3378 and 3198 cm^{-1} representing the $\nu_{\text{N-H}}$, $\nu_{\text{O-H}}$ and $\nu_{\text{O-H}}$ bands. This indicates the coordination of the ligand to the Cu(II) ion. The coordination of the

pyridine ring to the metal is also suggested by the shift in the ν_{pyr} band from 1475 cm^{-1} in the ligand to 1484 cm^{-1} .

The structure was unambiguously confirmed by X-ray crystallography. Crystals suitable for X-ray crystal analysis were grown by dissolving the sample in warm (approx. $40 \text{ }^\circ\text{C}$) acetonitrile. The solution was allowed to cool slowly to room temperature and stand for several days in the dark to yield small green crystals. The crystals were found to contain two different Cu(II) species which together form a triclinic unit cell (**Figure 2.35**).

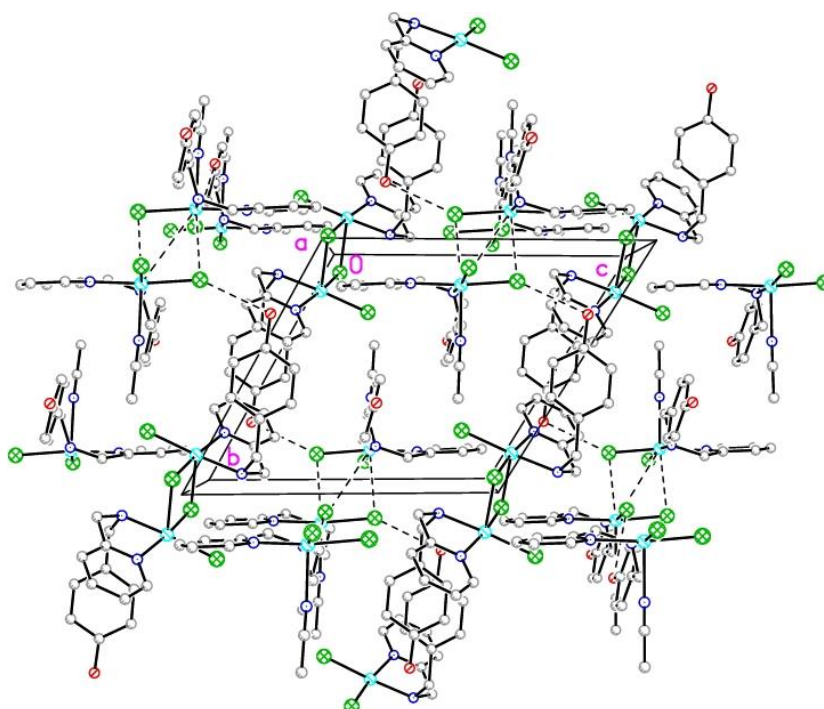


Figure 2.35. Unit cell of **2.19**

At the vertices of the cell there are dimers of a five-coordinate Cu(II) centre bound in a bidentate fashion by the ligand, a terminal chloride and two bridging chloride ligands (**Figure 2.36**). The geometry of 5-coordinate compounds can be described by the geometry parameter τ , which describes the degree of distortion from the square pyramidal to trigonal bipyramidal geometry.⁸⁷ The value is calculated by Addison's equation $\tau_5 = \frac{\beta - \alpha}{60^\circ}$, where β and α are the two largest coordination angles with a value of 0 signifying an ideal square pyramidal geometry and 1 representative of a trigonal bipyramidal structure. The Cu(II) centre in this structure has a τ_5 value of 0.15, indicating a square pyramidal coordination geometry.

The CuCl_2 dimer is planar with Cl-Cu-Cl bond lengths of 2.302 and 2.695 Å and a bond angle of 84.54° for the Cu-Cl-Cu bond. The terminal chloride occupies one of the corners of the square planar arrangement with a bond length of 2.257 Å and an angle of 176.89° with respect to the *trans* nitrogen. These molecules interact with the dimers of neighbouring unit cells via π - π stacking, with the aryl rings displaying a parallel displaced arrangement and a length of 3.395 Å. **2.19** is coordinated in a bidentate fashion with a bite angle of 82.25° with bond lengths of 2.010 and 2.036 Å for the Cu- N_{pyr} and Cu- N_{amine} interactions respectively, significantly shorter than the Cu-Cl bonds and reflects the greater binding affinity of the ligand.

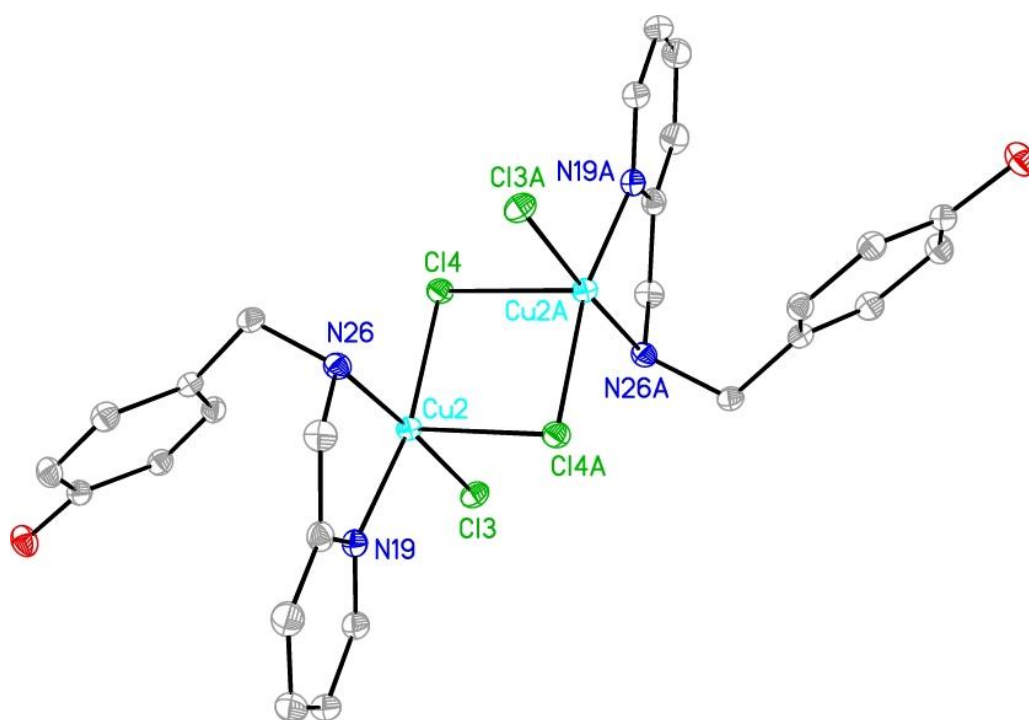


Figure 2.36. Crystal structure of the chloride bridged dimer of **2.19**

Encapsulated in the unit cell are two molecules of a mononuclear pentacoordinate Cu(II) complex. This adopts a square pyramidal geometry with two terminal chloride ligands and an acetonitrile molecule occupying the axial position (**Figure 2.37**). This species has a τ_5 value of 0.07 which indicates a less distorted square pyramidal structure than the previously describe bridged dimer. The Cu-Cl bonds display equal lengths of 2.313 Å and a Cl-Cu-Cl angle of 93.53° , similar to the coordination of the terminal chlorides in the bridged species. The bidentate ligand exhibits a bite angle of 82.6° , similar to the angle observed in the dimeric complex. The Cu-N bond lengths are slightly longer in this species than the previously described dimer with a Cu- N_{pyr}

length of 2.025 Å and a Cu-N_{amine} length of 2.046 Å. The acetonitrile ligand in the axial position shows a bond length of 2.302 Å, significantly shorter than the 2.692 Å bond length of the axial chloride of the dimeric species. The Cu(II) centre shows a weak interaction with a chloride ligand of another molecule with a distance of 2.997 Å. As the elemental analysis suggests the presence of one water molecule, it can be proposed that this occupies the axial position in place of the acetonitrile molecule which is observed in the crystal structure of the compound.

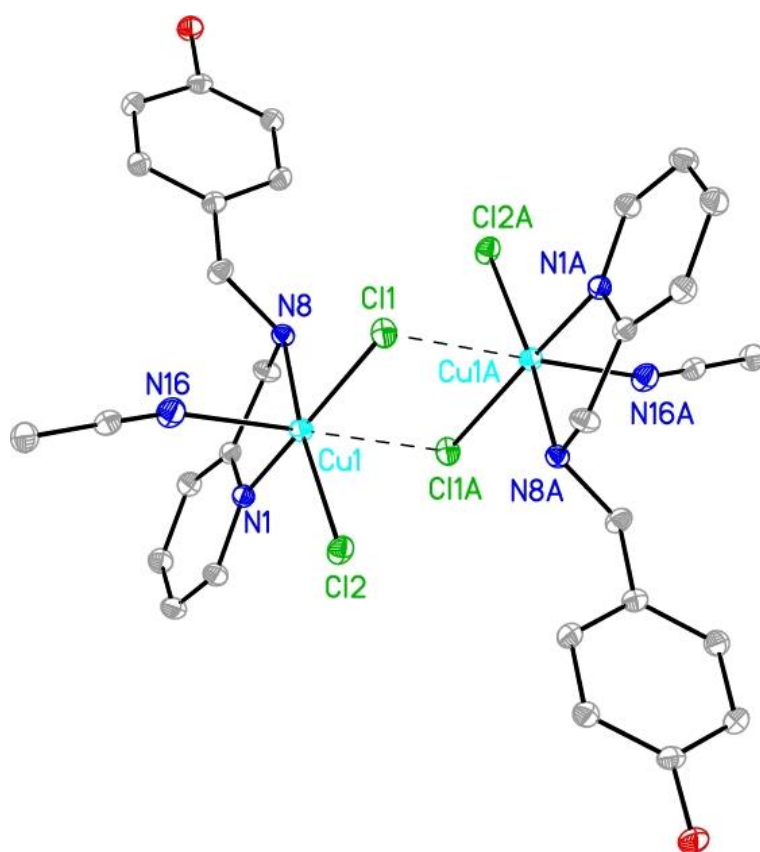
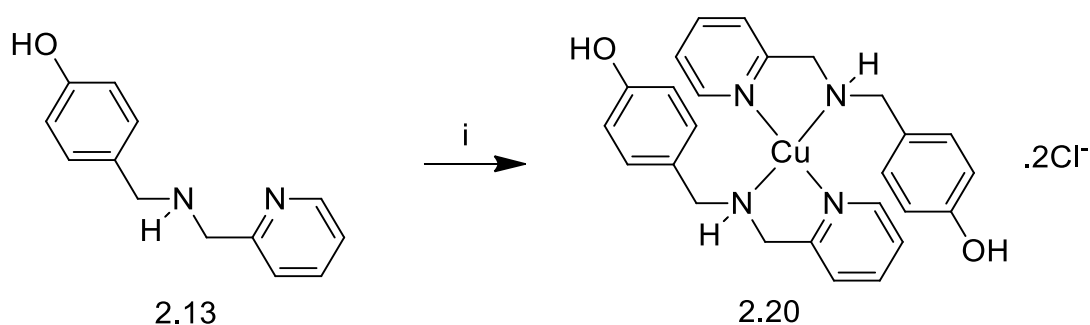
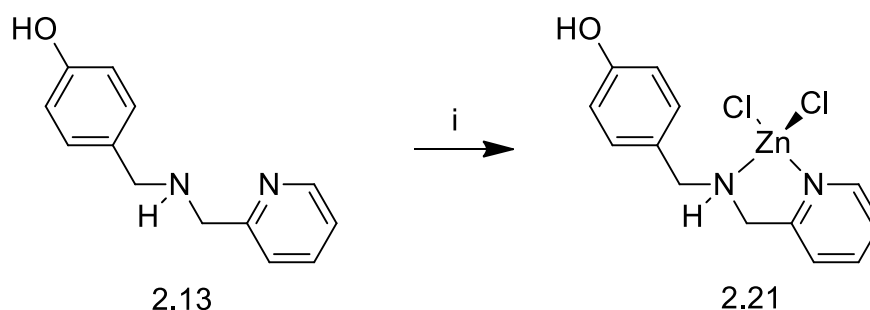


Figure 2.37. Mononuclear complex observed in the crystal structure of **2.19**



Scheme 2.15. Reagents and conditions: i) $\text{CuCl}_2 \cdot 2\text{H}_2\text{O}$, EtOH, 93%

The 2:1 Cu(II) complex **2.20** of ligand **2.13** was prepared by reacting $\text{CuCl}_2 \cdot 2\text{H}_2\text{O}$ with a threefold excess of ligand **2.13** in ethanol at room temperature to yield the product as a blue green powder (**Scheme 2.15**). Elemental analysis indicates the formation of the 2:1 complex. The IR spectra exhibits characteristic shifts in bands from 3430 cm^{-1} and 1475 cm^{-1} in the free ligand to 3340 cm^{-1} and 1489 cm^{-1} in the complex, which confirms that the metal binding occurs through the two chelating nitrogen atoms. As the Cu-Cl IR bands occur below 400 cm^{-1} and a crystal structure could not be obtained, the coordination of the chloride cannot be confirmed. It is possible that the complex could exist as an octahedral 6-coordinate complex or the 4-coordinate complex with two chloride counter ions as depicted in **Scheme 2.15**. Given that the reaction was done with three equivalents of a chelating ligand and only a 2:1 complex with two chlorides present was obtained, it is likely that this system favours a 4-coordinate geometry. This can be deduced as the conditions used could allow for a 6-coordinate structure with 3 strongly coordinating chelating ligands yet only two for found to coordinate with the metal centre.



Scheme 2.16. Reagents and conditions: i) ZnCl_2 , EtOH, 50%

The reaction of equimolar amounts of **2.13** with ZnCl_2 in ethanol at room temperature produces the 1:1 complex **2.21** which precipitated as a light brown powder (**Scheme 2.16**). The 1:1 coordination of the ligand to the metal was confirmed by elemental analysis and it is supported by the IR spectrum of the compound. This shows characteristic signals of the $\nu_{\text{N-H}}$ and $\nu_{\text{O-H}}$ stretches at 3415 cm^{-1} and 3233 cm^{-1} and a shift in the ν_{pyr} band from 1475 cm^{-1} to 1480 cm^{-1} when compared to **2.13**. The ^1H NMR reveals slight downfield shifts in the spectrum

following complexation with the electron withdrawing Zn(II) cation. The largest shift observed occurs in the Pyr-H signal which resonates at 7.77 ppm in the free ligand and following complexation is observed at 7.91 ppm.

The precise structure of the compound was confirmed by X-ray crystallography. Crystals suitable for X-ray analysis were grown by slow evaporation of the filtrate over several weeks to yield pale brown rhombic crystals. (**Figure 2.38**).

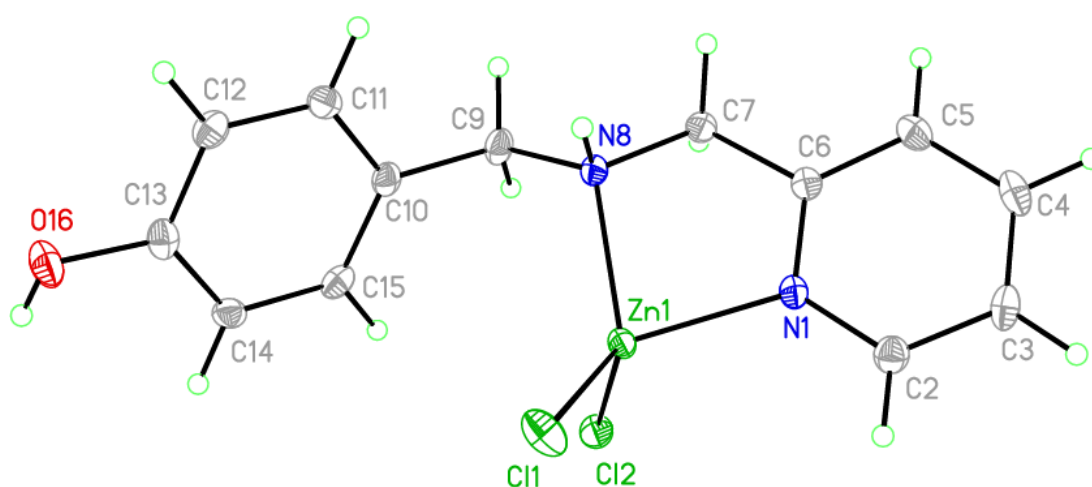


Figure 2.38. Crystal structure of **2.21**

As is typical for Zn(II) complexes, the compound adopts a 4-coordinate structure. (**Figure 2.38**). Each zinc atom is bound in a bidentate fashion by the ligand through the two nitrogen atoms with almost identical bond lengths of 2.059 and 2.056 Å, unlike **2.20** where there was a noted difference in the Cu-N bond lengths. The two chloride ligands present display bond lengths of 2.232 and 2.209 Å which are shorter than those of the analogous Cu(II) complex. The elongation of one of these chloride bond lengths may be explained by its hydrogen bonding with both the phenolic H atom of a neighboring molecule and an amine H as seen in the crystal packing diagram (**Figure 2.39**). The primary intermolecular interactions observed in the crystal structure are π -stacking interactions between phenolic aromatic rings. These participate in two separate parallel displaced interactions; one with a displacement angle of 21.59° and a distance of 3.369 Å and the other with a distance of 3.845 Å

and a displacement angle of 55.39°. The pyridine ring is also involved with π -stacking with the phenolic ring, in this case in a T-shaped manner with a distance of 2.741 Å.

The ligand binds the metal with a bite angle of 83.21° and two chloride ligands bind with a Cl-Zn-Cl angle of 116.28°. These angles are significantly different from the ideal angle of 109.5° for tetrahedral structures and more close resemble those of a trigonal pyramidal geometry (90 and 120° respectively). The geometry parameter for 4-coordinate structures can be calculated using Okuniewski's equation:⁸⁸ $\tau'_4 = \frac{\beta - \alpha}{360^\circ - \theta} + \frac{180^\circ - \beta}{180^\circ - \theta}$ where β and α are the largest coordination angles and θ is 109.5°, the ideal angle of a tetrahedral geometry. A square planar geometry is denoted by a value of 0, whereas tetrahedral geometry gives a value of 1. The Zn(II) complex has a value of $\tau'_4 = 0.88$ which reveals a distorted trigonal pyramidal ($\tau'_4 = 0.85$) coordination geometry.

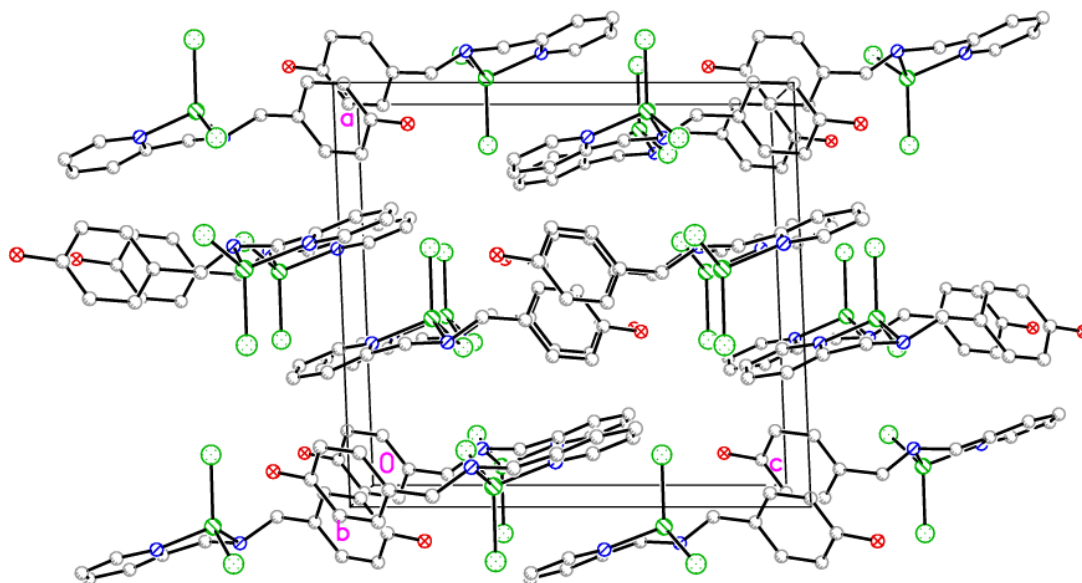
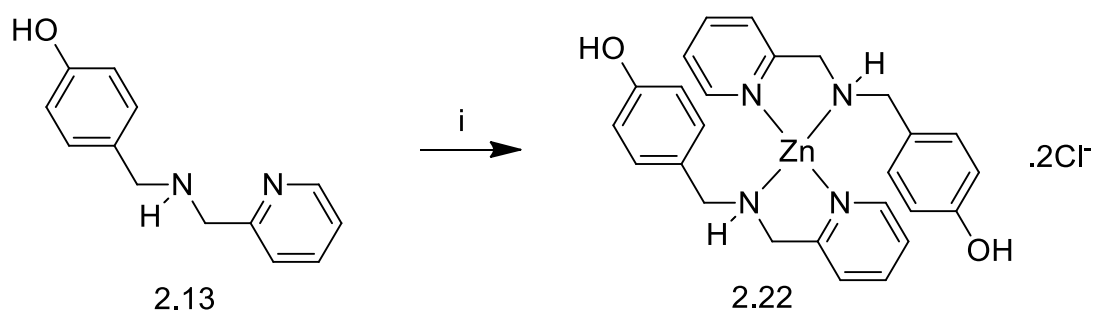


Figure 2.39. Unit cell of 2.21



Scheme 2.17. Reagents and conditions: i) ZnCl_2 , EtOH, 88%

The 2:1 Zn(II) complex **2.22** of ligand **2.13** was synthesized by reacting ZnCl_2 with a threefold excess of ligand **2.22** in ethanol at room temperature to yield the product as a white powder (**Scheme 2.17**). The formation of the 2:1 binding of Zn(II) to the ligand is confirmed by elemental analysis. The IR spectra exhibits characteristic shifts in band from 3430 cm^{-1} of the free ligand to 3395 and 3158 cm^{-1} for the $\nu_{\text{N-H}}$ and $\nu_{\text{O-H}}$ stretches and from 1475 cm^{-1} to 1489 cm^{-1} representing the ν_{pyr} . This confirms that the metal binding occurs through the two chelating nitrogen atoms. As with **2.20**, it is possible that the compound could exist as either an octahedral 6-coordinate complex or a 4-coordinate complex with two chloride counter ions. However, the coordination of the chloride cannot be confirmed as the $\nu_{\text{Zn-Cl}}$ occurs at a lower wavelength than was studied. Given that the IR spectra for **2.20** and **2.22** are almost identical (**Figure 2.40**), it can be assumed that they are symmetrically equivalent and therefore exhibit similar coordination geometry.

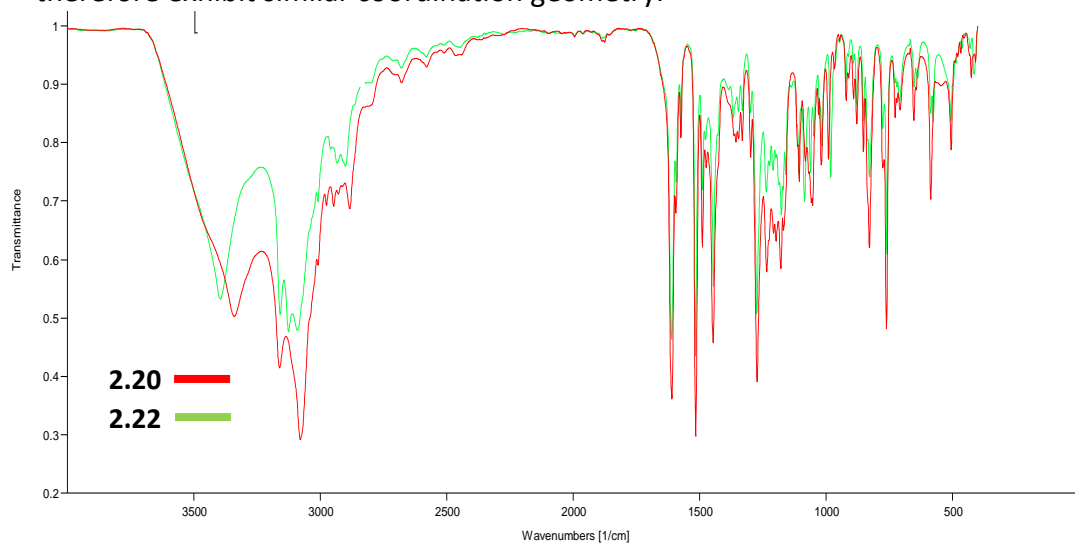


Figure 2.40. IR spectra of **2.20** and **2.22**

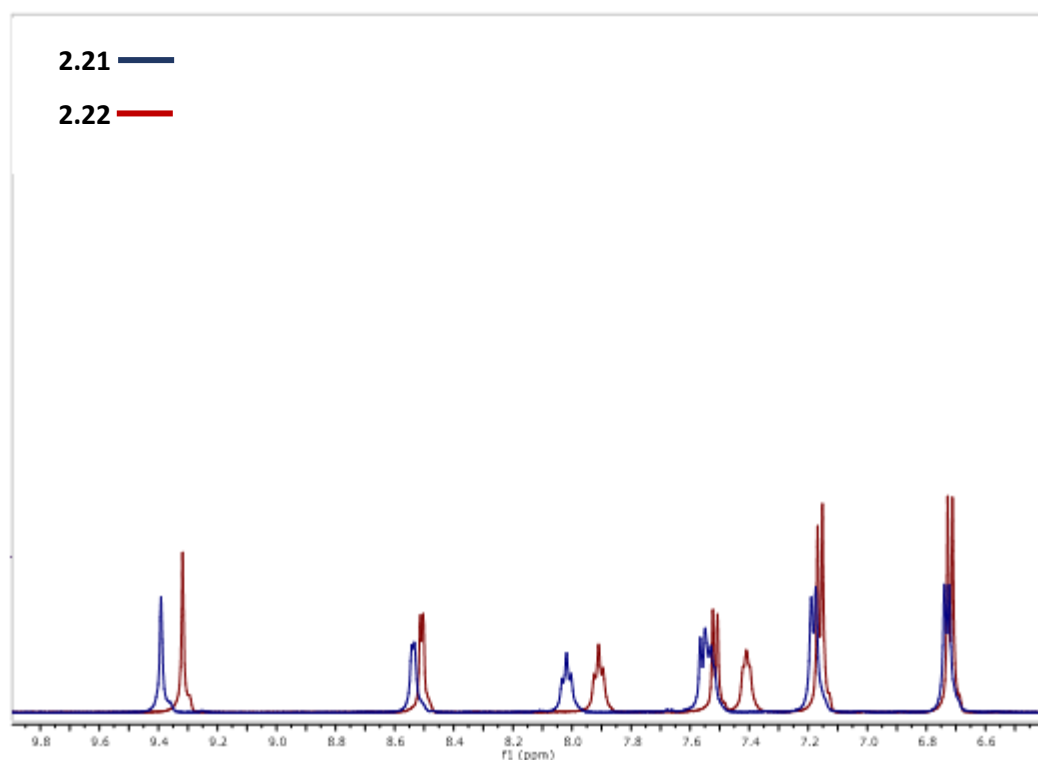
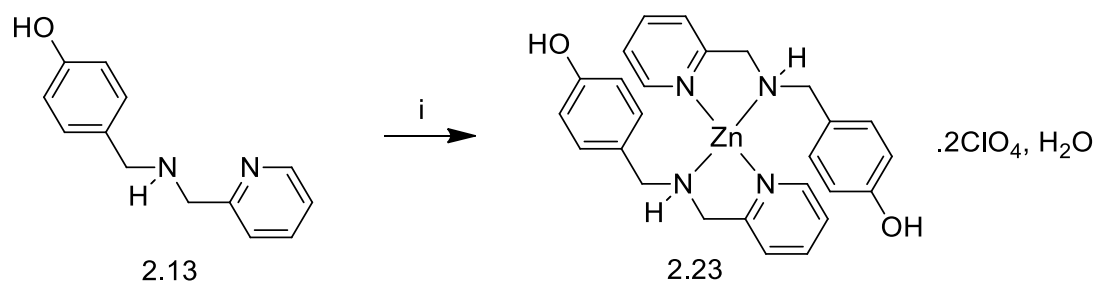


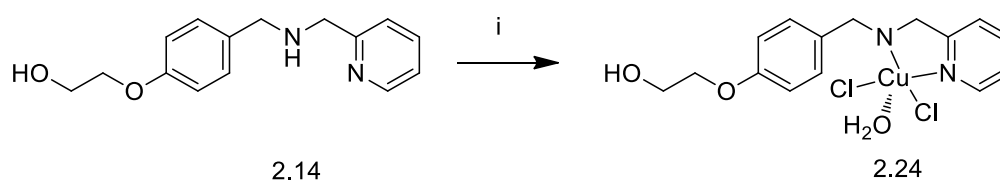
Figure 2.41. NMR Spectra of **2.21** and **2.22**

From the NMR of **2.21** and **2.22**, we can see that the 1:1 complex exhibits signals downfield of those of the 2:1 complex. This indicates that the the ZnCl_2 moiety is more electron withdrawing than the $[\text{Zn}(\mathbf{2.13})]^{2+}$ fragment despite the ligand not possessing a negative charge. This could be explained by the shorter Zn-N bond length as seen from the crystal structure of **2.21** which could offer better electron donation to the metal centre, thereby making it less electron withdrawing.



Scheme 2.18. Reagents and conditions: $\text{Zn}(\text{ClO}_4)_2 \cdot 6\text{H}_2\text{O}$, EtOH, 62%

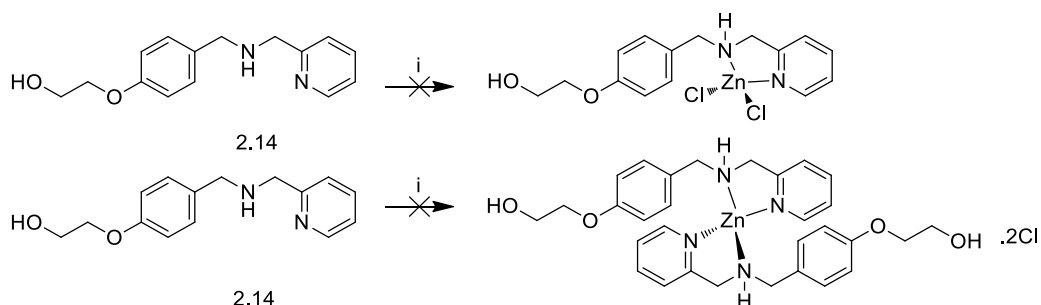
The perchlorate analogue of **2.22**, complex **2.23**, was synthesized by a similar method utilizing the direct reaction of $\text{Zn}(\text{ClO}_4)_2 \cdot 6\text{H}_2\text{O}$ with an excess of **2.13** at room temperature in ethanol. This yielded a hygroscopic brown solid which was collected by vacuum filtration (**Scheme 2.18**). Following lyophilization, the product was obtained as a light brown powder. Elemental analysis confirms the 2:1 binding of the ligand to the metal and also indicates the presence of one molecule of water. The $\nu_{\text{N-H}}$ shift cannot be determined due to the broad H_2O stretch which obscures the signal. However, the $\nu_{\text{C-N}}$ occurs as a broad signal at 1247 cm^{-1} in the ligand which shifts to 1222 cm^{-1} . This suggests the coordination of the secondary amine. The ν_{pyr} stretch exhibits a shift of 13 cm^{-1} , confirming the binding of the pyridine ring to the metal. Characteristic strong bands at 623 and 1090 cm^{-1} indicate the presence of the perchlorate anion and the absence of a second perchlorate band in the region of 650 cm^{-1} rules out perchlorate coordination to the metal.⁸⁹ This would suggest the 4-coordinate structure depicted above as the most likely structure of the complex.



Scheme 2.19. Reagents and conditions: i) $\text{CuCl}_2 \cdot 2\text{H}_2\text{O}$, EtOH, 62%

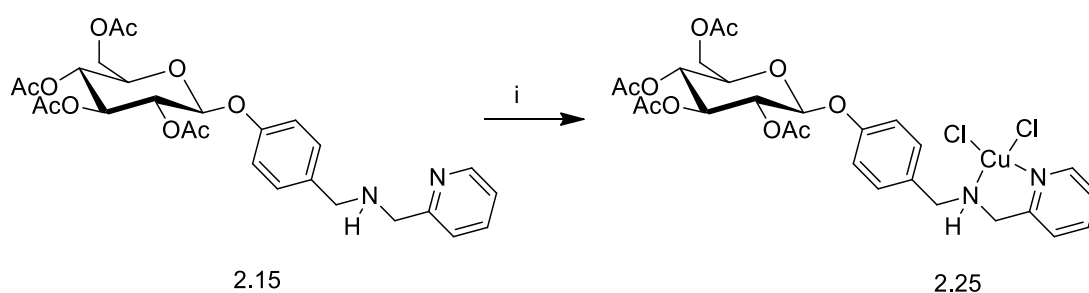
To see the effect of an alkyl hydroxyl group in place of a phenol group, the alkylated N_2 ligand **2.14** was reacted in a 1:1 stoichiometry with $\text{CuCl}_2 \cdot 2\text{H}_2\text{O}$ to generate complex **2.24** as a dark green solid (**Scheme 2.19**). The elemental analysis of the product confirms the 1:1 binding of the ligand and also reveals the presence of one water molecule, as was observed for the analogue **2.19**. As with ligand **2.13**, the $\nu_{\text{N-H}}$ and $\nu_{\text{O-H}}$ signals in the IR spectrum are observed as a single broad band at 3306 cm^{-1} . In the Cu(II) complex **2.24** these are observed as two distinct bands at 3437 and 3238 cm^{-1} . This confirms the binding of the secondary amine to the copper whereas the ν_{pyr} band shifts from 1474 to 1485 cm^{-1} , indicating Cu(II)- N_{pyr} coordination. Crystals suitable for X-ray analysis could not be obtained but considering the similarity to the

analogous compound **2.19** it could be proposed that the compound adopts a 5-coordinate square pyramidal geometry.



Scheme 2.20. Reagents and conditions: i) $ZnCl_2$ / $Zn(ClO_4)_2 \cdot 6H_2O$ / $Zn(NO_3)_2 \cdot 6H_2O$,
EtOH/*MeOH*/*MeCN*

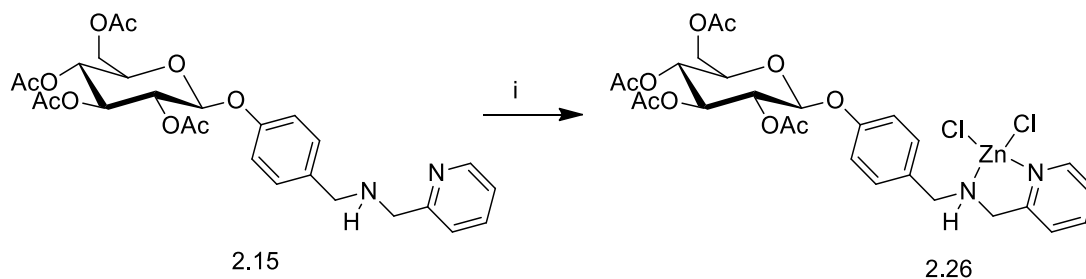
Rather surprisingly, the Zn(II) complex of **2.14** did not form as expected. Several salts and solvents were screened and in all cases no precipitation occurred. However, the addition of petroleum ether to the reaction mixture precipitated a strongly hygroscopic brown solid. A dark oil could also be separated from the reaction solvent after cooling in the freezer for several days. Upon lyophilization this yielded a brown, strongly hygroscopic solid which could not be satisfactorily characterized.



Scheme 2.21. Reagents and conditions: i) $CuCl_2 \cdot 2H_2O$, *EtOH*, 59%

Glucosylated ligand **2.15** was reacted with an equimolar amount of $CuCl_2 \cdot 2H_2O$ in ethanol to produce the complex **2.25** (Scheme 2.21). The 1:1 coordination of the ligand to the metal was determined by elemental analysis. Unlike the aglycon **2.19**, this compound does not show any water of coordination or solvation, which suggests a 4-coordinate geometry for the copper centre. The IR spectra reveals a shift in the ν_{N-H} band, which moves from 3427 cm^{-1} in the ligand to 3421 cm^{-1} in the Cu(II) complex

while the ν_{pyr} occurs at 1475 cm^{-1} in **2.15** and after complexation this shifts to 1486 cm^{-1} . This is a similar magnitude to the shift observed upon the formation of the aglycon complex **2.25** and indicates the participation of the pyridine ring in the coordination with the Cu(II) centre.



Scheme 2.22. Reagents and conditions: i) ZnCl_2 , EtOH, 52%

The Zn(II) complex of **2.15** was prepared by the reaction of the ligand with ZnCl_2 in ethanol to yield a beige precipitate (**Scheme 2.22**). As with the Cu(II) analogue the IR spectrum reveals shifts in the bands for the amine components of the molecule indicating their participation in the coordination with the metal with a 40 cm^{-1} shift observed in the $\nu_{\text{N-H}}$ and a shift of 11 cm^{-1} seen in the ν_{pyr} from 1474 cm^{-1} to 1486 cm^{-1} . Elemental analysis confirms the 1:1 binding of the metal with the ligand to form a 4-coordinate complex which likely adopts a trigonal planar geometry similar to that seen for **2.21**. ^1H NMR studies show a large downfield shifts in the aromatic signals caused by the deshielding effects of the Zn(II) cation (**Figure 2.42**). The Pyr-H signal occurring at 7.75 ppm in the free ligand shows a shift of almost 1 ppm upon complexation to 8.55, a significantly larger shift than was seen for the aglycon complex **2.21** which could suggest a stronger ligand-metal interaction.

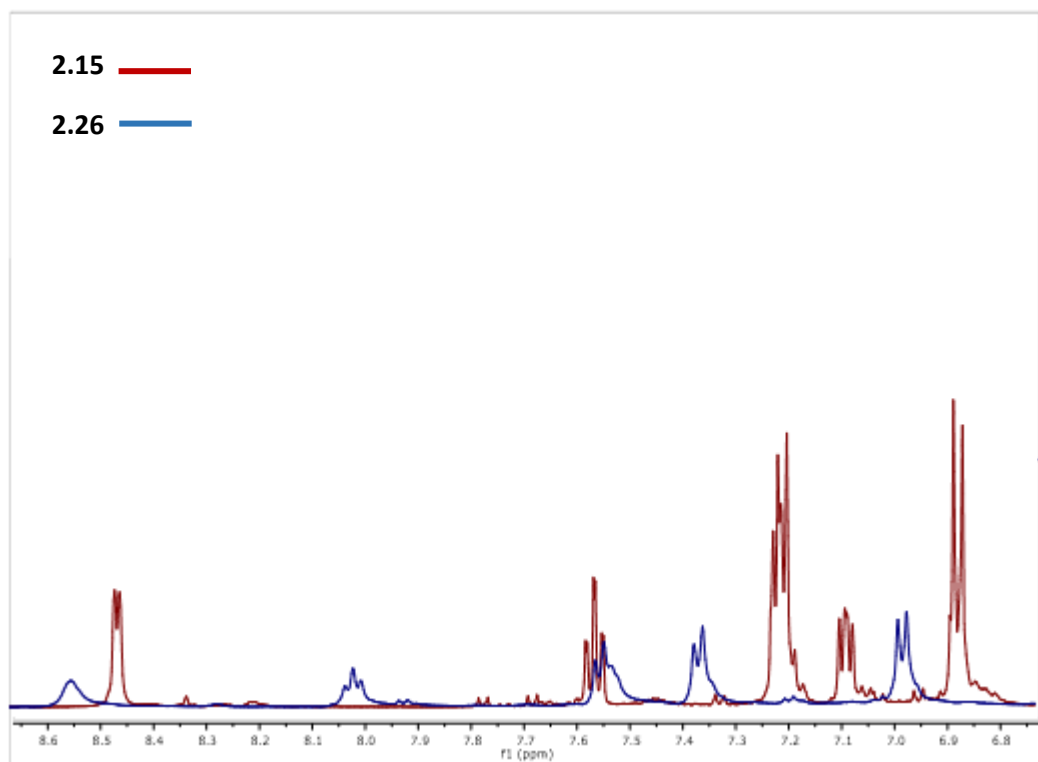
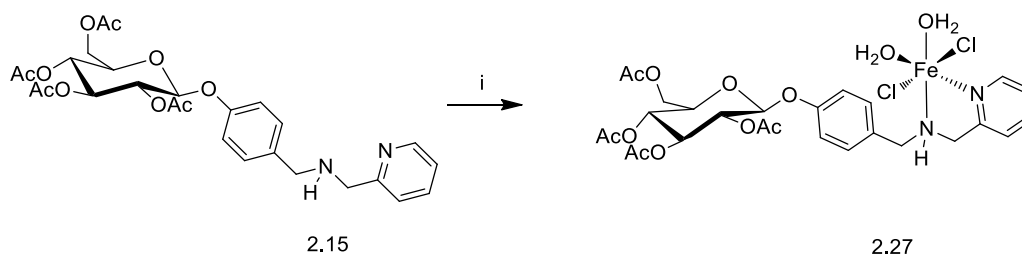


Figure 2.42. NMR spectra comparison of **2.15** and **2.26**



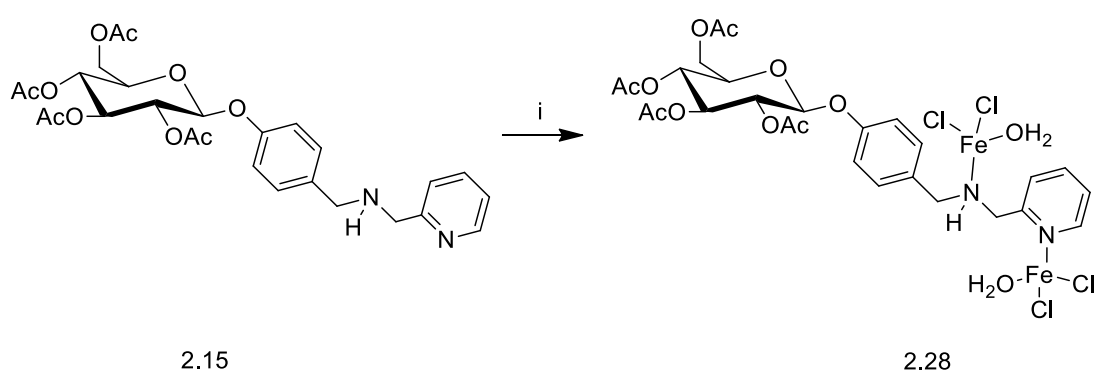
Scheme 2.23. Reagents and conditions: i) $\text{FeCl}_2 \cdot 4\text{H}_2\text{O}$, EtOH, 64%

The Fe(II) complex **2.27** was prepared by reacting ligand **2.15** with a solution of $\text{FeCl}_2 \cdot 4\text{H}_2\text{O}$ under an inert atmosphere (**Scheme 2.23**). In order to avoid the possible oxidation of the Fe(II) to Fe(III), the reaction was carried out on a Schlenk line using degassed solvents and a rigorously air-free environment. The ligand was dissolved in anhydrous, degassed ethanol and transferred by cannula to a solution of excess $\text{FeCl}_2 \cdot 4\text{H}_2\text{O}$ in degassed ethanol using a positive pressure of N_2 to immediately yield a pale brown precipitate. The reaction was stirred at room temperature for 3 h and the solvent was reduced by approximately half *in vacuo*. The reaction was allowed to stand overnight before being filtered under an inert atmosphere to yield a pale

brown solid. A small sample was isolated and immediately analyzed by IR spectroscopy and a separate sample was left exposed to air for one week. This showed no discoloration and its IR spectrum was identical to that of the sample which was analyzed immediately. This suggests that the compound is air stable.

The IR spectrum reveals changes in the $\nu_{\text{N-H}}$ band from 3427 cm^{-1} in the ligand to a broad band at 3435 cm^{-1} after the formation of the complex. This corresponds to the $\nu_{\text{N-H}}$ and $\nu_{\text{H}_2\text{O}}$ while the ν_{pyr} occurs at 1475 cm^{-1} in ligand which shifts to 1482 cm^{-1} . Elemental analysis suggests that two water molecules are present which are likely bound to the Fe(II) to give a 6 coordinate octahedral structure, as this is the most stable geometry for Fe(II). This is further supported by the fact that heating the complex overnight at $70\text{ }^\circ\text{C}$ did not induce any change in the complex by elemental analysis. This makes it unlikely that the water molecules observed are simple solvating the complex and are more likely coordinating to the metal centre.

Magnetic moment studies generated a value of 5.16 B.M which indicates a high spin d^6 configuration. This confirms that the iron species is in the Fe(II) oxidation state and no oxidation occurred. Although this is higher than the spin only approximation would predict (4.9 B. M), it is in the typical range of octahedral Fe(II) complexes (5.1-5.7 B. M) and reflects the spin-orbit coupling which the spin only approximation does not take into account.



Scheme 2.24. Reagents and conditions: i) $\text{FeCl}_2 \cdot 4\text{H}_2\text{O}$, EtOH, 85%

When ligand **2.15** was reacted in excess with $\text{FeCl}_2 \cdot 4\text{H}_2\text{O}$ under inert conditions identical to those used to synthesis **2.27**, a green brown precipitate was observed which yielded a dark green precipitate upon isolation. Elemental analysis suggests a

composition that corresponds to an unusual binuclear species with each Fe(II) coordinated to two chloride ligands, a water ligand and a monodentate complexation to the ligand. Drying of the complex overnight at 70 °C does not change the composition as determined by elemental analysis which suggests that the water molecules are directly coordinated to the metal. The binuclear nature of the compound is supported by the magnetic properties of the material which exhibits a μ_{eff} of 9.76 B.M which is close to the spin only predicted value of 9.8 B. M and greatly exceeds that of a mononuclear Fe(II) complex.

The IR spectrum of the compound shows a broad band at 3429 cm^{-1} , corresponding to the $\nu_{\text{H}_2\text{O}}$ which obscures the $\nu_{\text{N-H}}$ band. The corresponding $\nu_{\text{C-N}}$ cannot be assigned as it is obscured by the strong $\nu_{\text{C-O}}$ signal at 1230 cm^{-1} . The primary ν_{pyr} band at 1474 cm^{-1} shifts 5 cm^{-1} upon coordination of the metal. The less pronounced shifts in these bands compared to those exhibited by the **2.27** indicate weaker ligand-metal interactions.

It is possible the the complex exists as two 4-coordinate tetrahedral Fe(II) centres as depicted in **Scheme 2.24** or as a coordination polymer as depicted in **Figure 2.43**. utilising bridging chloride ligands. This would result in the Fe(II) having a larger coordination number which is more typical of Fe(II) chemistry. However, the magnetic moment values do not indicate any cooperativity between the two iron centres which makes this unlikely.

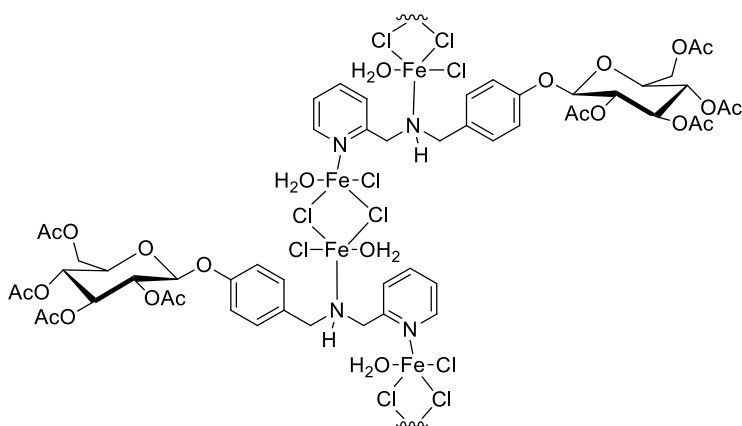
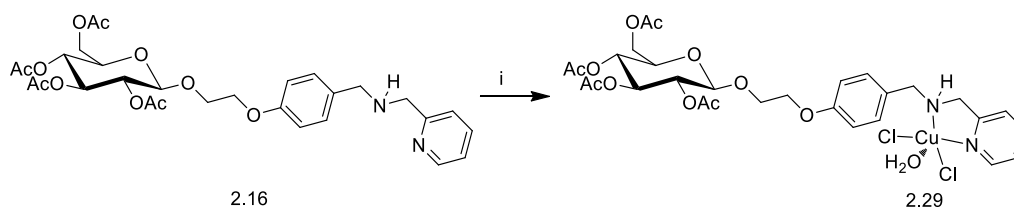


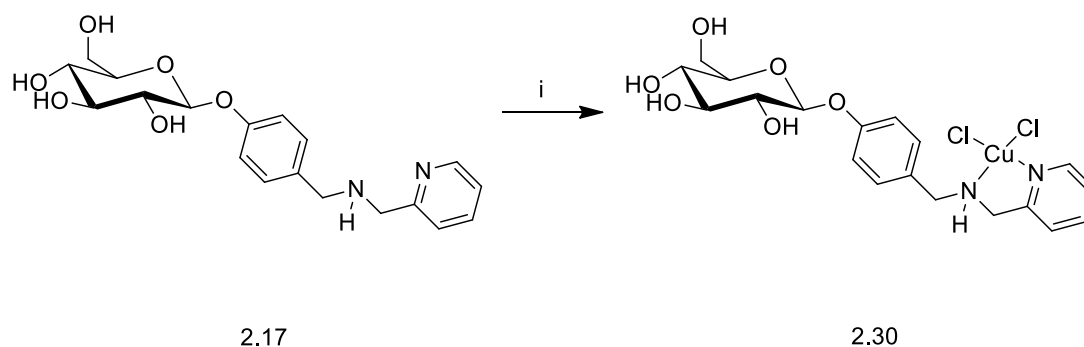
Figure 2.43. Proposed bridged metallopolymer arising from **2.28**



Scheme 2.25. Reagents and conditions: i) $\text{CuCl}_2 \cdot 4\text{H}_2\text{O}$, EtOH , 58%

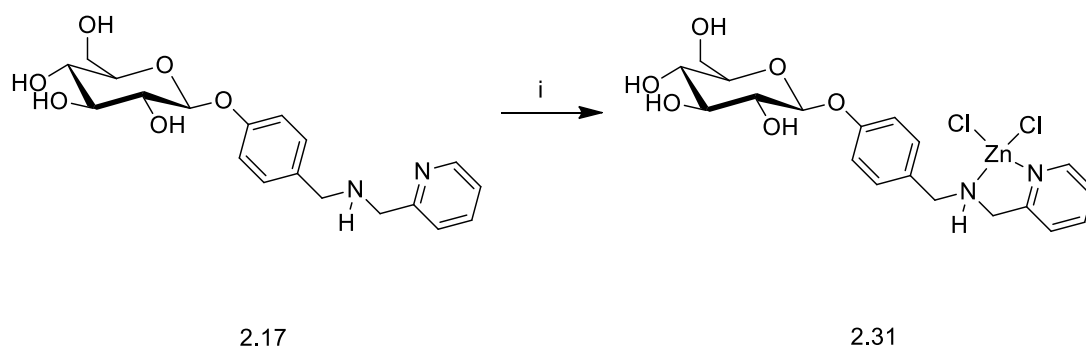
2.16 was reacted with $\text{CuCl}_2 \cdot 4\text{H}_2\text{O}$ in ethanol at room temperature to produce a green solid which, interestingly, formed a partial gel of the reaction solution (**Scheme 2.25**). The remaining solvent was decanted and the gelled substance was dried under high vacuum (0.01 mbar for 24 h). However, this was unsuccessful at removing the gelled ethanol. The substance was then dried under vacuum using Abderhalden's drying pistol with refluxing acetone as the heat source which was sufficient to remove the ethanol to yield the produce as a green solid. This was identified as the 1:1 complex by elemental analysis, which also indicated the presence of one water molecule. As the water remained after thorough drying of the compound both with heat and high vacuum, it can be proposed that it is coordinated to the metal to give a square pyramidal structure analogous to that observed in aglycon complex **2.19**.

The IR spectrum of **2.16** ligand exhibits a single band at 3412 cm^{-1} , while the ligand exhibits two bands in this region at 3442 and 3202 cm^{-1} corresponding to the $\nu_{\text{N-H}}$ and $\nu_{\text{H}_2\text{O}}$. The ν_{pyr} band shifts 6 cm^{-1} from 1477 to 1483 cm^{-1} upon complexation to the metal. This is a smaller shift than is observed upon the formation of the aglycon ligand and confirms the participation of the pyridine ring in binding the copper.



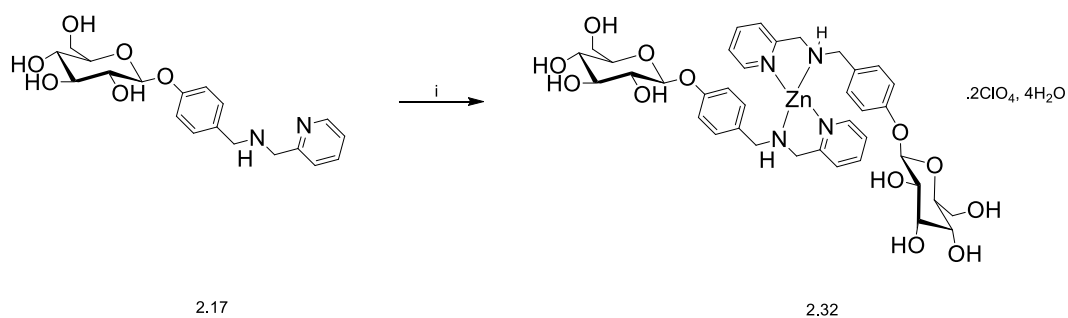
Scheme 2.26. Reagents and conditions: i) $\text{CuCl}_2 \cdot 4\text{H}_2\text{O}$, EtOH , 43%

The deprotected Cu(II) complex of **2.30** was synthesized by the reaction of CuCl₂·4H₂O with a stoichiometric amount of **2.17** in ethanol, which yielded the product as a pale green precipitate (**Scheme 2.26**). As with the acetylated **2.25**, a 1:1 coordination stoichiometry is revealed by elemental analysis. Unlike the aglycon and acetylglucosylated analogues, no water is observed coordinated to the metal centre. The IR spectrum of the ligand exhibits a very broad strong signal at 3379 cm⁻¹, corresponding to the ν_{O-H} and ν_{N-H} bands which are observed at 3405 cm⁻¹ in the Cu(II) complex. The ν_{pyr} band occurs at 1478 cm⁻¹ in **2.17** and after complexation this shifts to 1486 cm⁻¹. This is an almost identical shift which is effected by Cu(II) complexation to the acetyl protected ligand.



Scheme 2.27. Reagents and conditions: i) ZnCl₂, EtOH, 23%

Zn(II) complex **2.31** was synthesized by an identical method to **2.30** by the direct reaction of equimolar amounts of the ligand **2.17** and metal salt in ethanol (**Scheme 2.27**). Elemental analysis revealed the 1:1 coordination which would suggest a 4-coordinate geometry which is typically adopted by Zn(II) complexes. The IR spectrum shows a broad strong signal at 3430 cm⁻¹ corresponding to the ν_{O-H} and the ν_{N-H} bands, higher than that observed in the analogous Cu(II) complex. The ν_{pyr} band exhibits a shift of 8 cm⁻¹ with respect to the ligand which confirms the Zn(II)-Pyr coordination.



Scheme 2.28. Reagents and conditions: i) $\text{Zn}(\text{ClO}_4)_2 \cdot 6\text{H}_2\text{O}$, 55%

The 2:1 $\text{Zn}(\text{ClO}_4)_2$ complex **2.32** was prepared by the reaction of an ethanolic solution of the metal salt with an excess of the ligand **2.17** at room temperature to yield the product as a brown hygroscopic precipitate (**Scheme 2.28**). This produced a brown solid upon lyophilization for 24 h. Elemental analysis confirms the 2:1 coordination of the ligand to the metal in addition to four water molecules of solvation. The IR spectrum reveals a characteristic band at 3430 cm^{-1} corresponding to $\nu_{\text{N-H}}$ and $\nu_{\text{H}_2\text{O}}$ while a change in the ν_{pyr} at 1487 cm^{-1} confirms the coordination of the pyridine ring. Characteristic bands at 625 cm^{-1} and 1078 cm^{-1} indicates the presence of the perchlorate anion and the lack of a new band in the region of 650 cm^{-1} confirms that this is not coordinated directly to the metal.

2.3.3 Synthesis of the N_2O Series

Unlike the N_2 series of compounds, the imines of the N_2O series (**Figure 2.44**) showed remarkable stability towards hydrolysis. The imines of the N_2O series are stable under ambient conditions and require refluxing in the presence of water or acid to effect complete hydrolysis.

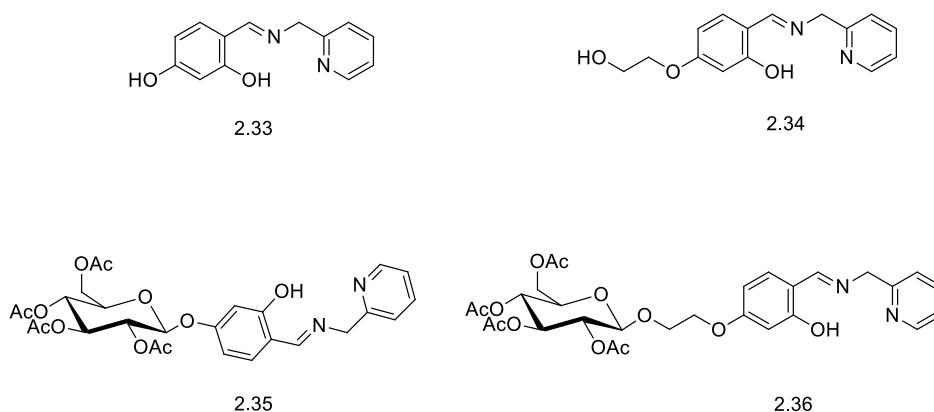


Figure 2.44. Ligands of the N_2O Series

This stability can be attributed to the intramolecular hydrogen bond between the *ortho*-phenolic proton and the lone pair of the imine (**Figure 2.45**). This bond can be clearly seen in the X-ray crystal structures of **2.33** and **2.34** and also in the shift of the *ortho*-phenolic group in the ^1H NMR spectra. These signals appear in the region of 13-14 ppm, a resonance frequency typically seen for carboxylic acids. This shows that the proton is highly deshielded by both the aromatic ring current and the hydrogen bonding to the imine.

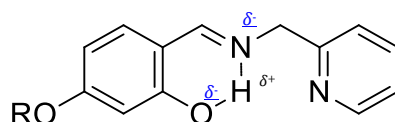
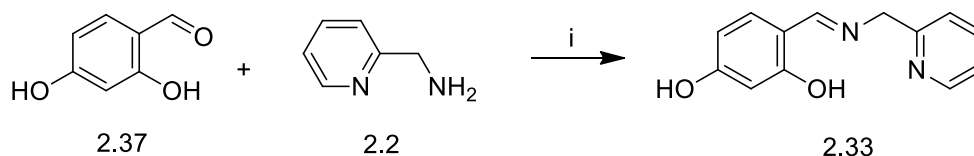


Figure 2.45. Hydrogen bonding observed in the N_2O series

The formation of the imine is highly thermodynamically favoured and is produced by stirring the aldehyde with 2-picolylamine **2.2** for several hours at room temperature without the need for acid catalysis or dehydrating agents.

Efforts were made to synthesize the corresponding amine N_2O ligands however these were unsuccessful. The use of hydride based reducing agents such as NaBH_4 or LiAlH_4 produced poor conversion and a difficult to separate mixture of starting material, degradation products and small amounts of product. This can be attributed to the acidic phenolic hydrogen reacting with the basic hydride to generate an electron rich delocalized aryl-imine with greatly reduced electrophilicity, which inhibits further reaction with hydrides. Catalytic hydrogenation of the imines did not generate the same degree of degradation of the starting material. However, even with the rather forcing conditions of heating at $50\text{ }^\circ\text{C}$ for 48 h with a 15 mol% loading of Pd/C, only ~40% conversion could be induced. This attests to the high thermodynamic stability of the imine ligands.



Scheme 2.29. i) EtOH, >98%

Ligand **2.33** (**Scheme 2.29**) was synthesized by stirring 2,4-dihydroxybenzaldehyde **2.37** and 2-picolylamine **2.2** in ethanol at room temperature, which formed a bright yellow precipitate. This generated the ligand in quantitative yield in 3 to 4 hours, which was collected by vacuum filtration and washed with cold ethanol. Crystals of the compound were grown by dissolving the compound in warm acetonitrile and letting the solution stand for several hours to yield amber, trapezoid-like crystals which were analysed by X-ray crystallography (**Figure 2.46**).

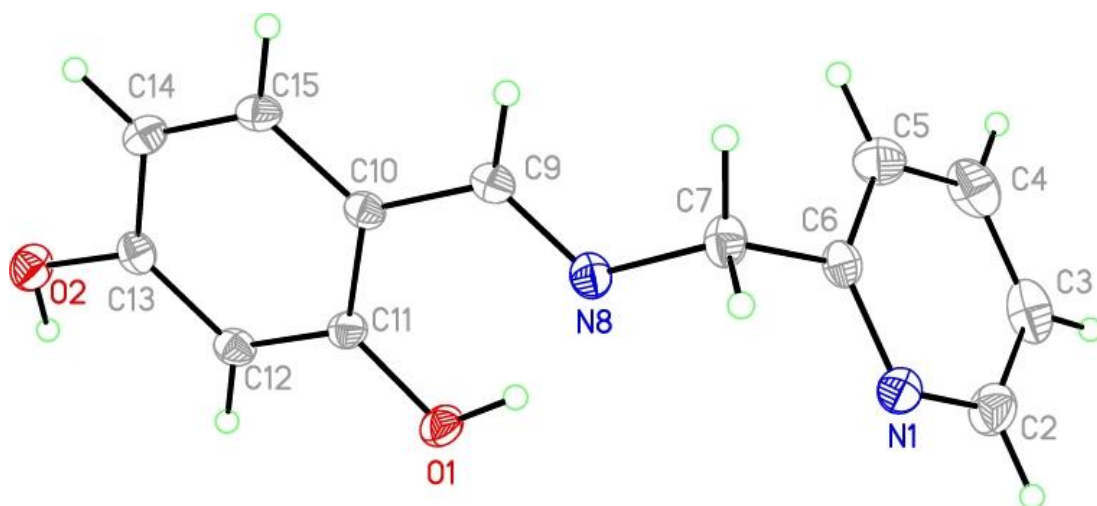


Figure 2.46. X-ray crystal structure of **2.33**

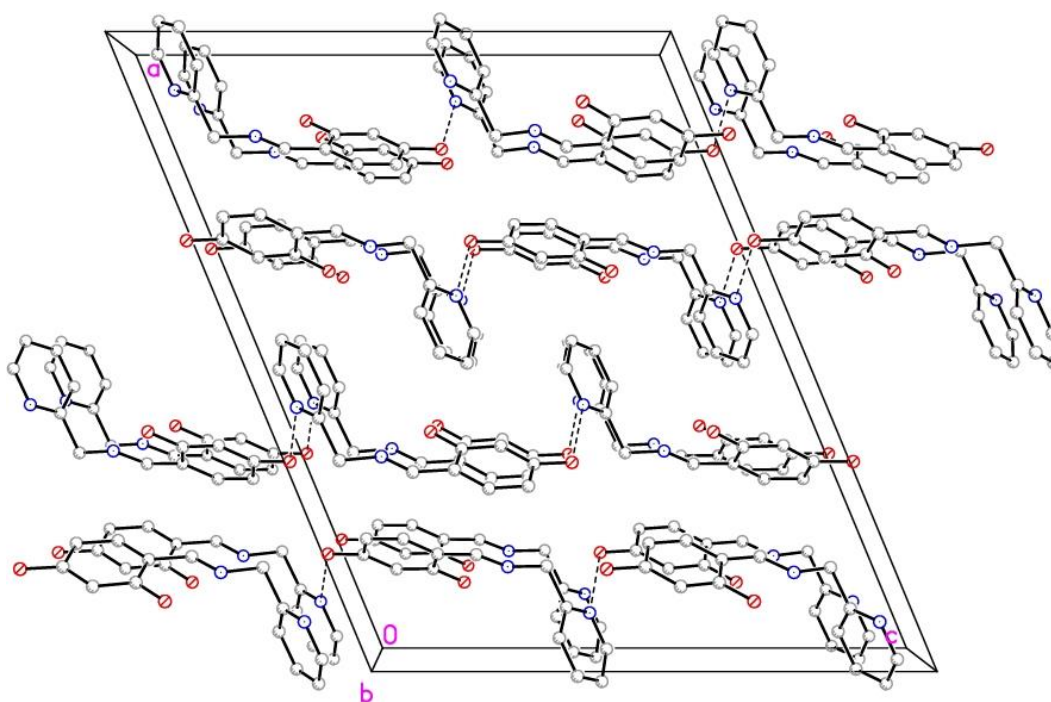
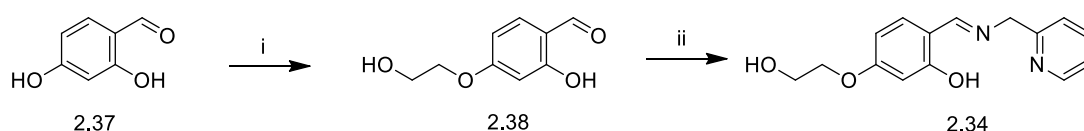


Figure 2.47. Unit cell of **2.33**

The compound crystallizes into a monoclinic unit cell which is primarily formed by intermolecular hydrogen bonding between the *para*-phenolic OH group and the pyridine nitrogen (**Figure 2.47**). Secondary intermolecular interactions are formed via T shaped π stacking between the electron rich dihydroxyaryl ring and the electron deficient pyridine ring. The imine is co-planar with the aryl ring indicating a high degree of conjugation while the pyridine ring is 77.69° out of plane with respect to this conjugated system. The compound clearly shows a strong hydrogen bond between the *ortho*-OH and the imine nitrogen with a distance of 1.702 \AA , which accounts for its greater stability compared to the N_2 imine analogue.



Scheme 2.30. Reagents and conditions: i) 2-chloroethanol, DBU, TBAI, IPA, 76%; ii) EtOH, 86%

Ligand **2.34** was made in two steps starting from 2,4-dihydroxybenzaldehyde **2.37** (**Scheme 2.30**). As with **2.33**, the aldehyde was alkylated with 2-chloroethanol using a microwave promoted synthesis. Although excess 2-chloroethanol was used, the reaction proved to be regiospecific for the *para* position and did not produce any of the *ortho*-alkylated product. This can be rationalized by steric hindrance from the nearby aldehyde and also its electronic effects. As it is moderately strong electron withdrawing group, the aldehyde draws electron density away from the phenolic OH group, therefore lowering the energy of the HOMO and reducing its nucleophilicity. As the *para* hydroxyl group is further away from the aldehyde, it does not suffer from this to the same degree and retains enough nucleophilicity to react with the 2-chloroethanol to generate **2.38**. This aldehyde was then stirred with 2-picolylamine **2.2** in ethanol at room temperature to yield the ligand as a yellow powder in a manner identical to **2.33**.

Single crystals suitable for X-ray analysis were obtained by dissolving the compound in hot acetonitrile and allowing it to cool overnight to yield long, needle like crystals.

The crystal structure of the compound shows strong similarities to that of **2.33** with a monoclinic unit cell and the molecules ordered by way of head to tail hydroxyl-pyridine hydrogen bonds (**Figure 2.48**) although there are no significant π stacking interactions.

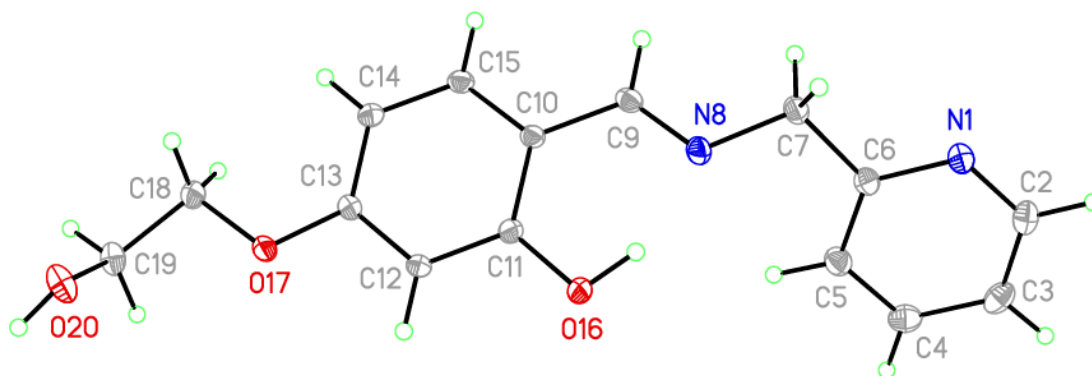


Figure 2.48. Crystal structure of **2.34**

As with the **2.33**, the compound shows a strong hydrogen bond between the *ortho*-phenolic hydrogen and the imine nitrogen with a bond length of 1.695 Å. The imine is co-planar with the aryl ring indicating the delocalized electron density. The pyridine ring is 49.75° out of this plane, significantly less than the value of 77.69° which was observed for the unalkylated compound **2.33**. The unit cell shows additional hydrogen bonding between the primary alcohol and the pyridyl nitrogen (**Figure 2.49**).

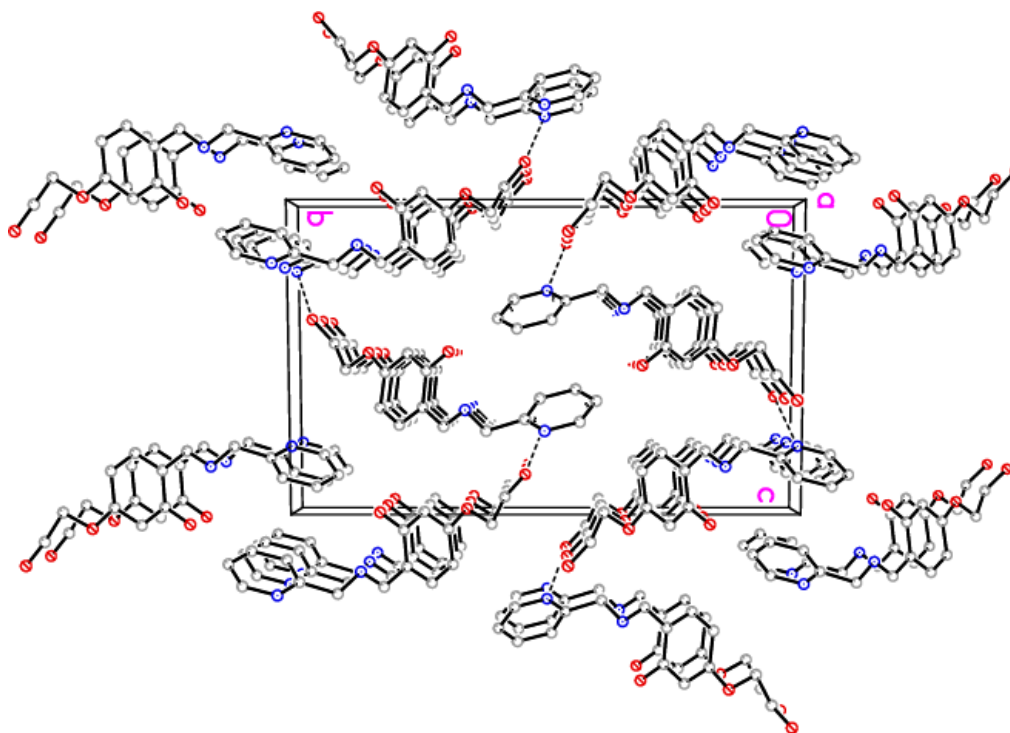
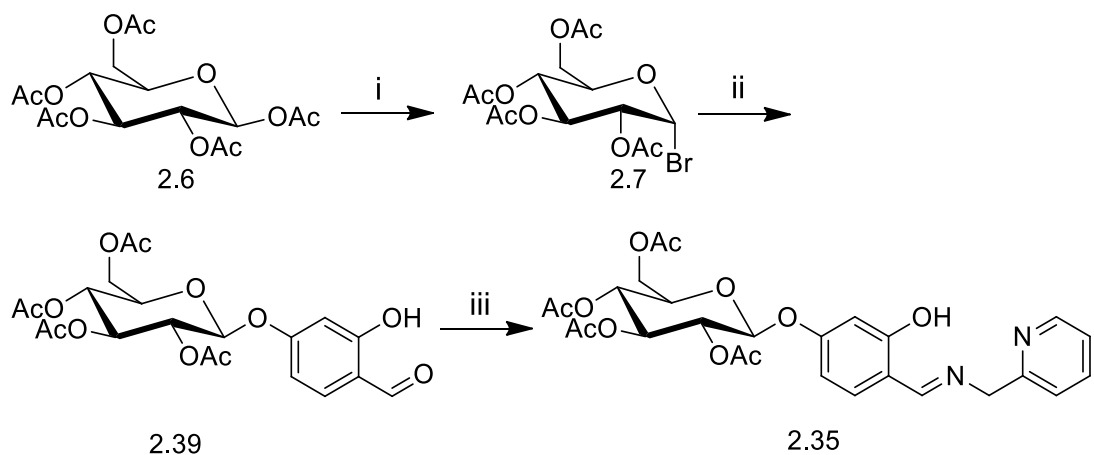
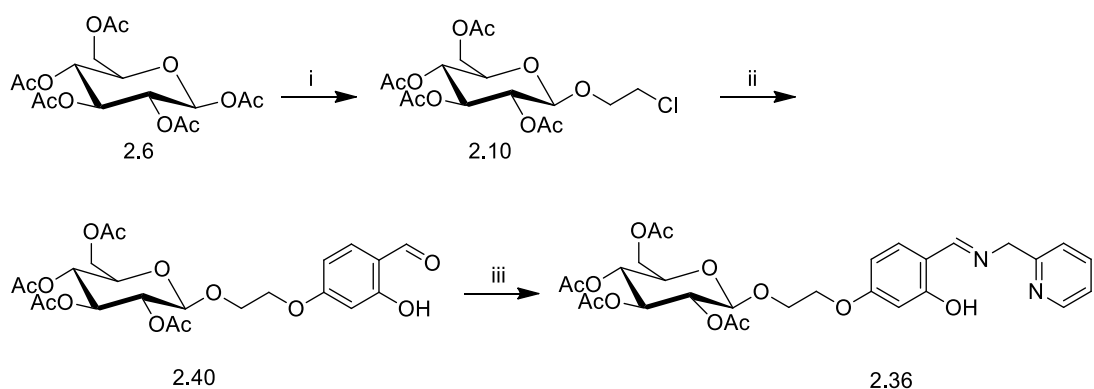


Figure 2.49. Unit cell of **2.34**



Scheme 2.31. Reagents and conditions: i) HBr/AcOH , 87%; ii) 2,4-dihydroxybenzaldehyde **2.37**, Ag_2CO_3 , 61%; iii) 2-picolylamine **2.2**, >98%

The glucosylated aldehyde **2.35** was synthesized in a manner similar to **2.8** using an Ag(I) promoted Koenigs-Knorr glycosylation of tetra-O-acetyl- α -D-glucopyranosyl bromide **2.7** (Scheme 2.31). Interestingly, silver carbonate proved to be effective in this reaction unlike the reaction using 4-hydroxybenzaldehyde **2.1** as the glucosyl acceptor where it did not produce satisfactory conversion (Scheme 4). The aldehyde **2.39** was obtained in moderate yield and was reacted directly with 2-picolylamine **2.2** in refluxing ethanol. This yielded the target compound **2.35** as an orange solid in quantitative yield upon evaporation of the solvent.



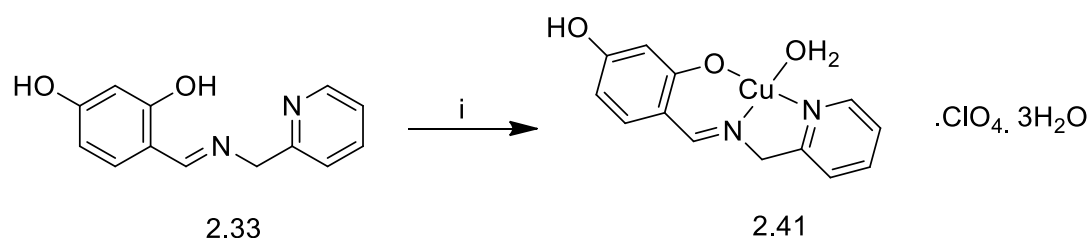
Scheme 2.32. Reagents and conditions: i) 2-chloroethanol, $\text{BF}_3 \cdot \text{OEt}_2$, DCM, 55%; ii) 2,4-dihydroxybenzaldehyde (**2.37**), DBU, TBAI, MeCN, 64%; iii) 2-picolylamine (**2.2**), 78%.

Ligand **2.36** was synthesized in a manner similar to **2.16** using the same intermediate **2.10** (Scheme 2.32). The ether synthesis was accomplished using microwave based methodology analogous to **2.38**. However, the choice of solvent played a crucial role in the success of the reaction. Using IPA as the solvent resulted in the deprotection of the acetyl groups on the sugar, in addition to the formation of the ether which was observed by NMR and mass spectroscopy. This is due to the DBU catalysed ester cleavage of the acetate protecting groups caused by the residual water present in the IPA. It was therefore decided to use anhydrous acetonitrile as the solvent which mitigated this problem, albeit with a slight reduction in the reaction yield compared to the non-glycosylated compound **2.38**.

The imine was then generated by refluxing **2.40** in ethanol with a stoichiometric amount of 2-picolyamine for 4 h. Precipitation of the product was induced by evaporation of approximately half of the solvent and cooling on ice to yield a bright yellow solid.

2.3.4 Coordination Chemistry of the N₂O Series

Initial investigations into the coordination chemistry of the N₂O series of ligands using the metal chloride salts which were used for the N₂ series produced predominantly hydrolysis of the ligand and the precipitation of the 2-picolyamine metal complexes. Perchlorate salts were therefore used which were less prone to inducing hydrolysis during complexation reactions.



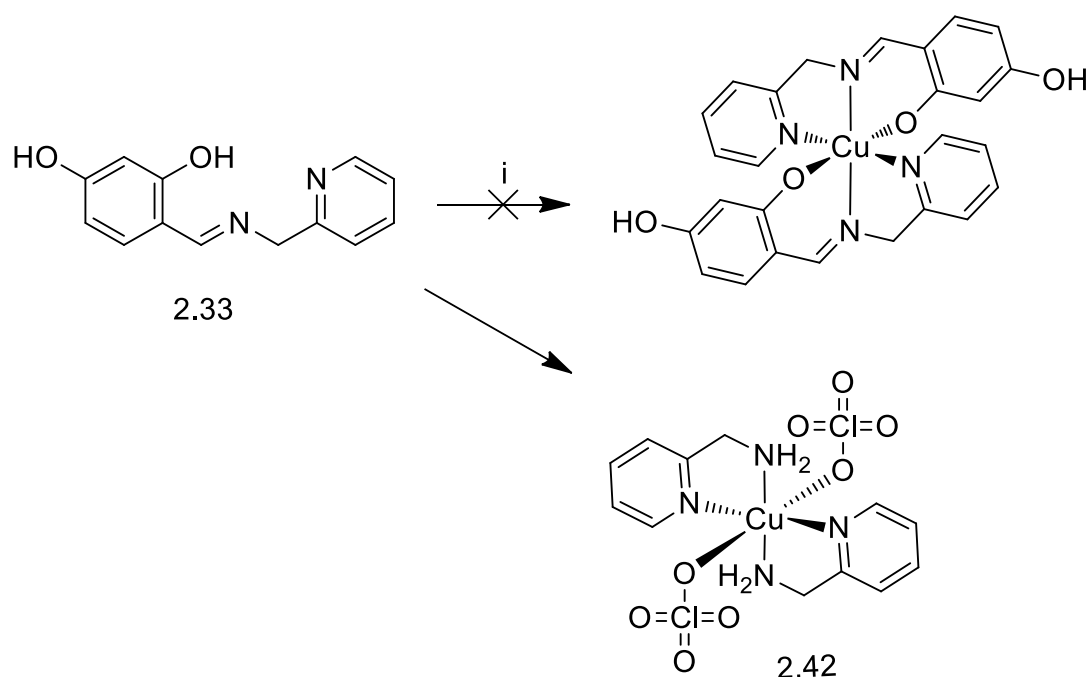
Scheme 2.33. Reagents and conditions: i) $\text{Cu}(\text{ClO}_4)_2 \cdot 6\text{H}_2\text{O}$, EtOH, 40%.

Direct reaction of the ligand **2.33** with $\text{Cu}(\text{ClO}_4)_2 \cdot 6\text{H}_2\text{O}$ in ethanol produced a dark green solid upon cooling (Scheme 2.33). Elemental analysis indicated that it contained four water molecules, a perchlorate anion in addition to the ligand and the

Cu(II) centre. The presence of one perchlorate anion suggests the monodeprotonation of either the ligand or one of the water molecules. Given that phenolic protons typically have pK_a values in the region of 4-10 and water has a pK_a of 15, it is most likely that the ligand is deprotonated as these phenolic protons are more acidic. This acidity is further increased upon complexation to a metal which makes it probable that it is the *ortho*-phenolic group which participates in binding to the metal which is deprotonated.

The IR spectrum reveals telling changes which identify the interactions of the Cu(II) with the ligand. The ν_{O-H} band occurs as a medium intensity, relatively sharp signal at 3435 cm^{-1} in the ligand. After complexation, there is a broad band at 3454 cm^{-1} and a broad band from 2950 to 3250 cm^{-1} which could be attributed to ν_{O-H} and ν_{H_2O} . The imine $\nu_{C=N}$ band shifts 11 cm^{-1} upon complexation from 1622 to 1633 cm^{-1} confirming its participation in the metal coordination while the ν_{pyr} shows a 10 cm^{-1} shift from 1480 to 1490 cm^{-1} . The presence of the perchlorate anion is clearly observed by the characteristic bands at 625 and 1088 cm^{-1} and the lack of a new band in the region of 650 cm^{-1} indicates that the perchlorate is not coordinated to the Cu(II) ion.

a



Scheme 2.34. Reagents and conditions: i) $\text{Cu}(\text{ClO}_4)_2 \cdot 6\text{H}_2\text{O}$, EtOH , 89%

Attempts were made to synthesize the 2:1 complex of **2.33** by refluxing three equivalents of the ligand with Cu(II) perchlorate and attempting to induce precipitation in the same manner as **2.40**. However, this did not produce the intended product (**Scheme 2.34**). Instead, hydrolysis of the ligand occurred and the 2-picolylamine produced reacted with the Cu(II) perchlorate to generate the compound **2.42** which precipitated as a lilac powder.

The structure of the product was identified by the synthesis of the bis-(2-picolylamine)diperchloratecopper complex **2.42** and a comparison of the IR spectra and elemental analyses. Unequivocal proof of the structure was confirmed by X-ray crystallography which matched the structure previously reported by Sarma (**Figure 2.50**).⁹⁰ This revealed an octahedral *trans*-[Cu(2-picolylamine)₂(ClO₄)₂] structure, contrary to an earlier report which erroneously identified it as a square planar [Cu(2-picolylamine)₂].2ClO₄ complex.⁹¹ The weak Cu-OCLO₃ interactions do not significantly alter the vibrational symmetry of the perchlorate anion and hence do not show easily identifiable peaks in the IR spectrum of the complex which would typically be used to determine the coordination of the perchlorate anion. This type of interaction has been described previously as 'semi-coordination'.⁹² Molar conductivity studies were also performed by Ramadan *et al.*⁹¹ which indicated the presence of two anions in solution. This is likely due to the dissociation and the perchlorate anions upon the dissolution of the compound. The weakness of the Cu(II)- ClO₄⁻ interaction is clearly seen in the crystal structure by the elongation of the Cu-O bond which has a length of 2.597 Å compared to the Cu-N bond lengths of 2.000 and 2.022 Å. The weakness of this bond can be attributed to weak coordinating ability of the perchlorate anion due to the delocalization of the negative charge across the perchlorate anion and also the Jahn-Teller distortion observed in octahedral d⁹ complexes. This causes distortion of the octahedral geometry which in this case elongates the Cu-O bond and weakens the interaction.

The crystal displays a triclinic unit cell (**Figure 2.51**) which exhibits hydrogen bonding between aromatic N-H groups and perchlorate Cl-O groups and also short interactions between the perchlorate anion and aromatic C-H. Surprisingly there are no π stacking interactions observed.

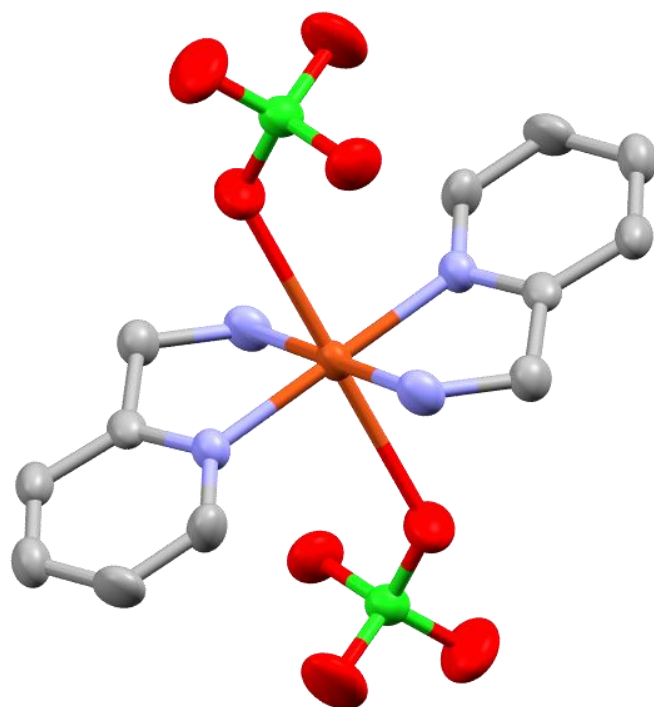


Figure 2.50. Crystal structure of **2.42**

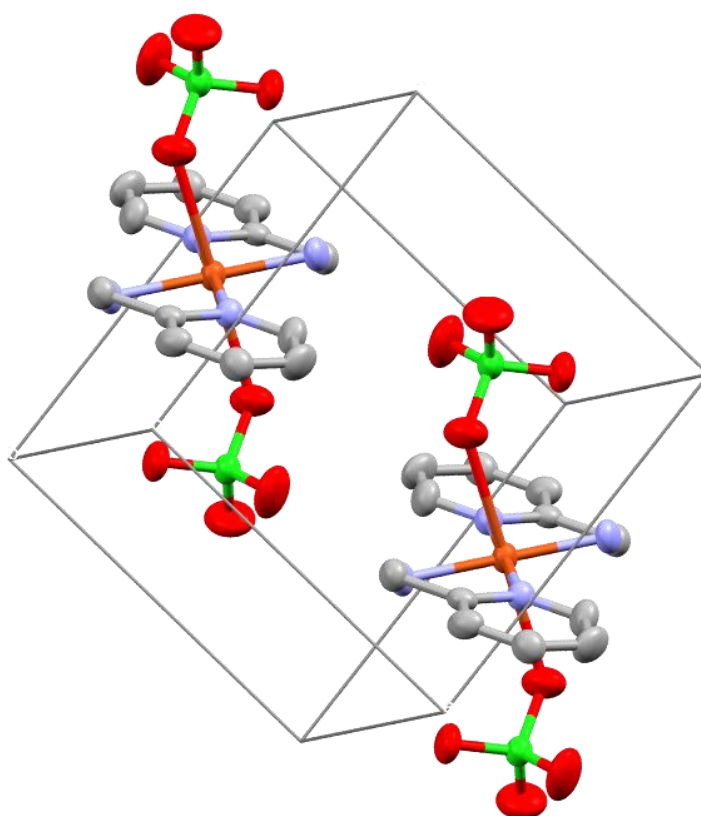
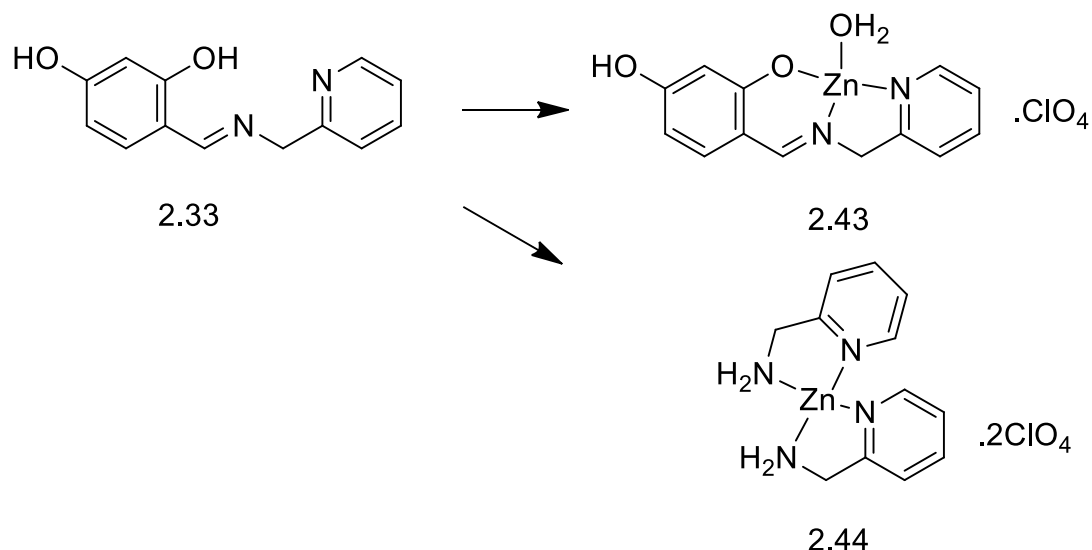


Figure 2.51. Unit cell of **2.42**

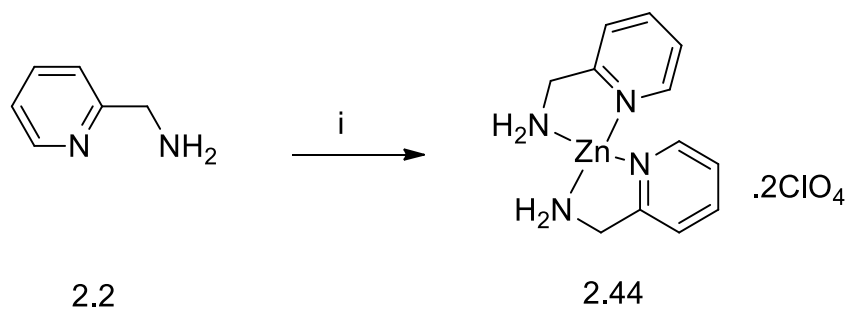


Scheme 2.35. Reagents and conditions: i) $Zn(ClO_4)_2 \cdot 6H_2O$, 94%

2.33 was reacted with $Zn(ClO_4)_2 \cdot 6H_2O$ in refluxing ethanol to produce a hygroscopic yellow solid (**Scheme 2.35**). This was lyophilized to yield a yellow powder which elemental analysis revealed to be the 1:1 complex **2.43**. Also present was one molecule of water present and one perchlorate anion, similar to the product observed for the 1:1 Cu(II) complex **2.41**. As only one perchlorate anion is present it can be deduced that the *ortho*-phenolic proton dissociated following the coordination of the Zn(II) ion. The IR spectrum shows a strong broad band at 3347 cm^{-1} corresponding to the ν_{H_2O} while the ν_{O-H} is present at 3307 cm^{-1} . The imine $\nu_{C=N}$ exhibits a sharp band at 1611 cm^{-1} while the ν_{pyr} shows a shift from 1480 to 1489 cm^{-1} upon complexation. The perchlorate anion shows bands at 625 and 1089 cm^{-1} and the absence of a new band in the region of 650 cm^{-1} rules out the possibility of coordination with the metal.

While the compound could be isolated and characterized in the solid state, it proved to be very susceptible to hydrolysis in solution. This made it difficult to obtain satisfactory 1H NMR data and impossible to obtain ^{13}C NMR data, as the complex undergoes hydrolysis over the time necessary to complete the NMR experiment. Only the 2, 4-dihydroxybenzaldehyde and $[Zn(2\text{-picolylamine})_2] \cdot 2ClO_4$ complex (**2.44**) were observed. The hydrolysis occurred in all solvents screened, namely in ethanol, MeOD, $CDCl_3$, anhydrous CD_3CN , d_8 -THF and d_6 -DMSO. This sensitivity towards hydrolysis is a crucial problem in the synthesis of this compound as the product will

hydrolyse with prolonged reaction time. This also made it impossible to generate the 2:1 Zn(II) complex as was also seen with the analogous Cu(II) complex. As with the Cu(II) complex, the [Zn(2-picolyamine)₂].2ClO₄ complex was synthesized directly and the characterization data compared to confirm the composition of the hydrolysis product (**Scheme 2.36**).



Scheme 2.36. Reagents and conditions: Zn(ClO₄)₂.6H₂O, EtOH, 94%.

The structure of the hydrolysis product was determined by X-ray crystallography of crystals which grew from an NMR sample of **2.43** in d₈-THF. This revealed the formation of 2:1 2-picolyamine Zn(II) complex **2.44** with non-coordinating perchlorate anions (**Figure 2.52**). The structure shows considerable disorder due to the multiple orientations of the perchlorate anion, therefore the perchlorate oxygen atoms modelled in two positions with occupancies of 69/31%.

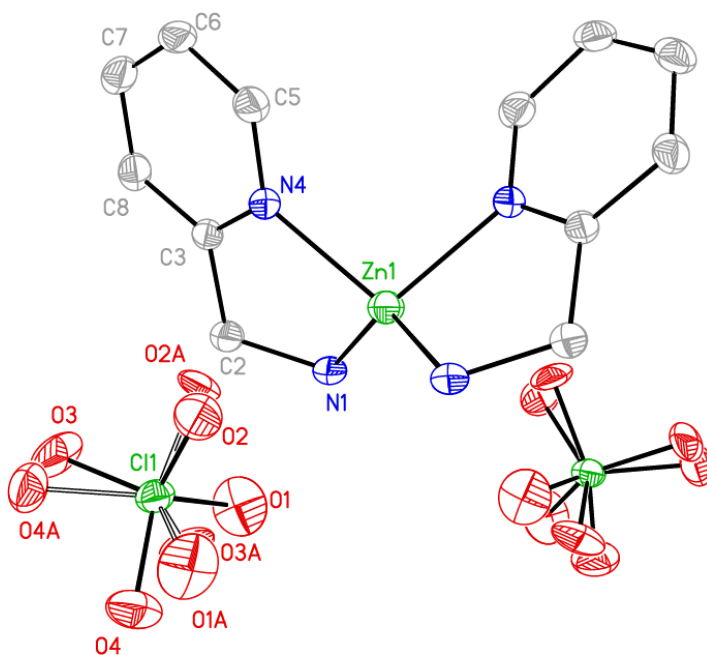


Figure 2.52. Crystal structure **2.44**

The structure reveals a 4-coordinate complex with the two bidentate 2-picolyamine ligands coordinated in a *syn* fashion, unlike the analogous Cu(II) complex where they were observed to orientate in an *anti* orientation. The structure is distorted and has a τ'_4 value of 0.70 which suggests a seesaw type geometry ($\tau'_4 = 0.64$).⁹³ This is an extremely unusual geometry for Zn(II) which has only been reported once in the literature to date for a zinc compound which contained Zn(0).⁹⁴

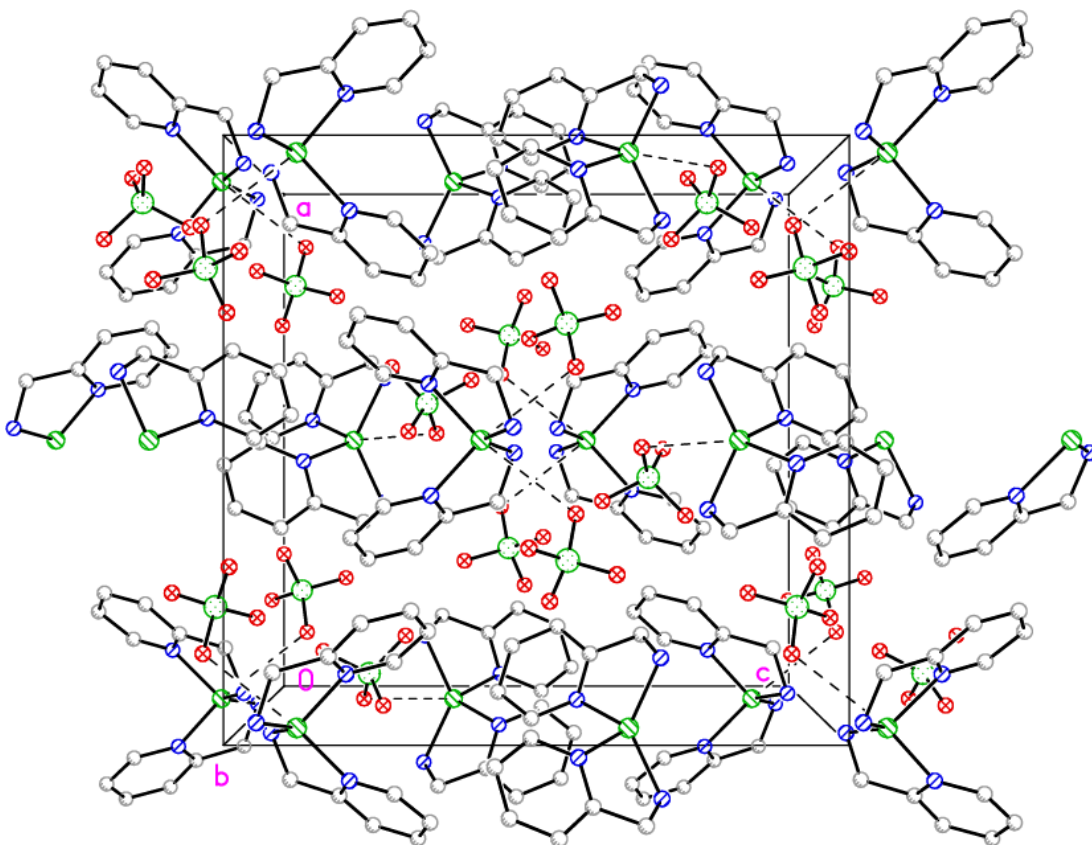
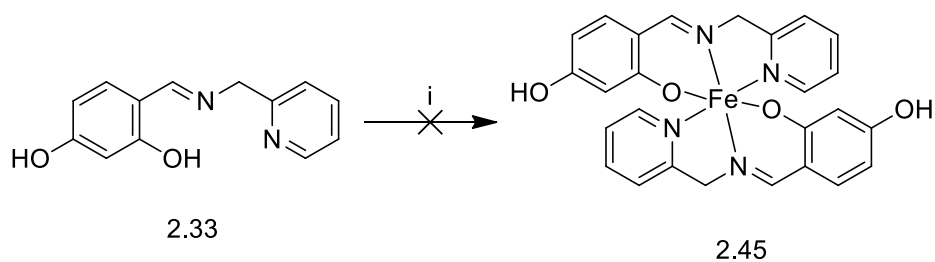


Figure 2.53. Unit cell of **2.44**

The unit cell displays a tetragonal crystal system and is displayed with only one possible orientation of the perchlorate anion for clarity (**Figure 2.53**). The primary intermolecular forces are hydrogen bonds between perchlorate anions and NH_2 groups with close contacts also observed between the perchlorate ion and pyridyl C-H's. Parallel displaced π stacking is also observed with a bond distance of 3.805 Å and a displacement angle of 15.57°.



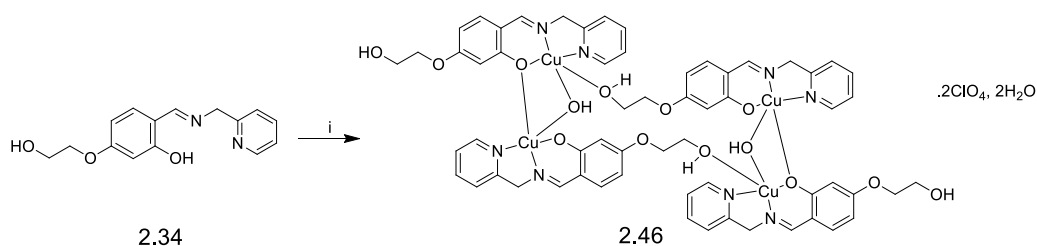
Scheme 2.37. Reagents and conditions: i) $\text{Fe}(\text{ClO}_4)_2 \cdot x\text{H}_2\text{O}$, MeOH, 45 °C

Attempts were made to synthesize an Fe(II) complex using inert conditions similar to those used to generate **2.41** and **2.43** (Scheme 37). Addition of the solution of $\text{Fe}(\text{ClO}_4)_2 \cdot x\text{H}_2\text{O}$ to a solution of excess ligand immediately produced a dark black solid which forms a deep brown solution when highly diluted. This colour is more typical of Fe(III) complexes and would suggest that oxidation of the Fe(II) has occurred, most likely by the redox active phenolic groups as degassed solvent was used. Reaction of the product with potassium ferrocyanide does not produce the deep blue colour which would be expected of an Fe(II) compound. However, this could be due to kinetic or thermodynamic inertness and is not unequivocal proof of the oxidation state of the metal. The reaction was repeated using $\text{Fe}(\text{ClO}_4)_3 \cdot \text{H}_2\text{O}$ and this yielded a similarly coloured product, however the IR spectrum and elemental analyses did not match those of attempted reaction to form **2.45**.

The IR spectrum indicates a strong interaction between the Fe centre and the imine due to the large shift in the $\nu_{\text{C=N}}$ stretch from 1622 to 1607 cm^{-1} and coordination of the pyridine ring is shown by the shift in the ν_{pyr} stretch from 1480 to 1475 cm^{-1} . No bands corresponding to the perchlorate anion are present in the spectra which indicates that the complex has reached neutrality by the deprotonation of the inner sphere ligands. The results of the elemental analysis did not correspond to any likely complexes of the ligand or hydrolysis products with the metal.

The material obtained is highly insoluble in all solvents with the exception of DMSO and DMF and exhibits a melting point above 300 °C which makes it likely that a polymeric material has formed. This is commonly encountered with Fe(III) which readily forms oxo and hydroxo bridged structures. Magnetic moment studies reveal that the iron is paramagnetic which suggests the presence of high spin Fe(II) or Fe(III)

however the molar susceptibility cannot be determined without knowledge of the molecular composition. This data does not provide enough evidence to suggest a likely structure for the complex formed. Extensive effort was exerted to grow crystals suitable for X-ray analysis, however these were unsuccessful.



Scheme 2.38. Reagents and conditions: i) $\text{Cu}(\text{ClO}_4)_2 \cdot 6\text{H}_2\text{O}$, EtOH, 42%

Upon reaction with an ethanolic solution of an excess of **2.34**, $\text{Cu}(\text{ClO}_4)_2 \cdot 6\text{H}_2\text{O}$ formed the bridged dimeric complex **1.38** as revealed by X-ray analysis (**Scheme 2.32**). The IR spectrum displays a single band 622 cm^{-1} with no extra peak observed in the region of 650 cm^{-1} which confirms that there is no interaction between the perchlorate ion and the Cu(II) centre. Elsewhere in the spectrum changes can be observed in a shift and broadening of the $\nu_{\text{O-H}}$ band found at 3267 cm^{-1} in the ligand which occurs at 3431 cm^{-1} in the metal complex. This can be attributed the interaction of the terminal alcohol with the copper centre. The imine $\nu_{\text{C=N}}$ shifts 12 cm^{-1} to 1641 cm^{-1} while the ν_{pyr} shifts from 1479 to 1489 cm^{-1} confirming its coordination with the Cu(II) centre.

The magnetic moment of the compound is significantly lower than the spin only approximation would predict. This can be explained by antiferromagnetic coupling between the copper atoms which is commonly observed in bridged polynuclear metal complexes. This effect leads to the partial quenching of the paramagnetism of the complex due to the close proximity of the metal ions joined by the bridging ligands. When the metal centres are ordered in such a close proximity the unpaired electrons of neighbouring copper atoms can align themselves in opposing directions, thus reducing the net magnetism of the molecule.

Crystals were obtained after storing the reaction filtrate in a freezer for one year. Upon analysis, this revealed a tetranuclear structure composed of two bridged binuclear subunits with two perchlorate counter ions and two water molecules of solvation. (**Figure 2.54**).

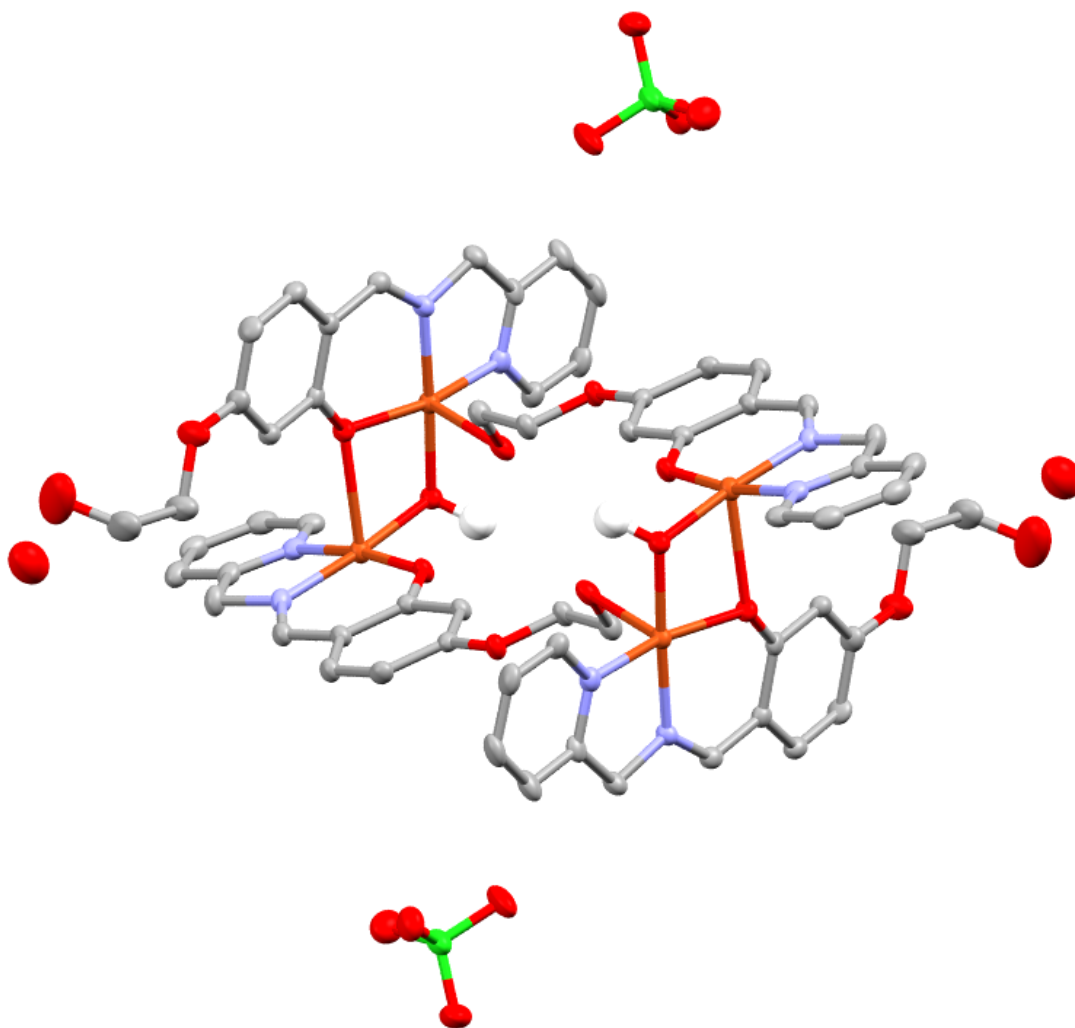


Figure 2.54. Crystal structure of **2.46**. Hydrogen atoms omitted for clarity.

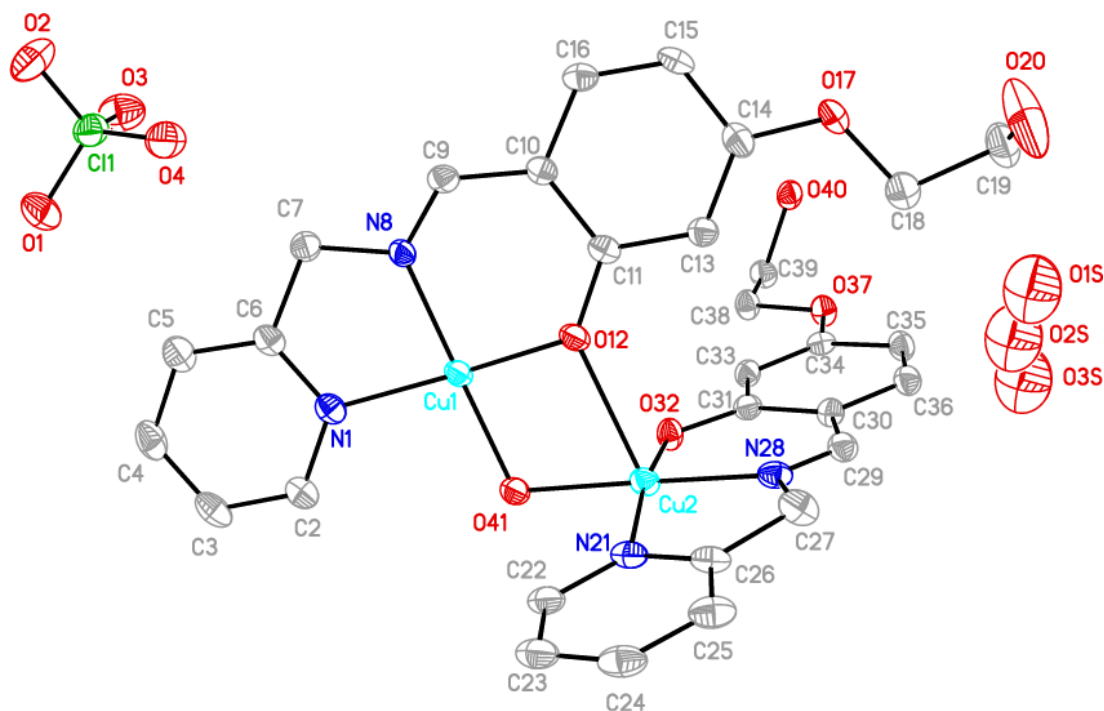


Figure 2.55. Asymmetric unit of **2.46** showing disorder water molecule position (32:49:19% occupancy). Hydrogen atoms omitted for clarity.

The compound exhibits two distinct 5-coordinate square pyramidal Cu(II) centres with N₂O₃ coordination spheres. One centre (Cu1 in **Figure 2.55**) is coordinated in a tridentate fashion by **2.34** which adopts a planar orientation and displays an N-N bite angle of 82.87° and an N-O bite angle of 92.54°. The N-Cu bond lengths are 1.940 and 1.994 Å which are shorter than those of the corresponding N₂ copper complex described *vide supra* which indicates the stronger binding of the metal by this ligand. The chelating phenoxide oxygen displays a similar bond length of 1.937°. The fourth coordination site of the planar arrangement is occupied by a hydroxide molecule which bridges the two Cu(II) centres. This displays a slight asymmetry in its coordination to both copper centres with O-Cu bond lengths of 1.919 and 1.934 Å and a μ-[Cu-O-Cu] angle of 107.91°. The axial position of the square pyramidal structure is occupied by the primary alcohol of another molecule of **2.34** to which forms the dimer. As is typically observed for square pyramidal structures, this bond is highly elongated with a length of 2.526 Å. The square pyramidal geometry is slightly distorted with a geometry index of τ₅ = 0.21.

The other Cu(II) centre present in the crystal (Cu2 in **Figure 2.55**) presents a similar N_2O_3 square pyramidal coordination sphere. This is comprised of the tridentate ligand **2.34**, a bridging hydroxide and a bridging phenoxide. Unlike the other Cu(II) centre, the phenoxide moiety of this ligand does not show any interaction with the other copper centre. The bite angles of the ligand are similar to that observed in the other copper centre with an N-N angle of 82.17° and an N-O angle of 94.00° . The imino N-Cu bond length is identical to that of the previously described copper centre however the pyridyl N-Cu bond is slightly longer with a length of 2.007 \AA . As is to be expected, the non-bridging phenoxide O-Cu bond is shorter than its counterpart in the other coordination centre measuring 1.926 \AA . The bridging hydroxide occupies the final planar coordination site *trans* to the imino nitrogen and is bonded at a distance of 1.934 \AA .

The axial position of this species is occupied by the bridging phenoxide of the ligand chelated to the other Cu(II) centre present in the asymmetric unit. The bond is longer than the equatorial bonds with a length of 2.400 \AA . However, it is shorter than that of the axial interaction observed in the other Cu(II) coordination sphere. The μ -[Cu-(Ph-O⁻)-Cu] angle is 16.72° smaller than that of the hydroxide bridge measuring 91.19° . The coordination geometry of this centre is closer to an ideal square pyramid with Addison's parameter $\tau_5 = 0.04$.

The crystal displays a triclinic unit cell and is composed entirely of a single tetranuclear complex (**Figure 2.56**). This forms relatively few intermolecular interactions with other molecules in the crystal with only two hydrogen bonds observed; perchlorate- $\mu(OH)$ and perchlorate-(CH_2OH). Other interactions observed are hydrophobic interactions between the CH_2 chains and the aromatic rings and parallel displaced π - π stacking between the pyridine and aryl ring with a distance of 4.094 \AA and a displacement angle of 32.57° .

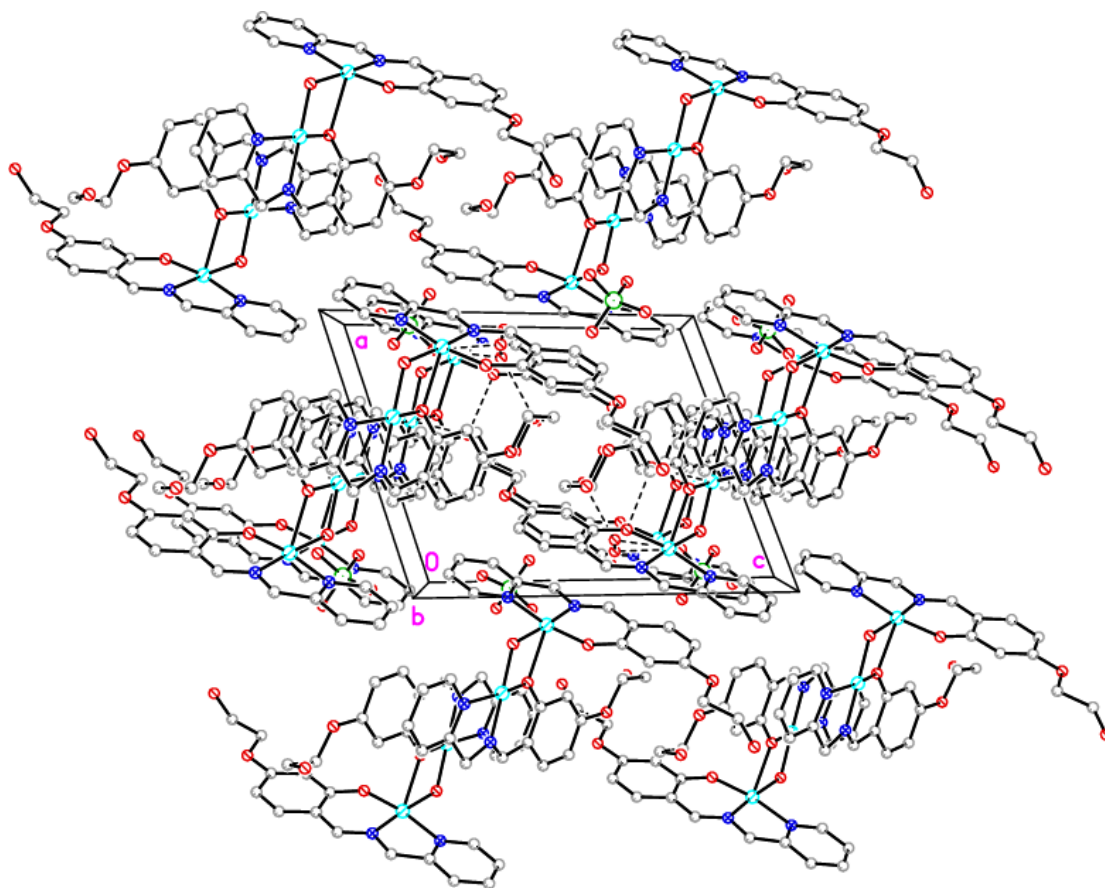
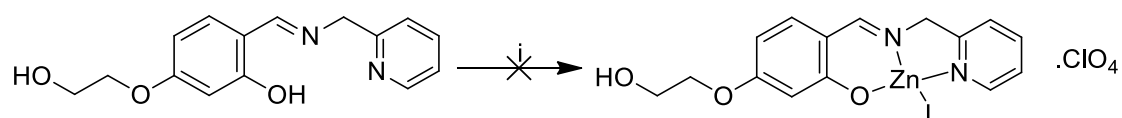


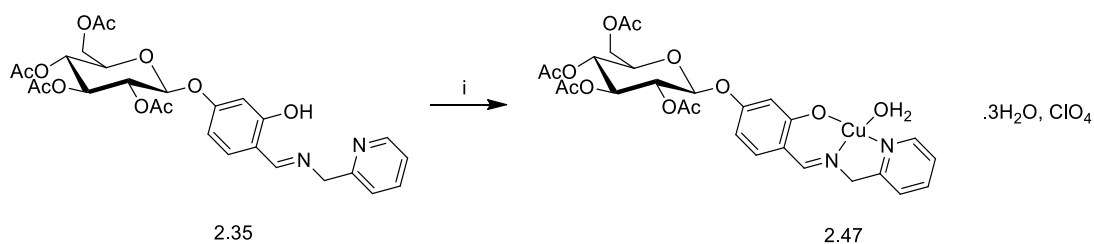
Figure 2.56. Unit cell of **2.46**



2.34

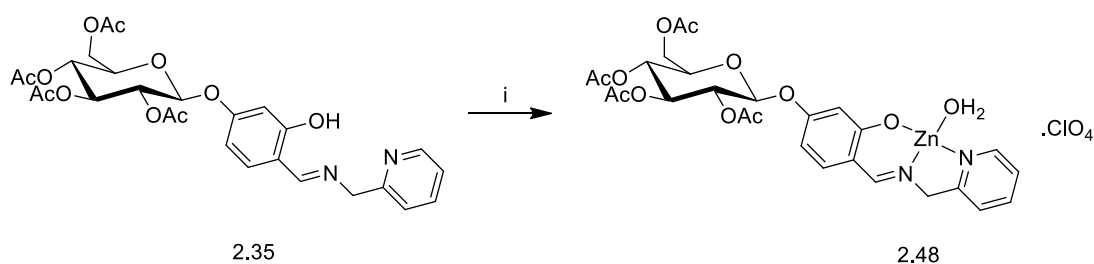
Scheme 2.39. Reagents and conditions: i) $\text{Zn}(\text{ClO}_4)_2 \cdot 6\text{H}_2\text{O}$ / $\text{Zn}(\text{NO}_3)_2 \cdot 6\text{H}_2\text{O}$ / ZnCl_2

Efforts towards the synthesis of the Zn(II) complex of **2.34** did not prove fruitful. All attempts made using different solvents, reaction temperatures and Zn(II) salts such as ZnCl_2 , $\text{Zn}(\text{ClO}_4)_2 \cdot 6\text{H}_2\text{O}$ and $\text{Zn}(\text{NO}_3)_2 \cdot 6\text{H}_2\text{O}$ failed to produce any identifiable complex other than the hydrolysis product **2.34**.



Scheme 2.40. Reagents and conditions: i) $\text{Cu}(\text{ClO}_4)_2 \cdot 6\text{H}_2\text{O}$, EtOH, 44%.

The Cu(II) complex of glycosylated ligand **2.35** was synthesized by the reaction of the **2.35** with $\text{Cu}(\text{ClO}_4)_2 \cdot 6\text{H}_2\text{O}$ in cold ethanol to produce a green precipitate (**Scheme 2.40**). The elemental analysis revealed a 1:1 complex with one perchlorate anion and four molecules of water, similar to the coordination sphere observed in the aglycon **2.41**. The IR spectrum shows an ill-defined broad band 3465 cm^{-1} corresponding to the $\nu_{\text{H}_2\text{O}}$ stretch while the imine $\nu_{\text{C}=\text{N}}$ exhibits a rather small shift from 1635 to 1628 cm^{-1} which is less than that seen upon the formation of **2.41** which could suggest a weaker binding interaction. Coordination of the pyridine ring is deduced by the shift from 1474 to 1483 cm^{-1} and the presence of the perchlorate anion is confirmed by the appearance of bands at 626 and 1110 cm^{-1} . Examination of the region around 650 cm^{-1} does not reveal any new peaks which makes the coordination of the perchlorate anion unlikely.



Scheme 2.41. Reagents and conditions: i) $\text{Zn}(\text{ClO}_4)_2 \cdot 6\text{H}_2\text{O}$, 39%

2.48 was synthesized by the direct reaction of the ethanolic solutions of the ligand **2.35** and $\text{Zn}(\text{ClO}_4)_2 \cdot 6\text{H}_2\text{O}$ (**Scheme 2.41**). The 1:1 coordination was confirmed by mass spectroscopy and also elemental analysis. The IR spectrum of the complex is nearly identical to that of **2.43** with identical shifts observed in the $\nu_{\text{H}_2\text{O}}$, $\nu_{\text{C}=\text{N}}$ and ν_{pyr} which suggests a similar coordination sphere with no coordination of the perchlorate anion (**Figure 2.57**). Both the ^1H NMR and ^{13}C NMR spectra showed hydrolysis of the metal complex in solution.

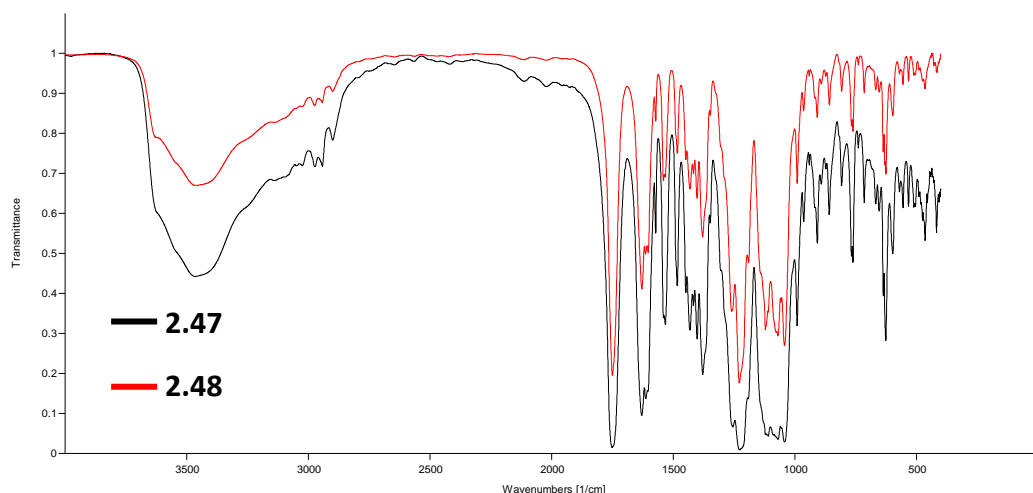
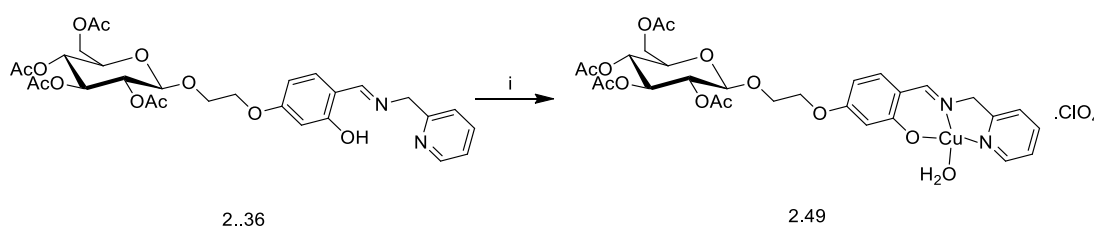
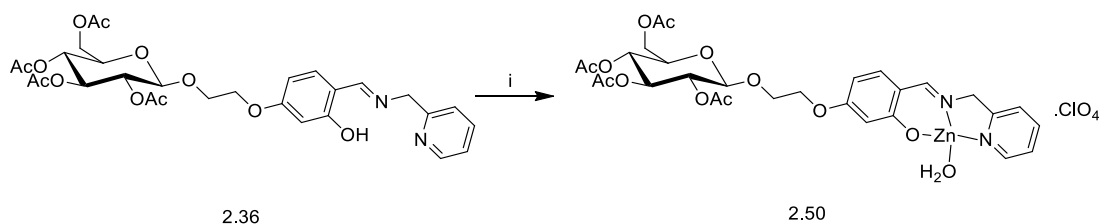


Figure 2.57. IR Spectra of **2.47** and **2.48**



Scheme 2.42. Reagents and conditions: i) $\text{Cu}(\text{ClO}_4)_2 \cdot 6\text{H}_2\text{O}$, 71%

$\text{Cu}(\text{II})$ complex **2.49** was synthesized by the reaction of **2.36** with $\text{Cu}(\text{ClO}_4)_2 \cdot 6\text{H}_2\text{O}$ in refluxing ethanol and cooling to produce a dark green solid (**Scheme 2.42**). Elemental analysis reveals the formation of the 1:1 complex with one perchlorate anion, analogous to the other $\text{Cu}(\text{II})$ complexes of the N_2O series. The IR spectrum exhibits a shift in the $\nu_{\text{O-H}}$ peak from 3467 to 3448 cm^{-1} which is significantly broader in the metal complex due to the overlapping $\nu_{\text{H}_2\text{O}}$ stretch. The imine $\nu_{\text{C=N}}$ band shows a small shift from 1630 to 1627 cm^{-1} similar to the shift observed in the complexes of the ligands featuring direct glycosylation. The coordination of the pyridine ring is inferred by the shift in the ν_{pyr} band from 1476 to 1489 cm^{-1} . It is proposed that the perchlorate anion is not coordinated to the copper centre due to the absence of a band in the 650 cm^{-1} region.



Scheme 2.43. Reagents and conditions: i) $\text{Zn}(\text{ClO}_4)_2 \cdot 6\text{H}_2\text{O}$. 64%

As with **2.49**, Zn(II) complex **2.50** was synthesized by the reaction of excess ligand **2.36** and the perchlorate salt in refluxing ethanol (**Scheme 2.43**). Upon cooling, this yielded the product as a white solid in addition to a sticky brown residue. The product was isolated by decanting the suspension in order to separate it from the brown residue which formed a brown oil upon exposure to air. The product darkened slightly to form a beige solid upon lyophilization for 24 h. This was shown by elemental analysis to be the 1:1 complex. As with compounds **2.47** and **2.48**, IR analysis reveals near identical spectra for both the Zn(II) and Cu(II) complexes of **2.36** with a broad $\nu_{\text{H}_2\text{O}}$ band at 3446 cm^{-1} and a shift in the ν_{pyr} to 1487 cm^{-1} . The $\nu_{\text{C=N}}$ does show a distinct shift to a higher wavenumber of 1436 cm^{-1} unlike the Cu(II) complex which caused it to vibrate at a lower energy. Both the ^1H NMR and ^{13}C NMR spectra showed hydrolysis of the metal complex in solution.

2.4 Conclusion

The aim of this work was to synthesize novel ligands and their glucosylated analogues and also to investigate their coordination chemistry. Two series of ligands, namely the N_2 and N_2O series, were obtained, characterized and their syntheses optimized. Their coordination chemistry with Cu(II), Zn(II) and in some cases Fe(II) was investigated and the resulting metal complexes were characterized by IR spectroscopy elemental analysis and, where applicable, NMR, magnetic susceptibility and X-ray crystallography.

The initial investigations into the N_2 imine ligands did not prove fruitful as the ligands were too prone to hydrolysis to be satisfactorily characterized or form stable metal complexes. The synthesis of the N_2 amine series of ligands was much more successful

however, it was not trivial as problems caused by the instability of the imine intermediates presented significant challenges. With optimized reaction conditions and meticulous attention to the reaction set up, the ligands can be synthesized in good yields and high purity. The N₂O series on the other hand was quite easily synthesized in high yield and purity stemming from the high thermodynamic stability of the hydrogen bond stabilized imine and their insolubility in ethanol, which allows for the precipitation of the product to drive the reaction to completion.

While the ligand synthesis presents more difficulty than the N₂O ligand series, the coordination chemistry of the N₂ series offers greater scope developing novel compounds. A wide selection of homo and heteroleptic complexes could be obtained with both chloride and perchlorate metal salts. The metal complexes are stable and could be completely characterized with ease. Several compounds were obtained as crystals which allowed for characterization by X-ray crystallography. These compounds would be expected to be more attractive as antikineto-plastic agents as they have superior stability in the solid and solution phase and therefore, are more likely to retain their composition *in vivo* for a longer time than the complexes of the N₂O series.

The coordination chemistry of the N₂O is rather limited with only heteroleptic 1:1 complexes obtained. The Lewis acid promoted hydrolysis of the N₂O proved to be a significant issue in the synthesis of stable metal complexes. Due to this, no homoleptic complexes were obtained and some of the complexes showed instability in solution which made complete characterization by NMR impossible. Several complexes were hygroscopic, which further presented difficulty in obtaining satisfactory characterization data. This instability is highly undesirable for bioactive compounds as it is possible that the compound will decompose *in vivo* before it can get to the site of action and the degradation products could present undesired side effects.

To the best of our knowledge, this work presents the first example of glycosylated Cu(II) and Zn(II) metallotherapeutics and also the first investigations into this strategy for the design of antiparasitic compounds.

Chapter 3: Biological Evaluation of Novel Antiparasitic Agents

3.1 Aim

The first aim of this chapter was to perform a preliminary evaluation the biological effects of a selection of compounds from the N₂ and N₂O series of compounds described in Chapter 2 (**Figure 3. 1**). Firstly, the compounds were studied to establish their *in vitro* safety in mammalian cells. Following this, their inhibitory effects towards the viability of *L. amazonensis* amastigotes and *T. cruzi* trypomastigotes were investigated *in vitro*. The compounds which showed the highest inhibitory activity were then studied further to gain information about their toxicity *in vivo* using the *Galleria mellonella* model. The biological evaluations of cytotoxicity and antiparasitic activity detailed in Sections 3.2.1, 3.2.2 and 3.2.3 were carried out by the group of Prof André Luis Souza dos Santos at the Microbiology Institute Paulo de Góes in Universidade Federal do Rio de Janeiro (UFRJ). All experiments were performed in triplicate, in three independent experimental sets. The data were analysed statistically by means of Student's t-test using EPIINFO 6.04 computer software. P values of 0.05 or less were considered statistically significant.

Following analysis of the data obtained from the above biological testing, it was attempted to establish a preliminary structure-activity relationship effected by the various modifications to the ligand core, namely glycosylation, alkylation, and metalation, on their antiparasitic activity. Finally, to investigate if the glycosylated compounds can act as pro-drugs, enzymatic hydrolysis studies were carried out.

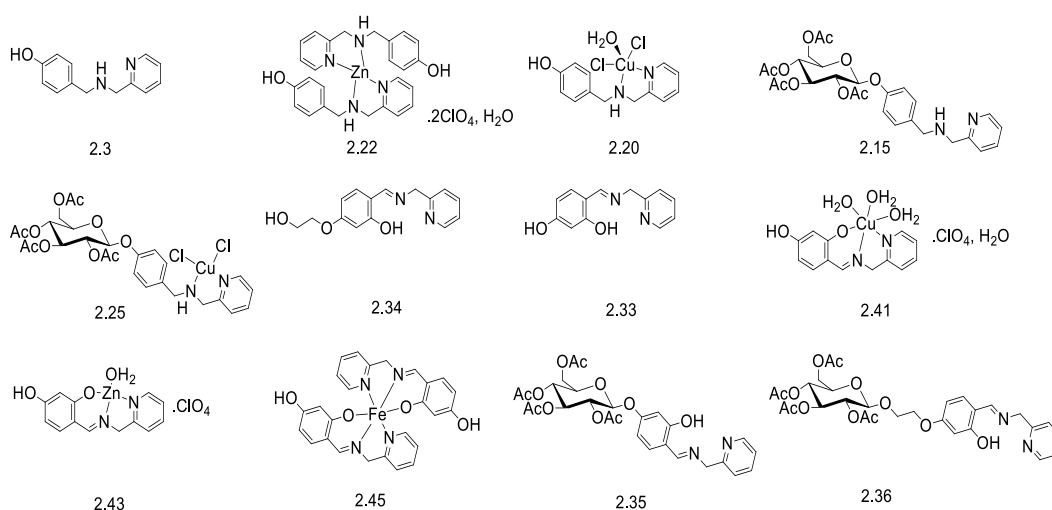


Figure 3. 1. Structures of compounds selected for biological investigation.

3.2 Results and Discussion

3.2.1 Evaluation of *In Vitro* Cytotoxicity to Macrophage Cells

The selected compounds (**Figure 3. 1**) were initially screened to assess their cytotoxicity. This testing was carried out by the group of Prof Santos at URFJ and was determined using RAW 264.7 murine macrophage cells. The compounds were administered across a range of concentrations and the viability of the macrophage cells was determined after 24 h using an MTT assay. The CC_{50} value, a measure of how much of a compound will inhibit the growth of a population of cells by 50%, was determined for each of the compounds and the results can be seen in **Figure 3. 2** and **Figure 3. 3**.

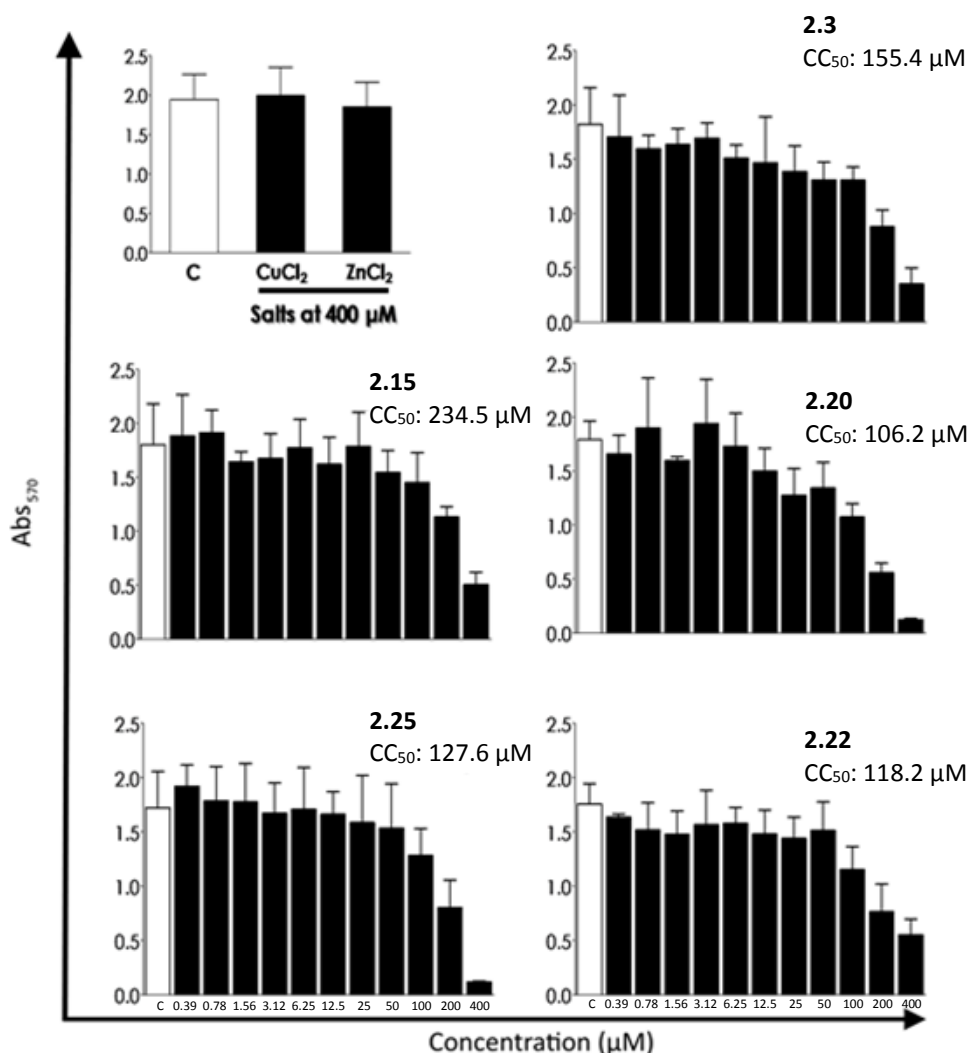


Figure 3. 2. Cytotoxicity of selected compounds on RAW macrophages. Mammalian cells (105 cells) were incubated in a 96-well plate for 48 h (RAW) in the absence (white bars) or in the presence of single doses of the compounds at a range of concentrations (black bars). Viability was determined spectrophotometrically at 570 nm by MTT assay.

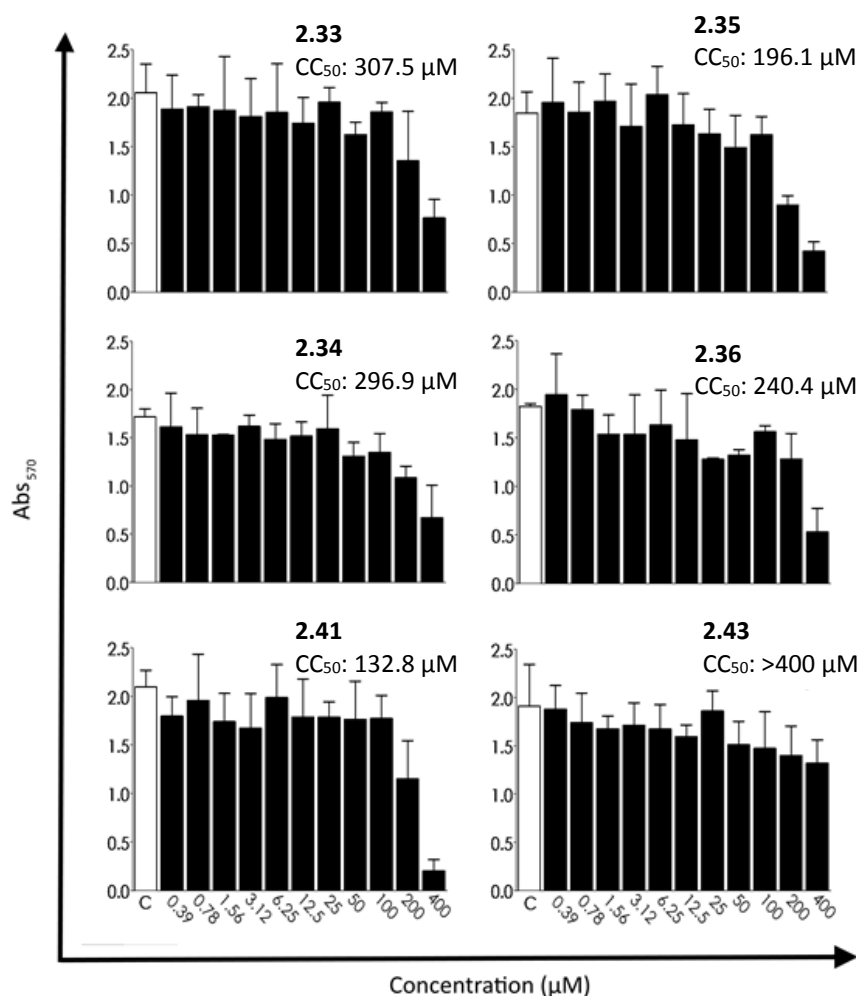


Figure 3. 3. Cytotoxicity of selected compounds on RAW macrophages. Mammalian cells (105 cells) were incubated in a 96-well plate for 48 h (RAW) in the absence (white bars) or in the presence of single doses of the compounds at a range of concentrations (black bars). Viability was determined spectrophotometrically at 570 nm by MTT assay.

From these results, we can see that the N₂ compounds are more cytotoxic than the corresponding compounds from the N₂O series, for example the aglycon ligand **2.3** is almost twice as cytotoxic as the N₂O analogue **2.33**. This trend can also be observed in the metal complexes of these ligands; the Zn(II) complex of **2.3** has a CC₅₀ value of 118.2 µM while the Zn(II) complex of **2.33** was so well tolerated by the cells that the CC₅₀ value was not determined as it was above the concentration range tested. However, this compound was found to be unstable in solution so it is likely that the tested compound is in fact a hydrolysis product.

Glycosylation of the N₂ ligands proved to be highly effective at decreasing the cytotoxicity of the compounds. This is clearly demonstrated by the increase of the

CC₅₀ value of **2.3** from 155.4 μM to 234.5 μM upon glycosylation with peracetylated glucose. This effect also occurs in the metal complexes with **2.25** exhibiting a cytotoxicity value of 21.4 μM higher than the aglycon analogue. Interestingly, the opposite effect was observed for the N₂O series of compounds; **2.35** presents with a CC₅₀ value more than 100 μM lower than **2.33** while the ligands featuring an ethylene group on the phenolic moiety also showed this effect. **2.36** displays a CC₅₀ value of 240.4 μM, while the parent aglycon is less toxic with a value of 296.9 μM.

Metalation of the N₂ compounds increases their cytotoxicity. The Zn(II) (**2.22**) and Cu(II) (**2.20**) complexes of **2.3** both exhibited lower CC₅₀ values than the parent ligand (118.2 μM and 106.2 μM vs 155.4 μM respectively). This was also seen for the Cu(II) complex (**2.25**) of the glucosylated ligand **2.15** which showed a reduction of 106.9 μM in the CC₅₀ value. The metal complexes of the N₂O series on the other hand showed no clearly identifiable trend. The ligand **2.33** possessed a CC₅₀ value of 307.5 μM while the Fe(II) complex **2.45** showed a similar value of 333.1 μM, the Cu(II) complex **2.41** was more cytotoxic with a value of 132.8 μM while the corresponding Zn(II) complex was well tolerated across the entire concentration range studied and therefore was not determined. CuCl₂·2H₂O and ZnCl₂ did not show any toxicity.

Overall these results are very promising as they demonstrate that the drugs are well tolerated by mammalian cells at relatively high dosages without affecting the viability of the cells. This attribute is an essential for drug candidates as it is necessary for them to be well tolerated by the host while the dosage is high for the compound to exert its therapeutic effect. The CC₅₀ values obtained show that the ligands and metal complexes of both the N₂ and N₂O series do not possess appreciable cytotoxicity and therefore could be administered to a mammal without expecting any significant toxic effects *in vivo*. This confirms that the compounds could have potential as agents for the treatment of parasitic diseases in humans.

3.2.2 Evaluation of Antileishmanial Activity

3.2.2.1 In Vitro Studies on *L. amazonensis* Viability

In order to assess the ability of the compounds to inhibit the growth of *L. amazonensis*, *in vitro* studies utilizing *L. amazonensis* promastigotes were performed

by Prof Santos and co-workers at URFJ. Metacyclic promastigotes are one of two structural forms of *L. amazonensis* which occur during the life cycle of the parasite. The promastigote form is significantly larger than the amastigote form and possesses a flagellum which allows it to be mobile inside the host organism. This form is present in the extracellular matrix and is responsible for the infection and proliferation of the parasite inside a mammalian host.⁹⁵

All compounds were administered to *L. amazonensis* promastigotes at an initial concentration of 50 μ M and the viability was examined after 72 h by motility and the lack of Trypan blue staining.⁹⁶ Of the twelve compounds assayed, seven of them were able to significantly inhibit the proliferation of the parasites (**Figure 3.4**). DMSO, ZnCl₂ and CuCl₂.4H₂O were used as controls and did not exhibit any antiparasitic activity. Following this preliminary investigation, the assay was repeated with compounds **2.3**, **2.22**, **2.20**, **2.33**, **2.43**, **2.41**, **2.45**, **2.34**, **2.15**, **2.25**, **2.35** and **2.36** at a lower concentration of 10 μ M and the viability of the parasites was quantified. As can be seen in **Figure 3. 5**, five of the compounds assayed retained the ability to effectively inhibit the proliferation of *L. amazonensis* promastigotes (**Figure 3. 6**).

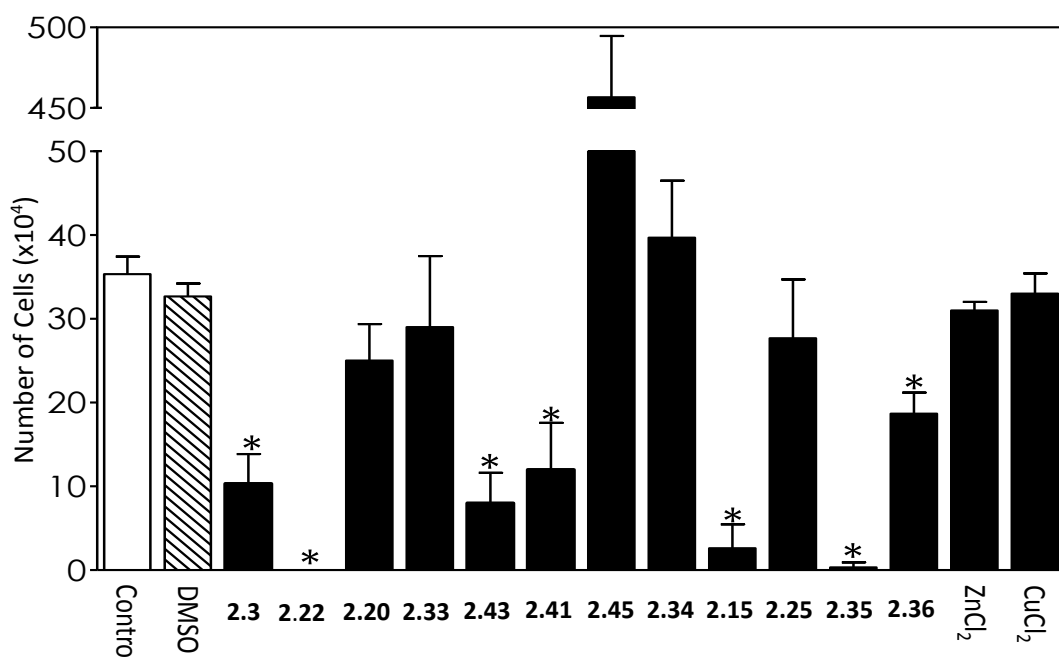


Figure 3. 4. Effects of selected compounds on the proliferative rate of *L. amazonensis* promastigotes. The proliferation of promastigotes was followed at 28 °C in absence/presence of the compounds (50 μ M). The viable parasites were counted by Trypan blue exclusion and motility in a Neubauer chamber after 72 h of incubation. Results are expressed as number of viable cells.

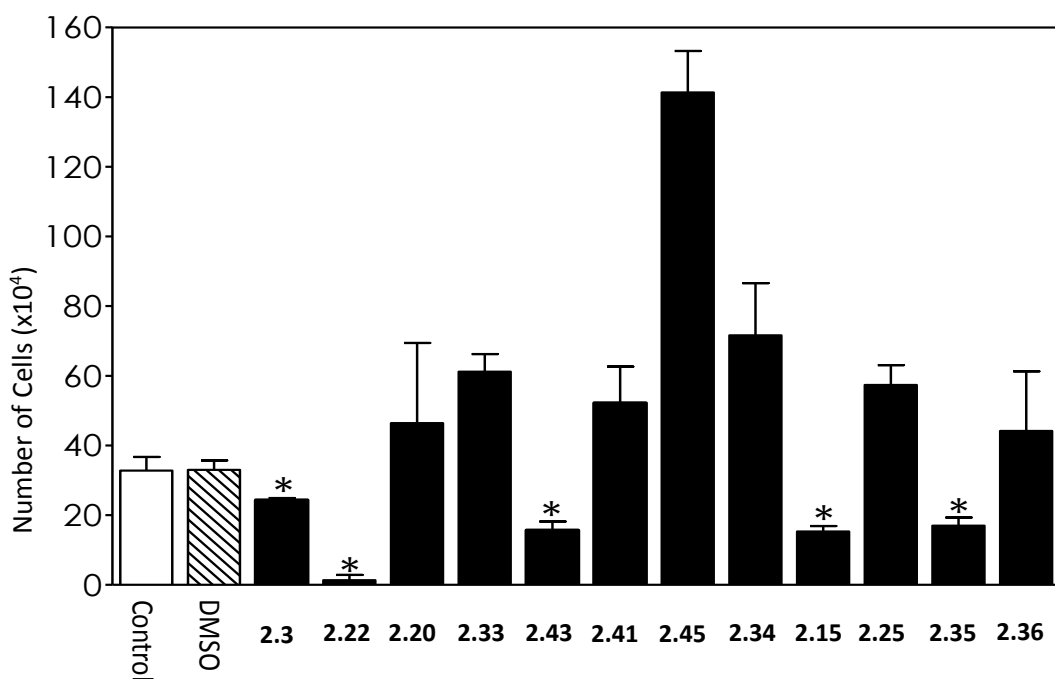


Figure 3. 5. Effects of selected compounds on the proliferative rate of *L. amazonensis* promastigotes. The proliferation of promastigotes was followed at 28 °C in absence/presence of the compounds (10 μ M). The viable parasites were counted by Trypan blue exclusion and motility in a Neubauer chamber after 72 h of incubation. Results are expressed as number of viable cells.

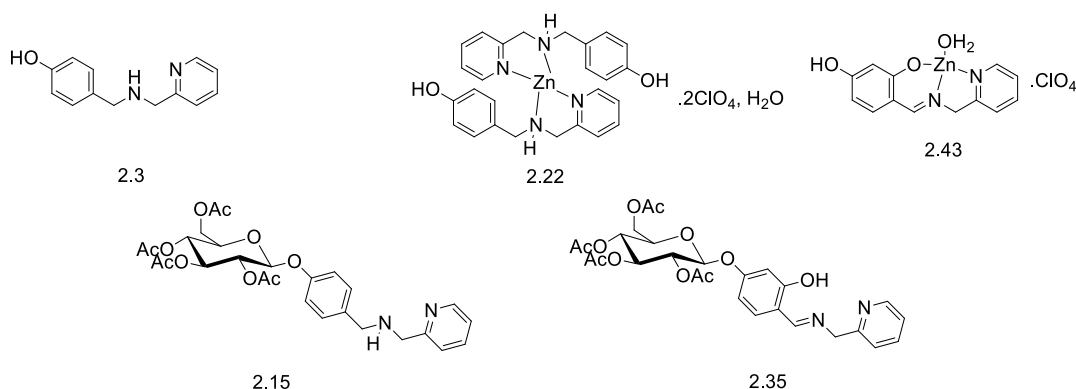


Figure 3. 6. Compounds capable of inhibiting the viability of *L. amazonensis* at 10 μ M.

Once the most efficacious compounds had been identified, their potency was determined by administering the compounds across a range of concentrations and determining the viability of the parasites. Using this data, the IC₅₀ value for each of the five compounds assayed could be determined. Amphotericin B, the current gold standard drug for the treatment of leishmaniasis, was also assayed (

Figure 3. 7).

From these values, it can be seen that the most potent compound is the Zn(II) complex **2.22** which is almost 20 times more efficacious than the ligand itself **2.3**. This non-metallated, aglycon ligand proved to be the least active of the five compounds selected for further study. Glucosylation of this ligand **2.15** also increased its activity to a lesser degree with a 3.5-fold increase in activity over the aglycon ligand **2.3**. Both compounds of the N₂O series assayed, namely the Zn(II) containing **2.43** or its hydrolysis products, and the glucosylated **2.35** showed only moderate antiparasitic activity. While all of the compounds assayed showed inferior activity to Amphotericin B, the activity of **2.22** exceeds that of the pentavalent antimonial drugs which are more commonly used to treat the disease.⁹⁷

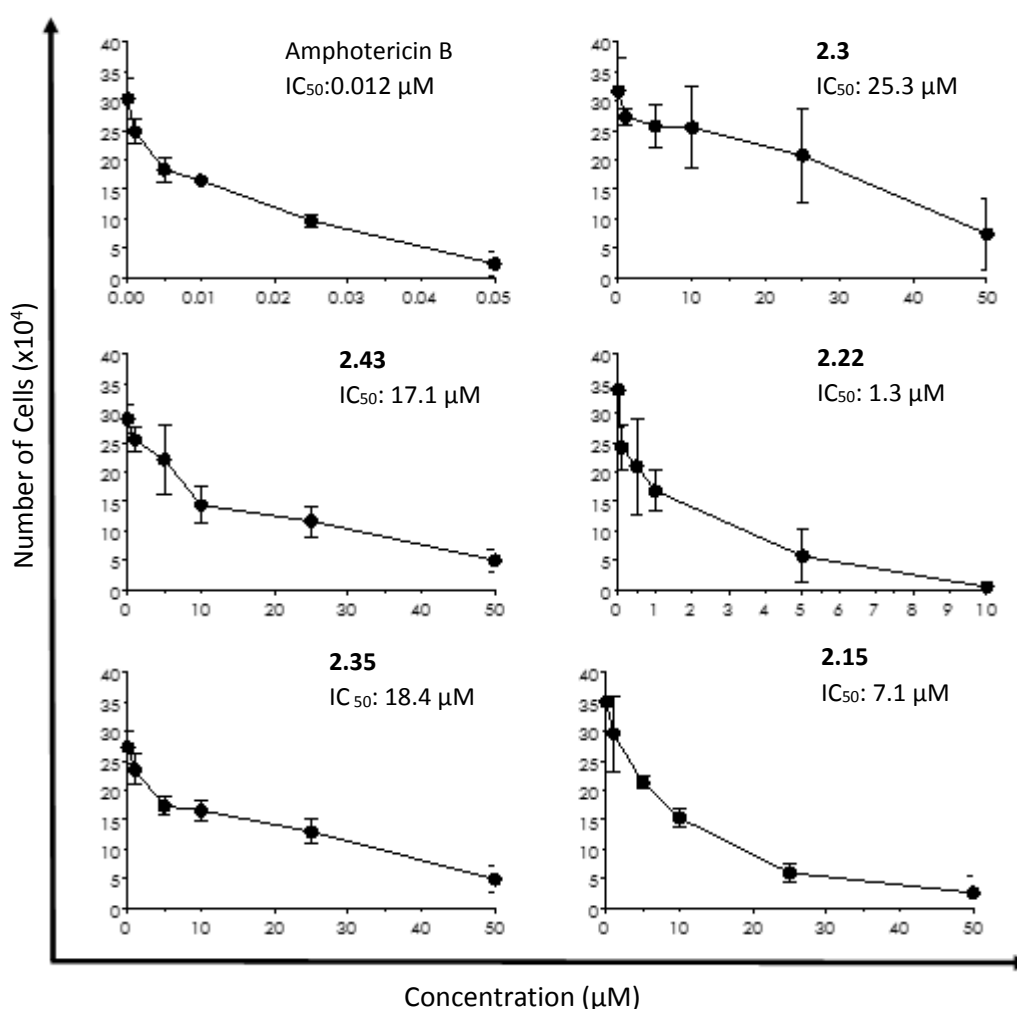


Figure 3. 7. IC₅₀ values determined for selected compounds. The viable parasites were counted by Trypan blue exclusion and motility in a Neubauer chamber after 24 h of incubation.

With these IC₅₀ values, it is possible to calculate the selectivity index (SI) for each of these compounds. This value describes the ratio between the dose of a compound needed to affect its desired pharmacological effect (in this case the inhibition of *L. amazonensis* viability), and the dose which is toxic to healthy mammal cells (RAW 246.7 murine macrophages). This data is presented in **Table 3.1**.

Compound	RAW CC ₅₀ (μM)	<i>L. amazonensis</i> IC ₅₀ (μM)	RAW/ <i>L.</i> <i>amazonensis</i> SI
2.3	155.4	25.3	6.1
2.15	234.5	7.1	33
2.22	118.2	1.3	90.9
2.35	196.1	18.4	10.7
2.43	>400	17.1	>23.4
Amp. B	37.4	0.012	3.1

Table 3. 1. Summary of antileishmanial activity and selectivity indices.

The data shows that all of the five compounds selected have selective antileishmanial activity. The least selective of the compounds studied was **2.3** which presented with an SI of 6.1 which indicates only a moderate selectivity for antileishmanial activity compared to its toxicity to RAW cells. However, its glucosylated analogue **2.15** is over 5 times more selective with an SI of 33, highlighting the benefit of carbohydrate conjugating in improving the tolerance of the compounds by mammalian cells. Of the N₂O compounds, glucosylated ligand **2.35** showed a moderate selectivity of 10.7. This was exceeded by the aglycon Zn(II) complex **2.43**, or its hydrolysis products, which showed an improved SI of >23.4. However, since the exact CC₅₀ value was not determined, an accurate value for the selectivity of the compound cannot be deduced.

Of the compounds assayed, the Zn(II) complex **2.22** is by far the most efficacious. Its low IC₅₀ value coupled with its high CC₅₀ value demonstrate that it is a highly selective antileishmanial compound with an SI of 90.9. This SI value far exceeds that of the compounds currently used to treat Leishmaniasis; miltefosine (SI: 0.2),⁹⁸ amphotericin B (SI: 3.1) and paromomycin (SI: 25).⁹⁹ This is an exceptional result and

clearly identifies this compound as worthy of further investigation as a novel antileishmanial therapy.

3.2.2.2 *L. amazonensis* Promastigote Morphology Studies

In order to gain an insight into the effects that the compounds have on the parasites, *L. amazonensis* were administered with the most efficacious compounds **2.3**, **2.22**, **2.15**, **2.43** and **2.35** at IC₅₀ concentrations and their morphology was examined using light microscopy after 24 h (**Figure 3. 8**). These studies were performed by Prof Santos and co-workers at URFJ.

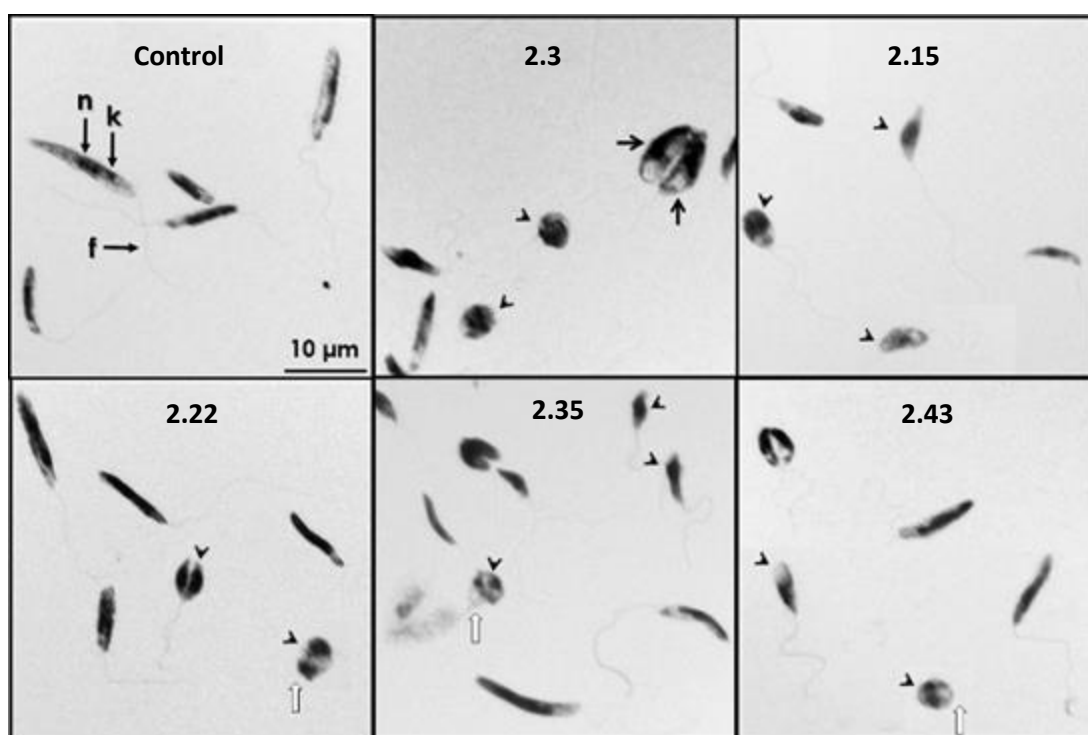


Figure 3. 8. Effects of selected compounds on the morphology of *L. amazonensis*.

Untreated parasites used as a control show a clearly defined kinetoplast (**k**), a central nucleus (**n**) and a long flagellum (**f**) attached to the cell body. Treatment of the parasites with the compounds induced several changes to the morphology of the parasites, namely the rounding in shape of the cell body coupled with a reduction in cell size (arrow head), swelling of the cell body (black arrow) and the loss of the flagellum (white arrow). Parasites were also treated with DMSO which did not cause any changes in the morphology.

The most common morphological change effected by the compounds are a rounding in shape of the cell which is coupled with a reduction in the size of the promastigote. This would suggest that the compounds are involved in inhibiting the development of the kinetoplast cytoskeleton which causes the loss of the elongated cell body that the parasites typically display. This change was caused by all of the compounds studied which may indicate a general response of the parasites to a toxic event. Both Zn(II) compounds **2.22** and **2.43** and the glycosylated N₂O ligand **2.35** treated cells showed a loss of flagellum by several of the parasites in addition to the reduced cell size and loss of cell structure. Interestingly, parasites treated with **2.3** also showed swelling of the cell body. This may be related to the damage to the cytoskeleton as the cells retain their typical length but lose their defined shape. In addition, the parasites appear to lose the distinct structure of the DNA containing nuclei and kinetoplasts which could indicate that the compounds act through the disruption of DNA replication and localization. This effect has been observed to be caused by compounds which are known to interfere with these processes, showing visible changes to these organelles.^{100,101,102,103} However, a more detailed study would need to be performed to investigate this in detail.

While the mode of action cannot be determined from these observations, it does demonstrate the significant damage effected by the compounds on the parasites and the morphological changes that result from this damage.

3.2.2.3 Insights Gained from Biological Studies of *L. amazonensis*

From these studies, it can be seen that all compounds from the N₂ series show potent antileishmanial activity with the exception of the copper complexes **2.20** and **2.25**. The N₂O aglycon ligands showed no significant activity however both metalation and glycosylation granted these compounds a degree of antileishmanial activity. The alkylation of the *para* phenolic group significantly decreases the activity of the compounds. When assayed at 50 μM, the direct glucose conjugate **2.35** showed an almost 20-fold improvement in leishmanial inhibition when compared to **2.36**, which contains an ethylene linker. A similar but less pronounced difference is also observed in the aglycon ligands **2.34** and **2.33**.

The Cu(II) complexes **2.20**, **2.25** and **2.41** did not show significant inhibitory effects with the exception of **2.41** which showed slightly less than half the proliferation of *L. amazonensis* when compared to the control. Complexation of the antileishmanial ligands **2.3** and **2.15** with Cu(II) served to reduce their *in vitro* activity which suggests that this metal interferes with the mechanism by which the N₂ compounds exert their antileishmanial effects.

Both Zn(II) complexes **2.22** and **2.43** showed highly enhanced activity over their parent ligands **2.3** and **2.33**, with **2.22** showing complete inhibition of parasite growth at 50 μM and almost complete inhibition at 10 μM. ZnCl₂ did not show any activity which clearly demonstrates the synergistic effect of complexing the metal with the ligand, which possesses only moderate antileishmanial activity in isolation. This could occur by three possible mechanisms;

- 1) The Zn(II) complexes may act through entirely new mode of action inside the cell than the parent ligand.
- 2) The complex may increase the uptake of the ligand into the cell and enhance its therapeutic effect by enacting its antiparasitic action through the same mechanism as the ligand in isolation.
- 3) The compounds may behave as ionophores to provide an enhanced uptake of the metal into the cell. The coordination of the metal to an organic ligand increases its lipophilicity and therefore its ability to cross the cell membrane by passive diffusion. The complex could dissociate inside the cell wherein the ligand could affect its antileishmanial effects as seen by **2.3** in isolation with additional, synergistic antiparasitic activity coming from the metal ion independent of the ligand.

As discussed in Chapter 2, Zn(II) complexes have successfully been used to treat *Leishmania* infections *in vivo*. As demonstrated in this study, complexation with Zn(II) can be used to enhance the activity of antikineto-plastic compounds. The cause of the antileishmanial activity of Zn(II) remains unclear although several modes of action have been proposed. Work by the group of Al-Mulla Hummadi has observed that Zn(II) complexes possess immunomodulatory properties and increases the number and activity of peritoneal macrophages in a murine model infected with *L. tropicana*

and *L. major*. They propose that this occurs by the activation of NADPH-oxidase bound to the surface of the macrophage membrane which causes a respiratory burst, leading to increased phagocytosis.¹⁰⁴ In addition to this immunoregulatory activity, Zn(II) has also been shown to directly inhibit several enzymes associated with the Embden-Meyerhof pathway which is responsible for glucose metabolism in a dose-dependent manner.¹⁰⁵ Rice *et al* have established that for their structurally similar 2-picolylamine derived Zn(II) complexes, the presence of Zn(II) is essential for the uptake of the ligand into the cell, when evaluated using *L. major*. While they could not establish a mode of action, their preliminary experiments lead them to propose that it involves the disruption of the parasite membrane.³⁶ Given the similarity of the chelating moiety of their compounds to the N₂ series of compounds which we investigated, it is likely that they share a common mechanism of action.

Interestingly, the Fe(II) compound **2.45** showed a remarkable increase in the viability of the parasites. Promastigotes treated with the compound proliferated at a rate thirteen times higher than the control population. This unusual observation can be attributed to the fact that iron is an essential nutrient for kinetoplastic parasites. It is utilised in the mitochondria of the parasites as a component of both heme and iron-sulfur clusters which play an essential role in the electron transport chain.¹⁰⁶ Recently, Mitra *et al* have identified it as a key modulator of the transformation of the promastigote form to the amastigote stage of the parasite life cycle. This work demonstrated that reducing iron uptake by knocking out a single gene which encodes a mitochondrial iron transmembrane transport protein severely limits the growth of *L. amazonensis*.¹⁰⁷

This effect can be explained by the inhibition of iron generated reactive oxygen species (ROS) in the cell. ROS, most importantly H₂O₂, are emerging to be not just toxic by-products of cellular respiration, but are in fact a key regulator of cell differentiation.^{108,109} Iron is widely utilized in nature due to its capacity for redox activity which allows for Fenton type chemistry that can both form and passivate ROS.¹¹⁰ This redox behaviour is essential for the formation of H₂O₂ in the cell by the conversion of O₂⁻ into H₂O₂ by superoxide dismutase. H₂O₂ has been identified as one of the main signalling molecules that induce the formation of infectious forms of *L.*

amazonensis. Most significantly, this has been directly correlated to the levels of iron uptake by the parasite.¹¹¹ It can therefore be proposed that **2.45** increases the uptake of iron inside the cell and thereby increases cell differentiation via this H₂O₂ signalling process, however, further investigation is needed to prove this hypothesis. Given that **2.45** was well tolerated by RAW cells (CC₅₀: 333.1 μM), it would appear that this redox activity occurs as a controlled process inside the cell, as indiscriminate ROS generation inside a mammalian cell would cause significant oxidative stress and therefore a low CC₅₀ value.

3.2.2.4 Conclusion of *L. amazonensis* Studies

These studies indicate that all the compounds selected for study are well tolerated by RAW murine macrophage cells and therefore are expected to be well tolerated in a mammalian body. The *in vitro* studies on the antileishmanial activity identified five compounds which warranted further study into their antileishmanial activity. These experiments determined the IC₅₀ values and selectivity indices of the chosen compounds. The morphological changes that these compounds affect were identified using light microscopy and structural defects were characterised. From these investigations, we identified Zn(II) complex **2.22** as a highly attractive potential therapeutic due to its high potency and its exceptional selectivity which exceeds that of the drugs currently used to treat the disease.

3.2.3 Evaluation of Antitrypanosomal Activity

3.2.3.1 *In Vitro* Studies on *T. cruzi* Viability

As with *L. amazonensis*, studies were carried out on all of the compounds selected to identify any potentially antichagasic activity. The studies were carried out by Prof Santos and coworkers at URFJ using *T. cruzi* metacyclic trypomastigotes. These are one of the two forms of the parasite which are present in infected humans and are responsible for both the initial infection from the disease vector and for the spread of the infection between regions of the body. In this stage of its life cycle, the parasite

possesses a long flagellum which allows it to swim inside the bloodstream of the host and thereby quickly infect different organ systems within the infected body.

All compounds were administered to *T. cruzi* trypomastigotes at an initial concentration of 50 μ M and the viability was examined after 24 h by motility and the lack of Trypan blue staining.⁹⁶ Of the twelve compounds assayed, seven of them were able to significantly inhibit the proliferation of the parasites (

Figure 3. 9). DMSO, ZnCl₂ and CuCl₂.4H₂O were used as controls and did not exhibit any antiparasitic activity.

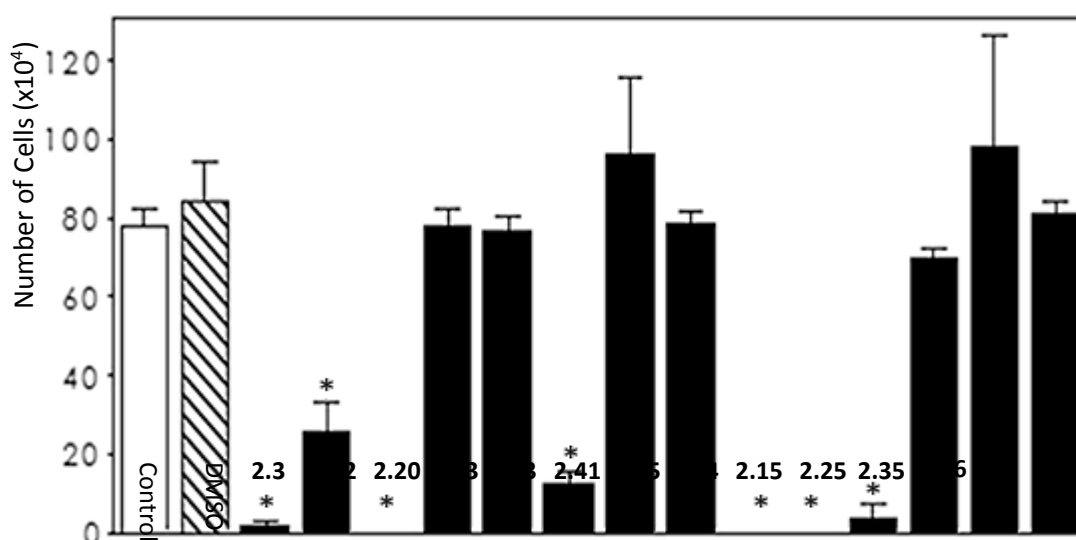


Figure 3. 9. Effects of selected compounds on the proliferative rate of *T. cruzi* trypomastigotes. The proliferation of trypomastigotes was followed at 28 °C in absence/presence of the compounds (50 μ M). The viable parasites were counted by Trypan blue exclusion and motility in a Neubauer chamber after 72 h of incubation. Results are expressed as number of viable cells.

Compounds **2.13**, **2.22**, **2.20**, **2.41**, **2.15**, **2.25** and **2.35** were then assayed at a concentration of 10 μ M and the viability of the trypomastigotes was quantified as before (**Figure 3.10**). From these studies, six compounds were identified which showed good antiparasitic activity and could reduce the proliferation of the trypomastigotes (**Figure 3. 11**).

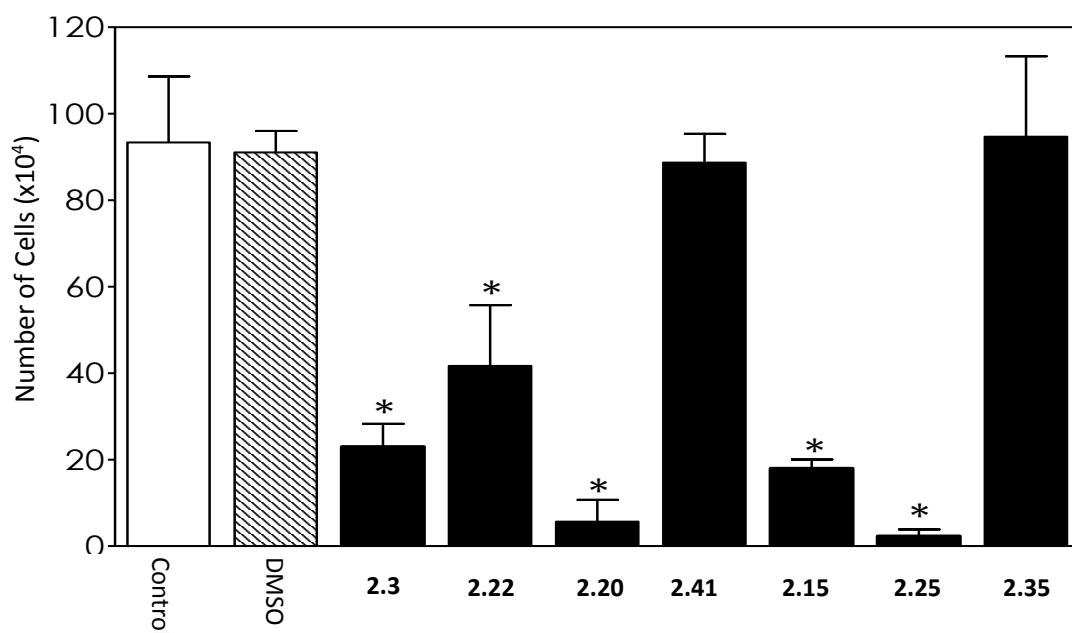


Figure 3. 10. Effects of selected compounds on the proliferative rate of *T. cruzi* trypomastigotes. The proliferation of trypomastigotes was followed at 28 °C in absence/presence of the compounds (10 μ M). The viable parasites were counted by Trypan blue exclusion and motility in a Neubauer chamber after 72 h of incubation. The results are expressed as number of viable cells.

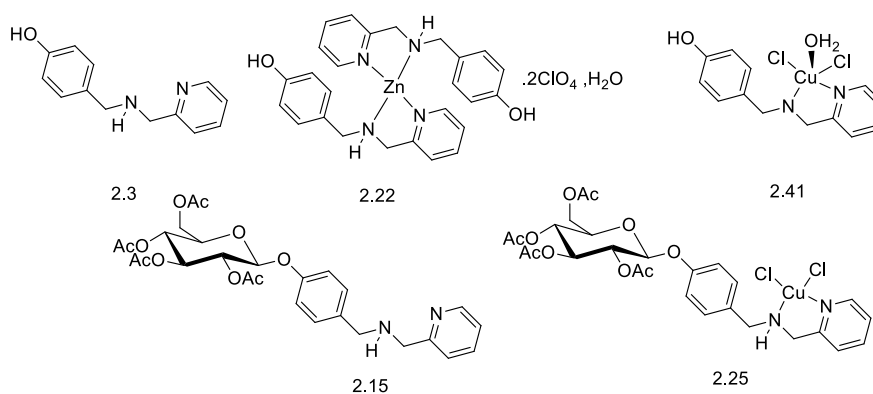


Figure 3. 11. Compounds capable of inhibiting the viability of *T. cruzi* promastigotes at 10 μ M.

With these compounds identified, it was then determined how potent their antichagasic activity was by administering them across a range of concentrations and examining the viability of the trypomastigotes. From this study, the IC₅₀ value the SI of each of the compounds were determined. Benznidazole, a compound currently used in the clinic to treat Chagas disease, was also assayed (**Figure 3. 12**).

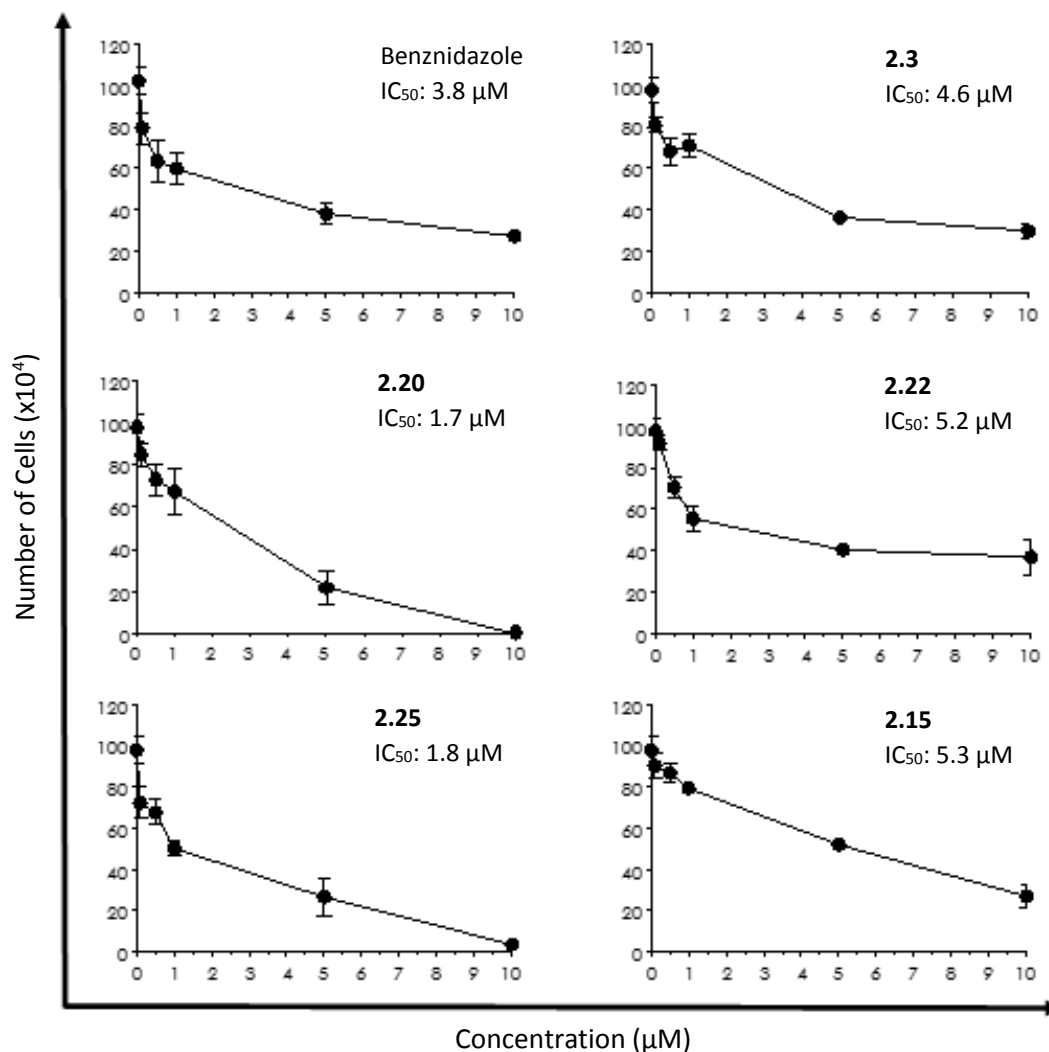


Figure 3. 12. IC₅₀ values determined for selected compounds. The viable parasites were counted by Trypan blue exclusion and motility in a Neubauer chamber after 24 h of incubation.

These results show that the antiparasitic activity of the N₂ series is superior to that of the N₂O analogues. Of the N₂O compounds assayed, only the Cu(II) complex **2.41** was able to inhibit the growth of *T. cruzi* trypomastigotes and this was only effective at the high concentration of 50 µM. The Cu(II) containing compounds **2.20** and **2.25** all displayed the highest activity for each of their respective series, which clearly demonstrates the importance of Cu(II) to their antiparasitic activity. The highest activity was observed for the N₂ Cu(II) complex **2.20** which had an IC₅₀ value of 1.7 µM while its glucosylated analogue **2.25** showed an almost identical value of 1.8 µM. Contrary to this, the free ligands showed reduced activity when compared to their Cu(II) analogues. The activity of the non-metallated aglycon and glucose conjugate **2.3** and **2.15** are once again very similar with values of 4.6 µM and 5.3 µM

respectively. The Zn(II) N₂ complex **2.22** showed inferior activity to both the free ligand **2.3** and Cu(II) analogue **2.20** with an IC₅₀ value of 5.2 μM. The results of these experiments are very promising as both **2.20** and **2.25** show more than twice the activity of benznidazole, the drug currently used to treat Chagas disease.

Using these IC₅₀ values, the SI values were calculated with respect to RAW cells and are presented in **Table 3.1**.

Compound	RAW CC ₅₀ (μM)	T. cruzi IC ₅₀ (μM)	RAW/T. cruzi SI
2.3	155.4	4.6	33.8
2.15	234.5	5.3	44.2
2.22	118.2	5.2	22.7
2.25	127.6	1.8	70.9
2.20	106.2	1.7	62.5
Benznidazole	182.1	3.8	47.9

Table 3. 2. Summary of antitrypanosomal activity and selectivity indices.

These studies show that all of the compounds display highly selective toxicity towards the trypomastigotes when compared to RAW mammalian cells. The Zn(II) compound **2.22** showed the least selective *T. cruzi* inhibition of all the compounds studied with a moderate SI of 22.7. The free N₂ ligand **2.3** displayed a good selectivity of 33.8 which was exceeded by its glucosylated analogue **2.15** which presented a 30% improvement in its SI which was determined to be 44.2. The highest selectivity, however, was exhibited by the Cu(II) complexes **2.20** and **2.25**. While both **2.20** and its glucosylated analogue **2.25** show almost identical IC₅₀ values, the SI of **2.25** is superior to that of **2.20** with a very high SI of 70.9. The activity of this compound far exceeds that of benznidazole in both its IC₅₀ value (3.8 μM vs 1.8 μM) and its selectivity (70.9 vs 47.9). These results clearly demonstrate the remarkable activity of **2.25** and highlight its potential as a novel antichagasic agent.

3.2.3.2 *T. cruzi* Trypomastigote Morphology Studies

As with *L. amazonensis*, the effects of the selected compounds on the morphology of *T. cruzi* trypomastigotes was investigated by Santos *et al* at URFJ. Compounds **2.3**,

2.15, 2.20, 2.25 and 2.22 were administered at their IC₅₀ values and the parasites were examined after 24 h using light microscopy.

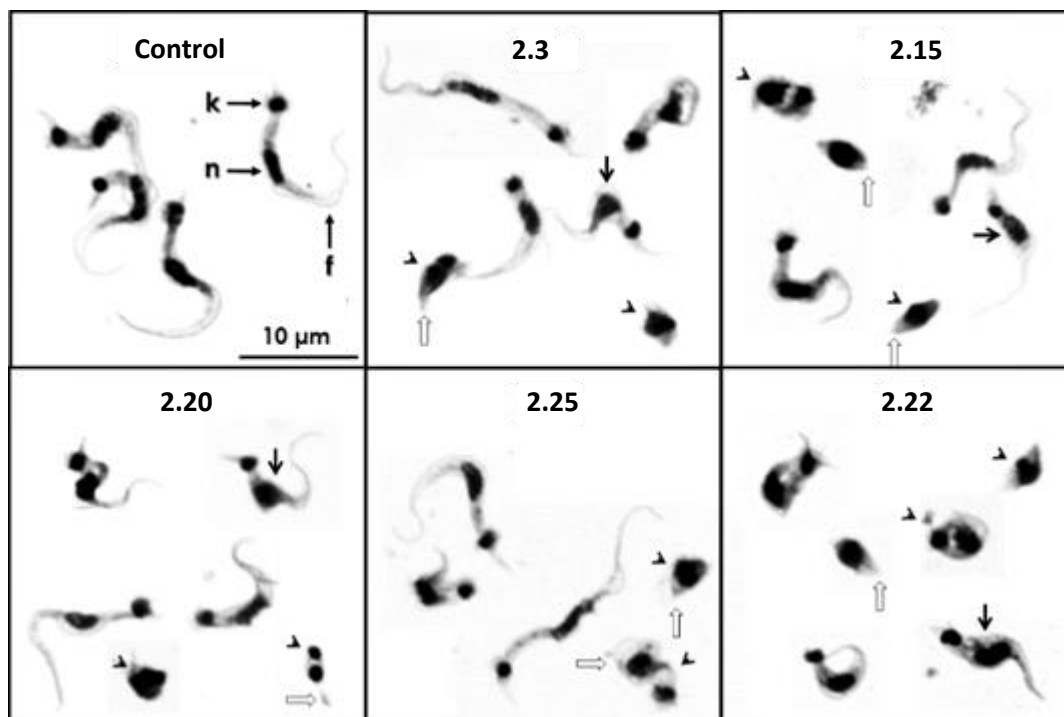


Figure 3. 13. Effects of selected compounds on the morphology of *L. amazonensis*

Untreated parasites used as a control show a clearly defined kinetoplast (**k**), a central nucleus (**n**) and a long flagellum (**f**) attached to the cell body. Treatment of the parasites with the compounds induced several changes to the morphology of the parasites, namely the rounding in shape of the cell body coupled with a reduction in cell size (arrow head), swelling of the cell body (black arrow) and the loss of the flagellum (white arrow). Parasites were also treated with DMSO which did not cause any changes in the morphology.

Similar to the studies on *L. amazonensis*, the most common morphological defect seen was the reduction in cell size together with a loss of the typical elongated shape of the cell. This structural damage was induced by all of the compounds studied. The cells that showed this damage also displayed a loss of distinct kinetoplasts and nuclei which would suggest that the production or localization of DNA was inhibited. The loss of flagellum was also observed to be caused by all of the compounds studied and was only observed in trypomastigotes which also showed a reduction in cell size and rounding of the cell body. It could therefore be inferred that the loss of flagellum is

linked to the same underlying biological process which gives rise to the loss of cell structural integrity.

Another effect observed to be caused by **2.3**, **2.15**, **2.20** and **2.22** was the swelling of the cell body of several of the parasites. These parasites retained the distinct kinetoplast and nucleus organelles in addition to their flagellum. The swelling is localized to the nucleus of the trypomastigote which could support the hypothesis that these compounds interfere with the DNA replication process.

3.2.3.3 Insights Gained from Biological Studies of *T. cruzi*

These studies show that the N₂ series of compounds are superior antiparasitic agents than their N₂O counterparts, similar to the results observed for the evaluation of antiparasitic activity in *L. amazonensis* (Section 3.2.2). All of the N₂ compounds assayed were capable of inhibiting the growth of *T. cruzi* trypomastigotes at a concentration of 10 µM whereas only the Cu(II) containing N₂O compound **2.41** and the glycosylated **2.35** showed antichagasic activity at the high concentration of 50 µM. The aglycon ligand **2.33** and its alkylated analogue **2.34** showed no activity which highlights the contribution of the glucose moiety to the activity of the compounds. Interestingly, the compound which featured an ethylene linker between the carbohydrate and the aromatic ring did not show inhibition of the trypomastigote growth whatsoever. This mirrors the observed activity of the compounds towards *L. amazonensis* and could suggest that a *para* phenolic group is essential to the activity of the compounds, as it is possible that the compounds conjugated directly to glucose (**2.15**, **2.25**, **2.35** and **2.36**) could be enzymatically cleaved to reveal the phenolic aglycon.

While all of the N₂ compounds showed good activity, there was a clear activity enhancement caused by both complexation to Cu(II) and glycosylation of the ligand; **2.3** showed less activity than the glycosylated compound **2.15** and Cu(II) complex **2.20**. Complexation to Zn(II), however, reduced the activity with **2.22** showing the less activity than the free ligand **2.3**. The Zn(II) containing N₂O complex **2.43** did not show any *T. cruzi* inhibition whatsoever. In addition to enhancing the inhibitory effects of the complexes, complexation to Cu(II) significantly increased the SI of the

compounds (62.5 vs 33.8 for the aglycon N₂ ligands **2.3** and **2.20**, and 70.9 vs 44.2 for the glucosylated analogues **2.15** and **2.25**). The free CuCl₂·2H₂O salt did not show any inhibitory activity however, which proves that the activity does not come from the Cu(II) ion alone. This data clearly demonstrates the synergistic effects that arise from the combination of the N₂ ligand scaffold with Cu(II). This may occur by:

- 1) The Cu(II) complexes having a unique antiparasitic mode of action to the free ligand such as ROS generation by the redox active Cu(II) centre.
- 2) The Cu(II) may not be involved in the antitrypanosomal activity directly but the complex may undergo increased uptake into the cell with respect to the ligand in isolation. This would lead to an increased uptake inside the cell and therefore a higher therapeutic effect than seen for the ligand alone.
- 3) The compounds may behave as ionophores to provide an enhanced uptake of the metal into the cell with respect to the simple CuCl₂·H₂O salt. The coordination of the metal to an organic ligand increases its lipophilicity and therefore its ability to cross the cell membrane by passive diffusion. This could dissociate inside the cell wherein the ligand could affect its antitrypanosomal effects in the same mode as **2.3** in isolation, with additional, synergistic antiparasitic activity coming from the metal ion independent of the ligand. This may not be possible for CuCl₂·2H₂O as this has extremely poor lipophilicity and therefore cannot pass into the cell via passive diffusion.

The efforts to develop Cu(II) antitrypanosomal drugs and investigations of their mode of action has been detailed in Chapter 2. While detailed knowledge on their precise mechanism of action is sparse, several biological effects have been determined. These include DNA scission,⁵⁴ inhibition of the farnesyl diphosphate synthase enzyme,⁵⁵ DNA intercalation⁵² and interactions with proteins involved in cell wall synthesis and microtubule formation such as tubulin, fibronectin and integrin.⁵⁴ The data we have obtained is insufficient to establish a likely mode of action but as our ligand scaffold varies significantly from the phenanthroline derivatives used by some of these authors it is probable that these compounds do not share a common mechanism to account for their antitrypanosomal activity.

The Fe(II) complex **2.45** did not show any inhibitory activity and in fact increase the viability of the parasites by approximately 25%. This is a much less pronounced growth enhancement than was observed in the studies of *L. amazonensis*. Iron is known to be an essential and growth rate limiting nutrient for *T. cruzi*.^{112,113} Inhibition of iron uptake has been shown to inhibit growth of the parasites and this is likely due to the fact that *T. cruzi* utilizes only iron containing superoxide dismutase (Fe-SOD) for detoxification of superoxide radicals unlike other organisms which possess Fe-SOD, Cu/Zn-SOD and/or Mn-SOD.^{114,115} It can therefore be proposed that compound **2.45** acts to increase the amount of bioavailable Fe in the growth medium and this could explain the increased viability of the trypomastigotes.

3.2.3.4 Conclusions of *T. cruzi* Biological Studies

These studies identified five compounds which showed good antitrypanosomal activity. These compounds were studied further and the IC₅₀ values were determined. These studies identified the Cu(II) N₂ compounds **2.20** and **2.22** as the most potent antitrypanosomal agents with almost identical IC₅₀ values of 1.7 µM and 1.8 µM respectively. The glycosylated compound **2.22**, however, showed a superior SI value of 70.9 which identifies this as the most attractive compound for further study. The morphological changes induced by these compounds were identified using light microscopy and structural defects were characterised. The results of these studies are remarkable as they indicated that **2.22** is both more potent and more selective than benznidazole, the drug currently used to treat the disease.

3.2.4 In Vivo Immunogenicity in *G. mellonella*

3.2.4.1 *Galleria Mellonella* as a Toxicology Model for the Analysis of Drug Candidates

Insects are an extremely useful model for the preliminary study of the *in vivo* toxicity of novel drug candidates. This analysis typically employs the use of animal models such as mice, rabbits or dogs which is expensive, labour intensive, requires specialist training and full ethical approval. Insect models offer a practical alternative for preliminary screening as they are cheap, do not require the same ethical approval as mammalian trials and the studies can be carried out easily with minimal training.

Results are typically obtained in 24-48 h which offers a significant advantage over mammalian studies which are typically quite time intensive, making them prohibitively expensive for the routine analysis of drug candidates. On the other hand, insect based assays can be used to quickly screen a large number of compounds with minimal time investment.

The innate immune systems of *G. mellonella* and mammals have been shown to bear many similarities.^{116, 117, 118} These include the cuticle, which provides a physical barrier which prevents the entry of pathogens into the insect in a similar manner to the skin of mammals. The innate immune system also involves a cellular response to threats, which in humans occurs by the phagocytosis of pathogens by macrophages and neutrophils. In *G. mellonella* this function is carried out by haemocytes which are found in the haemolymph, a fluid which fills the cavity of the insect analogous to blood in mammals. These similarities, in addition to many others, have led to the use of *G. mellonella* as an insect model to investigate drug toxicity.^{119, 120, 121, 122}

The studies using *G. mellonella* are very simple to perform; the test solutions are administered by injection directly into the haemocoel (body cavity) of the larvae through the last left pro-leg. The base of the pro-leg can be opened by applying gentle pressure to the sides of the larvae and this opening will close after the removal of the syringe without leaving a scar which minimises the chance of bacterial infection that could lead to a false positive result for immunogenicity. They are then incubated and any immune response can be easily identified by visual inspection of the cuticle without the need for any of the blood tests which would be required to gain the same information in a mammalian model.

3.2.4.2 *G. mellonella* Studies

Due to the insolubility of **2.43** in purely aqueous solutions, DMSO toxicity studies were first performed which established that concentrations of up to 20% could be safely administered without showing any toxicity in the larvae. *G. mellonella* larvae were then inoculated with **2.3, 2.15, 2.20, 2.22, 2.25, 2.33, 2.35, 2.41, 2.43** and **2.45** (**Figure 3.14**). This was carried out at concentrations of 1, 10 and 100 μM as solutions

in PBS buffer with 10% DMSO. The larvae were monitored every 24 h for viability and evidence of an immune reaction (**Figure 3. 17**).

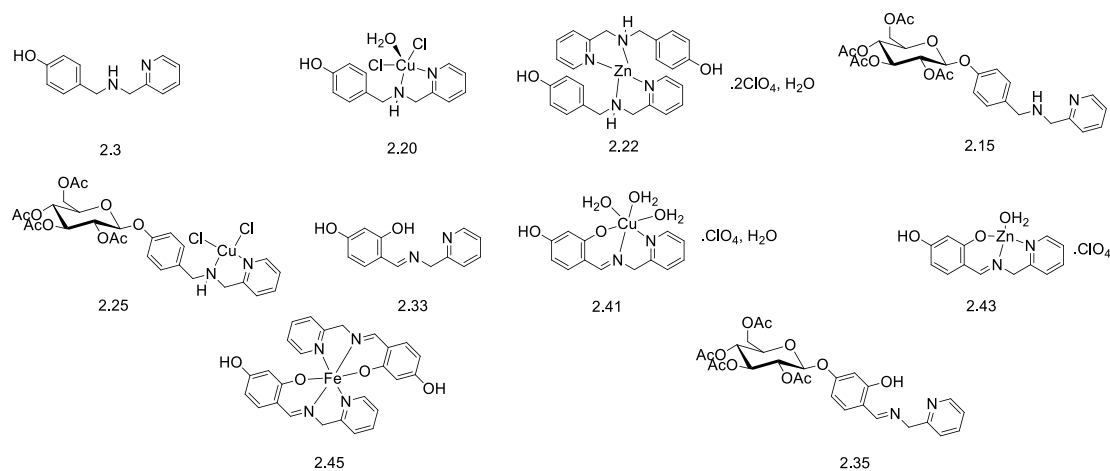


Figure 3. 14. Compounds studied for toxicity in *G. mellonella*



Figure 3. 15. *G. mellonella* larvae immediately following inoculation.

Upon inspection at 24 h and 48 h, all of the larvae studied were found to have survived treatment with the compounds and exhibited the behaviour typical of healthy larvae (**Figure 3. 16**). Most significantly, none of the larvae studied showed discolouration of their cuticle. This discolouration is caused by a melanisation process in the larvae and would indicate a response by their immune system to the presence of the compounds.

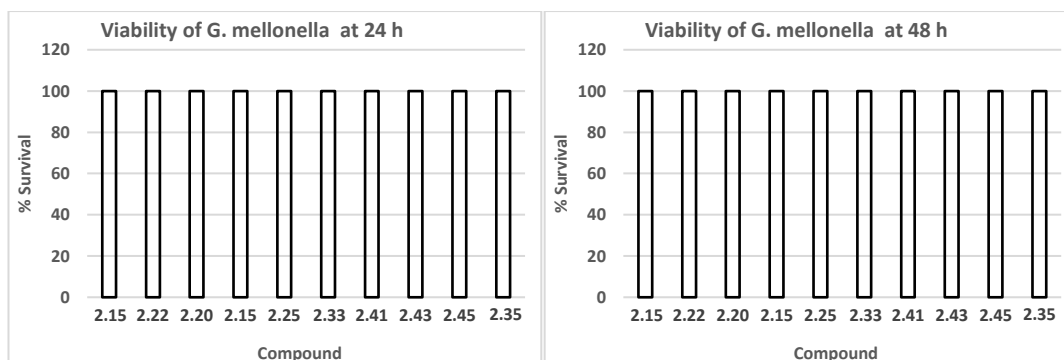


Figure 3. 16. Viability of *G. mellonella* at 24 h and 48 h

The results of these experiments are highly encouraging and suggest that these compounds are very well tolerated *in vivo*. The fact that all of the larvae used in the study survived together with the fact that none of the compounds tested provoked an immune response show that these compounds have extremely low toxicity.

G. mellonella has been successfully used as a model to study a variety of *in vivo* properties such as drug efficacy, metabolism, microbial virulence and toxicity and these effects have been positively correlated with studies in mice that show similar results which validates the use of the *G. mellonella* model.^{123, 124} It can therefore be expected that these results would also translate to low toxicity in higher organisms such as mammals.



Figure 3. 17. *G. mellonella* 48 h after inoculation.

These results provide further support to the *in vitro* studies carried out in RAW murine cells. Together these experiments have proven that these compounds have low toxicity both *in vitro* and *in vivo*. This is a vital step in the development of novel therapeutics and the toxicological information gathered from these experiments indicate that these compounds show promise for further development as safe antiparasitic drugs.

3.2.5 Susceptibility of Compounds to Enzymatic Hydrolysis

The investigations into the antileishmanial and antitrypanosomal activity of the library of compounds showed that the compounds which have an alkyl group on the *para* phenolic group (**2.34** and **2.36**) did not display any activity. This would indicate that a phenolic hydroxyl group at this position is essential to the antiparasitic activity of the compounds. While compounds **2.15**, **2.25** and **2.35** do not bear a phenolic OH group, hydrolysis of the glycosidic bond would result in a hydroxylated sugar residue and a redox active phenolic group on the ligand moiety (**Figure 3. 18**). This prompted us to investigate if these glycosides could be acting as pro-drugs.

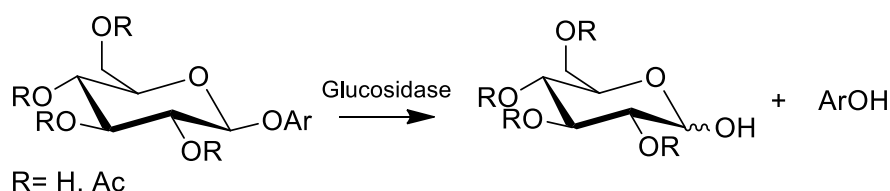
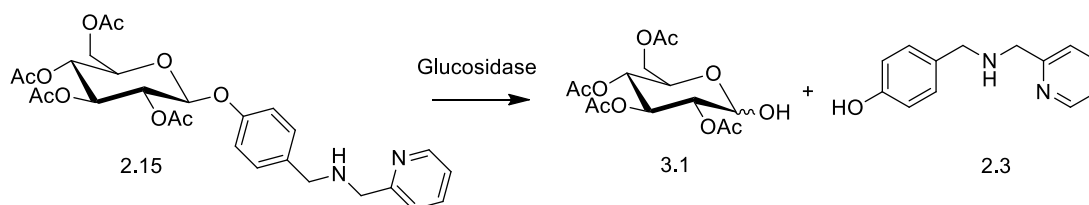


Figure 3. 18. Enzymatic hydrolysis of glycosylated ligands.

Glucose conjugation has successfully been used as a pro-drug strategy which takes advantage of the glucosidase enzymes that are ubiquitous in nature to cleave a glucosylated compound and reveal an active drug moiety.^{60,125,126,127} To investigate whether or not the compounds in question could act in this manner, their susceptibility to cleavage by glucosidase enzymes was studied. *In vivo*, glucosidase recognise per-hydroxylated sugars as the substrate. However, since some of the compounds described here bear acetyl protecting groups, we decided to investigate both the acetylated compounds **2.15** and **2.25** together with the deprotected analogues **2.17** and **2.30**.

To do this, the compounds were first incubated with phosphate buffer alone at physiological pH and temperature as a control to establish the stability of the glycosidic bond in aqueous solution. It was found that the products were stable at pH 7.4 in phosphate buffer as was determined by HPLC analysis. Once the stability was determined, the compounds were then incubated with a β -glucosidase enzyme, obtained from almonds, for 24 h in phosphate buffer at pH 7.4. Prior to these studies, the activity of the enzyme was verified using 4-nitrophenyl- β -D-glucopyranoside, a standard compound used for the validation and quantification of activity of β -glucosidase.¹²⁸ The resulting solutions were analysed using HPLC and HRMS to detect the consumption of the glycoside and to determine the nature of the products, if any, that were generated. If hydrolysis of the glycosidic bond occurs, this would be confirmed by the presence of the aglycon ligand in solution. HPLC studies were carried out using a SunFire C18 5 μ m 4.6x 100mm column at room temperature with a flow rate of 1 mL/min and a 0-20 % MeCN: H₂O mobile phase gradient over 30 min.

3.2.5.1 Results of Enzymatic Hydrolysis Studies



Scheme 3. 1. Hydrolysis of **2.15** by β -glucosidase.

The hydrolysis of **2.15** by β -glucosidase would produce the aglycon ligand **2.3** as a product (**Scheme 3. 1**). Thus, the observance of **2.3** after incubation of **2.15** with the enzyme would offer proof that the proposed hydrolysis has occurred. However, as β -glucosidase recognizes per-hydroxylated sugars and **2.15** is per-acetylated, it is possible that the enzyme does not recognize this molecule and instead recognizes a partially or completely deprotected compound formed by the chemical hydrolysis of

the compound in aqueous solution. In a physiological environment, this transformation would likely be carried out by esterases which are ubiquitous in the cell.

Figure 3. 19 shows the chromatogram of **2.15** before and after incubation for 24 h with β -glucosidase. From these chromatograms, it can be seen that the peaks at 11.2 min and 12.7 min which correspond to **2.15** have almost entirely disappeared upon reaction with the enzyme. This could suggest that this compound is susceptible to the action of β -glucosidase. While the initial trace of **2.15** shows more than one species in solution, this is to be expected as the compound is in aqueous solution at pH 7.4 and therefore exists as an equilibrium of protonated and unprotonated species.

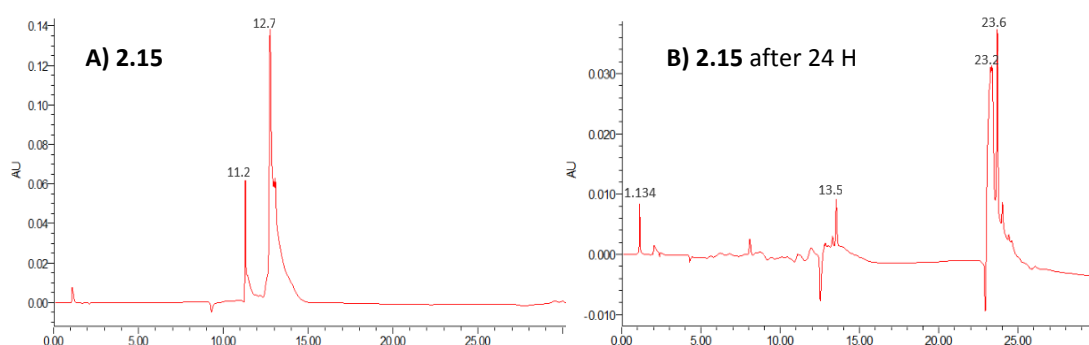


Figure 3. 19. HPLC traces of **2.15** A) before and B) after incubation with β -glucosidase.

From the HRMS data of the solution after enzymatic treatment (**Figure 3. 20**), we can see that the most abundant ions detected correspond to the ligand **2.15** ($m/z=545.213$) and its deacetylation products. However, the aglycon **2.3** is present in the sample which confirms that hydrolysis of the glycosidic bond has occurred to some extent. It can be inferred that i) the acetylated compound is only weakly susceptible to the action of β -glucosidase or ii) **2.15** must be partially or completely deacetylated before hydrolysis can take place. As the HPLC trace indicates that **2.15** has disappeared, it is likely that this is due to both the hydrolysis of the glycosidic bond, which is confirmed by the presence of **2.3**, in the mass spectrum, deacetylation of **2.15**, or degradation.

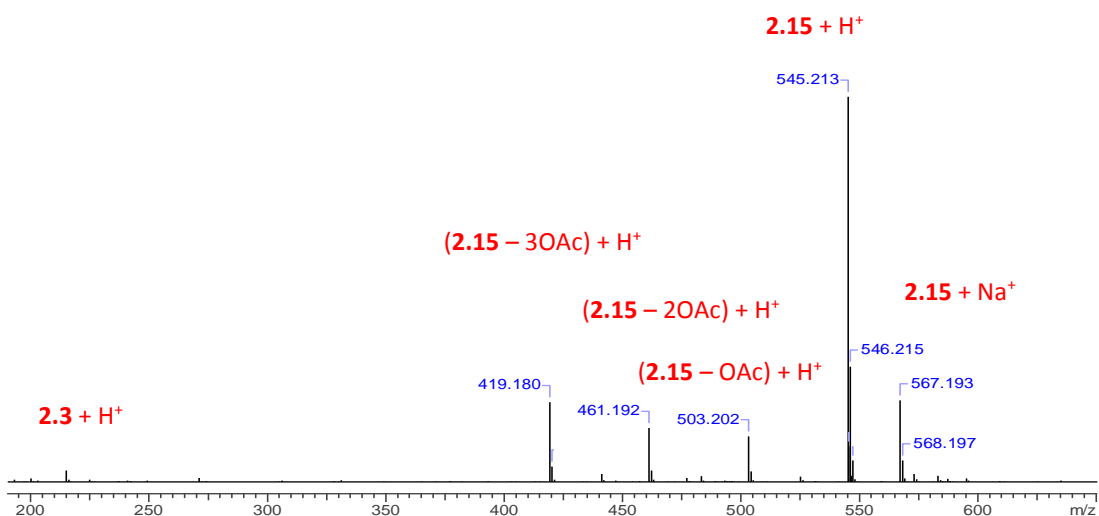
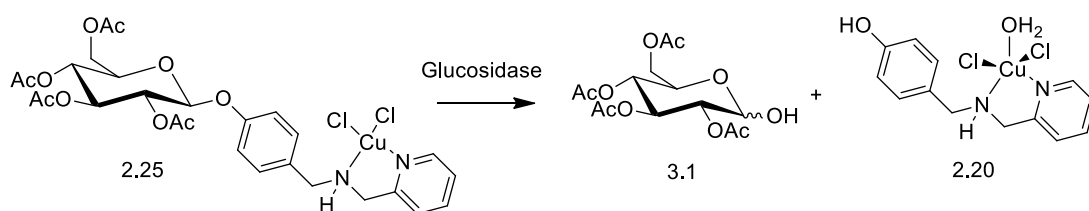


Figure 3. 20. ESI⁺ HRMS spectrum of **2.15** following incubation with β -glucosidase.



Scheme 3. 2. Hydrolysis of **2.25** by β -glucosidase.

Cu(II) complex **2.25** treated with β -glucosidase under the same conditions as **2.15** (**Scheme 3. 2**). The HPLC trace of Cu(II) complex **2.25** shows multiple species in solution which could be due to hydrolysis of the chloride ligands on the metal (**Figure 3.21**). Following incubation with the enzyme, the peaks at 0.9 and 1.2 min disappeared completely from the trace. This could indicate a reaction of the compound with the enzyme or deacetylation products.

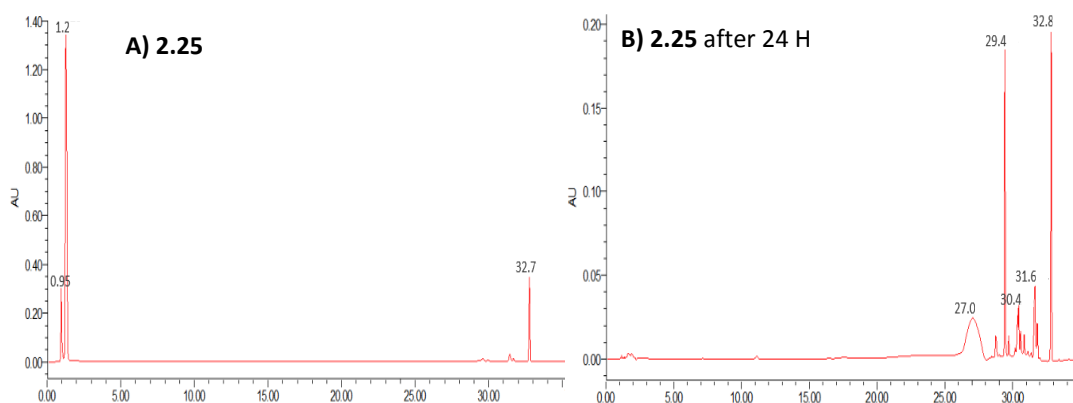


Figure 3.21. HPLC traces of **2.25** A) before and B) after incubation with β -glucosidase.

The HRMS data from the experiment utilizing **2.25** shows peaks corresponding to hydrolysis products (**Figure 3. 22**). The non-metallated aglycon species **2.3** is observed which indicates that the metal complex has dissociated, either in the aqueous solution or by ionisation inside the mass spectrometer.

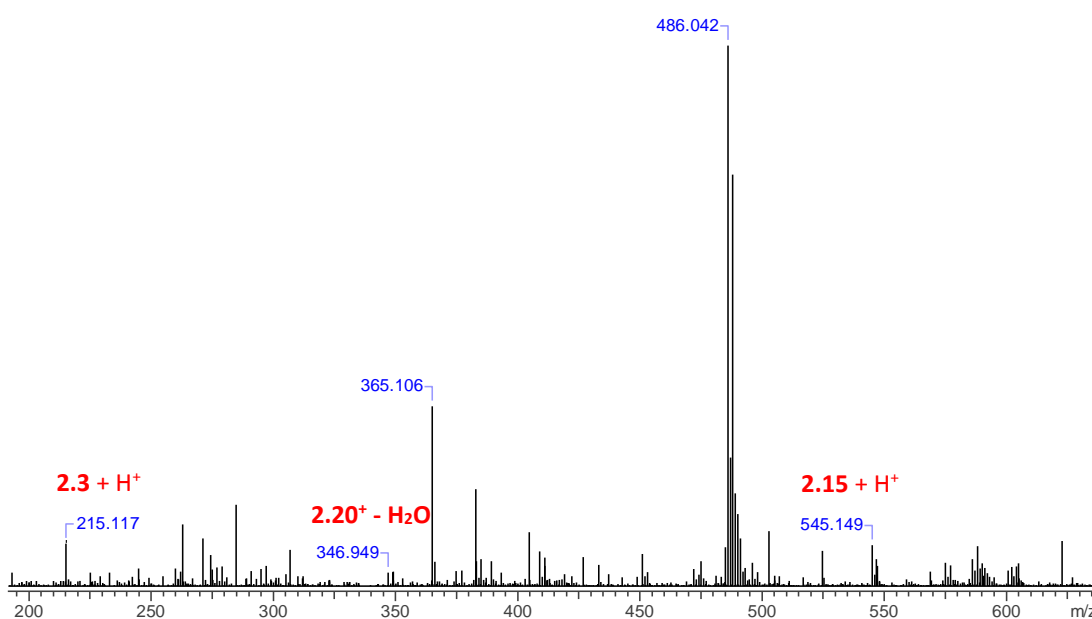


Figure 3. 22. ESI⁺ HRMS spectrum of **2.25** following incubation with β -glucosidase.

While the starting material **2.25** was not observed, the free ligand **2.15** was observed in the mass spectrum, indicating that the metal complex had partially dissociated. The incomplete hydrolysis of the ligand could be attributed to the presence of Cu(II) in solution which is known to inhibit the activity of β -glucosidase.¹²⁹

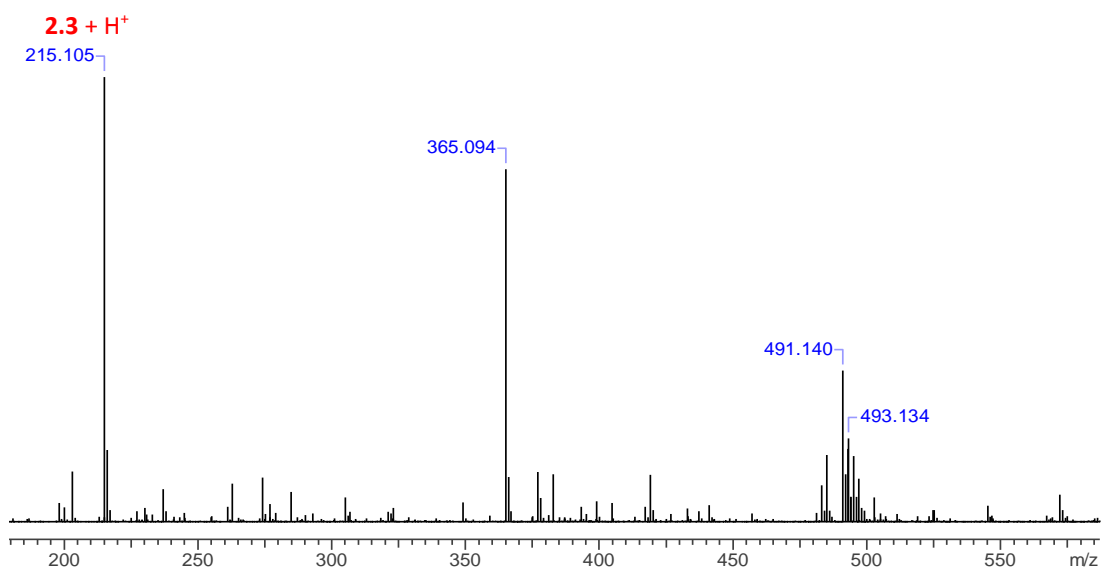
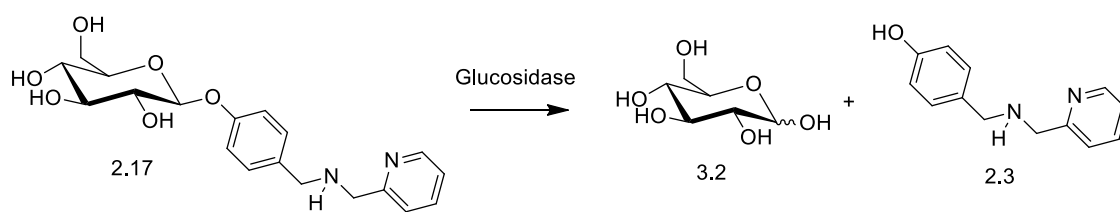


Figure 3. 24. ESI⁺ HRMS spectrum of **2.26** following incubation with β -glucosidase.



Scheme 3. 4. Hydrolysis of **2.25** by β -glucosidase.

As was seen with the acetylated analogue **2.15**, the HPLC trace of deprotected ligand **2.17** showed multiple species in solution, likely due to multiple protonation states as for its acetylated analogue (**Figure 3. 25**). These are rapidly eluted due to the highly polar nature of deprotected molecule and hence the peaks show very similar retention times but are sufficiently well resolved to be clearly distinguished.

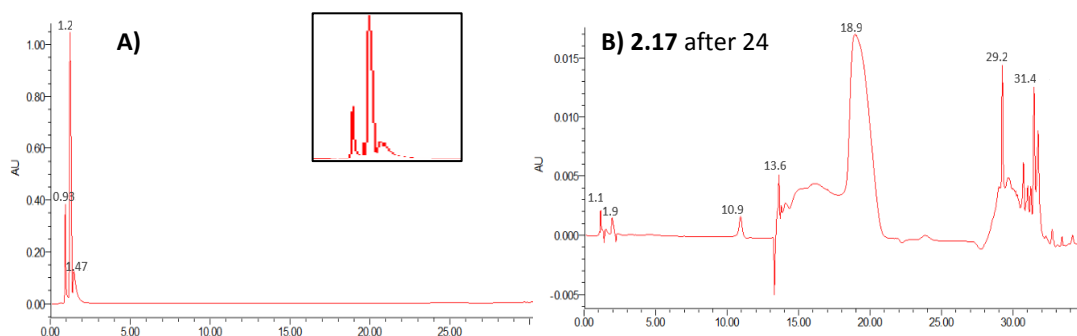


Figure 3. 25. HPLC traces of **2.17** A) before and B) after incubation with β -glucosidase.

The mass spectrum of **2.17** reveals that the primary ion detected is the aglycon **2.3** which confirms that the glycoside **2.17** is a substrate for the β -glucosidase enzyme (**Figure 3. 26**). No adducts of starting glycoside could be detected, unlike the reaction with the acetylated analogue **2.15**, which would suggest that compound has been completely hydrolysed after 24 h.

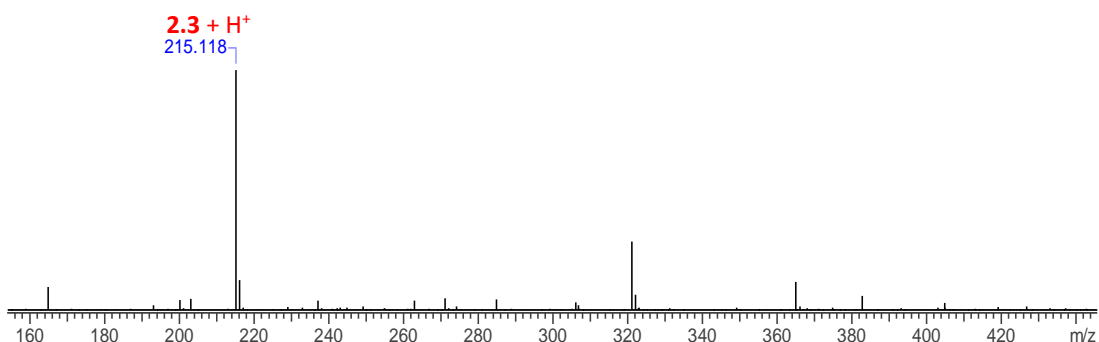
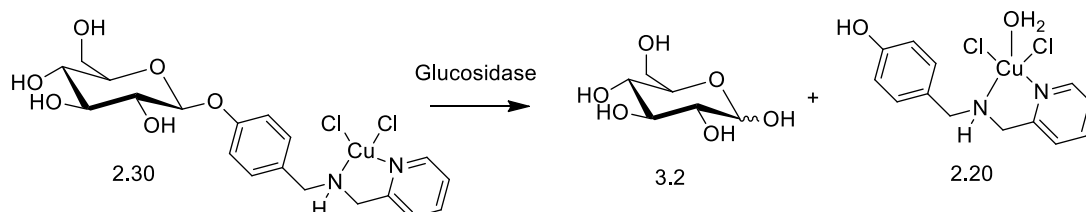


Figure 3. 26. ESI⁺ HRMS spectrum of **2.17** following incubation with β -glucosidase.



Scheme 3. 5. Hydrolysis of **2.30** by β -glucosidase.

Incubation of the per-hydroxylated Cu(II) complex **2.30** with β -glucosidase for 24 h resulted in an almost complete disappearance of the peak corresponding to **2.30** in the HPLC chromatogram (**Figure 3. 27**). This suggests **2.30** has been completely hydrolysed by the enzyme (**Scheme 3. 5**). As with the free ligand **2.17**, **2.30** is rapidly eluted due to the highly polar nature of the molecule.

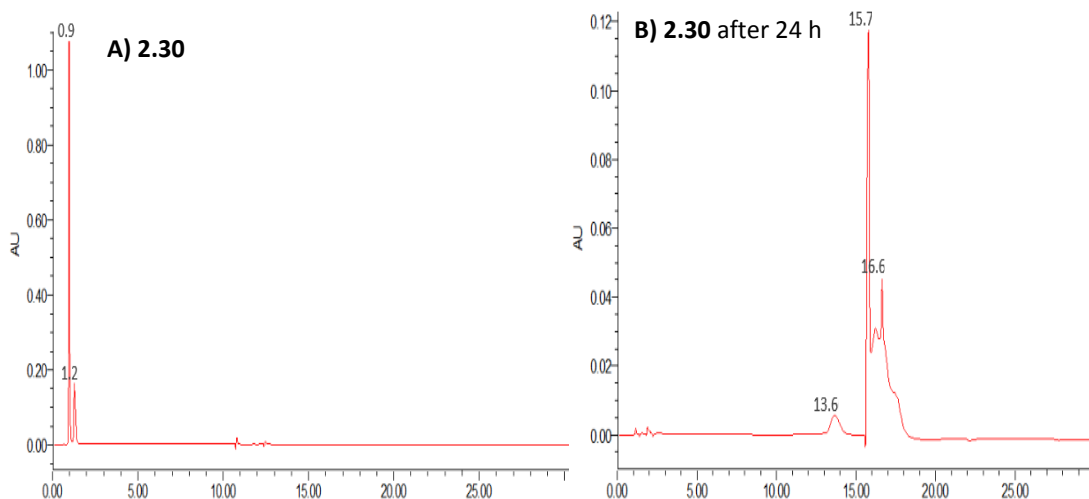


Figure 3. 27. HPLC traces of **2.30** A) before and B) after incubation with β -glucosidase.

Analysis by HRMS (**Figure 3. 28**) shows the presence both the aglycon Cu(II) complex **2.20** and the free aglycon ligand **2.3** which confirms that hydrolysis of the glycosidic bond has occurred. Also observed are peaks corresponding to the starting compound, one which shows the presence of a water adduct of **2.30** which has lost a chloride ligand ($m/z = 491.149$) and another of the free ligand **2.17** ($m/z = 377.171$).

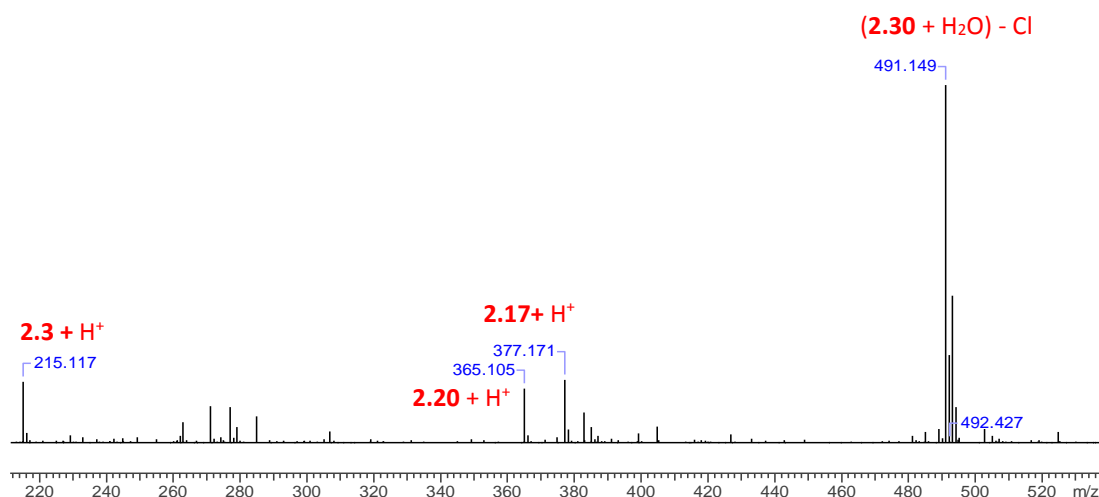
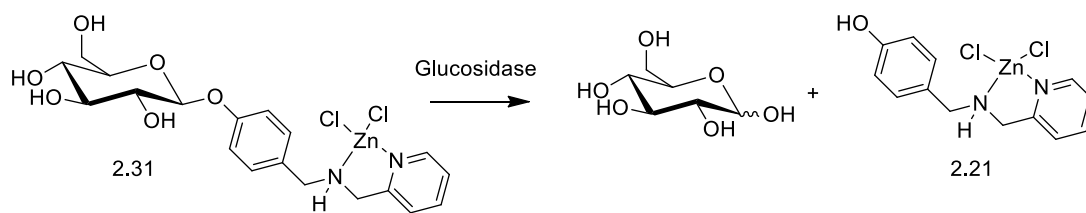


Figure 3. 28. ESI⁺ HRMS spectrum of **2.30** following incubation with β -glucosidase.



Scheme 3. 6. Hydrolysis of **2.31** by β -glucosidase.

The deprotected Zn(II) complex **2.31** was incubated with β -glucosidase for 24 h (**Scheme 3. 6**). The HPLC trace of **2.31** shows a single peak at $t = 1.2$ while the trace of the sample taken after incubation with the enzyme shows three major peaks at $t = 1.1, 13.0$ and 25.2 min (**Figure 3. 29**). While the retention time is not identical, the peak at $t = 1.1$ min in the hydrolysis study could correspond to the starting material which occurred at 1.2 min which would indicate that complete hydrolysis of the compound has not occurred. The variation in retention times could be explained by a variation in the temperature of the column between the two runs.

The HRMS spectrum shows the most abundant ion detected corresponds to the aglycon ligand **2.3**, indicating that hydrolysis of the ligand and dissociation of the metal complex has occurred (

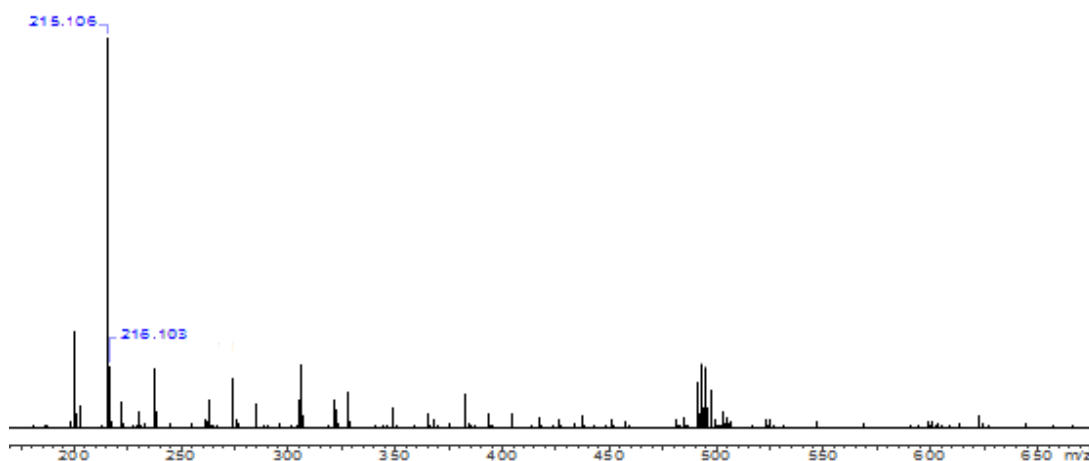


Figure 3. 30). None of the starting complex **2.31** or the free ligand **2.17** can be observed in the spectrum which demonstrates that the compound is in fact highly susceptible to the action of β -glucosidase.

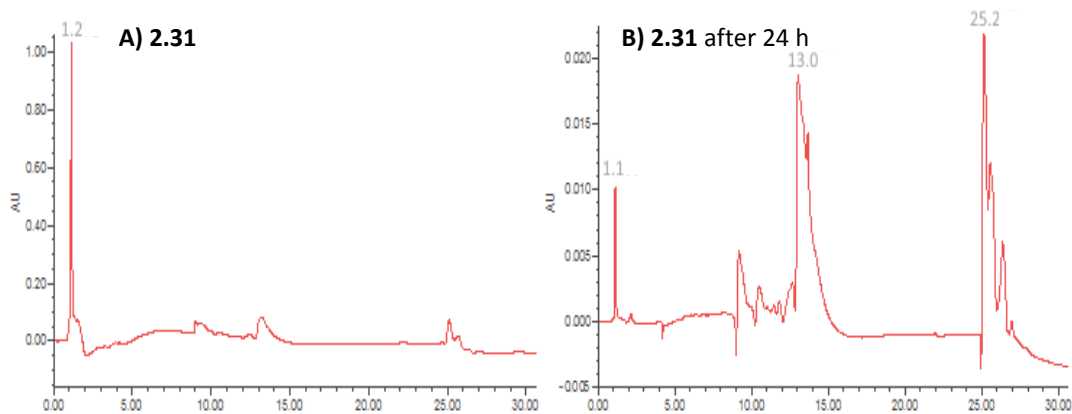


Figure 3. 29. HPLC traces of **2.31** A) before and B) after incubation with β -glucosidase.

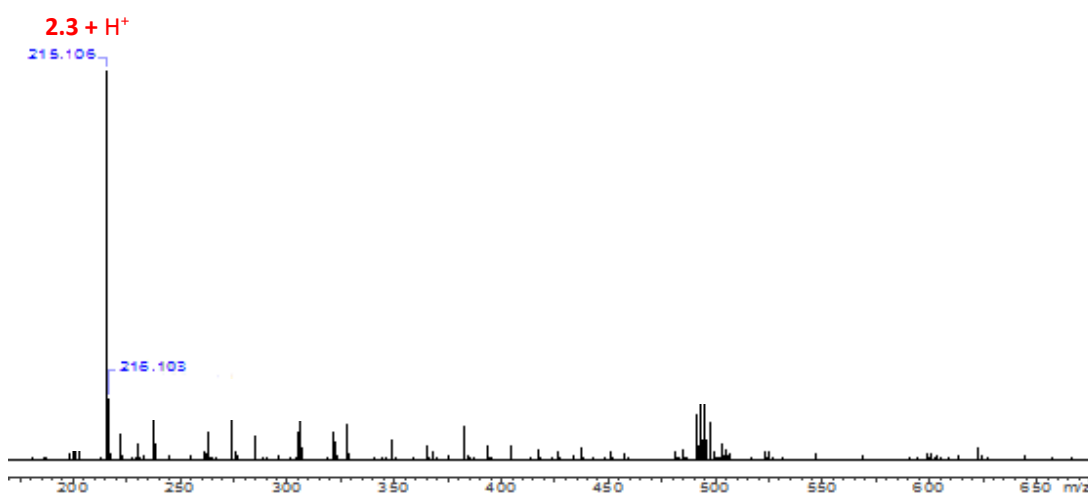
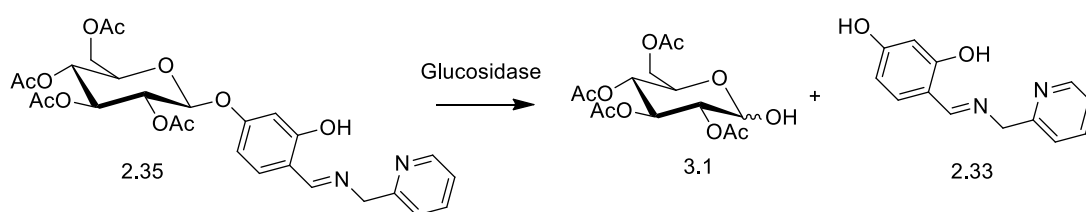


Figure 3. 30. ESI⁺ HRMS spectrum of **2.31** following incubation with β -glucosidase.



Scheme 3. 7. Hydrolysis of **2.35** by β -glucosidase.

HPLC analysis of the N_2O ligand **2.35** shows a single peak in the chromatogram which disappears entirely upon reaction with β -glucosidase for 24 h (**Figure 3. 31**). This may suggest that the compound is susceptible to the action of β -glucosidase or that hydrolysis of either the ester protecting groups or imine bond has occurred (**Scheme 3. 7**).

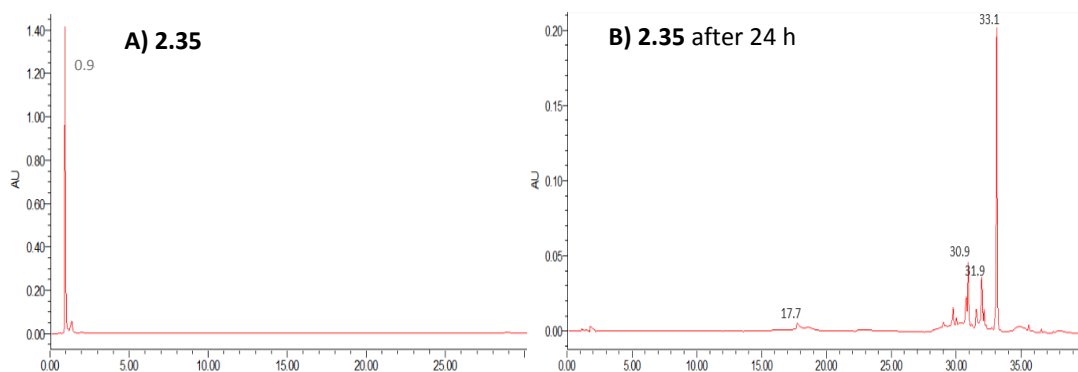


Figure 3. 31. HPLC traces of **2.35** A) before and B) after incubation with β -glucosidase.

The analysis of the mass spectrum presents a significant challenge due to the large number of species present (**Figure 3. 32**). None of the most abundant peaks correspond to adducts of the starting material, products of hydrolysis the glycosidic bond, deacetylation of the ligand or hydrolysis of the imine bond. However, closer examination of spectrum can lead to some tentatively assignments which correspond to expected products (**Figure 3. 33**). If **2.35** has been hydrolysed by the enzyme, it is expected that adducts of the aglycon **2.20** would be observed in the mass spectrum (**Scheme 3. 7**). While the abundance of the ions is low, masses corresponding to **2.33** + Na⁺, **2.33** + K⁺ and **2.33** + 2Na⁺-H⁺ can be observed in the spectrum. Coupled with the HPLC analysis which demonstrated that the none of the starting material remains, this could suggest that this compound is susceptible to the action of glucosidases.

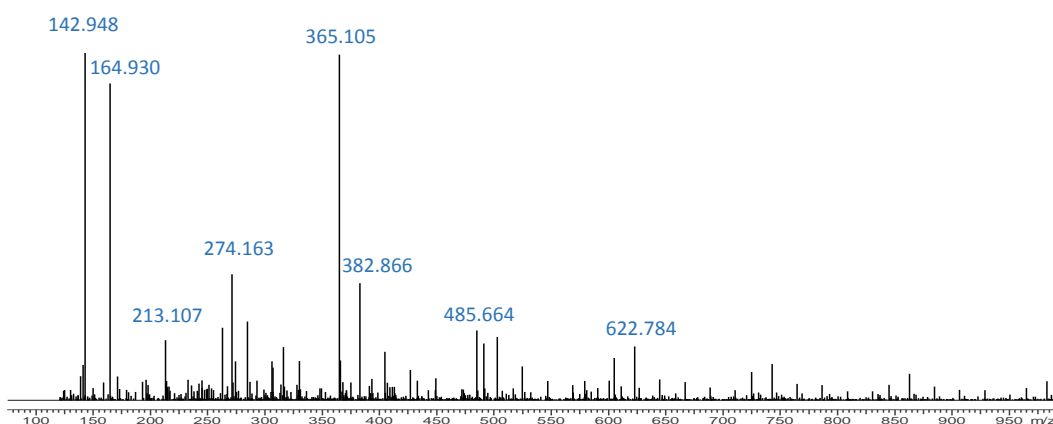


Figure 3. 32. ESI⁺ HRMS spectrum of **2.35** following incubation with β -glucosidase.

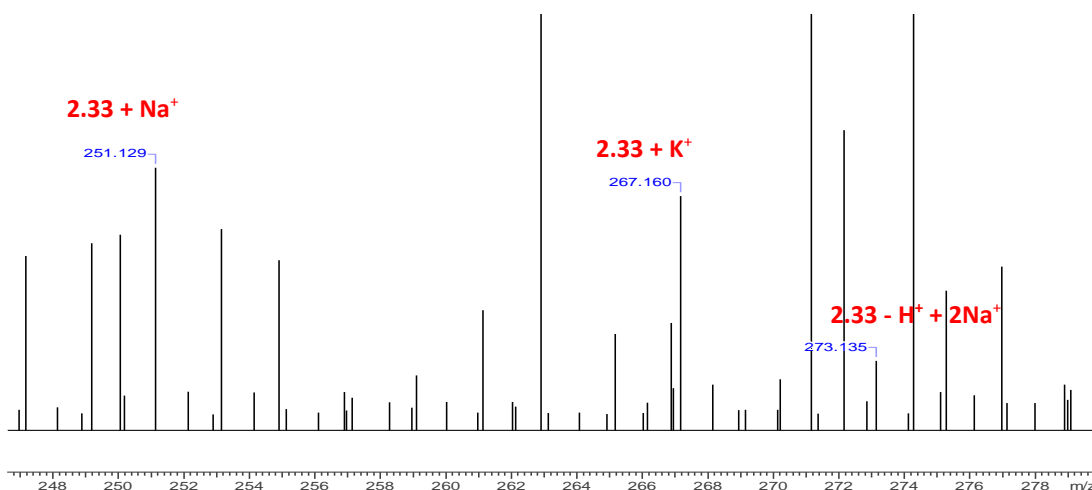


Figure 3. 33. ESI⁺ HRMS spectrum of **2.35** following incubation with β -glucosidase, 247-280 m/z.

3.2.5.2 Conclusion of Glucosidase Studies

These studies indicate that the glycosylated compounds **2.15**, **2.17**, **2.25**, **2.26**, **2.30**, **2.31** and **2.35** undergo hydrolytic reactions upon treatment with glucosidase enzymes at physiological pH and temperature. The presence of the aglycon ligand in solution after 24 h incubation was detected by HRMS analysis and the disappearance of the starting compound was determined by HPLC. These observations suggest that the glycosylated compounds could potentially be cleaved *in vivo* to produce the aglycon ligands and metal complexes. It was not clear that acetylated compounds **2.15** and **2.25** were as susceptible to hydrolysis as their deprotected analogues **2.17** and **2.30**. This is to be expected given that the natural substrates for the enzyme are per-hydroxylated glycosides. This study indicates that these compounds have undergone hydrolysis by β -glucosidase. Once administered to the parasite, it is possible that these compounds may inhibit the viability of *T. cruzi* and *L. amazonensis* by a pro-drug mechanism involving the enzymatic hydrolysis of the sugar moiety.

3.3 Conclusion

The aim of this chapter was to perform a preliminary evaluation of the biological effects of a selection of compounds from the N₂ and N₂O series of compounds. The toxicity of the compounds was investigated *in vivo* in RAW mammalian cells which found that they were well tolerated with minimal toxicity. Selected compounds were studied *in vivo* using the *G. mellonella* model which further demonstrated that the

compounds are not cytotoxic at the concentrations required for them to exert their antiparasitic effects.

The inhibitory effects towards *L. amazonensis* amastigotes and *T. cruzi* trypomastigotes were investigated *in vitro*. From this study, we identified two compounds which show exceptional activity as antikineto-plastic agents. Zn(II) complex **2.22** was shown to be more potent and selective than the currently used miltefosine and pentavalent antimonial therapies. While its potency was inferior to amphotericin B, it possesses superior selectivity. Considering that **2.22** is not structurally related to any of the currently used antileishmanial therapies, it is not expected to share any common resistance. This fact, together with the multitude of problems associated with the use of amphotericin B, demonstrate that **2.22** is a highly attractive candidate for further investigation as a novel therapy for Leishmaniasis.

The investigations into the antichagasic activity of these compounds found that the Cu(II) complex **2.25** shows exceptional activity towards *T. cruzi* trypomastigotes. Both its potency and selectivity exceed that of Benznidazole which clearly identifies this compound as a promising lead compound for further development of novel antichagasic therapies.

The studies into the antiparasitic activity of these compounds yielded vital information about the structure-activity relationships relevant to their activity. The N₂ series of compounds was discovered to be far superior than the corresponding N₂O analogues as antiparasitic agents. Glycosylation was identified as a modulator of both antiparasitic activity and as a means to increase selectivity of the compounds by making them less cytotoxic to RAW cells. Metal complexation was also discovered to significantly increase their ability to inhibit the growth of *T. cruzi* and *L. amazonensis*. Interestingly, it was discovered that the activity of the compounds could be tuned by the choice of metal; Zn(II) was found to increase the activity and selectivity towards *L. amazonensis* while the Cu(II) compounds showed increased activity towards *T. cruzi*.

The functionalization of the *para* phenoxy group with a non- enzymatically labile group was found to inhibit the activity of the compounds. The susceptibility of selected phenolic glycoconjugates compounds towards enzymatic hydrolysis was therefore determined. This established that it is possible for these compounds to be hydrolysed by β -glucosidase and therefore it is plausible that they can act as pro-drugs.

**Chapter 4: Studies Towards the Synthesis of a Galactosyl-
1,2,3-Triazolyl Derived Macrocyclic**

4.1 Introduction

4.1.1 Carbohydrate functionalized macrocycles

Macrocycles are rather loosely defined by IUPAC as being large cyclic molecules.¹³⁰ They are highly attractive compounds because of their interesting biological and physicochemical properties which stems from the conformational restriction caused by the macrocyclic ring.^{131,132,133} In particular, macrocycles containing carbohydrates have attracted considerable attention, both as pendant groups and as constituents of the macrocyclic ring.^{134, 135, 136} This attention stems from the widespread occurrence of carbohydrates in nature for recognition and cell signalling and also their utility in synthesis; they are cheap, abundant, stereochemically pure starting materials that offer substantial structural versatility. A single carbohydrate can adopt several different forms, namely open chain, α/β -furanose and α/β pyranose and this array of functional diversity grants carbohydrates significant utility in the design and synthesis of functional macrocyclic compounds.

4.1.2 Carbohydrates as Pendant Groups

Carbohydrates are commonly seen as pendant groups appended to macrocyclic rings such as porphyrins, crown ethers and polyene-lactones. Carbohydrates are attractive as pendant groups due to the relative ease of modification of the macrocycle. Upon the formation of the macrocycle, different sugar motifs can be attached to the macrocyclic core and allow late stage diversification in the synthesis.^{68, 137, 138}

Glycosylated macrocycles often display potent biological activities. For example, the macrolide class of antimicrobial drugs features a macrocyclic lactone ring and pendant deoxy saccharide groups. This includes the commonly prescribed antibiotics amphotericin B and erythromycin (**Figure 4. 1**). While these typically act by binding to sterols on the cell surface and forming pores which disrupt membrane integrity, they are also known to act as immunomodulators.^{139,140,141} Studies have suggested that they may function through several different mechanisms including coordination to endogenous metals, ROS generation and electron transfer.^{142,143}

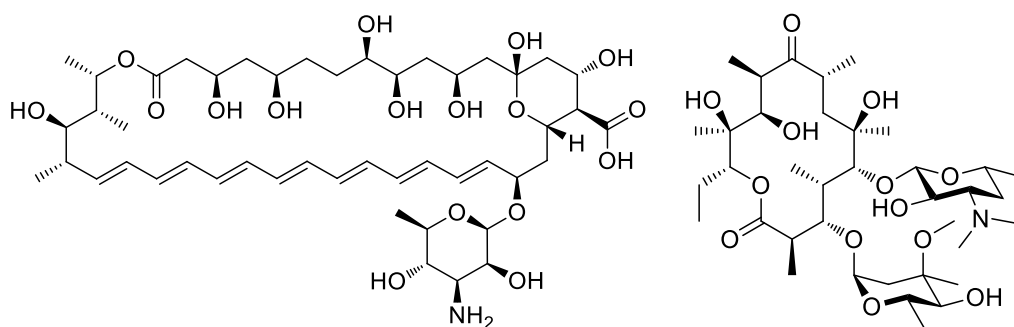


Figure 4. 1. Chemical structures of Amphotericin B and Erythromycin.

As was discussed in Chapter 2, carbohydrate conjugation is often employed as a means to improve solubility and drug targeting in cells. This strategy has been investigated using carbohydrates appended to macrocyclic rings. In one example, work by Vicente and co-workers appended various carbohydrates to a porphyrin ring using the copper promoted azide-alkyne cycloaddition (CuAAC). The metal complexes of these macrocycles were investigated for the potential use as targeted photosensitizing anticancer therapeutics.¹⁴⁴ They found that the galactose conjugate was selectively taken up by HEp2 cells and localized preferentially in the cells lysosome.

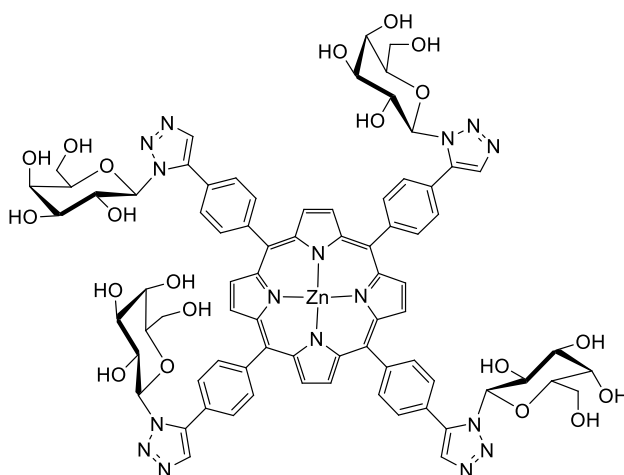


Figure 4. 2. Structure of galactose conjugated porphyrin synthesized by Vicente and co-workers.¹⁴⁴

Stephan and co-workers have successfully functionalized 14-azacrown-4 with various carbohydrate moieties (**Figure 4. 3**).¹⁴⁵ This was done to improve the binding of the molecule to concanavalin A, a lectin, with the aim of developing a targeting ligand for

use with metals such as ^{99m}Tc , ^{90}Y and other metals commonly used for radiopharmaceutical therapeutics and diagnostics.

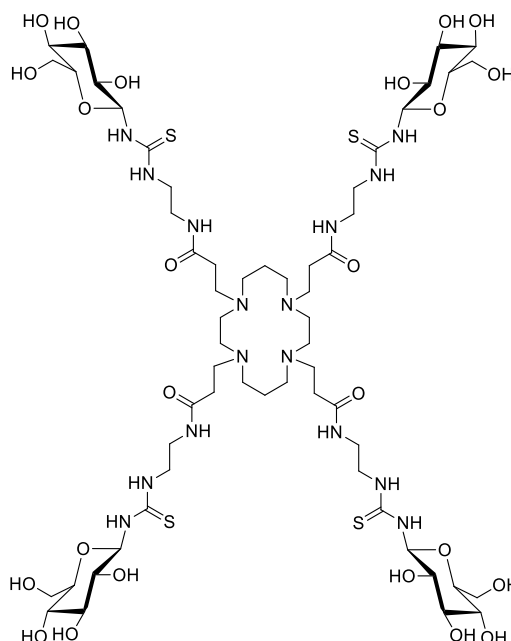


Figure 4. 3. Example of glucose functionalized azacrown synthesized by Stephan and co-workers.¹⁴⁵

From this work, they were able to quantify the change in binding affinity of different compounds based on the glycosylation motifs appended to the macrocyclic ring. These glycosylated macrocycles were found to bind much more strongly to concanavalin A than glucose, an observation attributed to the glycoclustering effect.

4.1.3 Carbohydrates as Internal Ring Constituents

Carbohydrates are commonly used as scaffolds upon which to build a macrocycle. This has many benefits as the rigid conformation of the carbohydrate, typically a ${}^4\text{C}_1$ conformation for a pyranose sugar, can offer a degree of preorganization to the open chain precursor and allow for a more efficient macrocyclization reaction than a purely linear chain molecule. The multifunctional nature of carbohydrates allows the possibility of linkage through any of the hydroxyl groups to generate structural diversity. The chiral nature of the sugar permits the synthesis of chiral cavities which offers potential for use of the molecules as asymmetric catalysts and chiral recognition.

As with the pendant carbohydrate macrocycles detailed above, molecules which have carbohydrates embedded in the macrocycle ring often display attractive biological profiles stemming from their conformational rigidity and dense functionality.

One such example of this is the macrocyclic analogue of Sialyl Lewis X (SLe^X) synthesized by Tsai and co-workers.¹⁴⁶ SLe^X is a tetrasaccharide often found on glycoproteins and serves as a ligand for selectins. These are carbohydrate recognising proteins that are involved in several important immunological processes including neutrophil extravasation, lymphocyte recirculation and platelet adhesion.¹⁴⁷ By synthesizing a macrocyclic scaffold, all the recognition elements are pre-organized in a defined manner which lowers the entropy upon binding with selectin. This proved to have a dramatic effect as the macrocycle was found to be 1000 times more potent than natural SLe^X at binding P-selectin.

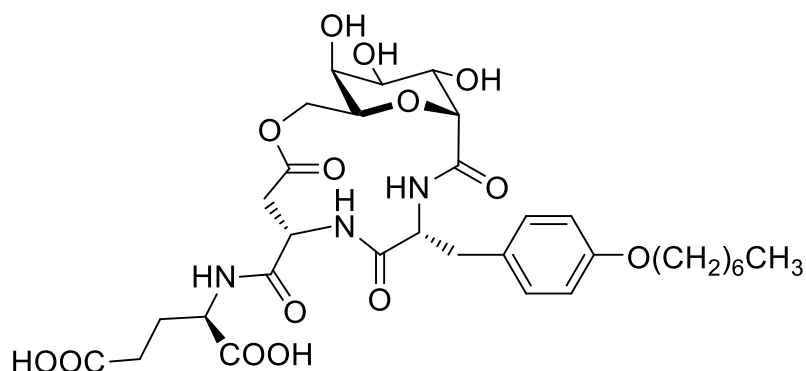


Figure 4. 4. SLe^X mimic synthesized by Tsai and co-workers.

Carbohydrate macrocycles have been investigated for their host-guest chemistry. Kessler *et al* synthesized macrocycles based on a glucosyluronic acid methylamine framework (**Figure 4. 5**). This is a dipeptide isostere that mimics a Gly-Ser sequence held in a β -turn conformation.¹⁴⁸ They found that the ring closing amide coupling reaction formed dimer, trimer, tetramer and hexamer macrocycles. Binding studies of the hexameric species with *p*-nitrophenol and benzoic acid were carried out using NMR titrations and found that the host-guest behaviour of the compound closely mimicked that of α -cyclodextrin.

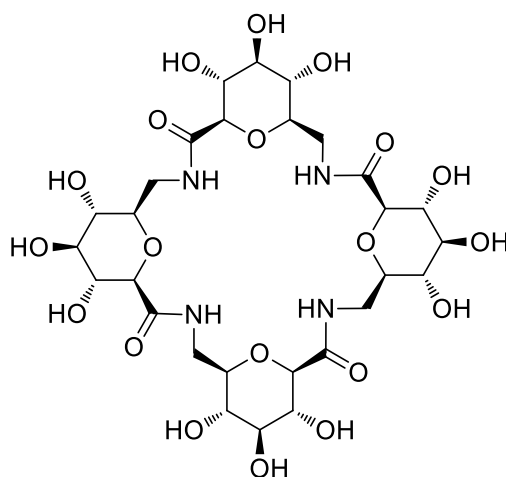


Figure 4. 5. Cyclodextrin mimic synthesized by Kessler and co-workers.¹⁴⁹

Carbohydrates have been widely used as scaffolds to synthesize chiral crown ethers incorporating two adjacent sugar hydroxyl groups as part of the cavity. These are attractive as chiral catalysts in their own right or as metal chelators. This methodology was exploited by Bakó and co-workers who synthesized several carbohydrate derived lariat crown ethers (**Figure 4. 6**), and studied their influence on the stereochemical outcome of the Darzens reaction (**Figure 4. 7**).¹⁵⁰

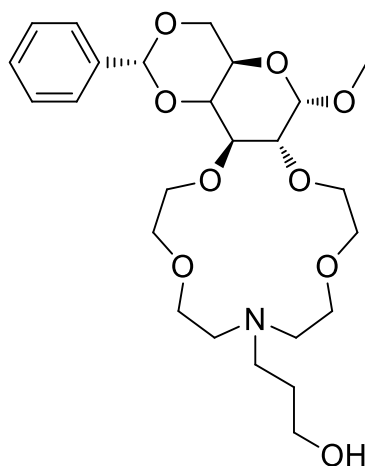


Figure 4. 6. Glucose derived crown ether investigated by Bakó and co-workers.¹⁵⁰

They found that the compounds could successfully catalyse the reaction to give *ee* values between 43% and 96%. Interestingly, they found that by replacing the glucose catalyst with one derived from mannose, which possesses inverted stereochemistry at the C-2 position, they could alter the enantioselectivity of the reaction and preferentially obtain the opposite enantiomer. This result clearly demonstrates the utility of carbohydrate macrocycles as highly effective and tunable catalysts.

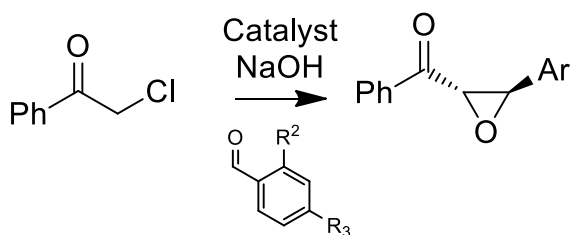


Figure 4. 7. Darzens reaction studied by Bakó.

4.1.4 Carbohydrate Macrocycles Containing Triazole Rings

The CuAAC reaction has been widely applied to the synthesis of macrocycles. The popularity of the reaction stems from its mild conditions, high functional group tolerance and high reliability. This makes it an ideal reaction for the ring closing step of a macrocycle synthesis.

Fields and co-workers have synthesized a collection of galactose derived macrocycles using CuAAC methodology and investigated their susceptibility to the action of enzymatic sialylation using *T. cruzi* trans-sialidase.¹⁵¹

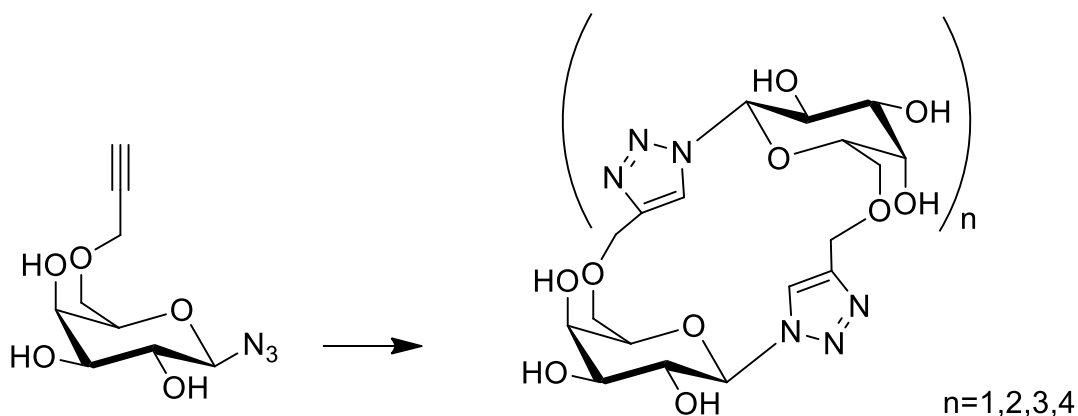


Figure 4. 8. Synthesis of triazole containing macrocycles used by Field and co-workers.¹⁵¹

This reaction was carried out in a microwave and produced macrocycles consisting of 2-5 saccharide subunits which were separated by HPLC. The reaction temperature, catalyst loading and reaction time were varied but they found that this had little effect on the yield and ratio of the macrocycles produced in the reaction. The concentration of the reactants however, did influence the amount of larger oligomer produced in the reaction, which increased with higher concentrations. These macrocycles were subject to sialylation with *T. cruzi* trans-sialidase. The researchers

found that the macrocycles consisting of 2 and 3 sugar subunits could be successfully sialylated using this enzymatic methodology.

The Gin research group has investigated using the CuAAC methodology to synthesize cyclodextrin mimics.¹⁵² They used an $\alpha(1\rightarrow4)$ linked trimannose unit as their central building block to synthesize a macrocycle containing 6 sugar subunits.

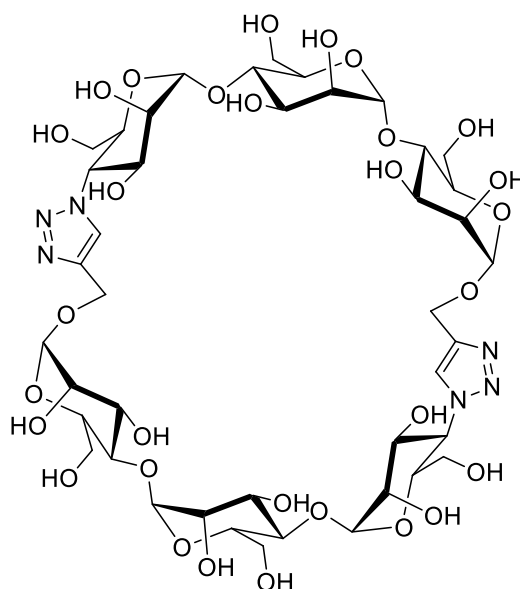


Figure 4. 9. Cyclodextrin mimic synthesized by Gin and coworkers.¹⁵²

This work found that the trimannose unit form the dimerized hexasaccharide macrocycle preferentially under CuAAC reaction conditions. Studies on the host-guest chemistry of the macrocycle found that it mimicked the behaviour of β -cyclodextrin to bind 8-anilino-1-naphthalenesulfonate, a fluorescent dye.

Listokowski and co-workers have used sucrose as a scaffold to build triazole linked macrocycles. They found that by using CuAAC methodology they could synthesize both the desired disucrose macrocycle together with two monomeric macrocycles.¹⁵³ Rather surprisingly, they found that both 1,4 and 1,5 substituted triazoles were formed under these conditions. By performing the reaction under thermal conditions without any catalysis, they found that they could produce the dimeric macrocycle exclusively without the formation of the monomeric species.

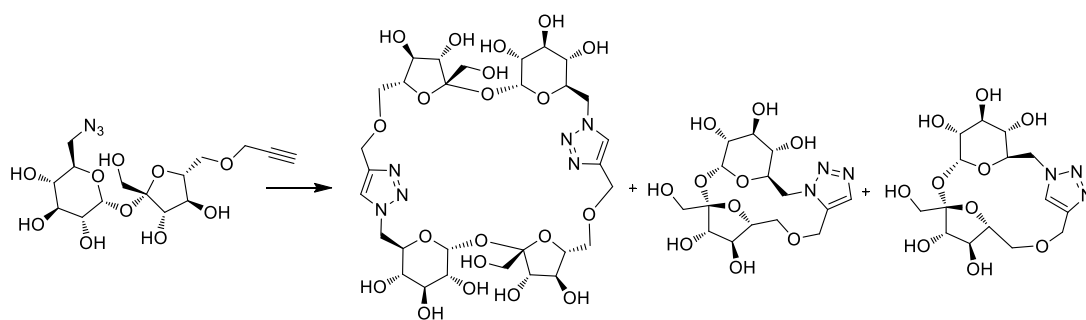


Figure 4. 10. *Macrocycles prepared by Listkowski and coworkers.*¹⁵³

4.1.5 Macrocyclization Strategies

There are numerous approaches that can be followed for the synthesis of macrocycles. The ring closing reaction to complete the macrocycle is typically the most difficult due to the entropy barrier that must be overcome to favour the intramolecular collision of the two reacting functional groups, as there are more conformations that result in intermolecular reactions than intramolecular ones. This intramolecular reaction is in competition with the intermolecular reaction that would produce dimers, trimers and oligomers which must be avoided. Due to the conformational constraint of the ring, the larger dimers and trimers are typically more favourably formed than monomeric species. In addition to the bond strain caused by the deviation of bond angles from their lowest energy conformation, Pitzer strain, also known as torsional strain, can often occur in macrocycles.¹⁵⁴ This is repulsion caused by the adoption of an eclipsed conformation of two adjacent substituents instead of the more stable staggered conformation. It is for these reasons that the formation of macrocyclic compounds is highly unfavourable with respect to the formation of their respective linear oligomers and hence present difficult synthetic targets.

To form the macrocyclic ring, it is therefore preferable to use a reaction that is reliable, high yielding and occurs in one step in a non-reversible manner. This ensures that the monomeric macrocycle, can be obtained in preference to the thermodynamically favoured oligomers. To this end a wide variety of reactions have been investigated such as esterification,^{155,156} Pd catalysed coupling reactions,^{157,158}

olefin metathesis¹⁵⁹ and CuAAC reactions.^{160,161} The CuAAC reaction is an important approach for the synthesis of non-naturally occurring macrocycles. This is due to the high reliability of the reaction, mild reaction conditions and high functional group tolerance which grants it a very wide substrate scope.¹⁶²

This reaction has two possible reactions pathways; one featuring a mononuclear σ -bonded copper acetylide and the other which proceeds via a binuclear intermediate. This binuclear complex has a σ -bonded acetylide in addition to an additional π -bond to another copper centre which is also bonded to the σ -bonded copper centre.¹⁶³ It is this binuclear pathway which is believed to be the primary pathway which the reaction proceeds through (**Figure 4. 11**). This is due to the increased polarity of the triple bond and therefore it exhibits increased reactivity with the azide dipole. In addition to this, the N_3 -Cu interactions direct the approach of the alkyne to azide moiety and control the regiochemistry of the reaction which forms the 1,3 disubstituted triazole exclusively.¹⁶⁴

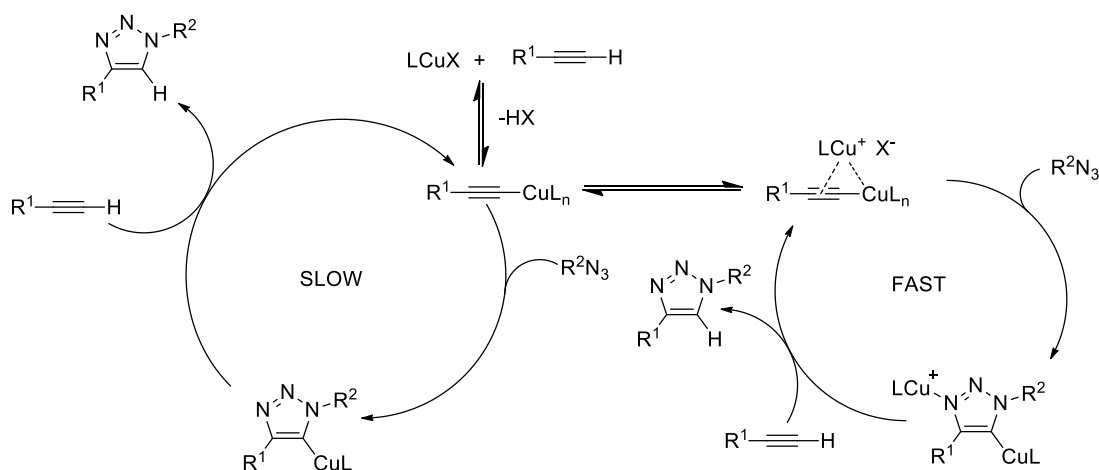


Figure 4. 11. Mechanism of the CuAAC.¹⁶³

Often the structure of a macrocycle will present more than one possible point for ring closure. When developing a synthetic route to a target, factors such as preorganisation must be considered.¹⁶⁵ This can occur in either the starting molecule or the reaction intermediate through hydrogen bonding, dipole-dipole interactions, π stacking or anion/cation templating. Choice of solvent can also play a crucial role

in stabilizing favourable transition states through hydrogen bonding which can alter the ratio of monomer to oligomers formed in the reaction.

One common strategy to increase the probability of an intramolecular reactions, and therefore avoid the formation of dimers, trimers and oligomers, is to use pseudo-high dilution conditions. High dilution is known to favour the production of cyclic products over linear molecules as it minimizes the likelihood of intermolecular collisions. The intramolecular reaction is first order as both reactants are present in the same molecule with a rate law of $r=k[A]$, where r is the rate of reaction, k is the rate constant and $[A]$ is the concentration of the uncyclized starting material. The intermolecular reaction is dependent on the reaction of two discrete molecules in solution and is therefore a second order reaction with a rate law of $r=k[A]^2$. As the rate of this reaction is proportional to the square of the concentration of the substrate, dilution has greater effect on reducing the rate of the bimolecular reaction compared to the monomolecular reaction. This difference can be exploited to favour the intramolecular reaction.¹⁶⁶ Pseudo-high dilution utilizes the dropwise addition of the open chain reactant into a solution of reaction promotor. A single drop of reactant is therefore diluted in the volume of the promotor and is present in an extremely low effective concentration. This provides a much high dilution than dissolving the entire quantity of the starting material in the same volume of solvent at once.

4.2 Aim

The aim of this work was to investigate the synthesis of a conformationally constrained macrocycle built upon a carbohydrate scaffold with CuAAC methodology. We envisage that this can be accomplished by the functionalization of the carbohydrate with an alkyne moiety in the C-6 position and a unit bearing an azide group in the C-1 position. This would allow for the use of the CuAAC reaction to close the ring in a high efficient manner.

As outlined above, small, conformationally restricted macrocycles are attractive due to their unique chemical and biological properties, stemming from their high degree of preorganization and rigidity. For our synthesis, galactose was chosen as the core

carbohydrate given the ease of regioselective manipulation of the C-6 position and the possibility to stereoselectively generate the β -glycoside of the azide containing fragment with participating protecting groups. This is important as it would leave both the alkyne and azide fragments orientated with a *syn* relationship with respect to the carbohydrate ring. This should allow for a lower energy conformation with the alkyne and azide moieties in close proximity which is necessary for the cycloaddition to generate the target macrocycle to occur.

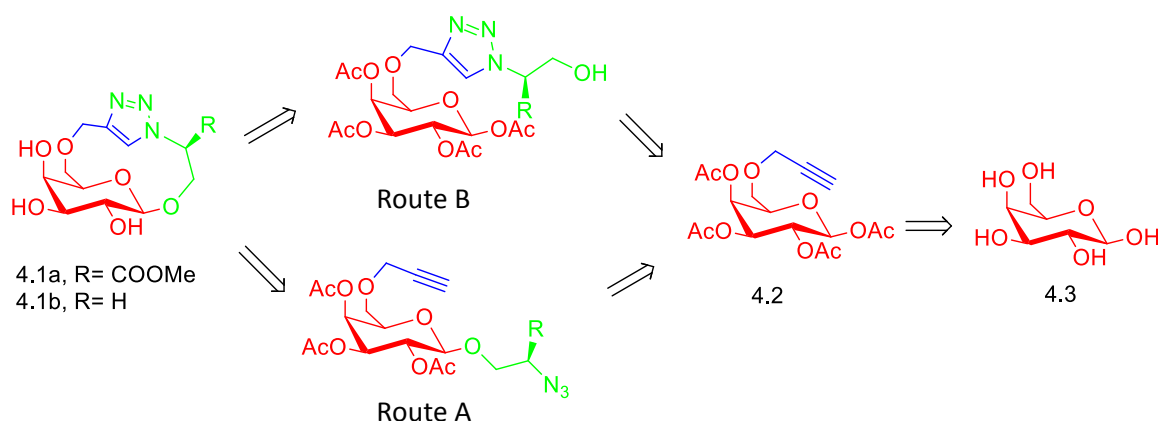


Figure 4. 12. Route to the target macrocycles **4.1a** and **4.1b**. The galactose unit shown in red, the ethylene moiety in green and the alkyne derived unit in blue.

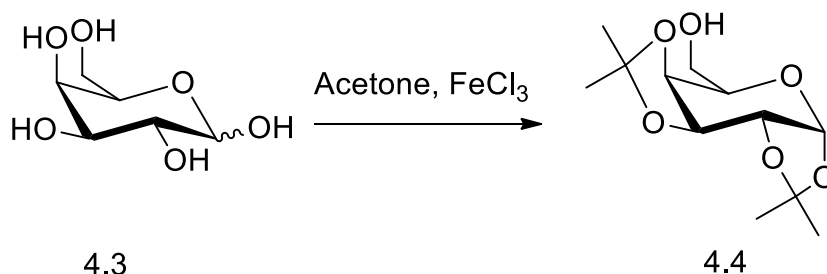
The preliminary investigations focused on the intramolecular cycloaddition of 2-azidoethyl to form the desired macrocycles **4.1a** and **4.1b** (Route A). Alternatively, an intramolecular glycosylation route could be followed which entails the tethering of the glycosyl acceptor to the C-6 position and then using a glycosylation reaction to form the macrocycle (Route B)

Two different types of acceptors were investigated. Initially, the glycosylation of *N*-Fmoc-L-serine methyl ester was explored. These derivatives would lead to macrocycles bearing a methyl ester which could be further functionalized. Structurally simpler 2-azidoethanol derivatives were also investigated, in order to establish the most favourable route to macrocyclization.

4.3 Results and Discussion

4.3.1 Investigations into the Synthesis of a Serine Derived Macrocycle 4.1a

4.3.1.1 Synthesis of Peracetylated Galactosyl Donor 4.2

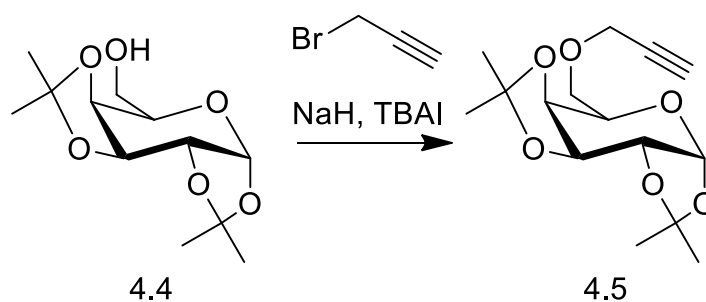


Scheme 4. 1. Reagents and conditions: Acetone, FeCl₃, 75%

The first reaction of the sequence is the protection of galactose with isopropylidene groups (**Scheme 4. 1**).¹⁶⁷ Isopropylidene protecting groups are extremely useful in carbohydrate chemistry as they allow selective manipulation of a single hydroxyl group by spanning two different pairs of hydroxyl groups in the saccharide. In the case of galactose, this strategy allows the regioselective reaction of the C-6 hydroxyl group.

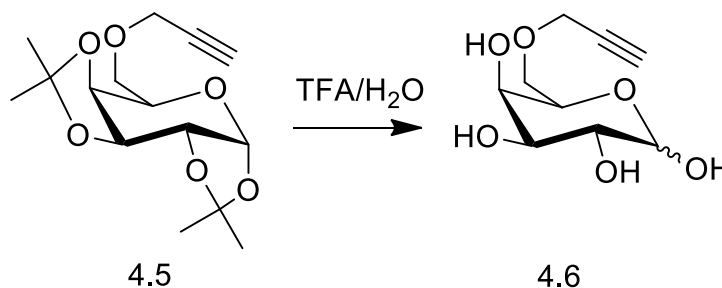
This selectivity arises from the preference of acetone to form cyclic 5-membered rings with vicinal diols. For this to occur with a cyclic carbohydrate it is necessary for the two hydroxyl groups on the ring to be in a *cis* orientation to each other. The *trans* configuration generates ring strain in the isopropylidene ring and the conformational rigidity of the pyranose prevents the twisting of the ring to adopt a more favourable conformation. As a result, galactose forms two isopropylidene rings; one spanning the C-1 and C-2 hydroxyl groups and the other formed between the C-3 and C-4 positions leaving the C-6 hydroxyl group unprotected.

Acetonide protection requires acid catalysis and to this end a range of catalysts were screened for the generation of diacetone galactose including H₂SO₄,¹⁶⁸ ZnCl₂,¹⁶⁹ and I₂.¹⁷⁰ While these did successfully generate the target compound, they showed problems with reproducibility when performed on a multigram scale. FeCl₃ proved to be the most efficient catalyst for the protection reaction and produces the protected compound **4.4** on scales up to 7 g with a consistent yield of 70-75%.¹⁶⁷



Scheme 4. 2. Reagents and conditions: Propargyl bromide, NaH, TBAI, 89%

The functionalization of the C-6 hydroxyl group to form **4.5** was carried out by the reaction of the isopropylidene protected compound with propargyl bromide utilizing TBAI as a catalyst (**Scheme 4. 2**).¹⁷¹ Initial reactions were carried out using sodium hydroxide as the base however these did not affect satisfactory conversion so it was decided to investigate the use of sodium hydride. Despite having a pK_{AH} that drastically exceeds that of the alkyne (42 vs ~26), the reaction proceeds smoothly using a threefold excess of base to form the product in high yield of 89%. The product can be purified by simple filtration through a silica plug with no trace of side products generated by the deprotonation of the alkyne starting material.



Scheme 4. 3. Reagents and conditions: TFA/H₂O, 97%

Compound **4.5** was then deprotected under acidic conditions (**Scheme 4. 3**). Various conditions were screened including catalytic TFA, Dowex H⁺ and HCl. However, the isopropylidene protecting groups proved to be very resistant to hydrolysis and these attempts unsuccessful. The reaction was eventually effected in high yield using the very forcing conditions of 66 % TFA in H₂O to generate **4.6** without any degradation observed.¹⁵¹

Following the rigorous drying of the deprotected saccharide **4.6** to ensure the removal of as much water as possible, the remaining hydroxyl groups were then

protected with acetyl groups to generate **4.2**. The acetylation reaction was carried out at 80 °C in acetic anhydride utilizing sodium acetate as a base. These conditions favour the formation of the β -anomer over the more thermodynamically stable α -anomer.

The selectivity of this reaction arises from the relative rate of mutarotation at the anomeric centre and the rate of acetylation. When acetic anhydride and a weak, non-nucleophilic base are used, the rate of mutarotation between the α and β -hydroxyl anomers is faster than the acetylation reaction. As the equatorial hydroxyl group is more nucleophilic than the axial α anomer, the kinetic β -product can be obtained preferentially over the thermodynamic α - product (**Figure 4. 13**)

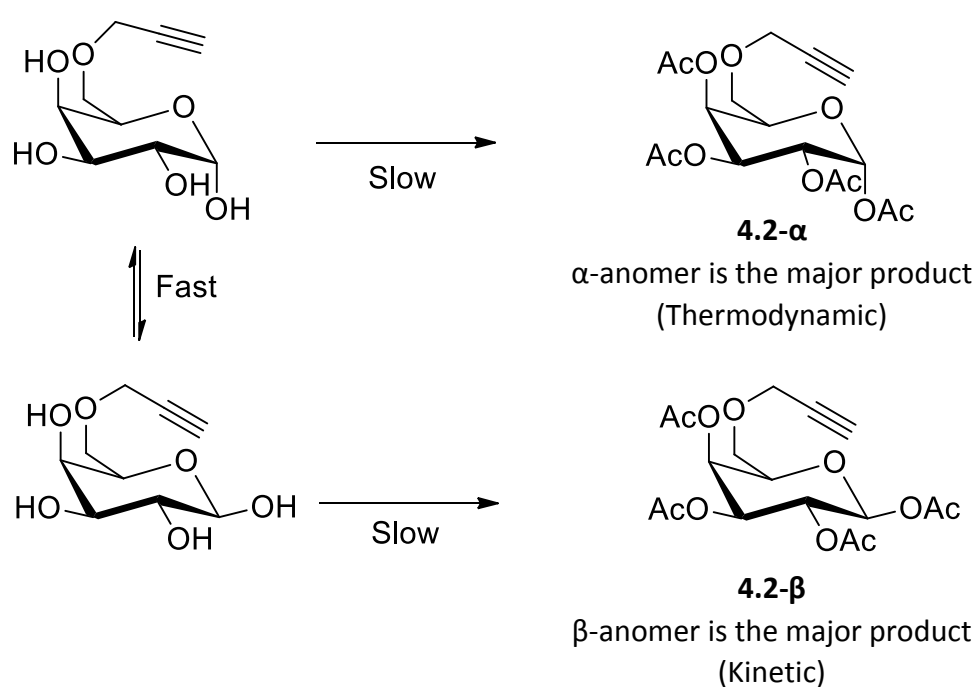
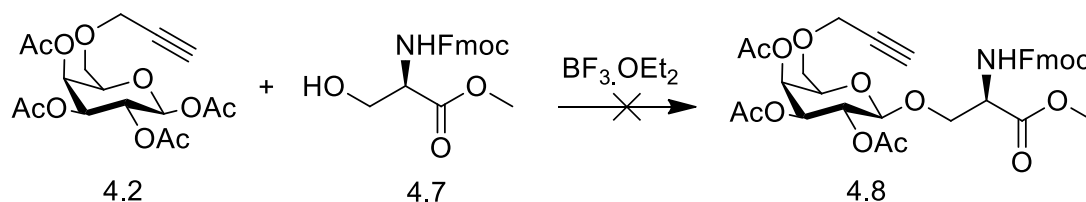


Figure 4. 13. Diastereoselective acetylation of **4.4**.

This reaction produced **4.2** in moderate yield of 74% in an α/β ratio of approximately 16:84% as determined by NMR spectroscopy. All though the compound has been reported as the pure β -anomer,¹⁵¹ these diastereomers did not prove separable by column chromatography. It was therefore decided to use the mixture of anomers for the next steps of the synthesize and purify the mixture upon further derivatization.

4.3.1.2 Glycosylation Studies with *N*-Fmoc-L-Serine Methyl Ester

4.3.1.2.1 Acetyl Donor



Scheme 4. 4. Reagents and conditions: $\text{BF}_3 \cdot \text{OEt}_2$, 0-25 °C, 18h.

The glycosylation of **4.2** presented significant challenges. The reaction of *N*-Fmoc-L-serine methyl ester **4.7** with donor **4.2** utilizing $\text{BF}_3 \cdot \text{OEt}_2$ as the reaction promotor did not affect the desired conversion to the target galactoside (**Scheme 4. 4**). Instead, acetyl transfer was observed from the donor **4.2** to the amino acid acceptor to generate the *O*-acetyl ester **4.9** (**Figure 4. 14**), in addition to the formation of dehydroalanine **4.10**.

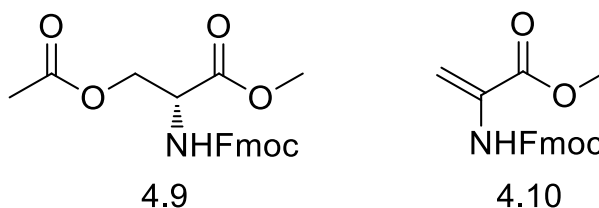
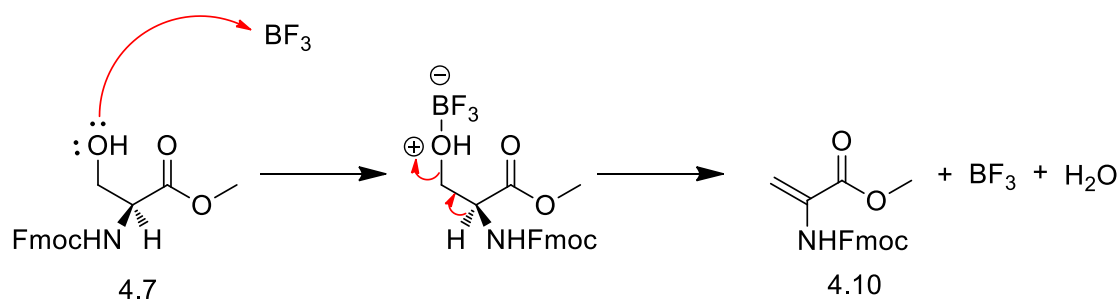


Figure 4. 14. Structure of *O*-acetylated by product **4.9** and elimination product **4.10**.

This is formed by the Lewis acid promoted elimination of the hydroxyl group, made possible by the presence of the electron withdrawing *N*-Fmoc and methyl ester groups which increase the acidity of the α -hydrogen. This proceeds through an E2 mechanism considering that the molecule is a primary alcohol which cannot form a stable cation necessary for an E1 and the lack of base prevents the E1cb pathway (**Scheme 4. 5**).



Scheme 4. 5. Formation of dehydroalanine product **4.10** by BF_3 .

Extensive efforts were made to avoid these side reactions including varying reaction temperatures, stoichiometries and order of addition, however, these difficulties persisted. SnCl_4 was also screened as a reaction promotor but this too was unable to effectively produce the desired galactoside. It was reasoned that the source of these problems were caused the disarmed character of the acetylated donor together with the poor nucleophilicity of the serine acceptor. Acetylated donors are known to be deactivated coupling partners in chemical glycosylation due to the electron withdrawing nature of the acetyl group which destabilizes the cationic oxocarbenium intermediate and therefore inhibits its formation. Serine derivatives are also a poor nucleophile due to the internal hydrogen bond between the hydroxyl group and the carboxyl lone pair. This forms a stable 5-membered ring and reduces the ability of the oxygen to behave as a nucleophile (**Figure 4. 15**).

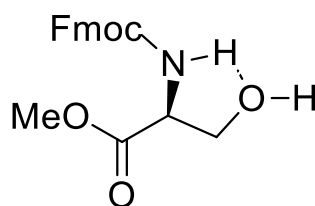


Figure 4. 15. Hydrogen Bonding in **4.7**.

4.3.1.1.2 Thioglycoside Donors

Due to these drawbacks, it was decided to explore the use of more reactive glycosyl donors. Thioglycosides are a very attractive class of glycosyl donors due to their high reactivity, mild activation conditions and stability. Since their first use by Ferrier and co-workers in 1973,¹⁷² thioglycosides have become extremely popular in

carbohydrate chemistry for the construction of a wide variety of oligosaccharides and glycoconjugates.¹⁷³ They are typically prepared from the corresponding acetyl donor utilizing Lewis acid promoters such as $\text{BF}_3 \cdot \text{OEt}_2$ or SnCl_4 and either an alkyl or aryl thiol. While a multitude of activating methods have been developed, these can be divided into three broad categories: 1) Metal salts; 2) halonium reagents; 3) organosulfur reagents.

1) *Metal salts*

The first usage of thioglycoside donors utilized soft, thiophilic cations such as Hg(II) and Ag(I) .¹⁷² These salts are often toxic and typically require stoichiometric amounts to effect complete conversion of the donor. The use of these salts as promoters necessitates high reaction temperatures which can lead to the formation of complex side products and therefore these salts are rarely used in glycosylation reactions.

2) *Halonium Reagents:*

Cationic halogen species such as Br^+ and I^+ are highly thiophilic and as a result have found widespread use as activators for thioglycosides under much milder conditions than the previously used metal salts. This approach was first introduced by Nicolaou in 1983 when he reported the successful activation of a selection of thioglycosides using NBS.¹⁷⁴ Iodinium based systems employing NIS/ TfOH or NIS/ AgOTf have been shown to be more efficient activators of thioglycosides, likely due to the softer nature of the I^+ cation. These systems were developed by the groups of Fraser-Reid and van Boom and since their publication in 1990 they have become the standard methods for the activation of thioglycosides in carbohydrate chemistry.^{175,176}

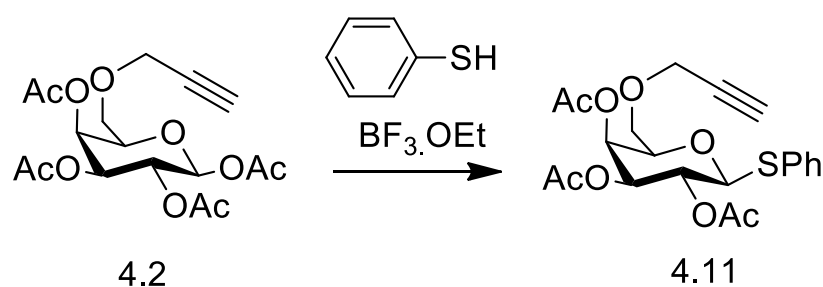
3) *Organosulfur Reagents:*

Another widely used method for the activation of thioglycosides is organosulfur reagents. These utilize a cationic sulfur containing molecule, usually generated *in situ*, to act as a soft electrophile to activate the thioglycoside. The first reported example of this was by Fügedi who used dimethyl(thiomethyl)sulfonium triflate (DMTST) as a reaction promotor to generate a selection of disaccharides.^{177,178} This reagent is generally used freshly prepared by the reaction of dimethyl disulfide and

methyl trifluoromethanesulfonate due to its high reactivity and hydroscopic nature. The safety hazards associated with using methyl trifluoromethanesulfonate has led researchers to develop alternative activating agents based on the same principle as DMTST. Commonly used substitutes include dimethyl(thiomethyl)sulfonium tetraaflouoroborate (DMTSTF), dimethyl disulphide/ triflic anhydride ($\text{Me}_2\text{S}_2/\text{Tf}_2\text{O}$) and S-(4-Methoxyphenyl) benzenethiosulfinate/ trifluoromethanesulfonic anhydride.^{179,180} A variety of organoselenium promoters have also been investigated.^{181,182}

4.3.1.1.2.1 Glycosylation Studies of *N*-Fmoc-L-Serine Methyl Ester Utilizing Thiophenyl Glycosides

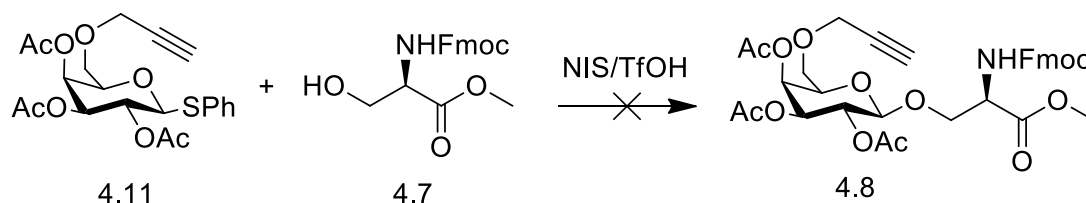
A thiophenol based galactose donor **4.11** (**Scheme 4. 6**) was initially investigated for its reactivity with *N*-Fmoc-L-serine methyl ester. To generate the thioglycoside from **4.2**, it was reacted with thiophenol using SnCl_4 as a promotor using conditions identical to those used to generate the thiophenol donor from the peracetylated analogue.¹⁸³ These proved unsuccessful and a mixture of starting material and degradation products were observed upon workup. Interestingly, a deep red colour developed during the reaction which is not generally observed during glycosylations using SnCl_4 . As the colour change is not seen for the analogous reaction of peracetylated galactose with thiophenol, it is unlikely that it arises from the displacement of the chloride ligands by thiophenol and instead arises from an interaction between the Sn(IV) and the alkyne moiety of the saccharide. This colour disappears upon quenching the reaction with a saturated aqueous solution of NaHCO_3 which would suggest that this is a weak interaction and that all of the tin is converted to SnO_2 .



Scheme 4. 6. Reagents and conditions: Thiophenol, $\text{BF}_3 \cdot \text{OEt}_2$, 0-25 °C, 61%

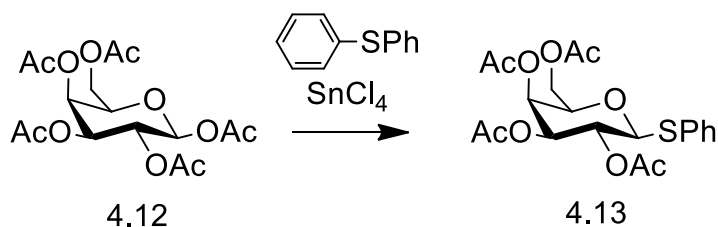
Galactosyl **4.11** was instead obtained in good yield using $\text{BF}_3 \cdot \text{OEt}_2$ as the reaction promotor, without the production of the degradation products observed as was the case when SnCl_4 was used (**Scheme 4. 6**).

4.11 was then subject to glycosylation with *N*-Fmoc-L-serine methyl ester **4.7** using the NIS/TfOH activating system. While the intended glycoside could be detected by mass spectrometry, it was formed in trace amounts and the bulk of the material recovered consisted of starting material **4.11**, the galactose hemiacetal and unidentifiable complex by-products. A range of stoichiometries were screened, as were the reaction temperature however no significant improvement could be obtained (**Scheme 4. 7**).



Scheme 4. 7. Reagents and conditions: NIS/TfOH, 0-25 °C

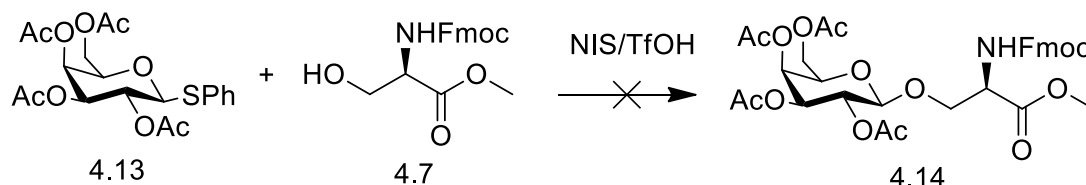
It was postulated that a possible cause of the side reactions and poor reactivity was the formation of an iodonium species between the alkyne moiety and the I^+ generated from the activator solution. We therefore conducted studies using a thiophenol galactose donor bearing an acetate group at the C-6 position in place of the intended alkyne.¹⁸³



Scheme 4. 8. Reagents and conditions: Thiophenol, SnCl_4 , 0-25 °C, 94%

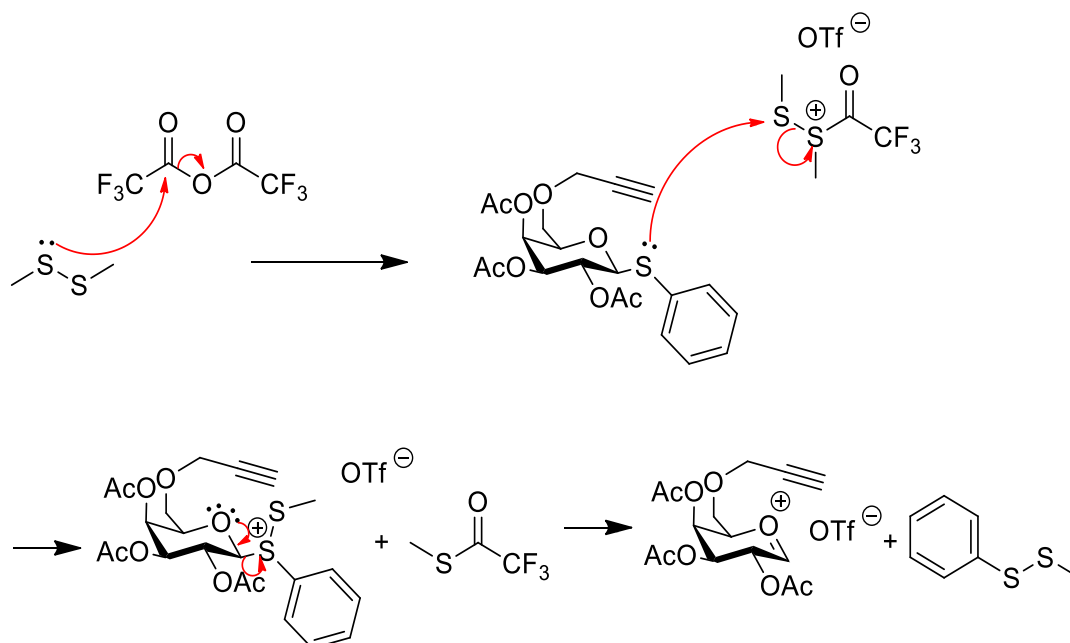
This was prepared as per literature methods and reacted with *N*-Fmoc-L-serine methyl ester using the NIS/TfOH activator system (**Scheme 4. 9**). While the reaction mixtures did produce a less complex mixture of products as determined by thin layer

chromatography (TLC), it was not successful at generating the glycosylation product **4.8**. As with the alkyne functionalized donor, various stoichiometries and reaction temperatures were screened, however, these too were not able to generate the desired product.



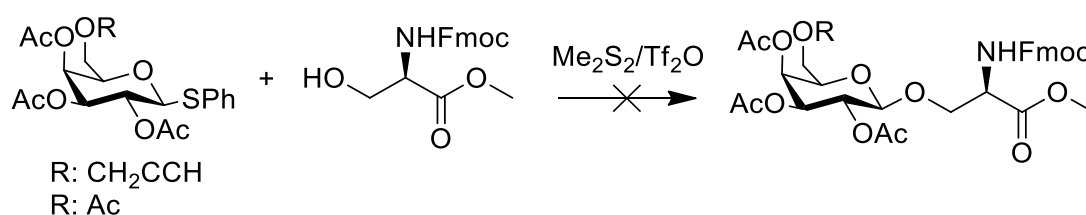
Scheme 4. 9. Reagents and conditions: NIS/TfOH, 0-25 °C

It was reasoned that the disarmed nature of **4.11** was impeding the reaction and that a stronger activator might overcome this problem. The Me₂S₂/Tf₂O system, initially developed by Fügedi and co-workers, was explored, as it is known to be highly active and can completely activate disarmed donors at temperatures as low as -78 °C.¹⁸⁰ This activity is due to the higher thiophilicity of the sulfonium cation generated by the activator solution, which is more readily attacked by the anomeric thiol (**Scheme 4. 10**).



Scheme 4. 10. Mechanism of activation by the dimethyl disulphide/triflic anhydride system.

Reacting thiophenyl galactoside **4.11** with *N*-Fmoc-L-serine methyl ester using freshly prepared $\text{Me}_2\text{S}_2/\text{Tf}_2\text{O}$ at $-42\text{ }^\circ\text{C}$ produced a complex mixture of by-products and starting materials, similar to the studies utilizing acetyl based donors (**Scheme 4.11**). While trace amounts of the intended product could be observed by mass spectrometry, it was not formed in sufficient amounts to allow isolation. This reaction was repeated several times with increasing stoichiometries of activator and *N*-Fmoc-L-serine methyl ester **4.7**, however, no improvement could be achieved. Conducting the reaction at the comparatively high temperature of $0\text{ }^\circ\text{C}$ and allowing longer reaction times were also insufficient to allow for the generation of the target glycoside **4.8**. Studies using the $\text{Me}_2\text{S}_2/\text{Tf}_2\text{O}$ system were also carried out using the peracetylated galactose thiophenyl donor **4.1** lacking the alkyne functionality at the C-6 position with identical results the studies using **4.11**.



Scheme 4. 11. Reagents and conditions: $\text{Me}_2\text{S}_2/\text{Tf}_2\text{O}$, $0\text{ }^\circ\text{C}$ or $-42\text{ }^\circ\text{C}$, no product recovered.

4.3.1.1.2.2 Glycosylation Studies of *N*-Fmoc-L-Serine Methyl Ester Utilizing Thioethyl Glycosides

The poor results of this approach demonstrated that the thiophenyl donor is not reactive enough to form the desired galactoside **4.8** with *N*-Fmoc-L-serine methyl ester. In efforts to achieve a reactive glycosylation partner while still retaining the disarming acetyl protecting groups at the C-2 position to control the stereochemistry of the glycosylation, we therefore decided to investigate a thioethyl galactoside donor **4.15** (**Figure 4. 16**). Thioethyl based donors are known to be more than twice as reactive as glycosyl donors than their thiophenyl analogues.¹⁸⁴

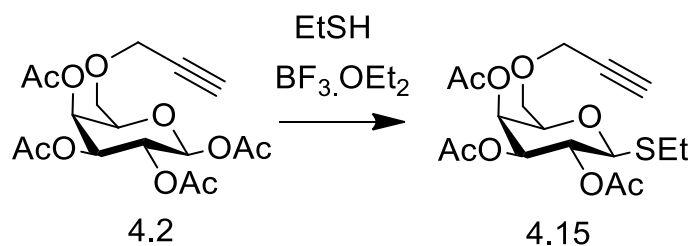
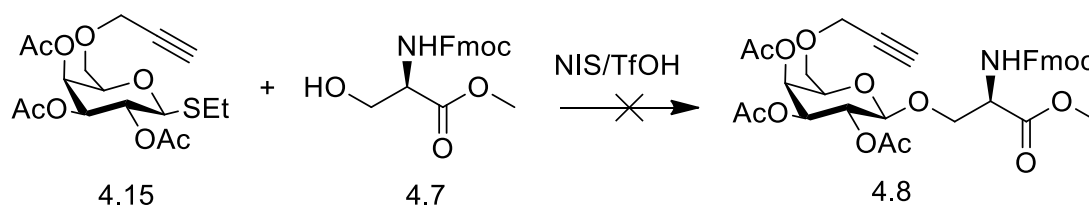


Figure 4. 16. Reagents and conditions: EtSH, BF₃.OEt₂, 0-25 °C, 45%

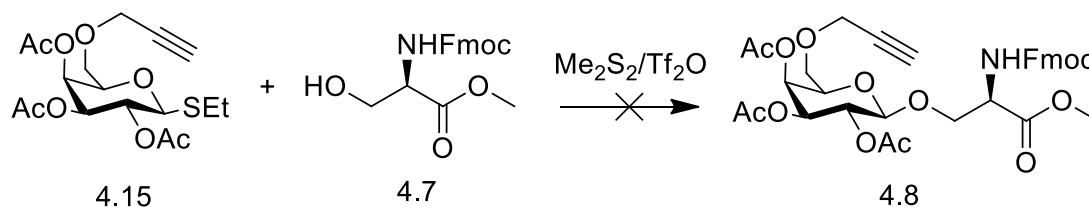
The synthesis of the thioethyl donor presented significant difficulty. Standard glycosylation conditions using BF₃.OEt₂ or SnCl₄ produced only very small amounts of the intended product **4.15** when **4.2** was reacted with thioethanol, even with prolonged reaction times and activation of the donor at room temperature. The majority of the material recovered was the unreacted acetyl donor **4.2** which suggests that the activation of the anomeric acetyl was being inhibited by the presence of thioethanol in the reaction mixture, most likely by the formation of a BF₃.SEt adduct which is unreactive towards **4.2**. After extensive optimization, a pre-activation protocol was developed. This entails the activation of **4.2** by the slow addition of a 50% solution of BF₃.Et₂O in DCM at 0 °C over 15 mins and stirring for a further 15 mins to ensure the activation of the anomeric acetate. Thiophenol is then added dropwise over 15 min and the reaction is allowed to warm to room temperature and stir overnight. This protocol was able to effect complete reaction of **4.2** however, the reaction did produce significant amounts of by-products which presented challenges during purification. Using this method, thioethyl galactoside **4.15** was successfully obtained in a moderate yield of 45%.

4.15 was then reacted with *N*-Fmoc-L-serine methyl ester **4.7** using the NIS/TfOH activating system. As with the thiophenyl derived donor **4.11**, no product could be recovered from the reaction (**Scheme 4. 12**). Unlike the reactions using **4.11**, very little of the unreacted donor was recovered indicating that the thioethyl donor was indeed more active.

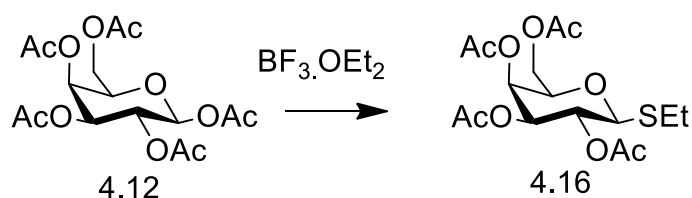


Scheme 4. 12. Reagents and conditions: NIS/TfOH, 0-25 °C, No product recovered.

The reaction was studied using the $\text{Me}_2\text{S}_2/\text{Tf}_2\text{O}$ promotor system and analysis of the reaction crude showed more promise; the intended glycoside **4.8** could be observed by mass spectroscopy and complete activation of the donor was observed by TLC analysis. Despite extensive efforts to optimize the reaction further, the target molecule could only be generated in trace amounts. Increasing reaction time lead to the generation of dehydroalanine **4.10**, likely caused by either the reaction of residual Tf_2O with the N-Fmoc-L-serine methyl ester **4.7** to promote elimination or the direct reaction of the hydroxyl group of **4.7** with the activated sulfonium present in the reaction promotor solution. A reaction utilizing first the $\text{Me}_2\text{S}_2/\text{Tf}_2\text{O}$ activator system followed by the later addition of NIS/TfOH was performed to see if a mixed activator strategy would show more success, however this did not yield any improvement over either activation strategy in isolation (**Scheme 4. 13**).



Scheme 4. 13. Reagents and conditions: $\text{Me}_2\text{S}_2/\text{Tf}_2\text{O}$, 0 °C or -42 °C, no product recovered.

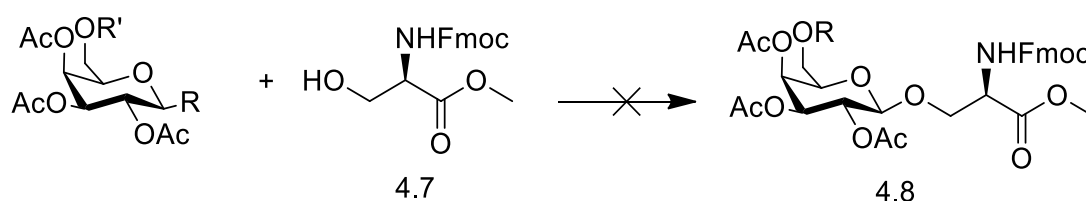


Scheme 4. 14. Reagents and conditions: Thioethanol, $\text{BF}_3 \cdot \text{OEt}_2$, 0-25 °C, 92%

As with previous investigations, the reaction with a peracetylated thiopethyl galactose donor lacking the alkyne functionality at the C-6 position was also

investigated (Donor **4.16**, **Scheme 4. 14**).¹⁸⁵ These studies however, did not reveal any improved outcome over the reactions utilizing **4.12**.

The attempted glycosylation studies of **4.7** are summarized in **Table 5. 1**. It became evident that the primary problem lay not with the reactivity of the galactosyl donor, but with the poor reactivity of the *N*-Fmoc-L-serine methyl ester acceptor **4.7**. The poor nucleophilicity of the serine hydroxyl group is caused by the hydrogen bond with the nitrogen of the carbamate group. This hydrogen bond severely hampers its reactivity even when reacted with thioethyl donors utilizing the strong glycosylation promotor system of Me₂S₂/Tf₂O.



Scheme 4. 15. Attempted routes to **4.8**.

R	R'	Activation	Outcome
OAc	Ac (4.12) CH ₂ C≡CH (4.2)	BF ₃ .OEt ₂	No product recovered. Acyl migration and elimination observed.
OAc	Ac (4.12) CH ₂ C≡CH (4.2)	SnCl ₄	No product recovered. Elimination observed.
SPh	Ac (4.13) CH ₂ C≡CH (4.11)	NIS/ TfOH	No product recovered.
SPh	Ac (4.13) CH ₂ C≡CH (4.11)	Me ₂ S ₂ / Tf ₂ O	No product recovered.
SEt	Ac (4.16) CH ₂ C≡CH (4.15)	NIS/ TfOH	No product recovered.
SEt	Ac (4.16) CH ₂ C≡CH (4.15)	Me ₂ S ₂ / Tf ₂ O	Trace conversion observed. Elimination observed.

Table 5. 1. Summary of *N*-Fmoc-L-Serine Methyl Ester Glycosylation Studies

The use of this acceptor is further complicated by the acidity of the α -hydrogen of the molecule. Due to the presence of the electron withdrawing methyl ester and the Fmoc carbamate groups, the proton is readily deprotonated which allows for the elimination of the hydroxyl group when it is activated by either a Lewis acid or an electrophile, both of which are utilized for the activation of acetyl, thiophenyl and thioethyl donors. The substitution of the Fmoc protecting group was considered but carbamate groups such as Boc or Cbz are also electron withdrawing and likely to allow the elimination reaction to proceed. Less electron withdrawing groups such as Bn or Tr were also contemplated but given the difficulty in removal that these groups can present, it was decided to abandon the pursuit the *N*-Fmoc-L-serine methyl ester galactoside.

4.3.2 Investigations into the Synthesis of a 1, 2, 3-Triazolyl-Ethylene Derived Macrocycle

Given the problems encountered with the glycosylation of *N*-Fmoc-L-serine methyl ester discussed above, it was decided to simplify the glycosyl acceptor in the hopes that this would be more amenable to glycosylation. To this end, we decided to use 2-azidoethanol as it would generate the same 12-membered sized macrocyclic ring, but it lacks the functional groups that reduce the nucleophilicity of *N*-Fmoc-L-serine methyl ester in glycosylation reactions. Furthermore, the use of the azide functionality on the molecule does not require the use of electron withdrawing protecting groups which reduces the likelihood of an elimination reaction occurring, particularly when the electron withdrawing ester group is also absent. Our new target therefore became **4.1b** (Figure 4. 17).

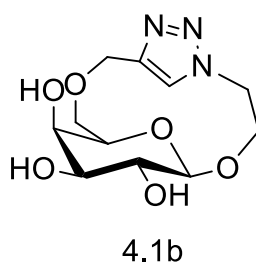
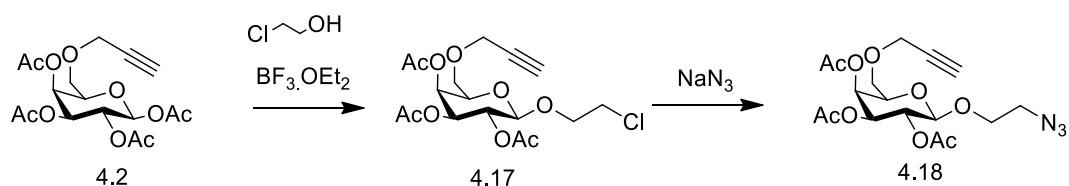


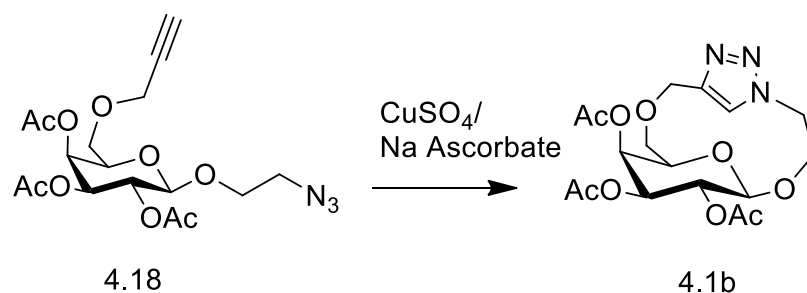
Figure 4. 17. Azidoethanol derived macrocycle **4.1b**.

4.3.2.1 CuAAC Macrocyclization Approach (Route A)



Scheme 4. 16. Reagents and conditions: 1) $\text{BF}_3 \cdot \text{OEt}_2$, 2-chloroethanol, 0-25 °C, 49%, 2) NaN_3 , 80°C, 83%

Acetylated donor **4.2** was glycosylated with 2-chloroethanol in DCM using a 50% solution of $\text{BF}_3 \cdot \text{OEt}_2$ in DCM. Following purification, this yielded **4.17** stereospecifically as the β -anomer in a moderate yield of 49%. This was then subjected to azide-halide exchange (**Scheme 4. 16**). **4.17** was reacted in DMF for 2 days at 80 °C in order to achieve sufficient conversion of the starting material to yield the product with a yield of 83%. This reaction is typically carried out at higher temperatures and frequently utilizes catalytic iodide. However these conditions were not used in order to avoid the possibility of a thermally promoted Huisgen cycloaddition which can occur at temperatures of 100 °C and above.¹⁸⁶



Scheme 4. 17. Reagents and conditions: Sodium Ascorbate, CuSO_4 .

With the azide/alkyne precursor **4.18** in hand, the cyclization of the compound was performed. This was carried out using $\text{CuSO}_4 \cdot 5\text{H}_2\text{O}$ / sodium ascorbate as the reaction catalyst (**Scheme 4. 17**). Pseudo-high dilution conditions were used and the substrate **4.18** (0.025M solution in MeCN) was added dropwise (approximately one drop every 5 seconds) to the solution of catalyst and reaction was allowed to stir at room temperature for 10 days before being worked up. Analysis of the crude mixture by TLC proved impossible, as the products were strongly retained by the TLC plate. However, conversion of the starting glycoside **4.18** was complete as determined by

TLC analysis. Attempts to purify the compound by crystallization, trituration or chromatography in strongly eluting mobile phases proved unsuccessful.

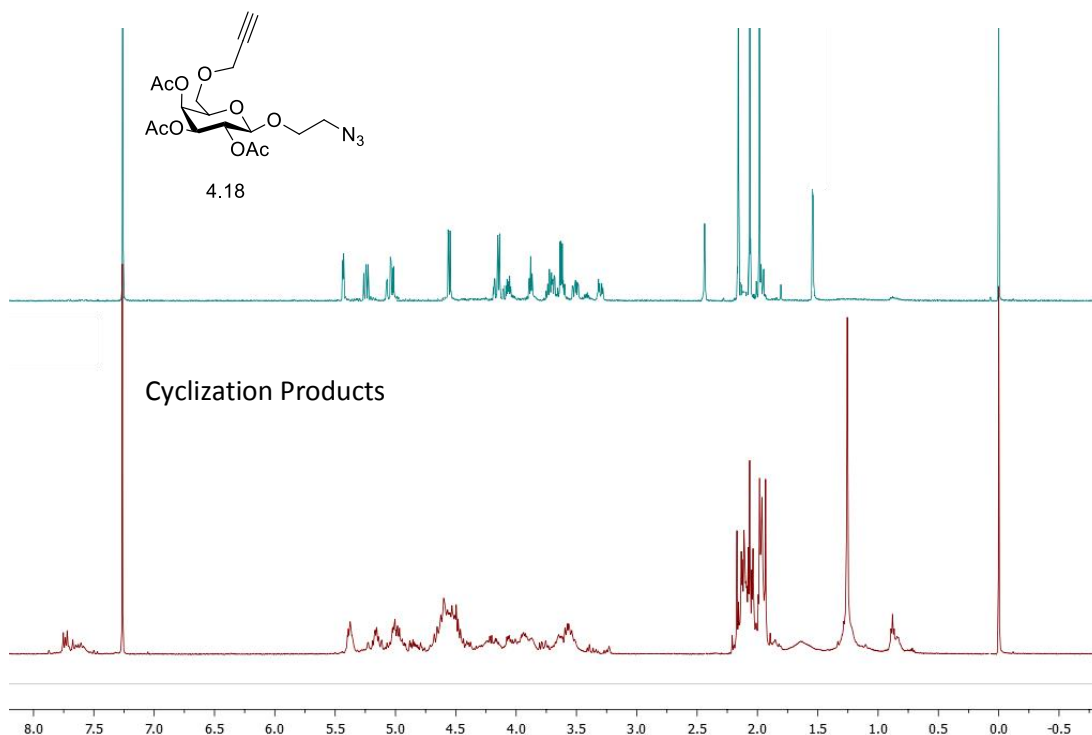


Figure 4.18. ¹H NMR spectra of **4.18** (blue) and the products of the cyclization reaction (red).

The ¹H NMR spectrum of the reaction crude is quite poorly resolved with broad signals compared to that of **4.18** (Figure 4.18). This is likely due to the mixture of compounds present in the sample. The 7.5-7.8 ppm region shows a large number of new peaks corresponding to triazole C-H signals which clearly demonstrates that a number of products was formed during the reaction. A range of ¹³C spectra, homo/heteronuclear 2D experiments, ¹H decoupled experiments and DOSY NMR experiments were carried out in an effort to try and elucidate the nature and number of species present in the sample but these did not provide any data that could determine the products generated with any degree of certainty.

From the mass spectrum obtained from the crude reaction product, it is clear that a mixture of products had formed (Figure 4.19). Strong signals corresponding to the monomeric product (**4.1b**, [M+Na]⁺: 436.134 m/z), dimer (**4.19**, [2M+H]⁺: 827.294 m/z), trimer (**4.20**, [3M+2H]²⁺: 620.725 m/z) and pentamer (**4.21**, [5M+2H]²⁺: 1034.366 m/z), which could be present as cyclic or open chain oligomers, are clearly

observable. This indicates that the formation of the monomeric macrocycle is not highly favourable, even under the highly dilute conditions used.

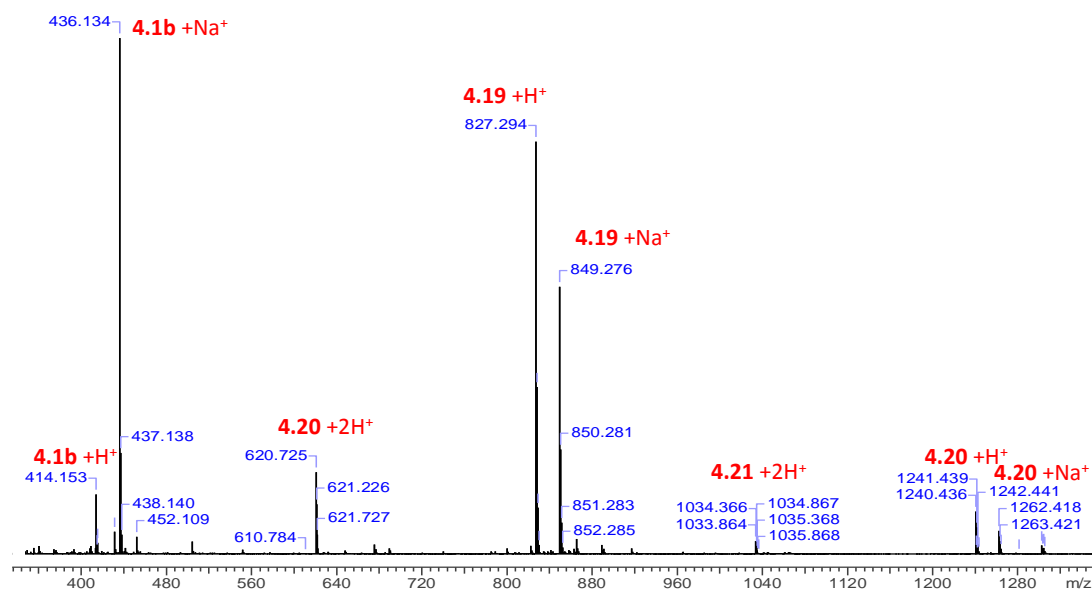


Figure 4. 19. ESI+ mass spectrum of cyclization crude.

To confirm that the observed base peak was the monomeric macrocycle and not a dimer+2H⁺ signal, we inspected the isotopic distribution (**Figure 4. 20**). This can be used to identify signals which correspond to dimeric and trimeric products which generate the same mass as the monomer when their charge is equal to the number of monomer units which make up the molecule. When a dimer is present, a signal with a m/z of [M+X⁺] +0.502 is expected, due to the presence of a single ¹³C atom in place of a ¹²C in the molecule.^{187, 188}

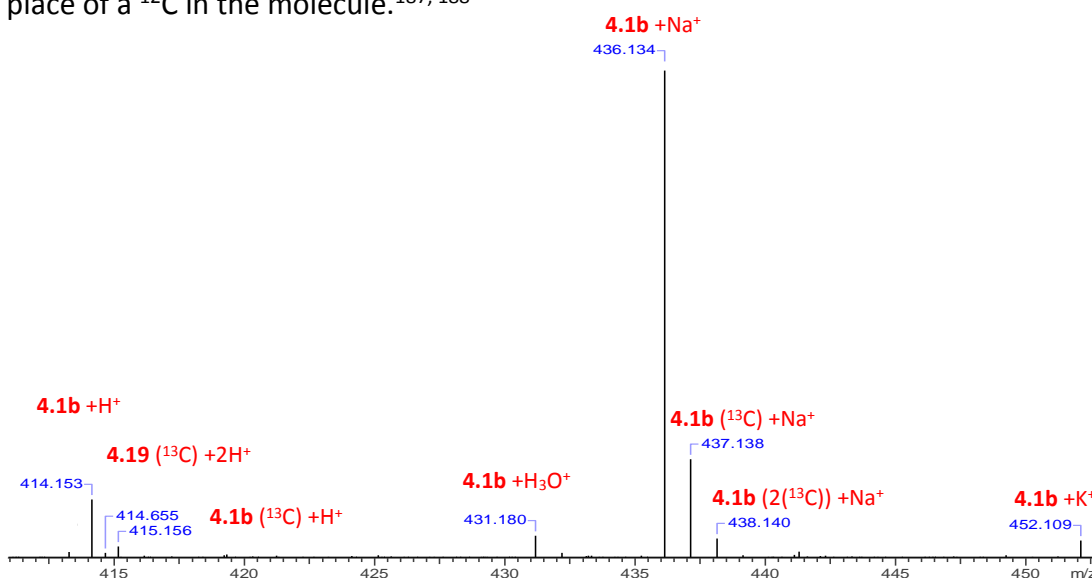


Figure 4. 20. ESI+ mass spectrum of cyclization crude, 410-455 m/z range.

From this data, we can see that a signal corresponding to $[4.1b+H^+] +0.502$ is present at 414.655 m/z, indicating the presence of dimer **4.19** +2H⁺. This value means that we cannot accept the m/z value of 414.153 as conclusive evidence of the monomer as this could also indicate **4.19**+2H⁺. However, analysis of the more abundant Na⁺ adduct does not show an ion corresponding to $[4.1b+Na^+] +0.502$. This isotope pattern provides definitive proof that a mass corresponding to the monomeric macrocycle is present in the sample. As the **4.18** is not observable by TLC or NMR, we can be confident that this is indeed the macrocyclic product and not unreacted starting material.

Inspection of the 826-860 m/z range of the spectrum yields similar results (**Figure 4. 21**). The proton adducts of the dimer **4.19** also show the presence of a peak with a m/z value of $[4.19+H^+] +0.502$, indicating the that a tetramer, **4.22**, is present in the product. The K⁺ adduct is present also but does not show a signal corresponding to $[4.19+K^+] +0.502$ so we can conclude that the dimer **4.19** is present.

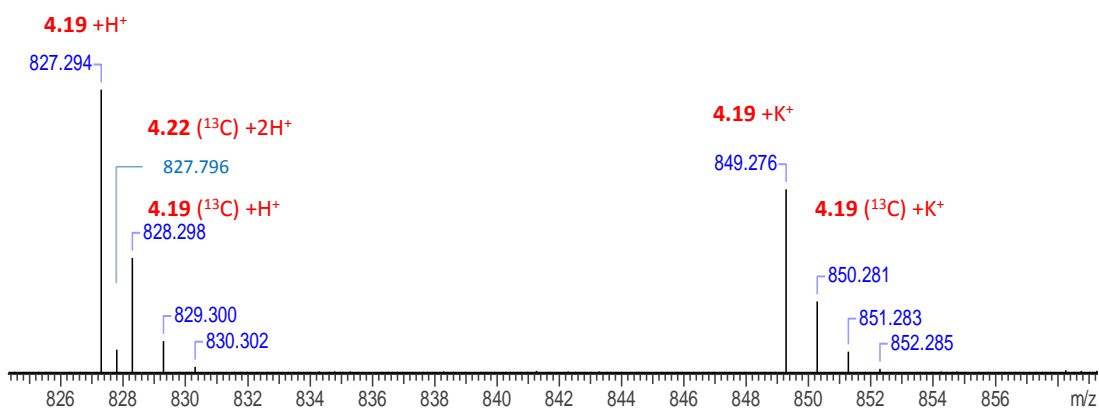


Figure 4. 21. ESI+ mass spectrum of cyclization crude, 826-860 m/z range.

A similar analysis of the 1033-1038 m/z range indicates the presence of the pentameric product **4.21** in the reaction mixture. While the monocationic adducts of **4.21** are too large to be observable in the mass range studied, the formation of this compound can be determined by the observation of dicationic fragments seen in this m/z region (**Figure 4. 22**). This shows the expected masses of the diprotic adduct and the diprotic adduct of a molecule containing an atom of ¹³C. Interestingly, it also

shows a m/z of $[4.21+H^+] + 0.502$, thus showing that decamer has formed during the reaction.

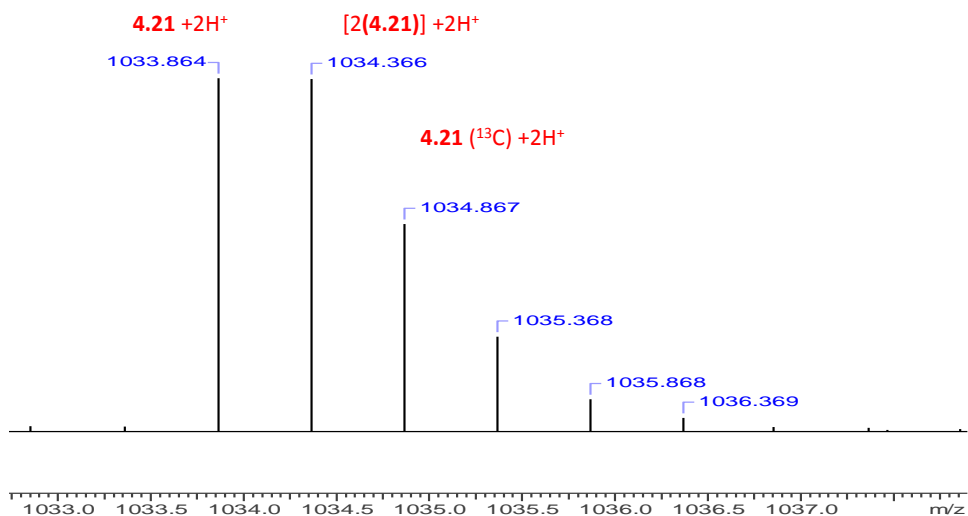


Figure 4. 22. ESI+ mass spectrum of **4.16**, 1033-1038 m/z range.

Finally, the upper range of the spectrum was analysed to glean more information about the compounds produced during the reaction (**Figure 4. 23**). Similar to the other ions studied, the protic adducts of the trimer **4.20** show the presence of a compound with m/z of $[4.20+H^+] + 0.502$, indicating that a hexamer is present.

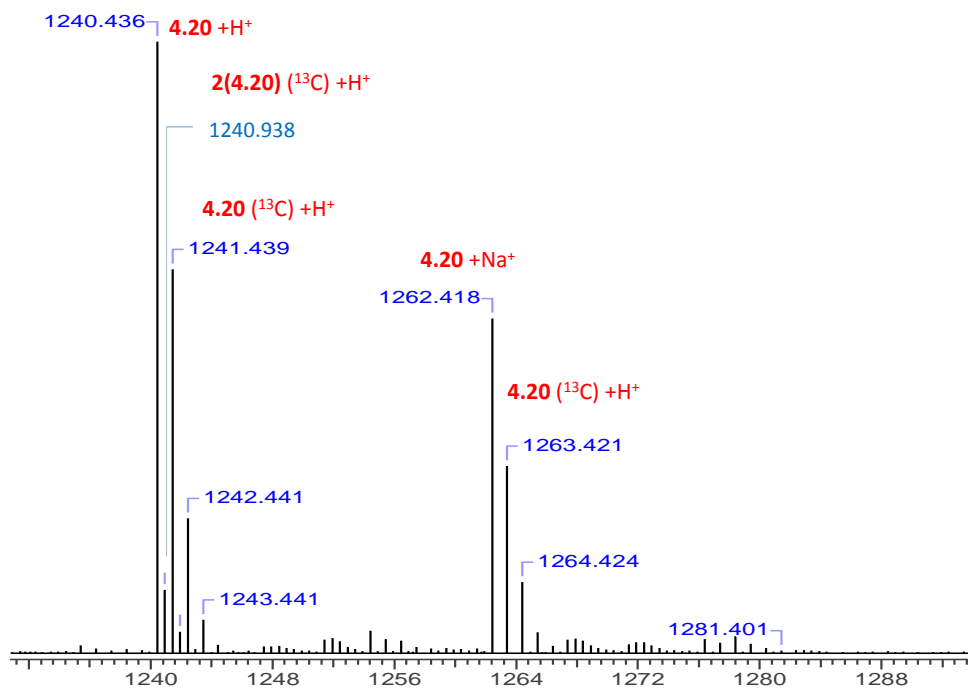


Figure 4. 23. ESI+ mass spectrum of cyclization crude, 1230-1330 m/z range.

This mass spectral data, together with the NMR data, shows that this route to the macrocycle is highly problematic. The abundance of oligomeric products observed

show that this route does not favour the formation of the desired monomeric macrocycle. A closer evaluation of the mechanism of the reaction can be used to explain this (**Figure 4. 24**).

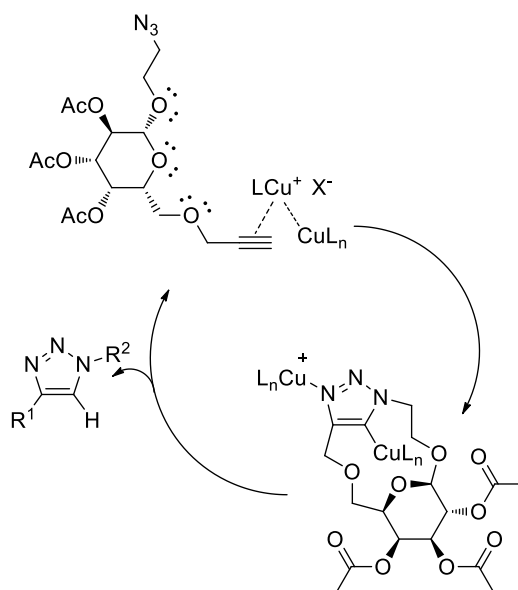


Figure 4. 24. Mechanism for the formation of **4.16**. Reagents and conditions: **4.18**, $\text{CuSO}_4 \cdot 6\text{H}_2\text{O}$, sodium ascorbate.

The formation of a dicopper species is necessary for the cycloaddition to occur. As can be seen from **Figure 4. 24**, this would place one of the copper atoms, together with its inner sphere ligands, inside the cavity of the macrocycle. While some stabilization may occur from the interactions between the Cu(I) ion and the lone pairs present on the oxygen atoms of the ring, it is likely that the steric bulk of the copper complex would disfavour the ring closing in such a manner and would instead form the larger oligomers observed in the mass spectrum of the reaction product.

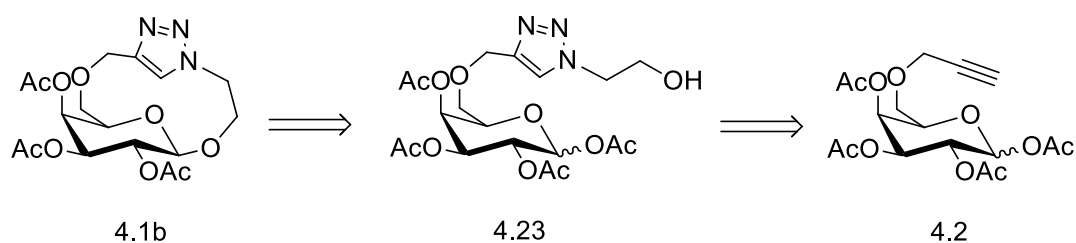
In addition to the steric effects preventing the intramolecular closure of the ring, there are electronic effects that must be considered. The macrocyclic ring has three oxygen atoms, two of which are bonded to the same carbon atom, and these each bear lone pairs of electrons (**Figure 4. 24**). Each of these oxygen atoms possesses a dipole moment associated with this electron density and this causes electronic repulsion between these groups. This repulsion would likely raise the energy of a conformation in which the azide and alkyne groups are in close enough proximity to react in an intramolecular manner, especially considering that the reaction was carried out at room temperature.

The data presented above is taken from a single macrocyclization reaction. Attempts were made to obtain the target macrocycle by varying the solvent and catalyst loadings however these did not produce any significant change in the outcome of the reaction.

4.3.2.2 Intramolecular Glycosylation Route (Route B)

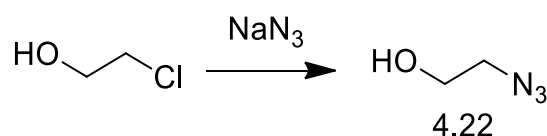
Owing to these difficulties, we decided to explore alternative strategies to obtain the target macrocycle. We also decided to investigate the feasibility of using an intramolecular glycosylation reaction to form the macrocyclic ring (**Scheme 4. 18**).

4.3.2.2.1 Studies Using Acetyl Donor 4.23



Scheme 4. 18. Route to macrocycle using a ring closing glycosylation.

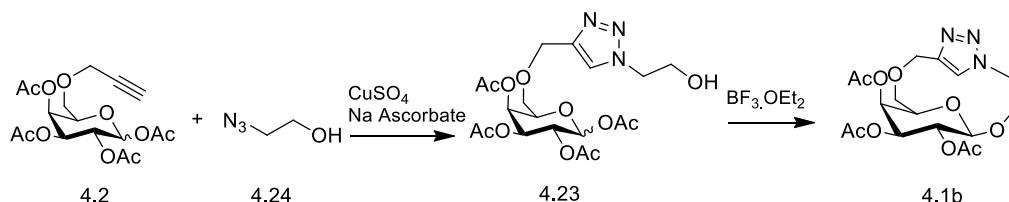
The initial attempts used acetyl galactosyl donor **4.2**. This was first reacted with 2-azidoethanol to generate the triazole- alcohol compound **4.23** which could then take part in an intramolecular glycosylation reaction to give the target **4.1b** (**Scheme 4. 18**).



Scheme 4. 19. Reagents and conditions: Sodium azide, 80 °C, 48 h, 3.07 g.¹⁸⁹

2-azidoethanol **4.22** was generated from the reaction of 2-chloroethanol with sodium azide in refluxing water for 2 days (**Scheme 4. 19**). Despite longer reaction times, full conversion of chloride to the azide derivative could not be achieved. This could be explained by the volatile nature of 2-chloroethanol which means that a fraction would be in the vapour phase and therefore unable to react with the aqueous azide solution. Due to the explosive nature of low molecular weight azides,

it was decided to avoid distilling the reaction mixture and instead use the mixture of compounds for the next reaction as 2-chloroethanol will not participate in the CuAAC reaction. The unreacted 2-chloroethanol was then safely removed by high vacuum upon completion of the reaction.



Scheme 4. 20. Reagents and conditions: CuSO₄/ Sodium Ascorbate, 96 %, 2) BF₃.OEt₂, 0-25 °C, 81% based on recovered material.

2-azidoethanol was then reacted with **4.2** utilizing catalytic CuSO₄.5H₂O and sodium ascorbate to promote the cycloaddition between the azide and alkyne. The reaction went smoothly with the total conversion of the starting material observed by TLC. As was observed with the previously studied triazole compounds, the product **4.23** showed an R_f value of 0 in TLC unless extremely polar eluents were used, such as 70% MeOH in DCM with triethylamine. In these cases, extreme streaking on the plate was observed. This prevented the separation by column chromatography of the α and β-anomers present in the CuAAC product, as the starting material contained both the α and β-anomeric acetyl group. Attempts to isolate the β-anomer by crystallization were unsuccessful.

With the triazole precursor **4.23** in hand, we attempted the synthesis of the macrocycle by intramolecular glycosylation. The reaction was carried out under pseudo-high dilution conditions by the dropwise addition of the substrate to a solution of BF₃.OEt₂. A 0.042 M solution of **4.23** in DCM was added dropwise at a rate of approximately 0.05 ml/min to a 0.21 M solution of 3 equivalents of BF₃.OEt₂ in DCM at 0 °C under anhydrous conditions and was stirred for 48 h. This produced a complex mixture of products which, as with previous efforts to synthesize the macrocycle, proved to be inseparable by chromatography. Attempts to purify the mixture by trituration and crystallization were also unsuccessful.

Analysis of the ^1H NMR spectrum of the reaction crude clearly indicates the presence of multiple products in the sample which complicates the analysis, however, it does reveal significant information about the outcome of the reaction. The $\text{H}_{\beta-1}$ of the acetyl donor **4.23** can be seen as a doublet at 5.65 ppm in (Figure 4. 25). In the reaction crude, this peak has almost entirely disappeared, indicating that a small amount of the starting material was not activated during the reaction. Most importantly however, are the new peaks in the 7.5-7.8 ppm region which correspond to the triazolyl C-H signal. This presents as a single sharp peak in **4.23** at 7.62 ppm whereas the spectrum of the reaction crude shows at least 5 poorly defined peaks indicative of a mixture of species. While one of these can be attributed to the starting material **4.21**, the nature of the rest cannot be determined. The signals which occur upfield from this region are poorly defined and cannot be assigned with any confidence. Analysis of the ^{13}C spectra, homo/heteronuclear 2D experiments, ^1H decoupled experiments and DOSY NMR suggested some tentative assignments, however, no information into the precise structure of the compounds present could be determined with any degree of certainty.

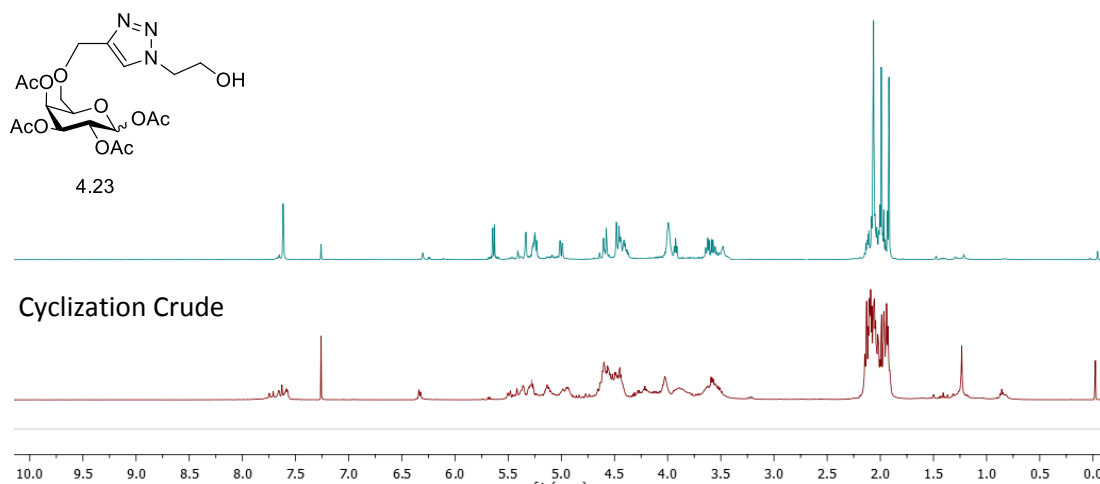


Figure 4. 25. ^1H NMR of **4.23** (blue) and the cyclization crude (red).

Analysis of the mass spectrum of the reaction crude shows an m/z signal corresponding to **4.1b** which confirms the formation of the desired macrocycle. Only trace amounts of dimer and trimer could be observed in the mass spectrum of the compound with a total ion counts of 0.3% and 0.1% respectively (Figure 4. 26).

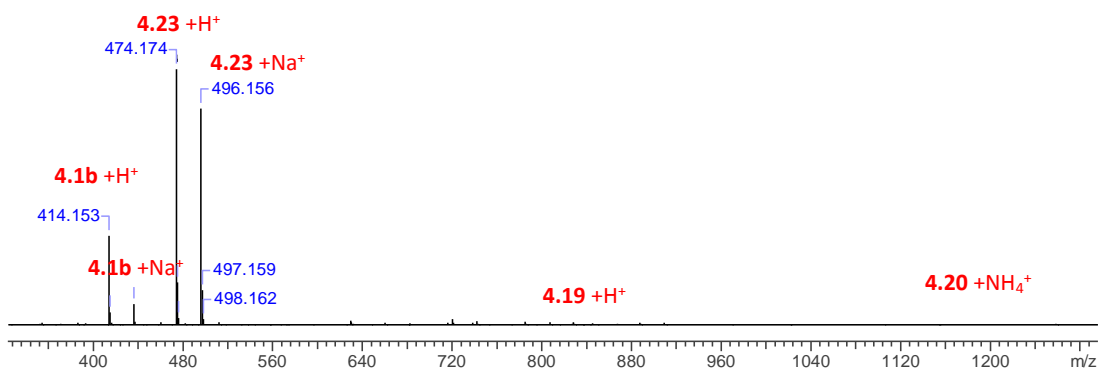


Figure 4. 26. ESI+ mass spectrum of the intramolecular glycosylation crude.

To confirm that the observed base peak was the monomeric macrocycle and not a dimer+2H⁺ signal, we inspected the isotopic distribution as before. No signal corresponding to a m/z of M+ 0.5017 was detected in the spectra and we can therefore be confident that the desired macrocycle was formed (**Figure 4. 27**).

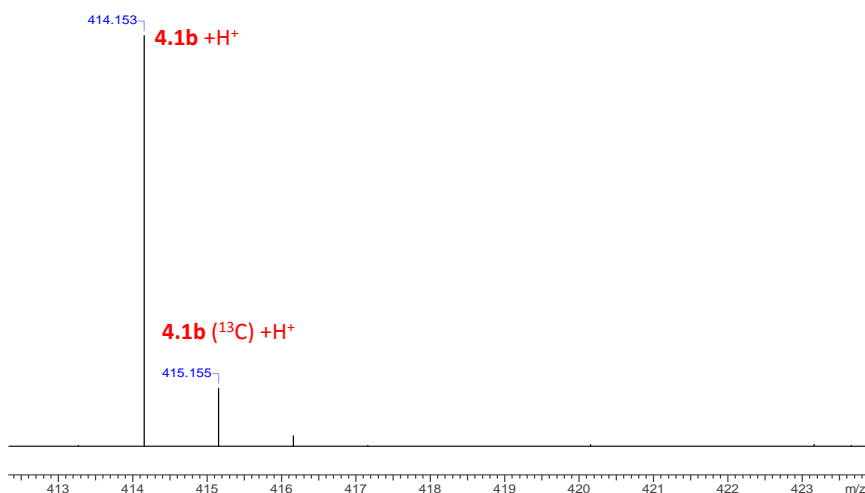


Figure 4. 27. ESI+ mass spectrum of intramolecular glycosylation crude, 423-423 m/z range.

The complicated spectrum could arise not just from the presence of a mixture of monomer, dimer, trimer and starting material, it is also possible that different conformers of the monomer could be present in the mixture. It was hypothesized that due to the rigidity of the monomeric macrocycle, multiple conformations could be formed which could be conformationally locked at room temperature due to the small cavity which could restrict rotation.

In order to investigate this, we undertook variable temperature NMR studies. At high temperatures, the macrocycle would have enough energy to convert between different conformations, thus any possible conformers would appear equivalent and

the signals corresponding to different conformations would coalesce into a single peak. Conversely, at lower temperatures the signals should appear more defined as intermolecular collisions are reduced and each conformer should be locked in its lowest energy state. We therefore examined the NMR spectra of the mixture at 40 °C and -60°C (**Figure 4. 28**). These appeared to be almost identical and therefore we can conclude that this hypothesis is incorrect.

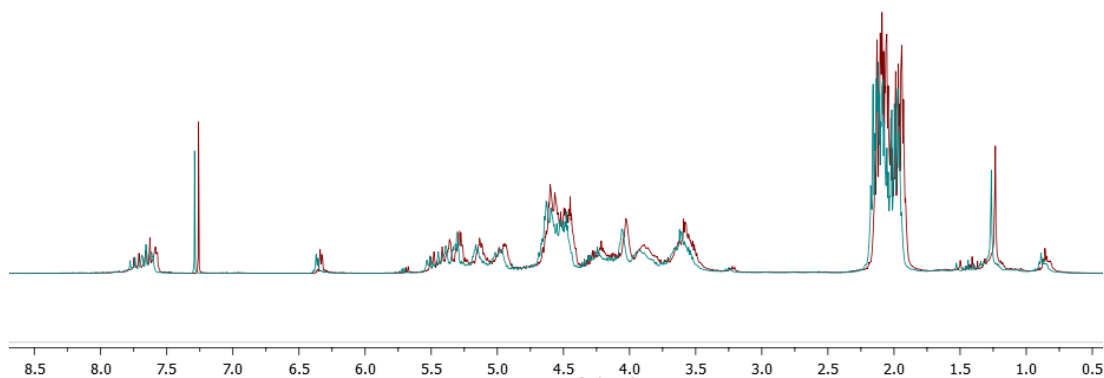
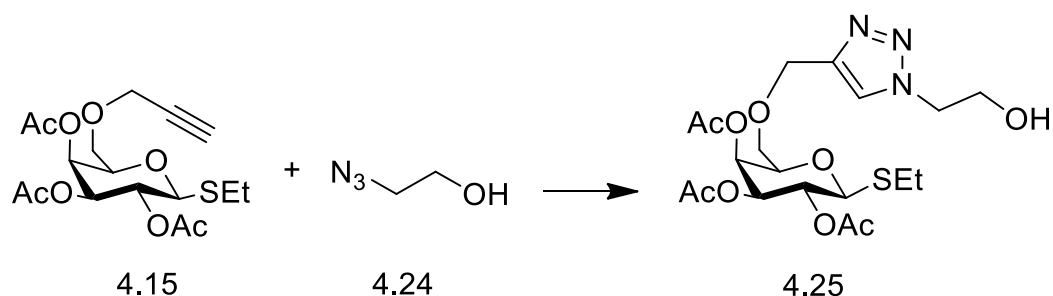


Figure 4. 28. ^1H NMR spectra of **4.16** at 40 °C (red) and -60°C (blue).

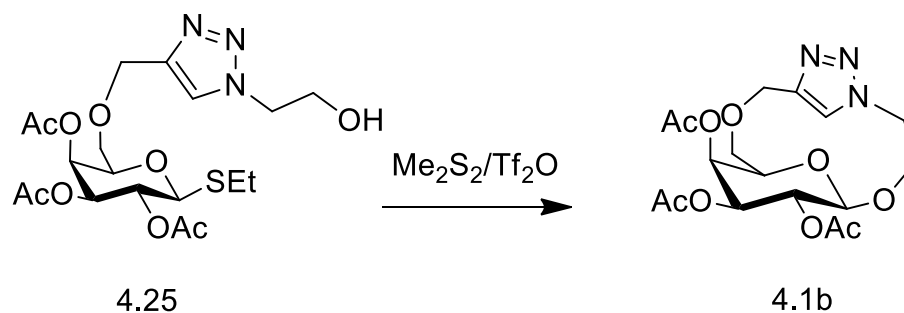
This route showed great promise as far fewer oligomeric products were produced than the previously studied CuAAC Route A. However, the reaction still produced a number of different compounds and did not go entirely to completion. In an effort to investigate whether or not a more active donor would give a cleaner reaction, we decided to study the same ring closing glycosylation route using a thiogalactoside donor. To this end, we investigated the thioethyl donor **4.12** as a coupling substrate for macrocyclization.

4.3.2.2.2 Thioglycoside Donor



Scheme 4. 21. Reagents and conditions: CuSO_4 , Na ascorbate, 96 %

As with the analogous acetyl donor, **4.15** was reacted with 2-azidoethanol using catalytic $\text{CuSO}_4 \cdot 6\text{H}_2\text{O}$ and sodium ascorbate. This product was also unsuitable for isolation by column chromatography due to high retention to silica, as was observed for the other triazole compounds.



Scheme 4. 22. Reagents and conditions: Me_2S_2 , Tf_2O , -42°C .

Triazole-thiogalactoside **4.25** was then cyclized using the $\text{Me}_2\text{S}_2/\text{Tf}_2\text{O}$ reaction promotor described *vide supra* under pseudo-high dilution conditions at -42°C . As with the acetyl donor **4.23**, a complex mixture of products was formed. These were inseparable by column chromatography, trituration and crystallization.

Comparison of the ^1H NMR spectra of starting material **4.25** and the crude reaction mixture shows a single peak at 7.57 ppm in **4.25** corresponding to the triazole C-H (**Figure 4. 29**). Upon glycosylation, this signal has disappeared and instead becomes a broad signal with at least 4 discernible peaks (**Figure 4. 30**). Similar to the spectra obtained from the cyclization of the acetyl donor **4.23**, the 3-6 ppm region was too poorly resolved due to the overlapping peaks to yield any reliable information into the nature of the products formed. Analysis of the ^{13}C spectra, homo/heteronuclear 2D experiments, ^1H decoupled experiments and DOSY NMR did not present any definitive evidence on the nature or number of the species formed during the reaction. Glycosylation reactions of the macrocycle utilizing higher reaction temperatures such as 0°C did not produce any significant differences in the reaction outcome.

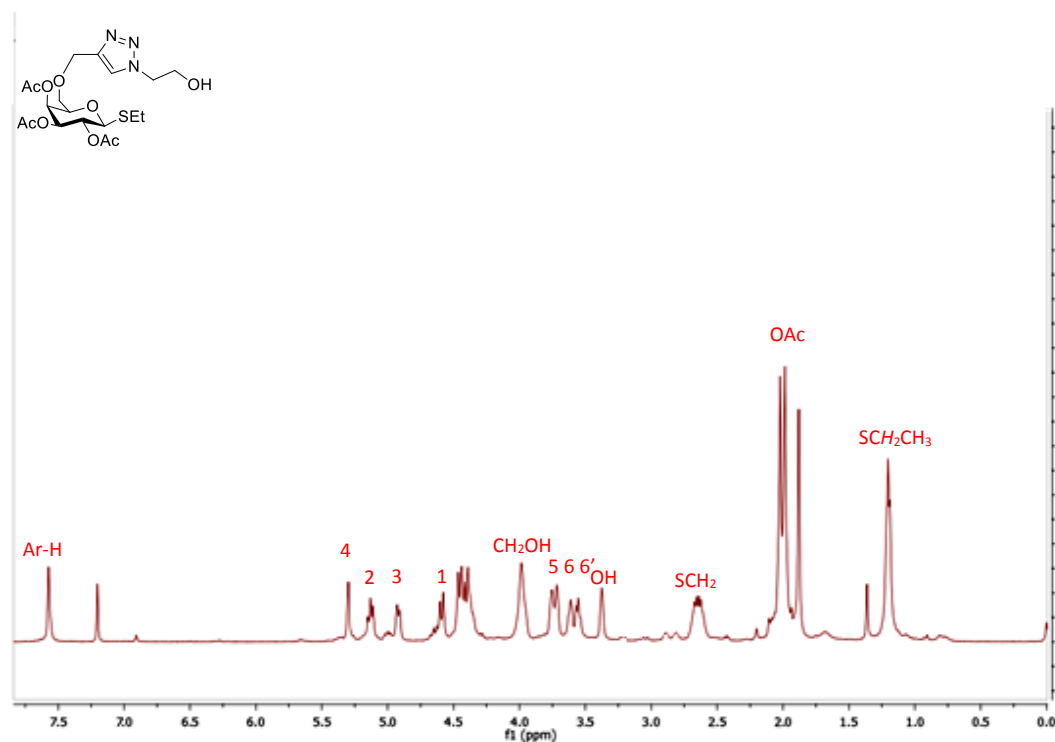


Figure 4. 29. ^1H NMR spectrum of **4.25**

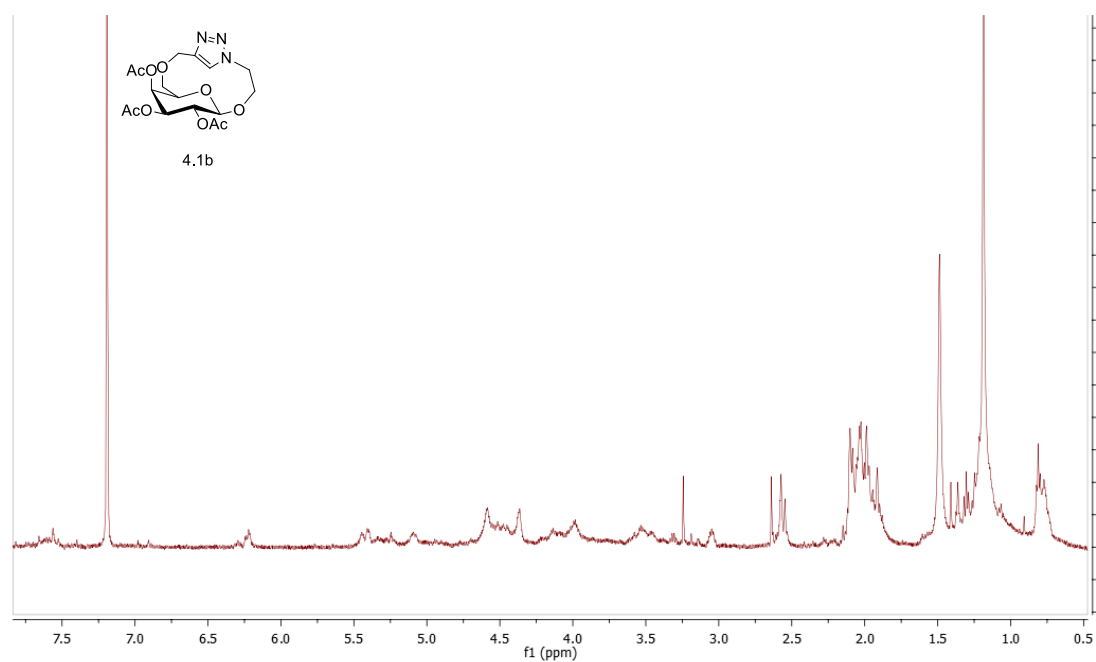


Figure 4. 30. ^1H NMR spectrum of **4.1b** formed by cyclization of **4.25**.

Analysis of the mass spectrum of the reaction crude proved to be more fruitful. From this, we can see that **4.1b** was formed by the m/z peak of 414.152, corresponding to **4.1b** + H^+ (Figure 4. 31). The nature of this signal was determined to be the

monomeric macrocycle and not the dimer+2H⁺ by the absence of a m/z of **4.16**+0.502. Also present in the spectrum is a peak corresponding to **4.19** +K⁺ with an ion count of 21.5% relative to **4.16**. While high molecular weight ions were observed, these did not correspond to the trimeric product **4.20**.

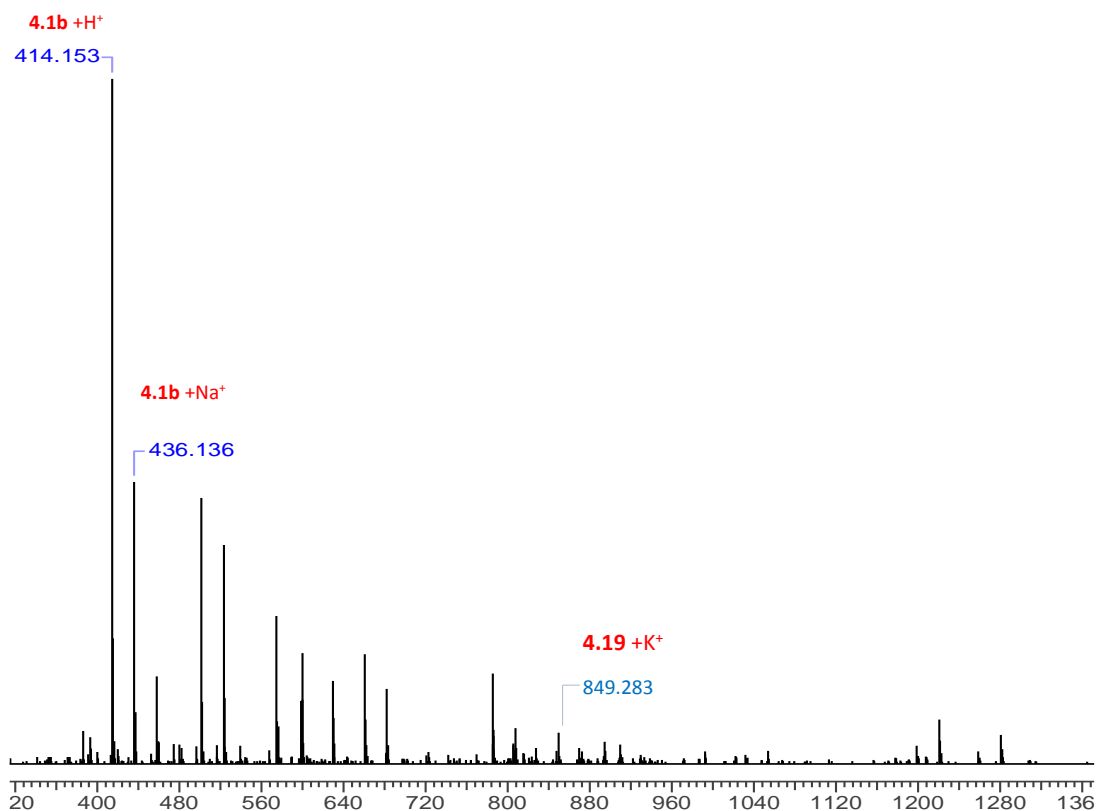
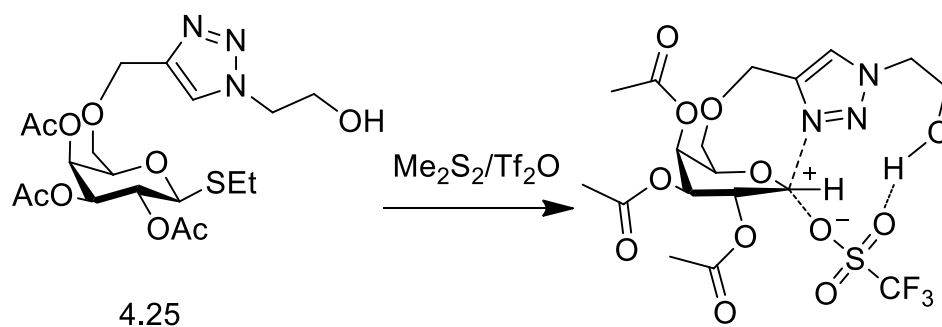


Figure 4. 31. ESI⁺ spectrum of the reaction crude of the intramolecular glycosylation of **4.25**.

The results of these studies suggest that the intramolecular glycosylation could be more favourable for the generation of the monomeric macrocycle. For both donors studied, **4.23** and **4.25**, this route generated far fewer oligomeric products, as determined by HRMS, however a number of reaction products is evident by NMR spectroscopy. This would suggest that it possesses a degree of selectivity for the intramolecular reaction rather than the intermolecular reaction that generates the oligomeric products. An examination of the intermediate generated during the reaction may explain this (**Scheme 4. 23**).



Scheme 4. 23. Proposed intermediate formed during the glycosylation of **4.23**.

Upon the formation of the oxocarbenium ion, the anomeric position adopts a sp^2 geometry which forces the pyranose ring to adopt a 4E envelope conformation.¹⁹⁰ In non-polar solvents, such as DCM, a close contact ion pair (CCIP) is formed between the oxocarbenium ion and the anion, in this case triflate.³ It could be proposed that the electrostatic interactions between the oxocarbenium ion and the triazole N lone pair of electrons acts to tether the chain over the pyran ring. The triflate ion (or acetate in the case of the reaction of **4.23**) could then form a hydrogen bond with the hydroxyl group to bring it in close proximity to the anomeric centre. This hydrogen atom could also hydrogen bond to a second nitrogen present on the triazole ring. With the hydroxyl group tethered in such a fashion in proximity to the anomeric centre, it would favour the intramolecular reaction to a greater degree than the CuAAC route which does not possess any favourable preorganization of the cavity.

4.4 Conclusion

The aim of this chapter was to investigate the synthesis of a conformationally constrained macrocycle built upon a carbohydrate scaffold. Initial investigations into a galactose-serine derived macrocycle did not yield any successful macrocyclization reactions but important information was gained into the reactivity of this system. The disarming nature of acetyl protecting groups is too great to allow the reaction of the galactoside donors with the serine acceptor, even when the thiogalactoside donors were reacted with the strongly activating Me_2S_2/Tf_2O promotor system. A further complication that prevents the synthesis of the target galactoside is the competing elimination reaction to form dehydroalanine ester **4.10**. This occurs in the

presence of Lewis acids such as $\text{BF}_3 \cdot \text{OEt}_2$ and SnCl_4 or electrophiles such as dimethylsulfide-sulfonium triflate generated by the $\text{Me}_2\text{S}_2/\text{Tf}_2\text{O}$ activating system. In order to achieve this target glycoside, less deactivating protecting groups should be used together with a donor group that does not require stoichiometric amounts of Lewis acid or strongly electrophilic reagents to react.

Investigations into the synthesis of a 2-azidoethanol derived macrocycle showed more success. Two routes were explored; Route A used a CuAAC reaction to form the ring and Route B used an intramolecular glycosylation. The studies using the CuAAC presented a wide variety of oligomers formed which suggests that this route does not offer any selectivity for the desired macrocycle. In addition, to the difficulties with the purification of the products and the identical mass of the cyclic and linear species, the presence of the target macrocycle cannot be conclusively proved.

The intramolecular glycosylation route proved to be the most promising route. This present fewer oligomeric products than the CuAAC route as suggested by HRMS analysis and a plausible hypothesis to explain this selectivity is presented. Importantly, this route allows for the unequivocal proof of the existence of the monomeric macrocycle by HRMS which is not possible for the CuAAC route. This work has generated the preliminary synthetic methodology for the successful synthesis of a conformationally constrained 12-membered macrocycle built upon a galactose scaffold. Further work remains, however, for the optimal employment of this strategy and the purification and complete characterization of these macrocyclic structures.

Chapter 5: Investigations into the Fluorescent Properties of Functionalized Imino-Pyridyl Compounds

5.1 Introduction

5.1.1 Fluorescence Spectroscopy

Fluorescence is defined as the emission of light from a compound in an electronically excited singlet state.¹⁹¹ A singlet excited state is one where the excited electron is spin paired to an electron in the ground state. This differs from phosphorescence which involves a triplet excited state, in which the excited electron has the same spin orientation as the unpaired electron in the ground state.

Under standard conditions, a molecule will occupy the lowest vibrational level (v_0) of their ground state electronic configuration (S_0). Upon absorption of a photon of appropriate energy, the molecule is elevated to occupy an excited electronic state ($S_n, n > 0$). For each excited state, there are also a number of vibrational states. After absorbing energy and reaching one of the higher vibrational levels of an excited state, the molecule will then lose vibrational energy and fall to the lowest vibrational level of the excited state. If the molecule occupies an electronic state higher than S_1 , it will undergo internal conversion and pass from the lowest vibrational level of the upper state to a higher vibrational level of a lower excited state without the emission of light. This process will repeat until the lowest vibrational level of the first excited state is reached (S_1, v_0). The relaxation between different excited state species can occur through a number of different processes such as internal conversion, intramolecular charge transfer, molecular collisions and conformational change. Upon reaching the lowest vibrational state of S_1 , it can then return to the ground electronic state S_0 together with the fluorescent emission of light.¹⁹²

Intersystem crossing (ISC) is another possible process that can occur when a molecule is in an excited state. ISC involves a 'forbidden' transition from a singlet excited state to a triplet excited state ($S_n \rightarrow T_n, n > 0$). This triplet excited state can undergo radiative emission upon relaxation to S_0 in a process known as phosphorescence. Phosphorescence is a slow process and typically occurs over timescales of 10^{-3} to 10^3 seconds, this differs significantly from fluorescence which occurs over 10^{-9} to 10^{-7} seconds. Phosphorescence is not usually seen in solution as there are many competing, non-radiative relaxation mechanisms. For this reason, the observed

phosphorescent intensity is typically significantly weaker than fluorescent emission.¹⁹² These various processes can be represented using a Jablonski diagram (Figure 5. 1).¹⁹³

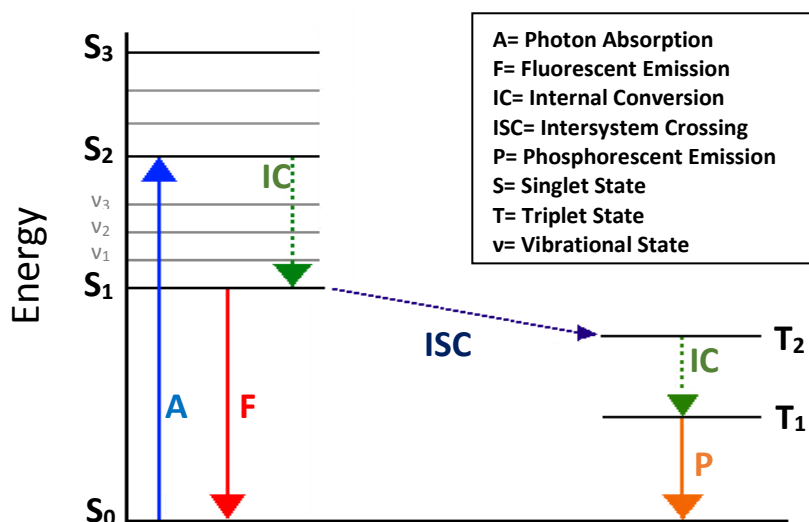


Figure 5. 1. Jablonski diagram depicting the electronic transitions giving rise to absorption, fluorescence and phosphorescence.¹⁹²

The energy of the emitted photon is typically less than that of the absorbed photon, as can be seen from **Figure 5. 1**, and therefore fluorescence occurs at longer wavelengths than the excitation light. This phenomenon was first observed by George Stokes in 1852 and allows for the distinction between the absorbed and emitted photons.¹⁹⁴ The difference between the band maxima of absorption and emission in a spectrum of the same electronic transition in a spectra is known as the Stokes shift in his honour.¹⁹⁵

5.1.2 Structural Attributes of Fluorophores

A fluorophore is a molecule or moiety that can exhibit fluorescence following excitation with light of an appropriate wavelength. These typically contain several fused aromatic rings such as those seen in the common fluorophores fluorescein, pyrene and anthracene. Another structural feature frequently found in fluorophores is a long chain of conjugated double bonds such as those present in cyanine fluorescent dyes (

Figure 5. 2).¹⁹⁵

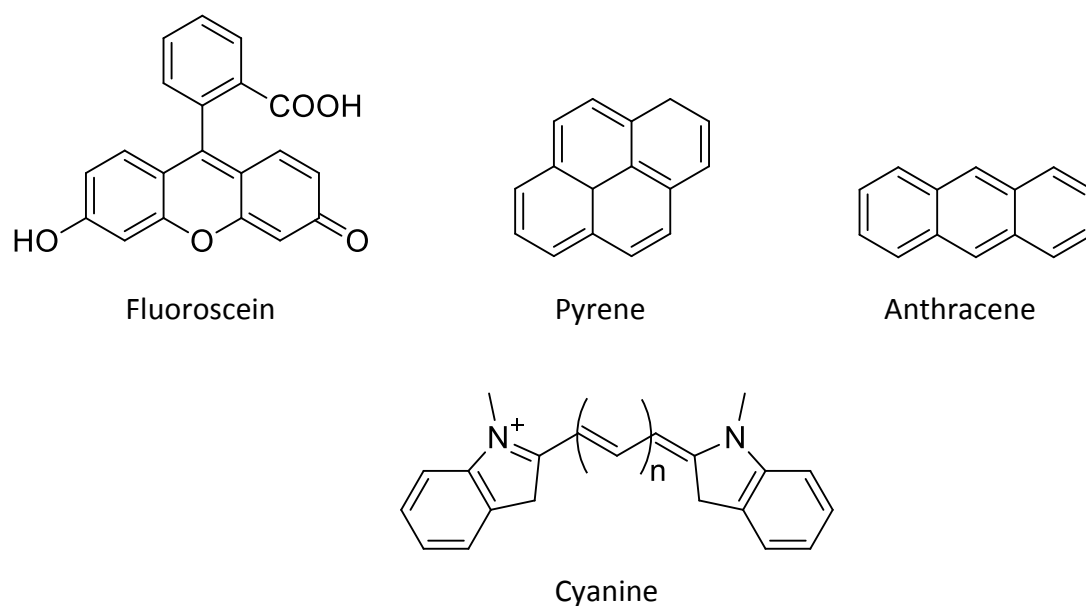


Figure 5. 2. Structures of common fluorophores.

The reason that highly conjugated and aromatic compounds often display fluorescence is due to their electronic structure. By virtue of their large, delocalized HOMO orbitals, these molecules have low lying $\pi \rightarrow \pi^*$ transitions. These transitions are characterized by high molar absorption coefficients and high fluorescent yields. However, when a heteroatom such as O or N is present in the π system, the lowest energy transition may be a $n \rightarrow \pi^*$ transition. The transitions of this type generally have molar absorption coefficients 10^2 lower than $\pi \rightarrow \pi^*$ transitions and have longer radiative lifetimes. Due to these longer radiative lifetimes, the observed fluorescent intensity is generally much lower than $\pi \rightarrow \pi^*$ transitions because of the competing non-radiative relaxation processes that occur. This effect is often observed in pyridine derived fluorophores.¹⁹²

5.1.3 Fluorescent glycosides

Glycosylated fluorophores are an attractive tool for the investigation of a wide variety of biological processes such as glycosidase activity,¹²⁸ antigen binding,¹⁹⁶ and the metabolism of sphingolipids.¹⁹⁷ These approaches take advantage of the low detection limit of fluorescent compounds and the highly sensitive nature of fluorometry to elucidate the details of these processes *in vitro*.

This approach has become a routine method for the analysis of glycohydrolase enzymes. Some of the most common substrates used are glycosides of 4-methylumbelliferyl (**Figure 5. 3**).

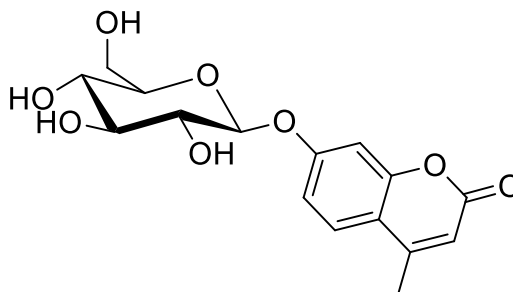


Figure 5. 3. 4-methylumbelliferyl- β -D-glucopyranoside.¹⁹⁸

These offer an improvement over chromogenic substrates such as 4-nitrophenol glycosides as they have a significantly lower limit of detection.¹⁹⁸ This class of fluorescent probes have been commercially available since the 1960's and have been used to identify, characterize and determine the kinetics of a range of glycosides.^{199, 200, 201, 202} 4-methylumbelliferone is released upon hydrolysis of the glycosidic bond of these probes and can be detected by fluorescent spectroscopy. This fluorophore is characterized by an 89 nm Stokes shift and is most effectively detected at basic pH's, as the phenolate is more electron donating and, together with the electron withdrawing lactone, constitutes a 'push-pull' system. Push-pull systems are frequently employed as fluorophores as they undergo intramolecular charge transfer from their neutral to zwitterionic state, a process that involves a low energy HOMO \rightarrow LUMO transition.^{203, 204, 205}

Due to the high pH requirement for the low-level detection of 4-methylumbelliferyl glycosides, researchers have developed fluorophores that retain high fluorescence under acidic conditions. Kaneshiki *et al* synthesized a lysotropic galactoside for the intracellular study of enzymatic activity.²⁰⁶ To this end, they utilized a dicyano-hydroquinonyl unit as the fluorophore of their probe (**Figure 5. 4**).

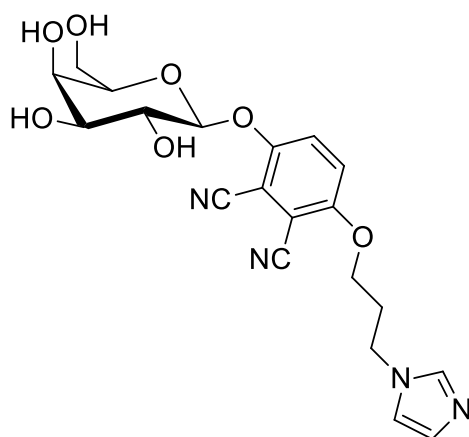


Figure 5. 4. Fluorescent probe synthesized by Kaneski et al.²⁰⁶

They found that this molecule exhibits the same maximum emission wavelength across the entire pH range while the excitation wavelength varied dependent on the protonation state of the phenol, revealed upon hydrolysis of the glycosidic bond. This indicates that emitting excited state is identical for both the phenol and phenolate state of the fluorophore. While the glycoside did show a degree of fluorescence, it was found that this did not occur at the maximum emission wavelength of the aglycon fluorophore. This allows it to be used as a probe for β -galactosidase activity, with the transition of interested showing a Stokes shift of 75 nm. The use of this probe to monitor β -galactosidase activity was validated *in vitro* using human lysosome homogenate.²⁰⁶

Work by the Brumer group has led to the development of resorufin based probes for glycosidase activity (**Figure 5. 5**).²⁰⁷ These were developed to fulfil the need for probes for the direct analysis of endogenous glycoside hydrolases and transglycosidases responsible for cell wall remodelling in plants.

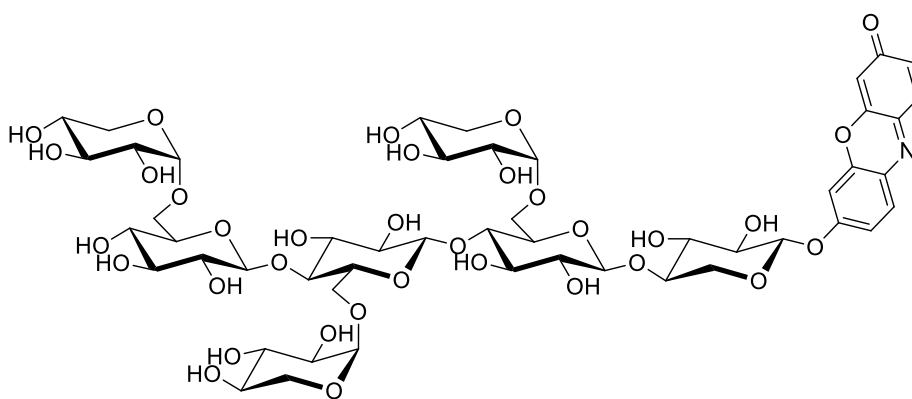


Figure 5. 5. Xylogluco-oligosaccharide probe developed by Brumer et al.²⁰⁷

The group used xylogluco-oligosaccharide, a substrate for xyloglucan endohydrolase, functionalized with resorufin as a fluorescent probe. Upon glucohydrolysis, the resorufin aglycon is released and exists in its deprotonated state in the plant apoplast. Similar to the 4-methylumbelliferone fluorophore, the deprotonated resorufin fluorophore is an example of a push-pull system. This fluorophore has a high fluorescent intensity and a Stokes shift of 14 nm. Importantly, the absorption/emission occurs at relatively long wavelengths of 571/585 nm which are longer than the wavelengths of autofluorescence observed in living tissue (< 400 nm). This makes the probe suitable for use in biological tissue and was successfully used by the group to monitor xyloglucan endohydrolase in plant tissue extracts.

Vocadlo *et al* have recently published a fluorogenic glycoside substrate for imaging glucocerebrosidase activity in living human cells.²⁰⁸ Their probe is initially non-fluorogenic but upon glucohydrolysis it becomes photochemically active. This is due to the design which incorporates a BODIPY fluorophore together with a Black Hole Quencher 2 moiety (**Figure 5. 6**). This group functions to quench the fluorescence of the BODIPY fluorophore by Förster Resonance Energy Transfer (FRET).

FRET occurs when the absorption band of a quenching molecule overlaps with the emission band of a fluorophore. The quenching group therefore absorbs the emitted energy of the fluorophore and disperses it through non-radiative processes, ultimately quenching the fluorescence of the system. This process requires both the emitting and quenching groups to be close to each other, such as this probe where they are appended to the same glucose scaffold. Upon cleavage of the quenching group, it disperses in solution and can no longer quench the fluorescence of the BODIPY fluorophore as it is no longer in close proximity to it.

Using this probe, the group were able to image and monitor the activity of glucocerebrosidase in human cells by the detection of the fluorophore which is rendered active by the activity of the enzyme. This is significant as the study of the activity of this enzyme in the lysosome has proven difficult to date. Given that this enzyme plays a central role in the mechanism of Gaucher's disease, this probe presents an important new tool for the study of the disease.

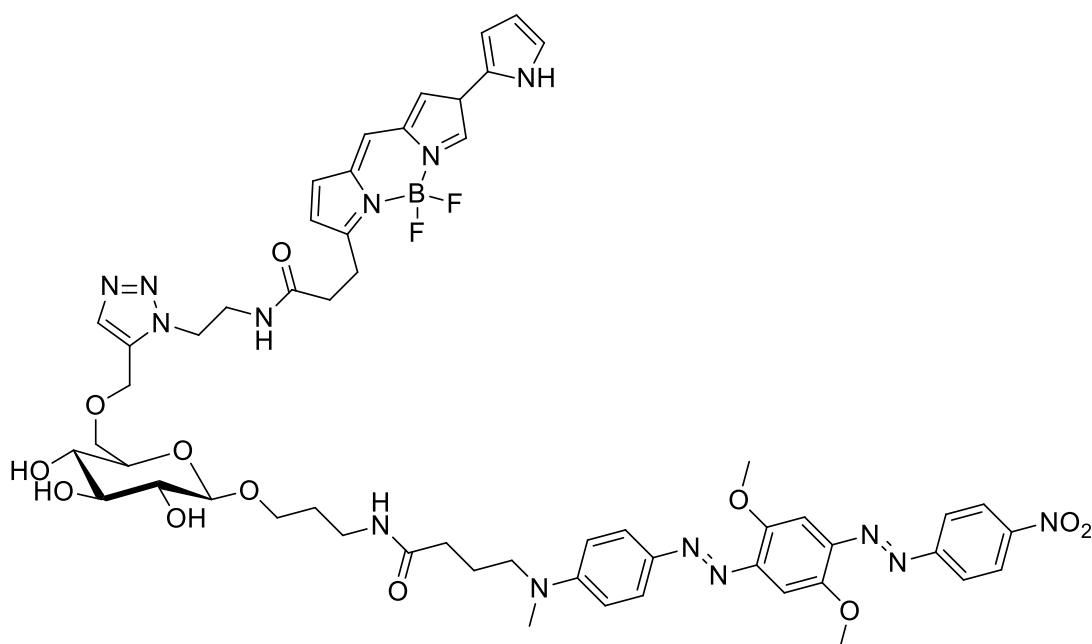


Figure 5. 6. Probe synthesized by Vocadlo *et al.*²⁰⁸

Panza *et al* have investigated the CD1a antigen binding properties using a dansyl-functionalized sulfatide probe.¹⁹⁶ Sulfatides are a class of galactose derived glycolipids containing a sulfate group and are involved in the adaptive immune response. They function by first binding to CD receptors to form a complex which can then be recognised as an antigen by T-cells.

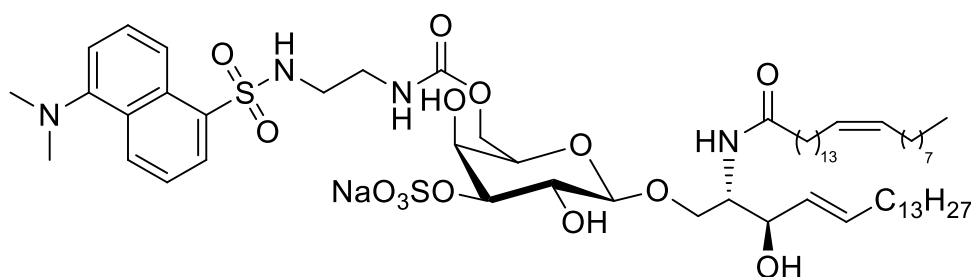


Figure 5. 7. CD1a probe investigated by Panza *et al.*¹⁹⁶

Using recombinant sCD1a immobilized on magnetic beads, the group found that the incorporation of the dansyl fluorophore at the C-6 position of the sugar did not inhibit its binding to the CD1a receptor. Furthermore, they established that the binding of the probe to the receptor is specific, as it can be displaced by unlabelled sulfatide but not by tripalmitin, a lipid unable to bind to CD1a. The detection of the fluorophore

was established by irradiating the compound at 351 nm and detecting emission at 530 nm, giving the probe a Stokes shift of 179 nm.

A similar approach was used by Bonin *et al* to investigate the localization of an α -galactosylceramide fluorescent probe.²⁰⁹ α -galactosylceramides are a class of immunomodulatory compounds which are capable of activating natural killer cells (NKT), a type of T-lymphocyte. They synthesized a BODIPY functionalized α -galactosylceramide and administered this to mice by intraperitoneal injection and monitored the activation-induced disappearance of NKT cells (**Figure 5. 8**).

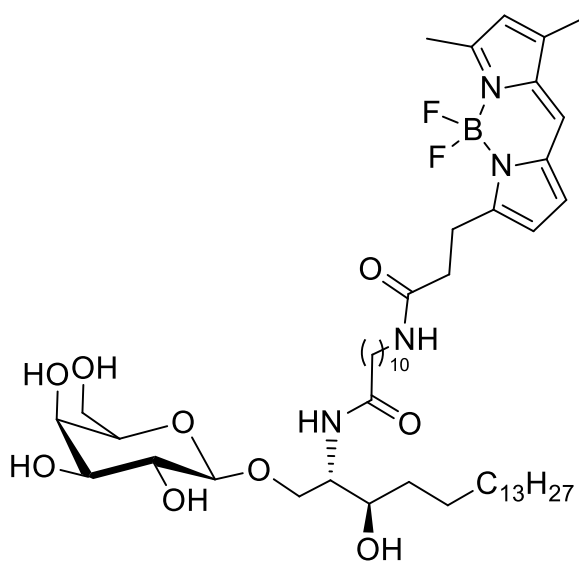


Figure 5. 8. α -galactosylceramide probe used by Bonin *et al*.²⁰⁹

They found that this probe had similar immunomodulatory activity to the known α -galactosylceramide immunomodulator KRN7000. Using fluorescent microscopy to inspect liver tissue taken from the mice administered with the probe, they were able to establish the localization of the compound within the liver. They found that the compound accumulated primarily in spleen and liver antigen presenting cells and, significantly, was not associated with NKT cells.

The Mitkovski group has used fluorescent probes to investigate the distribution of a galactoside analogue of the known cytotoxic compound duocarmycin (**Figure 5. 9**).²¹⁰ This molecule incorporates a coumarin based moiety which serves as both a fluorophore and a DNA intercalator. They then studied the cytotoxicity and localization of the galactoside prodrug and its aglycon in human lung cancer cells.

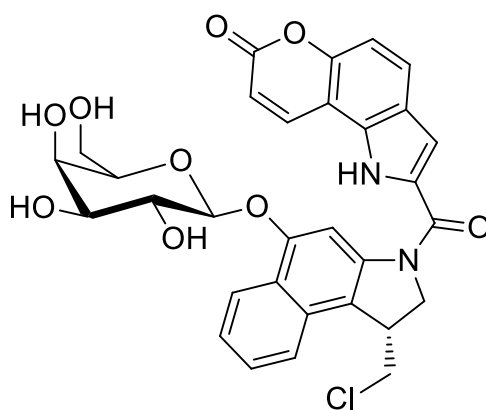


Figure 5. 9. Galactoside studied by Mitkovski et al.²¹⁰

From these studies, they found that both the galactoside and its aglycon displayed almost identical IC_{50} values. Using confocal laser scanning microscopy, they studied how these compounds are absorbed and localized within the cell. These studies showed that both the galactoside and aglycon penetrate the cell membrane within seconds and after several minutes accumulate within the mitochondria and ultimately cause cell death.

5.2 Aim

During the synthesis of **2.35** (Chapter 2), it was noticed that solutions of this compound appeared fluorescent when viewed under UV light at 254 nm. This effect was not observed for the corresponding aglycon **2.33**. Given that the compound does not feature a large, extended conjugated system typically present in other fluorescent moieties such as pyrene and anthracene, we hypothesized that this fluorescence could arise from the presence of the acetal functionality present in the glycosidic bond. Therefore, the aim of this work was to synthesize a selection of analogues of **2.35** and investigate their fluorescent properties.

The influence of several structural attributes on the photochemical properties of the system was explored by synthesising and studying the fluorescence of several analogues (**Figure 5. 10**). To do this, we sought to first investigate the nature of the glycoside attached to the ligand core. The aforementioned **2.35** features a β -glycosidic linkage and each acetyl group is in an equatorial configuration. We reasoned that the inversion of this chiral centre to an α -mannoside **5.1** could have a significant effect on the fluorescence, as this would change the orientation of the

lone pairs present on both oxygen atoms and therefore change the overall electronic structure of the bond. In addition, we wanted to investigate the effect that the retention of the β -glycosidic linkage with the inversion of a stereocenter at a position remote to the anomeric centre would have on the fluorescent behaviour. This could be achieved by studying a β -galactoside **5.2** which is the C-4 epimer of glucose.

To assess if the observed enhancement of fluorescence is unique to glycosides, we also aimed to explore a non-glycosidic groups appended to the N_2O core; the alkylated compound **2.34**, the acetal containing tetrahydropyran (THP) compound **5.3** and the ether linked menthol conjugate **5.4**.

Finally, DFT calculations were obtained in order to assist with the interpretation of the data obtained from the fluorescence studies. The calculations were performed by Dr C. Henchy (Dept. of Chemistry, Maynooth University).

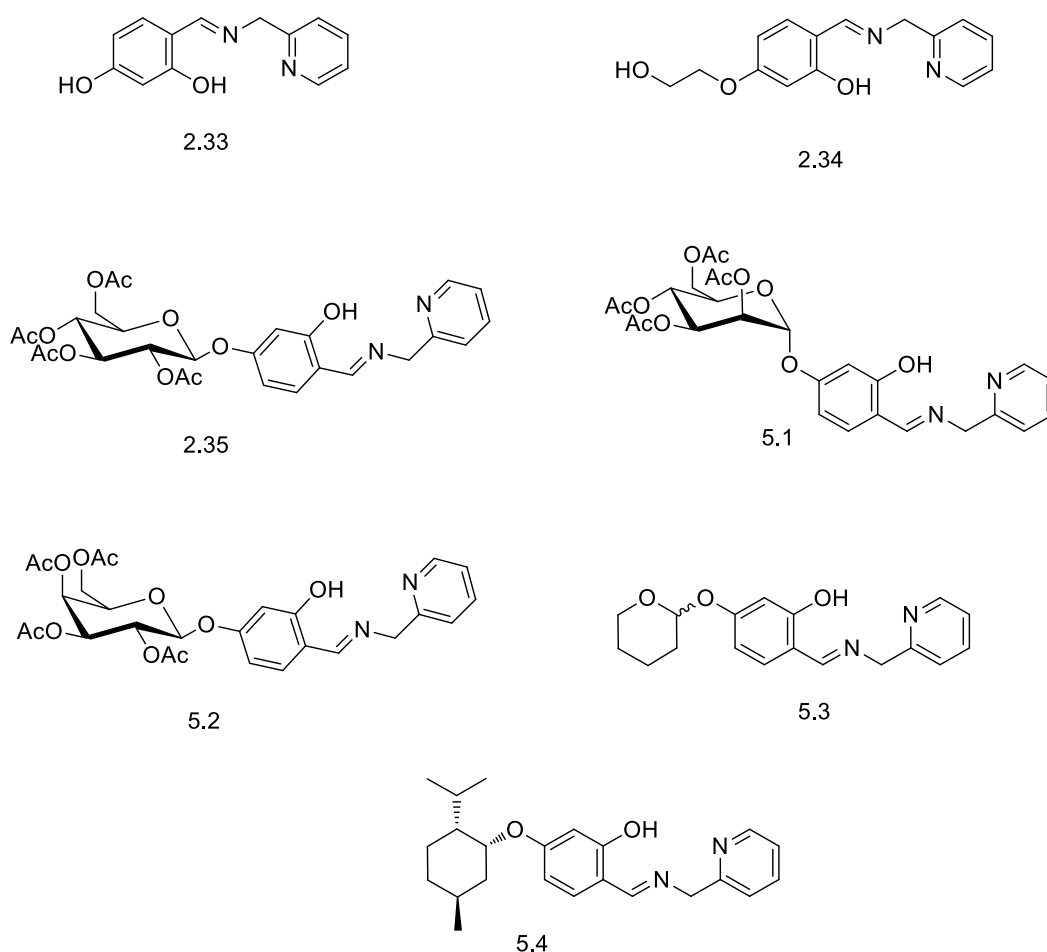
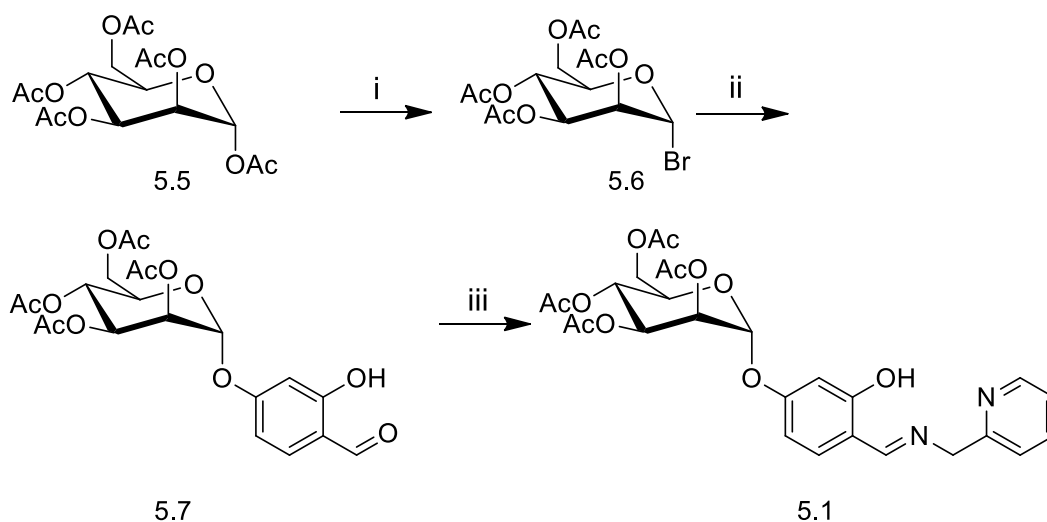


Figure 5. 10. Compounds Investigated for the Photochemical Behaviour.

5.3 Results and Discussion

5.3.1 Synthesis

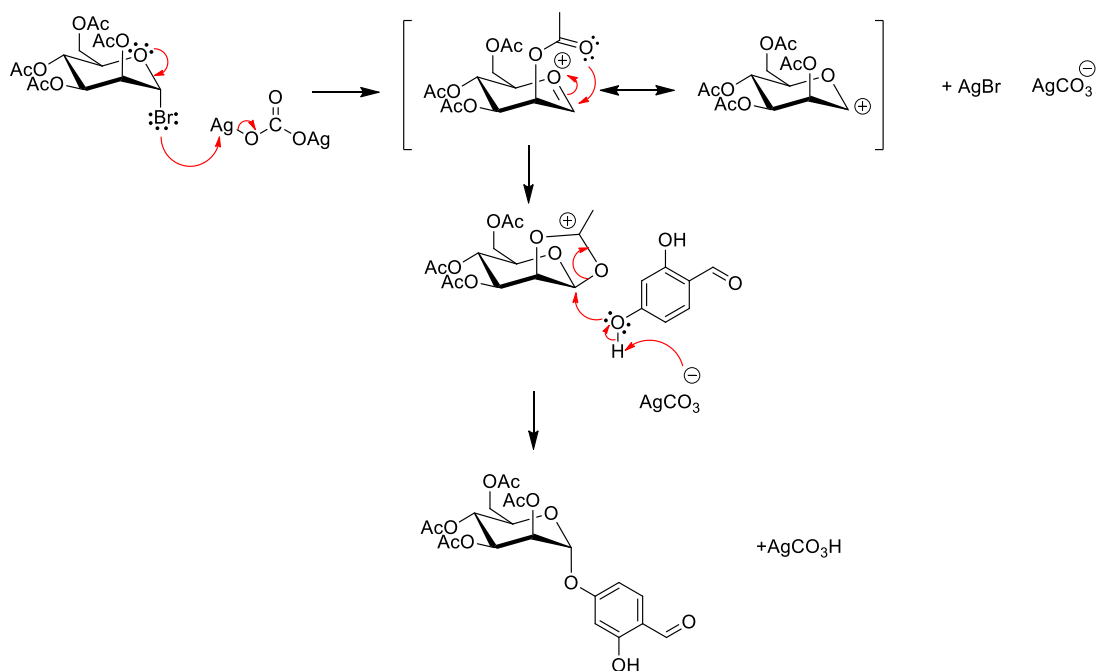
5.3.1.1 Synthesis of Mannoside 5.1



Scheme 5. 1. Reagents and conditions: i) HBr/AcOH, >98%; ii) 2,4-hydroxybenzaldehyde **2.37**, Ag₂CO₃, MeCN, 72%; iii) 2-picolylamine, EtOH, >98%

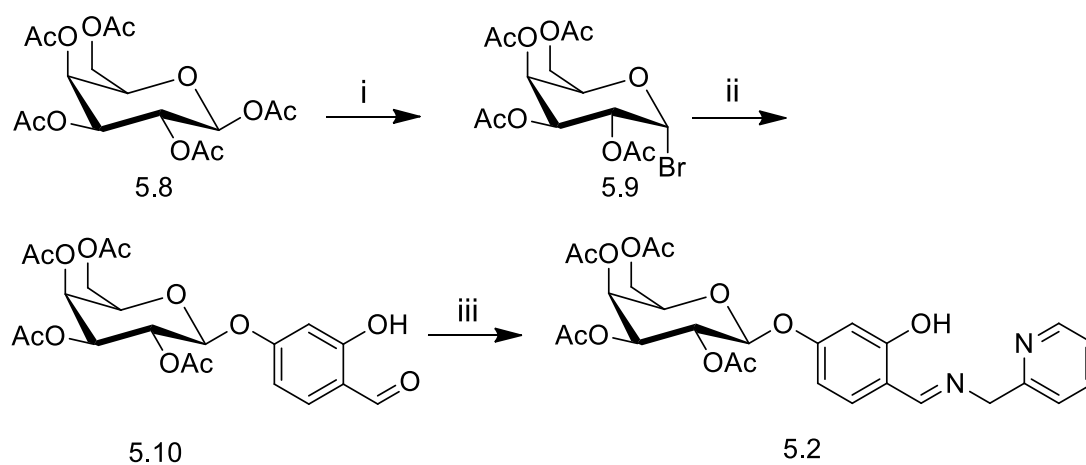
Mannoside **5.1** was synthesized in a manner analogous to the glucoside **2.35** described in Chapter 2 (**Scheme 5. 1**). Mannose pentaacetate **5.5** was brominated using HBr/AcOH to generate the bromide mannosyl donor **5.6**.²¹¹ This was then subject to Koenigs-Knorr glycosylation conditions with **2.37** to yield the galactoside **5.7** in good yield. Unlike the Koenigs-Knorr glycosylation of **2.39** which produced the β -glucoside, the reaction utilizing **5.6** produces **5.7** as the α -anomer stereospecifically. This arises because the acetyl group on the C-2 position is in the axial configuration unlike glucose and galactose. When the oxocarbenium ion is formed, the acetoxonium ring is therefore formed on the top face of the sugar (**Scheme 5. 2**). The nucleophile therefore can only attack from the bottom face of the pyranose ring to form the α -anomer exclusively. The stereochemistry was confirmed by the chemical shift of the anomeric proton in ¹H NMR and the ³J_{1,2} coupling constant of 1.7 Hz, which is characteristic of *cis*-glycosidic bonds.

The imine **5.1** was then prepared by refluxing **5.7** in anhydrous ethanol with 2-picolylamine overnight and reducing to dryness to produce a yellow oil.



Scheme 5. 2. Mechanism for the formation of **5.7**.

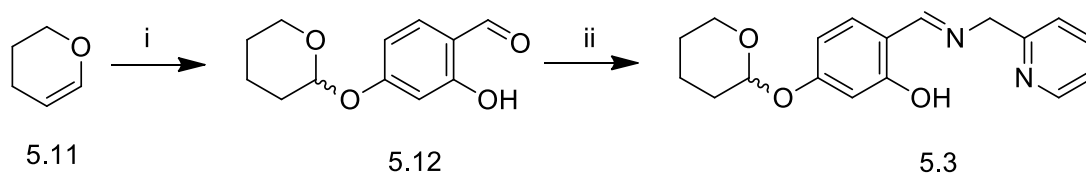
5.3.1.2 Synthesis of Galactoside **5.2**



Scheme 5. 3. Reagents and conditions: i) HBr/AcOH, 89%; ii) 2,4-hydroxybenzaldehyde **2.37**, Ag₂CO₃, MeCN, 66%; iii) 2-picolylamine, EtOH, >98%

The galactoside **5.2** was synthesized following the same route as the glucoside and mannoside **2.35** and **5.1**, respectively (**Scheme 5. 3**). Galactose pentaacetate **5.8** was brominated using HBr/AcOH to generate the aldehyde **5.10** as the expected β-anomer, as evidenced by the chemical shift of the H-1 proton.²¹² The target imine **5.2** was synthesized in quantitative yield by the reaction of **5.10** with 2-picolylamine in refluxing EtOH and the complete evaporation of the solvent.

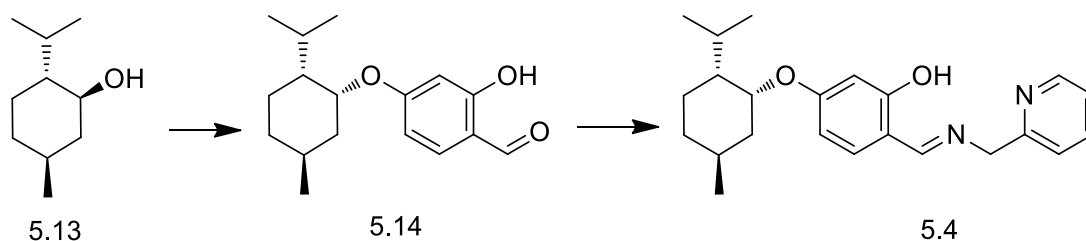
5.3.1.3 Synthesis of THP Derivative 5.3



Scheme 5. 4. Reagents and conditions: i) 2,4-hydroxybenzaldehyde **2.37**, PPTS, DCM, 90%; iii) 2-picolylamine, EtOH, >98%

The THP derived compound **5.3** was synthesized by first forming the THP conjugated aldehyde **5.12** (Scheme 5. 4). This was carried in anhydrous dichloromethane using catalytic pyridinium *p*-toluenesulfonate (PPTS) to produce the target compound as a racemic mixture in excellent yield.²¹³ This aldehyde was refluxed in ethanol overnight with 2-picolylamine to produce the target compound **5.3** in quantitative yield upon evaporation of the solvent.

5.3.1.4 Synthesis of Menthol Derivative 5.4

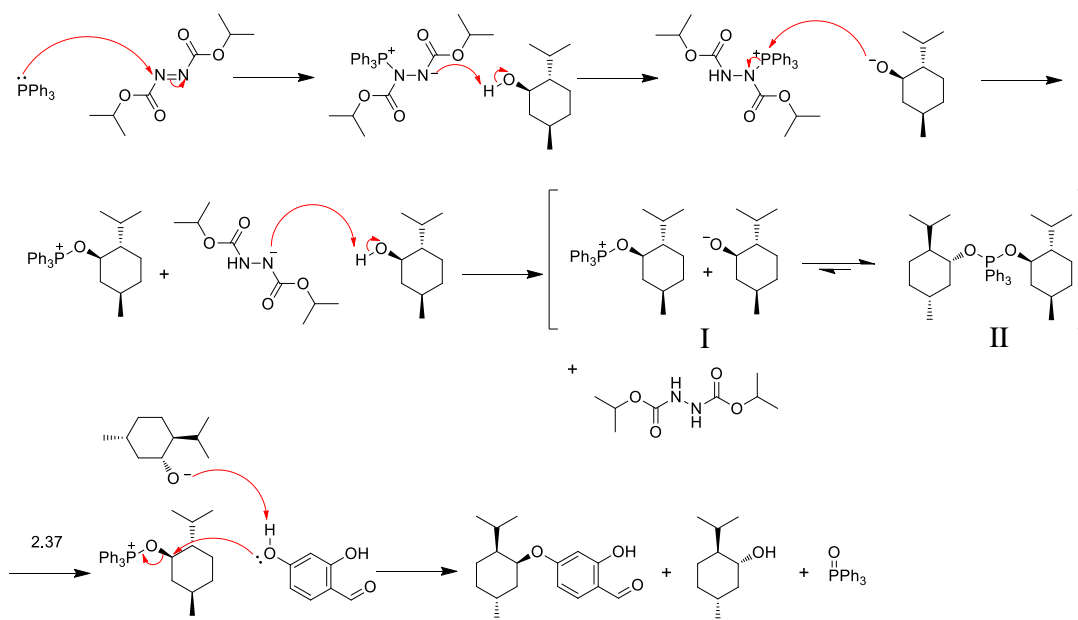


Scheme 5. 5. Reagents and conditions: i) 2,4-hydroxybenzaldehyde **2.37**, DIAD, PPh_3 , THF, 16 %; iii) 2-picolylamine, EtOH, >98 %

Our initial attempts to synthesize a sterically bulky ether had focused on an adamantane derivative. This could not be synthesized however, due to the structurally demanding nature of the bromoadamantane used in the reaction. This could not undergo S_N2 substitution due to the steric hindrance which prevents back side attack of the nucleophile. On the other hand, an S_N1 reaction cannot take place as the rigidity of the compound prevents the formation of a planar, sp^2 hybridized cation necessary for this reaction to occur. As an alternative to this sterically demanding conjugate, the menthol derivative **5.4** was investigated.

The synthesis of the menthol functionalised imine **5.4** begins with the Mitsunobu reaction of (-)-menthol with 2,4-dihydroxybenzaldehyde (**Scheme 5. 5**). This reaction proceeds with the inversion of stereochemistry at the C-O stereocenter of the menthol ring. This occurs because the hydroxyl group is eliminated in an S_N2 fashion after activation by DIAD/PPh₃ (**Scheme 5. 6**).

The reaction is quite low yielding (16 %), however, this is unsurprising due to the nature of reactants. Typically, a Mitsunobu reaction is conducted with both reactants in solution when the PPh₃/DIAD is added. The more acidic hydroxyl group, often a carboxylic acid, is deprotonated by the phosphonium-amide betaine and is ultimately eliminated by the nucleophilic attack of the less acidic hydroxyl group.²¹⁴ As the more acidic hydroxyl group, the phenol, is also the nucleophile in our intended reaction, a protocol involving the activation of the secondary hydroxyl group before the addition of the phenol was followed. Under these conditions, a (I) phosphonium-alkoxide betaine is generated, which is in equilibrium with the dialkoxyphosphorane (II).²¹⁵ Upon addition of **2.37**, the activated phosphonium-oxide (I) is then displaced and a molecule of menthol is regenerated, requiring two equivalents to be used in the reaction.



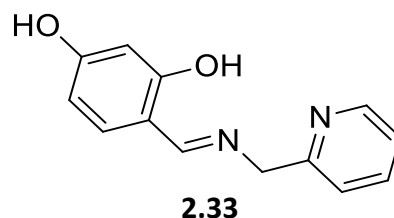
Scheme 5. 6. Mechanism of the Mitsunobu Reaction.²¹⁵

5.14 was then reacted with 2-picolylamine in refluxing ethanol to produce the target imine in quantitative yield as an orange oil.

5.3.2 Fluorescence Studies

With compounds **2.33**, **2.34**, **2.35**, **5.1**, **5.2**, **5.3** and **5.4** successfully synthesized and characterized, their photochemical behaviour was investigated. This was done by first determining the λ_{max} , the frequency that the molecule absorbs the most energy, and then examining the fluorescent emission of the molecule at this wavelength. This was carried out using both methanol and acetonitrile as solvents.

5.3.2.1 Fluorescence Studies of **2.33**



Solutions of **2.33** in acetonitrile and methanol were excited with light at λ_{max} frequencies and the resulting emission spectra were obtained (**Figure 5. 11** and **Figure 5. 12**). From these spectra, it can be seen the compound exhibits very weak emission. The 10 μM solution of **2.33** in acetonitrile shows a negligible emission of 1.706 a.u. at 296 nm when excited at 268 nm.

An identical solution of **2.33** in methanol was excited at 272 nm and the emission spectrum was collected. This did not show any fluorescence whatsoever.

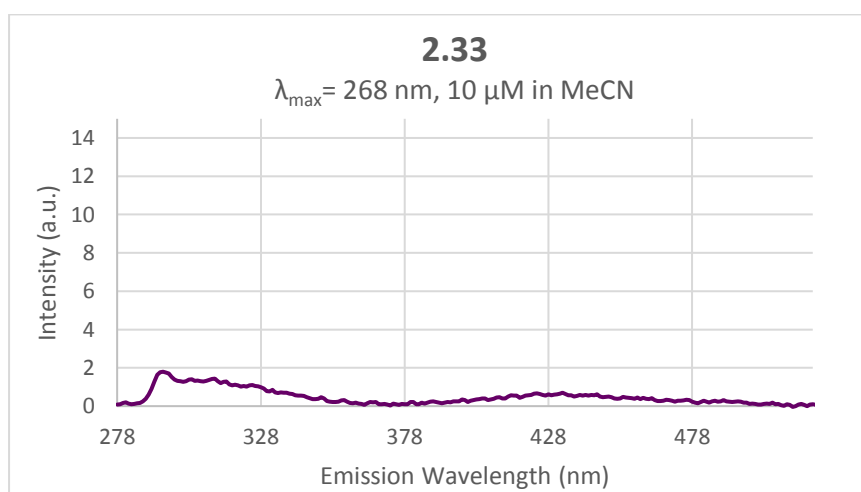


Figure 5. 11. Emission spectrum of **2.33** in acetonitrile.

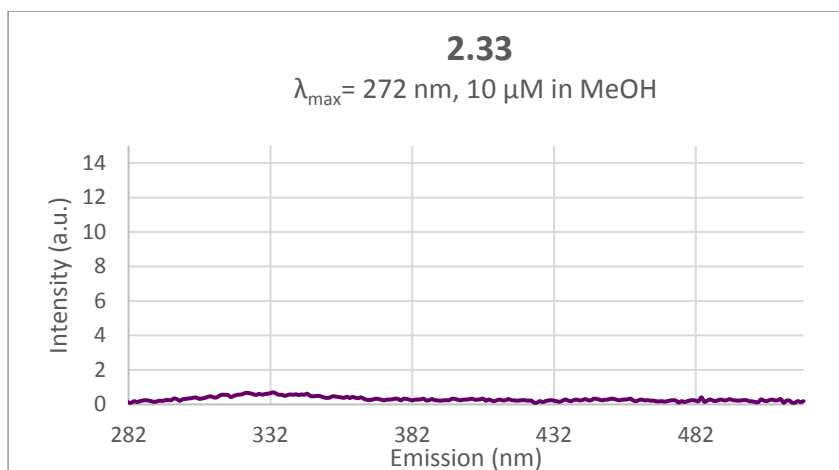
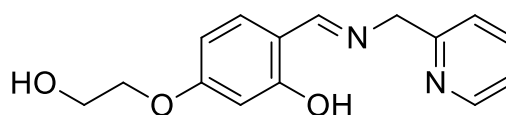


Figure 5. 12. Emission spectrum of **2.33** in methanol.

5.3.2.2 Fluorescence Studies of **2.34**



2.34

The alkylated ether compound **2.34** was investigated in a manner identical to **2.33** at wavelengths of 275 nm (methanol, **Figure 5. 13**) and 279 nm (acetonitrile, **Figure 5. 14**). These studies found that the compound does not show any fluorescent behaviour in either acetonitrile or methanol.

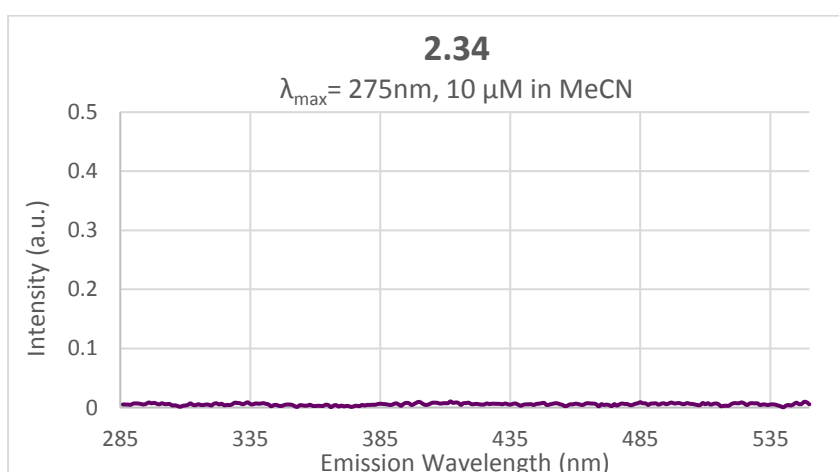


Figure 5. 13. Emission spectrum of **2.34** in acetonitrile.

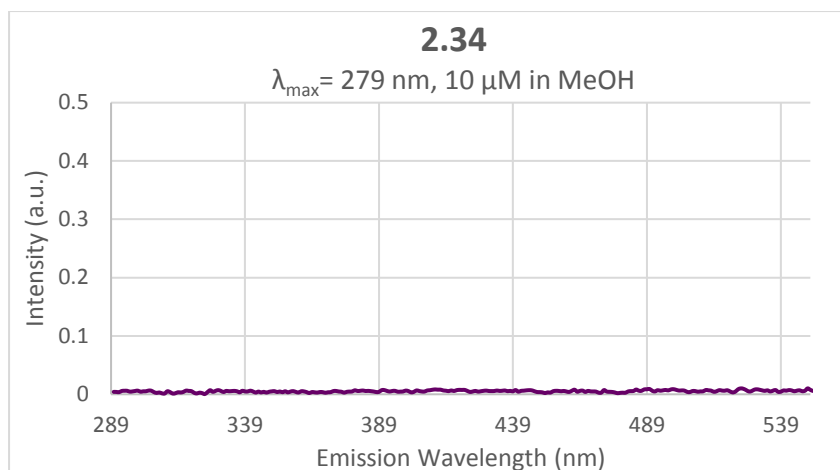
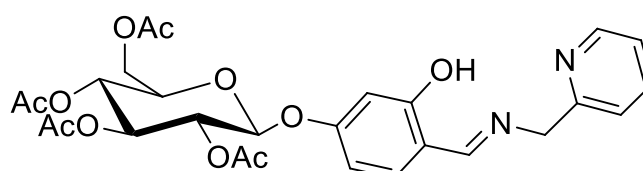


Figure 5. 14. Emission spectrum of **2.34** in methanol.

5.3.2.3 Fluorescence Studies of 2.35



2.35

The glucoside **2.35** was studied in both acetonitrile and methanol at a concentration of $10 \mu\text{M}$ (**Figure 5. 15** and **Figure 5. 16**). The acetonitrile solution was excited at 270 nm and the emission spectrum was collected. This showed a broad emission band centred at 428 nm, presenting a Stokes shift of 158 nm, with an intensity of 15.88 a.u. The solution in methanol showed a similar emission with the band centred at a slightly lower wavelength of 427 nm and a weaker emission intensity of 10.83 a.u. This has a similar Stokes shift of 155 nm, showing that the solvent has very little effect on the fluorescence of the compound.

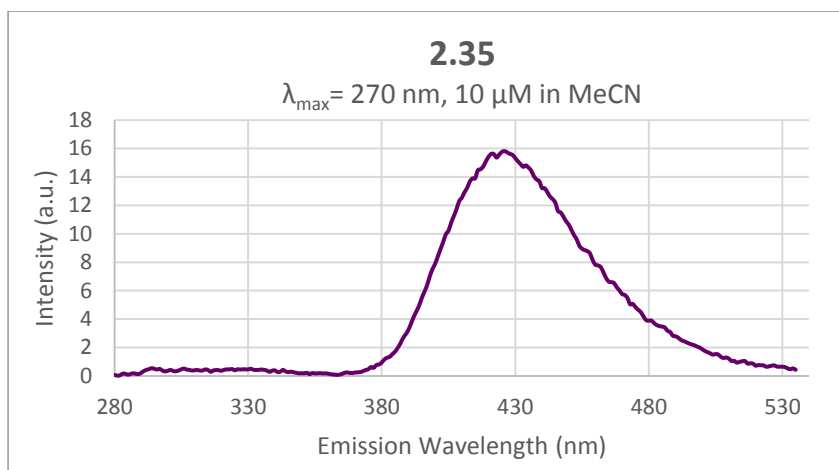


Figure 5. 15. Emission spectrum of **2.35** in acetonitrile.

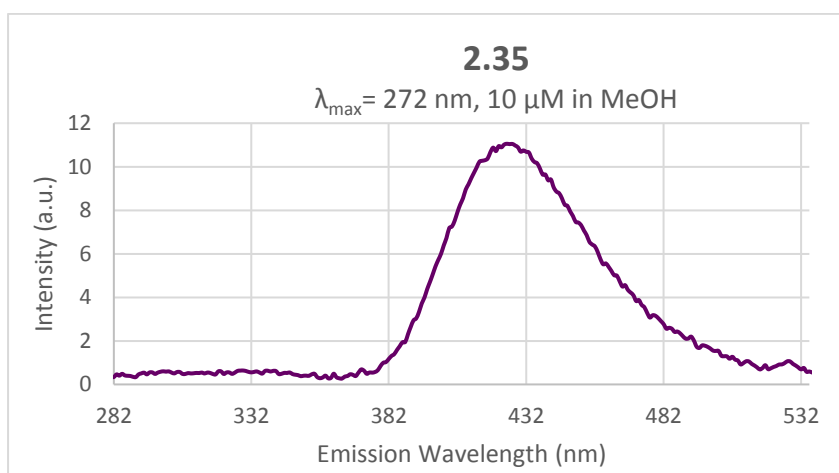
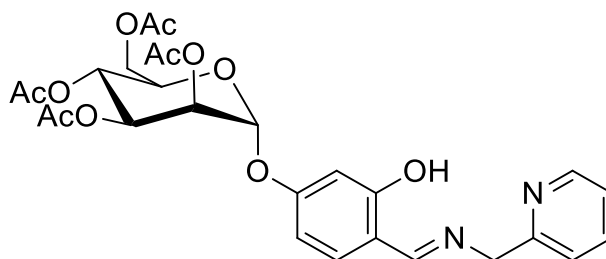


Figure 5. 16. Emission spectrum of **2.35** in methanol.

5.3.2.4 Fluorescence Studies of **5.1**



5.1

The mannose appended compound **5.1**, containing an α -glycosidic bond, did not show any fluorescent activity comparable to that of the β -glycosylated compounds

2.35 and **2.51**. When excited at its λ_{max} frequency of 269 nm in acetonitrile, it showed two broad emission bands centred at 310 nm and 437 nm (**Figure 5. 17**). These have very low intensities of 2.57 a.u. and 1.49 a.u. The presence of two emission bands suggests that there are two distinct excited states adopted upon irradiation. When the experiment is repeated using methanol as a solvent, no fluorescence is detected (**Figure 5. 18**).

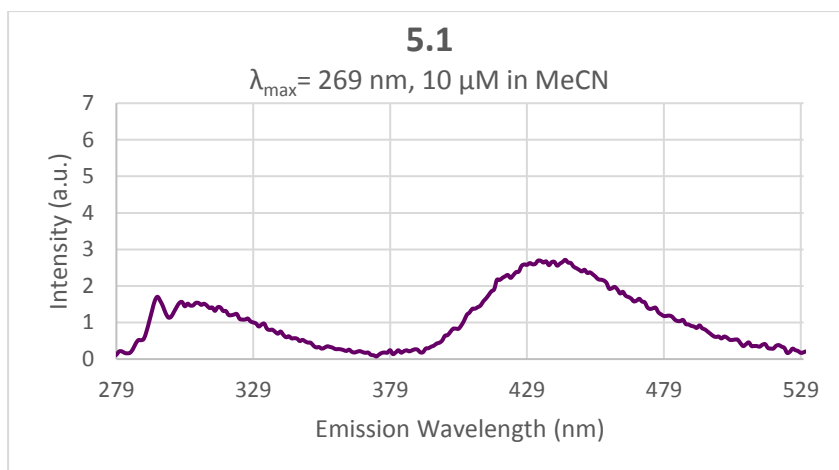


Figure 5. 17. Emission spectrum of **5.1** in acetonitrile.

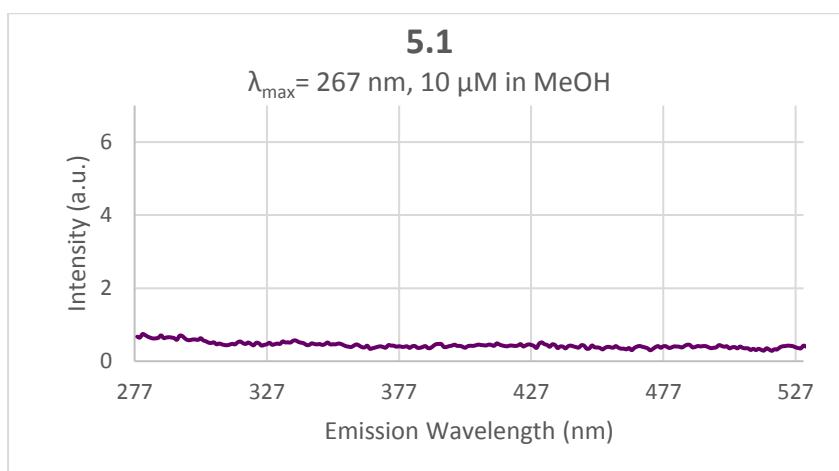
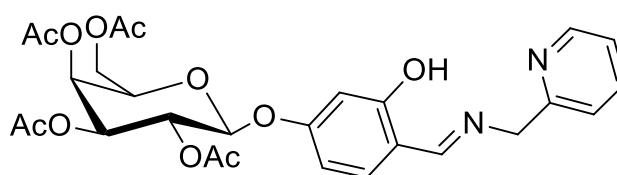


Figure 5. 18. Emission spectrum of **5.1** in methanol.

5.3.2.5 Fluorescence Studies of **5.2**



5.2

The galactoside **5.1**, possessing an axial C-4 hydroxyl group, showed fluorescent behaviour similar the glucoside **2.35**. When excited at 297 nm in acetonitrile, the compound showed a broad emission centred at 371 nm with an intensity of 20.22. This has a Stokes shift of 74 nm, less than half that of **2.35**. When the compound was excited at the same wavelength in methanol, it showed an emission band at the lower wavelength of 437 nm, giving it a Stokes shift of 140 nm which is similar to that of **2.35**. The intensity of the emission, however, was weaker than that observed in acetonitrile.

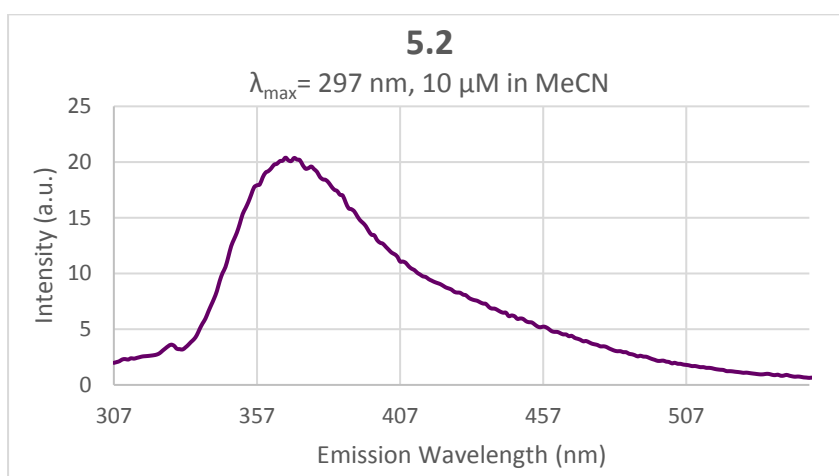


Figure 5. 19. Emission spectrum of **5.2** in acetonitrile.

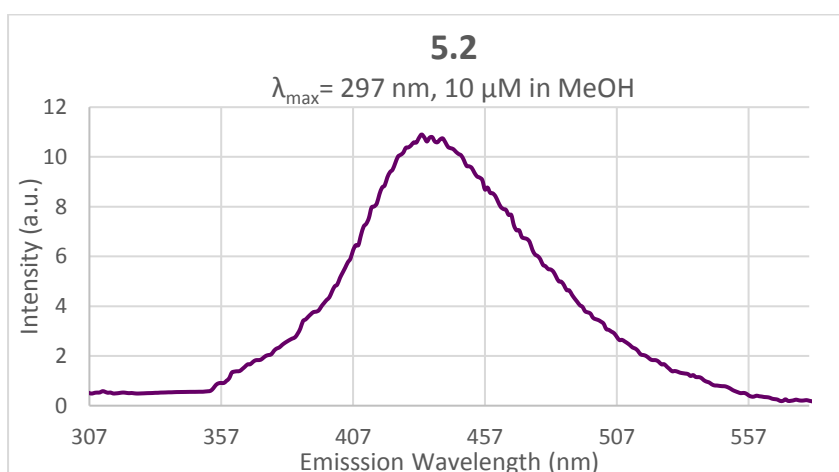
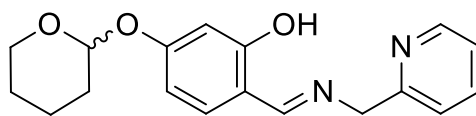


Figure 5. 20. Emission spectrum of **5.2** in methanol.

5.3.2.6 Fluorescence Studies of 5.3



5.3

The THP derived compound **5.3** was studied as the acetal linkage, while racemic, is identical to that of the glycosidic bond, but compound lacks the functionality on the pyran ring found on the glycosides. When **5.3** was studied in acetonitrile, a sharp, weak emission band was observed (**Figure 5. 21**). The Stokes shift of this emission is much larger than that observed for the glycosylated compounds with a value of 265 nm. The intensity of this emission is very low with a value of 2.23 a.u. The corresponding experiment in acetonitrile (**Figure 5. 22**) did not show this emission.

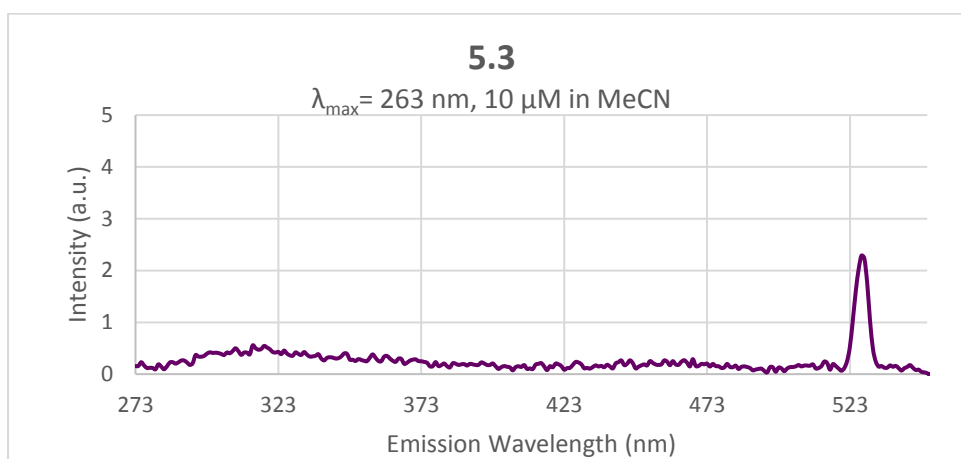


Figure 5. 21. Emission spectrum of **5.3** in acetonitrile.

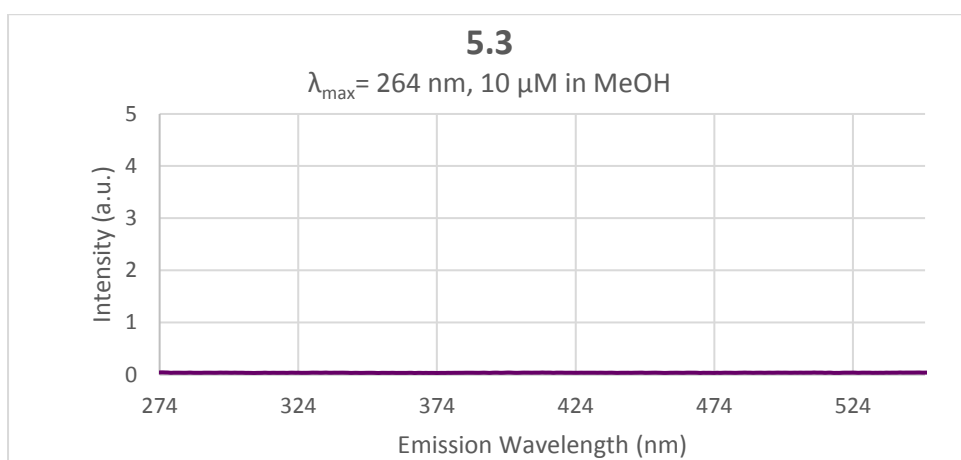
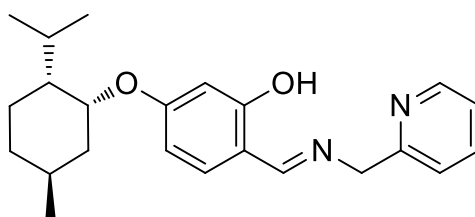


Figure 5. 22. Emission spectrum of **5.3** in methanol.

5.3.2.7 Fluorescence Studies of 5.4



5.4

5.4 was studied to investigate the effect of a sterically bulky, non-glycosidic ether linked group on the photochemical behaviour of the compound. When irradiated with light at 266 nm in acetonitrile, a broad, weak emission band is observed at 425 nm with an intensity of 2.77 a.u. (**Figure 5. 23**). This has a Stokes shift of 159 nm, almost identical to that of **2.35** which was 158 nm. The intensity, however, is weaker than either of the β -glycosides studied. The same experiment repeated in methanol showed two, extremely broad emissions at 331 nm and 437 nm with intensities of 1.83 a.u. and 1.51 a.u. respectively (**Figure 5. 24**). These are extremely weak and it can be concluded that this compound does not exhibit significant fluorescent behaviour.

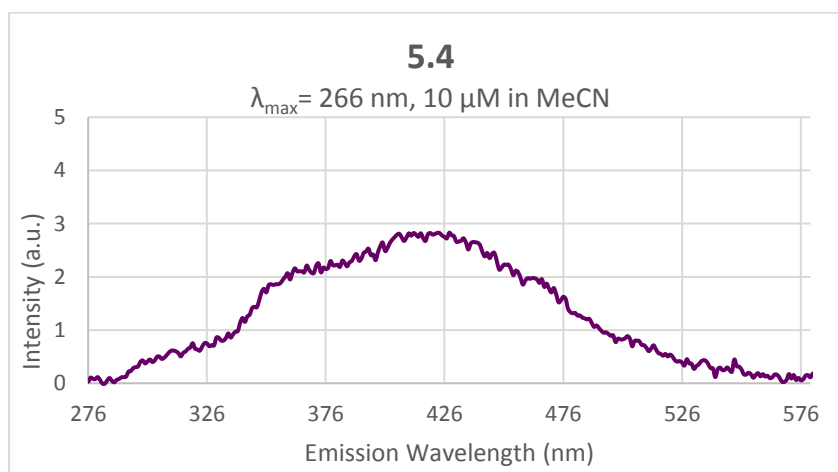


Figure 5. 23. Emission spectrum of **5.4** in acetonitrile.

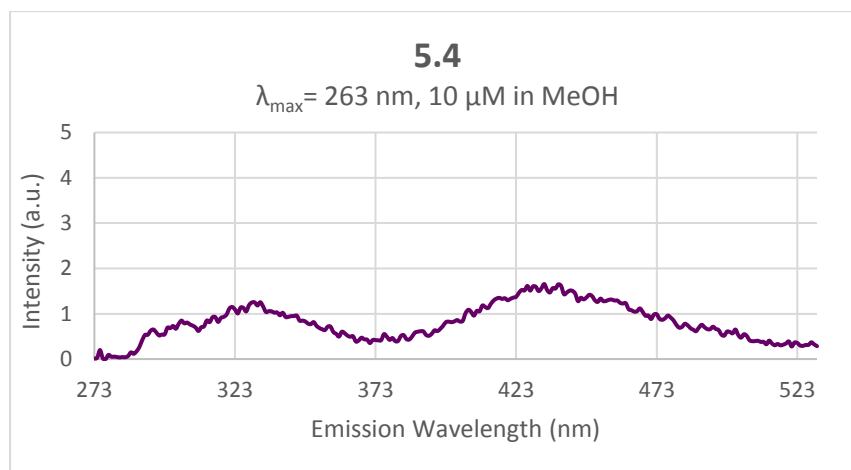


Figure 5. 24. Emission spectrum of **5.4** in methanol.

In summary, these fluorescence studies show that only the β -glycosylated compounds, **2.35** and **5.1**, show significant fluorescent activity (**Figure 5. 25**). This observation can be correlated with the fact that β -vanillin glucosides, a class of plant metabolites, also display fluorescence.²¹⁶ The α -linked mannoside **5.2** showed extremely weak fluorescence in acetonitrile and none in methanol. The acetal linked **5.3**, analogous to a glycosidic bond, showed only very weak fluorescence in acetonitrile. Neither the phenolic compound **2.33** nor the ether functionalised **2.34** showed significant photochemical activity while the ether linked menthol **5.4** showed a weak fluorescent emission. These results indicate that, while a β -glycoside moiety appears to grant a significant increase in the fluorescence of the N_2O scaffold, fluorescence of this moiety is not exclusive to β -glycosides as was proved by the weak but clearly identifiable fluorescent emission of **5.4**. This would indicate that the fluorescent activity arises not just from the electronic properties of the β -glycosidic bond but also the steric contribution of the appended group.

In addition, the solvent appears to play a role in the fluorescence of the compounds. The compounds which showed fluorescence presented with more intense emission in acetonitrile when compared to methanol. While acetonitrile and methanol are both water-miscible, polar solvents, methanol can function as a H-bond donor while acetonitrile cannot. As the compounds contain several H-bond acceptors, this means that the compounds will differ in their solvation shell in both solvents. It is therefore

likely that the compounds will adopt different conformations which can affect the electronic structure of the compounds and therefore change their fluorescent properties. This effect is well documented in pyridine type fluorophores.^{192,217,218}

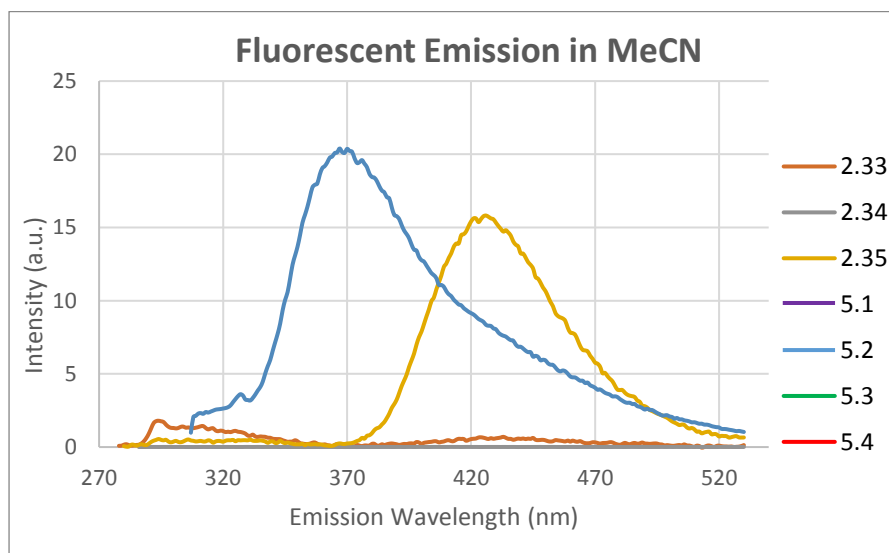


Figure 5. 25. Fluorescent emission of compounds studied in acetonitrile.

5.3.3 DFT Studies

In an effort to gain an insight into the electronic effects that are responsible for the differences observed in the fluorescent activity of **2.33**, **2.34** and **2.35**, a preliminary investigation of the electronic structure of these molecules was carried out using density functional theory (DFT). These studies were performed by Dr Christopher Henchy at Maynooth University using the Gaussian-03 software suite,²¹⁹ utilizing the B3LYP functional and 6-311++g(2d,2p) basis set. Excited states and electronic transitions were studied using Time-Dependent DFT calculations.

Taking the conformation found from the X-ray crystal structure of **2.3** as the ground state conformation (**Figure 5. 26, A**), the molecular orbital structure was generated. Once this was done, the vibrational structure and electronic transitions could be modelled. As expected, this found that the primary absorption involves the promotion of an electron from the HOMO orbital, molecular orbital 60 (MO-60) (**Figure 5. 26, B**), into the LUMO orbital (MO-61) (**Figure 5. 26, C**). These structures can give an insight into why this molecule lacks strong fluorescence.

As described above, fluorescence is typically observed in molecules that have extended networks of conjugated double bonds, as this gives a larger, extended HOMO. Due to this extended electronic network, both the HOMO energy and energy gap between the HOMO and LUMO is reduced, therefore making it more probable that an electronic transition will occur. **Figure 5. 26, B** shows that the major contributor to the HOMO of the molecule is the phenolic ring and imine functional group. Only a very slight contribution of electron density comes from the pyridine ring. This means that the HOMO effectively extends from the *p*-phenolic group to the end of the pyridine ring, giving it a much smaller HOMO than typical fluorophores such as anthracene or fluorescein, which have HOMOs that extend across several aromatic rings. The reason that the HOMO does not extend across the pyridine ring is likely due to the non-planar orientation of the pyridine ring with respect to the aryl ring, having a torsion angle of 81.87° as determined from the X-ray crystal structure. The orbitals of the pyridine ring, therefore, do not align well with those of the aryl ring and as a result, the HOMO does not extend across both rings.

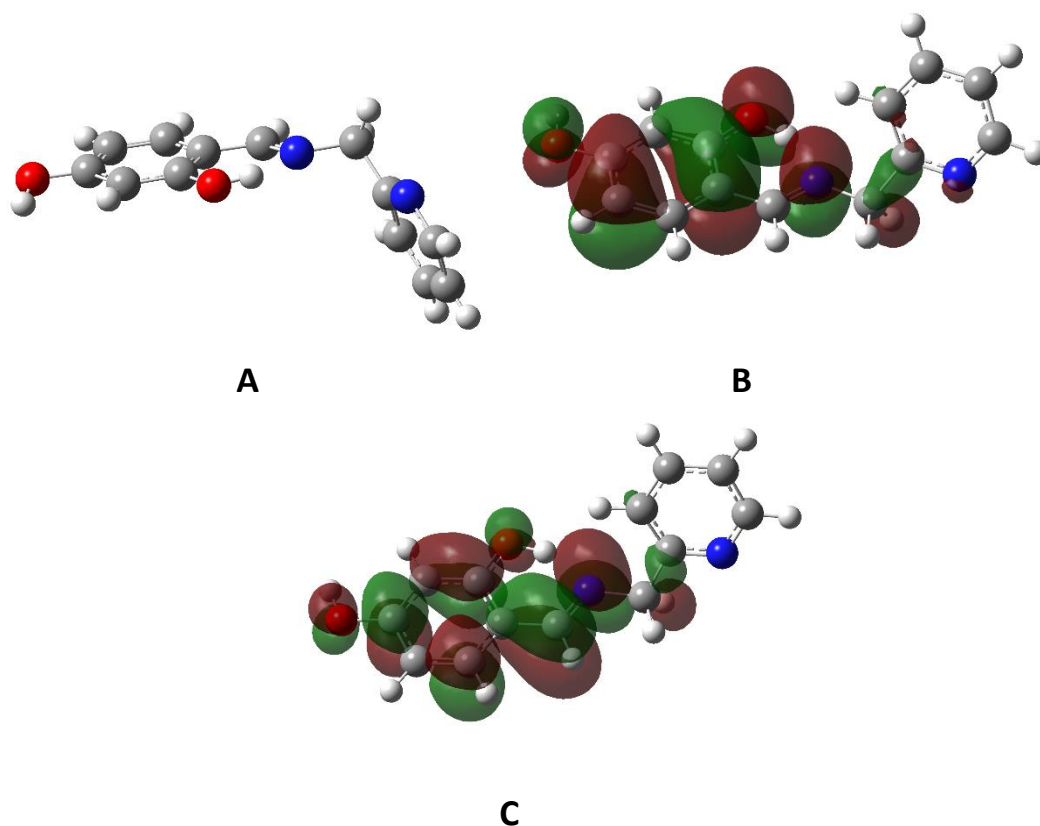


Figure 5. 26. A) Molecular structure of **2.33**; B) HOMO, MO-60; C) LUMO, MO-61

As with **2.33**, the ground state geometry of **2.34** was taken from the crystal structure of the compound. From this the molecular orbital structure and electronic transitions were generated. The principle electronic transition of this molecule is from the HOMO (MO-72) to LUMO (MO-73). The molecular orbital structure of **2.34** is very similar to that of **2.33**; the HOMO extends from the *p*-phenolic oxygen atom, across the aryl ring and terminates at the *m*-carbon atom of the pyridine ring. It is unsurprising, therefore, that the molecule does not exhibit fluorescence, as the HOMO is not significantly delocalized. This observation mimics the results obtained for **2.33**.

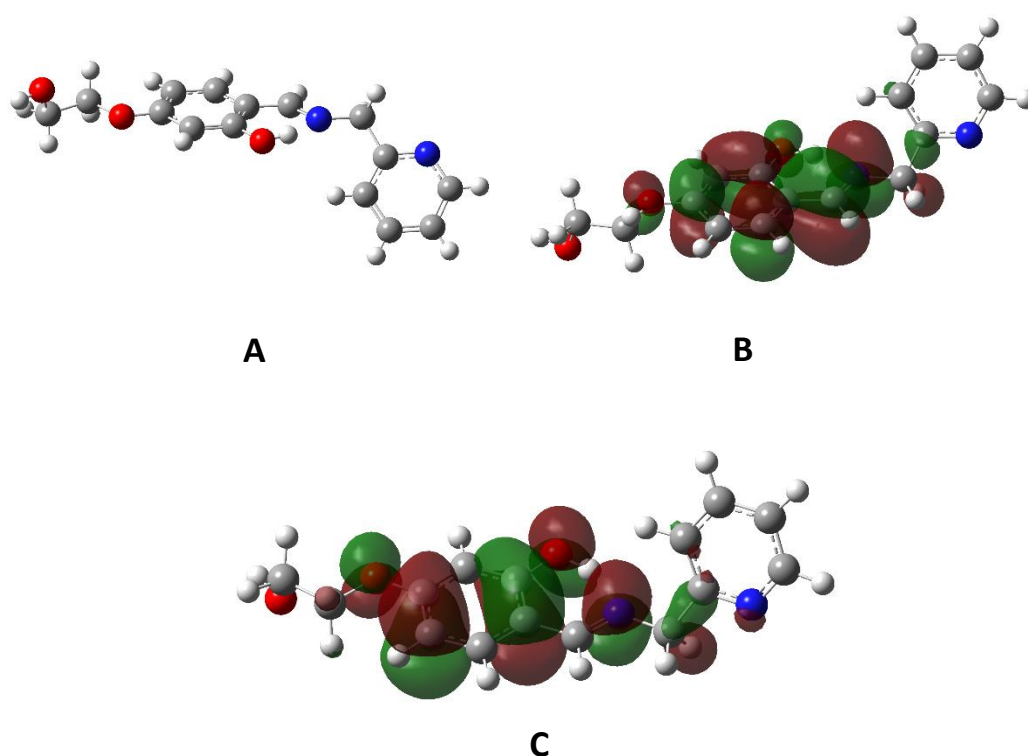


Figure 5. 27. A) Molecular structure of **2.34**; **B)** HOMO, MO-72; **C)** LUMO, MO-73

To analyse glucosylated compound **2.35**, the ground state geometry was first determined as no crystal structure could be obtained (**Figure 5. 28, A**). After the ground state geometry was validated using vibrational analysis, the electronic structure was generated in the same manner as above. The strongest predicted electronic transition was from the HOMO (**Figure 5. 28, B**) to the LUMO (**Figure 5. 28,**

C), as was the case for the **2.33** and **2.34**. The electronic structure of **2.35** shows striking differences to those described above. The HOMO of **2.35** is significantly larger, extending from the pyran oxygen atom, through the glycosidic bond and across both the aryl and pyridine ring. This extended electronic structure explains why this molecule exhibits fluorescence while the aglycon **2.33** does not, and could be attributed to the more planar arrangement of the two aromatic rings in **2.35**, which is predicted to be 33.21 °.

Interestingly, this structure reveals that the oxygen atom present in the pyranose ring contributes to the HOMO of the molecule, suggesting that the acetal functionality present in the glycosidic bond is an important contributor to the fluorescence of the molecule. As the acetal containing **5.3** did not show fluorescence while the ether linked **5.4** did, it is apparent that the glycosidic bond is not the only factor that influences the fluorescence. Steric bulk may contribute to the ground state conformation and allow for a more planar arrangement between the two aromatic rings. This could explain why the bulky, ether linked **5.4** exhibited fluorescence, albeit weak, while the acetal linked **5.3** compound did not. Further study is required to confirm this hypothesis.

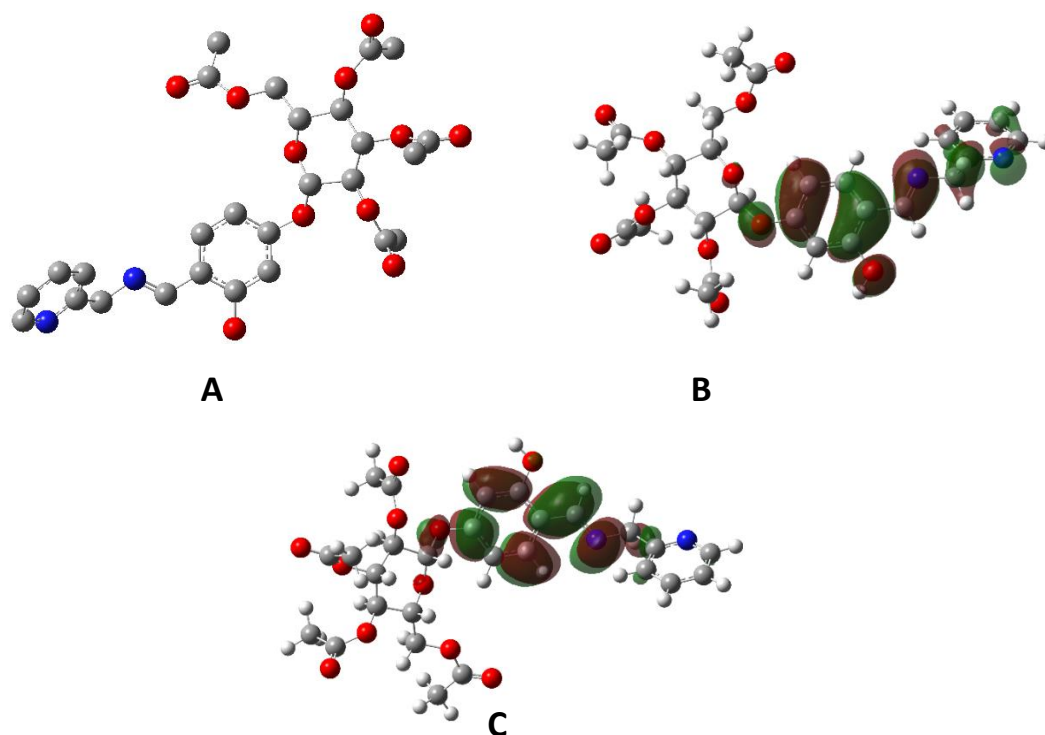


Figure 5. 28. A) Geometry optimized molecular structure of **2.35**; B) HOMO; C) LUMO.

5.4 Conclusion

The aim of this work was to synthesize and carry out a preliminary investigation of the fluorescent activity of a selection of N₂O derivatives. To this end a galactose, mannose, THP and menthol analogues of **2.35** were synthesized and characterized. These compounds, along with the previously described **2.33**, **2.34** and **2.35**, were studied by spectrofluorometry.

These studies found that the β -glycoside functionalized molecules **2.35** and **5.1** showed moderate fluorescence, while compounds **2.33**, **2.34**, **5.2**, **5.3** and **5.4** showed little to no fluorescence. In addition, the solvent used for analysis played a minor role in the fluorescence of the solutions. Solutions that used acetonitrile as the solvent showed an improved intensity of emission compared to those of methanol.

To aid in the analysis of these results, DFT studies were used to analyse the electronic structure of the molecules. These found that the HOMO orbital of **2.35**, which was found to be fluorescent, is comprised of electron density contributed by both aromatic rings and, importantly, the β -glycosidic bond. Conversely, **2.33** and **2.34**, which were not fluorescent, did not show this extended HOMO orbital. This difference in the electronic structure may explain the difference fluorescent activity between the glycosylated and non-glycosylated compounds.

Chapter 6: Experimental Details

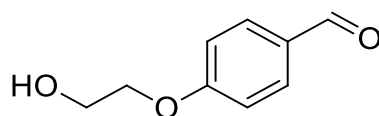
6.1 General Procedures

All chemicals purchased were reagent grade and used without further purification unless stated otherwise. Anhydrous dichloromethane and acetonitrile were freshly distilled over CaH_2 prior use. Ethanol was dried over 3 Å molecular sieves, which were flame dried prior to use. Reactions were monitored with thin layer chromatography (TLC) on Merck Silica Gel F₂₅₄ plates. Detection was effected by UV, charring in a mixture of 5 % sulfuric acid-ethanol or 6 % vanillin-ethanol. All glassware used for anhydrous reactions was flame dried under vacuum prior to use. NMR spectra were obtained on a Bruker Ascend 500 or a Bruker Avance 300 spectrometer using the residual solvent peak as internal standard. Chemical shifts are reported in ppm. Proton and carbon assignments were made with the aid of 1D and 2D NMR experiments (COSY, DEPT, HSQC, HMBC, NOESY, PSYCHE and TOCSY). Flash chromatography was performed with Merck Silica Gel 60. Microwave reactions were carried out using a CEM Discover Microwave Synthesizer. Optical rotations were obtained from an AA-100 polarimeter. $[\alpha]_D$ values are given in $10^{-1} \text{ cm}^2 \cdot \text{g}^{-1}$. The melting points were obtained using a Stuart Scientific SMP1 melting point apparatus and are uncorrected. Purity was confirmed by elemental analysis using a FLASH EA 1112 Series Elemental Analyzer with Eager 300 operating software. High resolution mass spectrometry was performed on an Agilent-LC 1200 Series coupled to a 6210 Agilent Time-Of-Flight (TOF) mass spectrometer equipped with an electrospray source in both positive and negative (ESI+/-) modes. Magnetic susceptibility measurements were carried out at room temperature using a Johnson Matthey Magnetic Susceptibility Balance with $[\text{HgCo}(\text{SCN})_4]$ as reference. Infrared spectra were obtained as a film on NaCl plates or as KBr disks in the region $4000\text{--}400 \text{ cm}^{-1}$ on a Perkin Elmer Spectrum 100 FT-IR spectrophotometer. The X-ray intensity data were measured using an Oxford Cryosystems low temperature device using a MiTeGen micromount and solved using the Bruker APEX Software Package. The X-ray crystal structures were analysed using Mercury 3.8 software.

Caution: Although not encountered in our experiments, perchlorate salts of metal ions are potentially explosive and should be manipulated with care.

6.2 Chapter 2

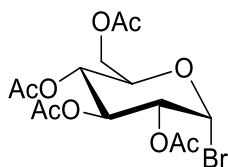
6.2.1 N₂ Series



2.4

To a solution of 4-hydroxybenzaldehyde (1 g, 0.0082 mol) and DBU (1.35 mL, 0.009 mol) in IPA (10 mL) was added a solution of 2-chloroethanol (1.65 mL, 0.0246 mol) and NaI (1.23 g 0.0082 mol) in IPA (15 mL) and heated to 120 °C in a microwave for 4 h. The solvent was removed *in vacuo* and the residue was suspended in EtOAc (30 mL) and washed with saturated sodium dithionite solution (30 mL), H₂O (2x30 mL), saturated NaHCO₃ solution (2x30 mL) and brine (30 mL). The organic solution was dried over Na₂SO₄ and the solvent was removed *in vacuo* to yield a heavy yellow oil. This was purified by column chromatography (3:2 Pet. Ether/EtOAc, R_f: 0.29) to yield the product as a clear oil (0.804 g, 59 %). ¹H NMR (500 MHz, CDCl₃) δ 9.88 (s, 1H, HC=O), 7.84 (d, *J* = 8.8 Hz, 2H, ArH), 7.02 (d, *J* = 8.8 Hz, 2H, ArH), 4.17 (t, *J* = 4.8 Hz, 2H, ArOCH₂), 4.01 (t, *J* = 4.8 Hz, 2H, CH₂OH), 2.16 (bs, 1H, OH). ¹³C NMR (126 MHz, CDCl₃) δ 190.9 (C=O), 163.8 (Ar), 132.2 (Ar), 130.4 (Ar), 114.9 (Ar), 69.7 (ArO-C), 61.3 (C-OH). IR (NaCl Plate): 3420, 2939, 2874, 2745, 1681, 1603, 1578, 1510, 1315, 1261, 1164, 1080, 1045, 833 cm⁻¹. HRMS *m/z* (ESI+): 167.0703 (C₉H₁₀O₃: [M+H]⁺ requires 167.07082)

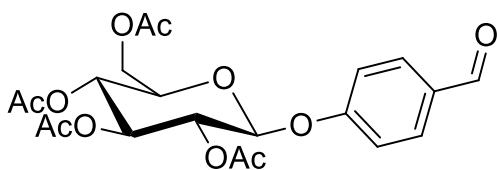
The NMR data is in agreement with that reported in the literature.²²⁰



2.7

Glucose pentaacetate (5 g, 0.0128 mol) was dissolved in HBr/AcOH (15 mL) with acetic anhydride (2 mL) under N₂ and stirred for 4 h at room temperature. This was diluted with DCM (30 mL) and washed with water (3 x 20 mL), saturated NaHCO₃ solution (30 mL) and brine (30 mL) before being dried with Na₂SO₄. The solvent was removed *in vacuo* to yield a clear oil which was diluted in Et₂O (20 mL) and cyclohexane (70 mL) was added. The solution was cooled on ice to precipitate the product as a white solid (4.525 g, 87 %). ¹H NMR (500 MHz, CDCl₃) δ 6.61 (d, *J* = 4.0 Hz, 1H, H-1), 5.56 (appt, *J* = 9.7 Hz, 1H, H-3), 5.16 (appt, *J* = 9.8 Hz, 1H, H-4), 4.84 (dd, *J* = 10.0, 4.1 Hz, 1H, H-2), 4.40 – 4.25 (m, 2H, H-5, H-6), 4.16 – 4.09 (m, 1H, H-6'), 2.10 (s, 3H, OAc), 2.10 (s, 3H, OAc), 2.05 (s, 3H, OAc), 2.03 (s, 3H, OAc). ¹³C NMR (126 MHz, CDCl₃) δ 170.6 (C=O), 169.9 (C=O), 169.8 (C=O), 169.54 (C=O), 86.65 (C-1), 72.2 (C-5), 70.7 (C-2), 70.3 (C-3), 67.3 (C-4), 61.0 (C-6), 20.7 (OAc), 20.7 (OAc), 20.7 (OAc), 20.6 (OAc).

The NMR data is in agreement with the data reported in the literature.²²¹

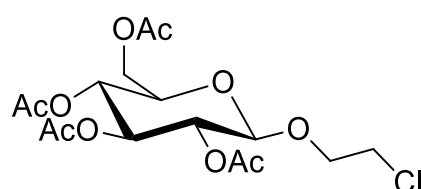


2.8

2.7 (5.68 g, 0.0138 mol), 4-hydroxybenzaldehyde (3.374 g, 0.0176 mol) and Ag₂O (8 g, 0.0345 mol) were dissolved in freshly distilled MeCN (80 mL) under N₂ in the dark and allowed to stir at room temperature for 17 h with approximately 1 g of molecular sieves. The solvent was removed *in vacuo* and the residue was then dissolved in EtOAc and filtered through a Celite plug. The solution was then washed with 1M HCl

(100 mL), NaHCO₃ solution (2x100 mL), brine (100 mL) and dried over Na₂SO₄. The solvent was removed *in vacuo* to yield an orange solid which was recrystallized from EtOH to yield the product as a white solid (3.933 g, 63 %). ¹H NMR (500 MHz, CDCl₃) δ 9.93 (s, 1H, C(=O)H), 7.85 (d, *J* = 8.7 Hz, 2H, Ar-H), 7.10 (d, *J* = 8.7 Hz, 2H, Ar-H), 5.41 – 5.26 (m, 2H, H-2, H-3), 5.27 – 4.88 (m, 2H, H-1, H-4), 4.29 (dd, *J* = 12.3, 5.5 Hz, 1H, H-6), 4.18 (dd, *J* = 12.3, 2.4 Hz, 1H, H-6'), 3.93 (ddd, *J* = 9.9, 5.5, 2.4 Hz, 1H, H-5), 2.07 (s, 3H, OAc), 2.06 (s, 3H, OAc), 2.06 (s, 3H, OAc), 2.05 (s, 3H, OAc). ¹³C NMR (126 MHz, CDCl₃) δ 190.8 (C(=O)H), 170.6 (C=O), 170.3 (C=O), 169.5 (C=O), 169.3 (C=O), 161.3 (Ar), 131.9 (Ar), 131.8 (Ar), 116.9 (Ar), 98.2 (C-1), 72.7 (C-2), 72.5 (C-5) 71.2 (C-3), 68.3 (C-4), 62.1 (C-6), 20.8 (OAc), 20.7 (OAc), 20.7 (OAc), 20.7 (OAc). IR (KBr Disk): 2963, 2850, 2747, 1754, 1692, 1505, 1422, 1380, 1233, 1038 cm⁻¹. HRMS *m/z* (ESI⁺): 475.1201 (C₂₁H₂₄O₁₁: [M+Na⁺]⁺ requires 475.1201). Mp: 145-146 °C. [α]_D²⁵: -0.17 (c 1, CH₂Cl₂)

The NMR characterisation data is in agreement with that reported in the literature.²²²

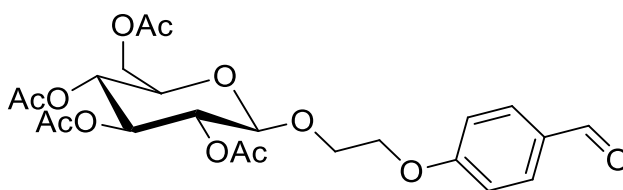


2.10

Glucose pentaacetate (2 g, 0.00512 mol) and 2-chloroethanol (1.03 mL, 0.01536 mol) were dissolved in DCM (15 mL) at 0 °C. A solution of BF₃·OEt₂ (1.89 mL, 0.01536 mol) in DCM (1.89 mL) was added dropwise via cannula over 8 min and the reaction was allowed to warm to room temperature and stirred for 17 h. This was then transferred to a separating funnel and washed with saturated NaHCO₃ solution (2 x 20 mL), H₂O (20 mL) and the combined aqueous layers were extracted with DCM (20 mL). The combined organic layers were then washed with brine (30 mL) and dried with Na₂SO₄ before the solvent was removed *in vacuo* to yield a transparent yellow oil. This was then recrystallized from hot ethanol (20 mL) to yield the product as a white solid (1.1633 g, 55 %). ¹H NMR (500 MHz, CDCl₃) δ 5.22 (t, *J* = 9.5 Hz, 1H, H-3), 5.09 (t, *J* =

9.7 Hz, 1H, H-4), 5.02 (dd, $J = 9.6, 8.0$ Hz, 1H, H-2), 4.58 (d, $J = 8.0$ Hz, 1H, H-1), 4.26 (dd, $J = 12.3, 4.8$ Hz, 1H, H-6), 4.15 (dd, $J = 12.3, 2.4$ Hz, 1H, H-6'), 4.13 – 4.06 (m, 1H, OCH), 3.80 – 3.73 (m, 1H, OCH), 3.71 (ddd, $J = 9.9, 4.7, 2.4$ Hz, 1H, H-5), 3.62 (t, $J = 5.7$ Hz, 2H, CH₂Cl), 2.09 (s, 3H, OAc), 2.06 (s, 3H, OAc), 2.03 (s, 3H, OAc), 2.01 (s, 3H, OAc). ¹³C NMR (126 MHz, CDCl₃) δ 170.7 (C=O), 170.4 (C=O), 169.5 (C=O), 169.5 (C=O), 101.2 (C-1), 72.7 (C-3), 72.0 (C-5), 71.1 (C-2), 70.0 (OCH₂), 68.4 (C-4), 61.9 (C-6), 42.6 (CH₂Cl), 20.8(OAc), 20.8(OAc), 20.7(OAc), 20.7 (OAc). IR (KBr Disk): 2969, 1749, 1434, 1380, 1223, 1173, 602cm⁻¹. HRMS m/z (ESI+): 411.1060 (C₁₆H₂₄ClO₁₀: [M+H]⁺ requires 411.10580). Mp: 114 °C Anal. Calcd for C₁₆H₂₃ClO₁₀: C, 46.78; H, 5.64. Found: C, 46.74; H, 5.63. $[\alpha]_D^{22}$: -15° (c= 4, CHCl₃)

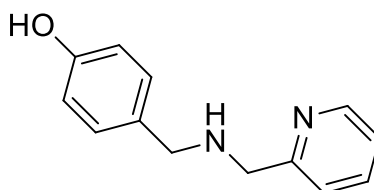
The characterisation data is in agreement with that reported in the literature.²²³



2.11

2.10 (6.278 g, 0.015 mol), 4-hydroxybenzaldehyde (3.733 g, 0.03 mol), TBAI (1.1 g, 0.003 mol) and K₂CO₃ (2 g, 0.015 mol) were dissolved in anhydrous DMF (80 mL) under N₂ in the dark with 3 Å molecular sieves. This was heated to 110 °C for 18 h and the solvent was removed *in vacuo* in the dark to yield a brown residue. The residue was diluted with EtOAc (80 mL) and washed with saturated sodium dithionite solution (50 mL), H₂O (2x50 mL), saturated NaHCO₃ (2x50 mL) and brine (50 mL). This was dried over Na₂SO₄ and the solvent was removed *in vacuo* to produce an orange oil which was purified by column chromatography (3:1 Pet. Ether/ EtOAc, Rf: 0.33) to yield the product as a yellow oil (6.479 g, 87 %). ¹H NMR (500 MHz, CDCl₃) δ 9.89 (s, 1H, HC=O), 7.84 (d, $J = 8.6$ Hz, 2H, Ar-H), 7.00 (d, $J = 8.6$ Hz, 2H, Ar-H), 5.23 (appt, $J = 9.5$ Hz, 1H, H-3), 5.10 (appt, $J = 9.7$ Hz, 1H, H-4), 5.02 (appt, $J = 10$ Hz, 1H, H-2), 4.67 (d, $J = 8.0$ Hz, 1H, H-1), 4.27 (dd, $J = 12.3, 4.7$ Hz, 1H, H-6), 4.24 – 4.09 (m, 4H, H-6', CHCH₂OAr), 3.97 (ddd, $J = 10.7, 6.6, 4.1$ Hz, 1H, CHCH₂OAr), 3.74 (ddd, $J = 9.9, 4.4, 2.3$ Hz, 1H, H-5), 2.08 (s, 3H, OAc), 2.03 (s, 3H, OAc), 2.00 (s, 3H, OAc), 1.92 (s, 3H, OAc).

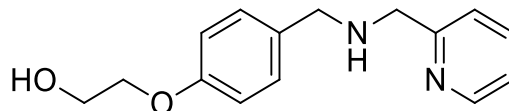
^{13}C NMR (126 MHz, CDCl_3) δ 190.7 (C=O), 170.6 (OAc), 170.2 (OAc), 169.4 (OAc), 169.3 (OAc), 163.6 (Ar), 132.0 (Ar), 130.2 (Ar), 114.8 (Ar), 101.05 (C-1), 72.7 (C-3), 71.9 (C-5), 71.1 (C-2), 68.3 (C-4), 67.92 ($\text{CH}_2\text{CH}_2\text{OAr}$), 67.4 ($\text{CH}_2\text{CH}_2\text{OAr}$), 61.9 (C-6), 20.7 (OAc), 20.6 (OAc), 20.6 (OAc), 20.5(OAc). HRMS m/z (ESI+): 497.1654 ($\text{C}_{23}\text{H}_{29}\text{O}_{12}$: $[\text{M}+\text{H}]^+$ requires 497.16590). IR (KBr Disk): 2977, 2953, 2926, 2890, 1744, 1700, 1609, 1578, 1511, 1448, 1377, 1255, 1228, 1170, 1137, 1043, 924, 839, 610, 520cm^{-1} . $[\alpha]_{\text{D}}^{24}$: -0.09 (c 0.5, CH_2Cl_2)



2.13

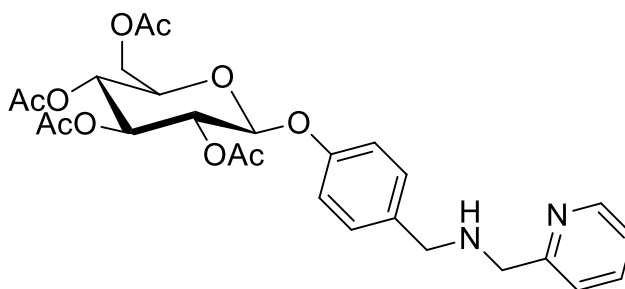
4-hydroxybenzaldehyde (10 g, 0.0818 mol), 2-aminomethylpyridine (8.76 mL, 0.085 mol) and Na_2SO_4 (15 g, 0.1 mol) were refluxed overnight in diethyl ether (200 mL). This was reduced to approximately 40 mL and cooled to -10°C in an ice/acetone/ NaCl bath and EtOH (100 mL, dried over molecular sieves) was added. NaBH_4 (9 g, 0.2379 mol) was added portion wise over 30min and allowed to warm to room temperature and stir overnight. The reaction was quenched with water (approximately 40 mL) and stirred until no more gas was generated. The EtOH was removed *in vacuo* and the reaction was extracted with 5 x 50 mL diethyl ether and the combined organic layers were washed with water (100 mL), brine (100 mL) and dried over Na_2SO_4 . The solvent was removed *in vacuo* to yield the product as a heavy brown oil (12.411 g, 71 %). ^1H NMR (300 MHz, CDCl_3) δ 8.52 (d, $J = 5.4$ Hz, 1H, pyr-H), 7.64 (td, $J = 7.7, 1.7$ Hz, 1H, pyr-H), 7.32 (d, $J = 7.7$ Hz, 1H, pyr-H), 7.18 (dd, $J = 7.0, 5.4$ Hz, 1H, pyr-H), 7.04 (d, $J = 8.4$ Hz, 2H, Ar-H), 6.62 (d, $J = 8.4$ Hz, 2H, Ar-H), 6.54 (s, 2H, N-H, O-H), 3.92 (s, 2H, CH_2), 3.72 (s, 2H, CH_2). ^{13}C NMR (126 MHz, CDCl_3) δ 158.8 (Pyr), 156.3 (Ar), 148.9 (Pyr), 137.2 (Pyr), 129.9 (Ar), 123.0 (Pyr), 122.5 (Pyr), 115.8 (Ar), 115.5 (Ar), 53.5 (Pyr CH_2), 52.8 (Ar CH_2). IR (KBr Disk): 3430, 3204, 3015, 2926, 1613, 1595, 1571, 1514, 1436, 1365, 1247, 1171, 831, 761, 564, 509cm^{-1} . HRMS m/z (ESI+): 215.1187, ($\text{C}_{13}\text{H}_{14}\text{N}_3\text{O}$: $[\text{M}+\text{H}]^+$ requires 215.1184). Elemental analysis calculated (%) for $\text{C}_{13}\text{H}_{14}\text{N}_3\text{O}$: C 72.87, H 6.59, N 13.07. Found: C 72.76, H 6.88, N 12.96.

Synthesized as per Brunner *et al*, however incomplete spectroscopic data was presented.⁸⁵



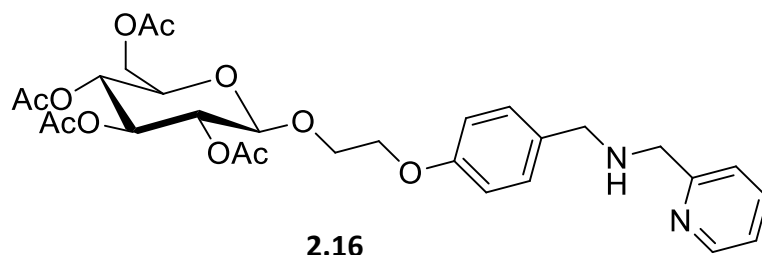
2.14

2.4 (1.523 g, 0.00916 mol) and 2-picolylamine (1.04 mL, 0.1 mol) were dissolved in EtOH (25 mL, dried over 3 Å molecular sieves) and refluxed for 3 h with MgSO₄ (2.21 g, 0.0183 mol) under N₂. This was cooled to -10 °C under Ar and solution of NaBH₄ (1.386 g, 0.0366 mol) in EtOH (20 mL, dried over molecular sieves) was added dropwise and the reaction was allowed to warm to room temperature and stir overnight. H₂O (approximately 25 mL) was added and the solution was heated to 80 °C for 30 min. The solvent was removed *in vacuo* and the residue was suspended in water to yield an orange solution the product was extracted with 5x30 mL portions of DCM. The combined organic layers were washed with brine, dried over Na₂SO₄ and the solvent was removed *in vacuo* to yield a heavy brown oil. By-products were removed by short path distillation (175 °C at 0.08 mbar) and the residue was further purified by column chromatography (0.8% MeOH in DCM, basic alumina stationary phase) to yield the product as a brown oil (1.609 g, 68 %). ¹H NMR (500 MHz, CDCl₃) δ 8.54 (d, *J* = 4.4 Hz, 1H, Pyr-H), 7.63 (apptd, *J* = 7.7, 1.7 Hz, 1H, Pyr-H), 7.35 – 7.28 (m, 1H, Pyr-H), 7.25 (d, *J* = 8.5 Hz, 2H, Ar-H), 7.15 (dd, *J* = 6.9, 5.3 Hz, 1H, Pyr-H), 6.83 (d, *J* = 8.6 Hz, 2H, Ar-H), 4.03 – 3.99 (m, 2H, CH₂OAr), 3.90 (s, 2H, CH₂Pyr), 3.90 – 3.87 (m, 2H, CH₂OH), 3.76 (s, 2H, CH₂Ar), 3.05 (bs, 2H, NH, OH). IR (NaCl Plate): 3306, 2928, 2862, 1610, 1594, 1570, 1511, 1474, 1454, 1435, 1367, 1301, 1247, 1175, 1085, 1051, 917, 985, 829, 761 cm⁻¹. HRMS *m/z* (ESI+): 259.1440 (C₁₅H₁₈N₂O₂: [M+H]⁺ requires 259.14465). Elemental analysis calculated (%) for C₁₅H₁₈N₂O₂: C 69.74, H 7.02, N 10.84. Found: C 69.38, H 7.09, N 10.77

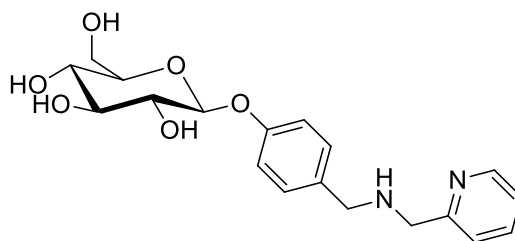


2.15

2.8 (1 g, 0.0022 mol) and 2-picolylamine (0.24 mL, 0.0022 mol) were stirred in EtOH (25 mL, dried over 3 Å molecular sieves) with MgSO₄ (3eq) for 4 h at 50 °C under N₂. This was filtered and cooled to approximately -10 °C in an ice/acetone/ salt bath under N₂ and AcOH (0.1 mL, 0.002 mol) was added immediately before the dropwise addition of a solution of NaBH₄ (0.333 g, 0.0088 mol) in EtOH (30 mL, dried over 3 Å molecular sieves). The solution was allowed to warm to room temperature and was stirred overnight before being quenched by the addition of water heating to 80 °C for 30 min until the precipitation of white boron salts had ceased. The solution dried *in vacuo* to yield a brown residue which was dissolved in water and extracted with EtOAc (5x40 mL). The combined organic layers were washed with brine (100 mL), dried with Na₂SO₄ and the solvent was removed *in vacuo* to yield the product as a heavy brown oil (0.934 g, 76 %). ¹H NMR (500 MHz, CDCl₃) δ 8.55 (d, *J* = 3.5 Hz, 1H), 7.67 (td, *J* = 7.6, 1.7 Hz, 1H), 7.33 – 7.28 (m, 3H), 7.21 (dd, *J* = 6.6, 5.1 Hz, 1H), 6.95 (d, *J* = 8.5 Hz, 2H), 5.27 (p, *J* = 9.4 Hz, 2H), 5.16 (t, *J* = 9.4 Hz, 1H), 5.06 (d, *J* = 7.3 Hz, 1H), 4.90 (s, 1H), 4.28 (dd, *J* = 12.2, 5.2 Hz, 1H), 4.22 – 4.12 (m, 1H), 3.99 (s, 2H), 3.88 (s, 2H), 3.86 – 3.79 (m, 1H), 3.70 (q, *J* = 7.0 Hz, 2H), 2.07 (s, 2H), 2.05 (s, 3H), 2.04 (s, 3H), 2.02 (s, 4H). ¹³C NMR (126 MHz, CDCl₃) δ 170.7 (C=O), 170.4 (=O), 169.5 (C=O), 169.4 (C=O), 159.5 (Pyr-C), 156.2 (Ar-C), 149.4 (Pyr-CH), 136.6 (Pyr-CH), 129.7 (Ar-C), 128.6 (Ar-CH), 122.6 (Pyr-CH), 122.2 (Pyr-CH), 117.2 (Ar-CH), 99.5 (C-1), 72.9 (C-4), 72.2 (C-5), 71.4 (C-3), 68.5 (C-2), 62.1 (C-6), 54.3 (PyrCH₂), 52.8 (ArCH₂), 20.8 (OAc), 20.8 (OAc), 20.7 (OAc), 20.7 (OAc). HRMS *m/z* (ESI⁺): 545.2139 (C₂₇H₃₂N₂O₁₀: [M+H⁺]⁺ requires 545.2135) IR (KBr Disk): 3427, 2945, 3922, 1751, 1610, 1592, 1511, 1474, 1435, 1369, 1235, 1214, 1069, 1042, 908, 831, 761, 600cm⁻¹. [α]_D²²: -0.07 (*c* 0.5, CH₂Cl₂), Elemental analysis calculated (%) for C₂₇H₃₂N₂O₂: C 59.55, H 5.92, N 5.14. Found: C 59.27, H 6.10, N 5.03.

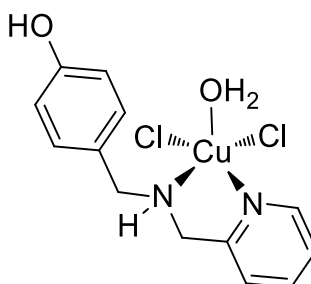


2.11 (6.436 g, 0.0129 mol) and 2-picolylamine (1.336 mL, 0.0129 mol) were refluxed in EtOH (25 mL, dried over 3 Å molecular sieves) with MgSO₄ (3.6 g) for 4 h under N₂. This was cooled to approximately -10 °C in an ice/acetone/ salt bath under N₂ and AcOH (0.74 mL, 0.0129 mol, dried over 3 Å molecular sieves) was added immediately before the dropwise addition of a solution of NaBH₄ (1.475 g, 0.0387 mol) in EtOH (30 mL, dried over 3 Å molecular sieves). The solution was allowed to warm to room temperature and was stirred overnight before being quenched by the addition of water heating to 80 °C for 30 min until the precipitation of white boron salts had ceased. The solution dried *in vacuo* to yield a brown residue which was dissolved in water and extracted with EtOAc (5x40 mL). The combined organic layers were washed with brine (100 mL), dried with Na₂SO₄ and the solvent was removed *in vacuo* to yield the product as an orange oil (3.229 g, 42.5%). ¹H NMR (500 MHz, CDCl₃) δ 8.56 (d, *J* = 4.0 Hz, 1H, Pyr-H), 7.64 (appt, *J* = 7.1 Hz, 1H, Pyr-H), 7.37 (appt, *J* = 8.6 Hz, 1H, Pyr-H), 7.26 (d, *J* = 6.5 Hz, 2H, Ar-H), 7.20 – 7.10 (m, 1H, Pyr-H), 6.87 (d, *J* = 6.5 Hz, 2H, Ar-H), 5.22 (appt, *J* = 9.5 Hz, 1H, H-3), 5.10 (appt, *J* = 9.7 Hz, 1H, H-4), 5.04 – 4.97 (m, 1H, H-2), 4.68 (d, *J* = 8.0 Hz, 1H, H-1), 4.26 (dd, *J* = 12.1, 3.8 Hz, 1H, H-6), 4.17 – 4.09 (m, 3H, H-6', OCH₂CH₂OAr), 3.91 (s, 2H, Pyr-CH₂), 3.78 (s, 2H, Ar-CH₂), 3.72 (ddd, *J* = 9.8, 4.4, 2.2 Hz, 1H, H-5), 3.64 – 3.55 (m, 1H, OCH₂CH₂OAr), 3.49-3.53 (m, 1H, OCH₂CH₂OAr), 2.07 (s, 3H, OAc), 2.03 (s, 3H, OAc), 2.00 (s, 3H, OAc), 1.93 (s, 3H, OAc). ¹³C NMR (126 MHz, CDCl₃) δ 170.7 (C=O), 170.3 (C=O), 169.4 (C=O), 169.4 (C=O), 159.4 (Pyr), 158.6 (Ar), 157.7 (Ar), 149.3 (Pyr), 136.5 (Pyr), 131.9 (Ar), 127.9 (Pyr), 122.5 (Pyr), 114.2 (Ar), 101.2 (C-1), 72.8 (C-3), 71.9 (C-5), 71.2 (C-2), 68.4 (C-4), 68.3 (CH₂Pyr), 67.3 (OCH₂CH₂OAr), 61.9 (C-6), 61.0 (OCH₂CH₂OAr), 60.9 (CH₂Ar), 20.9 (OAc), 20.7 (OAc), 20.6 (OAc), 20.5 (OAc). IR (NaCl Plate): 3385, 2970, 2932, 2883, 1755, 1611, 1512, 1435, 1367, 1231, 1070, 1040, 910, 832, 760, 596 cm⁻¹. HRMS *m/z* (ESI⁺): 589.2407 (C₂₉H₃₇N₂O₁₁: [M+H]⁺ requires 589.2392). [α]_D²³: -0.14 (c 0.5, MeOH). Anal. Calcd for C₂₉H₃₆N₂O₁₁: C, 59.18; H, 6.16; N, 4.76 Found: C, 59.17; H, 6.11; N, 4.45%



2.17

2.13 (2.656 g, 0.00487 mol) was dissolved in MeOH/H₂O (40/5 mL) and a drop of 5.4 M NaOMe solution was added. The reaction was stirred at room temperature for 1 hr and the pH was adjusted to approximately 9 using Dowex H⁺. The reaction was filtered and the solvent removed *in vacuo* to yield a brown oil which gave product as a light brown solid after lyophilisation for 48 h (1.836 g, quantitative yield). IR (KBr Disk): 3379, 2969, 2875, 1611, 1596, 1571, 1511, 1478, 1437, 1367, 1303, 1234, 1177, 1075, 1046, 1015, 896, 832, 763, 630, 559cm⁻¹. HRMS m/z (ESI⁺): 377.1697 (C₁₉H₂₅N₂O₆: [M+H]⁺ requires 377.1707). [α]_D²⁴: -0.11 (c 0.5, H₂O). Mp: 86-87 °C. Anal. Calcd for C₁₉H₂₄N₂O₆: C, 60.63; H, 6.43; N, 7.44 Found: C, 60.39; H, 6.56; N, 7.24%

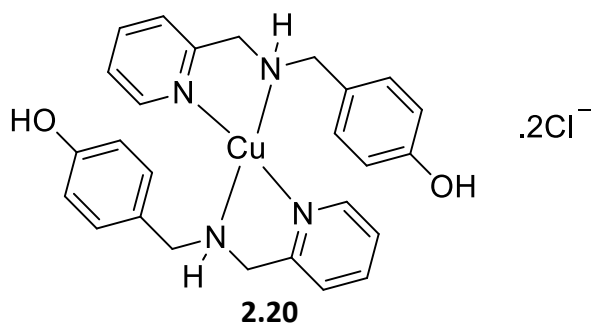


2.19

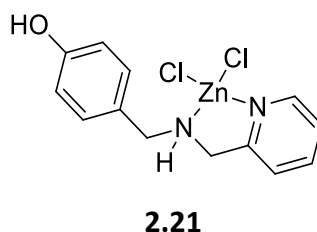
2.13 (0.438 g, 0.002 mol) was dissolved in EtOH (10 mL) and a CuCl₂·6H₂O solution (0.348 g, 0.002 mol in 10 mL EtOH) was added. A blue/green precipitate was formed and the reaction was allowed to stir at room temperature overnight. The solvent was reduced by half *in vacuo* and cooled on ice for 30 min and a green/blue solid was collected. This was washed with cold EtOH and dried under vacuum (0.525g, 69 %). IR (KBr Disk): 3495, 3377, 3198, 2970, 2918, 2873, 1610, 1516, 1484, 1444, 1234, 1217, 1049, 823, 768, 579, 510 cm⁻¹. Anal. Calcd for C₁₃H₁₆N₂Cl₂O₂Cu: C, 42.58; H, 4.40; N, 7.64. Found: C, 42.66; H, 4.39; N, 7.30%. Mp: 178 °C. μ_{eff}: 1.78 B.M.

Crystals suitable for X-ray analysis were obtained from a solution of the ligand in acetonitrile.

Empirical formula	$C_{56}H_{62}Cl_8Cu_4N_{10}O_4$	
Formula weight	1476.91	
Temperature	100(2) K	
Wavelength	0.71073 Å	
Crystal system	Triclinic	
Space group	$P\bar{1}$	
Unit cell dimensions	$a = 11.9914(6)$ Å	$\alpha = 113.9980(10)^\circ$.
	$b = 12.6755(6)$ Å	$\beta = 96.5800(10)^\circ$.
	$c = 12.6960(6)$ Å	$\gamma = 115.3470(10)^\circ$.
Volume	$1492.64(13)$ Å ³	
Z	1	
Density (calculated)	1.643 Mg/m ³	
Absorption coefficient	1.819 mm ⁻¹	
F(000)	752	
Crystal size	0.230 x 0.180 x 0.120 mm ³	
Theta range for data collection	1.874 to 30.211°.	
Index ranges	$-16 \leq h \leq 16, -17 \leq k \leq 17, -17 \leq l \leq 17$	
Reflections collected	58825	
Independent reflections	8816 [R(int) = 0.0282]	
Completeness to theta = 25.242°	100.0 %	
Absorption correction	Semi-empirical from equivalents	
Max. and min. transmission	0.7460 and 0.6898	
Refinement method	Full-matrix least-squares on F ²	
Data / restraints / parameters	8816 / 0 / 381	
Goodness-of-fit on F ²	1.030	
Final R indices [$I > 2\sigma(I)$]	R1 = 0.0223, wR2 = 0.0542	
R indices (all data)	R1 = 0.0292, wR2 = 0.0572	
Largest diff. peak and hole	0.423 and -0.420 e.Å ⁻³	



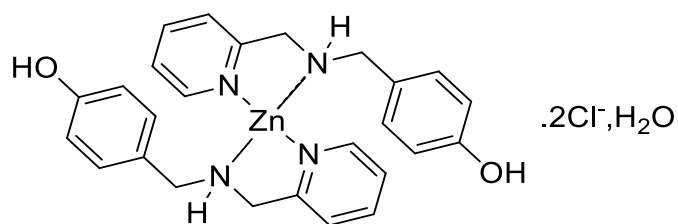
2.13 (0.613 g, 0.0028 mol) was dissolved in EtOH (10 mL) and a CuCl₂·6H₂O solution (0.163 g, 0.00093 mol, 0.33eq in 10 mL EtOH) was added. A green precipitate was formed and the reaction was allowed to stir at room temperature overnight. The solvent was reduced by half *in vacuo* and cooled on ice for 30 min and a green/blue solid. This was washed with cold EtOH and dried under vacuum (0.489 g, 62%). IR (KBr Disk): 3340, 3161, 3079, 2947, 2883, 1610, 1594, 1515, 1489, 1446, 1273, 1235, 1179, 1053, 828, 761, 585, 505 cm⁻¹. HRMS m/z (ESI+): 491.1523, (C₂₆H₂₈N₄O₂Cu: [M^{*}]⁺ requires 491.1508). Mp: 162-163°C. Anal. Calcd for C₂₆H₂₈N₄Cl₂O₂Cu: C, 55.47; H, 5.01; N, 9.95 Found: C, 55.46; H, 5.21; N, 9.73%. μ_{eff}: 1.89 B.M.



2.13 (0.425 g, 0.00198 mol) was dissolved in EtOH (10 mL) at and a solution of ZnCl₂ (0.270 g, 0.00198 mol in 10 mL EtOH) was added. A white precipitate was formed after several minutes stirring at room temperature and the reaction was allowed to stir overnight. This was reduced *in vacuo* by approximately half and cooled on ice to yield a brown precipitate. This was collected by filtration and washed with cold EtOH to yield a brown solid upon drying (0.349 g, 52 %). IR (KBr Disk): 3415, 3233, 3211, 3228, 1610, 1572, 1520, 1438, 1207, 1030, 835, 767, 509 cm⁻¹. Mp: 169-170 °C Anal. Calcd for C₁₃H₁₆N₂Cl₂O₂Zn: C, 44.54; H, 4.03; N, 7.99. Found: C, 44.01; H, 4.27; N, 7.79 %.

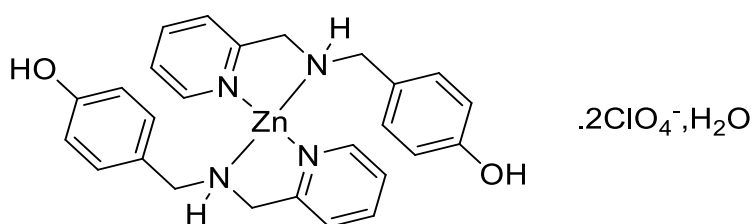
Crystals suitable for X-ray analysis were grown by slow evaporation of the filtrate over several weeks to yield pale brown rhombic crystals.

Empirical formula	C ₁₃ H ₁₄ Cl ₂ N ₂ OZn	
Formula weight	350.53	
Temperature	99.92 K	
Wavelength	0.71073 Å	
Crystal system	Monoclinic	
Space group	P2 ₁ /n	
Unit cell dimensions	a = 12.7884(7) Å	α = 90°.
	b = 8.3147(5) Å	β = 92.337(2)°.
	c = 13.8733(7) Å	γ = 90°.
Volume	1473.94(14) Å ³	
Z	4	
Density (calculated)	1.580 Mg/m ³	
Absorption coefficient	2.021 mm ⁻¹	
F(000)	712	
Crystal size	0.2 x 0.2 x 0.13 mm ³	
Theta range for data collection	2.857 to 28.420°.	
Index ranges	-16 ≤ h ≤ 17, -11 ≤ k ≤ 7, -18 ≤ l ≤ 18	
Reflections collected	13564	
Independent reflections	3684 [R(int) = 0.0487]	
Completeness to theta = 26.000°	99.9 %	
Absorption correction	Semi-empirical from equivalents	
Max. and min. transmission	0.7457 and 0.6619	
Refinement method	Full-matrix least-squares on F ²	
Data / restraints / parameters	3684 / 0 / 180	
Goodness-of-fit on F ²	1.019	
Final R indices [I > 2σ(I)]	R1 = 0.0323, wR2 = 0.0596	
R indices (all data)	R1 = 0.0548, wR2 = 0.0671	
Largest diff. peak and hole	0.389 and -0.435 e.Å ⁻³	



2.22

2.13 (0.858 g, 0.004 mol) was dissolved in EtOH (15 mL) and a solution of ZnCl₂ (0.177 g, 0.0013 mol in 10 mL EtOH) was added. A white precipitate was formed after several minutes stirring at room temperature and the reaction was allowed to stir overnight. The solvent was reduced *in vacuo* by approximately half and the solution was cooled on ice for 30 min. A white precipitate was collected by filtration and washed with cold EtOH (0.703 g, 90 %). IR (KBr Disk): 3395, 3158, 3125, 3090, 2900, 1611, 1592, 1574, 1516, 1489, 1445, 1366, 1274, 1236, 1176, 1085, 981, 828, 759, 506 cm⁻¹. Mp: 178-179 °C. Anal. Calcd for C₂₆H₃₀N₄Cl₂O₃Zn: C, 54.24 H, 5.56; N, 9.37. Found: C, 54.18; H, 5.19; N, 9.65%. ¹H NMR (500 MHz, DMSO) δ 9.32 (s, 1H, N-H), 8.51 (s, 1H, Pyr-H), 7.91 (t, 1H, Pyrr-H), 7.52 (ds, H, Pyr-H), 7.41 (bs, 1H, Pyr-H), 7.16 (d, 2H, Ar-H), 6.71 (d, 2H, Ar-H), 3.84 (s, 2H, Pyr-CH₂), 3.65 (s, 2H, Ar-CH₂). ¹³C NMR (126 MHz, DMSO) δ 157.1 (Pyr-C), 149.2 (Ar-C), 145.3 (Pyr-CH), 141.4 (Pyr-CH), 131.5 (Pyr-CH), 130.2 (Ar-CH), 125.4 (Ar-CH), 115.4 (Ar-CH), 56.8 (CH₂), 52.0 (CH₂).



2.23

To a solution of **2.13** (0.397 g, 0.00185 mol) in EtOH (10 mL) was added a solution of Zn (ClO₄)₂·6H₂O (0.229 g, 0.00061 mol) in EtOH (10 mL) at room temperature to immediately yield a beige precipitate. This was stirred for 5 h and the precipitate was collected by vacuum filtration to yield the product as a hygroscopic brown solid which was then freeze dried to yield the product as a brown powder (0.207 g, 62 %). ¹H

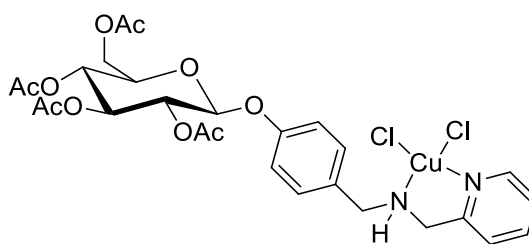
NMR (500 MHz, CD₃CN) δ 8.11 (bs, 2H, Ar-H), 8.05 – 8.00 (m, 2H, Ar-H), 7.49 (bs, 4H, Ar-H), 7.09 (bs, 4H, Ar-H), 6.77 (bs, 4H, Ar-H), 3.91 (bs, 4H, Pyr-CH₂), 3.64 (bs, 4H, Ar-CH₂). ¹³C NMR (126 MHz, DMSO) δ 157.1 (Pyr-C), 148.1 (Ar-C), 147.3 (Pyr-CH), 140.4 (Pyr-CH), 130.5 (Pyr-CH), 130.2 (Ar-CH), 124.1 (Ar-CH), 115.7 (Ar-CH), 56.6 (CH₂), 52.0 (CH₂). IR (KBr Disk): 3430, 2935, 2968, 1613, 1574, 1517, 1489, 1446, 1375, 1269, 1222, 1177, 1108, 1051, 928, 833, 764, 623, 509cm⁻¹. Mp: 161-163 °C. Anal. Calcd for C₂₆H₃₀N₄Cl₂O₁₁Zn: C, 43.93; H, 4.25; N, 7.88. Found: C, 44.02; H, 4.49; N, 8.20%



2.24

2.14 (0.200 g, 0.00077 mol) was dissolved in EtOH (10 mL) at room temperature and a solution of CuCl₂·2H₂O (0.158 g, 0.00092 mol) in EtOH (8 mL) was added to yield a green precipitate. This was stirred for 4 h and the product was collected by vacuum filtration and dried to yield the product as a dark green solid (0.189 g, 62.5 %).

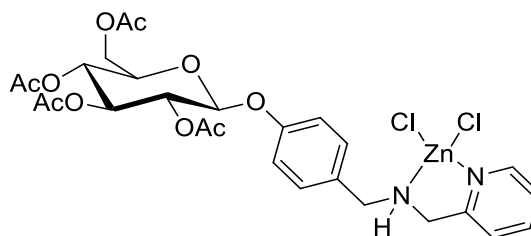
IR (KBr Disk): 3437, 3238, 2941, 2868, 1609, 1583, 1512, 1485, 1448, 1308, 1250, 1183, 1079, 1053, 918, 895, 841, 816, 767, 646, 598, 542cm⁻¹. Anal. Calcd for C₁₅H₂₀Cl₂CuN₂O₃: C, 43.86; H, 4.91; N, 6.82. Found: C, 43.34; H, 4.69; N, 6.29%. μ_{eff} : 1.86 B.M



2.25

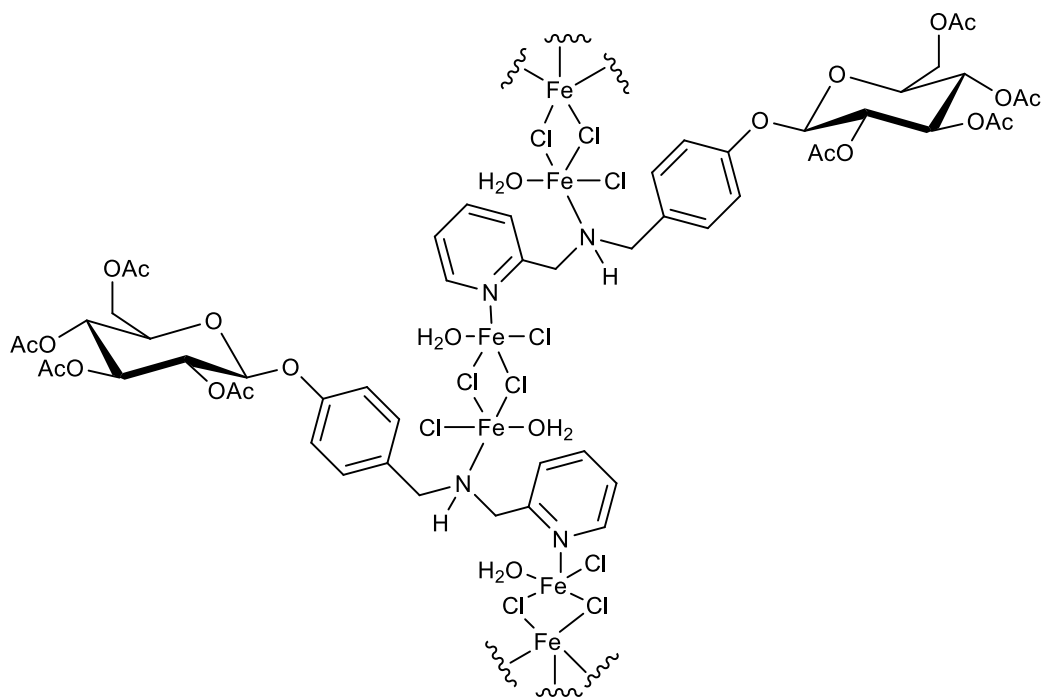
2.15 (0.294 g, 0.00054 mol) was dissolved in EtOH (10 mL) at room temperature and a solution of CuCl₂·2H₂O (0.110 g, 0.00065 mol) in EtOH (10 mL) was added and the reaction was allowed to stir overnight. The resulting green solution was allowed to stand for 3 days and a green precipitate was collected. This was washed with cold

EtOH and dried *in vacuo* to yield a green powder (0.216 g, 59 %). IR (KBr Disk): 3421, 2998, 2924, 2887, 1753, 1628, 1610, 1512, 1486, 1447, 1431, 1376, 1231, 1045, 908, 769, 600 cm^{-1} . Mp: 146-147 °C. Anal. Calcd for $\text{C}_{27}\text{H}_{32}\text{N}_2\text{Cl}_2\text{O}_{10}\text{Cu}$: C, 47.76; H, 4.75; N, 4.13. Found: C, 47.46; H, 4.85; N, 3.82%. μ_{eff} : 1.71 B.M



2.26

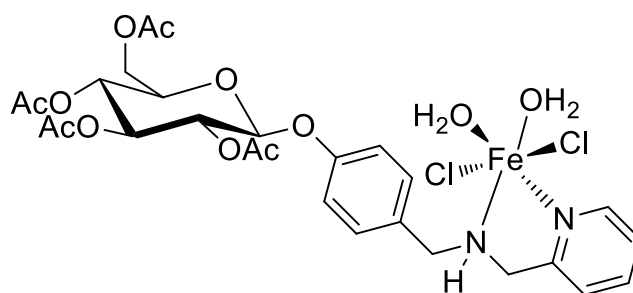
2.15 (0.200 g, 0.00036 mol) was dissolved in EtOH (15 mL) at room temperature and a solution of ZnCl_2 (0.049 g, 0.00036 mol) in EtOH (5 mL) was added which immediately formed a beige precipitate. The reaction was stirred for 4 h and the solid was filtered and washed with cold ethanol to yield the product as a beige solid (0.127 g, 52 %). ^1H NMR (500 MHz, DMSO) δ 8.57 (bs, 1H, Pyr-H), 8.02 (t, $J = 7.5$ Hz, 1H, Pyr-H), 7.59-7.53(m, 2H, Pyr-H), 7.36 (d, $J = 7.9$ Hz, 2H, Ar-H), 6.98 (d, $J = 7.8$ Hz, 2H, Ar-H), 5.57 (d, $J = 8.9$ Hz, 1H, H-1), 5.43 (t, $J = 7.9$ Hz, 1H, H-4), 5.07 (at, $J = 7.3$ Hz, 1H, H-2), 5.03 (at, $J = 7.5$ Hz, 1H, H-3), 4.27-4.23 (m, 1H, H-5), 4.19 (dd, $J = 9.3, 3.9$ Hz, 1H, H-6), 4.08 (ad, $J = 4.0$ Hz, 1H, H-6'), 3.88 (s, 2H, PyrCH₂), 3.79 (bs, 2H, ArCH₂), 2.03 (s, 3H, OAc), 2.03 (s, 3H, OAc), 2.02 (s, 3H, OAc), 1.98 (s, 3H, OAc). ^{13}C NMR (126 MHz, DMSO) δ 170.4 (C=O), 170.0 (=O), 169.8 (C=O), 169.6 (C=O), 156.2 (Pyr-C), 148.2 (Ar-C), 140.2 (Pyr-CH), 132.2 (Pyr-CH), 130.8 (Ar-C), 124.4 (Ar-CH), 124.2 (Ar-CH), 123.9 (Pyr-CH), 116.7 (Pyr-CH), 97.5 (C-1), 72.4 (C-4), 71.2 (C-5), 71.2 (C-3), 68.5 (C-2), 62.1 (C-6), 51.9 (PyrCH₂), 51.0 (ArCH₂), 20.9 (OAc), 20.8 (OAc), 20.8 (OAc), 20.7 (OAc). IR (KBr Disk): 3460, 3264, 2961, 2941, 1752, 1610, 1574, 1512, 1486, 1446, 1370, 1231, 1065, 1044, 910, 836, 768, 599 cm^{-1} . Mp: 123-124 °C. Anal. Calcd for $\text{C}_{27}\text{H}_{32}\text{N}_2\text{Cl}_2\text{O}_{10}\text{Zn}$: C, 47.63; H, 4.74; N, 4.11. Found: C, 47.26; H, 4.81; N, 4.04%



2.27

This reaction was carried out on a Schlenk line under a positive pressure of nitrogen. Flame dried glassware was used and the ethanol was dried over 3 Å molecular sieves and degassed using the freeze-pump-thaw method.

2.15 (0.366 g, 0.00067 mol) was dissolved in EtOH (10 mL) at room temperature to which a solution of FeCl₂·4H₂O (0.04 g, 0.00022 mol) in EtOH (5 mL) was added dropwise via cannula. This formed a deep green solution which was allowed to stir for 3 h before the solvent was reduced by approximately half *in vacuo* and left to stand overnight. This was then filtered under a flow of nitrogen to yield the product as an air stable green/grey solid (0.112 g, 60%). IR (KBr Disk): 3429, 2913, 1752, 1607, 1510, 1479, 1437, 1369, 1231, 1038, 1046, 909, 835, 766, 601 cm⁻¹. Mp: 149-150 °C. Anal. Calcd for C₂₇H₃₆N₂Cl₄O₁₂Fe₂: C, 38.88; H, 4.35; N, 3.36. Found: C, 38.89; H, 4.04; N, 3.30%. μ_{eff} : 9.76 B.M

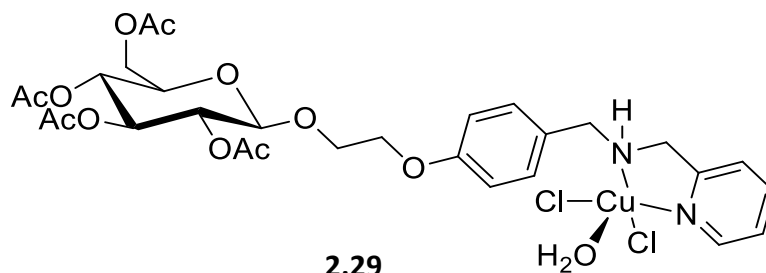


2.28

This reaction was carried out on a Schlenk line under a positive pressure of nitrogen. Flame dried glassware was used and the ethanol was dried over 3 Å molecular sieves and degassed using the freeze-pump-thaw method.

2.15 (0.266 g, 0.00048 mol) was dissolved in EtOH (10 mL) and was added dropwise via cannula to a solution of FeCl₂·4H₂O (0.116 g, 0.00057 mol) in EtOH (8 mL) which immediately produced a yellow brown precipitate. This was stirred for 3h at room temperature and the solvent was reduced *in vacuo* by approximately half and the solution was allowed to stand overnight. This was filtered under a stream of nitrogen to yield the product as a yellow brown solid (0.181 g, 53%).

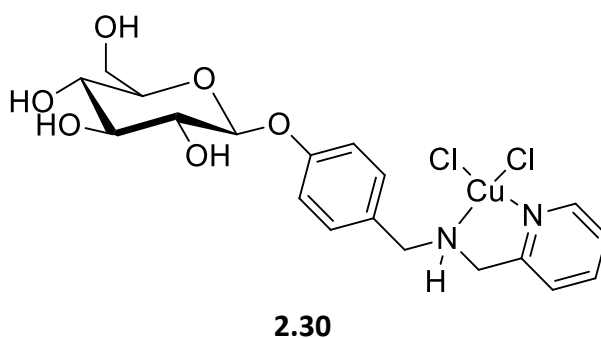
IR (KBr Disk): 3436, 3271, 2940, 1755, 1608, 1513, 1441, 1368, 1227, 1065, 1040, 907, 834, 777, 598 cm⁻¹. Mp: 141-142°C. Anal. Calcd for C₂₇H₃₆N₂Cl₂O₁₂Fe: C, 45.85; H, 5.13; N, 3.96. Found: C, 45.99; H, 4.77; N, 4.05%. μ_{eff} : 5.16 B.M.



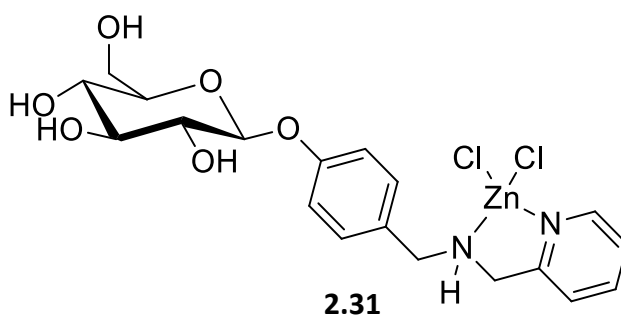
2.29

2.16 (0.74 3g, 0.0012 mol) was dissolved in EtOH (12 mL) and a solution of CuCl₂·2H₂O (0.258 g, 0.0015 mol) in EtOH (10 mL) was added to immediately yield a dark green solution. This was stirred for 4 h at room temperature and after standing for an hour, the solution had undergone partial gelation to yield a blue viscous gel like substance. This was filtered and dried *in vacuo* using Abderhaldens Drying Pistol using refluxing

acetone as the heat source to yield a dark green solid which was dried further by lyophilisation for 24 h to produce a green powder (0.499 g, 57.7 %). IR (KBr Disk): 3442, 3202, 2940, 2932, 2879, 1753, 1609, 1513, 1483, 1448, 1423, 1368, 1231, 1067, 1040, 913, 834, 773, 600 cm^{-1} . HRMS m/z (ESI+): 744.0897($\text{C}_{29}\text{H}_{36}\text{Cl}_2\text{CuN}_2\text{NaO}_{11}$: $[\text{M}+\text{Na}]^+$ requires 744.0889). Mp: 117-118°C. Anal. Calcd for $\text{C}_{29}\text{H}_{38}\text{Cl}_2\text{CuN}_2\text{O}_{12}$: C, 47.00; H, 5.17; N, 3.78 Found: C, 46.59; H, 5.11; N, 3.25 %. μ_{eff} : 1.98 B.M.

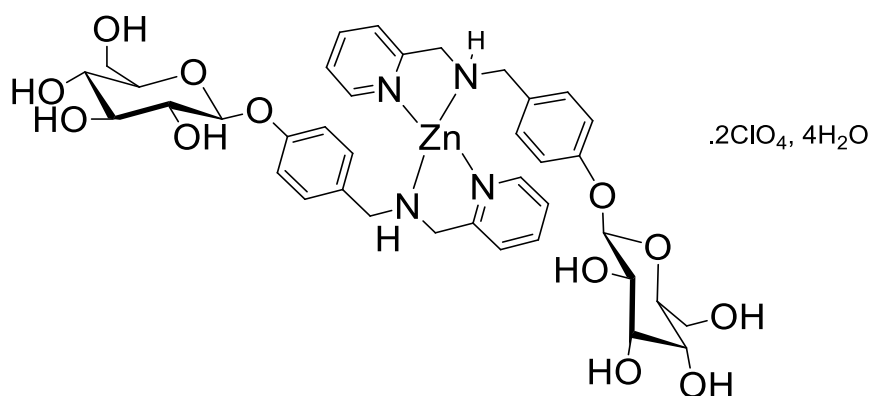


2.17 (0.200 g, 0.00053 mol) was dissolved in EtOH (15 mL) with sonication, and added to a stirring solution of $\text{CuCl}_2 \cdot 2\text{H}_2\text{O}$ (0.109 g, 0.00063 mol) in EtOH (8 mL) at room temperature to immediately yield a pale green solid. The reaction was stirred for 3 h and the product was collected by vacuum filtration and dried under vacuum (0.117 g, 43.2%). IR (KBr Disk): 3406, 2924, 2879, 1610, 1574, 1511, 1486, 1447, 1235, 1184, 1074, 1045, 896, 830, 767, 658, 628, 575, 419 cm^{-1} . HRMS m/z (ESI+): 532.0228 ($\text{C}_{19}\text{H}_{24}\text{Cl}_2\text{CuN}_2\text{O}_6\text{Na}$: $[\text{M}+\text{Na}]^+$ requires 532.0200). Mp: 140 °C. Anal. Calcd for $\text{C}_{19}\text{H}_{24}\text{Cl}_2\text{CuN}_2\text{O}_6$: C, 44.67; H, 4.74; N, 5.48. Found: C, 44.54; H, 5.17; N, 5.30%. μ_{eff} : 1.84 BM.



2.17 (0.300 g, 0.00079 mol) was dissolved in EtOH (15 mL) with sonication and added to a stirring solution of ZnCl_2 (0.130 g, 0.00095 mol) in EtOH (8 mL) at room

temperature to immediately yield a beige solid. The reaction was stirred for 3 h and the product was collected by vacuum filtration and dried by lyophilisation for 72 h to produce a pale yellow solid (0.092 g, 22.7%). ^1H NMR (500 MHz, D_2O) δ 8.21 (s, 1H, Pyr-H), 7.89 (s, 1H, Pyr-H), 7.51 – 7.43 (m, 1H, Pyr-H), 7.38 (d, J = 6.8 Hz, 1H, Ar-H), 7.11-7.08 (m, 1H, Pyr-H), 6.98(d, J = 6.8 Hz, 2H, Ar-H), 3.79 (s, 2H), 3.76 (bs, 2H), 3.72 (s, 2H), 3.69 (d, J = 9.8, 1H, H-6), 3.61 – 3.33(m, 6H). ^{13}C NMR (126 MHz, D_2O) δ 185.9 (Pyr), 154.2 (Pyr), 148.8 (Pyr), 140.1 (Pyr), 133.3 (Ar), 130.8 (Pyr), 124.2 (Ar), 119.4 (Ar), 117.7 (Ar), 99.5 (C-1), 77.8 (Glu-C), 76.6 (Glu-C), 73.5 (Gluc-C), 68.8 (Gluc-C), 59.1 (Pyr- CH_2), 51.6 (C-6), 50.7 (Ar- CH_2). IR (KBr Disk): 3430, 2920, 2873, 1610, 1512, 1446, 1236, 1074, 1043, 1015, 834, 767, 630, 565cm^{-1} . HRMS m/z (ESI+): 548.9894 ($\text{C}_{19}\text{H}_{24}\text{Cl}_2\text{ZnN}_2\text{O}_6\text{K}$: $[\text{M}+\text{K}]^+$ requires 548.9934). Mp: 127- 129 °C. Anal. Calcd for $\text{C}_{19}\text{H}_{24}\text{Cl}_2\text{N}_2\text{O}_6\text{Zn}$: C, 44.51; H, 4.72; N, 5.47. Found: C, 44.98; H, 4.99; N, 5.01%



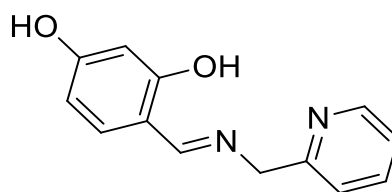
2.32

2.17 (0.216 g, 0.00057 mol) was dissolved in EtOH (15 mL) with sonication and a solution of $\text{Zn}(\text{ClO}_4)_2 \cdot 6\text{H}_2\text{O}$ (0.0854 g, 0.00028 mol) in EtOH (5 mL) was added to immediately produce a white precipitate. The reaction was stirred for 2 h at room temperature and reduced *in vacuo* to approximately 10 mL and the product was isolated by vacuum filtration and washed with cold ethanol to yield a sticky hygroscopic beige solid. This was lyophilized for 24 h to produce a beige solid.

^1H NMR (500 MHz, D_2O) δ 8.28 (s, 1H, Pyr-H), 7.94 (s, 1H, Pyr-H), 7.48 – 7.41 (m, 1H, Pyr-H), 7.38 (d, J = 7.0 Hz, 1H, Ar-H), 7.13-7.15 (m, 1H, Pyr-H), 7.00 (d, J = 7.0 Hz, 2H, Ar-H), 3.89 (s, 2H), 3.84 (d, J = 12.2 Hz, 2H), 3.72 (s, 2H), 3.68 (dd, J = 12.5, 5.4 Hz,

1H, H-6), 3.59 – 3.46 (m, 5H), 3.45 – 3.35 (m, 1H). ¹³C NMR (126 MHz, D₂O) δ 182.0 (Pyr), 156.5 (Pyr), 148.9 (Pyr) 138.4 (Pyr), 132 (Ar) 130.6 (Pyr), 124.6 (Ar), 124.3 (Ar), 116.9 (Ar), 100.2 (C-1), 76.2 (Glu-C), 75.6 (Glu-C), 72.9 (Gluc-C), 69.4 (Gluc-C), 60.6 (Pyr-CH₂), 51.6 (C-6) I, 50.1 (Ar-CH₂). IR (KBr Disk): 3421, 3282, 2922, 2879, 1610, 1575, 1512, 1487, 1446, 1397, 1303, 1237, 1183, 1121, 1078, 1015, 895, 833, 767, 625, 565cm⁻¹. Mp: 143-145°C. Anal. Calcd for C₃₈H₅₆Cl₂N₄O₂₄Zn: C, 41.90; H, 5.18; N, 5.14. Found: C, 42.17; H, 4.97; N, 4.99%

6.2.2 N₂O Series

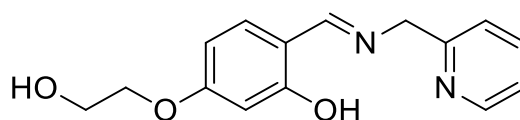


2.33

2,4-dihydroxybenzaldehyde (2 g, 0.0144 mol) and 2-picolylamine (1.49 mL, 0.0144 mol) were stirred at room temperature in EtOH (25 mL) for 4 h. The product precipitated out as a yellow solid which was collected by vacuum filtration and dried to give the product in a quantitative yield. ¹H NMR (500 MHz, CDCl₃) δ 8.60 (d, *J* = 4.9 Hz, 1H, Pyr-H), 8.25 (s, 1H, C(=N)H), 7.77 (dd, *J* = 8.5, 6.9 Hz, 1H, Pyr-H), 7.42 (d, *J* = 7.8 Hz, 1H, Pyr-H), 7.35 – 7.26 (m, 1H), 6.87 (d, *J* = 8.4 Hz, 1H, Ar-H), 6.29 (d, *J* = 2.2 Hz, 1H, Ar-H), 6.20 (dd, *J* = 8.4, 2.2 Hz, 1H, Ar-H), 4.83 (s, 2H, CH₂). ¹³C NMR (126 MHz, CDCl₃) δ 166.2 (C=N), 164.0 (Pyr), 160.8 (Pyr), 157.9 (Ar), 149.1 (Pyr), 137.8 (Pyr), 133.5 (Ar), 123.2 (Pyr), 123.05 (Ar), 112.5 (Ar), 107.3 (Ar), 103.4 (Ar), 64.3 (CH₂). IR (KBr Disk): 3435, 3064, 2763, 2676, 2618, 1621, 1442, 1331, 1271, 1120cm⁻¹. HRMS *m/z* (ESI+): 228.0905 (C₁₃H₁₂N₂O₂: [M+H]⁺ requires 228.0899). Mp: 159-160°C. Anal. Calcd for C₁₃H₁₂N₂O₂: C, 68.41; H, 5.30; N, 12.27 Found: C, 68.63; H, 5.44; N, 12.28%.

Crystals suitable for x-ray crystallography were grown by dissolving the sample in hot acetonitrile and letting the sample stand for several hours to yield pale orange trapezoid-like crystals.

Empirical formula	C ₁₃ H ₁₂ N ₂ O ₂	
Formula weight	228.25	
Temperature	99.92 K	
Wavelength	0.71073 Å	
Crystal system	Monoclinic	
Space group	C2/c	
Unit cell dimensions	a = 22.8835(13)	α = 90°.
	b = 5.7669(3) Å	β = 112.5980(15)°.
	c = 18.6703(10) Å	γ = 90°.
Volume	2274.7(2) Å ³	
Z	8	
Density (calculated)	1.333 Mg/m ³	
Absorption coefficient	0.092 mm ⁻¹	
F(000)	960	
Crystal size	0.28 x 0.2 x 0.2 mm ³	
Theta range for data collection	3.580 to 28.260°.	
Index ranges	-30 ≤ h ≤ 28, -7 ≤ k ≤ 5, -18 ≤ l ≤ 24	
Reflections collected	8049	
Independent reflections	2810 [R(int) = 0.0258]	
Completeness to theta = 25.242°	99.6 %	
Absorption correction	Semi-empirical from equivalents	
Max. and min. transmission	0.7457 and 0.7075	
Refinement method	Full-matrix least-squares on F ²	
Data / restraints / parameters	2810 / 0 / 163	
Goodness-of-fit on F ²	1.026	
Final R indices [I > 2σ(I)]	R1 = 0.0391, wR2 = 0.0949	
R indices (all data)	R1 = 0.0529, wR2 = 0.1034	
Extinction coefficient	0.0049(6)	
Largest diff. peak and hole	0.359 and -0.213 e.Å ⁻³	



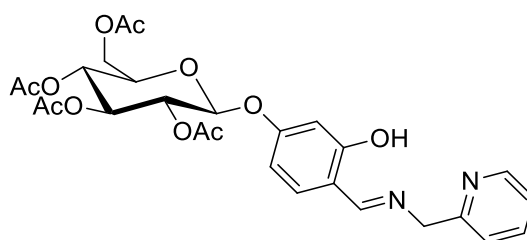
2.34

2.38 (0.954 g, 0.0052 mol) was dissolved in EtOH (20 mL, dried over 3 Å molecular sieves) at 35 °C and 2-picolylamine (0.54 mL, 0.0052 mol) was added. This was stirred overnight at room temperature under N₂ and the solvent was reduced *in vacuo* to approximately 10 mL and cooled on ice to yield a yellow precipitate which was filtered and washed with cold EtOH to give the product as bright yellow solid (1.217 g, 86%). ¹H NMR (500 MHz, CDCl₃) δ 13.83 (s, 1H, Ar-OH), 8.58 (d, *J* = 4.9 Hz, 1H, Pyr), 8.41 (s, 1H, C(=N)H), 7.69 (td, *J* = 7.7, 1.8 Hz, 1H, Pyr), 7.35 (d, *J* = 7.7 Hz, 1H, Ar-H), 7.22 – 7.20 (m, 1H, Ar-H), 7.18 (d, *J* = 8.9 Hz, 1H, Ar-H), 6.46 (m, 2H, Ar-H), 6.44 (d, *J* = 2.4 Hz, 1H, Ar-H), 4.89 (s, 2H, Pyr-CH₂), 4.18 – 4.06 (t, *J* = 4.9, 2H, ArO-CH₂), 4.01 – 3.92 (t, *J* = 4.9, 2H, CH₂OH). ¹³C NMR (126 MHz, CDCl₃) δ 166.1 (Ar-C), 164.2 (Ar-C), 161.1 (C=N), 157.7 (Pyr-C), 148.9 (Pyr-CH), 137.8 (Pyr-CH), 133.4 (Ar-CH), 123.2 (Pyr-CH), 123.0 (Pyr-CH), 112.3 (Ar-C), 107.3 (Ar-C), 103.3 (Ar-CH), 63.9 (CH₂). IR (KBr Disk): 3406, 3269, 2943, 2927, 2896.2, 1630, 1596, 1179.5, 1138, 1096, 1044, 844, 763, 614 cm⁻¹. HRMS *m/z* (ESI+): 273.1233 (C₁₄H₁₇N₂O₃: [M+H]⁺ requires 273.1239). Mp: 124 °C. Anal. Calcd for C₁₅H₁₄N₂O₃: C, 66.54; H, 5.92; N, 10.29 Found: C, 66.35; H, 6.05; N, 10.26%

Crystals suitable for x-ray crystallography were grown by dissolving the sample in hot acetonitrile and which yielded long needle shaped crystals upon cooling to room temperature.

Empirical formula	C ₁₅ H ₁₆ N ₂ O ₃	
Formula weight	272.30	
Temperature	99.99 K	
Wavelength	0.71073 Å	
Crystal system	Monoclinic	
Space group	P2 ₁ /c	
Unit cell dimensions	a = 5.3704(2) Å	α = 90°.
	b = 20.0520(5)	β = 100.5131(15)°.

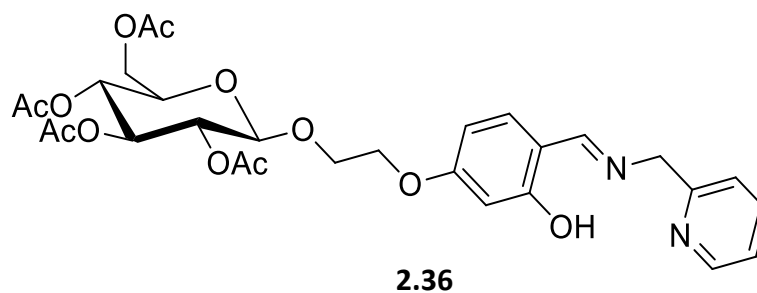
	$c = 12.4990(4) \text{ \AA}$	$\gamma = 90^\circ$.
Volume	1323.39(7) \AA^3	
Z	4	
Density (calculated)	1.367 Mg/m^3	
Absorption coefficient	0.096 mm^{-1}	
F(000)	576	
Crystal size	0.35 x 0.17 x 0.12 mm^3	
Theta range for data collection	2.622 to 33.144°.	
Index ranges	$-8 \leq h \leq 8$, $-30 \leq k \leq 30$, $-17 \leq l \leq 19$	
Reflections collected	32488	
Independent reflections	5038 [R(int) = 0.0495]	
Completeness to theta = 26.000°	99.9 %	
Absorption correction	Semi-empirical from equivalents	
Max. and min. transmission	0.7465 and 0.6856	
Refinement method	Full-matrix least-squares on F^2	
Data / restraints / parameters	5038 / 0 / 189	
Goodness-of-fit on F^2	1.037	
Final R indices [$I > 2\sigma(I)$]	R1 = 0.0487, wR2 = 0.1130	
R indices (all data)	R1 = 0.0774, wR2 = 0.1271	
Largest diff. peak and hole	0.408 and -0.272 e.\AA^{-3}	



2.35

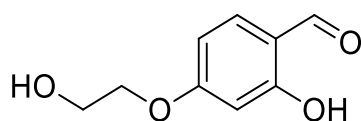
2.39 (1 g, 0.0021 mol) and 2-picolylamine (0.22 mL, 0.0021 mol) were refluxed in EtOH (20 mL, dried over 3 \AA molecular sieves) under N_2 for 6 h. The solvent was removed *in vacuo* to yield the product as an orange solid in a quantitative yield. ^1H NMR (500 MHz, CDCl_3) δ 13.72 (s, 1H, OH), 8.58 (d, $J = 4.9$ Hz, 1H, Pyr-H), 8.45 (s, 1H,

C(H)=N), 7.69 (apptd, $J = 7.8, 1.9$ Hz, 1H, Pyr-H), 7.34 (d, $J = 7.8$ Hz, 1H, Pyr-H), 7.21 (m, 2H, Pyr-H, Ar-H), 6.56 (d, $J = 2.3$ Hz, 1H, Ar-H), 6.50 (dd, $J = 8.5, 2.3$ Hz, 1H, Ar-H), 5.36 – 5.20 (m, 2H, H-1, H-2), 5.14 (m, 2H, H-3, H-4), 4.91 (s, 2H, CH₂-Pyr), 4.29 (dd, $J = 12.3, 5.7$ Hz, 1H, H-6), 4.18 (dd, $J = 12.3, 2.3$ Hz, 1H, H-6'), 3.89 (ddd, $J = 10.1, 5.7, 2.3$ Hz, 1H, H-5), 2.10 (s, 3H, OAc), 2.05 (s, 6H, OAc), 2.04 (s, 3H, OAc). ¹³C NMR (126 MHz, CDCl₃) δ 170.8 (C=O), 170.3 (C=O), 169.5 (C=O), 169.4 (C=O), 165.9 (C=N), 163.8 (Pyr), 160.2 (Ar), 157.9 (Ar), 149.6 (Pyr), 137.0 (Pyr), 132.9 (Pyr), 122.5 (Ar), 122.0 (Pyr), 114.6 (Ar), 108.2 (Ar), 104.2 (Ar), 98.3 (H-1), 72.8 (H-2), 72.3 (H-3), 71.1 (C-5), 68.3 (C-4), 64.6 (CH₂-Pyr), 61.9 (C-6), 20.8 (OAc), 20.7 (OAc), 20.7 (OAc), 20.7 (OAc). IR (KBr Disk): 3472, 3053, 3017, 2965, 2870, 1749, 1635, 1589, 1572, 1532, 1505, 1433, 1368, 1255, 1224, 1176, 1079, 1056, 749cm⁻¹. HRMS m/z (ESI⁺): 559.1895 (C₂₇H₃₁N₂O₁₁: [M+H]⁺ requires 559.1895). Mp: 77-78 °C. $[\alpha]_D^{23}$: -0.23° (*c* 2, CH₂Cl₂). Anal. Calcd for C₂₇H₃₀N₂O₁₁: C, 58.06; H, 5.41; N, 5.02 Found: C, 58.24; H, 5.42; N, 5.25%



2.40 (1.228 g, 0.00239 mol) and 2-picolylamine (0.247 mL, 0.00239 mol) were refluxed in EtOH (20 mL, dried over 3 Å molecular sieves) for 4 h under N₂. The solvent was reduced *in vacuo* to approximately 15 mL and the reaction was cooled on ice to yield the product as a pale yellow precipitate which was isolated by vacuum filtration (1.126 g, 78%). ¹H NMR (500 MHz, CDCl₃) δ 13.80 (s, 1H, Ar-OH), 8.58 (d, $J = 4.0$ Hz, 1H, Pyr-H), 8.41 (s, 1H, C(H)=N), 7.69 (td, $J = 7.7, 1.8$ Hz, 1H, Pyr-H), 7.35 (d, $J = 7.8$ Hz, 1H, Pyr-H), 7.21 (dd, $J = 7.0, 5.4$ Hz, 1H, Pyr-H), 7.19 – 7.14 (m, 1H, Ar-H), 6.44 – 6.39 (m, 2H, Ar-H), 5.22 (t, $J = 9.6$ Hz, 1H, H-3), 5.10 (t, $J = 9.7$ Hz, 1H, H-4), 5.02 (dd, $J = 9.6, 8.0$ Hz, 1H, H-2), 4.89 (s, 2H, CH₂-Pyr), 4.66 (d, $J = 8.0$ Hz, 1H, H-1), 4.27 (dd, $J = 12.3, 4.7$ Hz, 1H, H-6), 4.19 – 4.06 (m, 4H, H-6', OCH₂CH₂OAr, OCHCH₂OAr), 4.01 – 3.86 (m, 1H, OCH'CH₂OAr), 3.72 (ddd, $J = 10.1, 4.7, 2.4$ Hz, 1H, H-5), 2.08 (s, 3H, OAc), 2.03 (s, 3H, OAc), 2.00 (s, 3H, OAc), 1.96 (s, 3H, OAc). ¹³C NMR (126 MHz, CDCl₃) δ

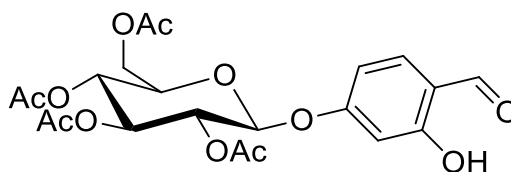
170.8 (C=O), 170.4 (C=O), 169.5 (C=O), 169.5 (C=O), 165.8 (C=N), 164.5 (Ar), 162.5 (Ar), 158.2 (Pyr), 149.5 (Pyr), 136.9 (Pyr), 133.1 (Ar), 122.5 (Pyr), 121.9 (Pyr), 112.9 (Ar), 106.8 (Ar), 101.8 (Ar), 101.2 (C-1), 72.8 (C-3), 72.0 (C-5), 71.2 (C-2), 68.4 (C-4), 68.1 (OC H₂CH₂OAr), 67.2 (OCH₂CH₂OAr), 64.2 (CH₂-Pyr), 61.9 (C-6), 20.8 (OAc), 20.7 (OAc), 20.7 (OAc), 20.7 (OAc). IR (KBr Disk): 3467, 2964, 2935, 2885, 1744, 1630, 1591, 1518, 1433, 1370, 1254, 1224, 1178, 1141, 1046, 981, 846, 606 cm⁻¹. HRMS m/z (ESI+): 603.2177 (C₂₉H₃₅N₂O₁₂: [M+H]⁺ requires 603.2190). [α]_D²³: -0.16° (c 2, CH₂Cl₂). Mp: 118-119 °C. Anal. Calcd for C₂₉H₃₄N₂O₁₂: C, 57.80; H, 5.69; N, 4.65 Found: C, 58.04; H, 5.68; N, 4.65%



2.38

2, 4-dihydroxybenzaldehyde (1 g, 0.0072 mol), 2-chloroethanol (0.97 mL, 0.0144 mol), DBU (1.07 mL, 0.0072 mol) and NaI (0.539 g, 0.0036 mol) were dissolved in IPA (25 mL) and heated in a microwave to 150 °C for 4 h. The solvent was removed *in vacuo* and the residue was dissolved in EtOAc (50 mL) and washed with NaHCO₃ solution (50 mL), H₂O (3 x 50 mL) and brine (50 mL) and the organic layer was then dried over Na₂SO₄. This yielded a brown oil was then purified by column chromatography (2:1 Pet Ether/EtOAc, R_f= 0.43) to give the product as a white solid (0.996 g, 76%). ¹H NMR (500 MHz, CDCl₃) δ 11.47 (s, 1H, Ar-OH), 9.72 (s, 1H, C(=O)H), 7.44 (d, *J* = 8.7 Hz, 1H, Ar-H), 6.57 (dd, *J* = 8.7, 2.3 Hz, 1H, Ar-H), 6.44 (d, *J* = 2.3 Hz, 1H), 4.15 – 4.12 (m, 2H, ArCH₂), 3.99 (m, *J* = 3.8 Hz, 2H, CH₂OH), 2.04 (s, 1H, CH₂OH). ¹³C NMR (126 MHz, CDCl₃) δ 194.5 (C=O), 165.8 (Ar), 164.4 (Ar), 155.4 (Ar), 135.4 (Ar), 115.4 (Ar), 108.6 (Ar), 69.7 (ArCH₂), 61.1 (CH₂OH). IR (KBr) Disk: 3462, 3446, 2959, 2921, 2865, 1804, 1648, 1495, 1232, 1168, 1047cm⁻¹. HRMS m/z (ESI+): 183.0661 (C₉H₁₀O₄: [M+H]⁺ requires 183.0657). Mp: 76-77 °C. Anal. Calcd for C₉H₁₀O₄: C, 59.34; H, 5.53. Found: C, 58.98.04; H, 5.55%

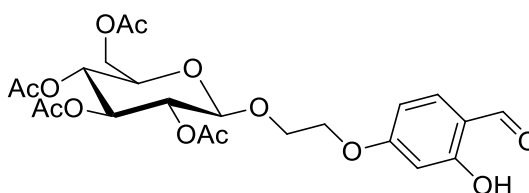
The NMR data is in agreement with that reported in the literature.²²⁴



2.39

2.7 (2 g, 0.0049 mol), 2, 4-dihydroxybenzaldehyde (1.344 g, 0.0097 mol) and Ag_2CO_3 (1.344 g, 0.0097 mol) were dissolved in MeCN (50 mL, dried over 3 Å molecular sieves) under N_2 in the dark and stirred overnight at room temperature. The solvent was removed *in vacuo* and the residue was dissolved in EtOAc (80 mL) with sonication and filtered through a Celite cake. The resulting solution was washed with 1M HCl (50 mL), saturated NaHCO_3 solution (3 x 50 mL) and brine (50 mL) and dried over Na_2SO_4 . The solvent was removed *in vacuo* to yield a dark brown oil which was purified by column chromatography (2:1 Pet. Ether/EtOAc, Rf: 0.13) to yield the product as a white solid (1.40 g, 61%). ^1H NMR (300 MHz, CDCl_3) δ 11.36 (s, 1H, OH), 9.76 (s, 1H), 7.46 (d, $J = 8.6$ Hz, 1H, Ar-H), 6.59 (dd, $J = 8.6, 2.3$ Hz, 1H, Ar-H), 6.54 (d, $J = 2.3$ Hz, 1H, Ar-H), 5.36 – 5.26 (m, 2H, H-1, H-2), 5.15 (m, 2H, H-3, H-4), 4.26 (dd, $J = 12.3, 5.9$ Hz, 1H, H-6), 4.17 (dd, $J = 12.3, 2.5$ Hz, 1H, H-6'), 3.91 (ddd, $J = 9.9, 5.9, 2.5$ Hz, 1H, H-5), 2.09 (s, 3H, OAc), 2.05 (s, 3H, OAc), 2.05 (s, 3H, OAc), 2.03 (s, 3H, OAc). ^{13}C NMR (75 MHz, CDCl_3) δ 194.8 (HC=O)H, 170.6 (OAc), 170.1 (OAc), 169.4 (OAc), 169.2(OAc), 164.0 (Ar), 163.2 (Ar), 135.4 (Ar), 116.7 (Ar), 109.6 (Ar), 103.6 (Ar), 97.7 (C-1), 72.5 (C-2), 72.4 (C-5), 70.9 (C-3), 68.1 (C-6), 61.9 (C-4), 20.6 (OAc). IR (KBr Disk): 3442, 2969, 2947, 2863, 1748, 1661, 1628. 1579, 1500, 1438, 1368, 1227, 1177, 1076, 1035, 979, 908, 802, 761 cm^{-1} . HRMS m/z (ESI+): 491.1167 ($\text{C}_{21}\text{H}_{24}\text{O}_{12}$: $[\text{M}+\text{Na}]^+$ requires 491.1166). Mp: 140-141 °C. $[\alpha]_{\text{D}}^{22}$: -6° (c= 0.5, CH_2Cl_2).

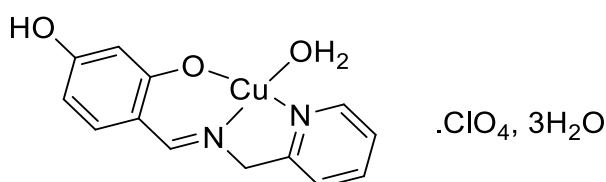
The NMR data is in agreement with reported data.²²⁵



2.40

2.10 (1 g, 0.0024 mol) and NaI (0.359 g, 0.0024 mol) in anhydrous MeCN (15 mL) was added a solution of 2,4-dihydroxybenzaldehyde (0.660 g, 0.0048 mol) and DBU (0.359

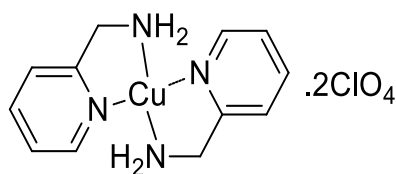
mL, 0.0024 mol) in anhydrous MeCN (10 mL) and the mixture was sealed in a microwave tube. This was heated in a microwave 125 °C for 4 h. The solvent was then removed *in vacuo* and the residue was dissolved in DCM (20 mL) and washed with H₂O (2x 20 mL), sat. NaHCO₃ solution (2x20 mL) and brine (20 mL) before being dried with Na₂SO₄ and the solvent was removed *in vacuo* to yield a heavy brown oil. This was purified by column chromatography (3:1 Pet. Ether/EtOAc, Rf: 0.17) to yield the product as dark yellow oil. ¹H NMR (500 MHz, CDCl₃) δ 11.39 (s, 1H, OH), 9.67 (s, 1H C(=O)H), 7.40 (d, *J* = 8.7 Hz, 1H, Ar-H), 6.49 (dd, *J* = 8.7, 2.3 Hz, 1H, Ar-H), 6.36 (d, *J* = 2.3 Hz, 1H, Ar-H), 5.18 (appt, *J* = 9.6 Hz, 1H, H-3), 5.05 (appt, *J* = 9.7 Hz, 1H, H-4), 4.97 (dd, *J* = 9.6, 8.0 Hz, 1H, H-2), 4.61 (d, *J* = 8.0 Hz, 1H, H-1), 4.22 (dd, *J* = 12.3, 4.7 Hz, 1H, H-6), 4.16 – 4.05 (m, 4H, H-6', OCH, CH₂Cl), 3.91 (dt, *J* = 9.6, 3.5 Hz, 1H, OCH'), 3.69 (ddd, *J* = 9.7, 4.7, 2.4 Hz, 1H, H-5), 2.03 (s, 3H, OAc), 1.98 (s, 3H, OAc), 1.95 (s, 3H, OAc), 1.91 (s, 3H, OAc). ¹³C NMR (126 MHz, CDCl₃) δ 194.4 (C(=O)H), 170.6 (OAc), 170.2 (OAc), 169.4 (OAc), 169.3 (OAc), 165.7 (Ar), 164.3 (Ar), 148.7(Ar), 135.4 (Ar), 115.4(Ar), 108.4 (Ar), 101.3(Ar), 101.0 (C-1), 72.7 (C-3), 71.9 (C-5), 71.1 (C-4), 68.3 (C-2), 67.7 (C-6), 67.4 (OCH₂), 61.8 (CH₂Cl), 20.7 (OAc), 20.6 (OAc), 20.5 (OAc), 20.5 (OAc). IR (KBr Disk): 3471, 2967, 1745, 1633, 1581, 1430, 1379, 1230, 1123, 1044, 989 cm⁻¹. HRMS *m/z* (ESI+): 513.1609 (C₂₃H₂₉O₁₃: [M+H]⁺ requires 513.1608). [α]_D²⁰: -2° (c = 0.25, CH₂Cl₂).



2.41

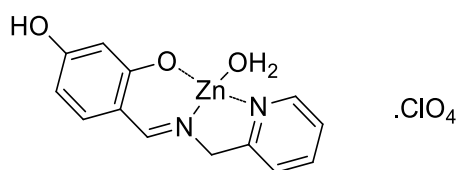
2.33 (0.5 g, 0.002 mol) was dissolved in EtOH (15 mL) and heated to reflux. A solution of Cu(ClO₄)₂·6H₂O (0.370 g, 0.001 mol) in EtOH (10 mL) was added upon which the reaction turned a dark green colour. This was refluxed for 5h after which it was reduced *in vacuo* to approximately 15 mL and cooled on ice to yield the product as a bluish green solid (0.158 g, 40 %). IR (KBr Disk): 3454, 3208, 3121, 2938, 2913, 2021, 1636, 1615, 1541, 1490, 1334, 1231, 1170, 1057, 625 cm⁻¹. Anal. Calcd for

$C_{13}H_{23}N_2ClO_9Cu$: C, 35.14; H, 3.86; N, 6.31. Found: C, 34.96; H, 3.75; N, 6.79 % μ_{eff} : 1.91 B.M.



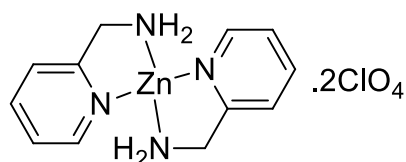
2.42

$Cu(ClO_4)_2 \cdot 6H_2O$ (0.2 g, 0.0005 mol) and 2-picolylamine (0.14 mL, 0.0010 mol) were stirred at room temperature in EtOH (10 mL) for 4h and cooled on ice for 30 min to yield a pale purple precipitate. This was collected by filtration and dried under vacuum (0.231 g, 89%). IR (KBr Disk): 3425, 3329, 3210, 3121, 2962, 2914, 1608, 1591, 1570, 1486, 1434, 1375, 1332, 1291, 1146, 1087, 1029, 945, 779, 626 cm^{-1} . HRMS m/z (ESI+) 279.0661 ($C_{12}H_{16}N_4Cu$: $[M]^+$ requires 279.0671). Anal. Calcd for $C_{12}H_{16}N_4Cl_2O_8Cu$: C, 30.11; H, 3.37; N, 11.70. Found: C, 30.16; H, 3.39; N, 11.74%. μ_{eff} : 2.01 B.M.



2.43

2.33 (0.750 g, 0.0032 mol) and $Zn(ClO_4)_2 \cdot 6H_2O$ (1.223 g, 0.0032 mol) were refluxed in EtOH (30 mL) for 4 h. This was reduced to approximately 15 mL *in vacuo* and cooled on ice to yield a hygroscopic yellow solid (0.859 g, 65 %). 1H NMR (500 MHz, CD_3CN) δ 8.52 (bs, 2H Pyr-H, HC(=N)), 8.11 (bs, 1H, Pyr-H), 7.61 (bs, 2H, Pyr-H), 7.44 (bs, 1H Ar-H), 6.60 (bs, 2H, Ar-H), 5.08 (bs, 2H, CH_2), 3.81 (bs, H_2O , OH). IR (KBr Disk): 3437, 3335, 3278, 3090, 2954, 2011, 1611, 1589, 1489, 1439, 1381, 1293, 1089, 1027, 625 cm^{-1} . Anal. Calcd for $C_{13}H_{15}N_2ClO_8Zn$: C, 38.07; H, 3.20; N, 8.65. Found: C, 37.89; H, 3.31; N, 8.40%



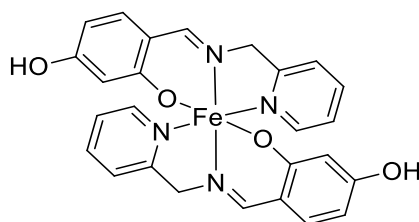
2.44

Zn(ClO₄)₂·6H₂O (0.723g, 0.0019 mol) and 2-picolylamine (0.4 mL, 0.0038 mol) were stirred at room temperature in EtOH (20 mL) for 4 h and cooled on ice for 30 min to yield a white precipitate which was collected by vacuum filtration and washed with cold EtOH and dried under vacuum (0.855 g, 94 %). ¹H NMR (500 MHz, DMSO) δ 8.30 (d, *J* = 2.9 Hz, 2H, Pyr-H), 8.05 (at, *J* = 7.2 Hz, 2H, Pyr-H), 7.59 (d, *J* = 7.9 Hz, 2H, Pyr-H), 7.56 – 7.50 (m, 2H, Pyr-H), 4.08 (s, 4H, CH₂), 3.91 (s, 4H, NH₂). ¹³C NMR (126 MHz, DMSO) δ 157.4 (Pyr-C), 146.8 (Pyr-CH), 139.7 (Pyr-C), 123.8 (Pyr-C), 123.5 (Pyr-C), 42.6 (CH₂). IR (KBr Disk): 3439, 3281, 3204, 3133, 2912, 1603, 1590, 1569, 1487, 1439, 1383, 1334, 1294, 1141, 1114, 1090, 1032, 1017, 940, 772, 636, 626cm⁻¹. Mp: Compound decomposes at 245 °C. Anal. Calcd C₁₂H₁₆N₄Cl₂O₈Zn: C 29.99, H 3.36, N 11.6. Found: C 29.51, H, 3.32, N 11.45%

Grey rhombic crystals suitable for X-ray analysis were obtained from the NMR sample of **2.43** prepared in d⁸-THF.

Empirical formula	C ₁₂ H ₁₆ Cl ₂ N ₄ O ₈ Zn	
Formula weight	480.56	
Temperature	99.99 K	
Wavelength	0.71073 Å	
Crystal system	Tetragonal	
Space group	I4 ₁ /a	
Unit cell dimensions	a = 14.9255(7) Å	α = 90°.
	b = 14.9255(7) Å	β = 90°.
	c = 15.3140(7) Å	γ = 90°.
Volume	3411.5(4) Å ³	
Z	8	
Density (calculated)	1.871 Mg/m ³	
Absorption coefficient	1.806 mm ⁻¹	
F(000)	1952	
Crystal size	0.18 x 0.12 x 0.1 mm ³	
Theta range for data collection	1.905 to 28.289°.	

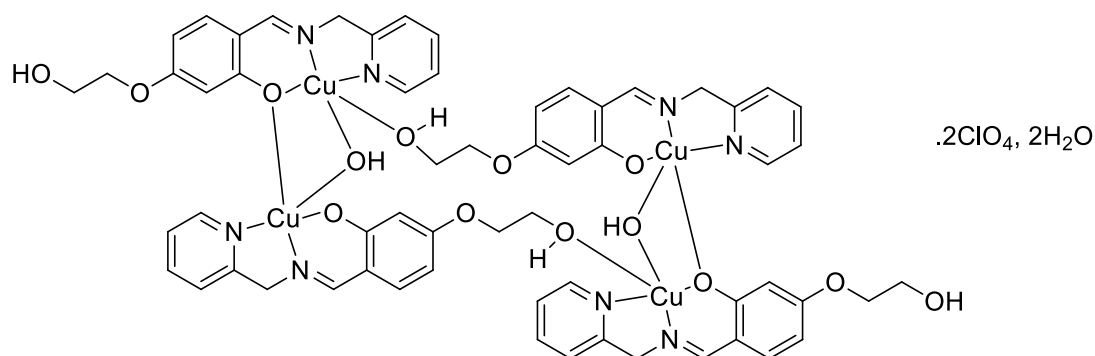
Index ranges	-19≤h≤19, -17≤k≤19, -20≤l≤18
Reflections collected	21050
Independent reflections	2120 [R(int) = 0.0436]
Completeness to theta = 26.000°	100.0 %
Absorption correction	Semi-empirical from equivalents
Max. and min. transmission	0.7457 and 0.6711
Refinement method	Full-matrix least-squares on F ²
Data / restraints / parameters	2120 / 0 / 160
Goodness-of-fit on F ²	1.280
Final R indices [I>2σ(I)]	R1 = 0.0500, wR2 = 0.0984
R indices (all data)	R1 = 0.0606, wR2 = 0.1018
Largest diff. peak and hole	0.381 and -0.528 e.Å ⁻³



2.45

The reaction was carried out on a Schlenk line under a positive pressure of nitrogen. Flame dried glassware was used and the methanol was dried over 3 Å molecular sieves and degassed using the freeze-pump-thaw method.

To a solution of **2.33** (1 g, 0.00438 mol) in MeOH (40 mL) at 45 °C was added a solution of Fe(ClO₄)₂.xH₂O (0.279 g, 0.00109 mol) in MeOH (15 mL) via cannula. The reaction immediately turned to a deep purple/black colour and was allowed to stir overnight at room temperature and was then left to stand for several hours. Approximately 15 mL of solvent was removed *in vacuo* and the resulting suspension was filtered under inert conditions to yield the product as air stable black solid (0.511 g). IR (KBr Disk): 3430, 2989, 1607, 1569, 1475, 1442, 1308, 1288, 1262, 1222, 1122, 1109, 1096, 762, 636 cm⁻¹. HRMS m/z (ESI+): 510.0964 (C₂₆H₂₂FeN₄O₄: [M]⁺ requires 510.09795). Mp: >300°C. Anal. Found: C 55.19, H, 3.95, N 8.77%



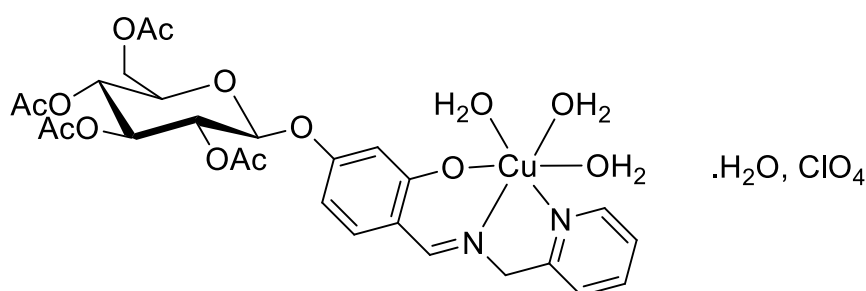
2.46

2.34 (0.230 g, 0.00084 mol) was heated to reflux in EtOH (10 mL, dried over 3Å molecular sieves) under N₂ and a solution of Cu(ClO₄)₂·6H₂O (0.155 g, 0.00042 mol) in EtOH (10 mL, dried over 3Å molecular sieves) was added and the reaction immediately turned a deep blue/green colour. This was refluxed for 4 h and the solvent was reduced by approximately half *in vacuo* and cooled on ice to yield the product as a dark green solid (0.154 g, 42%). IR (KBr Disk): 3431, 3074, 2936, 1641, 1609, 1572, 1532, 1489, 1431, 1400, 1306, 1238, 1220, 1180, 1147, 1103, 1043, 988, 848, 770, 622 cm⁻¹. HRMS m/z (ESI+): 334.0380 (C₁₅H₁₅N₂O₃: [M-(ClO₄)]⁺ requires 334.0378). Mp: 190-192 °C. Anal. Calcd for C₁₅H₁₅N₂ClO₇Cu: C, 41.48; H, 3.48; N, 6.45. Found: C, 41.99; H, 3.72; N, 6.51%. μ_{eff}: 1.83 B.M

Crystals were obtained after storing the reaction filtrate in a freezer for one year to produce small rhombic green crystals.

Empirical formula	C ₃₀ H ₃₃ ClCu ₂ N ₄ O ₁₂	
Formula weight	804.13	
Temperature	100.02 K	
Wavelength	0.71073 Å	
Crystal system	Triclinic	
Space group	P $\bar{1}$	
Unit cell dimensions	a = 11.4857(7) Å	α = 107.9394(19)°.
	b = 11.5834(7) Å	β = 100.493(2)°.
	c = 14.2410(9) Å	γ = 111.704(2)°.
Volume	1578.06(17) Å ³	
Z	2	

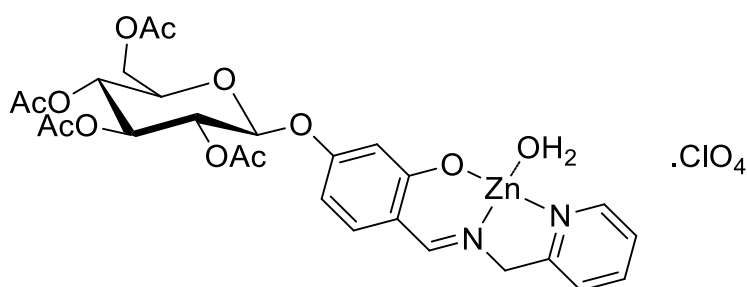
Density (calculated)	1.692 Mg/m ³
Absorption coefficient	1.505 mm ⁻¹
F(000)	824
Crystal size	0.12 x 0.08 x 0.05 mm ³
Theta range for data collection	1.595 to 26.387°.
Index ranges	-14 ≤ h ≤ 14, -14 ≤ k ≤ 14, -17 ≤ l ≤ 17
Reflections collected	32488
Independent reflections	6354 [R(int) = 0.0634]
Completeness to theta = 26.000°	98.3 %
Absorption correction	Semi-empirical from equivalents
Max. and min. transmission	0.7454 and 0.6274
Refinement method	Full-matrix least-squares on F ²
Data / restraints / parameters	6354 / 20 / 454
Goodness-of-fit on F ²	1.024
Final R indices [I > 2σ(I)]	R1 = 0.0383, wR2 = 0.0854
R indices (all data)	R1 = 0.0648, wR2 = 0.0934
Largest diff. peak and hole	1.152 and -0.698 e.Å ⁻³



2.47

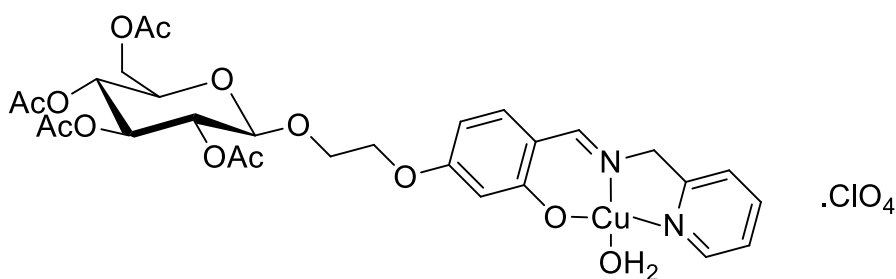
2.35 (0.2 g, 0.00036 mol) was dissolved in EtOH (15 mL, dried over 3Å molecular sieves) and cooled to 0 °C. Cu(ClO₄)₂ · 6H₂O (0.146 g, 0.00039 mol) was added to immediately produce a deep green colour and the reaction was stirred at 0 °C for 1.5 h. A green precipitate was collected by vacuum filtration and was washed with cold EtOH to yield the product as a green solid (0.125 g, 44 %). IR (KBr Disk): 3465, 2973, 2941, 2900, 1750, 1628, 1611, 1602, 1572, 1540, 1402, 1379, 1260, 1228, 1188, 1121, 1076, 1070, 1042, 990, 761, 636, 626 cm⁻¹. HRMS m/z (ESI⁺): 620.1057 (C₂₇H₂₉CuN₂O₁₁: [M-(4H₂O, ClO₄⁻)]⁺ requires 620.1067). Mp: 157-160 °C. [α]_D²²: -0.1° (c

0.2, DMSO). Anal. Calcd for $C_{27}H_{36}N_2ClO_{19}Cu$: C, 40.92; H, 4.73; N, 3.53. Found: C, 41.06; H, 4.44; N, 3.59. μ_{eff} : 1.87 B.M



2.48

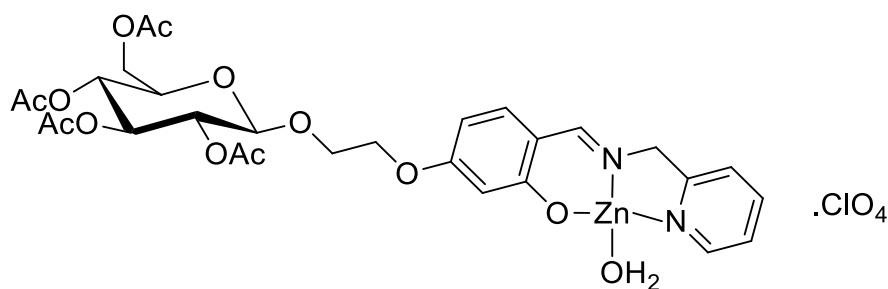
2.35 (0.2 g, 0.00036 mol) was dissolved in EtOH (15 mL, dried over 3 Å molecular sieves) and cooled to 0 °C. $Zn(ClO_4)_2 \cdot 6H_2O$ (0.146 g, 0.00039 mol) was added to immediately produce a beige colour and the reaction was stirred at 0 °C for 2 h. A beige precipitate was collected by vacuum filtration and was washed with cold EtOH to yield the product as a beige solid. IR (KBr Disk): 3463, 2969, 2946, 2901, 1750, 1629, 1611, 1602, 1572, 1540, 1402, 1379, 1260, 1228, 1188, 1121, 1076, 1070, 1042, 990, 761, 636, 626 cm^{-1} . HRMS m/z (ESI+): 739.0994 ($C_{27}H_{31}ClN_2O_{16}Zn$: $[M+H]^+$)⁺ requires 739.0726). Mp: 141-142 °C. $[\alpha]_D^{20}$: -0.21° (c 0.5, DMSO₂). Anal. Calcd for $C_{27}H_{31}N_2ClO_{16}Zn$: C, 43.80; H, 4.22; N, 3.78 Found: C, 44.29; H, 4.53; N, 4.04 %



2.49

2.36 (0.200 g, 0.00033 mol) was heated to reflux in EtOH (10 mL), dried over 3 Å molecular sieves) under N_2 to which a solution of $Cu(ClO_4)_2 \cdot 6H_2O$ (0.0615 g, 0.000165 mol) in EtOH (10 mL, dried over 3 Å molecular sieves) was added. The reaction was stirred at reflux for 4 h and reduced to approximately 15 mL *in vacuo* and cooled on

ice to yield the product as a deep green solid (0.183 g, 71 %). IR (KBr Disk): 3448, 2945, 2890, 1745, 1627, 1611, 1572, 1529, 1489, 1431, 1368, 1226, 1172, 1122, 1099, 1068, 1039, 910, 839, 768, 654, 623, 598 cm^{-1} . HRMS m/z (ESI+): 664.1325 ($\text{C}_{29}\text{H}_{33}\text{N}_4\text{O}_{12}\text{Cu}$: $[\text{M}-(\text{ClO}_4^-)]^+$ requires 664.1329). Mp: 132 $^\circ\text{C}$. $[\alpha]_{\text{D}}^{23}$: -0.2 $^\circ$ (c 0.5, DMSO). Anal. Calcd for $\text{C}_{29}\text{H}_{35}\text{ClCuN}_2\text{O}_{17}$: C, 44.51; H, 4.51; N, 3.58. Found: C, 44.32 H, 4.78; N, 3.44%. μ_{eff} : 1.81 B.M.



2.50

2.36 (0.200 g, 0.00033 mol) was heated to reflux in EtOH (10 mL, dried over 3 Å molecular sieves) under N_2 to which a solution of $\text{Zn}(\text{ClO}_4)_2 \cdot 6\text{H}_2\text{O}$ (0.0614 g, 0.000165 mol) in EtOH (10 mL, dried over 3 Å molecular sieves) was added. The reaction was stirred at reflux for 3 h and reduced to approximately 15 mL *in vacuo* and cooled on ice to yield the product as a hygroscopic white solid along with a sticky brown precipitate. The white solid was decanted from the reaction mixture as a suspension in cold EtOH and the remaining brown solid turned to an oil upon exposure to air overnight. The white solid darkened slightly upon exposure to air and was lyophilized for 24 h to yield a pale beige solid (0.082 g, 64 %). IR (KBr Disk): 3446, 2944, 2890, 1756, 1636, 1607, 1574, 1541, 1487, 1432, 1376, 1368, 1229, 1172, 1122, 1093, 1062, 1040, 909, 853, 766, 623, 599 cm^{-1} . HRMS m/z (ESI+): S1246.3436 ($\text{C}_{58}\text{H}_{67}\text{N}_4\text{O}_{24}\text{Zn}$: $[\text{M}+\text{H}]^+$ requires 1266.3431). Mp: 118-120 $^\circ\text{C}$. $[\alpha]_{\text{D}}^{23}$: -0.15 $^\circ$ (c 0.25, DMSO). Anal. Calcd for $\text{C}_{29}\text{H}_{35}\text{ClCuN}_2\text{O}_{17}$: C, 44.40; H, 4.50; N, 3.57. Found: C, 44.38 H, 4.89; N, 3.48%.

6.3 Chapter 3

G. mellonella Assay:

Sixth instar larvae of *Galleria mellonella* (the greater wax moth, which belongs to order Lepidoptera, family Pyralidae) were obtained from The Mealworm Company (Sheffield, England) and stored in wood shavings in the dark at 15 °C. Larvae chosen for experiments weighed between 0.17-0.23 g and displayed no discoloration on their cuticle. Five healthy larvae inoculated with each compound and were placed in sterile 9 cm Petri dishes containing a sheet of Whatman filter paper and a small amount of wood shavings. Compounds were tested at concentrations of 100, 10 and 1 µM. These were administered as solutions in 10 % DMSO in PBS buffer by inoculation of the larvae through the last left pro-leg directly into the haemocoel using a 300 µL Thermo Myjector syringe (29G) with the sterile test solutions (20 µL). Larvae were incubated at 30 °C and survival was assessed at 24 h and 48 h by response to physical stimulus.

Enzymatic Hydrolysis Susceptibility:

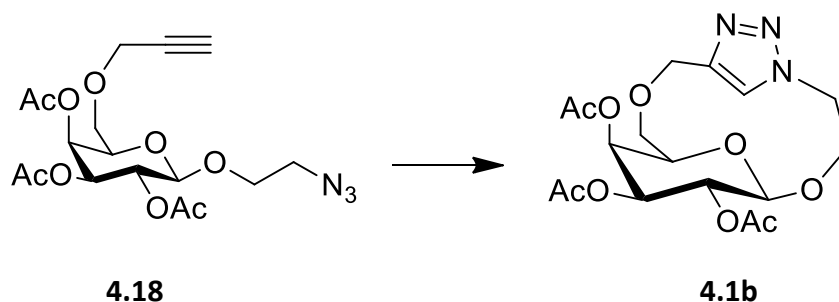
Compounds were dissolved in 5% DMSO in 1M phosphate buffer at pH 7.4 at a concentration of 0.02 M. of β-Glucosidase (1.7 mg (≥10.2 Units), from almonds, obtained from Sigma Aldrich, ≥6U/ mg) was added to 1 mL of substrate solution in a 1.5 mL Eppendorf tube. The solution was gently inverted several times and incubated at 37 °C for 24 h. Hydrolysis was monitored by HPLC and chromatogram changes were correlated with mass spectral analysis. Samples for HPLC and HRMS were filtered through a 0.45 µM syringe and diluted with H₂O prior to analysis.

HPLC studies were carried out using a SunFire C18 5 µm 4.6x 100mm column at room temperature with a flow rate of 1 mL/min. This was conducted using the following a gradient elution protocol:

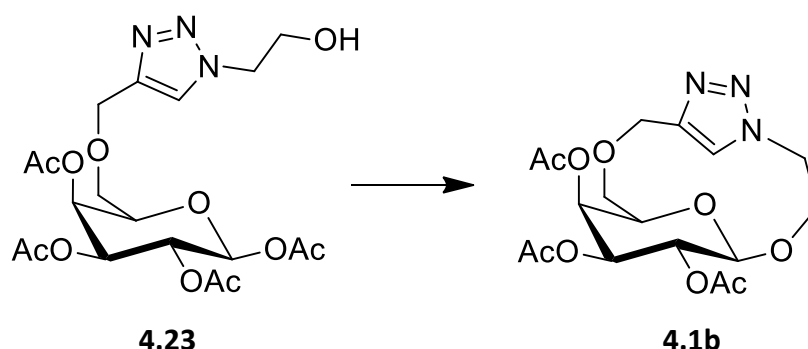
Time (min)	% H ₂ O	% MeCN
0	100	0
20	95	5
25	90	10

Following each run the system was flushed with 100% MeCN for 10 min and then 100% H₂O for 30 min to ensure no residue remained in the column.

6.4 Chapter 4

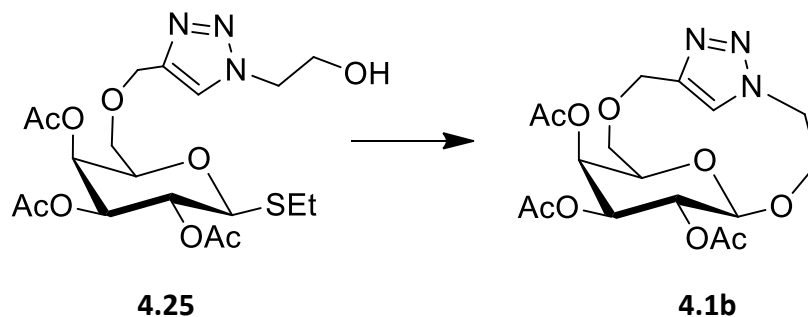


4.18 (0.100 g, 0.00024 mol) was dissolved in MeCN (40 mL) and added dropwise over 2 h to a solution of CuSO₄·5H₂O (0.0065 g, 0.00002 mol) and sodium ascorbate (0.0080 g, 0.00004 mol) in MeCN (25 mL). This was stirred at room temperature for 10 days and the solvent was removed *in vacuo*. The residue was suspended in DCM (15 mL) and was washed with water (3 x 5 mL) and the combined water layers were extracted with DCM (2 x 10 mL). The combined organic layers were washed with brined (20 mL) and dried over Na₂SO₄ and reduced *in vacuo* to yield a transparent yellow oil (0.081 g, 81 %, yield is based on the mass of recovered material).

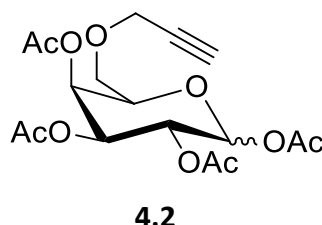


4.23 (0.100 g, 0.0021 mol) was dissolved in anhydrous DCM (50 mL) and was added dropwise over 3 h to a solution of BF₃·OEt₂ (0.77 mL, 0.0063 mol) in anhydrous DCM (30 mL) at 0 °C. This was allowed to warm to room temperature and stir for 48 h before it was transferred to a separating funnel and washed with NaHCO₃ solution (2

x 20 mL), H₂O (20 mL) and brine (20 mL). The organic layer was dried over Na₂SO₄ and the solvent was removed *in vacuo* to yield a yellow oil (0.071 g, 81%, yield is based on the mass of recovered material).



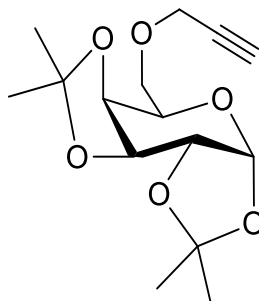
4.25 (0.064 g, 0.00027 mol) was dissolved in anhydrous DCM (40 mL) with 3Å molecular sieves at -42 °C in an MeCN/liquid N₂ bath. A 0.1M solution of promotor was prepared by adding trifluoromethanesulfonic anhydride (0.84 mL, 1 mmol) to a solution of dimethyl disulfide (0.10 mL, 1.1 mmol) in anhydrous DCM (7.5 mL) at 0 °C and stirring the mixture for 30 min to produce a yellow solution. 2 mL of this promotor solution (0.0004 mol) was added dropwise over 1 h and the reaction was allowed to stir overnight before it was quenched by the addition of 0.5 mL of triethylamine. The reaction mixture was transferred to a separating funnel and was washed with water (3x 10 mL). The combined aqueous layers were extracted with DCM (2 x 10 mL) and organic fractions were washed with brine (30 mL) and dried over Na₂SO₄. This was evaporated to yield a pale yellow oil (0.022 g, 34%, yield is based on the amount of recovered material).



4.6 (3 g, 0.0137 mol) was dissolved in Ac₂O (100 mL, 1.05 mol) with sodium acetate (1.123 g, 0.0137 mol) and heated to 80 °C for 20 h under N₂. Toluene (100 mL) was added and the was concentrated *in vacuo* to yield a brown residue. This was diluted with DCM (80 mL), washed with NaHCO₃ solution (4x 50ml), water (50 mL) and brine (100 mL) and then the organic layer was dried over Na₂SO₄. The solvent was removed

70.5 (C-4), 70.4 (C-3), 68.2 (C-2), 61.8 (C-6), 25.8 (CH₃), 25.7 (CH₃), 24.7 (CH₃), 24.2 (CH₃). HRMS m/z (ESI⁺): 283.1153 (C₁₂H₂₀NaO₆: [M + Na]⁺ requires 283.1158).

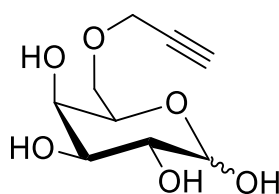
The characterization data is in agreement that reported in the literature.¹⁶⁷



4.5

4.4 (5.323 g, 0.0205 mol), propargyl bromide (5.51 mL, 0.0512 mol, 80 % solution in toluene) and TBAI (0.738 g, 0.002 mol) were dissolved in anhydrous THF (20 mL) under N₂. This was added dropwise via cannula to a solution of NaH (2.46 g, 0.00615 mol, stripped of oil) in anhydrous THF (30 mL) under N₂ at 0 °C. The reaction was allowed to warm to room temperature and was stirred overnight before being quenched with ice (20 g) and the THF was removed *in vacuo*. The residue was then diluted with DCM (30 mL) and washed with brine (2 x 30 mL) and dried with Na₂SO₄ and dried to a brown oil. This was filtered through a silica plug (4:1 Pet. Ether/ EtOAc) to yield a brown oil (5.443 g, 89 %). ¹H NMR (500 MHz, CDCl₃) δ 5.54 (d, *J* = 5.0 Hz, 1H, H-1), 4.60 (dt, *J* = 6.2, 3.1 Hz, 1H, H-3), 4.31 (dd, *J* = 5.0, 2.4 Hz, 1H, H-4), 4.28 – 4.24 (m, 1H, H-2), 4.23 (d, *J* = 2.4 Hz, 1H, CH₂C≡CH), 4.21 (d, *J* = 2.4 Hz, 1H, CH₂C≡CH), 4.02 – 3.97 (m, 1H, H-5), 3.77 (dd, *J* = 10.1, 5.3 Hz, 1H, H-6), 3.67 (dd, *J* = 10.1, 7.1 Hz, 1H, H-6'), 2.44 (t, *J* = 2.4 Hz, 1H, C≡CH), 1.54 (s, 3H, CH₃), 1.44 (s, 3H, CH₃), 1.34 (s, 3H, CH₃), 1.33 (s, 3H, CH₃). IR (KBr): 3273, 2925, 1382, 1211, 1070 cm⁻¹. HRMS m/z (ESI⁺): 299.1419 (C₁₅H₂₃O₆: [M + H]⁺ requires 299.1417).

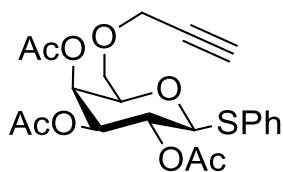
The characterization data is in agreement with that reported in the literature.¹⁷¹



4.6

4.5 (5.443 g 0.0182 mol) was dissolved in TFA/ H₂O (10 mL/5 mL) and stirred at room temperature for 4 h. The TFA was removed *in vacuo* to yield a dark brown solution which was diluted with H₂O and neutralised with basic Dowex Cl⁻. This was filtered and the solution was washed with DCM (2 x 20 mL) and the water was removed *in vacuo* to yield the product as a brown oil (3.855 g, 97 %). ¹H NMR (300 MHz, CD₃OD): δ 5.14 (d, *J* = 3.8 Hz, 1H, H_{α-1}), 4.46 (d, *J* = 7.5 Hz, 1H, H_{β-1}), 4.22-4.18 (m, 3H, CH₂C≡CH, H-5), 3.85-3.44 (m, 4H, H-2, H-3, H-4, H-6), 3.46-3.44 (m, 1H, H-6'), 2.85-2.83 (m, 1H, CH₂C≡CH). ¹³C NMR (75 MHz, CD₃OD): δ 98.1 (C_β -1), 94.1 (C_α -1), 76.0 (CH₂C≡CH), 74.9 (CH₂C≡CH), 71.3 (C-5), 70.5 (C-3), 70.4 (C-2), 70.3 (C-4), 69.9 (C-6), 59.8(CH₂C≡CH). HRMS *m/z* (ESI⁺): 219.0852 (C₉H₁₅O₆: [M + H]⁺ requires 219.0863).

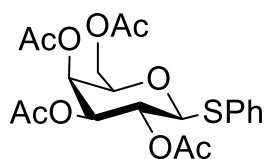
The characterization data is in agreement with that reported in the literature.¹⁵¹



4.11

4.2 (0.512 g, 0.0013 mol) and thiophenol (0.4 mL, 0.0039 mol) were dissolved in DCM (15 mL) at 0 °C. A solution of BF₃.OEt₂ (0.48 mL, 0.0039 mol) in DCM (0.5 mL) was added dropwise via cannula over 12 min and the reaction was allowed to warm to room temperature and stirred for 18 h. This was then transferred to a separating funnel and washed with saturated NaHCO₃ solution (2x 20 mL), H₂O (20 mL) and the combined aqueous layers were extracted with DCM (20 mL). The combined organic layers were then washed with brine (50 mL) and dried with Na₂SO₄ before the solvent was removed *in vacuo* to yield a dark yellow oil. This was purified by column chromatography (92:8 DCM/ diethyl ether, R_f: 0.32) to yield a clear oil. (0.346 g, 61 %). ¹H NMR (500 MHz, CDCl₃) δ 7.33-7.31 (m, 2H, Ar-H), 7.25- 7.22 (m, 2H, Ar-H), 7.13 – 7.13- 7.04 (m, 1H, Ar-H), 5.77 (d, *J* = 7.4 Hz, 1H, H-1), 5.66 – 5.43 (m, 2H, H-4, H-3), 4.92 – 4.74 (m, 1H, H-2), 4.44 (d, *J* = 2.8 Hz, 2H, CH₂C≡CH), 4.18- 4.14 (m, 1H, H-5), 3.67 (dd, *J* = 12.5, 4.7 Hz, 1H, H-6), 3.40 (dd, *J* = 12.3, 4.8 Hz, 1H, H-6'), 2.28-2.25 (bs,

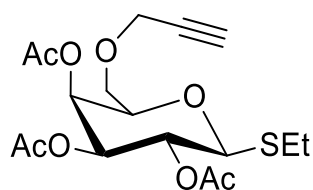
1H, CH₂≡CH), 2.08 (s, 3H, OAc), 1.98 (s, 3H, OAc), 1.95 (s, 3H, OAc). ¹³C NMR (126 MHz, CDCl₃) δ 172.3 (C=O), 171.8 (C=O), 171.1 (C=O), 134.0 (Ar-C), 131.5 (Ar-C), 129.9 (Ar-C), 128.7 (Ar-D), 89.3 (C-1), 79.9 (CH₂C≡CH), 75.2 (CH₂C≡CH), 74.1 (C-5), 71.5 (C-2), 69.3 (C-3), 68.5 (C-6) 67.9 (C-4), 58.6 (CH₂C≡CH), 21.3 (OAc), 21.3 (OAc), 22.9 (OAc). IR (NaCl): 2942, 2895, 2120, 1751, 1369, 1223, 1082, 1054 cm⁻¹. HRMS m/z (ESI⁺): 437.1266 (C₂₁H₂₅O₈S: [M+H]⁺ requires 437.1264). [α]_D²⁴: 0.12 (c 0.5, CH₂Cl₂).



4.13

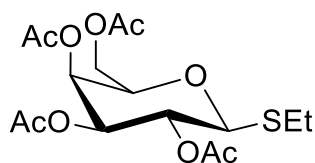
Galactose pentaacetate (1 g, 0.0026 mol) and thiophenol (0.45 mL, 0.0038 mol) were dissolved in DCM (20 mL) at room temperature. SnCl₄ (0.36 mL, 0.0031 mol) was added and the reaction was stirred for 5 h. This was then transferred to a separating funnel and washed with saturated NaHCO₃ solution (2x 20 mL), H₂O (20 mL) and the combined aqueous layers were extracted with DCM (20 mL). The combined organic layers were then washed with brine (50 mL) and dried with Na₂SO₄ before the solvent was removed *in vacuo* to yield an off white solid. This was purified by column chromatography (3:1 Pet. ether/ EtOAc, R_f: 0.31) to yield a white solid (1.075 g, 94%). ¹H NMR (500 MHz, CDCl₃) δ 7.52-7.48 (m, 2H, Ar-H), 7.33-7.27 (m, 3H, Ar-H), 5.42 (dd, *J* = 3.4, 1.0 Hz, 1H, H-4), 5.24 (dd, *J* = 9.9, 9.9 Hz, 1H, H-2), 5.06 (dd, *J* = 3.3, 9.9 Hz, 1H, H-3), 4.72 (d, *J* = 9.9 Hz, 1H, H-1), 4.20 (dd, *J* = 7.0, 11.3 Hz, 1H, H-6), 4.12 (dd, *J* = 6.2, 11.4 Hz, 1H, H-6'), 3.94 (ddd, *J* = 1.0, 6.1, 7.1 Hz, 1H, H-5), 2.12 (s, 3H, OAc), 2.10 (s, 3H, OAc), 2.05 (s, 3H, OAc), 1.98 (s, 3H, OAc). ¹³C NMR (125 MHz, CDCl₃) δ 170.3 (C=O), 170.2 (C=O), 170.0 (C=O), 169.6 (C=O), 132.7 (Ar), 132.8 (Ar), 129.1 (Ar), 128.3 (Ar), 86.8 (C-1), 74.5 (C-5), 72.2 (C-3), 67.3 (C-2), 67.2 (C-4), 61.8 (C-6), 20.8 (OAc), 20.7 (OAc), 20.5 (OAc), 20.5 (OAc).

The characterization data is in agreement with that reported in the literature.¹⁸³



4.15

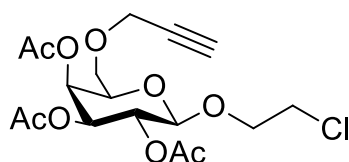
4.2 (1 g, 0.0026 mol) was dissolved in DCM (20 mL, anhydrous) with 3 Å molecular sieves under N₂ at 0 °C. A solution of BF₃·OEt₂ (0.98 mL, 0.0078 mol) in DCM (1.5 mL) was prepared under N₂ with 3 Å molecular sieves at 0 °C. This was added dropwise to the solution of (6-O-Propargyl)-1,2,3,4-tetra-O-acetyl-β-D-galactopyranoside over 10 min and this was allowed to stir for a further 15 min before EtSH (0.59 mL, 0.0078 mol) was added dropwise over 15 min. The reaction was then allowed to slowly warm to room temperature and stir overnight before being washed with NaHCO₃ solution (2x 20 mL) and brine (50 mL). This was dried over Na₂SO₄ and reduced *in vacuo* to yield a dark brown oil which was purified by column chromatography (2:3:1 Toluene/Pet. Ether/EtOAc, Rf: 0.28) to yield the product as a clear oil (0.336 g, 45 %). ¹H NMR (500 MHz, CDCl₃) δ 5.45 (dd, *J* = 3.4, 0.8 Hz, 1H, H-4), 5.21 (at, *J* = 10.0 Hz, 1H, H-3), 5.03 (dd, *J* = 10.0, 3.4 Hz, 1H, H-2), 4.47 (d, *J* = 10.0 Hz, 1H, H-1), 4.11 (qd, *J* = 15.9, 2.4 Hz, 2H, OCH₂C≡C), 3.86 (atd, *J* = 6.2, 0.9 Hz, 1H, H-5), 3.58 (addd, *J* = 24.2, 9.8, 6.3 Hz, 2H, H-6), 2.81 – 2.63 (m, 2H, SCH₂), 2.41 (t, *J* = 2.4 Hz, 1H, C≡CH), 2.13 (s, 3H, OAc), 2.04 (s, 3H, OAc), 1.96 (s, 3H, OAc), 1.26 (t, *J* = 7.5 Hz, 3H, SCH₂CH₃). ¹³C NMR (126 MHz, CDCl₃) δ 170.2 (C=O), 170.0 (C=O), 169.6 (C=O), 84.0 (C-1), 79.1 (CH₂C≡C), 76.6 (C-5), 75.1 (C≡CH), 72.1 (C-3), 67.9 (C-4), 67.6 (C-6), 67.5 (C-2), 58.6 (OCH₂C≡CH), 24.4 (SCH₂), 20.8 (OAc), 20.7 (OAc), 20.6 (OAc), 14.9 (CH₃). IR (NaCl Plate): 3275, 2970, 2933, 2875, 2116, 1750, 1432, 1370, 1245, 1224, 1100, 1081, 1056, 944, 920 cm⁻¹. HRMS *m/z* (ESI⁺): 411.1093 (C₁₇H₂₄O₈SNa: [M+Na]⁺ requires 411.1084). [α]_D²⁴: 0.08 (c 0.3, CH₂Cl₂).



4.16

Galactose pentaacetate (1 g, 0.0026 mol) and ethanethiol (0.39 mL, 0.0052 mol) were dissolved in anhydrous DCM (20 mL) at room temperature. A solution of $\text{BF}_3 \cdot \text{OEt}_2$ (1 mL, 0.0079 mol) in anhydrous DCM (1 mL) was added dropwise and the reaction was stirred overnight. This was then transferred to a separating funnel and washed with saturated NaHCO_3 solution (2 x 20 mL), H_2O (20 mL) and the combined aqueous layers were extracted with DCM (20 mL). The combined organic layers were then washed with brine (50 mL) and dried with Na_2SO_4 before the solvent was removed *in vacuo* to yield a yellow oil. This was purified by column chromatography (3:1 Pet. ether/EtOAc, Rf: 0.21) to yield a white solid (0.938 g, 92 %). ^1H NMR (500 MHz, CDCl_3) δ 5.44 (d, $J = 3.7$ Hz, 1H, H-1), 5.25 – 5.20 (m, 1H, H-4), 5.04 (dd, $J = 10.1, 3.7$ Hz, 1H, H-2), 4.48 (d, $J = 10.1$ Hz, 1H, H-3), 4.18 – 4.10 (m, 2H, H-6), 3.94–3.88 (m, 1H, H-5), 2.78 – 2.66 (m, 2H SCH_2CH_3), 2.18 (s, 3H, OAc), 2.05 (s, 3H, OAc), 2.02 (s, 3H, OAc), 2.00 (s, 3H, OAc), 1.27 (t, $J = 7.2$ Hz, 3H, SCH_2CH_3). ^{13}C NMR (125 MHz, CDCl_3) δ 170.3 (C=O), 170.1 (C=O), 170.0 (C=O), 169.5 (C=O), 83.9 (C-1), 74.2 (C-5), 71.7 (C-2), 67.1 (C-3), 67.0 (C-4), 61.3 (C-6), 24.3 (SCH_2CH_3), 20.7 (OAc), 20.6 (OAc), 20.6 (OAc), 20.5 (OAc), 14.7 (SCH_2CH_3).

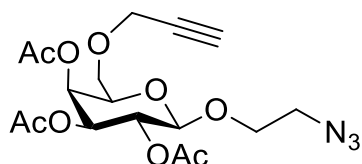
The characterization data is in agreement with that reported in the literature.¹⁸⁵



4.17

4.2 (0.933 g, 0.0024 mol) and 2-chloroethanol (0.583 mL, 0.0072 mol) were dissolved in anhydrous DCM (20mL) and cooled to 0 °C. A solution of $\text{BF}_3 \cdot \text{OEt}_2$ (0.89 mL, 0.0072 mol) in anhydrous DCM (1mL) was added dropwise by cannula over 5 min and the

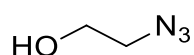
solution was allowed to warm to room temperature and stir overnight. The solution was then transferred to a separating funnel and washed with saturated NaHCO₃ solution (2x 20 mL), H₂O (20 mL) and the combined aqueous layers were extracted with DCM (20 mL). The combined organic layers were then washed with brine (50 mL) and dried with Na₂SO₄ before the solvent was removed *in vacuo* to yield a yellow oil. This was purified by column chromatography (2:1 Pet. ether/ EtOAc, Rf: 0.3) to yield a clear oil. (0.478 g, 49 %). ¹H NMR (500 MHz, CDCl₃) δ 5.43 (ad, *J* = 2.8 Hz, 1H, H-4), 5.23 (dd, *J* = 10.5, 8.0 Hz, 1H, H-2), 5.03 (dd, *J* = 10.5, 3.4 Hz, 1H, H-3), 4.53 (d, *J* = 8.0 Hz, 1H, H-1), 4.19 – 4.08 (m, 3H, H-5, OCH₂C≡CH), 3.87 (at, *J* = 6.4 Hz, 1H, OCH₂CH₂Cl), 3.81 – 3.70 (m, 1H, OCH₂CH₂Cl), 3.67 – 3.56 (m, 4H, H-6, OCH₂CH₂Cl), 2.44 (t, *J* = 2.3 Hz, 1H, C≡CH), 2.15 (s, 3H, OAc), 2.07 (s, 3H, OAc), 1.98 (s, 3H, OAc). ¹³C NMR (126 MHz, CDCl₃) δ 170.2 (C=O), 170.1 (C=O), 169.6 (C=O), 101.6 (C-1), 79.1 (C≡CH), 75.0 (C≡CH), 72.2 (C-5), 70.9 (C-3), 69.9 (C-2), 68.8 (C-4), 67.6 (CH₂C≡CH), 58.6 (C-6), 42.6 (CH₂CH₂Cl), 30.9 (CH₂CH₂Cl), 20.8 (OAc), 20.7 (OAc), 20.6 (OAc). IR (KBr Disk): 3264, 2969, 2156, 1751, 1437, 1382, 1221, 1171 cm⁻¹. HRMS *m/z* (ESI⁺): 407.1104 (C₁₇H₂₄ClO₉: [M+H⁺]⁺ requires 407.1103). [α]_D²¹: 0.1 (*c* 0.09, CH₂Cl₂).



4.18

4.17 (0.498g, 0.001 mol) was dissolved in DMF (20 mL) with H₂O (2 mL) and heated to 80 °C and NaN₃ (0.159 g, 0.002 mol) was added. The reaction was stirred for 48 h and the solvent was removed *in vacuo* to yield a yellow oil. This was diluted with DCM (50 mL) and washed with brine (3x 30 mL) and the combined brine layers were extracted with a further 20 mL of DCM. The combined organic layers were dried with Na₂SO₄ and the solvent was dried to give a pale yellow oil. This was purified by column chromatography (3:1 Pet. Ether/EtOAc, Rf: 0.23) to yield the product as a transparent oil (83 %, 0.343 g). ¹H NMR (500 MHz, CDCl₃) δ 5.45 – 5.41 (m, 1H, H-4), 5.24 (dd, *J* = 10.4, 8.0 Hz, 1H, H-3), 5.03 (dd, *J* = 10.4, 3.4 Hz, 1H, H-2), 4.56 (d, *J* = 8.0

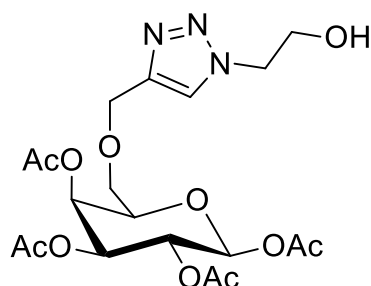
Hz, 1H, H-1), 4.19-4.14 (m, 2H, OCH₂C≡CH), 4.10 – 4.02 (m, 1H, OCH₂CH₂N₃), 3.88 (add, *J* = 6.1, 5.0 Hz, 1H, H-5), 3.77 – 3.66 (m, 1H, H-6), 3.62-3.66 (m, 2H, H-6', OCH₂'CH₂Cl), 3.55 – 3.46 (m, 1H, OCH₂CH₂Cl), 3.35 – 3.26 (m, 1H, OCH₂CH₂'N₃), 2.44 (t, *J* = 2.4 Hz, 1H, C≡CH), 2.16 (s, 3H, OAc), 2.06 (s, 3H, OAc), 1.98 (s, 3H, OAc). ¹³C NMR (126 MHz, CDCl₃) δ 170.2 (C=O), 170.1 (C=O), 169.5 (C=O), 101.2 (C-1), 79.1 (C≡CH), 75.0 (C≡CH), 72.3 (C-5), 71.1 (C-3), 68.8 (C-2), 68.4 (C-4), 67.7(CH₂C≡CH), 67.6 (C-6), 58.7 (CH₂CH₂Cl), 50.6 (CH₂CH₂Cl), 20.8 (OAc), 20.7 (OAc), 20.6 (OAc). IR (KBr Disk): 2987, 2962, 2155, 2103, 2109, 1760, 1380, 1227, 1053 cm⁻¹. HRMS *m/z* (ESI⁺): 415.1508 (C₁₇H₂₄N₃O₉: [M+H⁺]⁺ requires 415.1507). [α]_D²⁴: 0.13 (*c* 0.1, CH₂Cl₂).



4.22

2-chloroethanol (3 mL, 0.0447 mol) and NaN₃ (4 g, 0.0615 mol) were heated to 80 °C in H₂O (30 mL) for 48 h. The reaction was allowed to cool and the product was extracted with Et₂O (4 x 30 mL) and the combined organic layers were washed with brine (100 mL) and dried over Na₂SO₄ and the solvent removed *in vacuo* at room temperature to yield the product as a clear yellow oil (3.077 g, 85 %). ¹H NMR (500 MHz, CDCl₃) δ 3.76 – 3.63 (m, 2H, CH₂N₃), 3.37 – 3.35 (m, 2H, CH₂OH), 3.05 (bs, 1H, OH). ¹³C NMR (126 MHz, CDCl₃) δ 61.3 (CH₂N₃), 53.4 (CH₂OH).

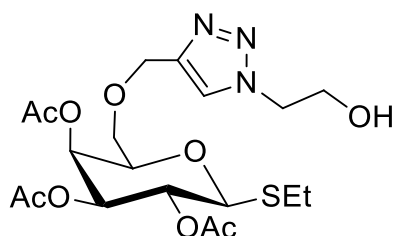
The characterization data is in agreement with that reported in the literature.¹⁸⁹



4.23

4.2 (0.100 g, 0.00026 mol) and 2-azidoethanol (0.05 mL, 0.00052 mol) were dissolved in MeCN (20 mL) along with CuSO₄·5H₂O (0.006 g, 0.00002 mol) and sodium ascorbate (0.008 g, 0.04 mmol) and stirred at room temperature overnight. The solvent was

removed *in vacuo* and the residue was dissolved in H₂O (20 mL) and DCM (20 mL). These were separated and the aqueous layer was extracted with a further 3 x 20 mL portions of DCM. The combined organic layers were washed with brine (50 mL), dried over Na₂SO₄ and the solvent was removed *in vacuo* to yield a clear oil (0.112 g, 92 %). ¹H NMR (500 MHz, CDCl₃) δ 7.62 (s, 1H, Ar-H), 5.64 (d, *J* = 8.3 Hz, 1H, H-1), 5.34 (d, *J* = 3.2 Hz, 1H, H-4), 5.25 (ad, *J* = 2.1 Hz, 1H, H-2), 5.00 (dd, *J* = 10.4, 3.2 Hz, 1H, H-3), 4.63 – 4.57 (m, 2H, OCH₂Ar), 4.50 – 4.42 (m, 2H, ArCH₂CH₂), 4.02 – 3.97 (m, 2H, ArCH₂CH₂), 3.92 (at, 1H, *J* = 6.4 Hz, H-5), 3.63 (dd, *J* = 9.6, 5.6 Hz, 1H, H-6), 3.60 – 3.54 (m, 1H, H-6'), 3.48 (bs, 1H, OH), 2.07 (s, 3H, OAc), 2.06 (s, 3H, OAc), 1.99 (s, 3H, OAc), 1.92 (s, 3H, OAc). ¹³C NMR (126 MHz, CDCl₃) δ 170.6 (C=O), 169.9 (C=O), 169.4 (C=O), 169.1 (C=O), 144.4 (Ar-C), 124.2 (Ar-H), 92.3 (C-1), 72.6 (C-5), 70.9 (C-3), 68.0 (C-2), 67.2 (C-4), 64.4 (OCH₂Ar), 61.0 (ArCH₂CH₂), 53.5 (C-6), 52.9 (CH₂OH), 20.8 (OAc), 20.6 (OAc), 20.6 (OAc), 20.5 (OAc). IR (NaCl Plate): 3274, 2967, 2931, 2874, 2116, 1748, 1432, 1371, 1223, 1154, 1100, 1055, 920 cm⁻¹. HRMS *m/z* (ESI+): 474.1717 (C₁₉H₂₈N₃O₁₁: [M+H]⁺ requires 474.1718). [α]_D²²: 0.21 (c 0.2, CH₂Cl₂).



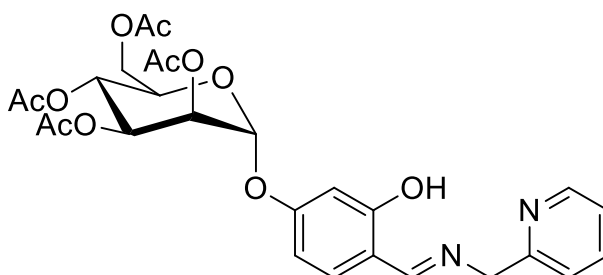
4.25

4.15 (0.100 g, 0.00025 mol) was dissolved in DMF/H₂O (15:1 mL) with 2-azidoethanol (0.6 mL, 0.0005 mol). CuSO₄·5H₂O (0.01 g, 15 mol%) and sodium ascorbate (0.016 g, 30 mol%) were added. The mixture was then sonicated for 5 min and stirred at room temperature for 2 h. The solvent was removed *in vacuo* and the residue was dissolved in H₂O (10 mL) and DCM (10 mL). These were separated and the aqueous layer was extracted with a further 3 x 10 mL portions of DCM. The combined organic layers were washed with brine (20 mL), dried over Na₂SO₄ and the solvent was removed *in vacuo* to yield a clear oil. This was dissolved in MeOH (15 mL) and was stirred with approximately 0.4 g of Chelex resin for 2 h before it was filtered and the solvent was evaporated to

produce a clear oil (0.117 g, 96 %). ^1H NMR (500 MHz, CDCl_3) δ 7.63 (s, 1H, Ar-H), 5.36 (ad, $J = 3.0$ Hz, 1H, H-4), 5.18 (at, $J = 10.0$ Hz, 1H, H-2), 4.97 (dd, $J = 10.0, 3.3$ Hz, 1H, H-3), 4.64 (d, $J = 12.7$ Hz, 1H, H-1), 4.53 – 4.37 (m, 4H, $\text{ArCH}_2\text{CH}_2\text{OH}$, OCH_2Ar), 4.08 – 3.98 (m, 2H, $\text{ArCH}_2\text{CH}_2\text{OH}$), 3.85 – 3.78 (m, 1H, H-5), 3.66 (dd, $J = 9.4, 5.4$ Hz, 1H, H-6), 3.60 (dd, $J = 9.4, 7.9$ Hz, 1H, H-6'), 3.23 (bs, 1H, OH), 2.81 – 2.62 (2, 3H, SCH_2), 2.08 (s, 3H, OAc), 2.04 (s, 3H, OAc), 1.93 (s, 3H, OAc), 1.26 (t, $J = 7.4$ Hz, 3H, SCH_2CH_3). ^{13}C NMR (126 MHz, CDCl_3) δ 170.9 (C=O), 170.2 (C=O), 169.7 (C=O), 144.7 (Ar-C), 124.2 (Ar-H), 84.1 (C-1), 67.8 (OCH_2Ar), 67.6 (C-5), 67.6 (C-3), 67.5 (C-4), 64.5 (C-6), 61.3 (C-2), 53.5 (ArCH_2CH_2), 53.0 (CH_2OH), 24.3 (SCH_2CH_3), 20.9 (OAc), 20.8 (OAc), 20.7 (OAc), 14.9 (SCH_2CH_3). IR (NaCl Plate): 3420, 3261, 2990, 2895, 1753, 1435, 1379, 1245, 1109, 1076, 944, 920 cm^{-1} . HRMS m/z (ESI+): 476.1693 ($\text{C}_{19}\text{H}_{29}\text{N}_3\text{O}_9\text{S}$: $[\text{M}+\text{H}]^+$ requires 479.1697), $[\alpha]_{\text{D}}^{23}$: 0.04 (c 0.1, MeOH).

6.5 Chapter 5

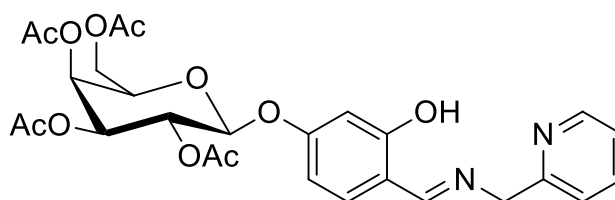
6.5.1 Synthesis



5.1

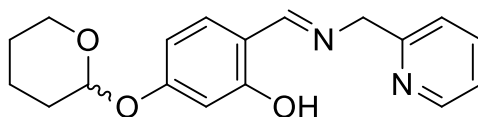
5.4 (1.125 g, 0.0024 mol) and 2-picolylamine (0.25 mL, 0.0024 mol) were refluxed overnight in EtOH (20 mL, dried over 3 Å molecular sieves) under N_2 . The solvent was removed *in vacuo* to yield the product as orange oil (1.339 g, >98 %). ^1H NMR (500 MHz, CDCl_3) δ 13.64 (bs, 1H, OH), 8.57 (dd, $J = 4.9, 0.8$ Hz, 1H, Pyr-H), 8.45 (s, 1H, C=N), 7.68 (atd, $J = 7.7, 1.8$ Hz, 1H, Pyr-H), 7.34 (d, $J = 7.8$ Hz, 1H, Pyr-H), 7.23 – 7.18 (m, 2H, Pyr-H, Ar-H), 6.70 (d, $J = 2.4$ Hz, 1H, Ar-H), 6.59 (dd, $J = 8.5, 2.4$ Hz, 1H, Ar-H), 5.55-5.19 (m, 2H, H-1, H-2), 5.43 (dd, $J = 3.5, 1.9$ Hz, 1H, H-3), 5.35 (at, $J = 10.0$ Hz, 1H, H-4), 4.90 (s, 2H, PyrCH_2), 4.35 – 4.25 (m, 1H, H-5), 4.09 – 4.03 (m, 2H, H-6), 2.20 (s, 3H, OAc), 2.04 (s, 6H, OAc), 2.03 (s, 3H, OAc). ^{13}C NMR (126 MHz, CDCl_3) δ 170.9 (C=O), 170.7 (C=O), 170.0 (C=O), 169.4 (C=O), 169.6 (C=N), 164.8 (Pyr), 160.8 (Ar),

157.9 (Ar), 149.6 (Pyr), 137.0 (Pyr), 132.9 (Pyr), 122.5 (Ar), 122.2 (Pyr), 115.0 (Ar), 109.2 (Ar), 104.2 (Ar), 98.3 (H-1), 72.6 (H-5), 71.3 (H-2), 71.0 (C-3), 68.8 (C-4), 64.7 (CH₂-Pyr), 62.0 (C-6), 20.8 (OAc), 20.8 (OAc), 20.7 (OAc), 20.7 (OAc). IR (NaCl Plate): 3489, 3105, 2968, 2879, 1751, 1639, 1591, 1582, 1505, 1438, 1370, 1224, 1176, 1079, 1056, 754cm⁻¹. HRMS m/z (ESI+): 559.1897 (C₂₇H₃₁N₂O₁₁: [M+H]⁺ requires 559.1895). $[\alpha]_D^{22}$: -2° (c= 0.25, CH₂Cl₂).



5.2

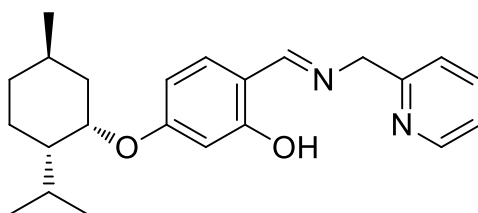
5.7 (1 g, 0.0021 mol) and 2-picolylamine (0.22 mL, 0.0021 mol) were refluxed in EtOH (20 mL, dried over 3Å molecular sieves) under N₂ for 8 h. The solvent was removed *in vacuo* to yield the product as an orange solid in a quantitative yield. ¹H NMR (500 MHz, CDCl₃) δ 13.76 (s, 1H, OH), 8.61 (d, *J* = 4.9 Hz, 1H, Pyr-H), 8.45 (s, 1H, C(H)=N), 7.69 (atd, *J* = 7.8, 2 Hz, 1H, Pyr-H), 7.36 (d, *J* = 7.8 Hz, 1H, Pyr-H), 7.20 (m, 2H, Pyr-H, Ar-H), 6.57 (d, *J* = 2.2 Hz, 1H, Ar-H), 6.51 (dd, *J* = 8.5, 2.2 Hz, 1H, Ar-H), 5.34 – 5.28 (m, 2H, H-1, H-2), 5.16-5.11 (m, 2H, H-3, H-4), 4.93 (s, 2H, CH₂-Pyr), 4.30 (dd, *J* = 12.6, 5.7 Hz, 1H, H-6), 4.18 (dd, *J* = 12.6, 2.2 Hz, 1H, H-6'), 3.88 (ddd, *J* = 10.1, 5.7, 2.2 Hz, 1H, H-5), 2.08 (s, 3H, OAc), 2.05 (s, 6H, OAc), 2.04 (s, 3H, OAc). ¹³C NMR (126 MHz, CDCl₃) δ 170.9 (C=O), 170.4 (C=O), 169.4 (C=O), 169.3 (C=O), 165.9 (C=N), 163.9 (Pyr), 160.8 (Ar), 157.7(Ar), 149.5 (Pyr), 137.2 (Pyr), 133.0 (Pyr), 122.8 (Ar), 122.1 (Pyr), 114.6 (Ar), 108.2 (Ar), 104.9 (Ar), 98.9 (H-1), 72.7 (H-5), 72.3 (H-3), 71.6 (C-2), 68.6 (C-4), 65.0 (CH₂-Pyr), 61.7 (C-6), 20.8 (OAc), 20.7 (OAc), 20.7 (OAc), 20.6 (OAc). IR (KBr Disk): 3420, 3017, 2965, 2877, 1748, 1637, 1589, 1576, 1505, 1439, 1367, 1224, 1180, 1079 cm⁻¹. HRMS m/z (ESI+): 559.1895 (C₂₇H₃₁N₂O₁₁: [M+H]⁺ requires 559.1895). Mp: 82-83 °C. $[\alpha]_D^{23}$: -0.2° (c 1, CH₂Cl₂).



5.3

5.9 (1 g, 0.0045 mol) and 2-picolylamine (0.46 mL, 0.0045 mol) were dissolved in anhydrous EtOH (20 mL). This was heated to 80 °C under N₂ for 18 h before the solvent was removed *in vacuo* to produce a dark orange oil in quantitative yield.

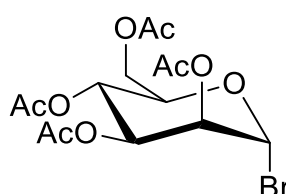
¹H NMR (500 MHz, CDCl₃) δ 8.56 (d, *J* = 4.8 Hz, 1H, Pyr-H), 8.42 (s, 1H, C=N), 7.68 (ddd, *J* = 7.8, 3.0, 1.5 Hz, 1H, Pyr-H), 7.35 (d, *J* = 7.8 Hz, 1H, Ar-H), 7.22 – 7.15 (m, Pyr-H, 2H), 6.64 (d, *J* = 2.3 Hz, 1H, Ar-H), 6.56 (dd, *J* = 8.5, 2.3 Hz, 1H, Ar-H), 5.45 (t, *J* = 3.1 Hz, 1H, t, *J* = 3 Hz, 1H, THP C(-O)₂H), 4.89 (s, 2H, PyrCH₂), 3.95 – 3.82 (m, 1H, THP C(O)-H), 3.67 – 3.54 (m, 1H, THP C(O)-H'), 2.05 – 1.91 (m, 2H, CH₂), 1.90 – 1.75 (m, 2H, THP CH₂), 1.75 – 1.43 (m, 2H, THP CH₂). ¹³C NMR (126 MHz, CDCl₃) δ 165.2 (C=N), 164.8 (Ar-O), 163.4 (Ar-O), 162.1 (Pyr-C), 148.3 (Pyr-H), 135.3 (Ar-H), 134.2 (Pyr-H), 124.3 (Pyr-H), 121.6 (Pyr-H), 116.8 (Ar-C), 109.4 (Ar-H), 103.7 (Ar-H), 97.3 (CH), 61.9 (CH₂), 30.1 (CH₂), 25.3 (CH₂), 19.1 (CH₂). IR (KBr Disk): 3289, 3075, 2867, 1621, 1442, 1331, 1271, 1241, 1120, 985 cm⁻¹. HRMS *m/z* (ESI⁺): 313.3709 (C₁₈H₂₁N₂O₃: [M+H]⁺ requires 313.3703). [α]_D²³: -5° (c 0.5, CH₂Cl₂).



5.4

5.14 (0.117 g, 0.00042 mol) and 2-picolylamine (0.044 mL, 0.00043 mol) were refluxed in EtOH (anhydrous, 10 mL) under N₂ for 3 h. The solvent was removed *in vacuo* to give the product as a bright yellow oil in a quantitative yield. ¹H NMR (500 MHz, CDCl₃) δ 13.7 (bs, 1H, OH), 8.48 (as, 1H, Pyr-H), 8.30 (s, 1H, HC=N), 7.58 (ad, *J* = 7.0 Hz, 1H, Pyr-H), 7.25 (ad, *J* = 7.5 Hz, 1H, Pyr-H), 7.17 – 7.00 (m, 2H Pyr-H, Ar-H), 6.37 (s, 1H, Ar-H), 6.33 (d, *J* = 8.4 Hz, 1H, Ar-H), 4.79 (s, 2H PyrCH₂), 4.58 (bs, 1H Cyclohexyl C(-O)H), 2.03 (ad, *J* = 13.5 Hz, 1H, CH), 1.70-1.63 (m, 2H), 1.61-1.52 (m, 2H), 1.47 (d, *J* = 12.7 Hz, 1H), 1.23 –

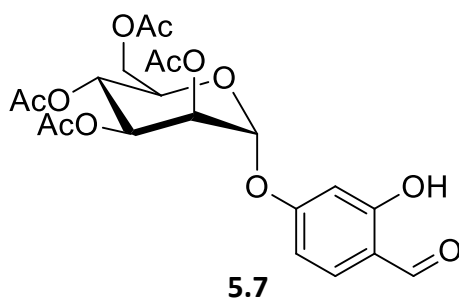
1.06 (m, 1H), 1.05 – 0.90 (m, 2H, CH₂), 0.85 (d, *J* = 6.4 Hz, 3H, CH₃), 0.74 (d, *J* = 6.5 Hz, 6H, isopropyl CH₃). ¹³C NMR (126 MHz, CDCl₃) δ 165.9 (C=N), 164.7 (Pyr), 162.6 (Ar), 158.4 (Pyr), 149.4 (Pyr), 136.9 (Ar), 133.0 (Pyr), 122.3 (Ar), 121.9 (Pyr), 112.2 (Ar), 107.9 (Ar), 102.5 (Ar), 73.6 (Cyclohexyl-C-O), 64.2 (PyrCH₂), 47.7 (Cyclohexyl-C), 37.7 (Cyclohexyl-C), 35.00 (Cyclohexyl-C), 29.39 (Cyclohexyl-C), 26, 24.9 (Cyclohexyl-C), 22.3 (Isopropyl-CH), 21.1 (Cyclohexyl-CH₃), 20.8 (Isopropyl-CH₃). IR (NaCl Plate): 3062, 2944, 2875, 1641, 1627, 1574, 1503, 1455, 1378, 1341, 1225, 1121, 990, 702cm⁻¹. HRMS *m/z* (ESI+): 367.2367 (C₂₃H₃₁N₂O₂: [M+H]⁺ requires 367.2380). . [α]_D²¹: +2 (c 0.2, CH₂Cl₂).



5.6

Mannose pentaacetate (1 g, 0.0026 mol) was dissolved in HBr/AcOH (7 mL) with acetic anhydride (1 mL) under N₂ and stirred for 4 h at room temperature. This was diluted with DCM (20 mL) and washed with water (3 x 10 mL), saturated NaHCO₃ solution (20 mL) and brine (30 mL) before being dried with Na₂SO₄. The solvent was removed *in vacuo* to yield a pale yellow oil (1.068 g, >98 %). ¹H NMR (300 MHz, CDCl₃) δ 6.28 (d, *J* = 1.6 Hz, 1H, H-1), 5.70 (dd, *J* = 10.2, 3.4 Hz, 1H, H-3), 5.43 (dd, *J* = 3.4, 1.6 Hz, 1H, H-2), 5.35 (at, *J* = 10.2 Hz, 1H, H-4), 4.31 (dd, *J* = 12.6, 5.0 Hz, 1H, H-6), 4.21 (ddd, *J* = 10.2, 5.0, 2.3 Hz, 1H, H-5), 4.12 (dd, *J* = 12.6, 2.3 Hz, 1H, H-6'), 2.16 (s, 3H, OAc), 2.09 (s, 3H, OAc), 2.06 (s, 3H, OAc), 1.99 (s, 3H, OAc).

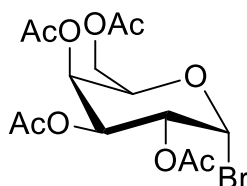
The NMR data is in agreement with the data reported in the literature.²¹¹



5.7

5.6 (2 g, 0.0049 mol), 2, 4-dihydroxybenzaldehyde (1.344 g, 0.0097 mol) and Ag₂CO₃ (1.344 g, 0.0097 mol) were dissolved in MeCN (50 mL, dried over 3 Å molecular

sieves) under N₂ in the dark and stirred at room temperature for 48 h. The solvent was removed *in vacuo* and the residue was dissolved in EtOAc (80 mL) with sonication and filtered through a Celite cake. The resulting solution was washed with 1M HCl (50 mL), saturated NaHCO₃ solution (3 x 50 mL) and brine (50 mL) and dried over Na₂SO₄. The solvent was removed *in vacuo* to yield a dark brown oil which was purified by column chromatography (2:1 Pet. Ether/EtOAc, Rf: 0.18) to yield the product as a white solid (1.40 g, 72 %). ¹H NMR (500 MHz, CDCl₃) δ 11.32 (s, 1H, OH), 9.77 (s, 1H, HC=O), 7.49 (dd, *J* = 8.8, 2.3 Hz, 1H, Ar-H), 6.72 (d, *J* = 8.8, 1H, Ar-H), 6.70 (d, *J* = 2.3 Hz, 1H, Ar-H), 5.58 (d, *J* = 1.7 Hz, 1H, H-1), 5.52 (dd, *J* = 10.0, 3.5 Hz, 1H, H-3), 5.43 (dd, *J* = 3.5, 1.7 Hz, 1H, H-2), 5.35 (at, *J* = 10.1 Hz, 1H, H-4), 4.29 (dd, *J* = 12.3, 5.7 Hz, 1H, H-6'), 4.06 (dd, *J* = 12.3, 2.4 Hz, 1H, H-6'), 4.01 (ddd, *J* = 10.1, 5.7, 2.3 Hz, 1H, H-5), 2.20 (s, 3H, OAc), 2.05 (s, 3H, OAc), 2.04 (s, 3H, OAc), 2.04 (s, 3H, OAc). ¹³C NMR (126 MHz, CDCl₃) δ 194.8 (HC=O), 170.5 (C=O), 169.9 (C=O), 169.9 (C=O), 169.6 (C=O), 164.0 (Ar-O), 162.2 (Ar-O), 135.4 (Ar-H), 116.7 (Ar-C), 109.3 (Ar-H), 104.1 (Ar-H), 95.5 (C-1), 69.6 (C-5), 69.0 (C-3), 68.6 (C-2), 65.8 (C-4), 62.0 (C-6), 20.8 (OAc), 20.6 (OAc), 20.6 (OAc), 20.5 (OAc). IR (KBr Disk): 3431, 2969, 2869, 1750, 1663, 1627, 1579, 1500, 1438, 1371, 1227, 1170, 1076, 1035, 979, 908 cm⁻¹. HRMS *m/z* (ESI⁺): 491.1167 (C₂₁H₂₄O₁₂Na: [M+Na]⁺ requires 491.1166). [α]_D²⁴: -8° (c = 0.5, CH₂Cl₂).

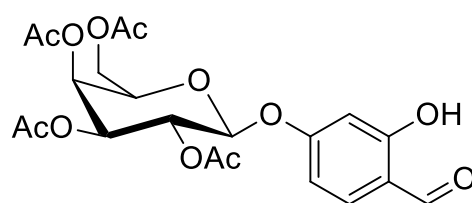


5.9

Galactose pentaacetate (1 g, 0.0026 mol) was dissolved in HBr/AcOH (7 mL) with acetic anhydride (1 mL) under N₂ and stirred for 4 h at room temperature. This was diluted with DCM (20 mL) and washed with water (3 x 10 mL), saturated NaHCO₃ solution (20 mL) and brine (30 mL) before being dried with Na₂SO₄. The solvent was removed *in vacuo* to yield a clear oil which was diluted in Et₂O (10 mL) and cyclohexane (50 mL) was added. The solution was cooled on ice to precipitate the product as a white solid (0.938 g, 89 %). ¹H NMR (300 MHz, CDCl₃) δ 6.64 (d, *J* = 3.9 Hz, 1H, H-1), 5.46 (dd, *J* = 3.3, 1.1 Hz, 1H, H-4), 5.35 (dd, *J* = 6.0, 3.3 Hz, 1H, H-3), 4.98

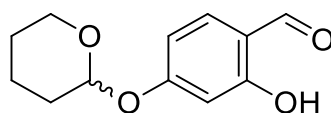
(dd, $J = 6.0, 3.9$ Hz, 1H, H-2), 4.46-4.43 (m, 1H, H-5), 4.14 (dd, $J = 11.5, 6.2$ Hz, 1H, H-6), 4.05 (dd, $J = 11.5, 6.9$ Hz, 1H, H-6'), 2.08 (s, 3H, OAc), 2.04 (s, 3H, OAc), 1.99 (s, 3H, OAc), 1.94 (s, 3H, OAc). ^{13}C NMR (75 MHz, CDCl_3) δ 170.5 (C=O), 170.1 (C=O), 170.0 (C=O), 169.8 (C=O), 87.9 (C-1), 70.97 (C-5), 67.9 (C-2), 67.7 (C-4), 67.0 (C-2), 60.8 (C-6), 20.4 (OAc), 20.3 (OAc), 20.2 (OAc), 20.2 (OAc).

The NMR data is in agreement with the data reported in the literature.²¹²



5.10

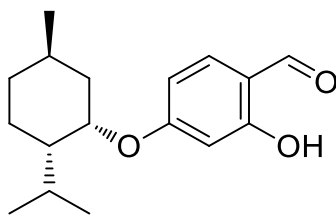
5.6 (0.900 g, 0.0022 mol), 2, 4-dihydroxybenzaldehyde (0.615 g, 0.0043 mol) and Ag_2CO_3 (0.605 g, 0.0043 mol) were dissolved in MeCN (25 mL, dried over 3 Å molecular sieves) under N_2 in the dark and stirred overnight at room temperature. The solvent was removed *in vacuo* and the residue was dissolved in EtOAc (40 mL) with sonication and filtered through a Celite cake. The resulting solution was washed with 1M HCl (25 mL), saturated NaHCO_3 solution (3 x 50 mL) and brine (50 mL) and dried over Na_2SO_4 . The solvent was removed *in vacuo* to yield a dark brown oil which was purified by column chromatography (2:1 Pet. Ether/EtOAc, Rf: 0.16) to yield the product as a white solid (1.40 g, 61%). ^1H NMR (500 MHz, CDCl_3) δ 11.35 (s, 1H, OH), 9.76 (s, 1H, HC=O), 7.46 (d, $J = 8.6$ Hz, 1H, Ar-H), 6.60 (dd, $J = 8.6, 2.2$ Hz, 1H, Ar-H), 6.55 (d, $J = 1.9$ Hz, 1H, Ar-H), 5.53 – 5.43 (m, 2H, H-1, H-2), 5.20 – 5.06 (m, 2H, H-3, H-4), 4.29 – 4.08 (m, 3H, H-5, H-6), 2.17 (s, 3H, OAc), 2.08 (s, 3H, OAc), 2.05 (s, 3H, OAc), 2.01 (s, 3H, OAc). ^{13}C NMR (126 MHz, CDCl_3) δ 194.8 (HC=O), 170.4 (C=O), 170.1 (C=O), 170.0 (C=O), 169.3 (C=O), 164.0 (Ar), 163.0 (Ar), 135.4 (Ar), 116.7 (Ar), 109.6 (Ar), 103.7 (Ar), 98.3 (C-1), 71.5 (C-5), 70.7 (C-2), 68.3 (C-3), 66.8 (C-4), 61.4 (C-6), 20.7 (OAc), 20.6 (OAc), 20.6 (OAc), 20.5 (OAc). IR (KBr Disk): 3459, 2971, 2863, 1755, 1665, 1579, 1432, 1375, 1230, 1177, 1073, 979, 908 cm^{-1} . HRMS m/z (ESI+): 469.1341 ($\text{C}_{21}\text{H}_{25}\text{O}_{12}$: $[\text{M}+\text{H}]^+$ requires 469.1340). Mp: 132-133 °C. $[\alpha]_{\text{D}}^{25}$: -1° ($c = 0.3$, CH_2Cl_2).



5.12

2,4-Dihydroxybenzaldehyde (1.0 g, 0.0072 mol) and 2,4-dihydro-2H-pyran (0.96 g, 0.0113 mol) were dissolved in anhydrous DCM (40 mL) with PPTS (0.175 g, 0.0007 mol). The reaction was stirred at ambient temperature for 4 h under N₂ and then washed with saturated NaHCO₃ solution (3 x 20 mL) and brine (50 mL). The organic fraction was dried over Na₂SO₄ and evaporated to yield a yellow oil. This was purified by column chromatography (5:1 Pet. Ether/EtOAc, Rf: 0.5) to produce the product as a pale yellow oil (1.439 g, 90 %). ¹H NMR (500 MHz, CDCl₃) δ 11.36 (s, 1H, OH), 9.72 (s, 1H, HC=O), 7.43 (d, *J* = 8.6 Hz, 1H, Ar-H), 6.65 (dd, *J* = 8.6, 1.9 Hz, 1H, Ar-H), 6.62 (s, 1H, Ar-H), 5.50 (t, *J* = 3 Hz, 1H, THP C(-O)₂H), 3.82 (td, *J* = 10.9, 3.0 Hz, 1H, THP C(O)-H), 3.66 – 3.56 (m, 1H, THP C(O)-H'), 1.86 (dt, *J* = 7.4, 3.5 Hz, 2H, THP CH₂), 1.77 – 1.64 (m, 2H, THP CH₂), 1.64 – 1.45 (m, 2H, THP CH₂). ¹³C NMR (126 MHz, CDCl₃) δ 194.6 (C=O), 164.4 (Ar-O), 164.2 (Ar-H), 135.3 (Ar-H), 109.4 (Ar-C), 103.7 (Ar-H), 96.3 (CH), 62.2 (CH₂), 29.9 (CH₂), 24.9 (CH₂), 18.4 (CH₂). IR (KBr Disk): 3431, 2969, 2869, 1750, 1663, 1627, 1579, 1500, 1438, 1371, 1227, 1170, 1076, 1035, 979, 908 cm⁻¹. HRMS *m/z* (ESI⁺): 223.0900 (C₁₂H₁₄O₄: [M+H]⁺ requires 223.0901).

The characterization data is in agreement with that reported in the literature.²¹³



5.14

Menthol (0.5 g, 0.00319 mol) and PPh₃ (3.147 g, 0.01276 mol) were dissolved in anhydrous THF (30 mL) under N₂ in a two-neck flask fitted with a thermometer and cooled to -10 °C in an ice/acetone/NaCl bath. DIAD (2.44 mL, 0.01276 mol) was added dropwise, ensuring that the temperature of the reaction never exceeded 5 °C. This

formed a bright yellow solution which was allowed to stir for 15 min to produce a cloudy white mixture to which was added a solution of 2, 4-dihydroxybenzaldehyde (1.657 g, 0.01276 mol) in anhydrous THF (15 mL) by cannula transfer to immediately form a deep red solution. This was allowed to gradually warm to room temperature and was stirred overnight after which it was reduced *in vacuo* to a heavy brown oil. This was dissolved in EtOAc (25 mL) and washed with saturated NaHCO₃ solution (3x 20 mL) and brine (50 mL) and was then dried with Na₂SO₄ and the solvent was removed *in vacuo* to produce a heavy red oil.

To remove TPPO and reduced DIAD by products,²²⁶ the oil was dissolved in toluene (30 mL) and MgCl₂ (3 g) was added and the mixture was heated to 60 °C for 2 h. A red precipitate was removed by vacuum filtration and the filtrate was concentrated *in vacuo* to yield a red oil which was purified by column chromatography (4:1 Cyclohexane/ Et₂O, Rf: 0.65) to yield the product as an amber oil (0.143 g, 16 %). ¹H NMR (500 MHz, CDCl₃) δ 11.48 (s, 1H, OH), 9.69 (s, 1H, C(=O)H), 7.40 (d, *J* = 8.7 Hz, 1H, Ar-H), 6.52 (dd, *J* = 8.7, 2.2 Hz, 1H, Ar-H), 6.42 (d, *J* = 2.1 Hz, 1H, Ar-H), 4.71 (ad, *J* = 1.4 Hz, 1H, OCH), 2.09 (add, *J* = 14.1, 2.1 Hz, 1H, CH), 1.83 – 1.72 (m, 2H, CH₂), 1.72 – 1.57 (m, 2H, CH₂), 1.53 (atd, *J* = 12.7, 3.3 Hz, 1H, CH), 1.46 – 1.39 (m, 1H, CH), 1.12 – 1.01 (m, 2H, CH₂), 0.92 (d, *J* = 6.7 Hz, 3H, CH₃), 0.83 (d, *J* = 6.7 Hz, 6H, isopropyl CH₃). ¹³C NMR (126 MHz, CDCl₃) δ 194.1 (C=O), 165.9 (Ar), 164.8 (Ar), 135.4 (Ar), 114.9 (Ar), 109.4 (Ar), 101.7 (Ar), 74.4 (Cyclohexyl-C-OAr), 47.6 (Cyclohexyl-C), 37.7 (Cyclohexyl-C), 34.8 (Cyclohexyl-C), 29.4 (Cyclohexyl-C), 24.8 (Cyclohexyl-C), 22.2 (Isopropyl C-H), 21.1 (CH₃), 20.7 (CH₃). IR (NaCl Plate): 2949, 2925, 2869, 1752, 1641, 1627, 1574, 1503, 1455, 1374, 1335, 1288, 1220, 1117, 980, 681cm⁻¹. HRMS *m/z* (ESI+): 277.1808 (C₁₃H₁₆O₇: [M+H]⁺ requires 277.1798). [α]_D²⁴: +3° (c 0.2, CH₂Cl₂).

6.5.2 Fluorescence Studies

Fluorescence spectra were obtained using a Jasco FP-6300 spectrofluorometer operating in emission mode using 1 cm quartz cuvette. Excitation and emission bandwidths were set at 2.5 nm. All experiments were carried out in triplicate using HPLC grade solvents at a concentration of 10μM. The λ_{max} was determined by UV/vis

spectroscopy at a concentration of 10 μM using a Perkin Elmer Lambda 35 spectrometer and Scan Lambda 35 software.

Chapter 7: Conclusions and Future Work

This thesis presents the results of a large body of research into the synthesis of functional glycosides and the investigation of their properties. From the work carried out on the synthesis of N_2 and N_2O ligands and an investigation of their coordination chemistry, it was identified that the N_2 ligands proved to be more difficult synthetic targets than the N_2O compounds. However, the N_2 series displayed better metal chelating ability, producing stable metal complexes which could be, in several cases, analysed by X-ray crystallography. The metal complexes of the N_2O series proved to be less stable and prone to hydrolysis in solution. Further work in this area should focus on diversifying the library of N_2 ligands with different carbohydrate moieties, in addition to non-carbohydrate biomolecules such as peptides and nucleobases. Furthermore, a wider variety of metals should be investigated and their properties studied. Another avenue of investigation which holds promise is the reduction of the N_2O imines to amines. Preliminary investigations into this reduction were carried out during this work, however, these studies were not exhaustive. Reduction of the imine bond would produce ligands which are not susceptible to hydrolysis, a problem which hampered work into the N_2O metal complexes in this work. As this problem likely stems from the acidity of the phenol groups, work should focus on reducing compounds already functionalized at the *para* position as these would have fewer acidic protons to react with the reducing agent.

The biological studies of these compounds identified very promising candidates for both Chagas disease and Leishmaniasis. The selectivity of the N_2 core was shown to be modulated by both the choice of metal and the incorporation of the carbohydrate moiety. The metal provides a means to target the desired parasite and the glucose moiety serves to increase in the tolerance of the compounds by mammalian cells. The identification of these structure-activity relationships allows for the design of highly specific antiparasitic compounds. Further work should focus on the elucidation of the mode of action of these compounds with the aim to further identify possibilities for the optimization of the structure of the antiparasitic compounds. The influence of the halide ligands and counterions present in the compounds on their antiparasitic activity should also be probed. The work presented here has focused on the use of chloride and perchlorate salts for the generation of the metal complexes.

Future work should investigate bromide ligands as metal complexes of these ligands are less prone to hydrolysis than the chlorides used in this work. Tetrafluoroborate counterions should also be tested as an alternative to perchlorate counterions as these are not explosive and are more amenable to a large scale synthesis which would be necessary if these compounds are to be synthesized on a scale necessary to carry out animal studies.

The research into the synthesis of a carbohydrate derived macrocycle has yielded several useful synthetic intermediates and studied several modes for their activation in glycosylation reactions. In addition, this work has identified problems associated with the use of serine as a building block due to the difficulties encountered when trying to perform glycosylation reactions with this molecule. Instead, an alternative route using 2-chloroethanol was investigated and this proved to be more successful. Two macrocyclization routes were explored and the reaction products were analysed by MS. These reactions have indicated the presence of the target macrocycle along with oligomeric by products and from these studies it was shown that an intramolecular glycosylation route holds promise for the synthesis of the monomeric macrocycle. A reason for this selectivity is presented based on the examination and comparison of the reaction mechanisms.

Future work on this should focus on exploring the ring closing glycosylation step with alternative glycosyl donors. Acetate based donors proved to generate less complex mixtures however the reaction was slow and it was difficult to achieve complete conversion of the starting material. Trichloroacetimidate donors should provide a higher reactivity which may overcome this while being activated using the same promotor which does not leave any products in the crude product, unlike the sulfur based promotors which were used for the thioglycoside glycosylations. The serine derived macrocycle may prove to be obtainable using an intramolecular glycosylation route following its so this strategy should be explored. In particular, InBr_3 has been recently shown to be a useful glycosylation promotor of acetylated sugars and amino acids and this could generate the target macrocycle from the intermediates developed in this work. Another avenue of exploration worth pursuing is the use of

templating cations to control the selectivity of the reaction for different sized macrocycles.

The studies on the photophysical properties revealed that the compounds containing a β -glycosidic linkage exhibited fluorescent behaviour while the α -glycosylated mannose derivative and the compounds containing non-carbohydrate moieties did not show fluorescence. A reason for this observation is proposed based on DFT studies of the glucosylated and non-glucosylated biaryl core which suggest that the pyran oxygen of the sugar moiety contributes electron density to the HOMO of the molecule. This electron donation appears to facilitate the fluorescent behaviour of the compounds with a β -glycoside moiety. While the fluorescent intensity of the compounds was quite low, this effect seems to be specific to sugars and therefore could have applications in fluorescent carbohydrate sensors. This avenue should be explored by exploring the use of these compounds to monitor glycosidase enzymes. In addition, modifications to the biaryl core should be explored in order to improve the water stability of the compounds and increase the fluorescent intensity of the compounds which would be necessary for their use as sensors with low detection limits.

Overall, the work presented here has explored a wide range of the synthetic chemistry of carbohydrates and the use of glycosylated molecules. From this I have succeeded in identifying compounds with extremely promising antiparasitic properties, developing synthetic intermediates and protocols for the generation of conformationally constrained macrocycles and investigated the influence of carbohydrate residues on the fluorescent properties of a novel biaryl fluorophore.

Bibliography

1. David Nelson , M. C., *Lehninger Principles of Biochemistry*. 2013.
2. Robyt, J., *Essentials of Carbohydrate Chemistry*. Springer: 1998.
3. Davis, B. G.; Fairbanks, A. J., *Carbohydrate Chemistry*. Oxford University Press: 2002.
4. Brandley, B. K.; Schnaar, R. L., Cell-surface carbohydrates in cell recognition and response. *J Leukoc Biol* **1986**, *40* (1), 97-111.
5. Klemm, D.; Heublein, B.; Fink, H. P.; Bohn, A., Cellulose: fascinating biopolymer and sustainable raw material. *Angewandte Chemie* **2005**, *44* (22), 3358-93.
6. Li, H.; Gao, X.; Liu, R.; Wang, Y.; Zhang, M.; Fu, Z.; Mi, Y.; Wang, Y.; Yao, Z.; Gao, Q., Glucose conjugated platinum(II) complex: antitumor superiority to oxaliplatin, combination effect and mechanism of action. *European journal of medicinal chemistry* **2015**, *101*, 400-8.
7. Carroux, C. J.; Rankin, G. M.; Moeker, J.; Bornaghi, L. F.; Katneni, K.; Morizzi, J.; Charman, S. A.; Vullo, D.; Supuran, C. T.; Poulsen, S. A., A prodrug approach toward cancer-related carbonic anhydrase inhibition. *J Med Chem* **2013**, *56* (23), 9623-34.
8. WHO Leishmaniasis Fact Sheet
<http://www.who.int/mediacentre/factsheets/fs375/en/> (accessed 08/07/16).
9. WHO, Leishmaniasis- Magnitude of the Problem. **2014**
10. Freitas-Junior, L. H.; Chatelain, E.; Kim, H. A.; Siqueira-Neto, J. L., Visceral leishmaniasis treatment: What do we have, what do we need and how to deliver it? *International journal for parasitology. Drugs and drug resistance* **2012**, *2*, 11-9.
11. Sangshetti, J. N.; Khan, F. A. K.; Kulkarni, A. A.; Arote, R.; Patil, R. H., Antileishmanial drug discovery: comprehensive review of the last 10 years. *Rsc Advances* **2015**, *5* (41), 32376-32415.

12. Polonio, T.; Efferth, T., Leishmaniasis: Drug resistance and natural products (Review). *International Journal of Molecular Medicine* **2008**, *22* (3), 277-286.
13. Navarro, M.; Gabbiani, C.; Messori, L.; Gambino, D., Metal-based drugs for malaria, trypanosomiasis and leishmaniasis: recent achievements and perspectives. *Drug Discov Today* **2010**, *15* (23-24), 1070-8.
14. Saravolatz, L. D.; Bern, C.; Adler-Moore, J.; Berenguer, J.; Boelaert, M.; den Boer, M.; Davidson, R. N.; Figueras, C.; Gradoni, L.; Kafetzis, D. A.; Ritmeijer, K.; Rosenthal, E.; Royce, C.; Russo, R.; Sundar, S.; Alvar, J., Liposomal Amphotericin B for the Treatment of Visceral Leishmaniasis. *Clinical Infectious Diseases* **2006**, *43* (7), 917-924.
15. Ramos, H.; Valdivieso, E.; Gamargo, M.; Dagger, F.; Cohen, B. E., Amphotericin B kills unicellular leishmanias by forming aqueous pores permeable to small cations and anions. *J Membr Biol* **1996**, *152* (1), 65-75.
16. Balana-Fouce, R.; Reguera, R. M.; Cubria, J. C.; Ordonez, D., The pharmacology of leishmaniasis. *General pharmacology* **1998**, *30* (4), 435-43.
17. Murray, H. W., Treatment of visceral leishmaniasis (kala-azar): a decade of progress and future approaches. *International journal of infectious diseases : IJID : official publication of the International Society for Infectious Diseases* **2000**, *4* (3), 158-77.
18. Yao, S., FDA approves Impavido to treat tropical disease leishmaniasis. *FDA NEWS RELEASE. U.S. Food and Drug Administration* 2014.
19. Croft, S. L.; Seifert, K.; Duchene, M., Antiprotozoal activities of phospholipid analogues. *Mol Biochem Parasitol* **2003**, *126* (2), 165-72.
20. Alvar, J.; Croft, S.; Olliaro, P., Chemotherapy in the Treatment and Control of Leishmaniasis. In *Advances in Parasitology*, David, H. M., Ed. Academic Press: 2006; Vol. Volume 61, pp 223-274.

21. Maarouf, M.; Lawrence, F.; Croft, S. L.; Robert-Gero, M., Ribosomes of Leishmania are a target for the aminoglycosides. *Parasitology Research* **1995**, *81* (5), 421-425.
22. Jhingran, A.; Chawla, B.; Saxena, S.; Barrett, M. P.; Madhubala, R., Paromomycin: uptake and resistance in Leishmania donovani. *Mol Biochem Parasitol* **2009**, *164* (2), 111-7.
23. Maarouf, M.; de Kouchkovsky, Y.; Brown, S.; Petit, P. X.; Robert-Gero, M., In vivo interference of paromomycin with mitochondrial activity of Leishmania. *Exp Cell Res* **1997**, *232* (2), 339-48.
24. Maarouf, M.; Adeline, M. T.; Solignac, M.; Vautrin, D.; Robert-Gero, M., Development and characterization of paromomycin-resistant Leishmania donovani promastigotes. *Parasite* **1998**, *5* (2), 167-173.
25. Farrer, N. J.; Sadler, P. J., Medicinal Inorganic Chemistry: State of the Art, New Trends, and a Vision of the Future. *Bioinorganic Medicinal Chemistry*, Wiley-VCH Verlag GmbH & Co. KGaA: 2011; pp 1-47.
26. Sesti-Costa, R.; Carneiro, Z. A.; Silva, M. C.; Santos, M.; Silva, G. K.; Milanezi, C.; da Silva, R. S.; Silva, J. S., Ruthenium complex with benzimidazole and nitric oxide as a new candidate for the treatment of chagas disease. *PLoS Negl Trop Dis* **2014**, *8* (10), e3207.
27. Wang, T.; Guo, Z., Copper in Medicine: Homeostasis, Chelation Therapy and Antitumor Drug Design. *Current Medicinal Chemistry* **2006**, *13* (5), 525-537.
28. Caballero, A. B.; Rodriguez-Dieguez, A.; Quiros, M.; Salas, J. M.; Huertas, O.; Ramirez-Macias, I.; Olmo, F.; Marin, C.; Chaves-Lemaur, G.; Gutierrez-Sanchez, R.; Sanchez-Moreno, M., Triazolopyrimidine compounds containing first-row transition metals and their activity against the neglected infectious Chagas disease and leishmaniasis. *Eur. J. Med Chem.* **2014**, *85*, 526-34.
29. Britta, E. A.; Silva, A. P.; Ueda-Nakamura, T.; Dias-Filho, B. P.; Silva, C. C.; Sernaglia, R. L.; Nakamura, C. V., Benzaldehyde thiosemicarbazone derived from

limonene complexed with copper induced mitochondrial dysfunction in *Leishmania amazonensis*. *PLoS One* **2012**, 7 (8), e41440.

30. da Silva Maffei, R.; Yokoyama-Yasunaka, J. K.; Miguel, D. C.; Uliana, S. R.; Esposito, B. P., Synthesis, characterization and evaluation of antileishmanial activity of copper(II) with fluorinated alpha-hydroxycarboxylate ligands. *Biometals* **2009**, 22 (6), 1095-101.

31. Harford, C.; Sarkar, B., Amino terminal Cu(II)- and Ni(II)-binding (ATCUN) motif of proteins and peptides: Metal binding, DNA cleavage, and other properties. *Accounts of Chemical Research* **1997**, 30 (3), 123-130.

32. Navarro, M.; Cisneros-Fajardo, E. J.; Sierralta, A.; Fernandez-Mestre, M.; Silva, P.; Arrieche, D.; Marchan, E., Design of copper DNA intercalators with leishmanicidal activity. *Journal of biological inorganic chemistry : JBIC : a publication of the Society of Biological Inorganic Chemistry* **2003**, 8 (4), 401-8.

33. Sharquie, K. E.; Najim, R. A.; Farjou, I. B.; Al-Timimi, D. J., Oral zinc sulphate in the treatment of acute cutaneous leishmaniasis. *Clin Exp Dermatol* **2001**, 26 (1), 21-6.

34. Bouma, M. J.; Snowdon, D.; Fairlamb, A. H.; Ackers, J. P., Activity of disulfiram (bis(diethylthiocarbamoyl)disulphide) and ditiocarb (diethyldithiocarbamate) against metronidazole-sensitive and -resistant *Trichomonas vaginalis* and *Tritrichomonas foetus*. *The Journal of antimicrobial chemotherapy* **1998**, 42 (6), 817-20.

35. Peniche, A. G.; Renslo, A. R.; Melby, P. C.; Travi, B. L., Antileishmanial Activity of Disulfiram and Thiuram Disulfide Analogs in an Ex Vivo Model System Is Selectively Enhanced by the Addition of Divalent Metal Ions. *Antimicrob Agents Chemother* **2015**, 59 (10), 6463-70.

36. Rice, D. R.; Vacchina, P.; Norris-Mullins, B.; Morales, M. A.; Smith, B. D., Zinc(II)-Dipicolylamine Coordination Complexes as Targeting and Chemotherapeutic Agents for *Leishmania major*. *Antimicrobial Agents and Chemotherapy* **2016**.

37. Pal, D. S.; Mondal, D. K.; Datta, R., Identification of Metal Dithiocarbamates as a Novel Class of Antileishmanial Agents. *Antimicrobial Agents and Chemotherapy* **2015**, *59* (4), 2144-2152.
38. Hassan Khan, N. U.; Zaib, S.; Sultana, K.; Khan, I.; Mougang-Soume, B.; Nadeem, H.; Hassan, M.; Iqbal, J., Metal complexes of tosyl sulfonamides: design, X-ray structure, biological activities and molecular docking studies. *RSC Adv.* **2015**, *5* (38), 30125-30132.
39. Chagas disease (American trypanosomiasis) Fact sheet. <http://www.who.int/mediacentre/factsheets/fs340/en/>.
40. Chagas Disease- Biology. <http://www.cdc.gov/parasites/chagas/biology.html>.
41. *Working to overcome the global impact of neglected tropical diseases*. World Health Organization Geneva, Switzerland, 2010.
42. Delespaux, V.; de Koning, H. P., Drugs and drug resistance in African trypanosomiasis. *Drug Resist Updat* **2007**, *10* (1-2), 30-50.
43. Urbina, J. A., New chemotherapeutic approaches for the treatment of Chagas disease (American Trypanosomiasis). *Expert Opinion on Therapeutic Patents* **2003**, *13* (5), 661-669.
44. Wilkinson, S. R.; Temperton, N. J.; Mondragon, A.; Kelly, J. M., Distinct mitochondrial and cytosolic enzymes mediate trypanothione-dependent peroxide metabolism in *Trypanosoma cruzi*. *The Journal of biological chemistry* **2000**, *275* (11), 8220-5.
45. Boiani, M.; Piacenza, L.; Hernandez, P.; Boiani, L.; Cerecetto, H.; Gonzalez, M.; Denicola, A., Mode of action of nifurtimox and N-oxide-containing heterocycles against *Trypanosoma cruzi*: is oxidative stress involved? *Biochem Pharmacol* **2010**, *79* (12), 1736-45.
46. Cancado, J. R., Long term evaluation of etiologic treatment of chagas disease with benznidazole. *Rev Inst Med Trop Sao Paulo* **2002**, *44* (1), 29-37.

47. Bermudez, J.; Davies, C.; Simonazzi, A.; Pablo Real, J.; Palma, S., Current drug therapy and pharmaceutical challenges for Chagas disease. *Acta Trop* **2016**, *156*, 1-16.
48. Viotti, R.; Vigliano, C.; Lococo, B.; Alvarez, M. G.; Petti, M.; Bertocchi, G.; Armenti, A., Side effects of benznidazole as treatment in chronic Chagas disease: fears and realities. *Expert Review of Anti-infective Therapy* **2009**, *7* (2), 157-163.
49. Moreno, S. N. J.; Docampo, R.; Mason, R. P.; Leon, W.; Stoppani, A. O. M., Different Behaviors of Benznidazole as Free-Radical Generator with Mammalian and Trypanosoma-Cruzi Microsomal Preparations. *Archives of Biochemistry and Biophysics* **1982**, *218* (2), 585-591.
50. Faundez, M.; Pino, L.; Letelier, P.; Ortiz, C.; Lopez, R.; Seguel, C.; Ferreira, J.; Pavani, M.; Morello, A.; Maya, J. D., Buthionine sulfoximine increases the toxicity of nifurtimox and benznidazole to Trypanosoma cruzi. *Antimicrob Agents Chemother* **2005**, *49* (1), 126-30.
51. Díaz de Toranzo, E. G.; Castro, J. A.; Franke de Cazzulo, B. M.; Cazzulo, J. J., Interaction of benznidazole reactive metabolites with nuclear and kinetoplasmic DNA, proteins and lipids from Trypanosoma cruzi. *Experientia* **1988**, *44* (10), 880-881.
52. Martins, D. A.; Gouvea, L. R.; Muniz, G. S. V.; Louro, S. R. W.; Batista, D. D. J.; Soeiro, M. D. C.; Teixeira, L. R., Norfloxacin and N-Donor Mixed-Ligand Copper(II) Complexes: Synthesis, Albumin Interaction, and Anti-Trypanosoma cruzi Activity. *Bioinorganic Chemistry and Applications* **2016**, *2016*, 11.
53. Nwaka, S.; Hudson, A., Innovative lead discovery strategies for tropical diseases. *Nat Rev Drug Discov* **2006**, *5* (11), 941-55.
54. Becco, L.; Rodriguez, A.; Bravo, M. E.; Prieto, M. J.; Ruiz-Azuara, L.; Garat, B.; Moreno, V.; Gambino, D., New achievements on biological aspects of copper complexes Casiopeinas(R): interaction with DNA and proteins and anti-Trypanosoma cruzi activity. *J Inorg Biochem* **2012**, *109*, 49-56.
55. Demoro, B.; Caruso, F.; Rossi, M.; Benitez, D.; Gonzalez, M.; Cerecetto, H.; Parajon-Costa, B.; Castiglioni, J.; Galizzi, M.; Docampo, R.; Otero, L.; Gambino, D.,

Risedronate metal complexes potentially active against Chagas disease. *J Inorg Biochem* **2010**, *104* (12), 1252-8.

56. Montalvetti, A.; Bailey, B. N.; Martin, M. B.; Severin, G. W.; Oldfield, E.; Docampo, R., Bisphosphonates Are Potent Inhibitors of Trypanosoma cruzi Farnesyl Pyrophosphate Synthase. *Journal of Biological Chemistry* **2001**, *276* (36), 33930-33937.

57. Gouvea, L. R.; Martins, D. A.; Batista Dda, G.; Soeiro Mde, N.; Louro, S. R.; Barbeira, P. J.; Teixeira, L. R., Norfloxacin Zn(II)-based complexes: acid base ionization constant determination, DNA and albumin binding properties and the biological effect against Trypanosoma cruzi. *Biometals* **2013**, *26* (5), 813-25.

58. K. Kapoor, V.; Kaur, A., Drug-Glycosidation and Drug Development. *Mini-Reviews in Medicinal Chemistry* **2013**, *13* (4), 584-596.

59. Li, T.; Gao, X.; Yang, L.; Shi, Y.; Gao, Q., Methyl 6-Amino-6-deoxy-d-pyranoside-Conjugated Platinum(II) Complexes for Glucose Transporter (GLUT)-Mediated Tumor Targeting: Synthesis, Cytotoxicity, and Cellular Uptake Mechanism. *ChemMedChem* **2016**, *11* (10), 1069-77.

60. Storr, T.; Merkel, M.; Song-Zhao, G. X.; Scott, L. E.; Green, D. E.; Bowen, M. L.; Thompson, K. H.; Patrick, B. O.; Schugar, H. J.; Orvig, C., Synthesis, Characterization, and Metal Coordinating Ability of Multifunctional Carbohydrate-Containing Compounds for Alzheimer's Therapy. *Journal of the American Chemical Society* **2007**, *129* (23), 7453-7463.

61. Schibli, R.; Dumas, C.; Petrig, J.; Spadola, L.; Scapozza, L.; Garcia-Garayoa, E.; Schubiger, P. A., Synthesis and in vitro characterization of organometallic rhenium and technetium glucose complexes against Glut 1 and hexokinase. *Bioconjug Chem* **2005**, *16* (1), 105-12.

62. Ferreira, C. L.; Lapi, S.; Steele, J.; Green, D. E.; Ruth, T. J.; Adam, M. J.; Orvig, C., ⁵⁵Cobalt complexes with pendant carbohydrates as potential PET imaging agents. *Applied radiation and isotopes : including data, instrumentation and methods for use in agriculture, industry and medicine* **2007**, *65* (12), 1303-8.

63. Banerjee, S. R.; Babich, J. W.; Zubieta, J., A new bifunctional amino acid chelator targeting the glucose transporter. *Inorganica Chimica Acta* **2006**, *359* (5), 1603-1612.
64. Gottschaldt, M.; Koth, D.; Muller, D.; Klette, I.; Rau, S.; Gorls, H.; Schafer, B.; Baum, R. P.; Yano, S., Synthesis and structure of novel sugar-substituted bipyridine complexes of rhenium and 99m-technetium. *Chemistry* **2007**, *13* (36), 10273-80.
65. Parmelee, D. J.; Walovitch, R. C.; Ouellet, H. S.; Lauffer, R. B., Preclinical evaluation of the pharmacokinetics, biodistribution, and elimination of MS-325, a blood pool agent for magnetic resonance imaging. *Invest Radiol* **1997**, *32* (12), 741-7.
66. Caravan, P., Protein-Targeted Gadolinium-Based Magnetic Resonance Imaging (MRI) Contrast Agents: Design and Mechanism of Action. *Accounts of Chemical Research* **2009**, *42* (7), 851-862.
67. Prata, M. I.; Santos, A. C.; Torres, S.; Andre, J. P.; Martins, J. A.; Neves, M.; Garcia-Martin, M. L.; Rodrigues, T. B.; Lopez-Larrubia, P.; Cerdan, S.; Geraldés, C. F., Targeting of lanthanide(III) chelates of DOTA-type glycoconjugates to the hepatic asialoglycoprotein receptor: cell internalization and animal imaging studies. *Contrast Media Mol Imaging* **2006**, *1* (6), 246-58.
68. Fulton, D. A.; Elemento, E. M.; Aime, S.; Chaabane, L.; Botta, M.; Parker, D., Glycoconjugates of gadolinium complexes for MRI applications. *Chemical communications* **2006**, (10), 1064-6.
69. Moats, R. A.; Fraser, S. E.; Meade, T. J., A "Smart" Magnetic Resonance Imaging Agent That Reports on Specific Enzymatic Activity. *Angewandte Chemie International Edition in English* **1997**, *36* (7), 726-728.
70. Urbanczyk-Pearson, L. M.; Femia, F. J.; Smith, J.; Parigi, G.; Duimstra, J. A.; Eckermann, A. L.; Luchinat, C.; Meade, T. J., Mechanistic investigation of beta-galactosidase-activated MR contrast agents. *Inorg Chem* **2008**, *47* (1), 56-68.

71. Milne, M.; Chicas, K.; Li, A.; Bartha, R.; Hudson, R. H., ParaCEST MRI contrast agents capable of derivatization via "click" chemistry. *Org Biomol Chem* **2012**, *10* (2), 287-92.
72. Miura, N.; Yamashita, M., Gadolinium compound and contrast medium for mri. Google Patents: 2008.
73. Roder, C.; Thomson, M. J., Auranofin: repurposing an old drug for a golden new age. *Drugs R D* **2015**, *15* (1), 13-20.
74. Thangamani, S.; Mohammad, H.; Abushahba, M. F.; Sobreira, T. J.; Hedrick, V. E.; Paul, L. N.; Seleem, M. N., Antibacterial activity and mechanism of action of auranofin against multi-drug resistant bacterial pathogens. *Sci Rep* **2016**, *6*, 22571.
75. Parsonage, D.; Sheng, F.; Hirata, K.; Debnath, A.; McKerrow, J. H.; Reed, S. L.; Abagyan, R.; Poole, L. B.; Podust, L. M., X-ray structures of thioredoxin and thioredoxin reductase from *Entamoeba histolytica* and prevailing hypothesis of the mechanism of Auranofin action. *J Struct Biol* **2016**, *194* (2), 180-90.
76. Chen, Y. S.; Heeg, M. J.; Brauschweiger, P. G.; Xie, W. H.; Wang, P. G., A carbohydrate-linked cisplatin analogue having antitumor activity. *Angew Chem Int Edit* **1999**, *38* (12), 1768-1769.
77. Ma, D. L.; Shum, T. Y.; Zhang, F.; Che, C. M.; Yang, M., Water soluble luminescent platinum terpyridine complexes with glycosylated acetylide and arylacetylide ligands: photoluminescent properties and cytotoxicities. *Chem. Comm.* **2005**, (37), 4675-7.
78. Liu, P.; Lu, Y.; Gao, X.; Liu, R.; Zhang-Negrerie, D.; Shi, Y.; Wang, Y.; Wang, S.; Gao, Q., Highly water-soluble platinum(II) complexes as GLUT substrates for targeted therapy: improved anticancer efficacy and transporter-mediated cytotoxic properties. *Chemical communications* **2013**, *49* (24), 2421-3.
79. Wu, M.; Li, H.; Liu, R.; Gao, X.; Zhang, M.; Liu, P.; Fu, Z.; Yang, J.; Zhang-Negrerie, D.; Gao, Q., Galactose conjugated platinum(II) complex targeting the Warburg effect for treatment of non-small cell lung cancer and colon cancer. *European journal of medicinal chemistry* **2016**, *110*, 32-42.

80. Florindo, P.; Marques, I. J.; Nunes, C. D.; Fernandes, A. C., Synthesis, characterization and cytotoxicity of cyclopentadienyl ruthenium(II) complexes containing carbohydrate-derived ligands. *Journal of Organometallic Chemistry* **2014**, *760*, 240-247.
81. Florindo, P. R.; Pereira, D. M.; Borralho, P. M.; Rodrigues, C. M.; Piedade, M. F.; Fernandes, A. C., Cyclopentadienyl-ruthenium(II) and iron(II) organometallic compounds with carbohydrate derivative ligands as good colorectal anticancer agents. *J Med Chem* **2015**, *58* (10), 4339-47.
82. Ott, I.; Koch, T.; Shorafa, H.; Bai, Z.; Poeckel, D.; Steinhilber, D.; Gust, R., Synthesis, cytotoxicity, cellular uptake and influence on eicosanoid metabolism of cobalt-alkyne modified fructoses in comparison to auranofin and the cytotoxic COX inhibitor Co-ASS. *Org Biomol Chem* **2005**, *3* (12), 2282-6.
83. Gottschaldt, M.; Pfeifer, A.; Koth, D.; Gorls, H.; Dahse, H. M.; Mollmann, U.; Obata, M.; Yano, S., Silver(I) complexes based on novel tripodal thioglycosides: synthesis, structure and antimicrobial activity. *Tetrahedron* **2006**, *62* (48), 11073-11080.
84. Rye, C. S.; Withers, S. G., Glycosidase mechanisms. *Curr Opin Chem Biol* **2000**, *4* (5), 573-80.
85. Brunner, H.; Dafinger, W.; Schönenberger, H., Synthesis of PtCl₂ complexes of pyridylmethylamine ligands and their activity against hormone-dependent mammary carcinoma. *Inorganica Chimica Acta* **1989**, *156* (2), 291-301.
86. Abdel-Magid, A. F.; Carson, K. G.; Harris, B. D.; Maryanoff, C. A.; Shah, R. D., Reductive Amination of Aldehydes and Ketones with Sodium Triacetoxyborohydride. Studies on Direct and Indirect Reductive Amination Procedures¹. *The Journal of Organic Chemistry* **1996**, *61* (11), 3849-3862.
87. Addison, A. W.; Rao, T. N.; Reedijk, J.; Vanrijn, J.; Verschoor, G. C., Synthesis, Structure, and Spectroscopic Properties of Copper(II) Compounds Containing Nitrogen Sulfur Donor Ligands - the Crystal and Molecular-Structure of Aqua[1,7-

Bis(N-Methylbenzimidazol-2'-yl)-2,6-Dithiaheptane]Copper(II) Perchlorate. *J Chem Soc Dalton* **1984**, (7), 1349-1356.

88. Okuniewski, A.; Rosiak, D.; Chojnacki, J.; Becker, B., Coordination polymers and molecular structures among complexes of mercury(II) halides with selected 1-benzoylthioureas. *Polyhedron* **2015**, *90*, 47-57.

89. Lewis, D. L.; Estes, E. D.; Hodgson, D. J., The infrared spectra of coordinated perchlorates. *Journal of Crystal and Molecular Structure* **1975**, *5* (1), 67-74.

90. Sarma, M.; Mondal, B., Nitric oxide reduction of copper(II) complexes: spectroscopic evidence of copper(II)-nitrosyl intermediate. *Inorg Chem* **2011**, *50* (8), 3206-12.

91. Ramadan, A. M.; ElNaggar, M. M., Synthesis, characterization and demonstration of superoxide dismutase-like activity of copper(II) chloride, bromide, nitrate, thiocyanate, sulphate, and perchlorate complexes with 2-methyl-amino pyridine. *Journal of Inorganic Biochemistry* **1996**, *63* (2), 143-153.

92. Brown, D. S.; Lee, J. D.; Melsom, B. G. A.; Hathaway, B. J.; Procter, I. M.; Tomlinson, A. A. G., The structure of $\text{Cu}(\text{en})_2(\text{BF}_4)_2$ and an infrared spectral criterion for "semi-co-ordinated" polyanions. *Chem. Commun. (London)* **1967**, *0* (8), 369-371.

93. Yang, L.; Powell, D. R.; Houser, R. P., Structural variation in copper(I) complexes with pyridylmethylamide ligands: structural analysis with a new four-coordinate geometry index, τ_4 . *Dalton Trans* **2007**, (9), 955-64.

94. Chu, T.; Belding, L.; Poddutoori, P. K.; van der Est, A.; Dudding, T.; Korobkov, I.; Nikonov, G. I., Unique molecular geometries of reduced 4- and 5-coordinate zinc complexes stabilised by diiminopyridine ligand. *Dalton Trans* **2016**, *45* (34), 13440-8.

95. Seguin, O.; Descoteaux, A., Leishmania, the phagosome, and host responses: The journey of a parasite. *Cell Immunol* **2016**.

96. Strober, W., Trypan Blue Exclusion Test of Cell Viability. In *Current Protocols in Immunology*, John Wiley & Sons, Inc.: 2001.

97. Mondal, S.; Roy, P.; Das, S.; Halder, A.; Mukherjee, A.; Bera, T., In vitro susceptibilities of wild and drug resistant leishmania donovani amastigote stages to andrographolide nanoparticle: role of vitamin E derivative TPGS for nanoparticle efficacy. *PLoS One* **2013**, *8* (12), e81492.
98. Loiseau, P. M.; Gupta, S.; Verma, A.; Srivastava, S.; Puri, S. K.; Sliman, F.; Normand-Bayle, M.; Desmaele, D., In vitro activities of new 2-substituted quinolines against Leishmania donovani. *Antimicrob Agents Chemother* **2011**, *55* (4), 1777-80.
99. Kalyan Roy, S. D., Subhasish Mondal, Anup Kumar Roy, Tanmoy Bera, The in Vitro effect of clarithromycin on amastigote of Leishmania donovani. *Int. J. Drug Dev. & Res.* **2013**, *5* (3), 425-431.
100. Simpson, L., Effect Of Acriflavin On The Kinetoplast Of Leishmania Tarentolae. *The Journal of Cell Biology* **1968**, *37* (3), 660.
101. Brun, R.; Leon, W., Effect of ethidium bromide on growth and morphology of Leishmania tarentolae promastigotes in vitro. *Acta Trop* **1978**, *35* (3), 239-46.
102. Leon, W.; Brun, R.; Krassner, S. M., Effect of berenil on growth, mitochondrial DNA and respiration of Leishmania tarentolae promastigotes. *J Protozool* **1977**, *24* (3), 444-8.
103. Mwololo, S. W.; Mutiso, J. M.; Macharia, J. C.; Bourdichon, A. J.; Gicheru, M. M., In vitro activity and in vivo efficacy of a combination therapy of diminazene and chloroquine against murine visceral leishmaniasis. *J Biomed Res* **2015**, *29* (3), 214-23.
104. Al-Mulla Hummadi, Y. M.; Najim, R. A.; Al-Bashir, N. M., The mechanism behind the antileishmanial effect of zinc sulphate. I. An in-vitro study. *Annals of tropical medicine and parasitology* **2005**, *99* (1), 27-36.
105. Al-Mulla Hummadi, Y. M.; Al-Bashir, N. M.; Najim, R. A., The mechanism behind the antileishmanial effect of zinc sulphate. II. Effects on the enzymes of the parasites. *Annals of tropical medicine and parasitology* **2005**, *99* (2), 131-9.

106. Crichton, R. R., Chapter 1 - An Overview of Metals and Selected Nonmetals in Biology. In *Biological Inorganic Chemistry (Second Edition)*, Elsevier: Oxford, 2012; pp 1-19.
107. Mitra, B.; Laranjeira-Silva, M. F.; Perrone Bezerra de Menezes, J.; Jensen, J.; Michailowsky, V.; Andrews, N. W., A Trypanosomatid Iron Transporter that Regulates Mitochondrial Function Is Required for *Leishmania amazonensis* Virulence. *PLoS Pathog* **2016**, *12* (1), e1005340.
108. Sena, L. A.; Chandel, N. S., Physiological roles of mitochondrial reactive oxygen species. *Mol Cell* **2012**, *48* (2), 158-67.
109. Reczek, C. R.; Chandel, N. S., ROS-dependent signal transduction. *Curr Opin Cell Biol* **2015**, *33*, 8-13.
110. De Freitas, J. M.; Meneghini, R., Iron and its sensitive balance in the cell. *Mutation research* **2001**, *475* (1-2), 153-9.
111. Mitra, B.; Cortez, M.; Haydock, A.; Ramasamy, G.; Myler, P. J.; Andrews, N. W., Iron uptake controls the generation of *Leishmania* infective forms through regulation of ROS levels. *The Journal of Experimental Medicine* **2013**, *210* (2), 401-416.
112. Lalonde, R. G.; Holbein, B. E., Role of iron in *Trypanosoma cruzi* infection of mice. *The Journal of clinical investigation* **1984**, *73* (2), 470-6.
113. Loo, V. G.; Lalonde, R. G., Role of iron in intracellular growth of *Trypanosoma cruzi*. *Infect Immun* **1984**, *45* (3), 726-30.
114. Arantes, J. M.; Francisco, A. F.; de Abreu Vieira, P. M.; Silva, M.; Araujo, M. S.; de Carvalho, A. T.; Pedrosa, M. L.; Carneiro, C. M.; Tafuri, W. L.; Martins-Filho, O. A.; Eloi-Santos, S. M., *Trypanosoma cruzi*: desferrioxamine decreases mortality and parasitemia in infected mice through a trypanostatic effect. *Exp Parasitol* **2011**, *128* (4), 401-8.
115. Arantes, J. M.; Pedrosa, M. L.; Martins, H. R.; Veloso, V. M.; de Lana, M.; Bahia, M. T.; Tafuri, W. L.; Carneiro, C. M., *Trypanosoma cruzi*: treatment with the iron

chelator desferrioxamine reduces parasitemia and mortality in experimentally infected mice. *Exp Parasitol* **2007**, *117* (1), 43-50.

116. Kavanagh, K.; Reeves, E. P., Exploiting the potential of insects for in vivo pathogenicity testing of microbial pathogens. *FEMS microbiology reviews* **2004**, *28* (1), 101-12.

117. Hoffmann, J. A., Innate immunity of insects. *Current opinion in immunology* **1995**, *7* (1), 4-10.

118. Kimbrell, D. A.; Beutler, B., The evolution and genetics of innate immunity. *Nature reviews. Genetics* **2001**, *2* (4), 256-67.

119. Dolan, N.; Gavin, D. P.; Eshwika, A.; Kavanagh, K.; McGinley, J.; Stephens, J. C., Synthesis, antibacterial and anti-MRSA activity, in vivo toxicity and a structure-activity relationship study of a quinoline thiourea. *Bioorg Med Chem Lett* **2016**, *26* (2), 630-5.

120. Desbois, A. P.; Coote, P. J., Wax moth larva (*Galleria mellonella*): an in vivo model for assessing the efficacy of antistaphylococcal agents. *The Journal of antimicrobial chemotherapy* **2011**, *66* (8), 1785-90.

121. Kellett, A.; O'Connor, M.; McCann, M.; Howe, O.; Casey, A.; McCarron, P.; Kavanagh, K.; McNamara, M.; Kennedy, S.; May, D. D.; Skell, P. S.; O'Shea, D.; Devereux, M., Water-soluble bis(1,10-phenanthroline) octanedioate Cu²⁺ and Mn²⁺ complexes with unprecedented nano and picomolar in vitro cytotoxicity: promising leads for chemotherapeutic drug development. *Medchemcomm* **2011**, *2* (7), 579-584.

122. Jander, G.; Rahme, L. G.; Ausubel, F. M., Positive Correlation between Virulence of *Pseudomonas aeruginosa* Mutants in Mice and Insects. *Journal of Bacteriology* **2000**, *182* (13), 3843-3845.

123. Brennan, M.; Thomas, D. Y.; Whiteway, M.; Kavanagh, K., Correlation between virulence of *Candida albicans* mutants in mice and *Galleria mellonella* larvae. *Fems Immunol Med Mic* **2002**, *34* (2), 153-157.

124. McCann, M.; Santos, A. L. S.; da Silva, B. A.; Romanos, M. T. V.; Pyrrho, A. S.; Devereux, M.; Kavanagh, K.; Fichtner, I.; Kellett, A., In vitro and in vivo studies into the biological activities of 1,10-phenanthroline, 1,10-phenanthroline-5,6-dione and its copper(II) and silver(I) complexes. *Toxicology Research* **2012**, *1* (1), 47-54.
125. Cai, T. B.; Lu, D.; Tang, X.; Zhang, Y.; Landerholm, M.; Wang, P. G., New Glycosidase Activated Nitric Oxide Donors: Glucose and 3-Morphorlinosydnonimine Conjugates. *The Journal of Organic Chemistry* **2005**, *70* (9), 3518-3524.
126. Cheng, H.; Cao, X.; Xian, M.; Fang, L.; Cai, T. B.; Ji, J. J.; Tunac, J. B.; Sun, D.; Wang, P. G., Synthesis and Enzyme-Specific Activation of Carbohydrate-Geldanamycin Conjugates with Potent Anticancer Activity. *Journal of Medicinal Chemistry* **2004**, *48* (2), 645-652.
127. Bonina, F.; Puglia, C.; Rimoli, M. G.; Melisi, D.; Boatto, G.; Nieddu, M.; Calignano, A.; La Rana, G.; De Caprariis, P., Glycosyl derivatives of dopamine and L-dopa as anti-Parkinson prodrugs: synthesis, pharmacological activity and in vitro stability studies. *J Drug Target* **2003**, *11* (1), 25-36.
128. Namchuk, M. N.; Withers, S. G., Mechanism of Agrobacterium beta-glucosidase: kinetic analysis of the role of noncovalent enzyme/substrate interactions. *Biochemistry* **1995**, *34* (49), 16194-202.
129. Geiger, G.; Furrer, G.; Funk, F.; Brandl, H.; Schulin, R., Heavy metal effects on beta-glucosidase activity influenced by pH and buffer systems. *J Enzyme Inhib* **1999**, *14* (5), 365-79.
130. Wilkinson, A. D. M. a. A., *IUPAC. Compendium of Chemical Terminology, 2nd ed.* Blackwell Scientific Publications: 2006.
131. Gibson, S. E.; Lecci, C., Amino acid derived macrocycles--an area driven by synthesis or application? *Angewandte Chemie* **2006**, *45* (9), 1364-77.
132. Crane, E. A.; Scheidt, K. A., Prins-type macrocyclizations as an efficient ring-closing strategy in natural product synthesis. *Angewandte Chemie* **2010**, *49* (45), 8316-26.

133. Venkatesan, S.; Sun, J.; Zhang, L.; Dubey, A.; Sykes, A.; Lin, T.-Y.; Hung, Y.-C.; Qiao, Q.; Zhang, C., An oligothiophene chromophore with a macrocyclic side chain: synthesis, morphology, charge transport, and photovoltaic performance. *RSC Adv.* **2016**, *6* (104), 102043-102056.
134. Xie, J.; Bogliotti, N., Synthesis and Applications of Carbohydrate-Derived Macrocyclic Compounds. *Chemical reviews* **2014**.
135. Dasari, B.; Jogula, S.; Borhade, R.; Balasubramanian, S.; Chandrasekar, G.; Kitambi, S. S.; Arya, P., Macrocyclic glycohybrid toolbox identifies novel antiangiogenesis agents from zebrafish assay. *Org Lett* **2013**, *15* (3), 432-5.
136. Ruttens, B.; Blom, P.; Van Hoof, S.; Hubrecht, I.; Van der Eycken, J.; Sas, B.; Van Hemel, J.; Vandekerckhove, J., Carbohydrate-based macrolides prepared via a convergent ring closing metathesis approach: in search for novel antibiotics. *J Org Chem* **2007**, *72* (15), 5514-22.
137. Bradley, D.; Williams, G.; Mbatha, G. B., The synthesis and characterisation of carbohydrate-functionalised porphyrazines. *Dyes and Pigments* **2011**, *88* (1), 65-74.
138. Kamioka, S.; Takahashi, T.; Kawauchi, S.; Adachi, H.; Mori, Y.; Fujii, K.; Uekusa, H.; Doi, T., Chiral tetraazamacrocycles having four pendant-arms. *Org Lett* **2009**, *11* (11), 2289-92.
139. Hartsel, S. C.; Benz, S. K.; Peterson, R. P.; Whyte, B. S., Potassium-selective amphotericin B channels are predominant in vesicles regardless of sidedness. *Biochemistry* **1991**, *30* (1), 77-82.
140. Altenburg, J.; de Graaff, C. S.; van der Werf, T. S.; Boersma, W. G., Immunomodulatory effects of macrolide antibiotics - part 1: biological mechanisms. *Respiration* **2011**, *81* (1), 67-74.
141. Wolf, J. E.; Stein, S. H.; Little, K. D.; Abegg, A. L.; Little, J. R., Amphotericin B selectively stimulates macrophages from high responder mouse strains. *Immunopharmacol Immunotoxicol* **1991**, *13* (3), 221-35.

142. Kovacic, P.; Cooksy, A., Novel, unifying mechanism for amphotericin B and other polyene drugs: electron affinity, radicals, electron transfer, autoxidation, toxicity, and antifungal action. *Medchemcomm* **2012**, *3* (3), 274-280.
143. Kovacic, P.; Kiser, P. F.; Feinberg, B. A., Are reduction potentials of antifungal agents relevant to activity? *Pharm Res* **1990**, *7* (3), 283-8.
144. Hao, E.; Jensen, T. J.; Vicente, M. G. H., Synthesis of porphyrin-carbohydrate conjugates using "click" chemistry and their preliminary evaluation in human HEP2 cells. *Journal of Porphyrins and Phthalocyanines* **2009**, *13* (1), 51-59.
145. Stephan, H.; Rohrich, A.; Noll, S.; Steinbach, J.; Kirchner, R.; Seidel, J., Carbohydration of 1,4,8,11-tetraazacyclotetradecane (cyclam): synthesis and binding properties toward concanavalin A. *Tetrahedron Letters* **2007**, *48* (50), 8834-8838.
146. Tsai, C. Y.; Huang, X. F.; Wong, C. H., Design and synthesis of cyclic sialyl Lewis X mimetics: a remarkable enhancement of inhibition by pre-organizing all essential functional groups. *Tetrahedron Letters* **2000**, *41* (49), 9499-9503.
147. Simanek, E. E.; McGarvey, G. J.; Jablonowski, J. A.; Wong, C.-H., Selectin–Carbohydrate Interactions: From Natural Ligands to Designed Mimics. *Chemical reviews* **1998**, *98* (2), 833-862.
148. von Roedern, E. G.; Kessler, H., A Sugar Amino Acid as a Novel Peptidomimetic. *Angewandte Chemie International Edition in English* **1994**, *33* (6), 687-689.
149. Locardi, E.; Stockle, M.; Gruner, S.; Kessler, H., Cyclic homooligomers from sugar amino acids: synthesis, conformational analysis, and significance. *J Am Chem Soc* **2001**, *123* (34), 8189-96.
150. Rapi, Z.; Bako, P.; Keglevich, G.; Szollosy, A.; Drahos, L.; Botyanszki, A.; Holczbauer, T., Asymmetric phase transfer Darzens reactions catalyzed by D-glucose- and D-mannose-based chiral crown ethers. *Tetrahedron-Asymmetr* **2012**, *23* (6-7), 489-496.

151. Campo, V. L.; Carvalho, I.; Da Silva, C. H. T. P.; Schenkman, S.; Hill, L.; Nepogodiev, S. A.; Field, R. A., Cyclooligomerisation of azido-alkyne-functionalised sugars: synthesis of 1,6-linked cyclic pseudo-galactooligosaccharides and assessment of their sialylation by *Trypanosoma cruzi* trans-sialidase. *Chemical Science* **2010**, *1* (4), 507-514.
152. Bodine, K. D.; Gin, D. Y.; Gin, M. S., Synthesis of readily modifiable cyclodextrin analogues via cyclodimerization of an alkynyl-azido trisaccharide. *J Am Chem Soc* **2004**, *126* (6), 1638-9.
153. Jarosz, S.; Lewandowski, B.; Listkowski, A., Towards sucrose macrocycles with higher symmetry via a 'Click Chemistry' route. *Synthesis*, **2008**, *2008* (6), 913-916.
154. Dubois, J. E.; Cossebarbi, A., Strain Release in Conformational and Geometric Adaptation of Moderately and Highly Congested Systems - Interplay of Small Structural Effects. *Structural Chemistry* **1991**, *2* (2), 89-105.
155. Takahashi, S.; Hosoya, M.; Koshino, H.; Nakata, T., Determination of absolute structure of macroviracins by chemical synthesis. *Org. Lett.* **2003**, *5* (9), 1555-8.
156. Ghosh, A. K.; Kassekert, L. A., Enantioselective Synthesis of Both Epimers at C-21 in the Proposed Structure of Cytotoxic Macrolide Callyspongiolide. *Org. Lett.* **2016**, *18* (13), 3274-7.
157. Hussain, A.; Yousuf, S. K.; Kumar, D.; Lambu, M.; Singh, B.; Maity, S.; Mukherjee, D., Intramolecular Base-Free Sonogashira Reaction for the Synthesis of Benzannulated Chiral Macrocycles Embedded in Carbohydrate Templates. *Advanced Synthesis & Catalysis* **2012**, *354* (10), 1933-1940.
158. Si, D.; Peczuh, M. W., Synthesis and structure of a carbohydrate-fused [15]-macrodilactone. *Carbohydrate research* **2016**, *434*, 113-120.
159. Jarikote, D. V.; Murphy, P. V., Metathesis and Macrocycles with Embedded Carbohydrates. *European Journal of Organic Chemistry* **2010**, *2010* (26), 4959-4970.

160. Billing, J. F.; Nilsson, U. J., C₂-symmetric macrocyclic carbohydrate/amino acid hybrids through copper(I)-catalyzed formation of 1,2,3-triazoles. *J. Org. Chem.* **2005**, *70* (12), 4847-50.
161. Dorner, S.; Westermann, B., A short route for the synthesis of "sweet" macrocycles via a click-dimerization-ring-closing metathesis approach. *Chem. Comm.* **2005**, (22), 2852-4.
162. Pasini, D., The click reaction as an efficient tool for the construction of macrocyclic structures. *Molecules* **2013**, *18* (8), 9512-30.
163. Jin, L.; Tolentino, D. R.; Melaimi, M.; Bertrand, G., Isolation of bis(copper) key intermediates in Cu-catalyzed azide-alkyne "click reaction". *Science Advances* **2015**, *1* (5).
164. Worrell, B. T.; Malik, J. A.; Fokin, V. V., Direct evidence of a dinuclear copper intermediate in Cu(I)-catalyzed azide-alkyne cycloadditions. *Science* **2013**, *340* (6131), 457-60.
165. Marti-Centelles, V.; Pandey, M. D.; Burguete, M. I.; Luis, S. V., Macrocyclization Reactions: The Importance of Conformational, Configurational, and Template-Induced Preorganization. *Chemical reviews* **2015**, *115* (16), 8736-834.
166. Jonathan W. Steed, D. R. T., Karl Wallace, *Core Concepts in Supramolecular Chemistry and Nanochemistry*. Wiley: 2007.
167. Midland, M. M.; Beck, J. J.; Peters, J. L.; Rennels, R. A.; Asirwatham, G., Synthesis and Conformational Analysis of 1,2:3,4-Di-O-isopropylidene- α -D-galactopyranose: A Nuclear Magnetic Resonance and Molecular Modeling Experiment. *Journal of Chemical Education* **1994**, *71* (10), 897.
168. Liu, H. W.; Nakanishi, K., Pyranose Benzoates - an Additivity Relation in the Amplitudes of Exciton-Split Cd Curves. *Journal of the American Chemical Society* **1982**, *104* (5), 1178-1185.

169. Timmer, M. S. M.; Dangerfield, E. M.; Cheng, J. M. H.; Gulab, S. A.; Stocker, B. L., Rapid synthesis of 1-deoxygalactonojirimycin using a carbamate annulation. *Tetrahedron Letters* **2011**, *52* (37), 4803-4805.
170. Kaliappan, K. P.; Subrahmanyam, A. V., A new versatile strategy for C-aryl glycosides. *Org Lett* **2007**, *9* (6), 1121-4.
171. Mereyala, H. B.; Gurralla, S. R.; Mohan, S. K., Study of metal and acid catalysed deprotection of propargyl ethers of alcohols via their allenyl ethers. *Tetrahedron* **1999**, *55* (37), 11331-11342.
172. Ferrier, R. J.; Hay, R. W.; Vethaviasar, N., A potentially versatile synthesis of glycosides. *Carbohydrate research* **1973**, *27* (1), 55-61.
173. Lian, G.; Zhang, X.; Yu, B., Thioglycosides in Carbohydrate research. *Carbohydrate research* **2015**, *403*, 13-22.
174. Nicolaou, K. C.; Seitz, S. P.; Papahatjis, D. P., A mild and general method for the synthesis of O-glycosides. *Journal of the American Chemical Society* **1983**, *105* (8), 2430-2434.
175. Veeneman, G. H.; van Leeuwen, S. H.; van Boom, J. H., Iodonium ion promoted reactions at the anomeric centre. II An efficient thioglycoside mediated approach toward the formation of 1,2-trans linked glycosides and glycosidic esters. *Tetrahedron Letters* **1990**, *31* (9), 1331-1334.
176. Konradsson, P.; Udodong, U. E.; Fraserreid, B., Iodonium Promoted Reactions of Disarmed Thioglycosides. *Tetrahedron Letters* **1990**, *31* (30), 4313-4316.
177. Fugedi, P.; Garegg, P. J., A Novel Promoter for the Efficient Construction of 1,2-Trans Linkages in Glycoside Synthesis, Using Thioglycosides as Glycosyl Donors. *Carbohydrate research* **1986**, *149* (1), C9-C12.
178. Andersson, F.; Fúgedi, P.; Garegg, P. J.; Nashed, M., Synthesis of 1,2--linked glycosides using dimethyl(methylthio) sulfonium triplate as promoter and thioglycosides as glycosyl donors. *Tetrahedron Letters* **1986**, *27* (33), 3919-3922.

179. Crich, D.; Smith, M., S-(4-Methoxyphenyl) benzenethiosulfinate (MPBT) trifluoromethanesulfonic anhydride: A convenient system for the generation of glycosyl triflates from thioglycosides. *Organic Letters* **2000**, 2 (25), 4067-4069.
180. Tatai, J.; Fugedi, P., A new, powerful glycosylation method: activation of thioglycosides with dimethyl disulfide-triflic anhydride. *Org Lett* **2007**, 9 (22), 4647-50.
181. Fukase, K.; Nakai, Y.; Kanoh, T.; Kusumoto, S., Mild but efficient methods for stereoselective glycosylation with thioglycosides: Activation by [N-phenylselenophthalimide-Mg(ClO₄)(2)] and [PhIO-Mg(ClO₄)(2)]. *Synlett* **1998**, 1998 (1), 84-+.
182. Ito, Y.; Ogawa, T., Novel Approaches to Glycoside Synthesis - Benzeneselenenyl Triflate as a Promoter of Thioglycosides - a New Method for O-Glycosylation Using Thioglycosides. *Tetrahedron Letters* **1988**, 29 (9), 1061-1064.
183. Li, Z.; Gildersleeve, J. C., Mechanistic studies and methods to prevent aglycon transfer of thioglycosides. *J Am Chem Soc* **2006**, 128 (35), 11612-9.
184. Lahmann, M.; Oscarson, S., Investigation of the reactivity difference between thioglycoside donors with variant aglycon parts. *Canadian Journal of Chemistry* **2002**, 80 (8), 889-893.
185. Calosso, M.; Charpentier, D.; Vaillancourt, M.; Bencheqroun, M.; St-Pierre, G.; Wilkes, B. C.; Guindon, Y., A new approach to explore the binding space of polysaccharide-based ligands: selectin antagonists. *ACS Med Chem Lett* **2012**, 3 (12), 1045-9.
186. Scarpaci, A.; Blart, E.; Montembault, V.; Fontaine, L.; Rodriguez, V.; Odobel, F., A new crosslinkable system based on thermal Huisgen reaction to enhance the stability of electro-optic polymers. *Chemical communications* **2009**, (14), 1825-7.
187. Strupat, K., Molecular Weight Determination of Peptides and Proteins by ESI and MALDI. In *Methods in Enzymology*, Academic Press: 2005; Vol. Volume 405, pp 1-36.

188. Thakur, S. S.; Deepalakshmi, P. D.; Gayathri, P.; Banerjee, M.; Murthy, M. R.; Balaram, P., Detection of the protein dimers, multiple monomeric states and hydrated forms of Plasmodium falciparum triosephosphate isomerase in the gas phase. *Protein engineering, design & selection : PEDS* **2009**, *22* (5), 289-304.
189. Fall, A.; Seck, I.; Diouf, O.; Gaye, M.; Seck, M.; Gomez, G.; Fall, Y., Synthesis of new triazolium-based ionic liquids and their use in the Morita-Baylis-Hillman reaction. *Tetrahedron Letters* **2015**, *56* (36), 5128-5131.
190. Broeker, J. L.; Hoffmann, R. W.; Houk, K. N., Conformational analysis of chiral alkenes and oxonium ions: ab initio molecular orbital calculations and an improved MM2 force field. *Journal of the American Chemical Society* **1991**, *113* (13), 5006-5017.
191. Lakowicz, J. R., *Principles of Fluorescence Spectroscopy*, 3rd Ed. 2006.
192. Valeur, B., In *Molecular Fluorescence*, Wiley-VCH Verlag GmbH: 2001; pp 3-19.
193. Jablonski, A., Efficiency of Anti-Stokes Fluorescence in Dyes. *Nature* **1933**, (131), 839-840.
194. Stokes, G. G., On the Change of Refrangibility of Light. *Philosophical Transactions of the Royal Society of London* **1852**, *142*, 463-562.
195. Jameson, D. M., *Introduction to Fluorescence*. CRC Press: 2014.
196. Franchini, L.; Compostella, F.; Donda, A.; Mori, L.; Colombo, D.; De Libero, G.; Matto, P.; Ronchetti, F.; Panza, L., Synthesis of a fluorescent sulfatide for the study of CD1 antigen binding properties. *European Journal of Organic Chemistry* **2004**, *2004* (23), 4755-4761.
197. Pagano, R. E.; Watanabe, R.; Wheatley, C.; Dominguez, M., Applications of BODIPY–Sphingolipid Analogs to Study Lipid Traffic and Metabolism in Cells. In *Methods in Enzymology*, Alfred, H. M.; Yusuf, A. H., Eds. Academic Press: 2000; Vol. Volume 312, pp 523-534.

198. van Tilbeurgh, H.; Loontjens, F. G.; De Bruyne, C. K.; Claeysens, M., Fluorogenic and chromogenic glycosides as substrates and ligands of carbohydrases. In *Methods in Enzymology*, Academic Press: 1988; Vol. Volume 160, pp 45-59.
199. Öckerman, P. A., Identity of β -glucosidase, β -xylosidase and one of the β -galactosidase activities in human liver when assayed with 4-methylumbelliferyl- β -D-glycosides studies in cases of Gaucher's disease. *Biochimica et Biophysica Acta (BBA) - General Subjects* **1968**, *165* (1), 59-62.
200. van Tilbeurgh, H.; Claeysens, M.; de Bruyne, C. K., The use of 4-methylumbelliferyl and other chromophoric glycosides in the study of cellulolytic enzymes. *FEBS Letters* **1982**, *149* (1), 152-156.
201. Szweda, R.; Spohr, U.; Lemieux, R. U.; Schindler, D.; Bishop, D. F.; Desnick, R. J., Synthesis of 4-Methylumbelliferyl Glycosides for the Detection of Alpha-D-Galactopyranosaminidases and Beta-D-Galactopyranosaminidases. *Can J Chem* **1989**, *67* (9), 1388-1391.
202. Lee, J. C.; Chang, S. W.; Liao, C. C.; Chi, F. C.; Chen, C. S.; Wen, Y. S.; Wang, C. C.; Kulkarni, S. S.; Puranik, R.; Liu, Y. H.; Hung, S. C., From D-glucose to biologically potent L-hexose derivatives: synthesis of alpha-L-iduronidase fluorogenic detector and the disaccharide moieties of bleomycin A2 and heparan sulfate. *Chemistry* **2004**, *10* (2), 399-415.
203. Demchenko, A., *Introduction to Fluorescence Sensing*. Springer: 2015.
204. Bures, F., Fundamental aspects of property tuning in push-pull molecules. *Rsc Advances* **2014**, *4* (102), 58826-58851.
205. Nepraš, M.; Almonasy, N.; Bureš, F.; Kulhánek, J.; Dvořák, M.; Michl, M., Fluorescence and photophysical properties of D- π -A push-pull systems featuring a 4,5-dicyanoimidazole unit. *Dyes and Pigments* **2011**, *91* (3), 466-473.
206. Miller, S. P. F.; French, S. A.; Kaneski, C. R., Synthesis and Characterization of a Novel Lysosomotropic Enzyme Substrate That Fluoresces at Intracellular Ph. *J Org Chem* **1991**, *56* (1), 30-34.

207. Ibatullin, F. M.; Banasiak, A.; Baumann, M. J.; Greffe, L.; Takahashi, J.; Mellerowicz, E. J.; Brumer, H., A real-time fluorogenic assay for the visualization of glycoside hydrolase activity in planta. *Plant Physiol* **2009**, *151* (4), 1741-50.
208. Yadav, A. K.; Shen, D. L.; Shan, X.; He, X.; Kermode, A. R.; Vocadlo, D. J., Fluorescence-quenched substrates for live cell imaging of human glucocerebrosidase activity. *J Am Chem Soc* **2015**, *137* (3), 1181-9.
209. Vo-Hoang, Y.; Micouin, L.; Ronet, C.; Gachelin, G.; Bonin, M., Total enantioselective synthesis and in vivo biological evaluation of a novel fluorescent BODIPY alpha-galactosylceramide. *Chembiochem* **2003**, *4* (1), 27-33.
210. Tietze, L. F.; Behrendt, F.; Pestel, G. F.; Schuberth, I.; Mitkovski, M., Synthesis, biological evaluation, and live cell imaging of novel fluorescent duocarmycin analogs. *Chem Biodivers* **2012**, *9* (11), 2559-70.
211. Abbott, S. D.; Gagnon, L.; Lagraoui, M.; Kadhim, S.; Attardo, G.; Zacharie, B.; Penney, C. L., Synthesis and activity of dipeptides, linked to targeting ligands, as specific NK cell enhancers. *J Med Chem* **1998**, *41* (11), 1909-26.
212. Kuznik, N.; Chrobaczynski, A.; Mika, M.; Miler, P.; Komor, R.; Kubicki, M., A new class of bioactivable self-immolative N,O-ligands. *European journal of medicinal chemistry* **2012**, *52*, 184-92.
213. Nicolaou, K. C.; Pfefferkorn, J. A.; Roecker, A. J.; Cao, G. Q.; Barluenga, S.; Mitchell, H. J., Natural product-like combinatorial libraries based on privileged structures. 1. General principles and solid-phase synthesis of benzopyrans. *Journal of the American Chemical Society* **2000**, *122* (41), 9939-9953.
214. Swamy, K. C.; Kumar, N. N.; Balaraman, E.; Kumar, K. V., Mitsunobu and related reactions: advances and applications. *Chemical reviews* **2009**, *109* (6), 2551-651.
215. Varasi, M.; Walker, K. A. M.; Maddox, M. L., A Revised Mechanism for the Mitsunobu Reaction. *J Org Chem* **1987**, *52* (19), 4235-4238.

216. Talamond, P.; Verdeil, J. L.; Conejero, G., Secondary metabolite localization by autofluorescence in living plant cells. *Molecules* **2015**, *20* (3), 5024-37.
217. Wenska, G.; Koput, J.; Pedzinski, T.; Marciniak, B.; Karolczak, J.; Golankiewicz, B., Effect of hydroxylic solvent on the fluorescence behavior of some bioactive 9-oxoimidazo[1,2-a]purine derivatives. *The journal of physical chemistry. A* **2006**, *110* (38), 11025-33.
218. Ando, Y.; Homma, Y.; Hiruta, Y.; Citterio, D.; Suzuki, K., Structural characteristics and optical properties of a series of solvatochromic fluorescent dyes displaying long-wavelength emission. *Dyes and Pigments* **2009**, *83* (2), 198-206.
219. Frisch, J. *Gaussian 09*, Gaussian, Inc.: Wallingford, CT, USA, 2009.
220. Chandrika, N. T.; Shrestha, S. K.; Ngo, H. X.; Garneau-Tsodikova, S., Synthesis and investigation of novel benzimidazole derivatives as antifungal agents. *Bioorganic & medicinal chemistry* **2016**, *24* (16), 3680-6.
221. Mangunuru, H. P. R.; Yerabolu, J. R.; Liu, D.; Wang, G. J., Synthesis of a series of glucosyl triazole derivatives and their self-assembling properties. *Tetrahedron Letters* **2015**, *56* (1), 82-85.
222. Ferrari, E., Synthesis, cytotoxic and combined cDDP activity of new stable curcumin derivatives. **2009**, *17* (8), 3043–3052.
223. Velasco-Torrijos, T.; Abbey, L.; O'Flaherty, R., A Concise Synthesis of Glycolipids Based on Aspartic Acid Building Blocks. *Molecules* **2012**, *17* (10), 11346-11362.
224. Hu, J. M.; Wang, X.; Qian, Y. F.; Yu, Y. Q.; Jiang, Y. Y.; Zhang, G. Y.; Liu, S. Y., Cytoplasmic Reactive Cationic Amphiphiles for Efficient Intracellular Delivery and Self-Reporting Smart Release. *Macromolecules* **2015**, *48* (16), 5959-5968.
225. Mora-Soumille, N.; Al Bittar, S.; Rosa, M.; Dangles, O., Analogs of anthocyanins with a 3',4'-dihydroxy substitution: Synthesis and investigation of their acid–base, hydration, metal binding and hydrogen-donating properties in aqueous solution. *Dyes and Pigments* **2013**, *96* (1), 7-15.

226. Lukin, K.; Kishore, V.; Gordon, T., Development of a Scalable Synthesis of Oxadiazole Based S1P1Receptor Agonists. *Organic Process Research & Development* **2013**, *17* (4), 666-671.

Appendix

Publications

- **Andrew Reddy**, Jessica Ramos-Ondono, Lorna Abbey and Trinidad Velasco-Torrijos, *Chromatography-free synthesis of acetyl-protected 2-chloroethyl and 2-azidoethyl O-glycopyranosides*, *Carbohydrate Chemistry: Proven Synthetic Methods*, Volume 4, edited by Christian Vogel and Paul Murphy, 2017.
- **Andrew Reddy**, Leandro Stefano Sangenito, Arthur de Azevedo Guedes, Marta Helena Branquinha, Kevin Kavanagh, John McGinley, André Luis Souza dos Santos and Trinidad Velasco-Torrijos, *Glycosylated Metal Chelators as Anti-Parasitic Agents with Tunable Selectivity*, (*Dalton Trans.*, 2017,**46**, 5297-5307)

Oral Presentations

- *Multifunctional Metalloglycosides with Tunable Selectivity as Novel Anti-Parasitic Agents*, 68th Irish Universities Chemistry Research Colloquium, University College Cork, 2016.
- *Carbohydrates as Scaffolds for Conformationally Constrained Macrocycles*, Supramolecular Chemistry Ireland Symposium, Maynooth University, 2015.
- *The Development of Glycoconjugated Metal Chelators*, Maynooth University Postgraduate Research Day, 2014.

Poster Presentations

- **Andrew Reddy**, Leandro Stefano Sangenito, Arthur de Azevedo Guedes, Marta Helena Branquinha, Kevin Kavanagh, John McGinley, André Luis Souza dos Santos and Trinidad Velasco-Torrijos, *Multifunctional Metalloglycosides with Tunable Selectivity as Novel Anti-Parasitic Agents*, 7th Irish Metals in Medicine Meeting, Dublin Institute of Technology, 2016.
- **Andrew Reddy**, John McGinley and Trinidad Velasco-Torrijos, *Glycosidic Metal Chelators as a Novel Therapy for Alzheimer's Disease*. 67th Irish Universities Chemistry Research Colloquium, Maynooth University, 2015 and also the CASE Symposium, Royal College of Surgeons, 2015.

- **Andrew Reddy**, Lorna Abbey and Trinidad Velasco-Torrijos, *The Influence of Diastereomeric Composition on the Gelation of Aspartic Acid Derived Glycolipids*, 65th Irish Universities Chemistry Research Colloquium, Trinity College Dublin, 2013.

Crystallographic Data

2.18

Empirical formula	$C_{20}H_{20}N_2O_2$	
Formula weight	320.38	
Temperature	99.99 K	
Wavelength	0.71073 Å	
Crystal system	Monoclinic	
Space group	$P2_1/n$	
Unit cell dimensions	$a = 12.4902(7)$ Å	$\alpha = 90^\circ$.
	$b = 9.8711(6)$ Å	$\beta = 90.197(2)^\circ$.
	$c = 13.6216(8)$ Å	$\gamma = 90^\circ$.
Volume	$1679.42(17)$ Å ³	
Z	4	
Density (calculated)	1.267 Mg/m ³	
Absorption coefficient	0.083 mm ⁻¹	
F(000)	680	
Crystal size	$0.31 \times 0.19 \times 0.17$ mm ³	
Theta range for data collection	2.991 to 29.557° .	
Index ranges	$-17 \leq h \leq 17$, $-13 \leq k \leq 13$, $-18 \leq l \leq 18$	
Reflections collected	19589	
Independent reflections	4678 [R(int) = 0.0872]	
Completeness to theta = 26.000°	99.9 %	
Absorption correction	Semi-empirical from equivalents	
Max. and min. transmission	0.7459 and 0.6692	
Refinement method	Full-matrix least-squares on F ²	
Data / restraints / parameters	4678 / 0 / 225	
Goodness-of-fit on F ²	1.018	
Final R indices [$I > 2\sigma(I)$]	R1 = 0.0658, wR2 = 0.1067	
R indices (all data)	R1 = 0.1316, wR2 = 0.1269	
Largest diff. peak and hole	0.252 and -0.286 e.Å ⁻³	

Atomic coordinates ($\times 10^4$) and equivalent isotropic displacement parameters ($\text{\AA}^2 \times 10^3$) for **2.18**. $U(\text{eq})$ is defined as one third of the trace of the orthogonalized U^{ij} tensor.

	x	y	z	$U(\text{eq})$
N(1)	6204(1)	362(2)	6252(1)	20(1)
C(2)	5341(2)	20(2)	6790(1)	23(1)
C(3)	4366(2)	636(2)	6691(1)	24(1)
C(4)	4254(2)	1660(2)	6006(2)	26(1)
C(5)	5132(2)	2031(2)	5456(2)	25(1)
C(6)	6092(1)	1354(2)	5590(1)	19(1)
C(7)	7030(2)	1672(2)	4938(2)	22(1)
N(8)	7290(1)	3114(2)	4953(1)	19(1)
C(9)	7801(2)	3516(2)	4030(1)	22(1)
C(10)	6989(1)	3643(2)	3217(1)	18(1)
C(11)	6957(1)	2764(2)	2422(1)	21(1)
C(12)	6218(2)	2916(2)	1669(1)	23(1)
C(13)	5482(2)	3967(2)	1709(1)	21(1)
C(14)	5488(2)	4852(2)	2504(2)	22(1)
C(15)	6235(2)	4673(2)	3246(1)	22(1)
O(16)	4775(1)	4094(2)	950(1)	29(1)
C(17)	7953(2)	3461(2)	5815(1)	22(1)
C(18)	8005(1)	4968(2)	5968(1)	20(1)
C(19)	7076(2)	5690(2)	6165(2)	25(1)
C(20)	7097(2)	7074(2)	6321(2)	25(1)
C(21)	8060(2)	7773(2)	6268(1)	21(1)
C(22)	8992(2)	7077(2)	6069(1)	23(1)
C(23)	8956(2)	5683(2)	5926(1)	21(1)
O(24)	8124(1)	9137(1)	6422(1)	28(1)

Bond lengths [\AA] and angles [$^\circ$] for **2.18**

N(1)-C(2)	1.349(2)	C(4)-C(5)	1.380(3)
N(1)-C(6)	1.339(2)	C(5)-H(5)	0.9500
C(2)-H(2)	0.9500	C(5)-C(6)	1.384(3)
C(2)-C(3)	1.368(3)	C(6)-C(7)	1.505(2)
C(3)-H(3)	0.9500	C(7)-H(7A)	0.9900
C(3)-C(4)	1.382(3)	C(7)-H(7B)	0.9900
C(4)-H(4)	0.9500	C(7)-N(8)	1.461(2)

N(8)-C(9)	1.467(2)	C(4)-C(3)-H(3)	120.6
N(8)-C(17)	1.474(2)	C(3)-C(4)-H(4)	120.6
C(9)-H(9A)	0.9900	C(5)-C(4)-C(3)	118.81(18)
C(9)-H(9B)	0.9900	C(5)-C(4)-H(4)	120.6
C(9)-C(10)	1.505(3)	C(4)-C(5)-H(5)	120.3
C(10)-C(11)	1.389(3)	C(4)-C(5)-C(6)	119.36(18)
C(10)-C(15)	1.386(3)	C(6)-C(5)-H(5)	120.3
C(11)-H(11)	0.9500	N(1)-C(6)-C(5)	122.03(17)
C(11)-C(12)	1.385(3)	N(1)-C(6)-C(7)	118.02(16)
C(12)-H(12)	0.9500	C(5)-C(6)-C(7)	119.86(17)
C(12)-C(13)	1.387(3)	C(6)-C(7)-H(7A)	109.3
C(13)-C(14)	1.393(3)	C(6)-C(7)-H(7B)	109.3
C(13)-O(16)	1.362(2)	H(7A)-C(7)-H(7B)	108.0
C(14)-H(14)	0.9500	N(8)-C(7)-C(6)	111.60(15)
C(14)-C(15)	1.384(3)	N(8)-C(7)-H(7A)	109.3
C(15)-H(15)	0.9500	N(8)-C(7)-H(7B)	109.3
O(16)-H(16)	0.93(3)	C(7)-N(8)-C(9)	110.43(15)
C(17)-H(17A)	0.9900	C(7)-N(8)-C(17)	111.25(15)
C(17)-H(17B)	0.9900	C(9)-N(8)-C(17)	112.01(15)
C(17)-C(18)	1.503(3)	N(8)-C(9)-H(9A)	109.4
C(18)-C(19)	1.389(3)	N(8)-C(9)-H(9B)	109.4
C(18)-C(23)	1.383(3)	N(8)-C(9)-C(10)	111.06(15)
C(19)-H(19)	0.9500	H(9A)-C(9)-H(9B)	108.0
C(19)-C(20)	1.383(3)	C(10)-C(9)-H(9A)	109.4
C(20)-H(20)	0.9500	C(10)-C(9)-H(9B)	109.4
C(20)-C(21)	1.388(3)	C(11)-C(10)-C(9)	122.66(17)
C(21)-C(22)	1.381(3)	C(15)-C(10)-C(9)	119.77(18)
C(21)-O(24)	1.365(2)	C(15)-C(10)-C(11)	117.58(18)
C(22)-H(22)	0.9500	C(10)-C(11)-H(11)	119.1
C(22)-C(23)	1.390(3)	C(12)-C(11)-C(10)	121.78(18)
C(23)-H(23)	0.9500	C(12)-C(11)-H(11)	119.1
O(24)-H(24)	0.94(2)	C(11)-C(12)-H(12)	120.3
C(6)-N(1)-C(2)	117.90(16)	C(11)-C(12)-C(13)	119.50(18)
N(1)-C(2)-H(2)	118.4	C(13)-C(12)-H(12)	120.3
N(1)-C(2)-C(3)	123.20(18)	C(12)-C(13)-C(14)	119.84(18)
C(3)-C(2)-H(2)	118.4	O(16)-C(13)-C(12)	117.86(18)
C(2)-C(3)-H(3)	120.6	O(16)-C(13)-C(14)	122.30(18)
C(2)-C(3)-C(4)	118.70(17)	C(13)-C(14)-H(14)	120.3

C(15)-C(14)-C(13)	119.32(18)	C(20)-C(19)-C(18)	121.39(18)
C(15)-C(14)-H(14)	120.3	C(20)-C(19)-H(19)	119.3
C(10)-C(15)-H(15)	119.0	C(19)-C(20)-H(20)	120.0
C(14)-C(15)-C(10)	121.96(18)	C(19)-C(20)-C(21)	120.00(18)
C(14)-C(15)-H(15)	119.0	C(21)-C(20)-H(20)	120.0
C(13)-O(16)-H(16)	109.0(17)	C(22)-C(21)-C(20)	119.58(17)
N(8)-C(17)-H(17A)	109.4	O(24)-C(21)-C(20)	122.23(17)
N(8)-C(17)-H(17B)	109.4	O(24)-C(21)-C(22)	118.17(17)
N(8)-C(17)-C(18)	111.35(15)	C(21)-C(22)-H(22)	120.2
H(17A)-C(17)-H(17B)	108.0	C(21)-C(22)-C(23)	119.55(17)
C(18)-C(17)-H(17A)	109.4	C(23)-C(22)-H(22)	120.2
C(18)-C(17)-H(17B)	109.4	C(18)-C(23)-C(22)	121.82(17)
C(19)-C(18)-C(17)	119.95(17)	C(18)-C(23)-H(23)	119.1
C(23)-C(18)-C(17)	122.40(17)	C(22)-C(23)-H(23)	119.1
C(23)-C(18)-C(19)	117.65(18)	C(21)-O(24)-H(24)	111.3(14)
C(18)-C(19)-H(19)	119.3		

Anisotropic displacement parameters ($\text{\AA}^2 \times 10^3$) for **2.18**. The anisotropic displacement factor exponent takes the form: $-2\pi^2 [h^2 a^{*2} U_{11} + \dots + 2 h k a^* b^* U_{12}]$

	U_{11}	U_{22}	U_{33}	U_{23}	U_{13}	U_{12}
N(1)	22(1)	18(1)	20(1)	-2(1)	1(1)	0(1)
C(2)	31(1)	19(1)	19(1)	-2(1)	4(1)	-2(1)
C(3)	25(1)	24(1)	24(1)	-7(1)	7(1)	-6(1)
C(4)	18(1)	24(1)	35(1)	-4(1)	1(1)	2(1)
C(5)	25(1)	20(1)	30(1)	4(1)	0(1)	1(1)
C(6)	21(1)	14(1)	21(1)	-4(1)	-1(1)	-3(1)
C(7)	21(1)	18(1)	26(1)	-1(1)	3(1)	0(1)
N(8)	20(1)	18(1)	20(1)	2(1)	0(1)	-3(1)
C(9)	16(1)	25(1)	26(1)	2(1)	2(1)	-1(1)
C(10)	14(1)	20(1)	22(1)	3(1)	3(1)	-3(1)
C(11)	16(1)	21(1)	26(1)	2(1)	5(1)	3(1)
C(12)	22(1)	23(1)	23(1)	-2(1)	2(1)	-1(1)
C(13)	18(1)	20(1)	25(1)	6(1)	-1(1)	-6(1)
C(14)	18(1)	18(1)	32(1)	3(1)	2(1)	3(1)
C(15)	21(1)	20(1)	24(1)	-2(1)	3(1)	-2(1)
O(16)	26(1)	28(1)	33(1)	2(1)	-10(1)	1(1)

C(17)	23(1)	19(1)	25(1)	2(1)	-3(1)	2(1)
C(18)	20(1)	21(1)	18(1)	1(1)	-3(1)	0(1)
C(19)	18(1)	23(1)	34(1)	1(1)	1(1)	-4(1)
C(20)	15(1)	23(1)	36(1)	-1(1)	1(1)	3(1)
C(21)	21(1)	18(1)	22(1)	1(1)	-3(1)	0(1)
C(22)	15(1)	26(1)	27(1)	2(1)	-2(1)	-3(1)
C(23)	17(1)	24(1)	22(1)	-1(1)	-1(1)	4(1)
O(24)	20(1)	19(1)	43(1)	-4(1)	-6(1)	1(1)

Hydrogen coordinates ($\times 10^4$) and isotropic displacement parameters ($\text{\AA}^2 \times 10^3$) for **2.18**

	x	y	z	U(eq)
H(2)	5415	-683	7262	28
H(3)	3777	365	7084	29
H(4)	3584	2100	5916	31
H(5)	5078	2744	4991	30
H(7A)	7660	1145	5160	26
H(7B)	6860	1394	4256	26
H(9A)	8345	2833	3847	27
H(9B)	8170	4395	4122	27
H(11)	7456	2039	2393	25
H(12)	6215	2305	1130	27
H(14)	4984	5572	2538	27
H(15)	6231	5274	3790	26
H(17A)	8686	3103	5721	27
H(17B)	7649	3027	6407	27
H(19)	6411	5223	6194	30
H(20)	6454	7546	6464	30
H(22)	9655	7546	6030	27
H(23)	9602	5209	5796	25
H(24)	7440(18)	9540(20)	6404(16)	37(6)
H(16)	4270(20)	4760(30)	1110(20)	60(8)

Torsion angles [$^\circ$] for **2.18**

N(1)-C(2)-C(3)-C(4)	0.0(3)	C(2)-N(1)-C(6)-C(5)	0.7(3)
N(1)-C(6)-C(7)-N(8)	-128.19(18)	C(2)-N(1)-C(6)-C(7)	-175.74(17)

C(2)-C(3)-C(4)-C(5)	-0.6(3)	C(11)-C(10)-C(15)-C(14)	-1.4(3)
C(3)-C(4)-C(5)-C(6)	1.2(3)	C(11)-C(12)-C(13)-C(14)	-0.4(3)
C(4)-C(5)-C(6)-N(1)	-1.3(3)	C(11)-C(12)-C(13)-O(16)	179.24(17)
C(4)-C(5)-C(6)-C(7)	175.04(18)	C(12)-C(13)-C(14)-C(15)	0.3(3)
C(5)-C(6)-C(7)-N(8)	55.3(2)	C(13)-C(14)-C(15)-C(10)	0.7(3)
C(6)-N(1)-C(2)-C(3)	0.0(3)	C(15)-C(10)-C(11)-C(12)	1.3(3)
C(6)-C(7)-N(8)-C(9)	-152.83(16)	O(16)-C(13)-C(14)-C(15)	-179.32(17)
C(6)-C(7)-N(8)-C(17)	82.14(19)	C(17)-N(8)-C(9)-C(10)	-158.94(16)
C(7)-N(8)-C(9)-C(10)	76.47(19)	C(17)-C(18)-C(19)-C(20)	179.27(19)
C(7)-N(8)-C(17)-C(18)	-166.47(15)	C(17)-C(18)-C(23)-C(22)	179.95(18)
N(8)-C(9)-C(10)-C(11)	-111.99(19)	C(18)-C(19)-C(20)-C(21)	0.9(3)
N(8)-C(9)-C(10)-C(15)	68.1(2)	C(19)-C(18)-C(23)-C(22)	-0.4(3)
N(8)-C(17)-C(18)-C(19)	62.2(2)	C(19)-C(20)-C(21)-C(22)	-0.7(3)
N(8)-C(17)-C(18)-C(23)	-118.10(19)	C(19)-C(20)-C(21)-O(24)	-179.53(19)
C(9)-N(8)-C(17)-C(18)	69.4(2)	C(20)-C(21)-C(22)-C(23)	-0.1(3)
C(9)-C(10)-C(11)-C(12)	-178.54(17)	C(21)-C(22)-C(23)-C(18)	0.6(3)
C(9)-C(10)-C(15)-C(14)	178.45(17)	C(23)-C(18)-C(19)-C(20)	-0.4(3)
C(10)-C(11)-C(12)-C(13)	-0.5(3)	O(24)-C(21)-C(22)-C(23)	178.81(18)

Hydrogen bonds for **2.18** [Å and °].

D-H...A	d(D-H)	d(H...A)	d(D...A)	<(DHA)
C(17)-H(17A)...O(16)#1	0.99	2.58	3.402(2)	141
O(24)-H(24)...N(1)#2	0.94(2)	1.75(2)	2.695(2)	174(2)
O(16)-H(16)...O(24)#3	0.93(3)	1.85(3)	2.779(2)	171(2)

2.19

Empirical formula	C ₅₆ H ₆₂ Cl ₈ Cu ₄ N ₁₀ O ₄	
Formula weight	1476.91	
Temperature	100(2) K	
Wavelength	0.71073 Å	
Crystal system	Triclinic	
Space group	P $\bar{1}$	
Unit cell dimensions	a = 11.9914(6)	α = 113.9980(10)°.
	b = 12.6755(6) Å	β = 96.5800(10)°.
	c = 12.6960(6) Å	γ = 115.3470(10)°.

Volume	1492.64(13) Å ³
Z	1
Density (calculated)	1.643 Mg/m ³
Absorption coefficient	1.819 mm ⁻¹
F(000)	752
Crystal size	0.230 x 0.180 x 0.120 mm ³
Theta range for data collection	1.874 to 30.211°.
Index ranges	-16≤h≤16, -17≤k≤17, -17≤l≤17
Reflections collected	58825
Independent reflections	8816 [R(int) = 0.0282]
Completeness to theta = 25.242°	100.0 %
Absorption correction	Semi-empirical from equivalents
Max. and min. transmission	0.7460 and 0.6898
Refinement method	Full-matrix least-squares on F ²
Data / restraints / parameters	8816 / 0 / 381
Goodness-of-fit on F ²	1.030
Final R indices [I>2σ(I)]	R1 = 0.0223, wR2 = 0.0542
R indices (all data)	R1 = 0.0292, wR2 = 0.0572
Largest diff. peak and hole	0.423 and -0.420 e.Å ⁻³

Atomic coordinates (x10⁴) and equivalent isotropic displacement parameters (Å²x 10³) for **2.19**. U(eq) is defined as one third of the trace of the orthogonalized U_{ij} tensor.

	x	y	z	U(eq)
C(2)	3174(1)	8490(1)	7358(1)	16(1)
C(3)	3369(1)	8433(1)	8425(1)	18(1)
C(4)	4474(1)	8416(1)	8872(1)	18(1)
C(5)	5355(1)	8479(1)	8244(1)	16(1)
C(6)	5095(1)	8537(1)	7178(1)	13(1)
C(7)	6046(1)	8688(2)	6501(1)	16(1)
C(9)	5098(1)	6872(1)	4318(1)	16(1)
C(10)	6307(1)	6755(1)	4355(1)	14(1)
C(11)	6195(1)	5517(1)	4074(1)	16(1)
C(12)	7283(1)	5374(1)	4094(1)	17(1)
C(13)	8514(1)	6484(1)	4417(1)	15(1)
C(14)	8646(1)	7724(1)	4700(1)	16(1)

C(15)	7546(1)	7849(1)	4663(1)	16(1)
C(17)	1253(1)	5171(1)	3654(1)	16(1)
C(18)	11(1)	3888(1)	3113(1)	20(1)
C(20)	3848(1)	3405(1)	10719(1)	18(1)
C(21)	4925(1)	3808(2)	10352(2)	22(1)
C(22)	4727(2)	3193(2)	9100(2)	24(1)
C(23)	3465(2)	2226(2)	8263(1)	22(1)
C(24)	2422(1)	1880(1)	8694(1)	16(1)
C(25)	1023(1)	821(2)	7837(1)	18(1)
C(27)	-571(1)	1566(1)	8301(1)	16(1)
C(28)	353(1)	3076(1)	8912(1)	15(1)
C(29)	746(1)	3923(1)	10183(1)	16(1)
C(30)	1565(1)	5317(1)	10747(1)	16(1)
C(31)	1992(1)	5889(1)	10027(1)	15(1)
C(32)	1622(1)	5067(1)	8764(1)	18(1)
C(33)	803(1)	3670(1)	8218(1)	17(1)
Cl(1)	4031(1)	8626(1)	3379(1)	17(1)
Cl(2)	2208(1)	9050(1)	5165(1)	17(1)
Cl(3)	2074(1)	2520(1)	12316(1)	17(1)
Cl(4)	-1041(1)	711(1)	10480(1)	16(1)
Cu(1)	3788(1)	8460(1)	5097(1)	13(1)
Cu(2)	1002(1)	1587(1)	10298(1)	13(1)
N(1)	4014(1)	8530(1)	6734(1)	13(1)
N(8)	5382(1)	8238(1)	5213(1)	13(1)
N(16)	2216(1)	6184(1)	4076(1)	20(1)
N(19)	2617(1)	2444(1)	9904(1)	15(1)
N(26)	82(1)	849(1)	8491(1)	15(1)
O(1)	9562(1)	6300(1)	4435(1)	19(1)
O(2)	2762(1)	7263(1)	10519(1)	20(1)

Bond lengths [Å] and angles [°] for **2.19**.

C(2)-N(1)	1.3484(16)	C(4)-H(4)	0.9500
C(2)-C(3)	1.3834(19)	C(5)-C(6)	1.3922(18)
C(2)-H(2)	0.9500	C(5)-H(5)	0.9500
C(3)-C(4)	1.3930(19)	C(6)-N(1)	1.3474(16)
C(3)-H(3)	0.9500	C(6)-C(7)	1.4988(18)
C(4)-C(5)	1.3899(19)	C(7)-N(8)	1.4792(16)

C(7)-H(7A)	0.9900	C(27)-H(27A)	0.9900
C(7)-H(7B)	0.9900	C(27)-H(27B)	0.9900
C(9)-N(8)	1.4866(17)	C(28)-C(33)	1.3911(19)
C(9)-C(10)	1.5177(18)	C(28)-C(29)	1.4010(18)
C(9)-H(9A)	0.9900	C(29)-C(30)	1.3869(19)
C(9)-H(9B)	0.9900	C(29)-H(29)	0.9500
C(10)-C(15)	1.3946(19)	C(30)-C(31)	1.3979(18)
C(10)-C(11)	1.3995(18)	C(30)-H(30)	0.9500
C(11)-C(12)	1.3912(18)	C(31)-O(2)	1.3712(17)
C(11)-H(11)	0.9500	C(31)-C(32)	1.3913(18)
C(12)-C(13)	1.3928(19)	C(32)-C(33)	1.392(2)
C(12)-H(12)	0.9500	C(32)-H(32)	0.9500
C(13)-O(1)	1.3723(15)	C(33)-H(33)	0.9500
C(13)-C(14)	1.3913(19)	Cl(1)-Cu(1)	2.3130(4)
C(14)-C(15)	1.3932(18)	Cl(2)-Cu(1)	2.3130(3)
C(14)-H(14)	0.9500	Cl(3)-Cu(2)	2.2571(4)
C(15)-H(15)	0.9500	Cl(4)-Cu(2)	2.3024(4)
C(17)-N(16)	1.1392(18)	Cl(4)-Cu(2)#1	2.6922(4)
C(17)-C(18)	1.4549(19)	Cu(1)-N(1)	2.0254(11)
C(18)-H(18A)	0.9800	Cu(1)-N(8)	2.0463(11)
C(18)-H(18B)	0.9800	Cu(1)-N(16)	2.3020(13)
C(18)-H(18C)	0.9800	Cu(2)-N(19)	2.0101(12)
C(20)-N(19)	1.3484(18)	Cu(2)-N(26)	2.0358(11)
C(20)-C(21)	1.383(2)	Cu(2)-Cl(4)#1	2.6922(4)
C(20)-H(20)	0.9500	N(8)-H(8)	0.863(18)
C(21)-C(22)	1.392(2)	N(26)-H(26)	0.854(19)
C(21)-H(21)	0.9500	O(1)-H(1)	0.8400
C(22)-C(23)	1.380(2)	O(2)-H(2A)	0.8400
C(22)-H(22)	0.9500	N(1)-C(2)-C(3)	122.53(12)
C(23)-C(24)	1.3910(19)	N(1)-C(2)-H(2)	118.7
C(23)-H(23)	0.9500	C(3)-C(2)-H(2)	118.7
C(24)-N(19)	1.3449(17)	C(2)-C(3)-C(4)	118.86(12)
C(24)-C(25)	1.505(2)	C(2)-C(3)-H(3)	120.6
C(25)-N(26)	1.4793(17)	C(4)-C(3)-H(3)	120.6
C(25)-H(25A)	0.9900	C(5)-C(4)-C(3)	118.93(12)
C(25)-H(25B)	0.9900	C(5)-C(4)-H(4)	120.5
C(27)-N(26)	1.4974(17)	C(3)-C(4)-H(4)	120.5
C(27)-C(28)	1.5068(19)	C(4)-C(5)-C(6)	118.96(12)

C(4)-C(5)-H(5)	120.5	H(18A)-C(18)-H(18B)	109.5
C(6)-C(5)-H(5)	120.5	C(17)-C(18)-H(18C)	109.5
N(1)-C(6)-C(5)	122.09(12)	H(18A)-C(18)-H(18C)	109.5
N(1)-C(6)-C(7)	116.38(11)	H(18B)-C(18)-H(18C)	109.5
C(5)-C(6)-C(7)	121.44(11)	N(19)-C(20)-C(21)	122.16(13)
N(8)-C(7)-C(6)	111.04(10)	N(19)-C(20)-H(20)	118.9
N(8)-C(7)-H(7A)	109.4	C(21)-C(20)-H(20)	118.9
C(6)-C(7)-H(7A)	109.4	C(20)-C(21)-C(22)	118.62(14)
N(8)-C(7)-H(7B)	109.4	C(20)-C(21)-H(21)	120.7
C(6)-C(7)-H(7B)	109.4	C(22)-C(21)-H(21)	120.7
H(7A)-C(7)-H(7B)	108.0	C(23)-C(22)-C(21)	119.30(14)
N(8)-C(9)-C(10)	114.00(11)	C(23)-C(22)-H(22)	120.3
N(8)-C(9)-H(9A)	108.8	C(21)-C(22)-H(22)	120.3
C(10)-C(9)-H(9A)	108.8	C(22)-C(23)-C(24)	119.13(14)
N(8)-C(9)-H(9B)	108.8	C(22)-C(23)-H(23)	120.4
C(10)-C(9)-H(9B)	108.8	C(24)-C(23)-H(23)	120.4
H(9A)-C(9)-H(9B)	107.6	N(19)-C(24)-C(23)	121.64(13)
C(15)-C(10)-C(11)	118.17(12)	N(19)-C(24)-C(25)	116.24(12)
C(15)-C(10)-C(9)	122.06(12)	C(23)-C(24)-C(25)	122.08(13)
C(11)-C(10)-C(9)	119.77(12)	N(26)-C(25)-C(24)	111.28(11)
C(12)-C(11)-C(10)	121.21(12)	N(26)-C(25)-H(25A)	109.4
C(12)-C(11)-H(11)	119.4	C(24)-C(25)-H(25A)	109.4
C(10)-C(11)-H(11)	119.4	N(26)-C(25)-H(25B)	109.4
C(11)-C(12)-C(13)	119.68(12)	C(24)-C(25)-H(25B)	109.4
C(11)-C(12)-H(12)	120.2	H(25A)-C(25)-H(25B)	108.0
C(13)-C(12)-H(12)	120.2	N(26)-C(27)-C(28)	113.40(11)
O(1)-C(13)-C(14)	122.30(12)	N(26)-C(27)-H(27A)	108.9
O(1)-C(13)-C(12)	117.72(12)	C(28)-C(27)-H(27A)	108.9
C(14)-C(13)-C(12)	119.98(12)	N(26)-C(27)-H(27B)	108.9
C(13)-C(14)-C(15)	119.77(12)	C(28)-C(27)-H(27B)	108.9
C(13)-C(14)-H(14)	120.1	H(27A)-C(27)-H(27B)	107.7
C(15)-C(14)-H(14)	120.1	C(33)-C(28)-C(29)	118.17(12)
C(14)-C(15)-C(10)	121.18(12)	C(33)-C(28)-C(27)	120.65(12)
C(14)-C(15)-H(15)	119.4	C(29)-C(28)-C(27)	121.15(12)
C(10)-C(15)-H(15)	119.4	C(30)-C(29)-C(28)	121.53(12)
N(16)-C(17)-C(18)	179.01(15)	C(30)-C(29)-H(29)	119.2
C(17)-C(18)-H(18A)	109.5	C(28)-C(29)-H(29)	119.2
C(17)-C(18)-H(18B)	109.5	C(29)-C(30)-C(31)	119.13(12)

C(29)-C(30)-H(30)	120.4	Cl(3)-Cu(2)-Cl(4)	93.148(13)
C(31)-C(30)-H(30)	120.4	N(19)-Cu(2)-Cl(4)#1	91.29(3)
O(2)-C(31)-C(32)	117.53(12)	N(26)-Cu(2)-Cl(4)#1	86.06(3)
O(2)-C(31)-C(30)	122.11(12)	Cl(3)-Cu(2)-Cl(4)#1	96.558(12)
C(32)-C(31)-C(30)	120.35(13)	Cl(4)-Cu(2)-Cl(4)#1	95.459(11)
C(31)-C(32)-C(33)	119.50(12)	C(6)-N(1)-C(2)	118.62(11)
C(31)-C(32)-H(32)	120.2	C(6)-N(1)-Cu(1)	114.24(8)
C(33)-C(32)-H(32)	120.2	C(2)-N(1)-Cu(1)	127.02(9)
C(28)-C(33)-C(32)	121.30(12)	C(7)-N(8)-C(9)	113.03(10)
C(28)-C(33)-H(33)	119.3	C(7)-N(8)-Cu(1)	109.53(8)
C(32)-C(33)-H(33)	119.3	C(9)-N(8)-Cu(1)	114.73(8)
Cu(2)-Cl(4)-Cu(2)#1	84.542(11)	C(7)-N(8)-H(8)	107.4(12)
N(1)-Cu(1)-N(8)	82.60(4)	C(9)-N(8)-H(8)	110.4(11)
N(1)-Cu(1)-N(16)	90.95(5)	Cu(1)-N(8)-H(8)	100.8(11)
N(8)-Cu(1)-N(16)	96.18(4)	C(17)-N(16)-Cu(1)	163.95(11)
N(1)-Cu(1)-Cl(2)	95.76(3)	C(24)-N(19)-C(20)	119.10(12)
N(8)-Cu(1)-Cl(2)	171.50(3)	C(24)-N(19)-Cu(2)	114.06(9)
N(16)-Cu(1)-Cl(2)	92.18(3)	C(20)-N(19)-Cu(2)	126.53(9)
N(1)-Cu(1)-Cl(1)	167.32(3)	C(25)-N(26)-C(27)	114.14(11)
N(8)-Cu(1)-Cl(1)	86.94(3)	C(25)-N(26)-Cu(2)	108.80(8)
N(16)-Cu(1)-Cl(1)	97.32(3)	C(27)-N(26)-Cu(2)	113.25(8)
Cl(2)-Cu(1)-Cl(1)	93.526(13)	C(25)-N(26)-H(26)	108.6(13)
N(19)-Cu(2)-N(26)	82.25(5)	C(27)-N(26)-H(26)	107.4(12)
N(19)-Cu(2)-Cl(3)	95.98(3)	Cu(2)-N(26)-H(26)	104.1(12)
N(26)-Cu(2)-Cl(3)	176.89(4)	C(13)-O(1)-H(1)	109.5
N(19)-Cu(2)-Cl(4)	167.96(3)	C(31)-O(2)-H(2A)	109.5
N(26)-Cu(2)-Cl(4)	88.26(3)		

Anisotropic displacement parameters ($\text{\AA}^2 \times 10^3$) for **2.19**. The anisotropic displacement factor exponent takes the form: $-2\pi^2 [h^2 a^{*2} U_{11} + \dots + 2 h k a^* b^* U_{12}]$

	U_{11}	U_{22}	U_{33}	U_{23}	U_{13}	U_{12}
C(2)	12(1)	16(1)	20(1)	9(1)	7(1)	7(1)
C(3)	16(1)	18(1)	20(1)	9(1)	10(1)	9(1)
C(4)	20(1)	18(1)	15(1)	9(1)	6(1)	10(1)
C(5)	15(1)	17(1)	16(1)	8(1)	4(1)	9(1)
C(6)	11(1)	12(1)	15(1)	6(1)	4(1)	6(1)

C(7)	12(1)	22(1)	15(1)	10(1)	5(1)	10(1)
C(9)	14(1)	14(1)	19(1)	6(1)	4(1)	8(1)
C(10)	14(1)	16(1)	15(1)	7(1)	6(1)	9(1)
C(11)	15(1)	14(1)	17(1)	8(1)	6(1)	7(1)
C(12)	19(1)	15(1)	19(1)	9(1)	8(1)	11(1)
C(13)	17(1)	20(1)	14(1)	9(1)	7(1)	12(1)
C(14)	14(1)	16(1)	18(1)	8(1)	7(1)	8(1)
C(15)	17(1)	15(1)	20(1)	9(1)	8(1)	10(1)
C(17)	17(1)	17(1)	17(1)	8(1)	6(1)	11(1)
C(18)	16(1)	14(1)	22(1)	6(1)	6(1)	5(1)
C(20)	16(1)	17(1)	20(1)	10(1)	4(1)	8(1)
C(21)	14(1)	23(1)	31(1)	16(1)	6(1)	8(1)
C(22)	20(1)	31(1)	36(1)	23(1)	16(1)	16(1)
C(23)	25(1)	28(1)	24(1)	16(1)	14(1)	17(1)
C(24)	18(1)	16(1)	18(1)	10(1)	8(1)	11(1)
C(25)	19(1)	19(1)	14(1)	7(1)	6(1)	10(1)
C(27)	13(1)	15(1)	15(1)	7(1)	1(1)	6(1)
C(28)	13(1)	16(1)	15(1)	8(1)	4(1)	8(1)
C(29)	16(1)	18(1)	16(1)	10(1)	6(1)	10(1)
C(30)	16(1)	17(1)	13(1)	7(1)	4(1)	9(1)
C(31)	14(1)	15(1)	16(1)	8(1)	5(1)	7(1)
C(32)	20(1)	19(1)	16(1)	11(1)	8(1)	10(1)
C(33)	19(1)	19(1)	13(1)	8(1)	5(1)	10(1)
Cl(1)	17(1)	15(1)	13(1)	7(1)	3(1)	6(1)
Cl(2)	14(1)	17(1)	24(1)	10(1)	5(1)	9(1)
Cl(3)	17(1)	21(1)	14(1)	8(1)	4(1)	11(1)
Cl(4)	14(1)	14(1)	19(1)	8(1)	7(1)	8(1)
Cu(1)	10(1)	14(1)	15(1)	8(1)	4(1)	7(1)
Cu(2)	12(1)	13(1)	13(1)	6(1)	4(1)	7(1)
N(1)	11(1)	13(1)	16(1)	7(1)	5(1)	6(1)
N(8)	12(1)	14(1)	13(1)	8(1)	5(1)	7(1)
N(16)	17(1)	18(1)	24(1)	9(1)	6(1)	9(1)
N(19)	16(1)	14(1)	16(1)	8(1)	5(1)	8(1)
N(26)	14(1)	12(1)	16(1)	6(1)	4(1)	6(1)
O(1)	16(1)	21(1)	26(1)	13(1)	10(1)	13(1)
O(2)	23(1)	15(1)	17(1)	7(1)	5(1)	6(1)

Hydrogen coordinates ($\times 10^4$) and isotropic displacement parameters ($\text{\AA}^2 \times 10^3$) for

2.19.

	x	y	z	U(eq)
H(2)	2420	8500	7055	19
H(3)	2759	8406	8845	22
H(4)	4622	8361	9595	21
H(5)	6123	8484	8538	19
H(7A)	6767	9649	6923	19
H(7B)	6437	8143	6510	19
H(9A)	4669	6642	3478	20
H(9B)	4466	6199	4487	20
H(11)	5360	4761	3865	19
H(12)	7188	4524	3889	20
H(14)	9484	8481	4918	19
H(15)	7640	8696	4850	20
H(18A)	-431	3905	3717	30
H(18B)	181	3148	2870	30
H(18C)	-552	3749	2386	30
H(20)	3979	3819	11573	22
H(21)	5783	4491	10943	27
H(22)	5452	3437	8824	29
H(23)	3310	1802	7405	27
H(25A)	827	984	7158	22
H(25B)	917	-86	7474	22
H(27A)	-1300	1388	8629	19
H(27B)	-957	1189	7407	19
H(29)	444	3534	10669	19
H(30)	1833	5876	11612	19
H(32)	1926	5456	8277	21
H(33)	546	3111	7354	21
H(1)	10254	7040	4673	28
H(2A)	3021	7650	11290	31
H(8)	5886(17)	8834(18)	5049(16)	16(4)
H(26)	-524(19)	30(20)	8232(17)	23(5)

Torsion angles [°] for **2.19**

N(1)-C(2)-C(3)-C(4) 0.0(2) C(2)-C(3)-C(4)-C(5) 1.1(2)

C(3)-C(4)-C(5)-C(6)	-1.0(2)	C(28)-C(29)-C(30)-C(31)	0.9(2)
C(4)-C(5)-C(6)-N(1)	-0.1(2)	C(29)-C(30)-C(31)-O(2)	177.50(12)
C(4)-C(5)-C(6)-C(7)	176.40(13)	C(29)-C(30)-C(31)-C(32)	-1.4(2)
N(1)-C(6)-C(7)-N(8)	-23.73(16)	O(2)-C(31)-C(32)-C(33)	-177.76(12)
C(5)-C(6)-C(7)-N(8)	159.56(12)	C(30)-C(31)-C(32)-C(33)	1.1(2)
N(8)-C(9)-C(10)-C(15)	-31.24(18)	C(29)-C(28)-C(33)-C(32)	0.0(2)
N(8)-C(9)-C(10)-C(11)	148.82(12)	C(27)-C(28)-C(33)-C(32)	177.90(12)
C(15)-C(10)-C(11)-C(12)	-0.2(2)	C(31)-C(32)-C(33)-C(28)	-0.5(2)
C(9)-C(10)-C(11)-C(12)	179.75(12)	C(5)-C(6)-N(1)-C(2)	1.16(19)
C(10)-C(11)-C(12)-C(13)	0.9(2)	C(7)-C(6)-N(1)-C(2)	-175.53(12)
C(11)-C(12)-C(13)-O(1)	179.51(12)	C(5)-C(6)-N(1)-Cu(1)	-175.07(10)
C(11)-C(12)-C(13)-C(14)	-0.9(2)	C(7)-C(6)-N(1)-Cu(1)	8.24(15)
O(1)-C(13)-C(14)-C(15)	179.76(12)	C(3)-C(2)-N(1)-C(6)	-1.1(2)
C(12)-C(13)-C(14)-C(15)	0.2(2)	C(3)-C(2)-N(1)-Cu(1)	174.61(10)
C(13)-C(14)-C(15)-C(10)	0.5(2)	C(6)-C(7)-N(8)-C(9)	-102.46(13)
C(11)-C(10)-C(15)-C(14)	-0.5(2)	C(6)-C(7)-N(8)-Cu(1)	26.81(13)
C(9)-C(10)-C(15)-C(14)	179.52(12)	C(10)-C(9)-N(8)-C(7)	-57.60(15)
N(19)-C(20)-C(21)-C(22)	-0.3(2)	C(10)-C(9)-N(8)-Cu(1)	175.85(9)
C(20)-C(21)-C(22)-C(23)	1.4(2)	C(23)-C(24)-N(19)-C(20)	2.4(2)
C(21)-C(22)-C(23)-C(24)	-0.6(2)	C(25)-C(24)-N(19)-C(20)	-179.59(12)
C(22)-C(23)-C(24)-N(19)	-1.3(2)	C(23)-C(24)-N(19)-Cu(2)	-171.50(11)
C(22)-C(23)-C(24)-C(25)	-179.20(13)	C(25)-C(24)-N(19)-Cu(2)	6.47(15)
N(19)-C(24)-C(25)-N(26)	14.18(17)	C(21)-C(20)-N(19)-C(24)	-1.6(2)
C(23)-C(24)-C(25)-N(26)	-167.86(13)	C(21)-C(20)-N(19)-Cu(2)	171.51(10)
N(26)-C(27)-C(28)-C(33)	105.20(14)	C(24)-C(25)-N(26)-C(27)	100.60(13)
N(26)-C(27)-C(28)-C(29)	-77.02(15)	C(24)-C(25)-N(26)-Cu(2)	-26.95(13)
C(33)-C(28)-C(29)-C(30)	-0.3(2)	C(28)-C(27)-N(26)-C(25)	-69.46(14)
C(27)-C(28)-C(29)-C(30)	-178.11(12)	C(28)-C(27)-N(26)-Cu(2)	55.78(13)

Hydrogen bonds for **2.19** [Å and °].

D-H...A	d(D-H)	d(H...A)	d(D...A)	<(DHA)
C(2)-H(2)...Cl(2)	0.95	2.77	3.3431(14)	120
C(3)-H(3)...Cl(4)#2	0.95	2.80	3.6274(14)	146
C(7)-H(7B)...Cl(3)#3	0.99	2.79	3.7061(13)	153
C(18)-H(18B)...Cl(3)#4	0.98	2.78	3.6015(15)	142
C(20)-H(20)...Cl(3)	0.95	2.71	3.2697(15)	118
O(1)-H(1)...Cl(2)#5	0.84	2.37	3.2099(11)	175

O(2)-H(2A)...Cl(1)#6	0.84	2.31	3.1412(11)	170
N(8)-H(8)...Cl(2)#7	0.863(18)	2.825(18)	3.6810(12)	172.1(15)
N(26)-H(26)...Cl(3)#1	0.854(19)	2.672(19)	3.5147(12)	169.1(16)

2.21

Empirical formula	C ₁₃ H ₁₄ Cl ₂ N ₂ OZn		
Formula weight	350.53		
Temperature	99.92 K		
Wavelength	0.71073 Å		
Crystal system	Monoclinic		
Space group	P2 ₁ /n		
Unit cell dimensions	a = 12.7884(7) Å	α = 90°.	
	b = 8.3147(5) Å	β = 92.337(2)°.	
	c = 13.8733(7) Å	γ = 90°.	
Volume	1473.94(14) Å ³		
Z	4		
Density (calculated)	1.580 Mg/m ³		
Absorption coefficient	2.021 mm ⁻¹		
F(000)	712		
Crystal size	0.2 x 0.2 x 0.13 mm ³		
Theta range for data collection	2.857 to 28.420°.		
Index ranges	-16 ≤ h ≤ 17, -11 ≤ k ≤ 7, -18 ≤ l ≤ 18		
Reflections collected	13564		
Independent reflections	3684 [R(int) = 0.0487]		
Completeness to theta = 26.000°	99.9 %		
Absorption correction	Semi-empirical from equivalents		
Max. and min. transmission	0.7457 and 0.6619		
Refinement method	Full-matrix least-squares on F ²		
Data / restraints / parameters	3684 / 0 / 180		
Goodness-of-fit on F ²	1.019		
Final R indices [I > 2σ(I)]	R1 = 0.0323, wR2 = 0.0596		
R indices (all data)	R1 = 0.0548, wR2 = 0.0671		
Largest diff. peak and hole	0.389 and -0.435 e.Å ⁻³		

Atomic coordinates ($\times 10^4$) and equivalent isotropic displacement parameters ($\text{Å}^2 \times 10^3$) for **2.21**. U(eq) is defined as one third of the trace of the orthogonalized U_{ij} tensor.

x	y	z	U(eq)
---	---	---	-------

Cl(1)	6317(1)	5323(1)	7553(1)	21(1)
Zn(1)	5582(1)	3137(1)	8169(1)	13(1)
N(1)	6178(2)	2476(2)	9509(1)	14(1)
C(2)	6326(2)	3385(3)	10308(2)	17(1)
Cl(2)	3854(1)	3103(1)	8151(1)	17(1)
C(3)	6727(2)	2758(3)	11167(2)	19(1)
C(4)	6988(2)	1147(3)	11204(2)	22(1)
C(5)	6834(2)	209(3)	10389(2)	19(1)
C(6)	6420(2)	902(3)	9550(2)	13(1)
C(7)	6155(2)	-86(3)	8661(2)	17(1)
N(8)	6129(2)	913(2)	7776(1)	13(1)
C(9)	5526(2)	102(3)	6969(2)	16(1)
C(10)	5603(2)	1043(3)	6048(2)	14(1)
C(11)	6458(2)	827(3)	5477(2)	15(1)
C(12)	6549(2)	1659(3)	4618(2)	17(1)
C(13)	5765(2)	2736(3)	4322(2)	16(1)
C(14)	4911(2)	2970(3)	4884(2)	16(1)
C(15)	4830(2)	2121(3)	5739(2)	16(1)
O(16)	5903(2)	3525(2)	3472(1)	22(1)

Bond lengths [Å] and angles [°] for **2.21**.

Cl(1)-Zn(1)	2.2318(6)	C(7)-H(7B)	0.9900
Zn(1)-N(1)	2.0557(18)	C(7)-N(8)	1.482(3)
Zn(1)-Cl(2)	2.2093(6)	N(8)-C(9)	1.493(3)
Zn(1)-N(8)	2.0593(19)	N(8)-H(8)	0.90(3)
N(1)-C(2)	1.348(3)	C(9)-H(9A)	0.9900
N(1)-C(6)	1.346(3)	C(9)-H(9B)	0.9900
C(2)-H(2)	0.9500	C(9)-C(10)	1.505(3)
C(2)-C(3)	1.380(3)	C(10)-C(11)	1.388(3)
C(3)-H(3)	0.9500	C(10)-C(15)	1.389(3)
C(3)-C(4)	1.381(3)	C(11)-H(11)	0.9500
C(4)-H(4)	0.9500	C(11)-C(12)	1.387(3)
C(4)-C(5)	1.381(3)	C(12)-H(12)	0.9500
C(5)-H(5)	0.9500	C(12)-C(13)	1.393(3)
C(5)-C(6)	1.385(3)	C(13)-C(14)	1.381(4)
C(6)-C(7)	1.508(3)	C(13)-O(16)	1.367(3)
C(7)-H(7A)	0.9900	C(14)-H(14)	0.9500

C(14)-C(15)	1.388(3)	Zn(1)-N(8)-H(8)	111.5(18)
C(15)-H(15)	0.9500	C(7)-N(8)-Zn(1)	106.25(14)
O(16)-H(16)	0.76(3)	C(7)-N(8)-C(9)	111.20(17)
		C(7)-N(8)-H(8)	105.0(17)
N(1)-Zn(1)-Cl(1)	114.66(6)	C(9)-N(8)-Zn(1)	115.65(14)
N(1)-Zn(1)-Cl(2)	109.95(6)	C(9)-N(8)-H(8)	106.8(17)
N(1)-Zn(1)-N(8)	83.22(8)	N(8)-C(9)-H(9A)	109.5
Cl(2)-Zn(1)-Cl(1)	116.28(2)	N(8)-C(9)-H(9B)	109.5
N(8)-Zn(1)-Cl(1)	118.49(6)	N(8)-C(9)-C(10)	110.60(18)
N(8)-Zn(1)-Cl(2)	109.65(6)	H(9A)-C(9)-H(9B)	108.1
C(2)-N(1)-Zn(1)	128.89(16)	C(10)-C(9)-H(9A)	109.5
C(6)-N(1)-Zn(1)	111.94(15)	C(10)-C(9)-H(9B)	109.5
C(6)-N(1)-C(2)	119.15(19)	C(11)-C(10)-C(9)	119.8(2)
N(1)-C(2)-H(2)	118.9	C(11)-C(10)-C(15)	118.4(2)
N(1)-C(2)-C(3)	122.2(2)	C(15)-C(10)-C(9)	121.8(2)
C(3)-C(2)-H(2)	118.9	C(10)-C(11)-H(11)	119.3
C(2)-C(3)-H(3)	120.7	C(12)-C(11)-C(10)	121.4(2)
C(2)-C(3)-C(4)	118.6(2)	C(12)-C(11)-H(11)	119.3
C(4)-C(3)-H(3)	120.7	C(11)-C(12)-H(12)	120.3
C(3)-C(4)-H(4)	120.3	C(11)-C(12)-C(13)	119.3(2)
C(3)-C(4)-C(5)	119.4(2)	C(13)-C(12)-H(12)	120.3
C(5)-C(4)-H(4)	120.3	C(14)-C(13)-C(12)	120.0(2)
C(4)-C(5)-H(5)	120.3	O(16)-C(13)-C(12)	116.5(2)
C(4)-C(5)-C(6)	119.4(2)	O(16)-C(13)-C(14)	123.5(2)
C(6)-C(5)-H(5)	120.3	C(13)-C(14)-H(14)	120.0
N(1)-C(6)-C(5)	121.2(2)	C(13)-C(14)-C(15)	119.9(2)
N(1)-C(6)-C(7)	116.91(19)	C(15)-C(14)-H(14)	120.0
C(5)-C(6)-C(7)	121.7(2)	C(10)-C(15)-H(15)	119.5
C(6)-C(7)-H(7A)	109.3	C(14)-C(15)-C(10)	121.0(2)
C(6)-C(7)-H(7B)	109.3	C(14)-C(15)-H(15)	119.5
H(7A)-C(7)-H(7B)	108.0	C(13)-O(16)-H(16)	111(3)
N(8)-C(7)-C(6)	111.65(18)		
N(8)-C(7)-H(7A)	109.3		
N(8)-C(7)-H(7B)	109.3		

Anisotropic displacement parameters ($\text{\AA}^2 \times 10^3$) for **2.21**. The anisotropic displacement factor exponent takes the form: $-2\pi^2 [h^2 a^{*2} U^{11} + \dots + 2 h k a^* b^*]$

U ¹²]	U ¹¹	U ²²	U ³³	U ²³	U ¹³	U ¹²
Cl(1)	16(1)	20(1)	27(1)	9(1)	-3(1)	-5(1)
Zn(1)	14(1)	12(1)	11(1)	1(1)	-1(1)	1(1)
N(1)	17(1)	15(1)	11(1)	1(1)	0(1)	1(1)
C(2)	18(1)	17(1)	17(1)	0(1)	0(1)	-1(1)
Cl(2)	14(1)	21(1)	17(1)	1(1)	3(1)	2(1)
C(3)	20(1)	25(1)	12(1)	-2(1)	-2(1)	-5(1)
C(4)	19(1)	29(1)	16(1)	5(1)	-5(1)	0(1)
C(5)	21(1)	17(1)	18(1)	4(1)	-1(1)	2(1)
C(6)	12(1)	15(1)	13(1)	1(1)	1(1)	-1(1)
C(7)	24(1)	12(1)	14(1)	1(1)	1(1)	3(1)
N(8)	15(1)	13(1)	10(1)	-1(1)	-1(1)	1(1)
C(9)	23(1)	15(1)	12(1)	-2(1)	0(1)	-4(1)
C(10)	17(1)	14(1)	12(1)	-3(1)	-2(1)	-2(1)
C(11)	16(1)	14(1)	16(1)	-2(1)	-2(1)	0(1)
C(12)	14(1)	20(1)	17(1)	-1(1)	4(1)	-2(1)
C(13)	19(1)	16(1)	14(1)	0(1)	-1(1)	-5(1)
C(14)	17(1)	13(1)	16(1)	-2(1)	-2(1)	2(1)
C(15)	16(1)	18(1)	15(1)	-5(1)	2(1)	-1(1)
O(16)	22(1)	27(1)	18(1)	10(1)	1(1)	0(1)

Hydrogen coordinates ($\times 10^4$) and isotropic displacement parameters ($\text{\AA}^2 \times 10^3$) for **2.21**

	x	y	z	U(eq)
H(2)	6148	4494	10278	21
H(3)	6821	3422	11721	23
H(4)	7270	688	11785	26
H(5)	7012	-900	10403	23
H(7A)	6683	-949	8603	20
H(7B)	5464	-601	8728	20
H(9A)	4782	8	7134	20
H(9B)	5805	-996	6878	20
H(11)	6993	93	5679	18
H(12)	7139	1496	4235	20

H(15)	4237	2280	6119	19
H(8)	6800(20)	960(30)	7602(19)	20(7)
H(16)	5390(30)	3910(40)	3290(20)	40(11)

Torsion angles [°] for **2.21**.

Zn(1)-N(1)-C(2)-C(3)	179.17(19)
Zn(1)-N(1)-C(6)-C(5)	179.93(19)
Zn(1)-N(1)-C(6)-C(7)	-3.8(3)
Zn(1)-N(8)-C(9)-C(10)	64.8(2)
N(1)-C(2)-C(3)-C(4)	0.3(4)
N(1)-C(6)-C(7)-N(8)	26.2(3)
C(2)-N(1)-C(6)-C(5)	-1.3(4)
C(2)-N(1)-C(6)-C(7)	175.0(2)
C(2)-C(3)-C(4)-C(5)	-0.5(4)
C(3)-C(4)-C(5)-C(6)	-0.2(4)
C(4)-C(5)-C(6)-N(1)	1.1(4)
C(4)-C(5)-C(6)-C(7)	-175.1(2)
C(5)-C(6)-C(7)-N(8)	-157.5(2)
C(6)-N(1)-C(2)-C(3)	0.6(4)
C(6)-C(7)-N(8)-Zn(1)	-33.8(2)
C(6)-C(7)-N(8)-C(9)	-160.4(2)
C(7)-N(8)-C(9)-C(10)	-173.9(2)
N(8)-C(9)-C(10)-C(11)	84.0(3)
N(8)-C(9)-C(10)-C(15)	-96.8(3)
C(9)-C(10)-C(11)-C(12)	179.2(2)
C(9)-C(10)-C(15)-C(14)	-179.5(2)
C(10)-C(11)-C(12)-C(13)	0.1(3)
C(11)-C(10)-C(15)-C(14)	-0.3(3)
C(11)-C(12)-C(13)-C(14)	0.2(3)
C(11)-C(12)-C(13)-O(16)	179.6(2)
C(12)-C(13)-C(14)-C(15)	-0.5(3)
C(13)-C(14)-C(15)-C(10)	0.6(3)
C(15)-C(10)-C(11)-C(12)	0.0(3)
O(16)-C(13)-C(14)-C(15)	-179.9(2)

Hydrogen bonds for **2.21** [Å and °]

	d(D-H)	d(H...A)	d(D...A)	<(DHA)
C(2)-H(2)...Cl(2)#1	0.95	2.96	3.632(2)	129
C(5)-H(5)...Cl(2)#2	0.95	2.96	3.551(2)	121
C(12)-H(12)...Cl(2)#3	0.95	2.73	3.655(3)	165
N(8)-H(8)...Cl(1)#4	0.90(3)	2.49(3)	3.353(2)	162(2)
O(16)-H(16)...Cl(1)#5	0.76(3)	2.52(3)	3.267(2)	168(3)

2.33

Atomic coordinates ($\times 10^4$) and equivalent isotropic displacement parameters ($\text{\AA}^2 \times 10^3$) for **2.33**. $U(\text{eq})$ is defined as one third of the trace of the orthogonalized U_{ij} tensor.

	x	y	z	U(eq)
N(1)	5850(1)	7126(2)	9278(1)	20(1)
O(1)	6255(1)	10023(2)	7190(1)	21(1)
C(2)	5274(1)	7143(2)	9310(1)	26(1)
O(2)	6725(1)	9517(2)	4918(1)	23(1)
C(3)	4831(1)	5428(3)	8996(1)	28(1)
C(4)	4985(1)	3594(3)	8624(1)	30(1)
C(5)	5577(1)	3557(2)	8585(1)	27(1)
C(6)	5996(1)	5351(2)	8916(1)	17(1)
C(7)	6639(1)	5416(2)	8867(1)	20(1)
N(8)	6596(1)	6618(2)	8156(1)	18(1)
C(9)	6814(1)	5578(2)	7703(1)	16(1)
C(10)	6795(1)	6657(2)	6992(1)	15(1)
C(11)	6505(1)	8842(2)	6751(1)	16(1)
C(12)	6471(1)	9804(2)	6051(1)	17(1)
C(13)	6737(1)	8638(2)	5595(1)	17(1)
C(14)	7040(1)	6495(2)	5837(1)	18(1)
C(15)	7060(1)	5539(2)	6521(1)	16(1)

Bond lengths [Å] and angles [°] for **2.33**.

N(1)-C(2)	1.3419(17)	C(2)-H(2)	0.9500
N(1)-C(6)	1.3375(16)	C(2)-C(3)	1.377(2)
O(1)-C(11)	1.3506(14)	O(2)-C(13)	1.3527(14)
O(1)-H(1)	0.96(2)	O(2)-H(2A)	0.95(2)

C(3)-H(3)	0.9500	C(6)-C(5)-C(4)	119.23(13)
C(3)-C(4)	1.383(2)	C(6)-C(5)-H(5)	120.4
C(4)-H(4)	0.9500	N(1)-C(6)-C(5)	122.20(12)
C(4)-C(5)	1.386(2)	N(1)-C(6)-C(7)	116.75(11)
C(5)-H(5)	0.9500	C(5)-C(6)-C(7)	121.03(12)
C(5)-C(6)	1.3838(18)	C(6)-C(7)-H(7A)	109.7
C(6)-C(7)	1.5093(17)	C(6)-C(7)-H(7B)	109.7
C(7)-H(7A)	0.9900	H(7A)-C(7)-H(7B)	108.2
C(7)-H(7B)	0.9900	N(8)-C(7)-C(6)	109.69(10)
C(7)-N(8)	1.4665(15)	N(8)-C(7)-H(7A)	109.7
N(8)-C(9)	1.2851(15)	N(8)-C(7)-H(7B)	109.7
C(9)-H(9)	0.9500	C(9)-N(8)-C(7)	117.87(11)
C(9)-C(10)	1.4509(16)	N(8)-C(9)-H(9)	119.3
C(10)-C(11)	1.4146(16)	N(8)-C(9)-C(10)	121.33(11)
C(10)-C(15)	1.4030(16)	C(10)-C(9)-H(9)	119.3
C(11)-C(12)	1.3942(16)	C(11)-C(10)-C(9)	121.25(10)
C(12)-H(12)	0.9500	C(15)-C(10)-C(9)	120.52(11)
C(12)-C(13)	1.3937(16)	C(15)-C(10)-C(11)	118.22(10)
C(13)-C(14)	1.4047(17)	O(1)-C(11)-C(10)	120.82(10)
C(14)-H(14)	0.9500	O(1)-C(11)-C(12)	118.99(11)
C(14)-C(15)	1.3756(16)	C(12)-C(11)-C(10)	120.19(11)
C(15)-H(15)	0.9500	C(11)-C(12)-H(12)	120.0
C(6)-N(1)-C(2)	117.94(11)	C(13)-C(12)-C(11)	120.06(11)
C(11)-O(1)-H(1)	106.9(12)	C(13)-C(12)-H(12)	120.0
N(1)-C(2)-H(2)	118.2	O(2)-C(13)-C(12)	122.24(11)
N(1)-C(2)-C(3)	123.50(13)	O(2)-C(13)-C(14)	117.41(11)
C(3)-C(2)-H(2)	118.2	C(12)-C(13)-C(14)	120.34(11)
C(13)-O(2)-H(2A)	110.8(11)	C(13)-C(14)-H(14)	120.4
C(2)-C(3)-H(3)	120.8	C(15)-C(14)-C(13)	119.18(11)
C(2)-C(3)-C(4)	118.31(12)	C(15)-C(14)-H(14)	120.4
C(4)-C(3)-H(3)	120.8	C(10)-C(15)-H(15)	119.0
C(3)-C(4)-H(4)	120.6	C(14)-C(15)-C(10)	121.97(11)
C(3)-C(4)-C(5)	118.82(13)	C(14)-C(15)-H(15)	119
C(5)-C(4)-H(4)	120.6		
C(4)-C(5)-H(5)	120.4		

Anisotropic displacement parameters ($\text{\AA}^2 \times 10^3$) for **2.33**. The anisotropic displacement factor exponent takes the form: $-2\pi^2 [h^2 a^{*2} U^{11} + \dots + 2 h k a^* b^* U^{12}]$

	U ¹¹	U ²²	U ³³	U ²³	U ¹³	U ¹²
N(1)	21(1)	21(1)	20(1)	-1(1)	9(1)	-1(1)
O(1)	26(1)	18(1)	23(1)	2(1)	13(1)	7(1)
C(2)	24(1)	29(1)	28(1)	1(1)	14(1)	4(1)
O(2)	26(1)	24(1)	20(1)	5(1)	11(1)	6(1)
C(3)	15(1)	39(1)	28(1)	12(1)	6(1)	2(1)
C(4)	24(1)	32(1)	29(1)	2(1)	4(1)	-11(1)
C(5)	30(1)	23(1)	27(1)	-5(1)	10(1)	-4(1)
C(6)	17(1)	20(1)	14(1)	4(1)	5(1)	0(1)
C(7)	18(1)	24(1)	18(1)	4(1)	8(1)	2(1)
N(8)	17(1)	19(1)	19(1)	2(1)	8(1)	0(1)
C(9)	12(1)	14(1)	18(1)	1(1)	4(1)	0(1)
C(10)	13(1)	14(1)	16(1)	-1(1)	4(1)	-2(1)
C(11)	13(1)	15(1)	19(1)	-2(1)	6(1)	0(1)
C(12)	16(1)	14(1)	20(1)	2(1)	5(1)	2(1)
C(13)	15(1)	19(1)	16(1)	1(1)	4(1)	-3(1)
C(14)	17(1)	19(1)	17(1)	-3(1)	6(1)	1(1)
C(15)	14(1)	14(1)	19(1)	-1(1)	4(1)	1(1)

Hydrogen coordinates ($\times 10^4$) and isotropic displacement parameters ($\text{\AA}^2 \times 10^3$) for **2.33**.

	x	y	z	U(eq)
H(2)	5167	8406	9562	31
H(3)	4429	5502	9034	34
H(4)	4690	2382	8400	36
H(5)	5695	2315	8334	32
H(7A)	6943	6233	9325	24
H(7B)	6795	3815	8866	24
H(9)	6991	4073	7835	19
H(12)	6268	11255	5885	21
H(14)	7229	5716	5532	22
H(15)	7260	4077	6679	20
H(2A)	6413(9)	10700(40)	4730(11)	50(5)
H(1)	6318(10)	9090(40)	7639(12)	57(6)

Torsion angles [°] for **2.33**.

N(1)-C(2)-C(3)-C(4)	-0.4(2)
N(1)-C(6)-C(7)-N(8)	-90.03(13)
O(1)-C(11)-C(12)-C(13)	178.80(11)
C(2)-N(1)-C(6)-C(5)	-0.48(18)
C(2)-N(1)-C(6)-C(7)	178.19(11)
C(2)-C(3)-C(4)-C(5)	0.1(2)
O(2)-C(13)-C(14)-C(15)	-179.78(11)
C(3)-C(4)-C(5)-C(6)	-0.1(2)
C(4)-C(5)-C(6)-N(1)	0.3(2)
C(4)-C(5)-C(6)-C(7)	-178.32(12)
C(5)-C(6)-C(7)-N(8)	88.65(14)
C(6)-N(1)-C(2)-C(3)	0.51(19)
C(6)-C(7)-N(8)-C(9)	-127.39(12)
C(7)-N(8)-C(9)-C(10)	-179.36(10)
N(8)-C(9)-C(10)-C(11)	-3.46(18)
N(8)-C(9)-C(10)-C(15)	177.23(11)
C(9)-C(10)-C(11)-O(1)	2.21(17)
C(9)-C(10)-C(11)-C(12)	-177.58(11)
C(9)-C(10)-C(15)-C(14)	178.82(11)
C(10)-C(11)-C(12)-C(13)	-1.41(18)
C(11)-C(10)-C(15)-C(14)	-0.52(17)
C(11)-C(12)-C(13)-O(2)	-178.94(11)
C(11)-C(12)-C(13)-C(14)	-0.18(18)
C(12)-C(13)-C(14)-C(15)	1.40(18)
C(13)-C(14)-C(15)-C(10)	-1.04(18)
C(15)-C(10)-C(11)-O(1)	-178.46(10)
C(15)-C(10)-C(11)-C(12)	1.74(17)

Hydrogen bonds for **2.33** [Å and °].

D-H...A	d(D-H)	d(H...A)	d(D...A)	<(DHA)
O(2)-H(2A)...N(1)#1	0.95(2)	1.76(2)	2.7106(14)	173.1(17)
O(1)-H(1)...N(8)	0.96(2)	1.70(2)	2.5772(13)	149.8(18)

2.34

Atomic coordinates ($\times 10^4$) and equivalent isotropic displacement parameters ($\text{\AA}^2 \times 10^3$) for **2.34**. $U(\text{eq})$ is defined as one third of the trace of the orthogonalized U_{ij} tensor.

	x	y	z	U(eq)
N(1)	-2556(2)	4976(1)	2831(1)	16(1)
C(2)	-2518(2)	5624(1)	3108(1)	19(1)
C(3)	-434(2)	5933(1)	3722(1)	19(1)
C(4)	1720(2)	5556(1)	4062(1)	20(1)
C(5)	1718(2)	4889(1)	3782(1)	18(1)
C(6)	-460(2)	4614(1)	3167(1)	14(1)
C(7)	-632(2)	3896(1)	2812(1)	16(1)
N(8)	1385(2)	3491(1)	3429(1)	15(1)
C(9)	2551(2)	3074(1)	2916(1)	14(1)
C(10)	4580(2)	2660(1)	3491(1)	12(1)
C(11)	5409(2)	2727(1)	4628(1)	13(1)
C(12)	7422(2)	2350(1)	5156(1)	15(1)
C(13)	8613(2)	1893(1)	4577(1)	13(1)
C(14)	7804(2)	1810(1)	3456(1)	14(1)
C(15)	5808(2)	2197(1)	2932(1)	14(1)
O(16)	4269(2)	3160(1)	5211(1)	18(1)
O(17)	10546(2)	1549(1)	5185(1)	17(1)
C(18)	11903(2)	1072(1)	4651(1)	17(1)
C(19)	14058(2)	817(1)	5490(1)	18(1)
O(20)	13097(2)	410(1)	6248(1)	22(1)

Bond lengths [\AA] and angles [$^\circ$] for **2.34**.

N(1)-C(2)	1.3430(15)	C(5)-C(6)	1.3909(16)
N(1)-C(6)	1.3414(14)	C(6)-C(7)	1.5043(16)
C(2)-H(2)	0.9500	C(7)-H(7A)	0.9900
C(2)-C(3)	1.3831(18)	C(7)-H(7B)	0.9900
C(3)-H(3)	0.9500	C(7)-N(8)	1.4567(14)
C(3)-C(4)	1.3824(18)	N(8)-C(9)	1.2834(15)
C(4)-H(4)	0.9500	C(9)-H(9)	0.9500
C(4)-C(5)	1.3836(17)	C(9)-C(10)	1.4517(15)
C(5)-H(5)	0.9500	C(10)-C(11)	1.4152(14)

C(10)-C(15)	1.3971(15)	N(8)-C(7)-C(6)	112.17(9)
C(11)-C(12)	1.3844(15)	N(8)-C(7)-H(7A)	109.2
C(11)-O(16)	1.3497(13)	N(8)-C(7)-H(7B)	109.2
C(12)-H(12)	0.9500	C(9)-N(8)-C(7)	118.82(10)
C(12)-C(13)	1.3934(15)	N(8)-C(9)-H(9)	119.5
C(13)-C(14)	1.3992(14)	N(8)-C(9)-C(10)	121.04(10)
C(13)-O(17)	1.3576(13)	C(10)-C(9)-H(9)	119.5
C(14)-H(14)	0.9500	C(11)-C(10)-C(9)	120.84(10)
C(14)-C(15)	1.3883(15)	C(15)-C(10)-C(9)	120.82(9)
C(15)-H(15)	0.9500	C(15)-C(10)-C(11)	118.32(10)
O(16)-H(16)	0.93(2)	C(12)-C(11)-C(10)	120.15(10)
O(17)-C(18)	1.4386(14)	O(16)-C(11)-C(10)	120.86(10)
C(18)-H(18A)	0.9900	O(16)-C(11)-C(12)	118.99(9)
C(18)-H(18B)	0.9900	C(11)-C(12)-H(12)	119.9
C(18)-C(19)	1.5024(16)	C(11)-C(12)-C(13)	120.26(10)
C(19)-H(19A)	0.9900	C(13)-C(12)-H(12)	119.9
C(19)-H(19B)	0.9900	C(12)-C(13)-C(14)	120.71(10)
C(19)-O(20)	1.4172(15)	O(17)-C(13)-C(12)	114.86(9)
O(20)-H(20)	0.89(2)	O(17)-C(13)-C(14)	124.43(10)
C(6)-N(1)-C(2)	118.11(10)	C(13)-C(14)-H(14)	120.7
N(1)-C(2)-H(2)	118.3	C(15)-C(14)-C(13)	118.51(10)
N(1)-C(2)-C(3)	123.31(11)	C(15)-C(14)-H(14)	120.7
C(3)-C(2)-H(2)	118.3	C(10)-C(15)-H(15)	119.0
C(2)-C(3)-H(3)	120.9	C(14)-C(15)-C(10)	122.03(10)
C(4)-C(3)-C(2)	118.21(11)	C(14)-C(15)-H(15)	119.0
C(4)-C(3)-H(3)	120.9	C(11)-O(16)-H(16)	105.1(13)
C(3)-C(4)-H(4)	120.4	C(13)-O(17)-C(18)	118.61(8)
C(3)-C(4)-C(5)	119.25(11)	O(17)-C(18)-H(18A)	110.3
C(5)-C(4)-H(4)	120.4	O(17)-C(18)-H(18B)	110.3
C(4)-C(5)-H(5)	120.5	O(17)-C(18)-C(19)	107.04(9)
C(4)-C(5)-C(6)	119.07(11)	H(18A)-C(18)-H(18B)	108.6
C(6)-C(5)-H(5)	120.5	C(19)-C(18)-H(18A)	110.3
N(1)-C(6)-C(5)	122.05(10)	C(19)-C(18)-H(18B)	110.3
N(1)-C(6)-C(7)	115.04(10)	C(18)-C(19)-H(19A)	109.8
C(5)-C(6)-C(7)	122.90(10)	C(18)-C(19)-H(19B)	109.8
C(6)-C(7)-H(7A)	109.2	H(19A)-C(19)-H(19B)	108.2
C(6)-C(7)-H(7B)	109.2	O(20)-C(19)-C(18)	109.52(10)
H(7A)-C(7)-H(7B)	107.9	O(20)-C(19)-H(19A)	109.8

O(20)-C(19)-H(19B) 109.8 C(19)-O(20)-H(20) 106.0(13)
 Anisotropic displacement parameters ($\text{\AA}^2 \times 10^3$) for **2.34**. The anisotropic displacement factor exponent takes the form: $-2\pi^2 [h^2 a^{*2} U^{11} + \dots + 2 h k a^* b^* U^{12}]$

	U ¹¹	U ²²	U ³³	U ²³	U ¹³	U ¹²
N(1)	15(1)	16(1)	18(1)	1(1)	2(1)	2(1)
C(2)	19(1)	16(1)	22(1)	2(1)	6(1)	4(1)
C(3)	26(1)	14(1)	21(1)	-1(1)	10(1)	-1(1)
C(4)	20(1)	20(1)	19(1)	-2(1)	3(1)	-5(1)
C(5)	15(1)	17(1)	19(1)	0(1)	1(1)	0(1)
C(6)	14(1)	14(1)	14(1)	2(1)	3(1)	0(1)
C(7)	14(1)	13(1)	18(1)	1(1)	-2(1)	1(1)
N(8)	16(1)	12(1)	16(1)	2(1)	0(1)	1(1)
C(9)	15(1)	13(1)	12(1)	2(1)	0(1)	-2(1)
C(10)	14(1)	11(1)	10(1)	1(1)	1(1)	-1(1)
C(11)	16(1)	12(1)	11(1)	0(1)	2(1)	1(1)
C(12)	19(1)	15(1)	10(1)	-1(1)	0(1)	3(1)
C(13)	14(1)	13(1)	12(1)	1(1)	1(1)	1(1)
C(14)	17(1)	14(1)	12(1)	-2(1)	2(1)	1(1)
C(15)	16(1)	14(1)	10(1)	-1(1)	2(1)	-1(1)
O(16)	24(1)	18(1)	12(1)	-2(1)	1(1)	9(1)
O(17)	19(1)	19(1)	12(1)	-1(1)	0(1)	8(1)
C(18)	18(1)	16(1)	16(1)	-1(1)	3(1)	4(1)
C(19)	15(1)	17(1)	22(1)	4(1)	3(1)	2(1)
O(20)	18(1)	26(1)	23(1)	10(1)	1(1)	2(1)

Hydrogen coordinates ($\times 10^4$) and isotropic displacement parameters ($\text{\AA}^2 \times 10^3$) for **2.34**.

	x	y	z	U(eq)
H(2)	-3998	5882	2869	22
H(3)	-482	6392	3904	23
H(4)	3185	5753	4485	24
H(5)	3183	4623	4005	21
H(7A)	-2291	3712	2906	19
H(7B)	-540	3871	2029	19
H(9)	2080	3036	2148	17
H(12)	7994	2404	5916	18
H(14)	8603	1494	3063	17

H(15)	5259	2147	2170	16
H(16)	2930(40)	3341(11)	4714(18)	51(6)
H(18A)	12555	1286	4044	20
H(18B)	10772	700	4354	20
H(19A)	15236	556	5131	22
H(19B)	15004	1197	5874	22
H(20)	14410(40)	311(10)	6763(17)	40(5)

Torsion angles [°] for **2.34**.

N(1)-C(2)-C(3)-C(4)	0.31(18)
N(1)-C(6)-C(7)-N(8)	-164.52(10)
C(2)-N(1)-C(6)-C(5)	-0.30(16)
C(2)-N(1)-C(6)-C(7)	-179.14(10)
C(2)-C(3)-C(4)-C(5)	-0.08(18)
C(3)-C(4)-C(5)-C(6)	-0.31(18)
C(4)-C(5)-C(6)-N(1)	0.51(17)
C(4)-C(5)-C(6)-C(7)	179.26(11)
C(5)-C(6)-C(7)-N(8)	16.65(16)
C(6)-N(1)-C(2)-C(3)	-0.12(17)
C(6)-C(7)-N(8)-C(9)	-135.51(11)
C(7)-N(8)-C(9)-C(10)	179.82(10)
N(8)-C(9)-C(10)-C(11)	-3.04(16)
N(8)-C(9)-C(10)-C(15)	178.61(10)
C(9)-C(10)-C(11)-C(12)	-177.06(10)
C(9)-C(10)-C(11)-O(16)	2.56(16)
C(9)-C(10)-C(15)-C(14)	178.01(10)
C(10)-C(11)-C(12)-C(13)	-1.29(17)
C(11)-C(10)-C(15)-C(14)	-0.38(16)
C(11)-C(12)-C(13)-C(14)	0.27(17)
C(11)-C(12)-C(13)-O(17)	-179.45(10)
C(12)-C(13)-C(14)-C(15)	0.67(17)
C(12)-C(13)-O(17)-C(18)	-179.26(10)
C(13)-C(14)-C(15)-C(10)	-0.61(17)
C(13)-O(17)-C(18)-C(19)	174.90(9)
C(14)-C(13)-O(17)-C(18)	1.03(16)

C(15)-C(10)-C(11)-C(12)	1.34(16)
C(15)-C(10)-C(11)-O(16)	-179.04(10)
O(16)-C(11)-C(12)-C(13)	179.08(10)
O(17)-C(13)-C(14)-C(15)	-179.63(10)
O(17)-C(18)-C(19)-O(20)	70.49(12)

Hydrogen bonds for **2.34** [\AA and $^\circ$].

D-H...A	d(D-H)	d(H...A)	d(D...A)	$\angle(\text{DHA})$
C(3)-H(3)...O(16)#1	0.95	2.64	3.2140(15)	119
C(7)-H(7B)...O(17)#2	0.99	2.62	3.5685(15)	161
C(9)-H(9)...O(17)#2	0.95	2.58	3.4699(13)	156
O(16)-H(16)...N(8)	0.93(2)	1.70(2)	2.5578(12)	152(2)
O(20)-H(20)...N(1)#3	0.89(2)	2.00(2)	2.8775(13)	174.6(19)

2.44

Atomic coordinates ($\times 10^4$) and equivalent isotropic displacement parameters ($\text{\AA}^2 \times 10^3$) for **2.44**. $U(\text{eq})$ is defined as one third of the trace of the orthogonalized U_{ij} tensor.

	x	y	z	$U(\text{eq})$
Zn(1)	5000	7500	4060(1)	27(1)
Cl(1)	2943(1)	8176(1)	5520(1)	21(1)
N(4)	4028(2)	7106(2)	3196(2)	20(1)
N(1)	4776(2)	6301(2)	4615(2)	26(1)
C(3)	3658(2)	6322(2)	3430(2)	19(1)
C(8)	3067(2)	5876(3)	2869(2)	24(1)
C(2)	3895(2)	5962(3)	4315(2)	24(1)
C(5)	3846(2)	7459(3)	2408(2)	24(1)
C(6)	3286(3)	7041(3)	1822(2)	28(1)
O(1)	3721(4)	7630(3)	5665(4)	41(1)
C(7)	2884(3)	6243(3)	2065(3)	29(1)
O(3)	2210(5)	7660(5)	5224(4)	47(2)
O(2)	3180(3)	8861(3)	4876(3)	32(1)
O(4)	2721(4)	8611(4)	6328(3)	38(1)
O(2A)	3297(6)	8167(9)	4666(6)	38(4)
O(1A)	3310(9)	7405(7)	6002(7)	33(3)

O(4A)	1957(8)	8036(9)	5447(9)	32(3)
O(3A)	3085(8)	8969(6)	5974(9)	43(3)

Bond lengths [Å] and angles [°] for **2.44**.

Zn(1)-N(4)#1	2.050(3)	O(1)-Cl(1)-O(2)	107.8(3)
Zn(1)-N(4)	2.050(3)	O(3)-Cl(1)-O(1)	111.4(4)
Zn(1)-N(1)#1	2.010(3)	O(3)-Cl(1)-O(2)	110.6(3)
Zn(1)-N(1)	2.010(3)	O(3)-Cl(1)-O(4)	110.2(4)
Cl(1)-O(1)	1.437(5)	O(4)-Cl(1)-O(1)	108.0(3)
Cl(1)-O(3)	1.413(5)	O(4)-Cl(1)-O(2)	108.7(3)
Cl(1)-O(2)	1.464(4)	O(2A)-Cl(1)-O(1A)	108.5(6)
Cl(1)-O(4)	1.436(4)	O(2A)-Cl(1)-O(4A)	107.4(7)
Cl(1)-O(2A)	1.410(8)	O(1A)-Cl(1)-O(4A)	107.1(7)
Cl(1)-O(1A)	1.474(10)	O(3A)-Cl(1)-O(2A)	114.6(7)
Cl(1)-O(4A)	1.491(13)	O(3A)-Cl(1)-O(1A)	110.9(6)
Cl(1)-O(3A)	1.388(9)	O(3A)-Cl(1)-O(4A)	108.0(7)
N(4)-C(3)	1.342(5)	C(3)-N(4)-Zn(1)	111.7(2)
N(4)-C(5)	1.345(5)	C(3)-N(4)-C(5)	119.8(3)
N(1)-H(1A)	0.9100	C(5)-N(4)-Zn(1)	127.6(3)
N(1)-H(1B)	0.9100	Zn(1)-N(1)-H(1A)	110.0
N(1)-C(2)	1.481(5)	Zn(1)-N(1)-H(1B)	110.0
C(3)-C(8)	1.399(5)	H(1A)-N(1)-H(1B)	108.3
C(3)-C(2)	1.501(5)	C(2)-N(1)-Zn(1)	108.7(2)
C(8)-H(8)	0.9500	C(2)-N(1)-H(1A)	110.0
C(8)-C(7)	1.376(6)	C(2)-N(1)-H(1B)	110.0
C(2)-H(2A)	0.9900	N(4)-C(3)-C(8)	120.7(3)
C(2)-H(2B)	0.9900	N(4)-C(3)-C(2)	117.1(3)
C(5)-H(5)	0.9500	C(8)-C(3)-C(2)	122.2(3)
C(5)-C(6)	1.376(5)	C(3)-C(8)-H(8)	120.5
C(6)-H(6)	0.9500	C(7)-C(8)-C(3)	119.0(4)
C(6)-C(7)	1.385(6)	C(7)-C(8)-H(8)	120.5
C(7)-H(7)	0.9500	N(1)-C(2)-C(3)	111.5(3)
N(4)-Zn(1)-N(4)#1	99.60(17)	N(1)-C(2)-H(2A)	109.3
N(1)#1-Zn(1)-N(4)#1	84.22(12)	N(1)-C(2)-H(2B)	109.3
N(1)-Zn(1)-N(4)	84.22(12)	C(3)-C(2)-H(2A)	109.3
N(1)#1-Zn(1)-N(4)	130.27(13)	C(3)-C(2)-H(2B)	109.3
N(1)-Zn(1)-N(4)#1	130.27(13)	H(2A)-C(2)-H(2B)	108.0
N(1)-Zn(1)-N(1)#1	129.99(19)	N(4)-C(5)-H(5)	119.0

N(4)-C(5)-C(6)	122.0(4)	C(7)-C(6)-H(6)	120.7
C(6)-C(5)-H(5)	119.0	C(8)-C(7)-C(6)	119.8(4)
C(5)-C(6)-H(6)	120.7	C(8)-C(7)-H(7)	120.1
C(5)-C(6)-C(7)	118.6(4)	C(6)-C(7)-H(7)	12

Anisotropic displacement parameters ($\text{\AA}^2 \times 10^3$) for **2.44**. The anisotropic displacement factor exponent takes the form: $-2h^2 a^* U_{11} + \dots + 2hk a^* b^* U_{12}$

	U ₁₁	U ₂₂	U ₃₃	U ₂₃	U ₁₃	U ₁₂
Zn(1)	29(1)	34(1)	18(1)	0	0	-16(1)
Cl(1)	23(1)	23(1)	16(1)	1(1)	-2(1)	-2(1)
N(4)	17(1)	27(2)	16(1)	-2(1)	0(1)	-1(1)
N(1)	24(2)	40(2)	14(2)	4(1)	-1(1)	-7(1)
C(3)	17(2)	23(2)	17(2)	-5(1)	2(1)	0(1)
C(8)	21(2)	27(2)	26(2)	-9(2)	1(2)	-2(2)
C(2)	24(2)	29(2)	18(2)	1(2)	0(1)	-6(2)
C(5)	20(2)	31(2)	22(2)	3(2)	2(1)	3(2)
C(6)	22(2)	47(2)	16(2)	-3(2)	1(1)	9(2)
O(1)	42(3)	25(3)	55(4)	5(2)	1(3)	14(2)
C(7)	22(2)	43(2)	23(2)	-14(2)	-2(2)	4(2)
O(3)	48(4)	64(5)	29(3)	14(3)	-15(3)	-44(4)
O(2)	33(2)	35(3)	28(2)	11(2)	0(2)	-7(2)
O(4)	43(3)	50(3)	22(2)	-8(2)	5(2)	4(2)
O(2A)	23(5)	77(10)	13(4)	4(5)	8(3)	8(5)
O(1A)	48(7)	29(5)	22(5)	3(4)	-16(5)	6(5)
O(4A)	23(6)	35(7)	36(7)	-5(5)	-4(5)	-6(5)
O(3A)	53(7)	14(5)	61(8)	-10(5)	-4(6)	-9(4)

Hydrogen coordinates ($\times 10^4$) and isotropic displacement parameters ($\text{\AA}^2 \times 10^3$) for **2.44**.

	x	y	z	U(eq)
H(1A)	5216	5910	4460	31
H(1B)	4777	6355	5207	31
H(8)	2797	5328	3041	29
H(2A)	3427	6140	4739	28
H(2B)	3911	5299	4292	28

H(5)	4112	8014	2251	29
H(6)	3178	7294	1263	34
H(7)	2483	5950	1677	35

Torsion angles [°] for **2.44**.

Zn(1)-N(4)-C(3)-C(8)	-171.4(3)
Zn(1)-N(4)-C(3)-C(2)	9.6(4)
Zn(1)-N(4)-C(5)-C(6)	168.2(3)
Zn(1)-N(1)-C(2)-C(3)	27.8(4)
N(4)-C(3)-C(8)-C(7)	1.4(5)
N(4)-C(3)-C(2)-N(1)	-25.6(5)
N(4)-C(5)-C(6)-C(7)	1.6(6)
C(3)-N(4)-C(5)-C(6)	0.0(5)
C(3)-C(8)-C(7)-C(6)	0.2(5)
C(8)-C(3)-C(2)-N(1)	155.5(3)
C(2)-C(3)-C(8)-C(7)	-179.7(3)
C(5)-N(4)-C(3)-C(8)	-1.5(5)
C(5)-N(4)-C(3)-C(2)	179.5(3)
C(5)-C(6)-C(7)-C(8)	-1.6(6)

Hydrogen bonds for **2.44** [Å and °].

D-H...A	d(D-H)	d(H...A)	d(D...A)	<(DHA)
N(1)-H(1A)...O(2)#1	0.91	2.50	3.086(6)	123
N(1)-H(1A)...O(4)#2	0.91	2.36	3.253(7)	167
N(1)-H(1A)...O(4A)#2	0.91	2.43	3.014(14)	122
N(1)-H(1B)...O(1)#3	0.91	2.50	3.404(7)	170
N(1)-H(1B)...O(4)#3	0.91	2.61	3.168(6)	120
N(1)-H(1B)...O(1A)#3	0.91	2.19	3.012(10)	150
C(8)-H(8)...O(3A)#4	0.95	2.56	3.353(10)	141
C(2)-H(2B)...O(1A)#2	0.99	2.53	3.290(15)	133
C(2)-H(2B)...O(3A)#4	0.99	2.37	3.242(11)	146
C(5)-H(5)...O(4A)#5	0.95	2.46	3.229(13)	138
C(6)-H(6)...O(3)#6	0.95	2.35	3.251(7)	158

2.46

Atomic coordinates ($\times 10^4$) and equivalent isotropic displacement parameters ($\text{\AA}^2 \times 10^3$) for **2.46** U(eq) is defined as one third of the trace of the orthogonalized U_{ij} tensor.

	x	y	z	U(eq)
Cu(1)	6145(1)	2655(1)	1113(1)	17(1)
N(1)	5889(3)	3407(3)	51(2)	19(1)
C(2)	6832(3)	4452(3)	-35(2)	22(1)
Cu(2)	8572(1)	3346(1)	2959(1)	18(1)
C(3)	6561(4)	4887(3)	-808(3)	27(1)
C(4)	5290(3)	4237(4)	-1527(3)	28(1)
C(5)	4322(3)	3150(4)	-1449(3)	28(1)
C(6)	4653(3)	2764(3)	-653(2)	20(1)
C(7)	3651(3)	1603(3)	-518(2)	21(1)
N(8)	4310(2)	1325(3)	305(2)	17(1)
C(9)	3642(3)	255(3)	440(2)	18(1)
C(10)	4094(3)	-113(3)	1253(2)	17(1)
C(11)	5425(3)	591(3)	1954(2)	16(1)
O(12)	6387(2)	1567(2)	1855(2)	19(1)
C(13)	5729(3)	217(3)	2786(2)	18(1)
C(14)	4767(3)	-806(3)	2916(2)	23(1)
C(15)	3446(3)	-1511(3)	2221(3)	23(1)
C(16)	3138(3)	-1164(3)	1416(2)	20(1)
O(17)	4975(2)	-1215(2)	3702(2)	32(1)
C(18)	6246(4)	-493(4)	4503(3)	36(1)
C(19)	6224(4)	-1284(4)	5171(3)	41(1)
O(20)	6210(4)	-2549(3)	4631(3)	75(1)
N(21)	9555(2)	2572(3)	2138(2)	21(1)
C(22)	9740(3)	2711(3)	1263(2)	22(1)
C(23)	10405(3)	2125(3)	733(3)	27(1)
C(24)	10916(3)	1386(3)	1117(3)	27(1)
C(25)	10743(3)	1244(3)	2017(3)	26(1)
C(26)	10056(3)	1861(3)	2518(3)	21(1)
C(27)	9813(3)	1759(3)	3494(3)	26(1)
N(28)	9199(2)	2630(3)	3896(2)	19(1)
C(29)	9138(3)	2870(3)	4834(2)	20(1)
C(30)	8515(3)	3629(3)	5317(2)	19(1)

C(31)	7923(3)	4291(3)	4851(2)	18(1)
O(32)	7914(2)	4296(2)	3916(2)	19(1)
C(33)	7319(3)	4994(3)	5406(2)	18(1)
C(34)	7252(3)	4994(3)	6366(2)	17(1)
C(35)	7822(3)	4331(3)	6828(2)	21(1)
C(36)	8447(3)	3682(3)	6313(2)	20(1)
O(37)	6653(2)	5616(2)	6934(2)	20(1)
C(38)	6013(3)	6261(3)	6469(2)	21(1)
C(39)	5462(3)	6938(3)	7216(2)	22(1)
O(40)	4385(2)	6022(2)	7394(2)	23(1)
O(41)	7979(2)	3915(2)	1900(2)	19(1)
Cl(1)	389(1)	2293(1)	-2132(1)	30(1)
O(1)	1253(3)	3136(3)	-2544(2)	36(1)
O(2)	-723(3)	1168(3)	-2998(2)	45(1)
O(3)	-64(3)	3093(3)	-1438(2)	42(1)
O(4)	1119(2)	1803(3)	-1568(2)	42(1)
O(1S)	8421(17)	-1890(20)	4322(11)	64(3)
O(2S)	8874(19)	-1150(20)	4433(10)	64(3)
O(3S)	9410(40)	-630(40)	4670(20)	64(3)

Bond lengths [Å] and angles [°] for **2.46**.

Cu(1)-N(1)	1.994(3)	C(4)-C(5)	1.389(5)
Cu(1)-N(8)	1.939(2)	C(5)-H(5)	0.9500
Cu(1)-O(12)	1.937(2)	C(5)-C(6)	1.382(4)
Cu(1)-O(41)	1.919(2)	C(6)-C(7)	1.505(4)
N(1)-C(2)	1.350(4)	C(7)-H(7A)	0.9900
N(1)-C(6)	1.347(4)	C(7)-H(7B)	0.9900
C(2)-H(2)	0.9500	C(7)-N(8)	1.463(4)
C(2)-C(3)	1.377(4)	N(8)-C(9)	1.288(4)
Cu(2)-O(12)	2.400(2)	C(9)-H(9)	0.9500
Cu(2)-N(21)	2.007(3)	C(9)-C(10)	1.428(4)
Cu(2)-N(28)	1.939(3)	C(10)-C(11)	1.422(4)
Cu(2)-O(32)	1.926(2)	C(10)-C(16)	1.422(4)
Cu(2)-O(41)	1.934(2)	C(11)-O(12)	1.323(4)
C(3)-H(3)	0.9500	C(11)-C(13)	1.411(4)
C(3)-C(4)	1.383(5)	C(13)-H(13)	0.9500
C(4)-H(4)	0.9500	C(13)-C(14)	1.378(4)

C(14)-C(15)	1.409(5)	C(35)-H(35)	0.9500
C(14)-O(17)	1.359(4)	C(35)-C(36)	1.367(4)
C(15)-H(15)	0.9500	C(36)-H(36)	0.9500
C(15)-C(16)	1.357(4)	O(37)-C(38)	1.439(4)
C(16)-H(16)	0.9500	C(38)-H(38A)	0.9900
O(17)-C(18)	1.426(4)	C(38)-H(38B)	0.9900
C(18)-H(18A)	0.9900	C(38)-C(39)	1.499(4)
C(18)-H(18B)	0.9900	C(39)-H(39A)	0.9900
C(18)-C(19)	1.509(5)	C(39)-H(39B)	0.9900
C(19)-H(19A)	0.9900	C(39)-O(40)	1.424(4)
C(19)-H(19B)	0.9900	O(40)-H(40)	0.8400
C(19)-O(20)	1.423(5)	O(41)-H(41)	0.9834
O(20)-H(20)	0.8400	Cl(1)-O(1)	1.460(3)
N(21)-C(22)	1.348(4)	Cl(1)-O(2)	1.434(3)
N(21)-C(26)	1.347(4)	Cl(1)-O(3)	1.444(3)
C(22)-H(22)	0.9500	Cl(1)-O(4)	1.435(2)
C(22)-C(23)	1.375(4)	N(8)-Cu(1)-N(1)	82.86(10)
C(23)-H(23)	0.9500	O(12)-Cu(1)-N(1)	165.65(10)
C(23)-C(24)	1.386(5)	O(12)-Cu(1)-N(8)	92.54(10)
C(24)-H(24)	0.9500	O(41)-Cu(1)-N(1)	98.18(10)
C(24)-C(25)	1.380(5)	O(41)-Cu(1)-N(8)	177.80(10)
C(25)-H(25)	0.9500	O(41)-Cu(1)-O(12)	85.99(9)
C(25)-C(26)	1.398(4)	C(2)-N(1)-Cu(1)	126.3(2)
C(26)-C(27)	1.497(5)	C(6)-N(1)-Cu(1)	115.1(2)
C(27)-H(27A)	0.9900	C(6)-N(1)-C(2)	118.6(3)
C(27)-H(27B)	0.9900	N(1)-C(2)-H(2)	119.0
C(27)-N(28)	1.470(4)	N(1)-C(2)-C(3)	122.0(3)
N(28)-C(29)	1.299(4)	C(3)-C(2)-H(2)	119.0
C(29)-H(29)	0.9500	N(21)-Cu(2)-O(12)	96.02(9)
C(29)-C(30)	1.425(4)	N(28)-Cu(2)-O(12)	104.37(9)
C(30)-C(31)	1.423(4)	N(28)-Cu(2)-N(21)	82.17(11)
C(30)-C(36)	1.419(4)	O(32)-Cu(2)-O(12)	93.26(8)
C(31)-O(32)	1.331(4)	O(32)-Cu(2)-N(21)	170.58(10)
C(31)-C(33)	1.411(4)	O(32)-Cu(2)-N(28)	94.00(10)
C(33)-H(33)	0.9500	O(32)-Cu(2)-O(41)	92.43(9)
C(33)-C(34)	1.383(4)	O(41)-Cu(2)-O(12)	73.82(8)
C(34)-C(35)	1.407(4)	O(41)-Cu(2)-N(21)	91.68(10)
C(34)-O(37)	1.362(4)	O(41)-Cu(2)-N(28)	173.42(10)

C(2)-C(3)-H(3)	120.2	O(17)-C(14)-C(15)	114.3(3)
C(2)-C(3)-C(4)	119.6(3)	C(14)-C(15)-H(15)	120.7
C(4)-C(3)-H(3)	120.2	C(16)-C(15)-C(14)	118.6(3)
C(3)-C(4)-H(4)	120.7	C(16)-C(15)-H(15)	120.7
C(3)-C(4)-C(5)	118.6(3)	C(10)-C(16)-H(16)	118.8
C(5)-C(4)-H(4)	120.7	C(15)-C(16)-C(10)	122.5(3)
C(4)-C(5)-H(5)	120.4	C(15)-C(16)-H(16)	118.8
C(6)-C(5)-C(4)	119.2(3)	C(14)-O(17)-C(18)	119.1(3)
C(6)-C(5)-H(5)	120.4	O(17)-C(18)-H(18A)	110.4
N(1)-C(6)-C(5)	122.1(3)	O(17)-C(18)-H(18B)	110.4
N(1)-C(6)-C(7)	116.0(3)	O(17)-C(18)-C(19)	106.6(3)
C(5)-C(6)-C(7)	122.0(3)	H(18A)-C(18)-H(18B)	108.6
C(6)-C(7)-H(7A)	109.7	C(19)-C(18)-H(18A)	110.4
C(6)-C(7)-H(7B)	109.7	C(19)-C(18)-H(18B)	110.4
H(7A)-C(7)-H(7B)	108.2	C(18)-C(19)-H(19A)	109.2
N(8)-C(7)-C(6)	109.9(2)	C(18)-C(19)-H(19B)	109.2
N(8)-C(7)-H(7A)	109.7	H(19A)-C(19)-H(19B)	107.9
N(8)-C(7)-H(7B)	109.7	O(20)-C(19)-C(18)	111.9(3)
C(7)-N(8)-Cu(1)	115.42(19)	O(20)-C(19)-H(19A)	109.2
C(9)-N(8)-Cu(1)	125.9(2)	O(20)-C(19)-H(19B)	109.2
C(9)-N(8)-C(7)	118.6(3)	C(19)-O(20)-H(20)	109.5
N(8)-C(9)-H(9)	117.0	C(22)-N(21)-Cu(2)	125.5(2)
N(8)-C(9)-C(10)	126.0(3)	C(26)-N(21)-Cu(2)	115.3(2)
C(10)-C(9)-H(9)	117.0	C(26)-N(21)-C(22)	119.2(3)
C(11)-C(10)-C(9)	123.2(3)	N(21)-C(22)-H(22)	119.0
C(11)-C(10)-C(16)	118.6(3)	N(21)-C(22)-C(23)	122.0(3)
C(16)-C(10)-C(9)	118.0(3)	C(23)-C(22)-H(22)	119.0
O(12)-C(11)-C(10)	122.9(3)	C(22)-C(23)-H(23)	120.5
O(12)-C(11)-C(13)	118.9(3)	C(22)-C(23)-C(24)	119.0(3)
C(13)-C(11)-C(10)	118.2(3)	C(24)-C(23)-H(23)	120.5
Cu(1)-O(12)-Cu(2)	91.19(8)	C(23)-C(24)-H(24)	120.2
C(11)-O(12)-Cu(1)	125.73(18)	C(25)-C(24)-C(23)	119.6(3)
C(11)-O(12)-Cu(2)	135.86(18)	C(25)-C(24)-H(24)	120.2
C(11)-C(13)-H(13)	119.4	C(24)-C(25)-H(25)	120.7
C(14)-C(13)-C(11)	121.1(3)	C(24)-C(25)-C(26)	118.6(3)
C(14)-C(13)-H(13)	119.4	C(26)-C(25)-H(25)	120.7
C(13)-C(14)-C(15)	121.0(3)	N(21)-C(26)-C(25)	121.5(3)
O(17)-C(14)-C(13)	124.7(3)	N(21)-C(26)-C(27)	116.0(3)

C(25)-C(26)-C(27)	122.4(3)	C(39)-C(38)-H(38B)	109.8
C(26)-C(27)-H(27A)	109.7	C(38)-C(39)-H(39A)	108.6
C(26)-C(27)-H(27B)	109.7	C(38)-C(39)-H(39B)	108.6
H(27A)-C(27)-H(27B)	108.2	H(39A)-C(39)-H(39B)	107.6
N(28)-C(27)-C(26)	109.7(3)	O(40)-C(39)-C(38)	114.5(3)
N(28)-C(27)-H(27A)	109.7	O(40)-C(39)-H(39A)	108.6
N(28)-C(27)-H(27B)	109.7	O(40)-C(39)-H(39B)	108.6
C(27)-N(28)-Cu(2)	115.7(2)	C(39)-O(40)-H(40)	109.5
C(29)-N(28)-Cu(2)	125.9(2)	Cu(1)-O(41)-Cu(2)	107.92(10)
C(29)-N(28)-C(27)	118.4(3)	Cu(1)-O(41)-H(41)	114.5
N(28)-C(29)-H(29)	117.3	Cu(2)-O(41)-H(41)	110.5
N(28)-C(29)-C(30)	125.3(3)	O(2)-Cl(1)-O(1)	108.21(16)
C(30)-C(29)-H(29)	117.3	O(2)-Cl(1)-O(3)	110.17(16)
C(31)-C(30)-C(29)	124.4(3)	O(2)-Cl(1)-O(4)	110.00(16)
C(36)-C(30)-C(29)	117.2(3)	O(3)-Cl(1)-O(1)	109.61(16)
C(36)-C(30)-C(31)	118.4(3)	O(4)-Cl(1)-O(1)	109.14(15)
O(32)-C(31)-C(30)	123.6(3)	O(4)-Cl(1)-O(3)	109.68(17)
O(32)-C(31)-C(33)	117.6(3)		
C(33)-C(31)-C(30)	118.8(3)		
C(31)-O(32)-Cu(2)	126.56(19)		
C(31)-C(33)-H(33)	119.6		
C(34)-C(33)-C(31)	120.8(3)		
C(34)-C(33)-H(33)	119.6		
C(33)-C(34)-C(35)	120.8(3)		
O(37)-C(34)-C(33)	124.2(3)		
O(37)-C(34)-C(35)	114.9(3)		
C(34)-C(35)-H(35)	120.5		
C(36)-C(35)-C(34)	118.9(3)	C(36)-C(35)-	
H(35)	120.5		
C(30)-C(36)-H(36)	118.9		
C(35)-C(36)-C(30)	122.3(3)		
C(35)-C(36)-H(36)	118.9		
C(34)-O(37)-C(38)	116.6(2)		
O(37)-C(38)-H(38A)	109.8		
O(37)-C(38)-H(38B)	109.8		
O(37)-C(38)-C(39)	109.4(2)		
H(38A)-C(38)-H(38B)	108.2		
C(39)-C(38)-H(38A)	109.8		

Anisotropic displacement parameters ($\text{\AA}^2 \times 10^3$) for **2.46**. The anisotropic displacement factor exponent takes the form: $-2\pi^2 [h^2 a^{*2} U^{11} + \dots + 2 h k a^* b^* U^{12}]$

	U ¹¹	U ²²	U ³³	U ²³	U ¹³	U ¹²
Cu(1)	16(1)	18(1)	19(1)	10(1)	9(1)	8(1)
N(1)	22(1)	21(1)	20(1)	9(1)	12(1)	12(1)
C(2)	26(2)	20(2)	23(2)	10(1)	12(1)	10(2)
Cu(2)	18(1)	21(1)	20(1)	10(1)	10(1)	11(1)
C(3)	37(2)	23(2)	34(2)	18(2)	21(2)	16(2)
C(4)	36(2)	38(2)	32(2)	25(2)	19(2)	27(2)
C(5)	26(2)	41(2)	34(2)	25(2)	17(2)	24(2)
C(6)	21(2)	26(2)	25(2)	14(1)	14(1)	16(2)
C(7)	17(2)	28(2)	23(2)	13(2)	8(1)	12(2)
N(8)	16(1)	21(1)	17(1)	10(1)	8(1)	9(1)
C(9)	16(2)	21(2)	18(2)	7(1)	9(1)	9(1)
C(10)	18(2)	17(2)	18(2)	7(1)	9(1)	9(1)
C(11)	18(2)	16(2)	21(2)	8(1)	11(1)	10(1)
O(12)	18(1)	19(1)	22(1)	12(1)	9(1)	7(1)
C(13)	18(2)	18(2)	18(2)	7(1)	7(1)	7(1)
C(14)	28(2)	23(2)	21(2)	12(1)	10(1)	11(2)
C(15)	22(2)	20(2)	29(2)	14(2)	14(1)	6(1)
C(16)	16(2)	19(2)	22(2)	7(1)	8(1)	7(1)
O(17)	30(1)	35(1)	27(1)	22(1)	7(1)	5(1)
C(18)	32(2)	34(2)	32(2)	19(2)	2(2)	5(2)
C(19)	46(2)	40(2)	31(2)	23(2)	7(2)	11(2)
O(20)	136(4)	65(2)	51(2)	42(2)	36(2)	54(2)
N(21)	16(1)	19(1)	23(1)	7(1)	8(1)	4(1)
C(22)	15(2)	24(2)	21(2)	6(1)	7(1)	5(1)
C(23)	19(2)	28(2)	24(2)	6(2)	10(1)	4(2)
C(24)	20(2)	26(2)	29(2)	3(2)	13(2)	7(2)
C(25)	20(2)	20(2)	36(2)	8(2)	12(2)	9(2)
C(26)	16(2)	17(2)	29(2)	8(1)	11(1)	5(1)
C(27)	30(2)	24(2)	35(2)	16(2)	19(2)	17(2)
N(28)	16(1)	19(1)	27(2)	10(1)	11(1)	9(1)
C(29)	20(2)	19(2)	24(2)	12(1)	8(1)	10(1)
C(30)	18(2)	20(2)	21(2)	10(1)	5(1)	9(1)
C(31)	15(2)	19(2)	18(2)	7(1)	6(1)	7(1)

O(32)	22(1)	25(1)	18(1)	12(1)	9(1)	16(1)
C(33)	17(2)	21(2)	20(2)	10(1)	6(1)	11(1)
C(34)	14(2)	16(2)	20(2)	6(1)	6(1)	6(1)
C(35)	24(2)	21(2)	16(2)	9(1)	6(1)	9(1)
C(36)	22(2)	21(2)	23(2)	12(1)	8(1)	11(1)
O(37)	25(1)	25(1)	19(1)	11(1)	11(1)	17(1)
C(38)	24(2)	27(2)	20(2)	12(1)	10(1)	16(2)
C(39)	22(2)	28(2)	24(2)	13(2)	12(1)	15(2)
O(40)	21(1)	34(1)	24(1)	16(1)	10(1)	17(1)
O(41)	18(1)	20(1)	21(1)	10(1)	8(1)	8(1)
Cl(1)	24(1)	28(1)	37(1)	18(1)	5(1)	11(1)
O(1)	42(2)	35(2)	45(2)	26(1)	21(1)	19(1)
O(2)	34(2)	35(2)	45(2)	8(1)	-7(1)	11(1)
O(3)	33(2)	43(2)	50(2)	14(1)	20(1)	18(1)
O(4)	28(1)	46(2)	60(2)	38(2)	7(1)	16(1)
O(1S)	73(7)	81(7)	53(4)	27(5)	27(4)	48(6)
O(2S)	73(7)	81(7)	53(4)	27(5)	27(4)	48(6)
O(3S)	73(7)	81(7)	53(4)	27(5)	27(4)	48(6)

Hydrogen coordinates ($\times 10^4$) and isotropic displacement parameters ($\text{\AA}^2 \times 10^3$) for **2.46**.

	x	y	z	U(eq)
H(2)	7709	4900	453	27
H(3)	7242	5628	-848	32
H(4)	5083	4527	-2062	34
H(5)	3443	2677	-1937	33
H(7A)	2956	1839	-329	26
H(7B)	3218	779	-1186	26
H(9)	2769	-344	-45	22
H(13)	6613	677	3265	22
H(15)	2786	-2215	2313	27
H(16)	2249	-1640	945	24
H(18A)	6409	442	4929	43
H(18B)	6958	-432	4190	43
H(19A)	7018	-731	5813	49
H(19B)	5426	-1456	5387	49
H(20)	6915	-2404	4487	113

H(22)	9401	3229	1006	27
H(23)	10511	2225	112	32
H(24)	11384	980	764	33
H(25)	11085	738	2289	32
H(27A)	9219	801	3340	31
H(27B)	10666	2050	4030	31
H(29)	9542	2509	5231	24
H(33)	6955	5474	5118	22
H(35)	7773	4333	7487	25
H(36)	8849	3252	6633	24
H(38A)	5286	5571	5807	25
H(38B)	6663	6947	6306	25
H(39A)	6186	7558	7895	26
H(39B)	5158	7502	6940	26
H(40)	3663	5823	6960	35
H(41)	8158	4873	2221	54(13)

Torsion angles [°] for **2.46**.

Cu(1)-N(1)-C(2)-C(3)	179.0(2)
Cu(1)-N(1)-C(6)-C(5)	-178.9(2)
Cu(1)-N(1)-C(6)-C(7)	1.3(3)
Cu(1)-N(8)-C(9)-C(10)	4.3(4)
N(1)-C(2)-C(3)-C(4)	-0.4(5)
N(1)-C(6)-C(7)-N(8)	-6.8(4)
C(2)-N(1)-C(6)-C(5)	-0.6(4)
C(2)-N(1)-C(6)-C(7)	179.6(3)
C(2)-C(3)-C(4)-C(5)	-0.5(5)
Cu(2)-N(21)-C(22)-C(23)	-178.7(2)
Cu(2)-N(21)-C(26)-C(25)	178.9(2)
Cu(2)-N(21)-C(26)-C(27)	-0.3(3)
Cu(2)-N(28)-C(29)-C(30)	4.6(5)
C(3)-C(4)-C(5)-C(6)	0.8(5)
C(4)-C(5)-C(6)-N(1)	-0.2(5)
C(4)-C(5)-C(6)-C(7)	179.5(3)
C(5)-C(6)-C(7)-N(8)	173.4(3)
C(6)-N(1)-C(2)-C(3)	0.9(4)
C(6)-C(7)-N(8)-Cu(1)	9.4(3)
C(6)-C(7)-N(8)-C(9)	-171.4(3)

C(7)-N(8)-C(9)-C(10)	-174.8(3)
N(8)-C(9)-C(10)-C(11)	-8.0(5)
N(8)-C(9)-C(10)-C(16)	166.9(3)
C(9)-C(10)-C(11)-O(12)	-6.3(5)
C(9)-C(10)-C(11)-C(13)	174.3(3)
C(9)-C(10)-C(16)-C(15)	-174.5(3)
C(10)-C(11)-O(12)-Cu(1)	22.4(4)
C(10)-C(11)-O(12)-Cu(2)	163.5(2)
C(10)-C(11)-C(13)-C(14)	0.2(4)
C(11)-C(10)-C(16)-C(15)	0.6(5)
C(11)-C(13)-C(14)-C(15)	0.0(5)
C(11)-C(13)-C(14)-O(17)	-179.2(3)
O(12)-C(11)-C(13)-C(14)	-179.1(3)
C(13)-C(11)-O(12)-Cu(1)	-158.2(2)
C(13)-C(11)-O(12)-Cu(2)	-17.1(4)
C(13)-C(14)-C(15)-C(16)	0.0(5)
C(13)-C(14)-O(17)-C(18)	4.6(5)
C(14)-C(15)-C(16)-C(10)	-0.3(5)
C(14)-O(17)-C(18)-C(19)	-173.0(3)
C(15)-C(14)-O(17)-C(18)	-174.6(3)
C(16)-C(10)-C(11)-O(12)	178.8(3)
C(16)-C(10)-C(11)-C(13)	-0.5(4)
O(17)-C(14)-C(15)-C(16)	179.3(3)
O(17)-C(18)-C(19)-O(20)	69.7(4)
N(21)-C(22)-C(23)-C(24)	-1.0(5)
N(21)-C(26)-C(27)-N(28)	-7.0(4)
C(22)-N(21)-C(26)-C(25)	-1.1(4)
C(22)-N(21)-C(26)-C(27)	179.7(3)
C(22)-C(23)-C(24)-C(25)	0.4(5)
C(23)-C(24)-C(25)-C(26)	-0.3(5)
C(24)-C(25)-C(26)-N(21)	0.6(5)
C(24)-C(25)-C(26)-C(27)	179.7(3)
C(25)-C(26)-C(27)-N(28)	173.8(3)
C(26)-N(21)-C(22)-C(23)	1.3(4)
C(26)-C(27)-N(28)-Cu(2)	11.5(3)
C(26)-C(27)-N(28)-C(29)	-167.6(3)
C(27)-N(28)-C(29)-C(30)	-176.5(3)
N(28)-C(29)-C(30)-C(31)	-3.1(5)

N(28)-C(29)-C(30)-C(36)	174.6(3)
C(29)-C(30)-C(31)-O(32)	-1.6(5)
C(29)-C(30)-C(31)-C(33)	179.0(3)
C(29)-C(30)-C(36)-C(35)	-177.1(3)
C(30)-C(31)-O(32)-Cu(2)	4.2(4)
C(30)-C(31)-C(33)-C(34)	-2.8(4)
C(31)-C(30)-C(36)-C(35)	0.7(5)
C(31)-C(33)-C(34)-C(35)	2.1(5)
C(31)-C(33)-C(34)-O(37)	-178.0(3)
O(32)-C(31)-C(33)-C(34)	177.8(3)
C(33)-C(31)-O(32)-Cu(2)	-176.4(2)
C(33)-C(34)-C(35)-C(36)	0.0(5)
C(33)-C(34)-O(37)-C(38)	2.5(4)
C(34)-C(35)-C(36)-C(30)	-1.4(5)
C(34)-O(37)-C(38)-C(39)	-177.6(3)
C(35)-C(34)-O(37)-C(38)	-177.7(3)
C(36)-C(30)-C(31)-O(32)	-179.3(3)
C(36)-C(30)-C(31)-C(33)	1.4(4)
O(37)-C(34)-C(35)-C(36)	-179.8(3)
O(37)-C(38)-C(39)-O(40)	-67.6(3)

Hydrogen bonds for **2.46** [Å and °].

D-H...A	d(D-H)	d(H...A)	d(D...A)	<(DHA)
C(2)-H(2)...O(3)#1	0.95	2.58	3.457(4)	154
C(7)-H(7A)...O(4)	0.99	2.47	3.142(4)	125
C(19)-H(19A)...O(2)#2	0.99	2.51	3.450(5)	157
O(20)-H(20)...O(1S)	0.84	1.70	2.531(17)	172
O(20)-H(20)...O(2S)	0.84	2.21	3.00(2)	156
C(22)-H(22)...O(41)	0.95	2.45	2.972(4)	114
C(23)-H(23)...O(4)#3	0.95	2.57	3.464(4)	158
C(27)-H(27B)...O(1S)#4	0.99	2.48	3.313(14)	142
O(40)-H(40)...O(32)#5	0.84	1.94	2.766(3)	170
O(41)-H(41)...O(1)#1	0.98	2.02	2.972(3)	163